Development, Anatomy, and Phylogenetic Relationships of Jawless Vertebrates and Tests of Hypotheses about Early Vertebrate Evolution

by

Tetsuto Miyashita

A thesis submitted in partial fulfillment of the requirements for the degree of

Doctor of Philosophy

in

Systematics and Evolution

Department of Biological Sciences
University of Alberta

ABSTRACT

The origin and early evolution of vertebrates remain one of the central questions of comparative biology. This clade, which features a breathtaking diversity of complex forms, has generated profound, unresolved questions, including: How are major lineages of vertebrates related to one another? What suite of characters existed in the last common ancestor of all living vertebrates? Does information from seemingly 'primitive' groups — jawless vertebrates, cartilaginous fishes, or even invertebrate outgroups — inform us about evolutionary transitions to novel morphologies like the neural crest or jaw? Alfred Romer once likened a search for the elusive vertebrate archetype to a study of the Apocalypse: "That way leads to madness."

I attempt to address these questions using extinct and extant cyclostomes (hagfish, lampreys, and their kin). As the sole living lineage of jawless vertebrates, cyclostomes diverged during the earliest phases of vertebrate evolution. However, precise relationships and evolutionary scenarios remain highly controversial, due to their poor fossil record and specialized morphology.

Through a comparative analysis of embryos, I identified significant developmental similarities and differences between hagfish and lampreys, and delineated specific problems to be explored. I attacked the first problem — whether cyclostomes form a clade or represent a grade — in a description and phylogenetic analyses of a new, nearly complete fossil hagfish from the Cenomanian of Lebanon. Aided by a detailed analysis of morphological characters, new phylogenetic trees recovered cyclostomes as a clade. This is the first morphological phylogeny to yield cyclostomes as monophyletic and therefore helps reconcile a major point of conflict between morphology- and molecule-based phylogenetics.

I tested the second problem — the assumption that living lampreys pass through a filter-feeding larval stage resembling ancestors of vertebrates — using a growth series of a fossil lamprey from the Late Devonian of South Africa. Surprisingly, these fossil lamprey larvae bear little morphological resemblance to larvae of living lampreys. Instead, the growth series reveals ontogenetic transition of traits that are consistent with the predatory habit of modern lamprey adults. Through comparison to other Paleozoic stem lampreys, I suggest that the filter-feeding larval stage evolved independently within vertebrates. Under this new scenario, larvae of living lampreys are a poor model with which to reconstruct primitive vertebrate characters.

For the third problem — how biting jaws evolved in vertebrates — I focused on one key feature of the jaw apparatus: the jaw joint. Using gene expression profiles and gene knockouts in lamprey and zebrafish embryos, I tested three hypotheses proposed to explain the origin of the jaw joint. Preliminary results suggest that a jaw joint may originate from a blood sinus pinched between two cartilages, or from a type of immature cartilaginous tissue. I describe a new genetic line of zebrafish that carries a mutation in the homeodomain-coding sequence of *nkx3.2* — a jaw joint marker gene. Homozygous mutants have fused upper and lower jaw cartilages, replicating *nkx3.2* morphants. At the adult stage, the mutants developed craniofacial phenotypes that resemble some of the jawless stem gnathostomes.

Finally, I propose an analytical pipeline to address a number of remaining questions in early vertebrate phylogeny: supertrees as a platform for future modular analyses of morphological characters. By sorting individual characters by different biological attributes, I hope to illustrate a view on early vertebrate evolution through understanding the dynamics of character evolution.

PREFACE

This thesis is an original work by Tetsuto Miyashita. The research, of this thesis is a part, received research ethics approval from the University of Alberta Research Ethics Board, title "Evolutionary origin of vertebrate jaws" on May 4, 2014, under ID AUP00000793. Some of the research conducted for this thesis forms part of collaborative projects:

Chapter 1 of this thesis is a revised version of a chapter for a book in press (*Evolution and Development of Fishes*, Cambridge University Press; edited by Z. Johanson, M. Richter, and C. Underwood). Title: Comparative development of cyclostomes. Authors: Tetsuto Miyashita, Stephen A. Green, Marianne E. Bronner. The manuscript was drafted by me. S.A.G. contributed photographs for Fig. 1.4. M.E.B. provided resources with which to conduct this work at California Institute of Technology.

Chapter 2 of this thesis presents results from collaboration led by Philip Currie at the University of Alberta. Synchrotron radiation scanning was conducted and the data processed by Phillip Manning at Mace Brown Museum of Natural History and colleagues. All other results, including interpretation of the results from synchrotron radiation scanning, are my own.

Chapter 3 of this thesis presents results from collaboration with Robert Gess at Albany Museum, who collected specimens described in the chapter. All results, including illustrations, phylogenetic and morphological analyses, and anatomical interpretations, are my own, unless cited otherwise.

Chapter 4 of this thesis presents results from collaboration with Ted Allison at the University of Alberta and Marianne Bronner at California Institute of Technology. Both Allison and Bronner provided laboratory space, resources, and animals. All results and interpretations are my own, unless cited otherwise.

Безмерное и бесконечное так же необходимо человеку, как и та малая планета, на которой он обитает.

The infinitely unfathomable is as essential for man as the little planet on which he dwells.

— *Demons*, Fyodor Dostoevsky

セロニアス・モンクはあの不可思議な和音を、理屈や論理で考え出したわけじゃあらない。彼はただしっかり目を見開いて、それを意識の暗闇の中から両手ですくい上げただけなのだ。大事なのは無から何かを創りあげることではあらない。諸君のやるべきはむしろ、今そこにあるものの中から、正しいものを見つけ出すことなのだ。

Thelonius Monk didn't need theories or logics to come up with those inexplicable chords. He only stared into darkness, keeping his eyes peeled and reaching out for the unfathomable. Nobody is asking y'all to create something out of nothing. Finding something right from what y'all have already got there — that's precisely what y'all gotta do.

— *Killing Commendatore*, Haruki Murakami
(Translation by T.M.)

ACKNOWLEDGEMENTS

When I entered the graduate program, my advisor Rich Palmer gave me Steven Weinberg's commencement address "Four Golden Lessons". In retrospect, the golden lessons were a development plan for me. As true as those lessons were, however, Weinberg overlooked one crucial item: the value of trust. The freedom and support given to me was the gift of confidence he had in me that — perhaps not so earned at the time but eventually — I will put it to a good use. I will continue to feel that confidence as I move on. Thank you, Rich. I will be measuring my success by whether you would be proud of (not so much what I accomplish but) how I develop myself as a student of biology. Using baseball reference, you have been a great manager. You took some heat for me, and still sent me out there to pitch a game.

If Rich was my equivalent of an MLB manager, Philip Currie would be that coach who believed in me through the farm system. No one else watched me growing up as long as you did, or brought me all the way up from the rookie league. Phil, I will be looking back to you constantly for exactly the same reasons with Rich. Keeping on this metaphor, Eva Koppelhus was my great General Manager without whom I would not have a contract with this team.

I have had an unparalleled squad of amazing coaches — Michael Coates, Ted Allison, Marianne Bronner, Philippe Janvier, Richard Strathmann, Richard Behringer, and Brian Hall. They served as *ad hoc* advisors, provided their lab spaces and resources for my thesis research, and took me under their wing when I was playing a visitor game. Of course, I would not be able to play without the ground-keeping crew, physical training team, and clubhouse staff — they are technicians in the labs who facilitated my work, collection managers and assistants at the museums who provided access to the specimens, staff at marine labs who let me have all the fun in the world (but not more than all that is there), field assistants who protected me from killing myself doing something stupid, library staff who went on a mission to obtain obscure references, department staff who made sure I am signing my real name in the right spot, and the University of Alberta IBD Clinic that has been providing my lifeline since 2009. They are too numerous to name individually here, but they will know when they find a box of chocolates.

It has been an honour to take the field with a talented and inspired group of players. First and foremost, they include my course mates from the 2010 Larval Biology class at Friday Harbor Laboratories and the 2013 Embryology class at the Marine Biological Laboratory. No words can describe the immense pleasure I felt to spend days, nights, and all hours in-between with people who share values and philosophies about science. It seemed as though I had lived just to share in these short but brilliant moments with such fabulous people. I look forward to more opportunities to cross paths with them. Next, they include members of the Allison lab (University of Alberta) and the Bronner lab (California Institute of Technology). They held my hand while I tested new waters, and were a great logistical and personal help at various stages of my thesis research. In particular, Phil Oel, Stephen Green, and Hugo Parker taught me all I know about molecular genetics, zebrafish, and lampreys. I am grateful to wonderful colleagues around the world. Some of them are close collaborators; others are fellow fieldworkers, family friends, discussion mates, conference companions, my students and volunteers, editors, and referees. Especially, I salute Federico Fanti and his family. We are the paleontology's best double-play combo.

I also thank those who play on the opposite side of the game. All different opinions aside, I have utmost respect for their work. One deserves a special mention: Dr. Shigeru Kuratani. He would be that pitcher who throws so hard a heater I just cannot hit, and I still tip my hat for sharing the field with such a dedicated player in this moment in time. As well, I bow to those past masters whom I only know by reading their work. I always wished I had friends that were Nils Holmgren, Torsten Gislen, Edwin Goodrich, or Walter Garstang.

My hat-off to funding agencies, including NSERC, Mitacs, and Killam Foundation.

I am grateful to family and friends home, here, and elsewhere. Although they might not be playing with me on the field, I would not have much to play for without them. In particular, my parents and my grandparents are the first to come to my mind for giving me the ball to play with. When I put on a uniform and take field, my thoughts still run to friends home. These are Kazuhiro Magome, Miyuki Tajima, Kaoru Kitahara, Mariko Takahashi, Yohei Shimizu, Yuki Wachi, Kanako Nozawa, Mariko Kurosu, and Hisao Nakagawa. My family-in-law have been always available in the bullpen to catch my warm-up tosses. Finally, my sincere thanks to Kesia Miyashita. If I ever get the ball to start Game 7 of World Series, there would be no other catcher I'd have sitting behind the plate and putting down the sign for me.

TABLE OF CONTENTS

Development, Anatomy, and Phylogenetic Relationships of Jawless Vertebrates and Tests of Hypotheses about Early Vertebrate Evolution

Chapter 3 — A Growth Series of a Devonian Stem Lamprey and Implications for the Origin of the Filter-feeding Larvae in Vertebrate Evolution

Chapter 4 — Testing Hypotheses about Evolutionary Origins of the Jaw Joint in Vertebrates

LIST OF TABLES

LIST OF FIGURES

Chapter 1
Introduction: Comparative Development of Cyclostomes and Outstanding Questions in Early Vertebrate Evolution*

> As if all passion, feeling, and interest had been worn out in the earlier ages of the world and had perished from its surface with its other departed monsters…
>
> — *Bleak House*, Charles Dickens

1.1 CYCLOSTOMES IN STUDIES OF VERTEBRATE EVOLUTION

In studies of the early evolution of vertebrates, hagfishes and lampreys figure disproportionately compared to the small fraction of living vertebrate species they represent (0.2%) (Nelson et al., 2016). These superficially anguilliform fishes represent the only living jawless and boneless vertebrate lineages. Together, they comprise the Cyclostomi Duméril, 1806. The crown-group Vertebrata consists of cyclostomes and gnathostomes (jawed vertebrates), and its node is the deepest root to which many vertebrate innovations (e.g., chondrocranium) can be traced (Fig. 1.1). Cyclostomes lack many traits that are otherwise widespread among vertebrates such as mineralized skeletons. For this reason, cyclostomes have generally been considered to retain primitive conditions relative to gnathostomes. This phylogenetic scheme and their supposedly primitive morphology make cyclostomes useful in setting a polarity for characters near the base of the Vertebrata. Perhaps surprisingly from a modern standpoint, this latter view gained wide acceptance only recently.

Cyclostomes were relegated to the sidelines in the search for vertebrate ancestry (or archetype) well into the 20th century. This treatment was not due to a misunderstanding of systematic relationships. Surely, early taxonomists recognized both hagfish and lampreys in the piscine grade — with the exception of Carl von Linnaeus and his followers who classified hagfish as 'vermes intestinalis' (Miyashita and Coates, 2016). Once ammocoetes were recognized as a larval stage of lampreys (Müller, 1856), and once the notochord was found in

---

* Large segments of this chapter are in press as a chapter in *Evolution and Development of Fishes*, Cambridge University Press; edited by Z. Johanson, M. Richter, and C. Underwood): Comparative development of cyclostomes, by Tetsuto Miyashita, Stephen A. Green, Marianne E. Bronner.

cephalochordates and tunicates (Kowalevsky, 1866a, 1866b), the apparent similarities between ammocoetes and cephalochordates reinforced the view of their close relationships near the base of the vertebrate branch (Haeckel, 1876).

Bypassing cyclostomes was more a matter of interpretation than of interrelationships. Cephalochordates were generally considered degenerate vertebrates at the time, and whether viewed as sharing a root exclusively with cephalochordates or representing an independent lineage, cyclostomes were interpreted in a similar vein (Gegenbaur, 1859; Huxley, 1874; Lankester, 1875; Cope, 1886, 1889; Dohrn, 1886; Patten, 1890). Dissenting views about degeneracy tended to interpret cyclostome morphology as highly specialized (Sewertzoff, 1899, 1913, 1916, 1927, 1931; Patten, 1912). The trust in elasmobranchs as classical models for the vertebrate archetype (Gegenbaur, 1859; Balfour, 1878; van Whijhe, 1882) probably influenced this oversight.

Still, the emphasis on elasmobranchs neither vanquished interest in cyclostomes nor ruled them out as relevant taxa for rooting vertebrate traits. Duméril (1806) himself postulated cyclostomes as an intermediate between a worm-like and a fish-like organization (Janvier, 1996a). Similarly, a series of works that proposed a crustacean-like vertebrate ancestor used cephalochordates and cyclostomes as a primitive form to bridge the arthropod grade to the gnathostome grade (Alcock, 1898; Gaskell, 1898, 1898, 1900, 1901, 1902, 1903, 1908). With cephalochordates falling outside of vertebrates (Wiley, 1894; Goodrich, 1901, 1902, 1909a), cyclostome morphology came to be considered in the light of its plesiomorphic state within vertebrates well into the 20th century (Goodrich, 1909b, 1930; Stensiö, 1927, 1932; Garstang, 1928; Holmgren and Stensiö, 1936; de Beer, 1937). This changing attitude is reflected in the fact that nearly every scenario for the vertebrate ancestry has fitted in cyclostomes — typically an ammocoete-like ancestor — near or at the origin of vertebrates since the mid-20th century (Leach, 1944; Romer, 1972; Willmer, 1974; Romer and Parsons, 1977; Northcutt and Gans, 1983; Mallatt, 1984, 1996; Jefferies, 1987; Gans, 1993; Gee, 1996). Interestingly, a revival of the nemertean hypothesis for the origin of vertebrates used hagfish, not ammocoetes, as a preferred model for primitive conditions (Jensen, 1960, 1963). Based on their characters, hagfish have often been evoked as more primitive than lampreys (e.g., physiological traits; visual system; lateral lines). The choice of a surrogate for ancestral states between cyclostome and stem gnathostome lineages remains a recurring theme in the comparative biology of cyclostomes.

Cyclostome research has come of age in modern times. Cladistic analysis of cyclostomes began with re-evaluation of phenotypic characters in support of paraphyly: lampreys and hagfish are successive outgroups with respect to gnathostomes (Løvtrup, 1977; Hardisty, 1982). This position was congruent with the revision of interrelationships of extinct jawless vertebrate lineages. Instead of spreading these 'ostracoderms' along the stems of hagfish, lampreys, and gnathostomes (Kiaer, 1924; Stensiö, 1927, 1958, 1964, 1968; Romer, 1945; Obruchev, 1964; Halstead, 1973a), phenotype-based parsimony analyses supported cyclostomes as paraphyletic and ostracoderms as lying along the stem of gnathostomes (Janvier, 1981, 1984, 1996b, 1996a, 2007, Forey, 1984, 1995; Forey and Janvier, 1993; Gagnier, 1993; Donoghue et al., 2000; Gess et al., 2006; Sansom et al., 2010b; Turner et al., 2010). On the other hand, molecular-based analyses almost unanimously favoured cyclostomes as a clade (Mallatt and Sullivan, 1998; Kuraku et al., 1999; Delarbre et al., 2000, 2002; Furlong and Holland, 2002; Yu et al., 2008; Near, 2009). Although it remains difficult to separate phylogenetic signal from long-branch attraction for cyclostomes (Near, 2009), recent phenotype-based analyses tend to constrain cyclostomes to a clade, which still results in 'ostracoderms' as stem gnathostomes (Heimberg et al., 2010; Conway Morris and Caron, 2014; Gabbott et al., 2016). Meanwhile, the rise of evolutionary developmental biology has provided strong motivation to use cyclostomes as a model for primitive conditions within vertebrates.

Vertebrate ancestry remains a chaotic topic despite these advances. As in other living chordate lineages, hagfish and lampreys each represent highly specialized long branches. So the information available at branch tips does not necessarily describe conditions at the root, unless there is unambiguous phylogenetic inference. As early workers conceded, it still is a matter of interpretation to dissect a cyclostome character into a combination of specialized, degenerate, derived, and/or primitive traits. An argument begins with and ends in a transformation series with presumed character polarity (e.g., Gans, 1993; Mallatt, 1996; Kuratani, 2012; Miyashita, 2016).

Following the great tradition of modern zoology, the main sources of inferences about deep evolutionary roots — therefore placed central to this thesis — remain development and the fossil record, bridged by comparative anatomy and phylogeny. Both development and fossil record being subjects and products of selection, these are leaky assumptions on their own. Nothing guarantees earlier developmental events to be better conserved than the later ones (Gould, 1977; Raff, 1996), or older fossils to be more primitive than the younger ones (Norell

and Novacek, 1992). Embryos and fossils provide inferences when viewed in patterns and trends. Comparative tools provide the power that delineates similarities and differences, generates phylogenetic trees, and confers strength to an inference. In this spirit, I organized this thesis around three main hypotheses to test:

1) Hagfish and lampreys represent an ancient lineage of specialized, predatory vertebrates (=cyclostomes), thereby splitting the crown group Vertebrata into cyclostomes and gnathostomes (Chapters 2 and 3).
2) Neither hagfish nor lampreys serve as a surrogate for the last common ancestor of living vertebrates: hagfish are specialized and degenerative (Chapter 2) and filter-feeding larvae of living lampreys evolved independently of the ancestor (Chapter 3).
3) The evolution of the jaw among gnathostomes required co-opting traits that are shared across vertebrates (Chapter 4).

Finally, I provide a preliminary outline of character analyses to yield an alternative to the evolutionary narrative based on a transformation series of archetypical, hypothetical ancestors (Chapter 5).

To provide the basis for my outlined approach in this chapter, I review development of cyclostomes in a comparative framework to try to infer primitive conditions within vertebrates. Detailed discussion of the cyclostome fossil record is deferred to the subsequent chapters (and references therein), but a primer is required before delving into the latter parts. I evaluate cyclostome affinity of several controversial forms and present a short summary of the state of knowledge about fossil jawless vertebrates in general. Finally, I briefly discuss the scheme of homology as intended in the thesis. This is neither a systematic treatment of nor a novel contribution to the concept of homology — rather, it is to minimize semantic confusions over my use of terms in this thesis. It is necessary because this thesis discusses similarities and identities at multiple levels from morphology to pathways to genes, across different temporal contexts (development and fossil record). The sections that follow are no exceptions, where development is described in both morphology and gene expression profiles, and where similarity is interpreted either phenetically or phylogenetically.

1.2 A BRIEF HISTORY OF RESEARCH ON CYCLOSTOME DEVELOPMENT

The early interest in cyclostomes was largely due to the apparent departure from typical vertebrate morphology — a motivation often viewed retrospectively in evolutionary or phylogenetic contexts (e.g., Richardson et al., 2010). However, the context was often comparative morphology ('bauplan', or general homology as defined by Owen, 1849) to early workers. In reading the early cyclostome literature, it is critical not to take the terms of character polarity out of that context as some modern workers did. Two citations of 'primitiveness' quoted by Richardson et al. (2010) illustrate this point (Beard, 1888; Johnston, 1905). In Beard's (1888) comparison of the pigmented pineal organ, whether or not the structure is a derived state in 'fishes' hinges on its presence in the 'primitive' group of cyclostomes. In Johnston's (1905) reconstruction of vertebrate neuromery, however, the term 'primitive' clearly refers to a hypothetical archetype with perfect neuromery. The 'primitiveness' in the latter is not be confused with a phyletically interpreted plesiomorphy, as in the former. With respect to such hypothetical archetypes, cyclostomes needed not represent an ancestral stock (or an intermediate grade). Confusingly, however, some authors advocated for phylogenetic implications. These include the proponents of the crustacean ancestry of vertebrates (Alcock, 1898; Gaskell, 1908).

Lampreys made headway in the study of cyclostome development. Beginning with the discovery of metamorphosis of ammocoetes into adult lampreys (Müller, 1856), observations on embryos and ammocoetes formed the foundation for focused comparisons (Table 1.1). Lampreys were not popular models in experimental embryology into the mid-20th century. The embryos have a large quantity of yolk granules in the tissues, which makes histological observation challenging. They are available only during a short spawning season (typically 2-3 months depending on the species; Renaud, 2011). The adults are semelparous (Renaud, 2011) so they are only good for a single spawning season. Nevertheless, developmental research continued in three main streams. Led by Hubert Damas's contributions, a series of descriptive works resolved conflicting observations of lamprey development in the early literature and set the new baseline for a comparative approach (Table 1.1). In the second stream, David Newth introduced lampreys to experimental embryology through grafting of the ectoderm to describe neural crest development and differentiations (Newth, 1950, 1951, 1956). In the third stream, morphologists and physiologists were motivated partly by lamprey-caused damage to the Great Lakes fisheries

to develop a more precise understanding of the developmental timetable and life history-related changes across metamorphosis (Table 1.1).

These three lines of research on lamprey development have converged in an evolutionary context. This revival began with structural, functional, and immunohistochemical analyses of cartilages and branchial structures in the larval stage or through metamorphosis (Table 1.1). Meanwhile, lampreys became a key taxon to revisit the long-standing questions about homology of trabecula cranii and head cavities. To my knowledge, the first characterization of gene expression in lampreys was that of the *Engrailed* cognate in the mandibular arch (Holland et al., 1993). Gene expression patterns have since become the main comparative tool in lamprey development to test hypotheses about the origins and early evolution of vertebrate- and gnathostome-specific traits (Table 1.1). Publication of the lamprey genome (*Petromyzon marinus*) further accelerated this line of research (Smith et al., 2013).

Hagfish embryos, on the other hand, were elusive. The first known collections came from Monterey Bay, California in the 1890's. Quock Tuck Lee from the Chinese Point fishing village of Pacific Grove (the future campus of the Hopkins Marine Station) began supplying eggs of the Pacific hagfish *Eptatretus stoutii* that contained embryos (Kohrs, 2013). These embryos generated several early publications that culminated in a monograph based on more than 800 specimens (Dean, 1899). Lee's departure from Pacific Grove in 1907 put an end to the brief period of successful collecting in Monterey Bay (Kohrs, 2013), and his collection site has never been rediscovered. The embryos collected by Lee constituted a single line of supply for the early literature on hagfish development (Table 1.2). The specimens acquired by Bashford Dean changed hands to LeRoy Conel, and their histological sections were later accessioned at the Museum of Comparative Zoology at Harvard University (Williston, 2016). Nils Holmgren and Bo Fernholm secured a total of three embryos of the Atlantic hagfish *Myxine glutinosa* in late stages of development (Holmgren, 1946; Fernholm, 1969), but these specimens are currently missing (B. Fernholm, pers. commn.).

Following this long struggle to obtain hagfish embryos, the success by Kinya Ota, Shigeru Kuratani, and colleagues took the cyclostome research community by a storm in 2007. They recovered embryos of the Japanese inshore hagfish *Eptatretus burgeri* from artificial spawning tanks and underwater cages (Ota and Kuratani, 2006, 2007, 2008). A series of publications using these embryonic materials followed (Table 1.2). The genome has yet to be

published for hagfish. Additionally, they obtained access to pre-hatching embryos of *Eptatretus atamii* from Tokyo Bay (Oisi et al., 2013a). Some of these field-collected embryos underwent hatching (R. Mimori, pers. commn.).

1.3 COMPARATIVE DEVELOPMENT OF CYCLOSTOMES

In this section, I present a summary of the comparative development of hagfish and lamprey. For hagfish, the description is based on the Dean-Conel collections of *Eptatretus stoutii* embryos (Fig. 1.2) and on the literature — particularly the recent contributions by Shigeru Kuratani's group. For lampreys, the description is based on *Petromyzon marinus* unless otherwise cited. Table 1.3 lists major points of comparison between these two taxa; Tables 1.4 and 1.5 describe the staging schemes of hagfish and lampreys, respectively; Tables 1.6 and 1.7 summarize known gene-expression patterns. Developmental stages are illustrated in Figs. 1.2 and 1.3.

Dean (1899) arranged his embryos of *E. stoutii* in an approximate order of development. Figure numbers assigned to each of these illustrations have been used as a surrogate for embryonic staging, but this practice is imprecise. Miyashita and Coates (2016) restaged Dean's embryos provisionally based on the Dean-Conel slide collection, and I follow this scheme in this chapter with the prefix MC. For lampreys, several staging schemes exist for different species. I follow Tahara's (1988) staging scheme for this thesis, indicated with the prefix T.

1.3.1 Life History and Reproductive Ecology

All living species of lampreys have a filter-feeding larval stage during which they are called ammocoetes. The duration of the larval stage differs among and within species, but typically lasts five to seven years in *Petromyzon marinus* (with the range from 2 to 19 years; Renaud, 2011). The duration of post-metamorphic adult stages also varies among and within species. It is shorter in populations of non-feeding adults than in those of feeding adults. In *P. marinus*, the ectoparasitic adult phase typically lasts for two years (Renaud, 2011). The number of eggs produced by a female lamprey varies at the levels of species, populations, and individuals and depending on whether the population is anadromous or not (Renaud 2011; Table 1.3).

In comparison, hagfish have no distinct larval stage, and the reproductive ecology is poorly known. The sex ratio for hagfish varies among populations and species — sometimes

equal as in *Eptatretus burgeri* and *E. cirrhatus* (Tsuneki et al., 1983; Martini and Beulig, 2013), sometimes males as few as 6% as in Gulf of Maine populations of *Myxine glutinosa* (Martini et al., 1998). Males sampled in the wild are seldom ripe with mature testis (Patzner, 1998). Ripe females typically carry under 30 eggs encapsulated in thick outer shell and with velcro-like anchor filaments (Patzner, 1998). Among three possible hypotheses about how fertilization occurs with low sperm production (in a burrow, a nest, or slime), release of sperm into the egg-containing slime seems most likely (Miyashita and Coates, 2016). However, Miyashita and Coates (2016) ruled out neither internal fertilization nor parthenogenesis. Although hagfish do not have any obvious external sexual organ, internal fertilization occurs in the absence of such structures — notably in coelacanths (Griffith and Thomson, 1973; Smith et al., 1975). On the other hand, parthenogenesis is known in several elasmobranchs (Feldheim et al., 2016; Dudgeon et al., 2017), although rare and facultative.

The most striking difference between hagfish and lampreys is the maximum fecundity per spawning, which differs by four orders of magnitude (Table 1.3). This difference is exaggerated because lampreys are semelparous. Even then, the lifetime fecundity for a female hagfish does not likely come close to that for a female lamprey. Both hagfish and lamprey hatch with a substantial yolk sac. Lampreys hatch at a relatively immature stage (T26) when the chondrocranium has not formed; hagfish hatchlings already have a complete chondrocranium (Dean, 1899; Neumayr, 1938; Oisi et al., 2013a201).

1.3.2 Descriptive Embryology

Egg size dictates differences in early embryogenesis between hagfish and lampreys. First cleavages are meroblastic and holoblastic, respectively (Figs. 1.2b, 1.3; Dean, 1899; Richardson et al., 2010). First cleavage in lampreys corresponds to left-right bilateralism in about a third of embryos (McCauley and Bronner-Fraser, 2006). Cleavages are typically radial (stages MC2 and T4-5). Blastomeres are smaller toward the animal pole (MC3-; T5-). In lampreys, yolk granules collect in the vegetal pole but remain abundant within and between developing tissues into the latest stages of embryogenesis (Nikitina et al., 2009). The yolk is mostly separate from the embryo in hagfish, but a syncytial zone forms at the boundary (MC3-4), probably arising from retarded division of marginal cells from the fourth cleavage forward (Dean, 1898; Miyashita and Coates, 2016).

From late blastula to gastrula, key differences in earlier stages dictate different modes of gastrulation. Hagfish do not develop a clearly defined blastcoel. Underneath the several-cell thick epiblast, the mesoendoderm consists of an equally thick layer of loose mesenchyme underlain by periblasts bordering the syncytial zone (MC4) (Dean, 1899). The periblasts probably form a ventral wall of the archenteron. Gastrulation is thought to proceed through ingression (Miyashita and Coates, 2016). Although embryonic extension at this stage is predominantly rearward, the overall pattern is reminiscent of amniotes ('primitive streak'). Lamprey blastulas have a clearly defined blastocoel (T9-16). The roof of the blastcoel thickens from two to three cells thick (T11) and thins to one cell thick during gastrulation (T13). Involution appears to be the primary cell movement during this time (von Kupffer, 1890; Hatta, 1907). The dorsal lip uplifts into a cone (T12) and then flattens as the blastocoel recedes and as the notochord anlage forms (T16). The blastopore remains externally visible as an anus long after gastrulation (T24) when the developing tail bud wraps around the edge of the yolk sac.

The stages from late gastrula to neurula have few points of comparison because these stages (MC5-9) appear to be underrepresented in Dean's collection of hagfish embryos. It is difficult to resolve a precise developmental order of the specimens currently available (Miyashita and Coates, 2016). The ectoderm is folded under the head plate toward the prechordal plate in the early neurula (MC5-6). The nasohypophyseal placode forms in this ectodermal membrane by MC8, but this space is secondarily closed externally by the ectodermal oropharyngeal membrane shortly thereafter (Oisi et al., 2013a). The resulting 'pouch' connects with the foregut forming the oropharyngeal cavity sometime at or immediately before the pharyngula stage (MC9-10). In lampreys, the foregut forms in the anterior end earlier than in hagfish (T17). At no point does the nasohypophyseal cavity connect with the foregut in this lineage, nor does the cavity secondarily close (von Kupffer, 1900; Oisi et al.. 2013a). Although Tahara (1988) described the stomodeum as open at T27, the mouth tends to open at T26 in the embryos of *Petromyzon marinus*. Precise timing for this is unclear in hagfish, but it has occurred by MC14.

From neurula to pharyngula, important embryonic events include somitogenesis, neural fold, and neural crest delamination. The onset of somitogenesis roughly coincides with appearance of the neural folds (hagfish: MC7; lampreys: T18-19) (Dean, 1899; Damas, 1944; Tahara, 1988). These events overlap with others to a great degree in hagfish embryos — somitogenesis and neural folds continue to form at the tail bud level while the embryo is well into

pharyngula stages (MC10-11) anteriorly. Curiously, cyclostomes and cephalochordates exhibit asymmetric arrangement of somites where the right side is slightly displaced posteriorly relative to the left side (Veit, 1939; Ota et al., 2007). Delamination and migration appear to correspond roughly with the formation of the hyomandibular pouch in both hagfish (MC9) and lampreys (T20-21) (Langille and Hall, 1988; McCauley and Bronner-Fraser, 2003; Ota et al., 2007). Just like in somitogenesis, neural crest development is not simultaneous along the long axis in hagfish. Brain regionalization is well underway by this time. Vesicles and rhombomeres are apparent in hagfish from stage MC7 onward (Dean, 1899; Conel, 1929). Although neural tube morphology is difficult to observe externally in lampreys, gene expression profiles clearly suggest regionalization (Sugahara et al., 2016; Parker and Krumlauf, 2017).

The pharyngula accompanies head protrusion in both hagfish (MC10) (Fig. 1.2j) and lampreys (T21) (Fig. 1.3). This process is particularly dramatic in hagfish, where the head plate lifts as the pharyngeal pouches form and the neural crest ectomesenchyme fills in the pharyngeal arches (Dean, 1899; Oisi et al., 2013a). These pouches roll up onto the lateral side of the body as they become displaced posteriorly (with the exception of the first [hyomandibular] pouch), and as the head extends around the previous animal pole (Dean 1899; Oisi et al., 2015). The tail bud also continues to extend and meets the head on the other side of the yolk at late stages (MC17) (Fig. 1.2q). The heart assumes its position behind the pharyngeal pouches much later in hagfish (MC14-16) (Dean, 1899) than in lampreys. The active respiratory pump begins late. The velar cartilages form only before hatching in hagfish, and they begin beating while still in the chondrogenic state in lampreys in T28 (Tahara, 1988). Still, nutrient uptake mainly comes from the yolk that remains prominent well after hatching (Piavis et al., 1971).

Lineage-specific features of adult cyclostome morphology begin to appear at these stages. In hagfish, the barbells form in MC12 but become arranged in precise positions later (MC15) (Dean, 1899; Oisi et al., 2013a). Slime glands also appear around this time. In lampreys, the prominent oral hood forms from the upper lip (posthypophsyeal process) from T27 to T30 (Tahara, 1988). Perhaps surprisingly given the difference in eye development between hagfish and lamprey adults, optic vesicles are nonetheless conspicuous in the hagfish neurula (MC8) (Dean, 1899), whereas they form internally relatively late in lampreys (T23) and become externally visible as eye spots well into the pharyngula stages (T27) (Tahara, 1988). Placode development generally seems to occur earlier in hagfish (MC6-7) than in lampreys (T22). They

can be morphologically distinguished even before the foregut is complete in hagfish, whereas placodes and their marker expression become prominent into stage T23 in lampreys (McCauley and Bronner-Fraser, 2002; Sauka-Spengler et al., 2007; Modrell et al., 2014).

1.3.3 Vertebrate Features from Neurula to Pharyngula

From the neurula stages forward, cyclostomes show truly vertebrate features in brain regionalization, neural crest, and placode-derived sensory ganglia. Although these traits may be visible morphologically at later stages of development, they are recognized primarily by gene expression profiles at these early stages. This is not because the expression profiles are unique to vertebrates — their major components exist outside vertebrates (Pani et al., 2012; Abitua et al., 2015; Stolfi et al., 2015). Rather, these are *bona fide* vertebrate features because these molecular traits are coupled with vertebrate-specific morphological characters.

The gnathostome-based scheme of regionalization largely applies to the developing brain in cyclostomes, both using morphological markers (ventricles and commisures) and molecular markers (region-specific expression of ligands, receptors, and transcription factors). Although a pallidum and cerebellum are difficult to delineate morphologically in cyclostomes, expression profiles mark the medial ganglionic eminence and the rhombic lip from which the two structures would otherwise develop in gnathostomes (Sugahara et al., 2016). In hagfish, the medial ganglionic eminence expresses *Hh2*, whereas lampreys lack expression of *Hedgehog* in this zone (Murakami et al., 2005; Sugahara et al., 2011, 2016). As for the rhombic lip, it is *Pax6*-positive in both lineages (hagfish: *Pax6*; lampreys: *Pax6B* somewhat ventrally but no expression of *Pax6A*) and does express more specific markers linked to cerebellar cell types (hagfish: *Atoh1*; lampreys: *Atoh1*, *Ptf1a*, *Wnt1*) (Sugahara et al., 2016). For these structures, hagfish follow the pattern observed in gnathostomes more closely; thus, lampreys appear to have diverged from the ancestral state (Sugahara et al., 2016). In addition to the anterior end of the neural tube and the mid-hindbrain boundary, the zona limitans intrathalamica is an important signaling centre in the diencephalon. Characteristic *Hh* expression appears in both hagfish (*Hh2*) and lampreys (*HhA*, *HhB*) (Murakami et al., 2005; Kano et al., 2010; Sugahara et al., 2011, 2016). An epiphysis still has not been identified in hagfish. For other genes involved in brain regionalization, Tables 1.6 and 1.7 present summaries of expression patterns. Although no comparative data are available for hagfish, reporter expression assays by Parker et al. (2014) revealed remarkable conservation of

the rhombomere-specific *Hox* regulatory networks in the hindbrain between lampreys and gnathostomes (Fig. 1.4d-f).

As in other vertebrates, neural crest arises as the neural plate borders fold and delaminate (McCauley and Bronner-Fraser, 2003; Ota et al., 2007). Migration routes of the ectomesenchyme are mapped well in lampreys but poorly in hagfish (Langille and Hall, 1988; McCauley and Bronner-Fraser, 2003; Oisi et al., 2013a). The patterns in lampreys are consistent with other vertebrates, but it is difficult to determine with precision how tightly the migration paths are constrained by the rhombomeric origins. Interestingly, *Snail* does not appear to be expressed in the ectomesenchyme in hagfish (Ota et al., 2007).

In parallel, neurogenic placodes give rise to the sensory capsules and ganglia in a manner consistent with gnathostome counterparts (Tables 1.6 and 1.7; Modrell et al. 2014). The exception here is the nasohypophyseal placode, which is tripartite (paired olfactory and single adenohypophyseal placodes) in gnathostomes. In cyclostomes, this placode is a single structure marked by similar expression profiles (hagfish: *Six3/6A*, *SoxB1*; lampreys: *Pax6A*) (Uchida et al., 2003; Oisi et al., 2013b). The anterior and posterior portions show different expression profiles (anterior: *Fgf8/17*; posterior: *PitxA*) and split from one another as the nasohypophyseal canal is completed (Uchida et al., 2003; Oisi et al., 2013b). The anterior portion associated with the telencephalon becomes the nasal cavity, whereas the posterior half associated with the hypothalamus. In hagfish, these stages roughly correspond with the closure of the nasohypophyseal canal (Oisi et al., 2013b).

1.3.4 Lineage-specific Features from Pharyngula to Larva/Juvenile

More lineage-specific features arise from the pharyngula stages forward. Expression profiles in the ectomesenchyme of the pharyngeal arches have been mapped extensively in lampreys from T25 to T28/29. They express the *Dlx*, *Hox*, and *Sox* families, the endothelin and FGF signalling pathways, downstream transcription factors (e.g., *Alx*, *Bapx*, *Barx*, and *Runx*), and their effectors (e.g., *Col2a*) (see Tables 1.6 and 1.7 for citations). In particular, *Dlx* genes have the characteristic dorsoventrally nested expression in the pharyngeal arches of gnathostomes. In cyclostomes, however, conflicting interpretations emerge. *Dlx* genes undergo independent duplication events in cyclostomes (Takechi et al., 2013), so a specific one-to-one comparison is difficult. To complicate matters further, Cerny et al. (2010) and Kuraku et al. (2010) used different species of

lampreys (*Petromyzon marinus* and *Lethenteron camchatsticum*, respectively). In hagfish, expression seems to be patterned dorsoventrally, but not in a comparable way to *P. marinus* (Fujimoto et al., 2013). In contrast, the collinear *Hox* expressions in the pharyngeal arches are readily comparable to those of gnathostomes (Takio et al., 2007). The pharyngeal pouches in lampreys deploy FGF signaling initiated in the pharyngeal endoderm, which is roughly comparable with gnathostomes (Jandzik et al., 2014). It is likely that significant modification to the signaling environment occurred in hagfish to allow the pouches to not form a permanent interface with the local ectoderm, and to migrate posteriorly.

The chondrocranial morphology is not as conserved as gene expression profiles (Fig. 1.5). Between cyclostomes and gnathostomes, two major differences in the condrocrania concern: (***a***) the cartilages arising from the trigeminal stream of neural crest ectomesenchyme; and (***b***) the cartilages of the branchial arches. As for the trigeminal crest-derived cartilages, those of the upper lip, velum, and lingual apparatus in cyclostomes have no exact counterparts in the palatoquadrate or Meckel's cartilage in jawed gnathostomes (asterisk [*] in Fig. 1.5; Miyashita, 2012; Kuratani et al., 2016). The cyclostome upper lip develops from the posthypophyseal process, which is premandibular in position but not delineated from the mandibular arch in expression profiles or cell lineages. The process is clearly visible by stage MC11-12 in hagfish (Oisi et al., 2013b). In lampreys, the mandibular mesoderm anterior to the hyomandibular arch around stage T21 is called a cheek process (Kuratani et al., 1999), which receives the trigeminal ectomesenchyme (Kuratani et al., 2001). From T24 to T25, the anterior portion becomes bulbous — this posthypophyseal process becomes an upper lip. Jawed gnathostomes do not develop a posthypophyseal process, but the palatoquadrate extends anteriorly from the mandibular arch (Shigetani et al., 2002; Cerny et al., 2004). In placoderms and osteichthyans, dermal jaw elements overwhelm the jaw cartilages, and the premandibular region contributes symphyseal elements of the upper jaw (Lee et al., 2001; Richman and Lee, 2003; Lee et al., 2004; Zhu et al., 2016). Posterior to the upper lip, the velum and lingual apparatus in cyclostomes does not correspond to the jaw cartilages of gnathostomes either (Miyashita, 2012; Kuratani et al., 2016). The cartilages of the velum arise as outpocketings of the mandibular arch into the hyomandibular pouch (MC12-14 in hagfish; T26-27 in lampreys) (Oisi et al., 2013b), whereas the lingual apparatus (MC12 in hagfish; T27-28 in lampreys, but not fully developed until the juvenile stage) sits in the

position occupied by a tongue in the crown-group gnathostomes (Holmgren, 1946; Johnels, 1948).

Numerous differences between hagfish and lamprey chondrocrania can be distilled into three main factors: heterochrony, premandibular configuration, and branchial morphology. Although hagfish hatch with a complete chondrocranium (Neumayr, 1938; Oisi et al., 2013a), larval lampreys only exhibit a part of the adult chondrocranium as cellular cartilages (parachordal cartilages and branchial bars; Johnels, 1948; Martin et al., 2009). The lateral mouth plate, velar cartilage, lingual apparatus, and hyoid arch have condensed but not chondrified, and the rest of the supporting skeleton in the head consists of mucocartilage, which is reduced during metamorphosis. Hagfish have an extensive upper-lip skeleton consisting of cartilaginous rods supporting the barbels (in place around MC14-15) (Miyashita, 2012). Also in hagfish, pharyngeal pouches except the most anterior (hyomandibular pouch) become gradually displaced posteriorly as they roll up onto the lateral side of the embryo and as the head extends forward off the yolk (MC12-16; Dean, 1899). These differences are in keeping with the large nasohypophyseal canal acting as a respiratory passage in hagfish — hence the large, pumping velum, incipient branchial cartilages, and a longitudinally elongate lingual apparatus — whereas in adult lampreys, the small velum functions as a valve, the branchial basket contacts to pump water, the lingual apparatus is housed within the branchial basket (Hardisty, 1981; Miyashita, 2012).

Other structures important in a comparative context with stem gnathostomes include the axial skeleton. The parachordal mesoderm chondrifies anteriorly to form the cranial base in both hagfish and lampreys. In addition, mesenchyme from the sclerotomes gives rise to cartilaginous nodules around the dorsal aorta in the tail of hagfish. *Pax1/9*- and *Twist*-expressing mesenchyme still occurs in the epithelialized sclerotomes at MC11 but readily migrates to the ventral side of the notochord by MC14 (Ota et al., 2011). Cartilaginous elements are identified as vertebrae (Ota et al., 2011, 2013) or as elements anatomically equivalent to the haemal arches of gnathostomes (Miyashita and Coates, 2016). In lampreys, the neural arches chondrify in juveniles. No strong inferences exist for or against a full set of vertebral elements in the last common ancestor of crown-group vertebrates. Among jawless stem gnathostomes, unequivocal vertebrae occur in *Euphanerops* and osteostracans (Janvier, 1996a; Janvier and Arsenault, 2007). Regardless of whether or not these vertebral elements are homologous with each other (Criswell et al., 2017a,

2017b), the *Pax1/9*- and *Twist*-expressing sclerotomes likely constitute a synapomorphy for crown-group vertebrates.

Another embryonic tissue of interest is somitic and lateral plate mesoderm. In addition to general muscle markers such as *Ma2* and *MrfA*, the head mesoderm is clearly differentiated from the trunk via expression of *Tbx1/10A* (hagfish: MC12 onward; lampreys: T23-27; Table 1.6) (Tiecke et al., 2007; Kuratani et al., 2016). Somatically derived muscles extend anteriorly onto the head in both hagfish (MC14-15) and lampreys (T25-28) (Damas, 1944). In the latter, the ventral portion below the otic capsule is marked by *EnA* (Kusakabe et al., 2011). *Pax3/7A* and *LbxA* are expressed generally along the ventral portions of myotomes, but expression domains are dorsoventrally greater in the first two anterior somites that extend onto the head (Kusakabe et al., 2011). Despite the lack of a clear morphological distinction between epaxial and hypaxial muscles, expression profiles confirm dorsoventral differentiation within the myotomes (Kusakabe and Kuratani, 2007). As for the lateral plate (marked by *HandA* expression), the cardiac and posterior lateral plate are distinguished by the expression domain of *Tbx20* and that of *Hox5i*, *Hox6w*, and *Myb*, respectively from T21-23 onward (Onimaru et al., 2011). Interestingly, the lateral plate in lampreys loses contact with the ectoderm through elimination of the somatopleure (T23-26 onward) and segregates to the coelomic lining by T30 (Tulenko et al., 2013).

1.3.5 Comparative Overview

How similar is development in hagfish and lampreys based on: (***a***) similarities and differences outlined in the previous sections; and (***b***) gene expression profiles summarized in Tables 1.6 and 1.7? Embryonic development differs between hagfish and lampreys markedly in early phases (up to neurulation) and moderately in late phases (after neural crest migration). Gene expression domains reported in the literature appear highly conserved during the in-between stages (MC9-12; T18-23) and continue to show similarities in later stages, barring morphological differences between hagfish and lampreys (Table 1.6). Qualitatively, this is consistent with the developmental hourglass model (Duboule, 1994; Raff, 1996), where the bottleneck corresponds to the pharyngula stages in vertebrates (Irie and Kuratani, 2011, 2014).

Gene expression profiles linked to the patterns established around the pharyngula stages are also highly conserved among vertebrates, and within cyclostomes. These include brain regionalization (the three signaling centers: Sugahara et al., 2016), neural crest development

(neural crest gene regulatory network: Green et al., 2015), hindbrain rhombomery (*Hox* regulation: Parker and Krumlauf, 2017), anteroposterior and dorsoventral patterning of pharyngeal arches (*Hox* and *Dlx* codes: Cerny et al., 2010; Kuraku et al., 2010). Minor differences between the lineages appear to be linked to genomic evolution. The pharyngeal *Dlx* codes are likely responsible for dorsoventral patterning of the pharyngeal arches across vertebrates (Cerny et al., 2010; Medeiros and Crump, 2012), but expression patterns of individual *Dlx* genes are difficult to compare because they were independently duplicated and lost in different lineages (Fujimoto et al., 2013; Takechi et al., 2013). Similarly, cyclostomes have at least four Hedgehog genes of unclear orthology, some of which have gnathostome-like expression domains in brain regionalization (Table 1.7; Kano et al., 2010; Sugahara et al., 2016). These differences document considerable distance between the major vertebrate lineages set apart by genomic evolution, and simultaneously imply strong developmental burden (Riedl, 1978) to conserve patterns and processes observed at phenotypic levels.

Critical for the subsequent chapters, a comparative analysis of development allows post-hatching, differentiated morphological traits to be linked to patterns established around the pharyngula stages. As revealed through contingency coding in the character list of Chapter 2, this hierarchical information helps identify non-independent character changes. For example, (***i***) hagfish and lampreys differ from gnathostomes in having a single nostril, extensive upper lip, and cartilages that cannot be compared to palatoquadrate or Meckel's cartilage (Janvier, 2007; Miyashita, 2016); and (***ii***) the two cyclostome lineages differ from each other in the position of the nasohypophyseal aperture (terminal in hagfish and dorsal in lampreys) and compositions of the upper lip cartilages and muscles (Fig. 1.4; Hardisty, 1982; Miyashita, 2012). Repeating from section **1.3.4**, cyclostome traits listed in (***i***) result from having a single nasohypophyseal placode wrapped around by the postoptic ectomesenchyme (Kuratani et al., 1999). This population of the ectomesenchyme gives rise to the posthypophyseal process, and its configuration — coupled with the secondary closure of the nasohypophyseal cavity in hagfish (Oisi et al., 2013b) — explain the traits grouped in (***ii***). Even in the absence of embryos, the traits listed in (***i***) indicate the cyclostome-like craniofacial development with a posthypophyseal process, whereas those in (***ii***) help identify hagfish- and lamprey-like morphology in those cyclostome-like stem taxa.

Although useful in identifying hierarchical orders of character development, this comparison alone cannot determine character polarity. In anlages of traits conserved across

vertebrates (including tripartite brain, neural crest, neurogenic placodes), none of the three lineages — hagfish, lampreys, and jawed vertebrates — depart markedly from others in gene expression profiles. Some notable exceptions are the alleged absence of *Snail* expression in the neural crest of hagfish (Ota et al., 2007) and of *Hedgehog* expression in the medial ganglionic eminence of lampreys (Sugahara et al., 2016). Discounting the minor differences correlated with gene orthology/paralogy, however, neither hagfish nor lampreys appear primitive. Determination of polarity is subject to the phylogenetic and character analyses in the subsequent chapters.

1.4 FOSSIL RECORD OF CYCLOSTOMES

Little space is required to provide a primer for fossil cyclostomes because there are so few. Most remain controversial because preserved suites of characters typically do not include those diagnostic to cyclostomes. Putative fossil cyclostomes are often little more than an anguilliform imprint with no trace of internal structures except, perhaps, a digestive tract and tooth-like elements indicating an anterior end. In addition, excellent summaries of fossil cyclostomes by Janvier (2015) and Janvier and Sansom (2016) already exist. Here, I will briefly review: (***a***) putative fossil cyclostomes (discussed in detail by Janvier 2015; Janvier and Sansom 2016); (***b***) the current status of phylogenetic schemes (reviewed in detail by Janvier 1996a, 2007, 2008); and (***c***) problematic fossil taxa recently proposed as cyclostomes.

1.4.1 Putative Fossil Cyclostomes

Only three fossils have been assigned to the stem of myxinoids. *Myxinikela siroka* is considered unambiguously as a stem myxinoid (Bardack, 1991, 1998) and is the only fossil myxinoid whose position is supported by a quantitative cladistic analysis (Gabbott et al. 2016). *Gilpichthys greenei* (Bardack and Richardson, 1977) is a presumed myxinod, and occurs in the same locality as *Myxinikela*: Francis Creek Shale (Mazon Creek), a Carboniferous Lägerstatte. Myxinoid affinity was proposed based on a pair of comb-like structures interpreted as keratinous teeth. *Myxineidus gononorum* (Poplin et al., 2001) is another putative myxinoid based on structures resembling the comb-like elements of *Gilpichthys*, but its large oral disc (Germain et al., 2014) implies a lamprey-like morphology instead. In addition, conodonts have been compared to myxinoids based on the proposed homology between the conodont apparatus and myxinoid

keratinous teeth (Krejsa et al., 1990). The homology, however, was questioned based on histological differences (Aldridge and Donoghue, 1998; Donoghue et al., 2000).

Lampreys have a richer fossil record. *Priscomyzon riniensis* (Gess et al. 2006) is chronologically the earliest occurrence among petromyzontiforms, followed by the Carboniferous *Mayomyzon pieckoensis* from the Francis Creek Shale (Bardack and Zangerl 1968, 1971) and *Hardistiella montanensis* from the Bear Gulch Limestone (Janvier and Lund, 1983; Lund and Janvier, 1986; Janvier et al., 2004). *Pipiscius zangerli* (Bardack and Richardson 1977) — another from the Fancis Creek Shale — was also suggested as a lamprey based on its peculiar oral disc. The radial arrangement of its teeth, however, is unlike any living lamprey and similar to the Cambrian vetulicolians (Shu et al., 1999). Finally, *Mesomyzon mangae* from the Early Cretaceous Lägerstatte Jehol Biota (Chang et al., 2006, 2014) represents the only non-Paleozoic (and freshwater) fossil cyclostome. It is unambiguously identified as a petromyzontiform and associated with both larval and metamorphic specimens.

1.4.2 Positions of 'Ostracoderms'

A grade of jawless stem gnathostomes — traditionally referred to as ostracoderms — has been variably assigned to cyclostome lineages in the literature. Cope (1889) was the first to recognize the dichotomy between Agnatha (jawless vertebrates) and Pisces (= Gnathostomata; jawed vertebrates). Stensiö (1927, 1964, 1968, 1968) regarded ostracoderms as paraphyletic, and grouped heterostracans with myxinoids and anaspids and osteostracans with petromyzontiforms. Opposing views — until the advent of cladistics — held that heterostracans are closer to gnathostomes, whereas the rest of ostracoderms (anaspids, osteostracans, and thelodonts) represent an intermediate group, or an ancestral stock, between cyclostomes and gnathostomes (Kiaer, 1924; Romer, 1945; Obruchev, 1964; Halstead, 1973b). Even after a series of cladistic analyses swept ostracoderms to the stem of gnathostomes (reviewed in Janvier 1996a, 2007), however, the anatomical interpretations of jawless stem gnathostomes has been influenced by the classification scheme of Stensiö (1927): anaspids and osteostracans are reconstructed typically as lamprey-like in nasohypophyseal, pharyngeal, and cardiac traits, whereas heterostracans are compared more closely with hagfish than with lampreys to interpret the nasohypophyseal and oropharyngeal morphology (e.g., Janvier 1996a, 2007, 2008). In support of this model-based approach, stem gnathostomes appear to share many morphological traits with cyclostomes in

these body regions. The most striking examples include the lamprey-like branchial pouches and histological characteristics of cartilages in the 'naked' anaspid *Euphanerops* (described and coded in characters 48-50, 101, and 102 in Chapter 2; Janvier and Arsenault, 2002; Janvier et al., 2006).

The development of modern cyclostomes is relevant to grouping these variations because the morphological traits are correlates of development. The nasohypophyseal morphology of jawless stem gnathostomes has two general states between the hagfish- and lamprey-like forms, represented by heterostracan and osteostracans, respectively (Janvier, 1996a). This variation is linked to the differences observed in modern cyclostome development (traits referred to in ***i*** and ***ii*** of the section **1.3.5 Comparative Overview**; Gai et al., 2010; Kuratani, 2012; Miyashita, 2016). Specific morphology supporting these interpretations is discussed, compared, and coded in Chapter 2. For the purpose of introduction, this is sufficient to confirm the current consensus that places the 'ostracoderm' lineages as stem gnathostomes.

1.4.3 Affinities of *Metaspriggina* and Other Cambrian Vertebrates

Metaspriggina (Fig. 1.6a) is among the most hopeful of the putative Cambrian vertebrates to be placed closer to crown-group vertebrates than to any other living deuterostome lineages (Conway Morris and Caron, 2014). An important question is whether *Metaspriggina* and other Cambrian 'vertebrates' (myllokunmingiids and yunnanozoans) have unambiguously vertebrate-specific traits, such as derivatives of neural crest, to place them potentially in the vertebrate crown.

A series of bipartite skeletal bars in the pharynx (Fig. 1.6a) are interpreted as cartilaginous branchial bars. Cartilages occur in the mesodermally derived pharyngeal bars of cephalochordates (Wright et al., 2001; Cole and Hall, 2004; Jandzik et al., 2015) so the branchial cartilages of *Metaspriggina* alone do not place the taxon among vertebrates, nor do they indicate the presence of neural crest in this taxon. Interestingly, both *Metaspriggina* and myllokunmingiids have a small prechordal head relative to their body. Given that the prechordal (premandibular) chondrocranium is well developed in cyclosotmes and gnathostomes, perhaps these Cambrian vertebrate-like animals diverged from the stem of vertebrates before the neural crest-derived ectomesenchyme formed a conspicuous prechordal head.

At any rate, these Cambrian forms have some unusual morphology. In *Metaspriggina*, serial trunk structures identified as myomeres (Conway Morris and Caron 2014) may be used as

an inference for its chordate affinity. However, it is difficult to postulate a taphonomic process in which typical chordate myomeres disintegrated into individual units and contracted into noodle-like structures, but still retained their integrity within each unit. Alternatively, the structures may represent thick, collagenous myosepta that connected trunk myomeres. One way or the other, these structures illustrate a challenge of interpreting the Cambrian stem 'vertebrates'.

1.4.4 Conodonts

Of all the Paleozoic forms assigned to vertebrates, none has attracted more controversy than conodonts (Sweet, 1988; Sweet and Donoghue, 2001). The fossil record of conodonts consists almost entirely of mineralized conodont elements, which constitute a prominent component of the Paleozoic microfossils (Sweet, 1988). Roughly coinciding with the rise of cladistic methods, the discovery of several body fossils (Briggs et al., 1983; Aldridge et al., 1986, 1992; Briggs, 1992; Gabbott et al., 1995) and the functional understanding of conodont apparatus (Aldridge et al., 1995; Purnell, 1994, 1995; Purnell and Donoghue, 1997; Goudemand et al., 2011) advanced the currently prevailing view that these small animals represent an early vertebrate lineage. The body fossils preserved: (***a***) a set of conodont elements in the oropharyngeal space; (***b***) paired pigmented structures near the anterior end that are interpreted as eyes; (***c***) a series of muscle blocks extending posterior to the eye to the tail; (***d***) a possible trace of a notochord; and (***e***) a midline fin wrapping around the tail (reviewed by Aldridge et al., 1993; Donoghue et al., 2000; Turner et al., 2010). The conodont elements have dentine and/or enamel-like tissues (Sansom et al., 1994; Donoghue, 2001). Despite their mineralized nature, the conodont elements have been compared to keratinous tooth plates of cyclostomes, both anatomically and functionally (Sweet, 1988; Krejsa et al., 1990; Goudemand et al., 2011; for counterpoints, see Aldridge and Donoghue, 1998).

The vertebrate affinity of conodonts was tested in a set of cladistic analyses through careful examination of decay indices, topological constraints, different taxonomic complements, multiple character coding schemes, various character partitions, and character weighting (Donoghue et al., 2000). In the subsequent phylogenies, conodonts have been resolved variably: (***a***) a stem gnathostome lineage (Donoghue and Smith, 2001; Conway Morris and Caron, 2014); (***b***) a stem cyclostome lineage (Sansom et al., 2010b; Keating and Donoghue, 2016); (***c***) collapsed at the crown vertebrate node (Gess et al., 2006; Gabbott et al., 2016; McCoy et al.,

2016); or (***d***) segregated outside the crown vertebrate node (Turner et al., 2010). Although often presented as a stem gnathostome (Donoghue et al., 2002, 2006), distribution of dentine and enamel-like tissues among paraconodonts and euconodonts suggest that the latter evolved independently from the rest of gnathostomes (Murdock et al., 2013). This questions the homology of enamel/oid tissues between conodonts and other vertebrate lineages.

Although conodonts continue to occupy a special position in the discussion of early vertebrates, the limited representation of conodonts in this thesis is proportionate to the amount of character information that they contribute to the comparison with cyclostomes. These characters are discussed individually in Chapter 2 (characters 28, 45, 56, 93, 104, 106, 109, 113, 115, 131, 141, 143, 151, 163). This treatment is in line with previous systematic reviews of early vertebrates (e.g., Janvier, 1996a, 2007, 2008, 2015; Donoghue and Keating, 2015). Their removal from a cladistic analysis did not affect tree topology significantly (Chapter 2). Instead, they are important potentially as a stem cyclostome lineage (Chapter 2). So the discussion of conodonts focuses on this aspect. Still, conodonts remain an uncertain factor in discussions about early vertebrate evolution until more information becomes available.

1.4.5 Status of *Palaeospondylus*

Palaeospondylus (Fig. 1.6b) has long been an enigma and placed on nearly as many branches as there are vertebrate lineages that cross the Devonian Period, including cyclostomes, jawless and jawed stem gnathostomes, and osteichthyans (Johanson et al., 2010, 2012). Recently, a myxinoid interpretation re-emerged (Hirasawa et al., 2016). Besides their anatomical interpretations, the conclusion of myxinoid affinity in the absence of falsifiability is difficult to evaluate. Their comparisons are not accompanied by: (***a***) a test of alternative interpretations of *Palaeospondylus*; (***b***) an attempt to retrodeform some conceivable taphonomic artifacts; or (***c***) a quantitative measure of similarities. And worse, a cladogram is presented without a supporting data matrix.

Hirasawa et al.'s (2016) comparison has at least several internal inconsistencies. The rostral plate of *Palaeospondylus* is compared to the nasal basket of hagfish. If true, the nasohypophyseal canal in *Palaeospondylus* would have been a blind sac or have taken an implausible path under the commissure of the palatal cartilages. This is because the rostral plate is attached to the ampyx across its entire width in *Palaeospondylus* (Fig. 1.6b). The putative velar skeleton of *Palaeospondylus* is a single V-shaped element under the otic capsules (Fig. 1.6b).

This reconstruction leaves little space for a joint with the hyoid arch, as present in both hagfish and lampreys. In addition, such a calcified, hard single element is functionally implausible as a pharyngeal pump (Strahan, 1958; Miyashita, 2012). Finally, the lingual apparatus is a longitudinally tripartite series of cartilages in hagfish and lampreys (Yalden, 1985). The hardest elements are the anterior and middle segments over which the dental plates slide (Clark and Summers, 2007). The dental plates consist of thin, soft cartilages supporting keratinous teeth, whereas the posterior segment is a soft, histologically tendon-like structure that provides structural support for the retractor and attachment sites for protractors (Robson et al., 2000). The calcified elements in *Palaeospondylus* are associated with dental plates and posterior lingual segment — opposite to the combination expected based on the biomechanics of the apparatus in living cyclostomes.

None of these inconsistencies alone rules out the myxinoid affinity of *Palaeospondylus*. However, careful evaluations are warranted when contrasting competing hypotheses. The observation of three semicircular canals in the otic capsule of *Palaeospondylus* questions the myxinoid affinity further (Johanson et al. 2017). Hirasawa et al. (2016) explain some of the discrepancies by comparing *Palaeospondylus* to an embryonic chondrocranium of hagfish. Unless such heterochronic event is justified in a broader comparative context, however, the hagfish-*Palaeospondylus* comparison becomes a circular argument where neither the assessment of similarities nor the phylogenetic position stands as a falsifiable hypothesis. At this moment, the myxinoid affinity is no more parsimonious or plausible than other proposed hypotheses.

1.4.6 Status of *Tullimonstrum*

Among all putative fossil cyclostomes, *Tullimonstrum* has the most preposterous appearance. The highly developed nervous and sensory systems — particularly the retina with melanosomes — suggest a position closer to vertebrates than to any other living invertebrate lineages (Clements et al., 2016; McCoy et al., 2016). The strikingly unique morphology of the proboscis and eyestalks precludes comparison with cyclostomes beyond superficial levels — the living cyclostome lingual apparatus or extraocular muscles do not fit in the respective body parts. Therefore, its status should be evaluated with those that allow a tighter comparative framework. Other characters cited as lamprey-like by McCoy et al. (2016) (arcualia, symmetric caudal fin, dorsal fin) are not diagnostic to lampreys. The single unambiguously lamprey-like character in

Tullimonstrum is three tectal cartilages (character 117 in McCoy et al., 2016). However, lampreys have only two tectal cartilages, and they cover the posthypophyseally derived snout (Johnels, 1948). This morphology differs markedly from a series of three small, nodulous skeletal structures in *Tullimonstrum*. In the branchial region, the thin skeletal bars are spaced so widely apart that they are anatomically inconsistent with the typical branchial bars in vertebrates. In both *Tullimonstrum* and *Pipiscius*, similarities with lampreys remain superficial. As a careful analysis of characters fails to enhance them (Sallan et al. 2017), a cautious approach and a set of unambiguously defined characters are required to test their positions as stem petromyzontiforms.

1.5 NOTES ON TERMINOLOGY AND HOMOLOGY

Following the above primers on cyclostome development and fossil record, I provide a brief account of conceptual terminology to reduce confusion in the following chapters. This thesis covers biological traits in multiple levels of organization, from genes to pathways to developmental processes (cell migration; differentiation) to structures to body regions, which are compared as interconnected properties, as individual units, or as transformation series. Conceptual terminology is diverse, and often inconsistent from one level to the other. Here, I explain my views rather than simply review definitions. Enforcement of definitions and consistencies will create even greater confusion because many require a context. For example, I will use traits, features, and characters somewhat interchangeably in descriptions — unless, of course, in a cladistic context. Whenever phylogenetic trees or matrices are discussed, a character assumes a cladistic character with discrete states, whereas a trait refers to either (***a***) a specific character state or (***b***) a collection of multiple, correlated character states. Similar to traits, the term "features" refers to a collection of discrete variants that do not necessarily assume cladistic characters.

Most other terms with implicit assumptions concern phylogenetic contexts. Jawed vertebrates are included in the following taxonomic terms: gnathostomes (total-group); crown-group (or crown) gnathostomes (crown group: chondrichthyans + osteichthyans); jawed gnathostomes or jawed vertebrates (placoderms + crown-group gnathostomes). So the term "gnathostomes" alone implies a total group, inclusive of the jawless stem members (Fig. 1.1). Jawed or crown gnathostomes will be specifically referred to as such, unless it is clear from the

context that the jawed forms or the crown-group lineages are intended. The same applies to cyclostome lineages. In the main text, hagfish and lampreys are preferred for readability, but they are also referred to as myxinoids and petromyzontiforms where cladistic attributes must be explicitly stated (e.g., crown myxinoid synapomorphy, instead of hagfish synapomorphy, because crown group and total group must be distinguished in this case). Cyclostomi (Myxinoidea + Petromyzontiformes) is a confusing taxon, as it has been suggested to be a clade and a grade. If cyclostomes are paraphyletic, the crown/stem designation does not make sense. Conveniently, cyclostomes were recovered as a clade in Chapter 2 — so in this thesis, the stem/crown designation is made without a footnote.

Although explicitly used in text only a handful of times, homology is the bedrock of comparative biology. The concept is assumed behind almost all terminology. Every reference to a character is a statement of a homology hypothesis without mentioning the term. The literature is insurmountably tall on the concept of homology, and even a superficial treatment goes well beyond the scope of this thesis. After all, the consensus on homology (just like in other diffuse concepts like species), if any, has not moved beyond the state Hall (1994) summarized — by quoting the statement 45 years preceding that — as:

> After examining the present status […] one arrives at disquieting results. A basic term of one of the most important zoological sciences […] cannot be exactly defined.
>
> (Szarski, 1949; p. 127)

Here, I list guidelines regarding homology as followed in this thesis.

1) Within this thesis, I treat homology as continuity of information (Van Valen, 1982) that is linked to knowledge of evolutionary origins (Hall, 1994). Specifically, transformation homology is intended; taxic homology is beyond the scope of this discussion (Carine and Scotland, 1999).

2) I accept three tests of homology by Patterson (1982): similarity, conjunction, and congruence. Among the three tests, similarity comes first.

3) I treat similarity as homology hypothesis (=primary homology: de Pinna, 1991). If the trait is an anatomical structure, its homology hypothesis corresponds to special homology *sensu* Owen (1849). In reverse, a homology hypothesis must pass Patterson's (1982) test of similarity but is not exposed to the test of congruence yet. It corresponds to orthology at the level of individual genes, to synteny at the level of genomes, and to specific gene regulatory network or character identity network at the level of pathways (Wagner, 1989, 1994, 2007, 2014).

4) To supplement the conjunction test, I use a hierarchy test. This test follows (***a***) the concept of incomplete homology as recognized by Gegenbaur (1859) and (***b***) the concept of depth of homology as postulated by Tautz (1999) to recognize hierarchical organization of a character. The test stipulates that a homology hypothesis assumes a reference to the context in which the traits are compared. Therefore: (***i***) a homology hypothesis must be made between the traits at a comparable level of organization; and (***ii***) a homology hypothesis at lower levels of organization (e.g., palatoquadrate) requires homology at upper levels (e.g., mandibular arch). In this particular example, palatoquadrate is a dorsal cartilage of the mandibular arch — thereby rendering the former character contingent on the latter. This hierarchical information allows contingency coding in Chapter 2.

However, the hierarchy is that of nested organization (from which the term is inseparable both semantically and epistemologically) and is not just a collection of temporally or spatially causal linkages. Following the preceding example, homology of cartilage (a recognizable tissue type) does not require the homology of chondrogenic cell lineages (e.g., palatoquadrate and occipital cartilages arise from different cell populations [neural crest and mesoderm]). Cartilages — as subject to the test of similarity at morphological and cytological levels — do not assume cell lineages as a critical attribute of similarity inseparable from the character. Likewise, developmentally transient features (e.g., populations of neural crest ectomesenchyme) are eligible to a homology hypothesis at that level; these homology hypotheses need not be subsumed by homologies of developmentally terminal states.

To clarify this even further, a hierarchical organization needs not extend all the way up the causal chain. This organization relates to how a character (or similarity) is defined. It does not necessarily describe causality; it only describes epistemological criteria required to

recognize the trait. Referring to the palatoquadrate-mandibular arch example once again, the homology hypothesis of 'mandibular arch' requires the homology of pharyngeal arches (as a mandibular arch is the pharyngeal arch I), but does not necessarily require the homology of the ectomesenchyme stream that fills it. So my hierarchical test does not create an infinite chain of conditional homology hypotheses that ends in a zygote. If such a chain exists with every causal link conserved across species, then new traits could only be derived through terminal addition or replacement — that way, the diverse body plans as observed today could hardly have evolved (Kuratani, 2016).

5) Consequently, this thesis does not uphold the view that homology is free of hierarchy (Wagner, 2014). Likewise, it does not uphold the suggestion that homology is resolved above the level of discrete character states (Wagner, 2014). Homology is treated essentially as a dimension-free, diffuse concept wholly dependent on the context.

6) Thus, this thesis envisions homology — or at least its hypothesis — to be ubiquitous. It is not an emergent property, but akin to a null hypothesis to explain any similarity in biological traits.

7) Due to the ubiquity of homology, the emphasis is not on whether or not two traits are homologous. Instead, it is on evolutionary history: how and what homologous traits were conserved and others modified (for example, see discussion on different models of co-option to explain the evolution of the jaw joint in Chapter 4).

8) Still, this view of homology could create an intractably large number of homology hypotheses (at every level of organization relevant to the character in question) to test for a single character change at a given node, as in Chapter 4. In principle, a distinct homology hypothesis cannot be reduced into another because that will fail both the conjunction and hierarchy tests.

9) To accommodate this problem, I accept deep homology (Shubin et al., 1997, 2009) at the outset as a way to refer to homologies at levels deeper than that at which the character is

defined. For example, a hypothesis of deep homology of the eyes between vertebrates and cephalopods (Arendt, 2003) — or that of the nerve cords between vertebrates and polychaetes (Denes et al., 2007) — is assumed to refer to a homology hypothesis at the level of pathways underlying the traits (=character identity network: Wagner, 2007), while discussing the evolution of the trait at the level of structure.

Therefore, deep homology is a homology hypothesis of a module. Only in this particular category, is homology an emergent property as it exists between modules. Consequently, deep homology is assumed more common than originally anticipated (Shubin et al., 1997, 2009): it is not restricted to mismatches between non-homologous morphological structures and homologous gene regulatory networks. Although I do not explicitly use the term "deep homology" elsewhere in this thesis, the need for such a modular construct follows my atomized view of homology, if not for shorthand to reduce complexity of information.

10) Related to deep homology, co-option refers to either a heterotopic/heterochronic shift or a duplication event at some level of organization. The former requires the loss of homology above or below the level at which the shift is identified. The latter fails the conjunction test at the level of organization where the trait was duplicated. This logical problem may be solved by invoking serial homology (Owen, 1849; Gegenbaur, 1859): duplicated traits are treated as a character unit. As an appendix to this issue, co-options and developmental-system drift (True and Haag, 2001) are often contrasted in the literature. This contrast is valid when explaining morphological traits (discontinuity of homology at the level of morphology through co-option at the level of gene regulatory network; continuity of homology at the level of morphology through developmental drift). Assuming co-option to be applicable at any level of biological organization, developmental system drift may be interpreted as a subcategory of broadly defined co-options.

11) As an added note, pleiotropy may pass the conjunction test as long as resolved at the levels of non-coding regulatory elements and pathways. As per the duplication event in the previous example, paralogy may be treated like serial homology so that orthology of paralogous genes is equivalent to a hypothesis of special homology. Orthologies that individual paralogous genes have with their counterparts are each considered as a single homology hypothesis; in

the absence of one-to-one orthology (implying independent duplication events), paralogues are considered collectively for a single homology hypothesis. As an example of the latter, *Hedgehog* genes in cyclostomes are considered collectively in comparison to *Shh* in gnathosotmes, even though individual *Hedgehog* genes cannot be compared as exclusive orthologues between cyclostomes and gnathostomes because of independent duplication events (Kano et al., 2010; Sugahara et al., 2016).

12) By incorporating deep homology, co-options, and serial homology to the paradigm of homology, this modular perspective reduces the number of traits to manage in a comparative analysis, and circumvents terminological confusion where historical inertia is strong. Consider digit numbers for an example. Morphological digit identity (digit I-V) refers to positional value, but polydactyly does not shift the digit identity. This is because each normal digit generates a homology hypothesis, and extra digits are then considered duplications in light of serial homology. To elaborate this point further, evolutionary digit loss may accompany developmental system drift, or a frame shift of digit identity during development (Wagner and Gauthier, 1999; Bever et al., 2011; Tamura et al., 2011). Without a modular perspective, the identity of the digit cannot be tested in stem birds in this case.

13) Although homology is postulated as dimension-free in principle, it must operate above developmental reaction norms (Schlichting and Pigliucci, 1998). In other words, homology only applies to patterns and processes under selective pressure. Specific distribution of capillaries can generate a homology hypothesis, but a single capillary branch cannot. In another example, a cartilaginous element (or a chondrogenic pathway, or a chondrocyte lineage) can generate a homology hypothesis, but a single chondrocyte cannot. This rule supplements the hierarchy test.

14) The principles outlined here do not entirely apply to general and serial homology *sensu* Owen (1849) and the subsequent homology concepts linked to these two categories (e.g., homotypie, homodynamie, homonymie, homonomie; Gegenbaur, 1859). It is difficult to apply the congruence and conjunction tests to these concepts. Nevertheless, two critical tests for these types of homology are similarity and hierarchy. As discussed by Miyashita (2016)

regarding the origin of the vertebrate jaw, serial homology of pharyngeal arches at pharyngula stages does not guarantee that of the differentiated pharyngeal skeletons.

Because of the hierarchy test, anatomical terminology used in character description influences matrix composition, and vice versa. This discussion concerns theory-neutral terminology (Brooks and Wiley, 1985; Grande and Rieppel, 1994). There is no comprehensive list of theory-neutral anatomical terms in vertebrate zoology, but examples include: (***a***) whether to refer to trigeminal nerve or cranial nerve V; (***b***) whether to refer to a posthypophyseal process or an upper lip; (***c***) whether to refer to vertebrae or axial skeletal condensation; and (***d***) whether to refer to spiracle, hyomandibular opening, or an opening between eye and otic capsule.

Some of these anatomical terms have subtle differences. As for example (***a***), trigeminal nerve innervates the premandibular and mandibular regions with three branches (ophthalmic, maxillary, and mandibular), and it is the fifth cranial nerve. The choice between these terms is essentially of no consequence, because no vertebrates have added or lost a ramus, and because cranial nerve V assumes no serial nature of the cranial nerves as a whole. However, three branches of the trigeminal nerve vary in compositions and innervation paths among vertebrate lineages (Song and Boord, 1993; Higashiyama and Kuratani, 2013). So the use of trigeminal nerve implies the homology of the tripartite organization, while accepting variations at lower levels in individual branches. In case (***b***), the posthypophyseal process refers to the premandibular region lateral to the nasohypophyseal placode in cyclostomes, which receives the postoptic stream of trigeminal ectomesenchyme (Kuratani, 2012). The upper lip, on the other hand, is more theory-neutral as a premandibular region overlapping the mouth and applicable to both cyclostomes and gnathostomes. In addition, the posthypophyseal process is a developmentally transient structure, whereas the upper lip is free of such temporal constraint. Thus, the choice between the two terms depends on phylogenetic and developmental contexts (see descriptions of characters 17, 66, 160, 161 in Chapter 2).

Other anatomical terms have stalk contrast. In example (***c***), the choice between vertebrae and axial skeletal condensation directly relates to the composition of characters 147-150 in Chapter 2. The question is at what levels the sclerotome-derived cartilaginous nodules in hagfish should be compared with vertebrae or vertebral elements in other lineages (Ota et al., 2011). To describe the hagfish elements as vertebrae is to assume (***i***) a vertebra in the common ancestor of

all living vertebrates and (***ii***) degeneration of the ancestral vertebrae within myxinoids (Ota et al., 2011). To ensure the greatest latitudes of character evolution, the more theory-neutral axial skeletal condensation was used for those characters. Finally, the spiracle as present in crown gnathostomes (most prominently in elasmobranchs) is referred to by three terms in case (***d***). The spiracle is an external opening of a hyomandibular pouch, and the term refers to its function in ventilation. To complicate this terminology in character composition, a distantly related lineage appears to have a similar structure: an opening behind the eye in amphiaspidiform heterostracans has been posited as a spiracle as well (Halstead, 1971). This opening in amphiaspidiforms has also been suggested to represent a posteriorly shifted nasohypophyseal opening (Janvier, 1974). In discussion of distribution of the spiracle (character 51, Chapter 2), I chose an external hyomandibular opening over a spiracle or an opening behind the eye. This choice is my statement that the essential attribute of the character is its relation to the hyomandibular pouch, and not its function or external position, even though the most theory-neutral term is probably the opening behind the eye.

As seen in these examples, no simple rule fits theory-neutral terminology. It may be non-consequential, important, or inappropriate to discussion of characters. Therefore, this thesis does not follow a one-fits-all guideline regarding theory-neutral terminology. It will be used wherever it is warranted (such as ‘axial skeletal condensations’ in characters 147-150 in Chapter 2).

1.6 PROSPECTUS

A survey of cyclostome development and fossil record provides rationales for the body of works presented in this thesis. The primer for cyclostome development forms a comparative basis for the next four chapters, but the available information will make sense only with phylogenetic inferences. For such inferences, however, the fossil record offers little in raw materials required to test hypotheses. My strategies are three-fold: (***a***) to increase information from the fossil record that bears on the hypotheses outlined at the outset; (***b***) to use phylogenetic methods in testing the hypotheses; and (***c***) to incorporate the information from development in the evolutionary narrative that arises from my hypothesis testing.

Primitive vertebrate traits are never straightforward to reconstruct. The practice often defies simple extension of developmental features shared between hagfish and lampreys, let alone

doing so based on features only observed in one of the two. This is not only because hagfish and lampreys differ in many aspects but also because they likely form a sister group (Fig. 1.1; Chapter 2). The interrelationships among hagfish, lampreys, and gnathostomes have been framed as a classical three-taxon problem (Forey, 1984; Delarbre et al., 2000, 2002). In a strict cladistic sense, this three-taxon scheme cannot infer primitive conditions for gnathostomes once hagfish and lampreys form a clade. It is gnathostomes that form an outgroup in that scheme.

Therefore, parsimony-informed decisions require an additional branch that either: (***a***) nests outside cyclosotmes and gnathostomes; or (***b***) breaks up the stem of gnathostomes. Invertebrate chordates are difficult to compare with vertebrates, but the traits present across vertebrates and absent in successive outgroups may be inferred as vertebrate synapomorphies. Examples include the neural crest (Green et al., 2015) and the hindbrain *Hox* regulatory network (Parker et al., 2016). Then the questions to ask would be: (***a***) to what degree, if any, do invertebrate chordates exhibit genomic traits underlying vertebrate synapomorphies; and (***b***) at what point and in what form did traits evolve along the stem of vertebrates (Chapters 2 and 3). On the other hand, the node of the crown-group Gnathostomata presents a different challenge (Chapters 4 and 5, Appendix). Inferences of primitive conditions leading to the clade of living jawed vertebrates require interpretation of fossils in at least one stem gnathostome lineage. Only then can cyclostomes serve as an outgroup with respect to those gnathostome branches. Where a parsimony-informed test is ambiguous, conflicting interpretations may only be discriminated by the arbitrarily defined criterion of likelihood. It creates a tenuous argument when such indirect inferences hinge on a chosen living model. Examples include a comparison between the ammocoete larvae of lampreys and cephalochordates (Chapter 3).

Nevertheless, parsimony is a blunt tool for dissecting evolutionary complexities. Regardless of whether one leans towards convergence or conservation, it is possible to interpret the characters in various ways to make the conflicting hypotheses of a transformation series maximally parsimonious. The likelihood a particular set of interpretations is correct can only be assessed qualitatively. In the following chapters, I will address these unresolved problems and unanswered questions that arise from a comparative review of cyclostomes

FIGURES

Fig. 1.1. Phylogenetic scheme for studying the comparative development of cyclostomes. The tree follows the current consensus regarding monophyly of cyclostomes and paraphyly of placoderms and acanthodians (tree drawn by T.M. according to phylogenetic analyses presented in Chapter 2 and sources cited in text). Dark silhouettes = extant lineages. Gray silhouettes = extinct lineages. Systematic positions of euconodonts, myllokunmingiids, and yunannozoans remain uncertain. It is likely that some, if not all, of these taxa fall out of crown-group vertebrates.

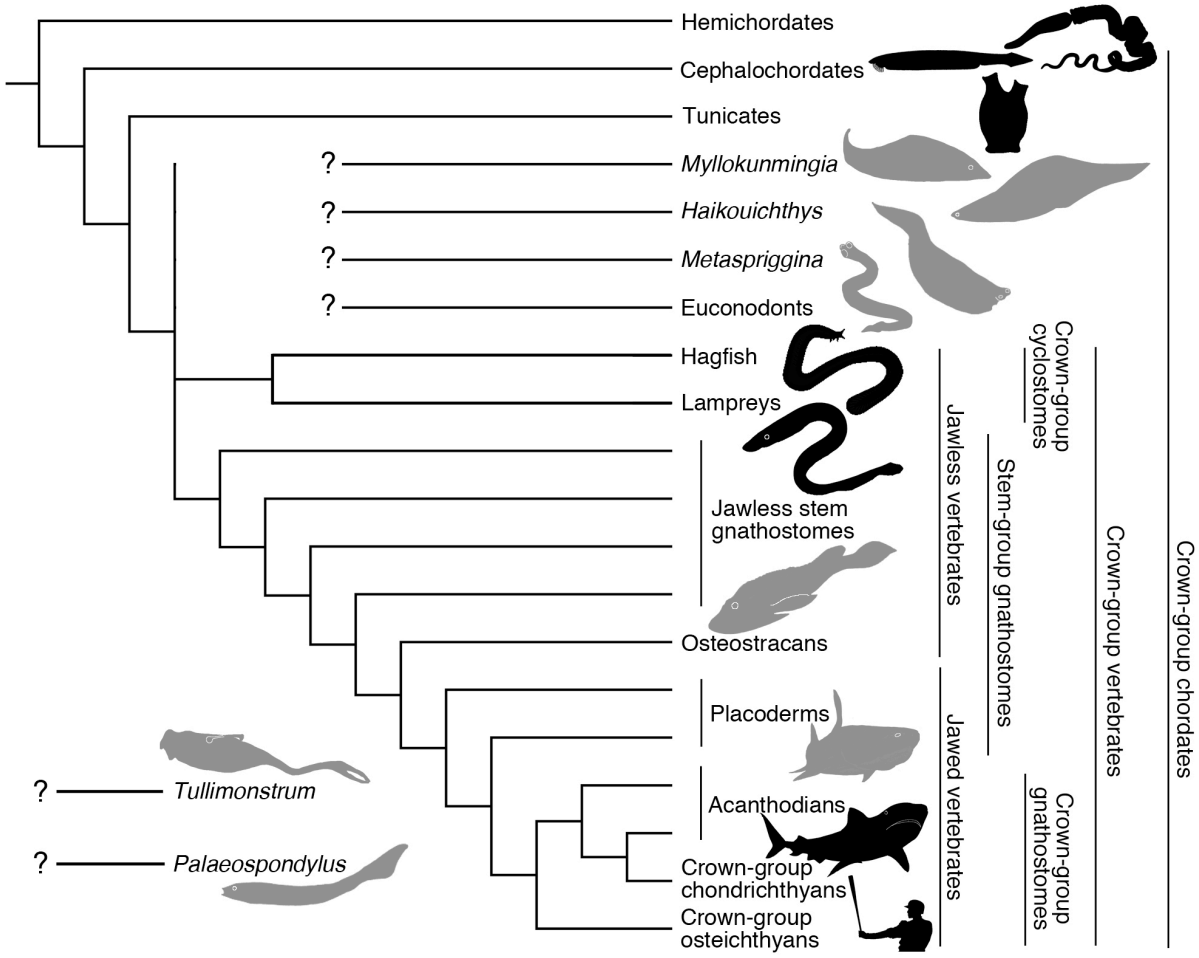
Hemichordates
Cephalochordates
Tunicates
?
Myllokunmingia
?
Haikouichthys
?
Metaspriggina
?
Euconodonts
Hagfish
Lampreys
Jawless stem gnathostomes
Osteostracans
Placoderms
Acanthodians
Crown-group chondrichthyans
Crown-group osteichthyans
?
Tullimonstrum
?
Palaeospondylus
Jawless vertebrates
Jawed vertebrates
Stem-group gnathostomes
Crown-group cyclostomes
Crown-group gnathostomes
Crown-group vertebrates
Crown-group chordates

Fig. 1.2. Development of the hagfish, *Eptatretus stoutii.* The plate is reproduced from Miyashita and Coates (2016) according to their provisional staging scheme (prefix = MC). (**b**-**s**) Original illustrations adopted from Dean (1899). (**a)** Egg capsules approx. 24 hours post deposition in captivity (photograph by T.M.). (**b**) MC2 at second (**b_1**), third (**b_2**), and fourth (**b_3**) cleavage viewed from the animal pole. (**c**) MC3 (blastula) indicated by an arrow. (**d**) MC4 (gastrula) in lateral view (**d_1**) and in close-up of the syncytial zone near the caudal end, demarcated by the presence of periblasts (**d_2**). (**e**) MC5 (late gastrula) indicated by an arrow. (**f**) MC6 (neurula) in dorsal view. (**g**) MC7 (late neurula) in dorsal view, dissected out from the egg capsule, with head pointing to the left. (**h**) MC8 (late neurula) in dorsal view. (**i**) MC9 (pharyngula) within egg capsule (**i_1**) and showing details of the head (**i_2**) in dorsal view. (**g**) MC10 (pharyngula) in dorsal view. (**k**) MC11 (pharyngula) in lateral view (**k_1**) and dissected out from the egg capsule with head pointing upwards (**k_2**). (**l**) MC12 (pharyngula) in egg capsule (**l_1**) and showing details of the head (**l_2**) in dorsal view. (**m**) MC13 (pharyngula) showing details of the head in dorsal view (**m_1**) and in lateral view (**m_2**). (**n**) MC14 (late embryo) showing details of the head in lateral view (**n_1**) and in dorsal view (**n_2**). (**o**) MC15 (late embryo) in egg capsule in lateral (**o_1**) and dorsal (**o_2**) views and showing details of the head in dorsal (**o_3**) and ventral (**o_4**) views. (**p**) MC16 (late embryo) showing details of the head in lateral view (**p_1**) and in egg capsule in ventral view (**p_2**). (**q**) MC17 (late embryo) showing details of the head in lateral view (**q_1**) and in egg capsule in ventral (**q_2**) and dorsal (**q_3**) views. (**r**) MC18 (near hatching) in egg capsule in ventral view (**r_1**) and showing details of the head from dorsal (**r_2**) and ventral (**r_3**) views. **S**, hatchling in right lateral view. Illustrations not to scale.

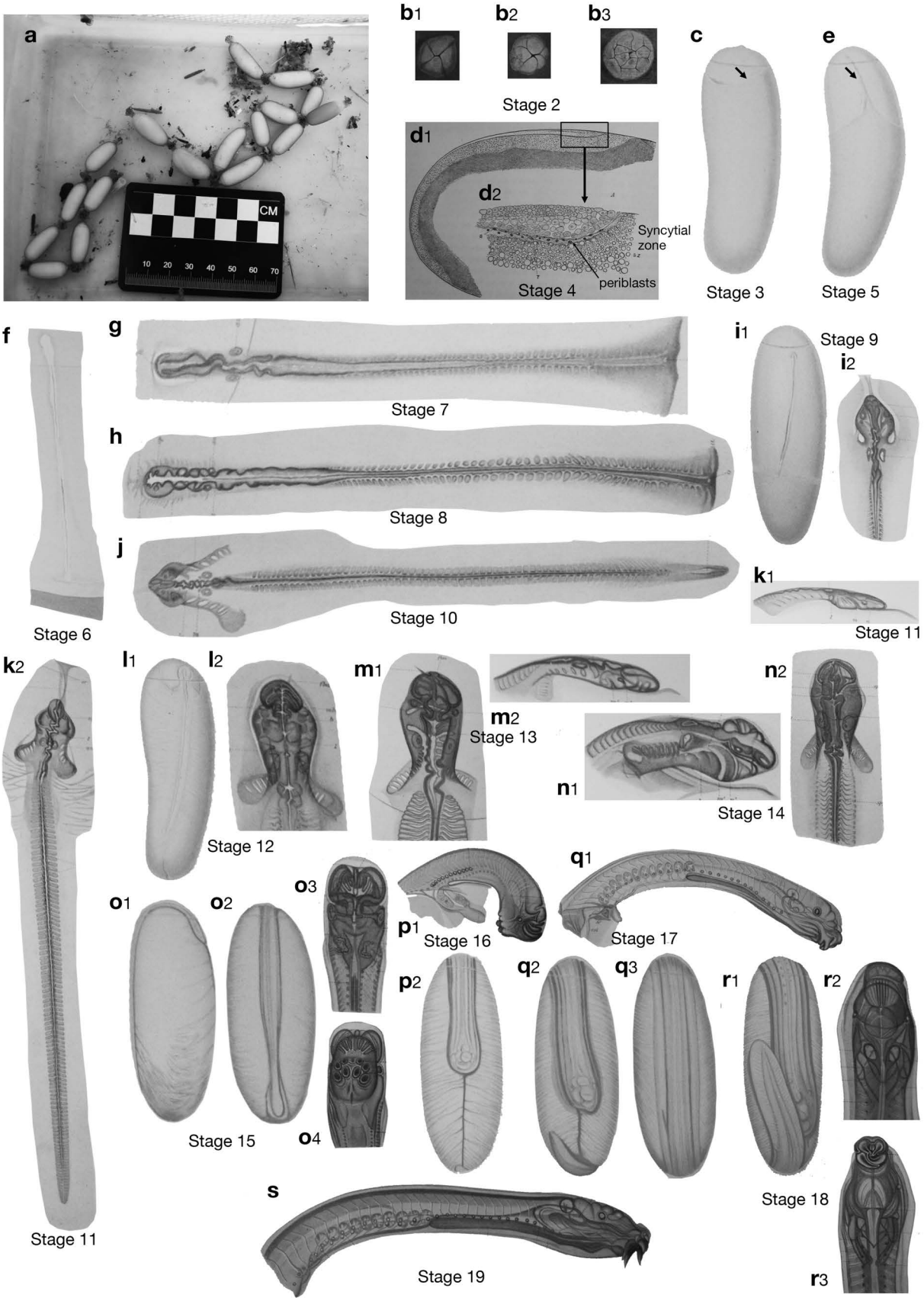
a
CM
10 20 30 40 50 60 70
b1
b2
b3
Stage 2
c
Stage 3
e
Stage 5
d1
d2
Syncytial zone
periblasts
Stage 4
f
Stage 6
g
Stage 7
h
Stage 8
i1
Stage 9
i2
j
Stage 10
k1
Stage 11
k2
Stage 11
l1
l2
Stage 12
m1
m2
Stage 13
n1
Stage 14
n2
o1
o2
o3
o4
Stage 15
p1
Stage 16
p2
q1
Stage 17
q2
q3
r1
r2
Stage 18
r3
s
Stage 19

Fig. 1.3. Schematic drawings of lamprey (*Lampetra* [*Lethenteron*] *reissneri*) embryonic stages according to Tahara (1988). Images shown are adapted from Tahara (1988), and shown with the animal pole at the top for early cleavage and gastrulation stages (T0 – T11). Gastrulation stages (T12 – T17) are shown with the location of the blastopore fixed towards the right. Later stages of embryogenesis (T18 - T30) are shown with anterior to the left and dorsal up.

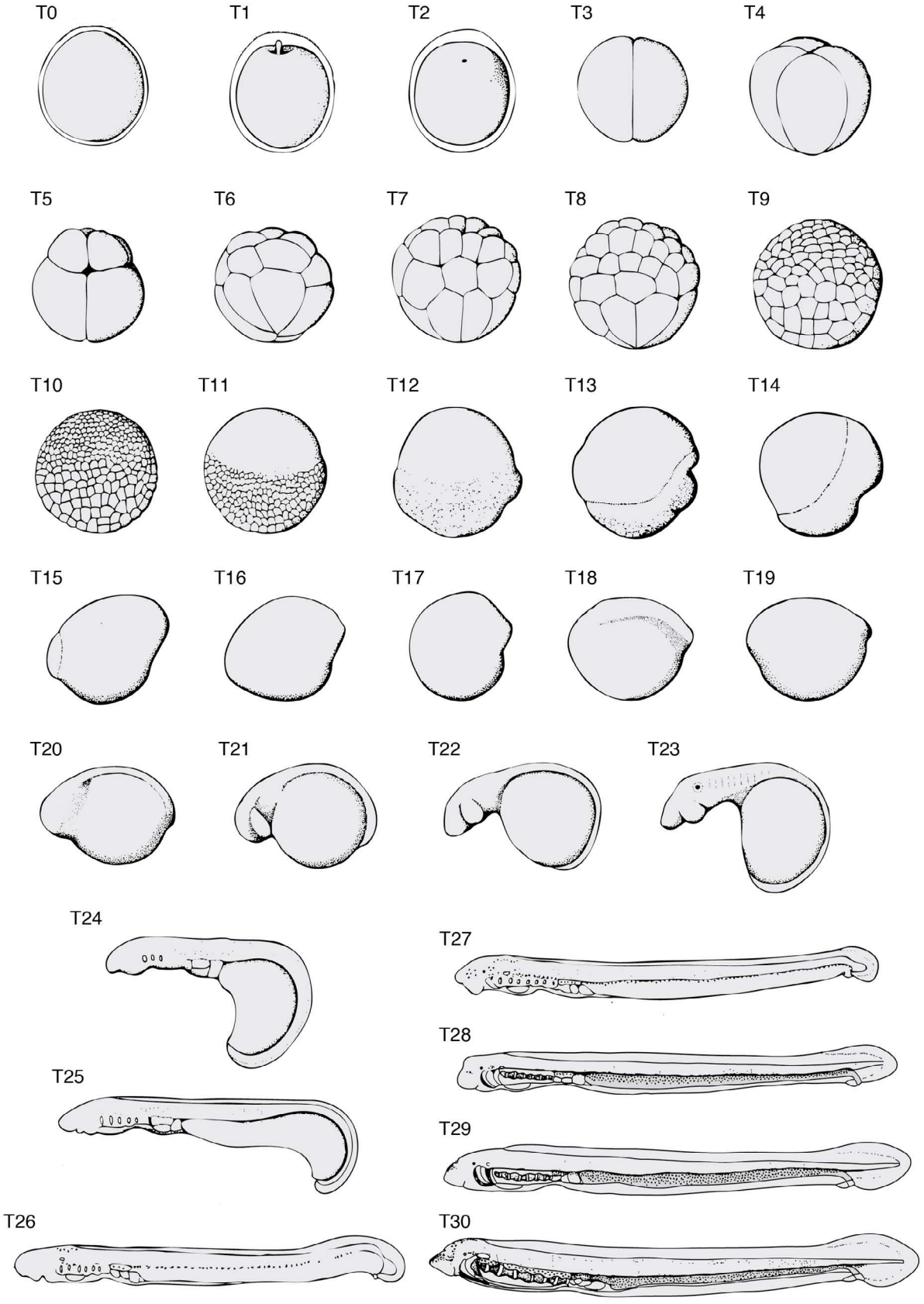
T0
T1
T2
T3
T4
T5
T6
T7
T8
T9
T10
T11
T12
T13
T14
T15
T16
T17
T18
T19
T20
T21
T22
T23
T24
T25
T26
T27
T28
T29
T30

Fig. 1.4. Representative gene-expression profiles in lamprey (*Petromyzon marinus*) at key stages of development using *in situ* hybridization (**a**-**c**) and fluorescent reporter expression assay (**d**-**f**). (**a**) *Zic-A* expression in dorsal neural tube and dorsal myotomes at T23. This transcription factor specifies the neural plate border prior to the delamination of neural crest cells. (**b**, **c**) A muscle marker *MyLC* (myosin light chain) is expressed in lateral myotomes at T23 (**b**) and at late T25/early T26 (**c**). (**d**-**f**) reporter expression assay of Pm1 *Hoxa2a* enhancer as described by Parker et al. (2014a) at T23 (**d**, **e**) and at T25 (**f**). Arrowheads indicate rhombomeres 3 and 5 in the hindbrain; arrows indicate position of the hyoid arch. The reporters are expressed in the hindbrain rhombomeres (r3 and r5) and the neural crest ectomesenchyme filling in the pharyngeal arches II rearward. Photographs were taken by Stephen A. Green (California Institute of Technology).

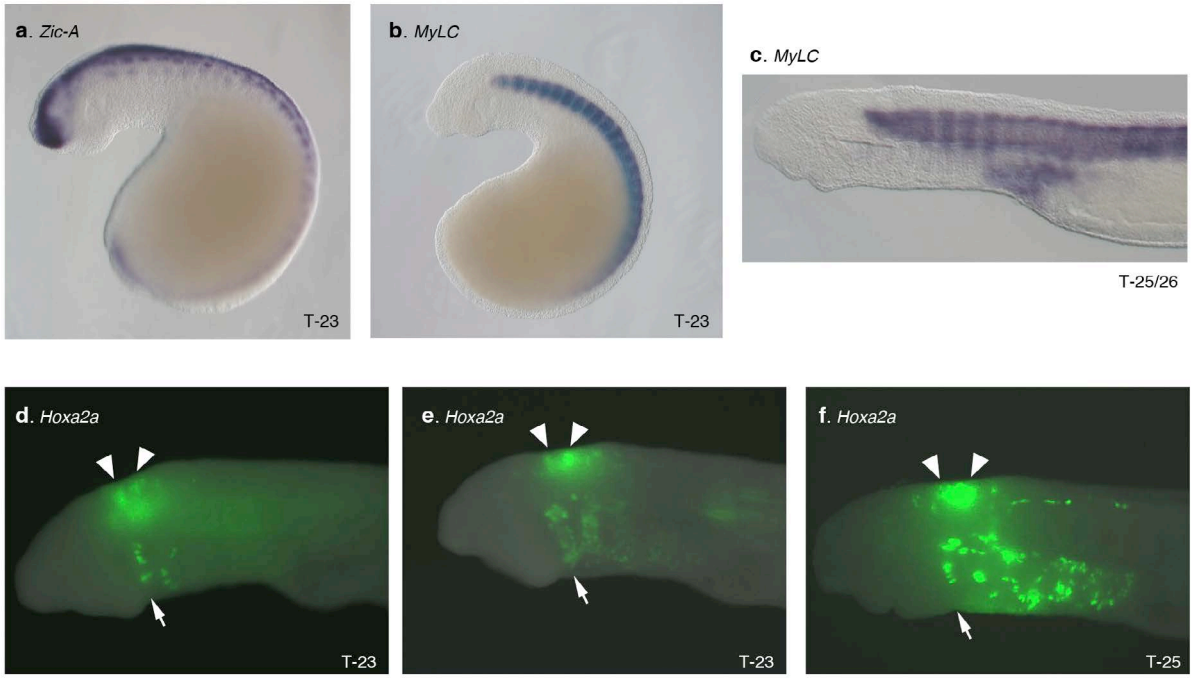
a. Zic-A
T-23
b. MyLC
T-23
c. MyLC
T-25/26
d. Hoxa2a
T-23
e. Hoxa2a
T-23
f. Hoxa2a
T-25

Fig. 1.5. Chondrocranial morphology of cyclostomes in left lateral view. (**a**) Hagfish *Myxine glutinosa* (redrawn after Cole, 1905). (**b**) Lamprey *Lampetra fluviatilis* (redrawn after Marinelli and Strenger, 1954). Asterisk (*) indicates cartilages derived from the ectomesenchyme of the posthypophyseal process (upper lip).

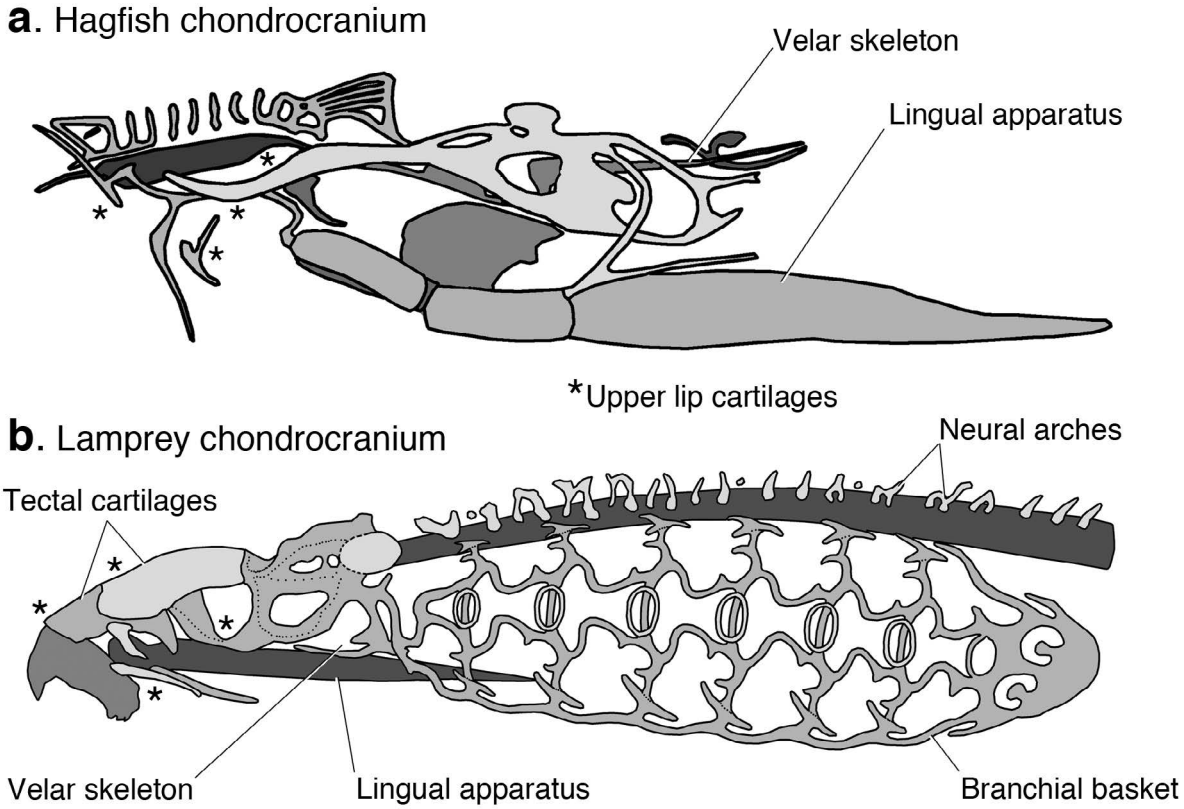
a. Hagfish chondrocranium
Velar skeleton
Lingual apparatus
*Upper lip cartilages
b. Lamprey chondrocranium
Neural arches
Tectal cartilages
Velar skeleton
Lingual apparatus
Branchial basket

Fig. 1.6. Two enigmatic early vertebrates. (**a**) *Metaspriggina walcotti* (Royal Ontario Museum 62933) from a Cambrian Lägerstatte in Kootenay National Park, Canada in dorsal view, showing branchial elements and myomeric structures among other preserved soft tissues. (**b**) *Palaeospondylus gunni* (Muséum national d'Histoire naturelle GBP 94) from the Early Devonian of Caithness, Scotland, showing some of the skeletal elements compared with those of hagfish, by Hirasawa et al. (2016).

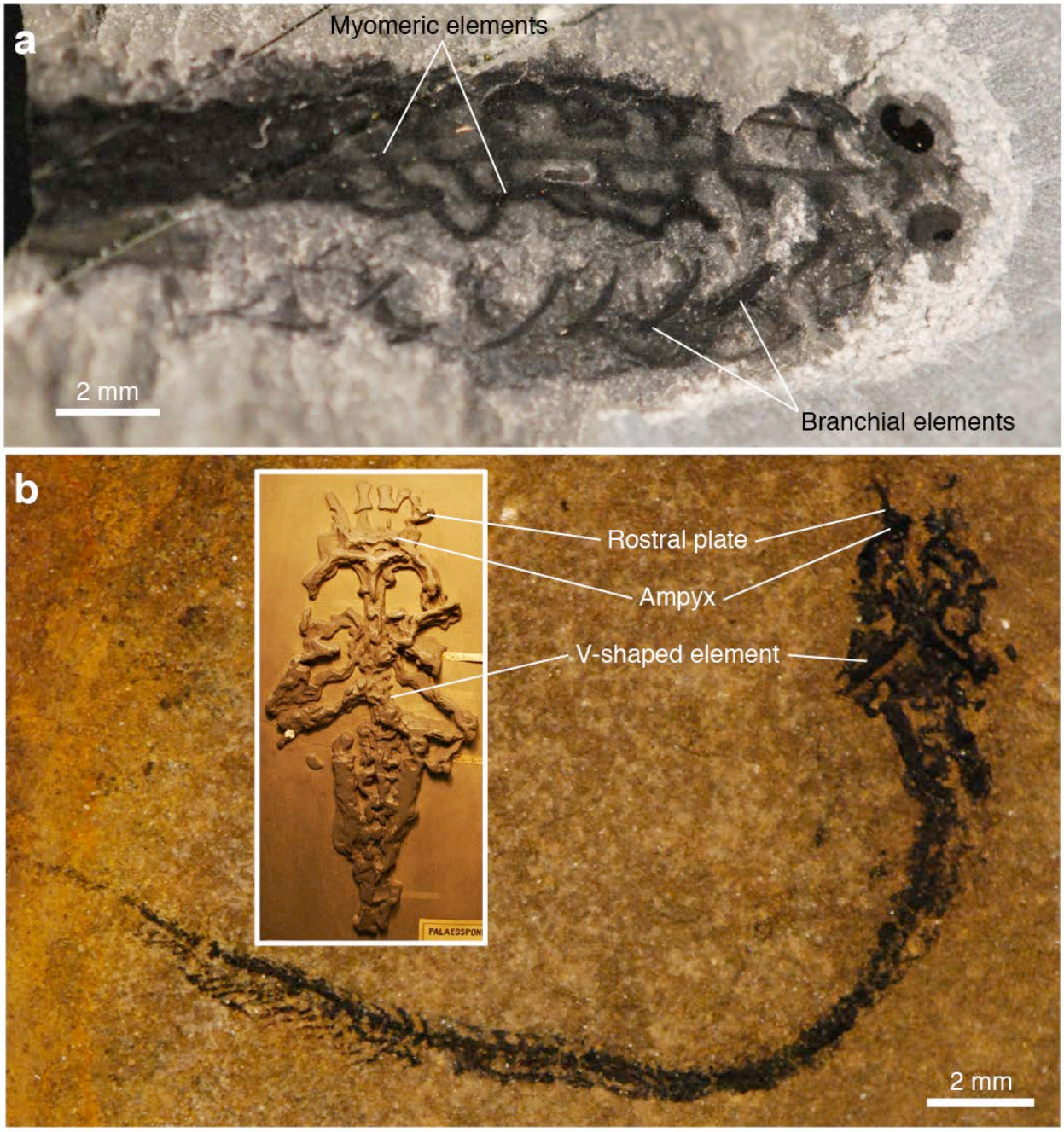
a
Myomeric elements
2 mm
Branchial elements
b
Rostral plate
Ampyx
V-shaped element
2 mm

TABLES

Table 1.1. Summary of the embryological and developmental biological literature on lampreys in a rough chronological order. Citations were grouped by a major topic and not duplicated between the topics.

Topics	References
Early works (the era of comparative morphology and embryology)	
General embryology and life history	Müller, 1856; Schultze, 1856; Calberla, 1877; Scott, 1880, 1881, 1882, 1887; Nuel, 1881; Shipley, 1887; Goette, 1890; Hasse, 1893; Owsjannikow, 1893
First cleavages, gastrulation, and germ layer formation	Shipley, 1885; von Kupffer, 1890; Hatta, 1907, 1915; Glaesner, 1910
Head, pharynx, and archenteron	Dohrn, 1886; Nestler, 1890; von Kupffer, 1890; Koltzoff, 1901; Hatta, 1923; Kieckebusch, 1928; Veit, 1939
Central and peripheral nervous systems	Freud, 1877, 1878; Wiedersheim, 1880; Ahlborn, 1883, 1884; Scott, 1883; Alcock, 1898; Johnston, 1905; Keibel, 1906, 1928, Tretjakoff, 1909a, 1909b, 1909c, 1913, 1927; Allen, 1916
Circulatory systems	Julin, 1887; Hatta, 1897, 1923; Cori, 1906; Keiser, 1914; Daniel, 1934
Musculoskeletal system	Schaffer, 1896; Schalk, 1913; Sewertzoff, 1913, 1916, Tretjakoff, 1926a, 1926b, 1929
Urogenital systems	Hatta, 1900; Wheeler, 1900; Okkelberg, 1921
The mid-20th century (the eve of evolutionary developmental biology)	
Developmental anatomy	Damas, 1935, 1942, 1944, 1948, 1951; Johnels, 1948; Lindström, 1949; Wedin, 1949
Experimental embryology (neural crest)	Newth, 1950, 1951, 1956
Developmental timetable and life history	Piavis, 1961, 1971; Smith et al., 1968; Wright and Youson, 1976, 1980; Youson and Potter, 1979; Tahara, 1988; Wright, 1989; Richardson and Wright, 2003; Yamazaki et al., 2003

Topics	References
The millennial (the rise of evolutionary developmental biology)	
Structural and immunohistochemical analyses of cartilages	Wright and Youson, 1982, 1983, Wright et al., 1983, 1988; Armstrong et al., 1987; Robson et al., 1993, 1993, 1997; McBurney and Wright, 1996; McBurney et al., 1996; Morrison et al., 2000
Branchial morphology	Mallatt, 1979, 1981, 1982; Moore and Mallatt, 1980
Trabecular cranii and head cavities	Langille and Hall, 1988; Kuratani et al., 1997, 1999, 2004; Horigome et al., 1999; McCauley and Bronner-Fraser, 2003
Nervous system, early evolution	Ueki et al., 1998; Ogasawara et al., 2000, 2001; Murakami et al., 2001, 2002, 2004, 2005; Uchida et al., 2003; Matsuura et al., 2008; Kano et al., 2010; Parker et al., 2011, 2014a, b; Sugahara et al., 2011, 2016; Higashiyama and Kuratani, 2014; Higashiyama et al., 2016;
Origin of the jaws	Tomsa and Langeland, 1999; Kimmel et al., 2001; Kuratani et al., 2001, 2013; Myojin et al., 2001; Cohn, 2002; Shigetani et al., 2002; Takio et al., 2004, 2007; Cerny et al., 2010; Kuraku et al., 2010
Neural crest and neurogenic placode, regulatory networks	Neidert et al., 2001; McCauley and Bronner-Fraser, 2002, 2004; Meulemans and Bronner-Fraser, 2002; Sauka-Spengler et al., 2002, 2007; Meulemans et al., 2003; Hammond and Whitfield, 2006; Hammond et al., 2009; Häming et al., 2011; Uy et al., 2012, 2015; Modrell et al., 2014; Lee et al., 2016
Musculature, early evolution	Kusakabe et al., 2003, 2004, 2011, Kusakabe and Kuratani, 2005, 2007; Suzuki et al., 2016
Branchial skeleton, early evolution	McCauley and Bronner-Fraser, 2006; Zhang et al., 2006; Ohtani et al., 2008; Martin et al., 2009; Cattell et al., 2011; Lakiza et al., 2011; Yao et al., 2011; Jandzik et al., 2014; Square et al., 2016a, 2016b
Origin of paired fins	Tiecke et al., 2007; Onimaru et al., 2011; Tulenko et al., 2013
Heart, pericardial space	Matsuura et al., 2008; Kokubo et al., 2010

Table 1.2. Chronology of the embryological and developmental biological literature on hagfish, adapted from Miyashita and Coates (2016). Abbreviations for generic names: *E.* = *Eptatretus*; *M.* = *Myxine*; *P.* = *Paramyxine*.

Year	Milestones	References
1890-1910		
	Successful early collecting efforts and preliminary accounts of embryos of *E. stoutii*; descriptive developmental anatomy of excretory organs.	Price (1896a, b, 1897, 1904); Dean (1898); Doflein (1899)
	Descriptive embryology of *E. stoutii* based on a nearly complete series.	Dean (1899)
	Development of the brain, pharynx, and nasohypophyseal cavity in *E. stoutii*.	von Kupffer (1899, 1900, 1906)
	Descriptive embryology of the mouth, gill pouches, and thyroid gland in *E. stoutii*.	Stockard (1906a, b)
1911-1940		
	Description of the brain development in *E. stoutii* based on the Dean-Conel sections.	Conel (1929, 1931b)
	Publication of the Bashford Dean festschrift part I ("*Archaic Fishes*").	Gudger & Smith (1933); Conel (1933)
	Description of the chondrocranial development in *E. stoutii*.	Neumayr (1938)
1941-1970		
	Neural crest development in *E. stoutii* based on the Dean-Conel sections.	Conel (1942)
	Detailed morphological description of two embryos of *M. glutinosa*.	Holmgren (1946)
	Pituitary development in *M. glutinosa*; no evidence for endostylar arrangement.	Fernholm (1969)
1971-2000		
	Re-examination of the Dean-Conel histological sections for the pituitary development suggests (incorrectly) an endodermal origin of the nasohypophyseal duct in *E. stoutii*.	Gorbman (1983); Gorbman & Tamarin (1985)
	Three-dimensional reconstruction of the Dean-Conel histological sections reveals lateral line and other neurogenic cranial placodes in *E. stoutii*.	Wicht & Northcutt (1995); Wicht and Tusch (1998)

Year	Milestones	References
2001-current		
	K.G. Ota and S. Kuratani began successful efforts to obtain embryos from *E. burgeri* in captivity; descriptive accounts of the newly obtained embryos.	Ota & Kuratani (2006, 2008); Kuratani & Ota (2007)
	Neural crest development in *E. burgeri* is similar to that in other vertebrates.	Ota et al. (2007)
	Expression of collagen type 2α1 genes in *E. burgeri*.	Ota & Kuratani (2010)
	Presence of sclerotomal cargilaginous elements in the caudal region of *E. burgeri*.	Ota et al. (2011, 2013, 2014)
	Transcriptome profiles in *E. burgeri*.	Takechi et al. (2011)
	Nasohypophyseal development in *E. burgeri* supports the pan-cyclostome pattern.	Oisi et al. (2013a)
	Description of the chondrocranial development in *E. burgeri* and *P. atamii*.	Oisi et al. (2013b)
	Partly dorsoventrally patterned expression of *Dlx* cognates in *E. burgeri*.	Fujimoto et al. (2013)
	'Hypobranchial' musculature and nerves in relation to pharyngeal pouches.	Oisi et al. (2015)
	Brain regionalization in *E. burgeri* comparable across vertebrates.	Sugahara et al. (2016)

Table 1.3. Key points at which to compare development between hagfish and lampreys. Sources are cited in text.

	Hagfish	Lampreys
Life history		
Larval stage	No distinct larval stage	Ammocoetes; metamorphosis
Sex ratio	Equal, or males significantly fewer (~6%) in some populations	Equal
Spawning	Iteroparous?	Semelparous
Fertilization	? — Unknown	External
Fecundity (per season)	10-70	370-304,800
Egg diameter	14-77 mm	0.38-1.37 mm
Egg morphology	Elongate; thick capsule (50-90 μm); anchor filaments; micropylar opening; opercular ring near animal pole	Round to elliptical; fertilization membrane; no anchor filaments, mycropylar opening, or opercular ring
Time to hatching	> 8 months	8 days – 1 month
Size at hatching	> 30-50 mm	2.6-7 mm
Embryology		
First cleavages	Meroblastic; discoidal	Holoblastic
Blastocoel	Not clearly defined	Well developed
Gastrulation	Ingression	Involution
Gastrula	'Primitive streak'	Externally visible blastopore and lip
Pharyngula	Head plate to protrusion	Head protrusion
Brain regionalization	No apparent departure from gnathostomes, except for the presence of epiphysis	*Nkx2.1/2.4A*, *Hh* not expressed in medial ganglionic eminence; *Pax6A* not expressed in rhombic lip
Neural crest	Lacks *Snail* expression	Nearly full complement of GRN
Sensory capsules	Prominent vesicles and placodes in early neurula	Vesicles and placodes in late neurula
Nasohypophyseal canal	Closed, and open secondarily; 'choana'	Remains open; no choana
Pericardium	Tucked under head late (MC14)	*In situ* at base of head protrusion

	Hagfish	Lampreys
Axial skeleton	Haemal arch-like cartilaginous nodules in tail	Neural arches in adult
Upper lips	Meeting at midline under nasohypophyseal canal and supporting barbels	Meeting at dorsal midline anterior to nasohypophyseal canal and supporting oral funnel
Lingual apparatus	Proportional in late embryos	Remains an anlage in larval stage
Branchial region	Pouches displaced posteriorly	Basket, separate from esophagus in adults
'Hypoglossal' nerves	No circumpharyngeal path	Circumpharyngeal path
Thyroid	No endostylic stage	Endostyle in larva
Hatching	Well past pharyngula	Pharyngula

Table 1.4. Staging scheme proposed by Miyashita and Coates (2016) for the hagfish *Eptatretus stoutii* based on observations on the Dean-Conel collections (histological sections of specimens described in Dean, 1899). Some phenotypic criteria overlap between stages temporally, and the chronological order of developmental events varies from one embryo to another — particularly across the neurula stages. The inconsistencies and coarse staging will only be resolved with a more densely sampled embryonic series. For further discussion, see Miyashita and Coates (2016). L = panel label in Fig. 1.2; MC = staging proposed by Miyashita and Coates (2016).

MC	Embryonic events	L
1	Fertilization; zygote	
2	Meroblastic cleavage (discoidal; asymmetric beyond eight cells)	b
3	Blastula (downgrowth of cellular cap; syncytial zone between blastomeres and yolk)	c
4	Early gastrula (neural axis as epiblastic thickening; blastoderm elongation)	d
5	Late gastrula (tail bud to blastopore lip; ‘primitive streak’)	e
6	Neurula (head plate; neural tube; stomodeum depressed; one third egg length)	f
7	Late neurula (brain compartments; rhombomeres; otic capsule; less than 54 somites)	g
8	Late neurula (oronasohypophyseal membrane; 59 somites; optic vesicle)	h
9	Late neurula-early pharyngula (hyomandibular pouch; foregut diverticulum)	i
10	Pharyngula (eyes; cranial nerves V, VII, VIII; five pharyngeal pouches; 73 somites)	j
11	Pharyngula (six to eight pharyngeal pouches; efferent pharyngeal arteries; 105 somites)	k
12	Pharyngula (embryo as long as egg; 9-12 pharyngeal pouches, onset of displacement)	l
13	Pharyngula (13-14 pharyngeal pouches, rolled into lateral side of body)	m
14	Late embryo (positional adjustment: e.g., heart tucked underneath head)	n
15	Late embryo (longer than yolk; nasohypophyseal opening, secondary; slime glands)	o
16	Late embryo (three quarters of circumference; pharyngeal pouches displaced)	p
17	Late embryo (nearly complete chondrocranium; tendon of lingual apparatus)	q
18	Late embryo (oral barbells folded; complete chondrocranium; caudal cartilages)	r
19	Hatchling; juvenile	s

Table 1.5. A summary of Tahara's (1988) staging scheme for lampreys based on *Lampetra reissneri*. Conspicuous phenotypic criteria relevant to this chapter were selected for each stage, but this list is not exhaustive. T= Tahara's stage, as indicated in Fig. 1.3.

T	Embryonic events
0	Unfertilized egg
1	Zygote, polar cone
2	Zygote, polar spot (polar cone absorbed into cytoplasm)
3	Two cells (first cleavage furrow from animal to vegetal pole)
4	Four cells (second cleavage furrow from animal pole, division meridional)
5	Eight cells (cleavage furrow horizontal or meridional)
6	12-16 cells (fourth cleavage from animal hemisphere, horizontal)
7	24-32 cells (fifth cleavage furrow in animal hemisphere)
8	Morula (sixth cleavage furrow from animal hemisphere)
9	Early blastula (seventh cleavage from animal hemisphere; blastocoel; segmentation cavity)
10	Mid blastula (expansion of blastocoel)
11	Late blastula (roof of blastocoel becomes thinner)
12	Gastrula, dorsal cone (blastocoel expands below equator; groove along vegetal yolk mass)
13	Gastrula, brow-shaped blastopore (roof and lateral wall of blastocoel one cell thick)
14	Gastrula, semi-circular blastopore (archenteron, mesoderm)
15	Gastrula, elliptical blastopore (archenteron tubular, with two-cell thick mesodermal roof)
16	Gastrula, flat dorsal lip (posterior protrusion; notochord; blastocoel vestigial)
17	Neurula, neural groove (neural plate with a groove, quarter of circumference; foregut)
18	Neurula, neural folds (groove one third of circumference; prechordal plate)
19	Neurula, neural folds elevated (somitic formation; groove a half of circumference)
20	Neurula, neural rod (neural fold closure; anterior protrusion; neural crest)
21	Head protrusion (posthypophyseal process; first pharyngeal pouches; liver; lateral plate)
22	Head protrusion, neural tube (otic placode; infundibulum; first myotome separate)
23	Head protrusion, stomodeum (upper lips fused; 25 somites; placodes; heart)
24	Hatching, nasal pit (four pharyngeal pouches; endostyle; pronephros; cardium + aortae)
25	Tail bud, heart beat (six to seven pharyngeal pouches; optic cup; nasohypophyseal canal)

T	Embryonic events
26	Tail bud, melanophores (eight pharyngeal pouches; chondrogenic condensation; mouth)
27	Tail bud, eye spots (posthypophyseal process expands; velum)
28	Velum beating (oral hood; gill contraction; intestinal lumen; pharyngeal arches irrigated)
29	Greenish bile in gall bladder (oral hood expansion; nasohypophyseal canal opening)
30	Ammocoete (digestive tract complete; torsion of liver and anterior intestine)

Table 1.6. Comparison of gene expression patterns between hagfish and lampreys, compiled from the literature. Documented gene expression patterns in hagfish are listed on the left side and set against lamprey counterparts where known and described. This comparison is restricted to homologues. Predicted or inferred orthologues are treated in the same row, and paralogues (if any) are also listed. A box with a solid line and shaded gray indicates cognates considered to have arisen by independent duplication events. No orthology can be determined between individual genes, but as a group they share a common evolutionary origin. This table is not an exhaustive list of paralogous genes present in each taxon (taxon-specific paralogues may exist but have not been isolated). Neither does it include negative results (lack of expression) unless specifically addressed in the original source. Temporal and spatial extent of the expression may be greater than described in the literature. Table 1.7 lists gene expression patterns in lampreys for which no counterpart has been described in hagfish. Abbreviations: CNS= central nervous system; EM= ectomesenchyme; NC= neural crest; NHP= nasohypophyseal placode; PA= pharyngeal arch (I-VII); PHP= posthypophyseal process; PNS= peripheral nervous system; SC= sclerotomes; ZLI= zona limitans intrathalamica; MC = developmental stages proposed by Miyashita and Coates (2016).

Hagfish			Lampreys			
Genes	**Contexts**	**Expression patterns**	**Genes**	**Contexts**	**Expression patterns**	**References**
Atoh1	CNS	Rhombic lip (MC15)	*Atoh1*	CNS	Hindbrain, dorsal (T27)	Sugahara et al. 2016
BGN/DCN	Skeleton	Mesenchyme ventral to notochord (MC15); cartilaginous matrix of 'vertebral' element (adult)				Ota et al. 2013
Col2A1a	Skeleton	Perichondral matrix, notochordal sheath, olfactory bulbs, keratinous tooth plates (juvenile)	*Col2a1a*	Skeleton	Somites (T23-30); non-pharyngeal ectoderm, epibranchial strip, perioral area (T24-30); head mesoderm (T25); pharyngeal ectoderm, lateral EM in PAs (T26-30); fin mesenchyme (T27)	Zhang et al. 2006; Sauka-Spengler et al. 2007; McCauley 2008; Ohtani et al. 2008; Ota & Kuratani 2010; Cattell et al. 2011
Col2A1b	Skeleton	Cartilages, notochord, epithelium (juvenile)	*Col2a1b*	Skeleton	Floor plate, notochord, hypochord (T23-30); non-pharyngeal ectoderm, epibranchial strip, perioral area (T24-30); pharyngeal ectoderm, lateral EM in PAs (T26-30); parachordal chondrocytes (T27)	Zhang et al. 2006; McCauley 2008; Ohtani et al. 2008; Ota & Kuratani 2010
Dlx1/4/6A	NC	PHP and PAs (MC12-13); lingual apparatus (MC14-15)	*DlxD*	NC	Anterior neural tube (dorsal), perioral ectoderm (T23); PAs, PHP (T23-27); hypothalamus, telenchephalon, nasal placode (T25-27)	Murakami et al. 2001, 2002; Myojin et al. 2001; Neidert et al. 2001; Cerny et al. 2010; Kuraku et al. 2010; Oisi et al. 2013b; Fujimoto et al. 2013; Kuratani et al. 2013
Dlx1/4/6B	NC	PAs (MC12-13); lateral side of otic capsule (MC14-15)	*DlxE*	NC	PHP, ventral PA I mesenchyme; weak in PAs, hypothalamus, telencephalon, nasal placode, otic vesicle (T26.5)	
Dlx1/4/6C			*DlxF*	NC	Ventral mesenchyme of PA I, nasal placode (T26.5)	Neidert et al. 2001; Cohn 2002; Shigetani et al. 2002; Cerny et al. 2010; Kuraku et al. 2010; Sugahara et al. 2011, 2013; Fujimoto et al. 2013
Dlx2/3/5A	NC	Otic vesicle (MC12-13)	*DlxA*	NC	Anterior neural tube (dorsal), perioral ectoderm (T23); EM (T23-27); non-mandibular PAs at mid-height and lateral, ventral PA I, PHP (T25-27); telencephalon, hypothalamus, otic vesicle, nasal placode (T26-27)	
Dlx2/3/5B	NC	PHP, PAs, and otic vesicle (MC12-13); chondrifying facial cartilages, lingual apparatus, and otic capsule (MC14-15)	*DlxC*	NC	EM (T22-27); perioral ectoderm (T23); PAs and PHP, hypothalamus, telencephalon, nasal placode (T25-27)	Kimmel et al. 2011; Neidert et al. 2001; Sauka-Spengler et al. 2007; Cerny et al. 2010; Kuraku et al.

Hagfish			Lampreys			
Genes	**Contexts**	**Expression patterns**	**Genes**	**Contexts**	**Expression patterns**	**References**
Dlx2/3/5C	NC	PHP and PAs (MC12-13); oropharyngeal floor (MC14-15)	*DlxB*	NC	Non-neural ectoderm (T17); PAs, PHP, mesenchyme around endostyle (T25-27)	2010; Oisi et al. 2013b; Fujimoto et al. 2013; Square et al. 2017
DlxΨ	NC	Chondrifying cranial cartilages and otic capsule (MC15-16)				Fujimoto et al. 2013
EmxB	CNS	Telencephalon (MC13-15)	*Emx*	Neural tube, mesoderm	Neural tube, mesoderm (T19-23); trigeminal and acousticofacial ganglia, velum (T24); telencephalon (T26)	Murakami et al. 2001; Myojin et al. 2001; Sugahara et al. 2016
Fgf8/17	Placodes, CNS	Nasal placode, mid-hindbrain boundary (MC9)	*Fgf8/17/18*	Pharynx	Pharyngeal pouch interface, nasal placode (T22-28); anteroventral telencephalon, epiphysis, PHP, perioral ectoderm (T24-26.5); mid-hindbrain boundary (T26)	Shigetani et al. 2002; Uchida et al. 2003; Oisi et al. 2013a; Sugahara et al. 2011, 2013; Jandzik et al. 2014
FoxG1	CNS	Telencephalon (MC13-15)				Sugahara et al. 2016
			FoxD-A	NC	Dorsal neural tube (T17); premigratory and migratory NC (T21-23); PHP (T23)	Sauka-Spengler et al. 2007
HandA	Lateral plate mesoderm	Mesenchyme derived from lateral plate (MC15)	*HandA*	Pharyngeal patterning	Heart, anterior mesenchyme (T23-26); cardiac ganglia (T24); ventral pharyngeal mesenchyme, ventral PA I (lower lip), lateral plate mesoderm (T24-27); caudal mesoderm (T25)	Cerny et al. 2010; Kuraku et al. 2010; Haming et al. 2011; Onimaru et al. 2011; Tulenko et al. 2013; Oisi et al. 2015; Square et al. 2017
Hh1	Placodes	Preoral gut diverticulum, hypothalamus (MC7-13); floor plate, notochord, pharyngeal endoderm (MC13)	*HhA*	CNS	Midline mesoderm (T18); prechordal plate (T19-21); notochord (T19-27); floor plate (T21-27); ZLI, endostyle (T24-27); hypothalamus, pharyngeal endoderm (T26-27)	Uchida et al. 2003; Murakami et al. 2005; Kano et al. 2010; Sugahara et al. 2011, 2013, 2016; Kuratani et al. 2013; Oisi et al. 2013a; Jandzik et al. 2014; Square et al. 2015b
Hh2	CNS	Hypothalamus, ZLI, medial ganglionic eminence, floor plate, notochord, pharyngeal endoderm (MC13-15); telencephalon (MC15)	*HhB*	CNS	Floor plate (T21-27); hypothalamus, ZLI (T23-27); notochord, pharyngeal endoderm (T24-27)	
Hh3	CNS	Pharyngeal endoderm (MC13); floor plate, notochord (MC13-15)	*HhC*	CNS	No expression in medial ganglionic eminence (T26-27)	
Hh4	Mesoderm	Notochord (MC13)	*HhD*	CNS	No expression in medial ganglionic eminence (T26-27)	
Lhx3/4A	Placodes	Hypophyseal placode (MC12)				Oisi et al. 2013a
			Lhx6/7/8A	PNS	PHP, PA I (T26-27.5)	Sugahara et al. 2011

Hagfish			Lampreys			
Genes	**Contexts**	**Expression patterns**	**Genes**	**Contexts**	**Expression patterns**	**References**
MyHCA	Myotomes	Myotomes, abaxial muscle precursors (MC15)	*MyHC1*	Myofibres	Lateral myotomes, adaxial later (T25-28)	Kusakabe & Kuratani 2005, 2007; Oisi et al. 2015
			MyHC2	Myofibres	Myotomes, adaxial later (T25-28); trunk musculature, hypobranchial muscles (T28)	
MyoD	Myotomes	Medial somites (MC14)				Ota et al. 2011
Nkx2.1/2.4	CNS	Hypothalamus (MC7-15); medial ganglionic eminence (MC15)	*Nkx2.1/2.4 (Ttf-1)*	CNS	Hypothalamus, endostyle (T21-27)	Murakami et al. 2001, 2005; Ogasawara et al. 2001; Uchida et al. 2003; Sugahara et al. 2011, 2013, 2016; Oisi et al. 2013a
			Nkx2.1/2.4 B	CNS	Hypothalamus (T26-27); telenchephalon, posterior tuberculum, rostral subpallium, endostyle (T27)	
			Nkx2.1/2.4 C	CNS	Hypothalamus (T26); telenchephalon, rostral subpallium, endostyle (T27)	
			OtxA	CNS	Anterior neural tube (T19,20); mid-hindbrain boundary (T22); hypothalamus, PA I, PHP (T23-28); fore-midbrain, epiphysis, optic stalk, nasal placode, olfactory epithelium, PAs (T24-28)	Ueki et al. 1998; Horigome et al. 1999; Tomsa & Langeland 1999; Murakami et al. 2001, 2002; Myojin et al. 2001; Uchida et al. 2003; Sugahara et al. 2016
			OtxB	NC	Eyes, optic stalk, epiphysis, olfactory epithelium, PHP, PA I (T25)	Ueki et al. 1998
OtxC	CNS	Mid-hindbrain boudnary (MC9)				Sugahara et al. 2016
Pax1/9	Somites, endoderm	Ventromedial epithelial somite (MC11); pharyngeal pouches (MC12); mesenchyme migrating ventral to notochord (MC14)	*Pax1/9*	Pharyngeal patterning	Pharyngeal pouches (T23.5-29); velum (T28-29)	Ogasawara et al. 2000; Ota et al. 2011; Oisi et al. 2013a
Pax3/7	NC, somites	Dorsal neural tube, dorsal somites (MC11-12); lateral somites (MC14)	*Pax7* (*Pax 3/7*)	Placodes, somites	Somites, adaxial at latest stage (T21-28); dorsal neural tube (T21-29); ophthalmic placode, trigeminal ganglia (T22-26); hypobranchial muscles (T28-29)	McCauley & Bronner-Fraser 2002; Kusakabe & Kuratani 2005; Ota et al. 2007, 2013; Modrell et al. 2014; York et al. 2017

Hagfish			Lampreys			
Genes	**Contexts**	**Expression patterns**	**Genes**	**Contexts**	**Expression patterns**	**References**
Pax6	NC, CNS	Anterior neural tube (MC11-12); telencephalon, pretectum, rhombic lip (MC13-15)	*Pax6*	CNS, NC	Anterior neural tube (T19); forebrain (T20-28); hindbrain, weak in rhombomere 4 (T20-28); trunk neural tube (T22-28); dorsal oral ectoderm (T23-26); optic vesicle (T24-26); ventral somites (T25-28); velum, PHP, nasal placode (T26-27); hypobranchial muscles (T29)	Murakami et al. 2001, 2002, 2004; Uchida et al. 2003; Ota et al. 2007; Kusakabe et al. 2011; Sugahara et al. 2011, 2016
			Pax6B	CNS	Forebrain, hindbrain (T27)	
PitxA (*Pitx2*?)	Placodes	Hypophyseal placode (MC7)	*PitxA*	CNS, pharynx	Ventral forebrain, foregut (T19-23); cardiac lateral plate (left side) (T24-26); hypophyseal placode, oral ectoderm, ZLI, anterior and ventral to mid-hindbrain boundary (T25-27); extraocular muscles (T27)	Uchida et al. 2003; Kokubo et al. 2010; Oisi et al. 2013a; Suzuki et al. 2016
Six3/6A	Placodes	NHP (MC7-12); prechordal plate, optic chiasma (MC7-9)				Oisi et al. 2013a
SnailA	NC	No expression in EM (MC11-12)	*SnailA*	NC	Neural ectoderm (T17); premigratory NC, neural tube (T22-23)	Ota et al. 2007; Sauka-Spengler et al. 2007; York et al. 2017
Sox9	NC, placodes	Otic capsule; EM (MC11-12)	*SoxE3* (*Sox 9*)	NC	Otic vesicle (T21-26); neural tube, especially anteriorly (T23, 24); somites (T24); cranial ganglia, EM (T24-26); pharyngeal chondrocytes (T26-30)	McCauley & Bronner-Fraser 2006; Ota et al. 2007; McCauley 2008; Ohtani et al. 2008; Lakiza et al. 2011; Yao et al. 2011; Uy et al. 2012
SoxB1 (*Sox2/3*)	Placodes	Anterior neural tube, NHP (MC7, 12)	*SoxB1a*	NC	Neural ectoderm (T17-27); PAs (T25-27)	Sauka-Spengler et al. 2007; Sauka-Spengler & Bronner-Fraser 2008; Uy et al. 2012; Oisi et al. 2013a
			SoxB1b	NC	Neural ectoderm (T17-27); PAs (T25-27)	
			SoxB2	NC	Neural ectoderm (T17-27); PAs, cranial ganglia (T25-27)	
SoxEa (*Sox10*)	NC	Motor neuron precursors; EM, pre-migratory only (MC11-12); chondrifhying mesenchyme (MC15)	*SoxE2* (*Sox 10*)	NC	Neural plate (T17-18); dorsal neural tube (T19-20); migratory NC (T21); otic and optic vesicles, EM (T22-26); PA II-VIII chondrocytes (T30)	McCauley & Bronner-Fraser 2003, 2006; Ota et al. 2007; Sauka-Spengler et al. 2007; McCauley

Hagfish			Lampreys			
Genes	**Contexts**	**Expression patterns**	**Genes**	**Contexts**	**Expression patterns**	**References**
			SoxE1	NC	Neural plate (T17-18); dorsal neural tube (T19-20); premigratory NC (T21); ganglia (T22-25); EM? (T24-26); parachordal chondrification (T26); pharyngeal chondrocytes (T26-30)	2008; Cattell et al. 2011; Lakiza et al. 2011; Oisi et al. 2013b; Jandzik et al. 2014, 2015
Tbx1/10A	Head mesoderm	Periotic mesenchyme, pharyngeal mesoderm (MC12); chondrifying parachordal mesenchyme (MC14-15)	*Tbx1/10A*	Head mesoderm	Pharyngeal mesoderm (T23-27); otic vesicle (T22-27); PHP (T26.5); caudal et ventral rectus (T27)	Sauka-Spengler et al. 2002; Hammond & Whitfield 2006; Tiecke et al. 2007; Oisi et al. 2013a, b; Suzuki et al. 2016
			Tbx1/10B	Head mesoderm	Otic vesicle (T20-26.5); pharyngeal endo-mesoderm (T23-26.5)	
Twist	Somites	Ventromedial epithelial somite (MC11); mesenchyme ventral to notochord (MC14)	*TwistA*	NC, somites	Ventral somites, cranial ganglia, PHP (T23-26); PAs (T26)	Sauka-Spengler et al. 2007; Ota et al. 2011
			TwistB	Mesoderm	Lateral plate (T17-23); mandibular mesoderm (T20-26); PAs, pronephric tubules (T26)	
			TwistC	NC	PHP, PA I (T23-26)	
			TwistD	NC	PHP, PA I (T26)	

Table 1.7. Gene expression patterns in lamprey embryos compiled from the literature except for those already listed in Table 1.6. This table is not an exhaustive list of paralogous genes. Neither does it include negative results (lack of expression) unless specifically addressed in the original source. Temporal and spatial extent of expression may be greater than described in the literature. For abbreviations, see Table 1.6.

Genes	Contexts	Expression patterns	References
Alx	NC	PHP, dorsal PA II dorsal and ventral PAs (T25-27); dorsal mandibular arch, medial portion of velum (T25-30); dorsal fin (T27)	Cattell et al. 2011; Square et al. 2017
AP2	NC	Non-neural ectoderm, neural plate border (T17); dorsal neural tube (T20, 21); EM, otic vesicle, PAs (T21-26)	Meulemans & Bronner-Fraser 2002; Sauka-Spengler et al. 2007; Lakiza et al. 2011
Ascl1	PNS	PHP mesoderm (tip) (T23-26); lens placode, hypophysis, trigeminal ganglia (T25-26); notochord (T26)	Haming et al. 2011
Bapx (*Nkx3.2*)	NC	Somites, paraxial mesoderm (T21-24); trigeminal ganglia (T24-25); pharyngeal endoderm, EM in ventral mandibular arch (T25); ventral pharyngeal mesenchyme (T26.5)	Cerny et al. 2010; Kuraku et al. 2010
Barx	NC	Ventral PA I (T25-30), PAs II-VII, medial to mesoderm (T26.5-30)	Cerny et al. 2010; Cattell et al. 2011
Bmp2/4A	Ectoderm	Ectoderm adjacent to neural plate (T18-22); trigeminal ganglia, pharyngeal endoderm (T22-26); kidney, somites (T23); PHP, heart (T24); epibranchial ganglia, nasohypophyseal placode, otic vesicle (T25-26); mouth, velum (T26)	Shigetani et al. 2002;Uchida et al. 2003; McCauley & Bronner-Fraser 2004
Bmp2/4B	Ectoderm	Trunk ectoderm (T22-24); perioral ectoderm (T24)	McCauley & Bronner-Fraser 2004
Bmp2/4C	Ectoderm	Neural folds (T20); trunk ectoderm (T22-24); mouth, ventral pharyngeal region (T24); otic vesicle, perioral ectoderm (T26)	McCauley & Bronner-Fraser 2004
Brn-3B	PNS	Cranial ganglia (T25)	Sauka-Spengler et al. 2007
Cad IA	NC, Mesoderm	Pre- and migratory NC (T17-21); pharyngeal arch, upper lip (oral mesenchyme) (T24-26); otic vesicle, dorsal pharyngeal mesoderm (T26)	Sauka-Spengler et al. 2007; York et al. 2017
Cad IIA	NC	Migratory NC (T17-22); cranial ganglia (T22-26)	Sauka-Spengler et al. 2007; York et al. 2017
ColC	Skeleton	Somites, around myotomes (T25); pharyngeal EM (T27)	Ohtani et al. 2008
EdnA	Pharynx	PHP (T22.5-25.5); pharyngeal mesoderm, restricted dorsally in posterior PAs at later stages (T23.5-27.5); ectoderm posterior to mouth (T24-26.5); PAs? (T25)	Kuraku et al. 2010; Square et al. 2016
EdnC	Pharynx	PHP (T23); mesenchyme posterior to mouth, posterior PAs, restricted dorsally; heart (T25.5-26.5)	Square et al. 2016
EdnE	Pharynx	Pharyngeal ectoderm and lateral EM in posterior PAs (T23.5-26.5)	Square et al. 2016

Genes	Contexts	Expression patterns	References
EdnrA	Pharynx	Anterior mesoderm (T22); heart, ventral pharyngeal mesenchyme (T22-26.5); lateral pharyngeal EM across chondrification (T24-29); trunk lateral plate, mid- and hind-brain boundary, ganglia for facial and glossopharyngeal nerves, rhombomeres 4-6 (T26)	Cerny et al. 2010; Kuraku et al. 2010; Jandzik et al. 2014; Square et al. 2016
EdnrB	Pharynx	Premigratory and migratory NC cells (T21-23); lateral pharyngeal EM, PHP, dorsal root ganglia (T25.5); melanocytes (T25.5-27)	Square et al. 2016, 2017
EnA	CNS	Mid-hindbrain boundary (T22-28); epibranchial muscles (T25-28)	Matsuura et al. 2008; Kusakabe et al. 2011; Square et al. 2015b
EnB	CNS	Mid-hindbrain boundary (T22-28)	Matsuura et al. 2008
EnC	Ectoderm	Pharyngeal ectoderm (T25-27); ventral trunk ectoderm (T27)	Matsuura et al. 2008
EnD	CNS, mesoderm	Mid-hindbrain boundary (T23-28); mesoderm in mandibular arch, somites (T23-30); PHP (T28-30)	Matsuura et al. 2008; Hammond et al. 2009
EphB	Neural tube	Perioral ectoderm (T24-26); thalamus, hindbrain (T25); neural tube (except forebrain) (T26); mesenchyme around endostyle, PAs (T26-27); mid-hindbrain (T27); retina (larva)	Suzuki et al. 2015
EphC	Hindbrain	Thalamus, tegmentum, rhombomeres 3 and 5, weakly in rhombomere 6 (T23- 26); PHP (T24-28); retina (T25-larva); otic vesicle (T28)	Murakami et al. 2004; Suzuki et al. 2015
Ets1a	NC	PAs, PHP, trigeminal and epibranchial placodes (T26)	Sauka-Spengler et al. 2007
Ets1b	NC	Endothelial and hematopoietic precursors (T17-24); nephrotomes (T24); PAs, PHP, trigeminal and epibranchial placodes (T24-26)	Sauka-Spengler et al. 2007
Fgf3	Pharynx	Lateral front of pharyngeal pouches (T23-26.5)	Jandzik et al. 2014
FgfrA	Pharynx	Medial pharyngeal endoderm (T22-26); chondrifying EM, heart (T26-27.5)	Jandzik et al. 2014
FgfrB	Pharynx	Anterior neural tube (T23.5-27); EM in PPP and PA I (T23.5-27); pharyngeal EM (ventral and lateral) (T26-28)	Jandzik et al. 2014
Follistatin	Placodes	Somites (T23-26); otic vesicle (T23-29); pharyngeal mesoderm (excl. PHP) (T25-29)	Hammond & Whitfield 2006; Hammond et al. 2009
Gdf5/6/7	Pharynx	Ventral mandibular arch, PAs II-VIII (T26.5)	Cerny et al. 2010
GFRa1	CNS, PNS	Neural tube, pharyngeal arches (T26-28)	Green et al. 2017
GliA	Neural tube, mesoderm, pharynx	Dorsal neural tube (T18-24); somites (T22-24); forebrain, mouth, PHP, PAs (T24-26)	Sugahara et al. 2011
Gsc	Pharynx	PHP, mandibular arc, anterior oblique et rectus, dorsal rectus (T26.5)	Cerny et al. 2010; Suzuki et al. 2016
GshA	PNS	Telencephalon, prethalamus, dorsal neural tube (T26)	Sugahara et al. 2011
Hox1w	Hindbrain, pharynx, somites	Rhombomere 4 (T21-26); posterior hindbrain, trunk neural tube, somites, lateral line ganglia, geniculate and petrosal placodes, posterior pharyngeal endoderm (T26)	Takio et al. 2007; Parker et al. 2015; Parker & Krumlauf 2017
Hox2	Hindbrain, pharynx	Rhombomeres 3 and 5, weak in other rhombomeres (r2-), trunk neural tube (T21-26); somites (T21); PAs II-VIII (T25-26)	Takio et al. 2004, 2007; Parker et al. 2015, 2016; Parker & Krumlauf 2017

Genes	Contexts	Expression patterns	References
Hox3d	Hindbrain, pharynx	Neural tube (not anteriorly) (T20-26); rhombomeres 4 and 5, weak in posterior hindbrain (T22-26); PAs III-VIII (T26)	Murakami et al. 2004; Takio et al. 2004, 2007; Parker et al. 2015, 2016
Hox4w	Neural tube	Neural tube posterior to r6 (T22-26)	Takio et al. 2004, 2007
Hox4x	Neural tube	Neural tube posterior to r6, PAs V-VIII (weak in III-IV) (T26)	Takio et al. 2004, 2007
Hox5i	Neural tube	Neural tube posterior to rhombomere 6, lateral plate mesoderm (T21-26)	Cohn 2002; Takio et al. 2004, 2007; Onimaru et al. 2011
Hox6/7m	Neural tube	Trunk neural tube (T26)	Takio et al. 2004, 2007
Hox6w	Neural tube	Trunk neural tube (T21-26); lateral plate mesoderm (T21-23)	Cohn 2002; Takio et al. 2004, 2007
Hox8p	Neural tube	Trunk neural tube (T26)	Takio et al. 2004, 2007
Hox9r	Neural tube	Posterior neural tube (T26-26.5)	Takio et al. 2007
Hox10a	Tail	Posterior neural tube, tail bud (T26-28)	Takio et al. 2007
Hox10s	Tail	Tail bud (T26-28)	Takio et al. 2007
Hox11T	Tail	Tail bud (T26-28)	Takio et al. 2007
Hoxq8	Neural tube	Trunk neural tube (T20-26)	Takio et al. 2004, 2007
HuC/D	PNS	Sensory ganglia (T22-29) (immunostaining)	Modrell et al. 2014
Id	NC	Neural plate border (T17); dorsal neural tube, ventral ectoderm (T20, 21); EM, trigeminal ganglia, PAs (T21-26)	Meulemans et al. 2003; Sauka-Spengler et al. 2007; Lakiza et al. 2011
Irx1/3	Neural tube	Neural tube (excluding forebrain) (T22-26); lateral plate mesoderm, nephridia (T24-26)	Onimaru et al. 2011
Isl1/2A	Mesoderm	Cardiac, pharyngeal, and splanchnic mesoderm (T22-26); trigeminal and epibranchial ganglia (T25-26)	Kokubo et al. 2010
Isl1/2B	CNS	Epiphysis, posteroventral telencephalon (mid-height), hypothalamus, neural tube (T26)	Sugahara et al. 2011
Kreisler	Hindbrain	Rhombomere 5 (T21-26)	Parker et al. 2015, 2016; Parker & Krumlauf 2017
Krox20	Hindbrain	Rhombomere 3 (T20-26); rhombomere 5 (T21-26)	Murakami et al. 2004; Parker et al. 2015, 2016; Parker & Krumlauf 2017
Lbx-A	Somites, neural tube	Ventral edge of somites, hypobranchial muscles, dorsal neural tube (hindbrain-trunk) (T26-28)	Kusakabe et al. 2011
MA1	Myofibres	PHP (T28)	Kuratani et al. 2004
MA2	Myofibres	Cardiac mesoderm, lateral myotomes (T22-29); PHP, pharyngeal mesoderm (T24-29)	Kuratani et al. 2004; Kusakabe & Kuratani 2005, 2007; McCauley & Bronner-Fraser 2006; Kokubo et al. 2010; Kusakabe et al. 2011
Mef2	Mesoderm	Somites, pharyngeal mesoderm, heart (T26)	Square et al. 2015b

Genes	Contexts	Expression patterns	References
Meis1/2a	Neural tube	Posterior telencephalon (mid-height), pretectum, hindbrain, trunk neural tube, epobranchial ganglia, PHP (T26)	Parker et al. 2014
Meis1/2b	Neural tube	Posterior telencephalon (mid-height), pretectum, hindbrain, trunk neural tube, epobranchial ganglia, PHP (T26)	Parker et al. 2014
Mrf-A	Myofibres	Somites (T22-29); heart (T24-29); hypobranchial muscles (T28-29)	Kusakabe et al. 2011
MsxA	NC	Non-neural ectoderm, neural plate border (T17); dorsal neural tube (T21); PHP, lower tip of mandibular arch (T26)	Sauka-Spengler et al. 2007; Cerny et al. 2010
MsxB	NC	Dorsal and ventral PAs, not in mandibular arch; perioral ectoderm; PHP (T26.5)	Cerny et al. 2010; Square et al. 2017
Myb	Hematopoiesis	Hematopoietic cells in lateral plate (T23-24)	Onimaru et al. 2011
n-Myc	NC	Neural ectoderm (T17); dorsal neural tube, EM (T21-22)	Sauka-Spengler et al. 2007; Sauka-Spengler & Bronner-Fraser 2008
NCAM	CNS	Neural tube, cranial ganglia derived from epibranchial placodes (T24-26)	York et al. 2017
NgnA	PNS	Cranial ganglia, branchial nerves (T22-25)	Sauka-Spengler et al. 2007; Uy et al. 2015
Nkx2.2	CNS	Diencephalon and posterior (T26)	Sugahara et al. 2011
Npn2	NC	EM (T26)	Sauka-Spengler et al. 2007
Pax2 (Pax 2/5/8)	NC, CNS	Mid-hindbrain boundary (T22-26); otic vesicle, pronephros (T22-25); spinal interneurons (T22); ventral PA I (T24-26); endostyle (T25)	Murakami et al. 2001; McCauley & Bronner-Fraser 2002, 2003
Phox2	PNS	Hindbrain, ventral pharyngeal mesenchyme (T22-26); mesenchyme at pharyngeal and vagal levels (T24-26); epibranchial ganglia (T25-26)	Haming et al. 2011; Green et al. 2017
Prdm1	Somites	Somites (T23-26); otic vesicle (T23-24)	Hammond et al. 2009
Prrx	NC	PHP, dorsal and ventral PAs but not in mandibular arch (T26.5)	Square et al. 2017
PtcA	Neural tube, somites	Anterior ectoderm (T18); ventral neural ectoderm, ventral forebrain (T19-23); somites (T21-26); otic vesicle (T23-26); neural tube, ZLI, PAs (T24-26)	Hammond & Whitfield 2006; Hammond et al. 2009; Sugahara et al. 2011
Ptf1a-A	CNS	Hindbrain (T27)	Sugahara et al. 2016
Ptf1a-B	CNS	No description of expression pattern	Sugahara et al. 2016
Ret	CNS, PNS	Neural tube, pharyngeal arches (T25-28)	Green et al. 2017
Robo	NC	EM (T26)	Sauka-Spengler et al. 2007
RunxA	Skeleton	Oral/PHP mesenchyme and cranial ganglia (T25-27); pharyngeal mesoderm (T26.5-27); pharyngeal pouches (T26.5-30)	Cattell et al. 2011
RunxB	Skeleton	Hindbrain and epibranchial ganglia (T26.5-27); endostyle (T27); heart, dorsal fin (T27-30); pharyngeal endoderm (T30)	Cattell et al. 2011
Sema3	Mesoderm	Pharyngeal mesoderm and ectodermal clefts (T26)	Sauka-Spengler et al. 2007

Genes	Contexts	Expression patterns	References
Sip1	CNS, NC	Premigratory NC (T22-23)	York et al. 2017
SoxC1 (*Sox 4/11/12*)	NC	Neural plate border (T17-18); dorsal neural tube (T19-20); NC derivatives (T21-25)	Uy et al. 2015
SoxC2	NC	Dorsal neural tube (T19-20); NC derivatives (T21-25)	Uy et al. 2015
SoxC3	NC	Neural plate (T17-18); lateral neural tube (T19-20); NC derivatives (T21-25)	Uy et al. 2015
SoxC4	NC	Neural plate border (T17-18); lateral neural tube (T19-20); NC derivatives (T21-25)	Uy et al. 2015
SoxD (Sox 5/6)	NC	Neural plate border (T17); EM, PAs, optic vesicle (T21-28); notochord (T24-25)	Ohtani et al. 2008; Uy et al. 2012
SoxF (*Sox 7/17/18*)	NC	Blastpore (T15-16); neural plate (T17); endostyle, heart, notochord (T23-26); PA I-II (T26)	Uy et al. 2012; Square et al. 2015b
Sp8/9A	CNS	Mid-hindbrain boundary, prethalamus, nasohypophyseal placode, telencephalon (mid-height), dorsal neural tube (T26)	Sugahara et al. 2011
SproutyA	Pharynx	Perioral ectoderm? (T26)	Sugahara et al. 2011
Tbx2/3A	Mesoderm, neural tube	Ventral pharyngeal mesenchyme (T24-26); conus anteriosus, atrioventricular canal, dorsal PAs, PPP, otic vesicle, trigeminal ganglia, dorsal thalamus (T26)	Kokubo et al. 2010
Tbx4/5	Mesoderm	Cardiac mesoderm, medial somites (T22-26); PAs III-VIII (T26)	Kokubo et al. 2010
Brachyury /Tbx 19	Head mesoderm	Axial mesoderm, notochord (T21-23); prechordal plate (T21, 22); pharyngeal endoderm, tail bud (T24-28); epiphysis, lower lip, nephrotome (T26)	Sauka-Spengler et al. 2003
Tbx20	Mesoderm	Cardiac mesoderm (T21-26); ventral pharyngeal mesenchyme (T23-26); PPP (T24-26); PAs, notochord? (T26)	Kokubo et al. 2010; Onimaru et al. 2011
Tfap2d	Neural tube	Forebrain (T25-265.)	Van Otterloo et al. 2012
Tyr	NC	Retina, melanocytes (T26.5)	Square et al. 2015b
Wnt1	CNS	Hindbrain (T27)	Sugahara et al. 2016
Zeb	CBS, NC	Premigratory NC (T22-23)	York et al. 2017
Zic-A	Somites, neural tube	Neural ectoderm (T17); dorsal neural tube (T21-26); dorsal myotomes (T22-26)	Sauka-Spengler et al. 2007; Kusakabe et al. 2011

Chapter 2

A Hagfish from the Cretaceous Tethys Sea and Monophyly of Cyclostomes

> And thus I clothe my naked villany
> With old odd ends stolen out of holy writ;
> And seem a saint, when most I play the devil
>
> — *The Life and Death of Richard III*, William Shakespeare

2.1 INTRODUCTION

Hagfish (myxinoids) represent a pivotal taxon to resolve early vertebrate phylogeny (Janvier, 2007). They may form a clade with lampreys to split the vertebrate crown group between cyclostomes and gnathostomes (Cyclostome Hypothesis: (Løvtrup, 1977; Stock and Whitt, 1992; Kuraku et al., 1999; Near, 2009; Heimberg et al., 2010), or they may fall outside the lamprey-gnathostome clade (Craniate Hypothesis: (Donoghue et al., 2000; Janvier, 2007; Near, 2009). With the Cyclostome Hypothesis supported by molecular datasets and the Craniate Hypothesis by morphological datasets, the dichotomy represents a classic case of conflict between molecular and morphological inferences in phylogenetics. This conflict remains difficult to resolve because of the patchy fossil record of stem taxa. Three soft-bodied Carboniferous forms (*Gilpichthys*, *Myxineidus*, and *Myxinikela*) have each been posited as stem myxinoids (Bardack and Richardson, 1977; Bardack, 1991; Poplin et al., 2001), but myxinoid affinities for the former two have been questioned (Germain et al., 2014; Gabbott et al., 2016; Janvier and Sansom, 2016). *Myxinikela* remains as a sole putative myxinoid with any degree of cladistic support (Gabbott et al., 2016). As these Carboniferous forms are only preserved with a handful of morphological structures, the inferences have been based on a few myxinoid- or cyclostome- diagnostic characters (potential keratinous teeth in *Gilpichthys*; a longitudinally elongate nasohypophyseal system in *Myxinikela*) and the general absence of lamprey-like traits (e.g., oral funnel, discrete dorsal fins) (Bardack and Richardson, 1977; Bardack, 1991; Poplin et al., 2001). Consequently, living hagfishes imply long ghost lineages, making it difficult to interpret the seemingly primitive yet highly specialized morphology of the group. These morphological characters include poorly developed visual, lateral line, and auditory systems that may be rudimentary or vestigial (Janvier,

2007) and an axial skeleton that may or may not be homologous with vertebral elements in other vertebrate lineages (Ota et al., 2011). This gap has complicated the task of finding congruence between the molecular and morphological data to resolve whether or not hagfish and lampreys form a clade with an exclusion of gnathostomes (Near, 2009). In this chapter, I describe a nearly complete hagfish fossil from the Late Cretaceous (Cenomanian) of Lebanon and present a new phylogeny of cyclostomes. With trace elements mapped by Synchrotron Rapid-Scanning X-Ray Fluorescence (SRS-XRF), the exquisitely preserved soft-tissue anatomy of this new hagfish is described to narrow the gap in the cyclostome fossil record.

2.2 SYSTEMATIC PALEONTOLOGY

Vertebrata Linnaeus, 1758

Cyclostomi Duméril, 1806

Myxinoidea Müller, 1834

Tethymyxine tapirostrum gen. et sp. nov.

2.2.1 Etymology

The generic name is derived from ‘Tethys’ after the Tethys Sea and ‘myxinos’ (Latinized Greek for ‘slimy fish’). The specific name is derived from two Latin roots, ‘tapir’ and ‘rostrum’ for the elongate tapering snout.

2.2.2 Holotype

BHI (Black Hills Institute of Geological Research) 6445. A complete body fossil.

2.2.3 Locality and Horizon

Hâdjula, Lebanon. Cenomanian, Upper Cretaceous (Hückel, 1970).

2.2.4 Diagnosis

A myxinoid with the following unique combination of characters: tapering nasohypophyseal profile; tentacular cartilage not extending beyond nasohypophyseal aperture; prebranchial length

nearly equal to branchial length; eight pairs of branchial pouches; 133 slime glands on one side; caudal fin not expanded into a round lobe.

2.3 METHODS, SUMMARY

BHI 6445 was scanned using Synchrotron Rapid-Scanning X-ray Fluorescence (SRS-XRF) at the Stanford Synchrotron Radiation Light-source, SLAC National Accelerator Laboratory. Three lines of phylogenetic analyses were performed: (***a***) maximum parsimony analyses; (***b***) non-clock Bayesian analyses; and (***c***) clock analyses. The morphological dataset was the same for all the analyses and included 60 taxa (Table S2.2) and 171 characters (Supplementary Information: **2.8.5 List of Characters**).

For the parsimony analyses, heuristic search was used with no topological constraint. The main analysis included the 52 core taxa (Table S2.2). I followed this with 22 different taxonomic combinations. For the non-clock-based Bayesian analyses, each analysis was run for five million generations with two runs of four chains, without topological constraint, and sampling every five thousand generations. To facilitate comparison of different taxonomic combinations, all MCMC searches used the same set of priors. For the tip-dated clock, two analyses were performed — one with molecular data only and the other with both molecular and morphological data. The dataset for molecular clock includes 80 taxa (Table S2.3). These are: 29 non-cyclostome modern taxa with mitochondrial genome; 11 living cyclostome taxa with mitochondrial genome or 16S/COI sequences and morphological data; 35 fossil taxa transferred from the morphological dataset; 13 fossil taxa with tip dates only to constrain some nodes. Each analysis was run for 50 million generations. For full description, see Supplementary Information: **2.8.2 Methods**.

2.4 DESCRIPTION

In visible light, BHI 6445 (Fig. 2.1) is preserved in full-body outline with soft tissues (body length = 313 mm). The trunk lies on its left side, whereas the head was twisted counter-clockwise to expose the ventral side. The preserved tissues are rich in P, S, Fe, and Cu (Figs. 2.1c, S2.3). These tissues are inferred to be: (**a**) composed of collagenous extracellular matrix (e.g., chondrocranium); (**b**) enclosed by a highly vascularized epithelial sheet (e.g., branchial pouches);

or (**c**) secreted keratin (e.g., slime and tooth-like apparatus). The preservation of structures and imprints is partly obscured by glue and paint as revealed in high concentrations of Cl, Fe, Mg, and S and low concentrations of Ti, V, P, and Cu mapped by Synchrotron Rapid-Scanning X-ray Fluorescence (SRS-XRF) (Figs. 2.1c, S2.3). The original outlines of the body are distinguished by high concentrations of P, As, Cl, Zn, and Cu and low concentrations of Si, Ti, Mn, Fe, and Ca relative to the surrounding matrix (Figs. 2.1c, S2.3). Distributions of these elements differentiate some structures against the background (e.g., the paucity of Si and Ti in keratinous structures).

The preservation of branchial pouches and slime suggests that BHI 6445 was rapidly buried (Sansom et al., 2011, 2013a). Although the mode of preservation is similar to that of the Early Cretaceous freshwater lamprey *Mesomyzon* from the Jehol Group of China, the preserved integument and muscles obscure internal structures in the specimens of *Mesomyzon* (Chang et al., 2006) (for detailed discussion, see Supplementary Information: **2.8.1. Taphonomy and Paleoecological Implications**). The integument is not preserved to such an extent in BHI 6445, which allows delineation of internal structures. The preserved structures and imprints are partly obscured by S-rich glue and paint as revealed through the SRS-XRF mapping (Figs. 2.1c, S2.3), but can be distinguished clearly from organically bound S through X-ray absorption spectroscopy (Fig. S2.4). In the head and mid-section of the trunk, the structural preservation is distinguished by surface topography under the dark colored paint. The overall characteristics clearly reject non-myxinoid hypotheses for the identitty of BHI 6445. The absence of a mineralized skeleton, paired fins, and jaws rules out anguilliform gnathostomes like the coeval eel *Luenchelys* (Forey et al., 2003). BHI 6445 is not a lamprey either because it does not have an oral sucker, tectal cartilages, branchial basket, dorsal fins, and other skeletal and proportional features of lampreys that would have been present given the state of preservation (Sansom et al., 2013a). Instead, BHI 6445 has characters diagnostic of myxinoids, including an elongate nasohypophyseal portion of the chondrocranium, posteriorly placed branchial pouches, and slime glands.

Tethymyxine has a small head relative to its body size. The prebranchial length of BHI 6445 is shorter than that in the living hagfishes, relative to the total body length (13 % versus 20-30%) or to the length of the branchial series (130% versus 150%) (Fernholm, 1998). As a consequence, the first branchial pouch sits more anteriorly than in living hagfish species, leaving a relatively short space for the lingual apparatus to occupy. The snout tapers towards the nasohypophyseal aperture (nostril). This region is obscured by paint (Fig 1c), but slight

differences in topography of preserved elements demarcate the outline. The nasohypophyseal barbels are preserved with the sigmoidal tentacular cartilage on the left side of BHI 6445. The barbels sit behind the aperture as in the living genus *Rubicundus* (Fernholm, 1991; Fernholm and Quattrini, 2008; Kuo et al., 2010; Fernholm et al., 2013) (Fig. 2.2c), but differs from it in lacking a protruded nasohypophyseal tube. Unlike all living hagfishes, the tentacular cartilages do not extend beyond the nasohypophyseal aperture (Fig. 2.2b-d). The tentacular cartilage is fused posteriorly with the lateral element of the anterior lingual cartilages.

Both left and right parts of the keratinous tooth plates are preserved in association with the anterior lingual cartilages in BHI 6445. Although several cusps can be identified by the distributions of Ca, Mn, Fe, Ni, and Hg (Fig. S2.3), precise cusp number and shape cannot be determined. Unlike the preservation of comb-like tooth plates in *Gilpichthys* from Mazon Creek (Bardack and Richardson, 1977), the plates may have been pyrolysated in BHI 6445 as seen in the scales of coeval actinopterygians (Forey et al., 2003; Saitta et al., 2017). The posterior lingual cartilage is preserved under the dark-colored paint, and this is corroborated by the distribution of S and P (Fig. S2.3). This mode of preservation also applies to the amorphous nasohypophyseal and labial connective tissues in BHI 6445, and is consistent with the fact that the element consists of highly vacuolated and elastic 'pseudocartilage' in living hagfish (Robson et al., 2000). The cartilages of the upper lip are represented in fragments. Presumably the missing counterpart has some of these elements from the right side of the animal. The upper lip cartilages from the left side are difficult to expose by manual preparation. The cartilages posterior to this main part of the head are likely detached visceral arches, but it is not possible to document the morphology in further detail.

Tethymyxine has eight pairs of branchial pouches. This number is greater than in *Rubicundus* spp. (n=5) (Fernholm, 1991; Fernholm and Quattrini, 2008; Kuo et al., 2010) and most other living hagfishes (n=4~7), equal to some species of *Eptatretus* and *Nemamyxyne*, and smaller than in some species of *Eptatretus* (n=14 in *E. polytrema*) (Fernholm, 1998). A structure immediately behind the branchial series is topographically and morphologically consistent with a heart (Fig. 2.1d, e). The intestine extends between the anterior and posterior liver lobes. These visceral tissues have different textures and colors that allow clear delineation under natural light (Fig. S2.2). However, the element mapping by SRS-XRF (Fig. S2.3) shows similar compositions among these tissues in the levels of Ca, Fe, Ni, Zn, P, and Hg concentrations.

Identified for the first time in any fossil cyclostome, slime glands are preserved in an uninterrupted series of infillings that extends nearly the entire length of the body on the ventral side. The infillings are distinguished from other tissues by surface profile, high Ca, P, and S concentrations, and higher levels of Cl, Ti, Mn, Fe, Cu, As, and Zn relative to the matrix (Figs. 2.1, S2.2, S2.3; Table S2.1). The chemical mapping is consistent with the fact that a major component of hagfish slime is tightly coiled, mucin-coated α-keratin threads (Fudge and Gosline, 2004; Winegard et al., 2014) — pyrolysates of which are characterized by calcium phosphatic content (Saitta et al., 2017). Slime glands are an apomorphy of myxinoids (Fernholm, 1998). The number of the slime glands (*n*=133 on the right) is greater than in most known living hagfishes (*n*=70~110) but close to that of *R. eos* (*n*=128~130) (Fernholm, 1998). The end of the tail is obscured by paint, but it is possible to outline the body by relatively high concentrations of Cu, P, S, and Fe (contained in paint, but higher in preserved tissues) (Figs. 2.1c, S2.3, S2.4; Table S2.1). The notochord is difficult to identify optically, but can be delineated with the high P and S concentrations along the dorsal midline (Figs. S2.3, S2.4b, c). The tail tapers rather than expanding into a round lobe.

2.5 PHYLOGENETIC ANALYSIS

Tethymyxine has myxinoid apomorphies not identified in other fossil taxa. These traits include the posteriorly placed branchial series and slime glands, which are absent, missing, or ambiguous in *Myxinikela* and other putative fossil cyclostomes (Gabbott et al., 2016). Both maximum parsimony and Bayesian analyses resolved *Tethymyxine* within the myxinoid crown group, sister to species of the living genus *Rubicundus* (Fig. 2.2) with strong Bremer and bootstrap supports (Fig. S2.5). *Myxinikela* was resolved as a stem myxinoid, whereas other Carboniferous forms (*Gilpichthys*, *Hardistiella*, *Mayomyzon*, *Myxineidus*) and *Priscomyzon* were found along the stem of lampreys. Other non-armoured fossil jawless vertebrates either formed a polytomy at the crown node of vertebrates (*Achanarella*, *Ciderius*, *Cornovichthys*, and *Pipiscius*) or fell into the gnathostome stem (*Euphanerops* and *Jamoytius*). Controversial Cambrian forms (*Haikouella*, *Haikouichthys*, *Metaspriggina*, and *Myllokunmingia*) were nested outside the crown node of vertebrates. Posited previously as a stem myxinoid (Hirasawa et al., 2016) or as a gnathostome (Johanson et al., 2017), *Palaeospondylus* was consistently resolved outside cyclostomes, whereas

another controversial taxon *Tullimonstrum* (Clements et al., 2016; McCoy et al., 2016; Sallan et al., 2017) either nested outside the vertebrate crown group or collapsed the node of cyclostomes (Figs. S2.6, S2.8; Tables S2.8, S2.10). Euconodonts were resolved as a stem cyclostome lineage (Figs. 2.2, S2.5-S2.8).

Using tip ages as calibration points, divergence estimates obtained from a Bayesian fossilized birth-death model placed the crown myxinoid node between the end Permian and early Cretaceous times (earlier than previous molecular clock estimates: Cretaceous – Eocene; (Kuraku and Kuratani, 2006)) and the crown lamprey node between the Triassic and early Jurassic times (prior to the complete separation of Gondowana from Laurasia; younger than previous molecular clock estimates: Permian; (Kuraku and Kuratani, 2006)) (Fig. 2.2). The interval of estimates for the crown node of cyclostomes extends into Proterozoic times, but this node likely falls in Cambrian to Silurian times, with the mean near the end-Cambrian mass extinction and the following Great Ordovician Biodiversification Event (Servais et al., 2010) (Table S2.11; Supplementary Information: **2.8.3 Results of Phylogenetic Analyses**). These results predict substantially longer stems for the crown myxinoid and lamprey nodes than for the crown cyclostome node, which is consistent with the highly divergent morphology, development, and genomes of the living cyclostomes (Janvier, 2007; Oisi et al., 2013b).

2.6 DISCUSSION

For the first time based on a morphological dataset, parsimony and Bayesian analyses converged on cyclostome monophyly: hagfish and lampreys formed a clade to the exclusion of gnathostomes. This clade corroborates the topology consistently supported by molecular data (Kuraku et al., 1999; Near, 2009; Heimberg et al., 2010). Cyclostome monophyly was stable across multiple taxonomic combinations under both maximum parsimony and Bayesian inferences (Table S2.7, S2.9). Instead, these tests highlighted instability at the base of gnathostomes. Anaspids (birkeniids, *Euphanerops*, *Jamoyitus*, and *Lasanius*) were within a few extra steps of falling into cyclostomes or nesting outside of crown vertebrates when the full set of taxa was considered. These alternative topologies even became shorter in parsimony analyses and/or had greater clade support in Bayesian analyses in multiple taxon sampling schemes than the consensus topology based on the full dataset (Figs. S2.5-S2.8; Tables S2.7-2.10;

Supplementary Information: **2.8.3 Results of Phylogenetic Analyses**). Under Bayesian inferences, even astraspids, arandaspidiforms, and heterostracans formed a polytomy at the crown vertebrate node or became resolved as stem cyclostomes when a few poorly known and unstable taxa were removed from the analysis (Fig. S2.8c, d). Although the cyclostome node has historically generated considerable debate (Janvier, 2007; Near, 2009), these new analyses imply that a truly unstable node in early vertebrate phylogeny may be that of the total group Gnathostomata rather than that of the crown group Cyclostomi.

These profound new interpretations supported by the new analyses were facilitated by increased taxon/character sampling and an enhanced contingency coding method (Brazeau, 2011). Character contingency has presented a challenge to the coding of cyclostomes in a cladistic dataset in which more than a third of all characters may be related to mineralized skeletons. Specifically in myxinoids, the absence of traits is difficult to interpret — for example, whether absence (e.g., electroreceptors: Braun and Northcutt, 1997)) represents an ancestral or secondary condition, or whether underdeveloped traits (e.g., vertebrae: Ota et al., 2011)) are rudimentary or vestigial. However, not all absence is additive. For characters of the mineralized skeletal matrix, attributes of a mineralized skeleton are not simply absent in myxinoids: they are inapplicable in this lineage. I mapped character contingency using such developmental and functional hierarchies with insights from the embryological observations in *Eptatretus* (Oisi et al., 2013b) and other vertebrate taxa (full description in **2.8 Supplementary Information**). This contingency coding removed, on average, 70% of character information from non-vertebrate outgroups and 32% from cyclostomes as inapplicable rather than absent (Fig. S2.12). The most parsimonious trees on the basis of this new dataset did not provide unambiguous support for many of the previously proposed synapomorphies of cyclostomes (e.g., lingual apparatus: optimized at the crown node only under delayed character transformation) (Yalden, 1985). Instead, the crown group of cyclostomes is united by two unambiguous character changes: keratinous tooth plates and migration of postotic myomeres to position of eyes (Fig. 2.2d, e; Table S2.6). In the same trees, optimization for both accelerated and delayed character transformations predicted secondary loss between the total and crown nodes of the Myxinoidea for many traits that are absent in the modern species, including: extrinsic eye musculature, pineal organ, electroreceptors, internal taste buds, lateral line in trunk, and neural arches of vertebral

column. Therefore, living hagfish are best interpreted as degenerative or vestigial in these respects.

2.7 CONCLUSION

Cyclostome interrelationships are critical to understanding where the crown vertebrate node falls among hagfish, lampreys, and gnathostomes. However, the paucity of fossil occurrences has made it difficult to test phylogenetic hypotheses or constrain divergence times. In this chapter, I reported *Tethymyxine tapirostrum* — a fossil hagfish from the early Late Cretaceous (Cenomanian) of Lebanon. The soft tissue anatomy of the holotype indicates that the suite of characters unique to living hagfish appeared before Cretaceous times. *Tethymyxine* elicited a re-evaluation of morphological characters for interrelationships of jawless vertebrates (**2.8 Supplementary Information**). By addressing contingency among correlated characters, these phylogenetic analyses based solely on morphological data recovered cyclostomes as a clade, and placed the new taxon nested within the hagfish crown group. Tip-dated trees predicted early Mesozoic origins for crown groups of hagfish and lampreys. These results potentially resolve the long-simmering morphological-molecular conflict near the base of the Vertebrata. They rejected the Craniate Hypothesis and implied that hagfish are highly specialized — and perhaps somewhat 'degenerate' — vertebrates. My analyses further suggest that: (***a***) controversial Cambrian forms are nested outside the vertebrate crown group; (***b***) *Palaeospondylus* and *Tullimonstrum* are best considered non-cyclostomes; (***c***) euconodonts lie in the stem of cyclostomes; and (***d***) anaspids remain highly unstable in the deepest sections of the gnathostome stem. These topologies suggest either that cyclostomes secondarily lost mineralized skeletons, or that mineralized skeletons evolved twice in vertebrates.

FIGURES

Fig. 2.1. *Tethymyxine tapirostrum* gen. et sp. nov, a fossil hagfish from the Cenomanian of Lebanon. Holotype (BHI 6445) in right lateral view: (**a**) photograph; (**b**) interpretive drawing; (**c**) false-color composite of distributions of four selected chemical elements (cyan=calcium; magenta=zinc; yellow=iron; black=manganese; HZ, 99.9% threshold) from Synchrotron Rapid-Scanning X-Ray Fluorescence (SRS-XRF). The visceral anatomy of BHI 6445 in composite photograph (**d**) and interpretive drawing (**e**). The cranial anatomy of BHI 6445 in interpretive drawing (**f**). **Abbreviations: int**, intestine; **lg**, left branchial pouch; **lva**, liver, anterior lobe; **lvp**, liver, posterior lobe; **rg**, right branchial pouch.

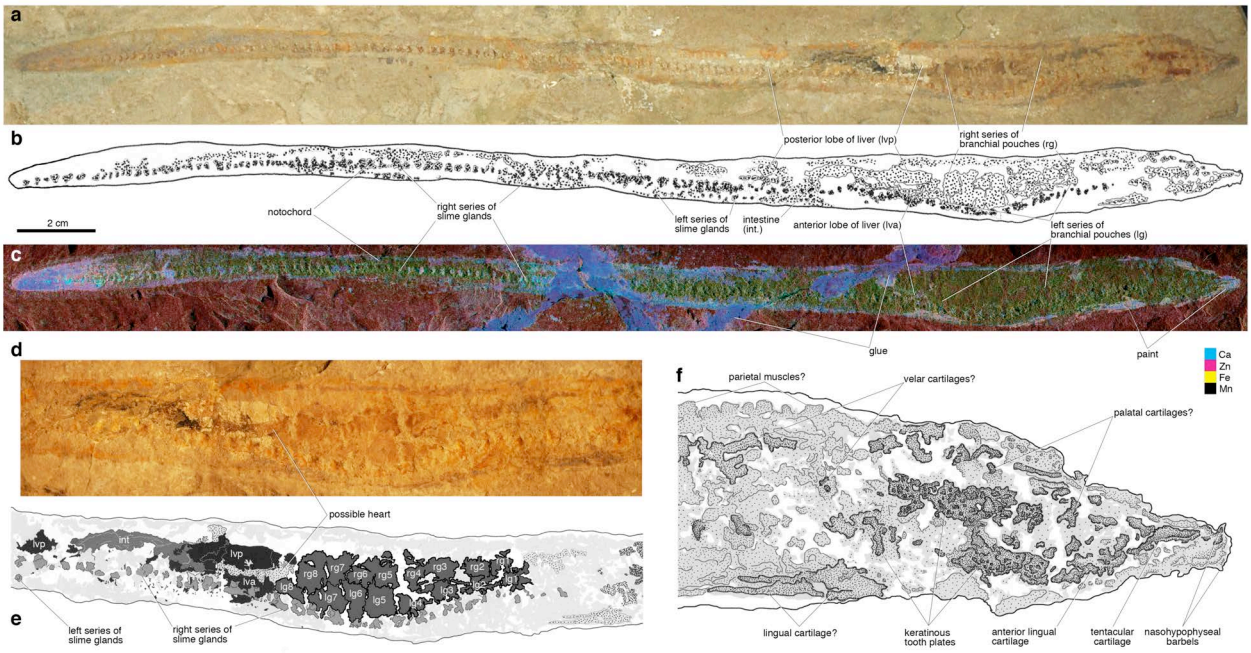
a
b
posterior lobe of liver (lvp)
right series of branchial pouches (rg)
notochord
right series of slime glands
left series of slime glands
intestine (int.)
anterior lobe of liver (lva)
left series of branchial pouches (lg)
2 cm
c
glue
paint
Ca
Zn
Fe
Mn
d
possible heart
int
lvp
lva
rg8
rg7
rg6
rg5
rg4
rg3
rg2
rg1
lg8
lg7
lg6
lg5
lg4
lg3
lg2
lg1
e
left series of slime glands
right series of slime glands
f
parietal muscles?
velar cartilages?
palatal cartilages?
lingual cartilage?
keratinous tooth plates
anterior lingual cartilage
tentacular cartilage
nasohypophyseal barbels

Fig. 2.2. *Tethymyxine* nests within the hagfish crown group; cyclostomes form a monophyletic clade, and hagfish crown lineages originated in the early Mesozoic. (**a**) A time-scaled phylogenetic tree with 95% highest posterior density (HPD) intervals for node ages based on a relaxed mitogenomic clock. Nodes are set at means of HPD distributions, except those constrained only by tip ages of fossil taxa (set at the median between node and tip ages). The tree follows the maximum parsimony analysis where it conflicts between the parsimony and Bayesian analyses: polytomy at the stem of vertebrates (resolved in Bayesian analysis); polytomy at the crown node of vertebrates (resolved differently across multiple taxonomic combinations); anaspids as a basal grade of gnathostomes (resolved as cyclostomes in multiple taxonomic combinations) (see **2.8 Supplementary Information**; Figs. S2.4-S2.8; Tables S2.1-S2.12). Comparison of the nasohypophyseal profiles in crown-group hagfishes: (**b**) *Tethymyxine tapirostrum*; (**c**) *Rubicundus eos*; (**d**) *Eptatretus stoutii*. The illustrations for **c** and **d** are based on Fernholm et al. (2013). An inset shows two unambiguous character changes supporting the node of the crown group Cyclostomi: keratinous tooth-like apparatus (**e**) and anteriorly migrated postotic myomeres (**f**).

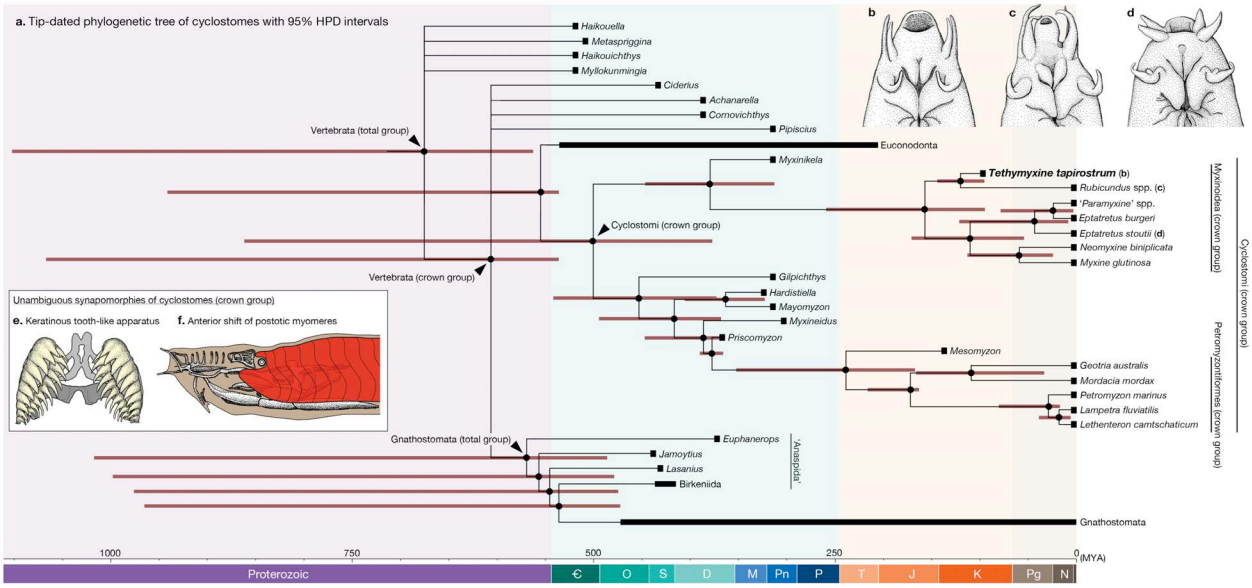
a. Tip-dated phylogenetic tree of cyclostomes with 95% HPD intervals
Haikouella
Metaspriggina
Haikouichthys
Myllokunmingia
Ciderius
Achanarella
Comovichthys
Pipiscius
Vertebrata (total group)
Euconodonta
Myxinikela
Tethymyxine tapirostrum (b)
Rubicundus spp. (c)
'Paramyxine' spp.
Eptatretus burgeri
Eptatretus stoutii (d)
Neomyxine biniplicata
Myxine glutinosa
Myxinoidea (crown group)
Cyclostomi (crown group)
Cyclostomi (crown group)
Vertebrata (crown group)
Gilpichthys
Hardistiella
Mayomyzon
Myxineidus
Priscomyzon
Petromyzontiformes (crown group)
Mesomyzon
Geotria australis
Mordacia mordax
Petromyzon marinus
Lampetra fluviatilis
Lethenteron camtschaticum
Unambiguous synapomorphies of cyclostomes (crown group)
e. Keratinous tooth-like apparatus
f. Anterior shift of postotic myomeres
Gnathostomata (total group)
Euphanerops
Jamoytius
Lasanius
Birkeniida
'Anaspida'
Gnathostomata
b
c
d
1000
750
500
250
0
(MYA)
Proterozoic
Є
O
S
D
M
Pn
P
T
J
K
Pg
N

2.8 SUPPLEMENTARY INFORMATION

2.8.1 Taphonomy and Paleoecological Implications

Holotype of *Tethymyxine tapirostrum* (BHI 6445) is exquisitely preserved. The preservation of branchial pouches suggests the early stage of decay when buried (Sansom et al., 2011, 2013a). In comparison to a decay series of a modern hagfish (*Myxine glutinosa*) under controlled conditions, the organs preserved in BHI 6445 include the intestine (onset of loss in *M. glutinosa*: 2 days post-mortem), slime glands (4 days), heart (6 days), branchial pouches (15 days), barbels and liver (48 days), myomeres and caudal fin (63 days), chondrocranium and keratinous tooth plates (200 days) (Sansom et al., 2011, 2013a). Among them, the gut is partly preserved in BHI 6445, and the slime glands represent α-keratin infillings. Some other organs are not preserved, even though they are expected to be present in the slab of BHI 6445, including: nasopharyngeal duct, pharyngocutaneous duct, and mouth (4 days) and inflection of myomeres (11 days) (Sansom et al., 2011, 2013a). On the basis of this combination, BHI 6445 may be best compared to decay stage 2 of modern hagfish, between the onset of loss of heart and of branchial pouches (Sansom et al., 2011, 2013a).

The mode of preservation is similar to the specimens of *Mesomyzon mengae* from the Lower Cretaceous Jehol Group of China (Chang et al., 2006, 2014). Compared to the modern river lamprey *Lampetra fluviatilis*, the organs prone to rapid disintegration but preserved in the specimens of *Mesomyzon* include: branchial cartilages (11 days), pericardiac cartilage (135 days), branchial lamellae, chondrocranium, and otic capsules (207 days) (Sansom et al., 2011, 2013a). This combination would place the adult specimens of *Mesomyzon* between the decay stage 1 (loss of branchial cartilages) and 2 (loss of kidney) (Sansom et al., 2011, 2013a). In specimens of *Mesomyzon*, the external organs such as the epidermis and myomeres are preserved so well that they obscure internal structures. Therefore, it is difficult to constrain the morphology of the skeletons and visceral tissues in this taxon. This is not the case in BHI 6445. Like in typical vertebrate fossils from the Cenomanian limestone of Hâdjula (Hückel, 1970; Forey et al., 2003), the soft integument is only discerned at the outline, perhaps within a decay halo, which allows delineation of internal structures. These observations based on decay sequences of modern relatives cannot be assumed to replicate the taphonomy of fossil taxa precisely (Parry et al., 2017). However, these comparisons indicate: (***a***) the tissues that tend to be lost relatively early

post-mortem are non-equivocally preserved in BHI 6445 (e.g., intestine, branchial pouches, keratin); and thus (***b***) taphonomic artifacts are unlikely to explain the presence of myxinoid synapomorphies (e.g., posteriorly displaced branchial pouches) or the absence of characters diagnostic to other known vertebrate lineages.

Paleoecological implications remain unclear for the occurrence of a hagfish. The Cenomanian limestone of Hâdjula has been interpreted as a mass-death assemblage of shallow, coastal, marine fauna of an inter-reef basin on the carbonate platform (Hückel, 1970; Forey et al., 2003; Lüning et al., 2004) — seemingly an unexpected environment in which to find a hagfish. Living hagfish generally inhabit deep (> 400 m), high-salinity (> 30 ppt), low-temperature (< 20 ºC) regimes, especially at low latitudes (Martini, 1998). However, they may transiently occupy benthic habitats shallower than 50 m (Martini, 1998). If similar ecological constraints applied to *Tethymyxine*, it would suggest that the holotype and only specimen of *Tethymyxine* does not represent a resident population in the Cenomanian of Hâdjula. However, it is difficult to compare the occurrence of *Tethymyxine* with the ecology of modern hagfish in the absence of precise paleoclimatic estimates or geochemical indicators for local environmental conditions.

2.8.2. Methods

2.8.2a SRS-XRF

BHI 6445 was scanned by SRS-XRF (Bergmann et al., 2012) at the Stanford Synchrotron Radiation Light-source, SLAC National Accelerator Laboratory. Experiments were conducted with an incident beam energy of either 13.5 keV (flux calculated between 10^{10} and 10^{11} photons s^{-1}) or 3.15 keV (flux ~10^{9} photons s^{-1}) and a beam diameter of 50 μm defined by a pinhole. Fluoresced x-rays were detected using a single element Vortex silicon drift detector. SRS-XRF maps from SSRL were processed from the raw detector count raster files using a custom MATLAB script that converted the data array into 8 bit tiff images clipped at various contrast percentiles. Image subtraction was performed using ImageJ via the built-in image subtraction function, and the image correlation was completed using the CorrelationJ plugin.

Energy dispersive spectra for quantification were obtained from single points at SSRL. The SSRL spectra were collected at a single point (50 μm spot size) for 100 live seconds. DLS point spectra were also collected at a single point (50 μm spot size) for 30 live seconds. All EDS spectra were fitted using PyMCA from fundamental parameters of the experiment using a

Durango apatite (fluoroapatite) mineral standard with known element concentrations for calibration. 2σ errors on concentration were calculated using the standard deviation of peak area for each element output by PyMCA. The concentrations of each element are an average of 3 individual EDS spectra taken within a few hundred microns of each other on the same specimen.

The results from SRS-XRF were analyzed primarily through spatial distribution of trace elements (Figs. S2.3, S2.4). Several elements have similar concentrations in the fossil and the matrix. The Ca signal appears relatively reduced throughout the fossil tissue compared to the high Ca content of the embedding limestone matrix. Thus, absolute Ca contents may be high in the tissues, but it is difficult to contrast specific tissues against the background on the basis of distributions alone. However organically bound Ca may be distinguished from inorganically bound Ca using spectral features. In the case of S, the spectrum is clearly different between the preserved tissues and the glue that shows only inorganic S (Fig. S2.4). The inorganic S and other organic S species (with peak energies equivalent to theoretical values for methionine sulphoxide, sulphonate, and cysteine) in the matrix are oxidation products diffused away from BHI 6445. Higher S levels in the tissues relative to the matrix (Table S2.1) imply that mass transfer of S was from the fossil outwards. However, spectroscopy shows relatively high levels of organic S in the matrix as well, which is a function of the biogenic nature of the Hâdjoula limestones. The XANES spectroscopy confirms that the organic S species present in both the matrix and fossil are different and requires further detailed study via this method to quantify the compositional variance.

The curatorial artifacts (glue and paint) can be easily identified in SRS-XRF, highlighting potential advantage of applying this method to fossils. An ‘N-shaped’ repair in the center of the specimen is highlighted by the glue, which showed elevated levels of Ti, V, Mn, and Fe. The distributions of Ni, Cu, Zn, P, S, As and Hg were predominantly controlled by soft tissues. These results are consistent with the observation that Cu, As, Fe and Hg naturally accumulate in the tissues of extant hagfish (Chiu and Mok, 2011). In particular, hagfish are predisposed to hyperacumulate Hg. As for Ni, the living hagfish *Eptatretus stoutii* takes up this element via a high affinity-low capacity transport pathway, which mainly accumulates the element in the brain, gills, and heart (Glover et al., 2015). The high levels of P and S in BHI 6445 may be attributed to the presence of polysulphate peptides in the skin (Kennedy, 1986). Thus, the levels of these elements observed in BHI 6445 are expected for a myxinoid. Although the concentrations of Hg

were below detection limits on a single point, the SRS-XRF maps indicate the presence of this element. A cadaver decay island appears to surround BHI 6445. This decay halo may be due to the mass-transfer of elements from the organism to the embedding matrix. The fossil still has elevated levels of several elements (P, S, As, Cl, Zn and Cu) relative to the matrix. Fe distributions also indicate a small decay halo.

2.8.2b Phylogenetic analyses, overview

Three sets of phylogenetic analyses were performed: (1) maximum parsimony analyses; (2) non-clock Bayesian analyses; and (3) clock-based Bayesian analyses. The morphological dataset is common among all analyses. It contains 60 taxa (Table S2.2) and 171 characters (**2.8.5 List of Characters**). Among 60 taxa, eight are designated as reserves (used to explore alternative taxonomic combinations). *Palaeospondylus* (in two different coding strategies) and *Tullimonstrum* have been proposed as a stem myxinoid (Hirasawa et al., 2016) and a stem petromyzontiform (McCoy et al., 2016), respectively, but both hypotheses have been evaluated critically (Sallan et al., 2017). Anaspids (=birkeniids), myxinoids (=living hagfishes), petromyzontids (=living lampreys), thelodonts, and crown gnathostomes (=chondrichthyans and osteichthyeans) replace their subgroup taxa in some of the parsimony analyses. The core of the dataset therefore consists of the remaining 52 taxa. Rationales for taxon and character sampling are discussed in detail in **2.8.4 Character and Taxon Sampling**.

The purpose of combining parsimony and Bayesian analyses is to identify robustly supported clades. Parsimony and model-based analyses often result in conflicting topologies even using the same morphological datasets. The debate is ongoing about which method outperforms others, and which method should be favored (Spencer and Wilberg, 2013; Wright and HIllis, 2014; Guillerme and Cooper, 2016; Hunt and Slater, 2016; O'Reilly et al., 2016, 2017; Brown et al., 2017; Goloboff et al., 2017; Puttick et al., 2017). For my analyses, it is critical to avoid confusing those two questions. Bayesian methods tend to be more accurate than parsimony, but parsimony appears to be more precise (greater resolution) (O'Reilly et al., 2016, 2017). Probabilistic methods require proper estimates of parameters or priors (Hunt and Slater, 2016; Nascimento et al., 2017). The factors to consider for my dataset are: (***a***) it contains a large proportion of taxa that are highly incomplete (Table S2.2); (***b***) missing entries are asymmetrically distributed, and characters based on soft tissues are underrepresented; (***c***) I enhanced contingency

coding for the current dataset; and (***d***) morphological datasets consistently supported cyclostomes as a grade under parsimony. The presence of incomplete and unstable taxa (***a***) favors precision over accuracy. Although biased distribution of missing entries (***b***) and historical trends (***d***) suggest probabilistic methods as a suitable option, the enhancement of contingeny coding (***c***) questions this. How degrees of contingency in morphological datasets impact the performance of probabilistic methods remains unclear (Harrison and Larsson, 2016; Nascimento et al., 2017). Under parsimony, contingency coding has predictable outcomes (Brazeau, 2009). Therefore, I used maximum parsimony as a primary line of phylogenetic analyses, and ran Bayesian analyses to highlight areas of agreement and disagreement with the results of the parsimony analysis.

2.8.2c Maximum parsimony analyses

For the parsimony analyses, I used PAUP* 4.0a152 (Swofford, 2017) (heuristic search; 10,000 random sequence additions; TBR; outgroup: Hemichordata) with no topological constraint. The main analysis included the 52 core taxa (retained + new in Table S2.2). I followed this with 22 different taxonomic combinations: addition of *Palaeospondylus* and/or *Tullimonstrum*; deletion of taxa predicted to be unstable; substitution of some taxa by suprageneric taxa (anaspids, myxinoids, petromyzontids, thelodonts, and crown gnathostomes). The Bremer support values (decay indices) were calculated for the main analysis of the core 52 taxa. The bootstrap analysis for this taxon set was run under heuristic search for 1,000 replications.

2.8.2d Non-clock Bayesian analyses

For the non-clock Bayesian analyses, I used MrBayes ver.3.2.5 (Huelsenbeck et al., 2015). Each analysis was run for five million generations with two runs of four chains, without topological constraint, and sampling every five thousand generations. To facilitate comparison of different taxonomic combinations, all MCMC searches with MrBayes used the same set of priors:

Datatype = Standard
Coding = Variable
# States = Variable, up to 10
Symmetric Dirichlet is fixed to 2.00
Rates = Gamma
Alpha_symdir

Type = Symmetric diricihlet/beta distribution alpha_i parameter

Prior = Symmetric dirichlet with fixed (2.00) variance parameter

Alpha

Type = Shape of scaled gamma distribution of site rates

Prior = Exponential(1.00)

Ratemultiplier

Type = Partition-specific rate multiplier

Prior = Dirichlet(1.00)

Tau

Type = Topology

Prior = All topologies equally probable a priori

Subparam. = V

V

Type = Branch lengths

Prior = Unconstrained: GammaDir (1.0, 0.1000, 1.0, 1.0)

Relative burnin = 25.0%

Due to a large amount of time required for individual rounds of analyses, I took a heuristic approach to find the combinations of taxa for maximum resolution. I removed an arbitrarily selected taxon sequentially from each analysis until the topology was better resolved, and then added taxa back in until the resolved nodes collapsed.

2.8.2e Tip-dated Bayesian analyses

For the tip-dated clock, two analyses were conducted — one with molecular data only and the other with both molecular and morphological data (total evidence). I used Fossilized Birth Death model in BEAST 2.4.5 (Bouckaert et al., 2014) (gamma site model: HKY, kappa = 2.0 [molecular]; Lewis MK [morphology]; clock model: relaxed clock, log normal). The dataset for molecular clock includes 80 taxa (Table S2.3). These are: 29 non-cyclostome modern taxa with mitochondrial genome; 11 living cyclostome taxa with mitochondrial genome or 16S/COI sequences and morphological data; 35 fossil taxa transferred from the morphological dataset; 13 fossil taxa with tip dates to calibrate the remaining internal nodes. Those 29 non-cyclostome modern taxa were selected to provide a broad phylogenetic coverage and multiple internal nodes

calibrated deeply so that a few long lineages do not skew calibration across the tree. The invertebrate outgroups (ambulacrarians, cephalochordates, and tunicates) were broken up into multiple living taxa. Likewise, chondrichthyans and osteichthyans were each divided into representative living lineages.

In order to generate reasonable calibrations for the nodes of non-cyclostomes, 13 fossil taxa were used as hard minima (Table S2.3, Notes). As for graptolites, crinoid, ischnacanthiform, and ctenacanthiform, the oldest occurrences were imported from the Paleobiology Database (Fox, 1968; Antia, 1981; Melo, 1988; Maletz, 2017; n.d.). Other taxa were selected from the literature (Gross, 1968; Carroll, 1969; Chang, 198119; Long, 1988; Milner and Sequeira, 1993; Jenkins et al., 1997; Zhu et al., 2009; Luo et al., 2011, 2015). Tree priors were used to constrain relationships of these taxa according to consensus in the literature. Several internal nodes could not be calibrated reasonably by tips, either because little consensus exists about relationships of stem taxa, or because fossil calibration is unreasonably shallow despite agreement among divergence estimates by multiple molecular clock analyses. This is the case for the internal nodes of actinopterygians, cephalochordates, chondrichthyans, and euarchontoglires (Table S2.3, Notes); so these nodes were given priors following the previous molecular clock analyses (Hurley et al., 2007; Janečka et al., 2007; Santini et al., 2009; Inoue et al., 2010; Licht et al., 2012; Near et al., 2012, 2014; Betancur-R et al., 2013; Broughton et al., 2013; Renz et al., 2013; Dornburg et al., 2014; Yue et al., 2014; Friedman, 2015) (Tables S2.4, S2.5). The crown node of enteropneusts was given fossil calibration for *Saccoglossus testa* (Cameron, 2016) so that low preservation potentials can be modeled better (Tables S2.3-S2.5).

As for the 11 living cyclostome taxa, they correspond readily to morphological operational taxonomic units (OTUs) used in the parsimony and non-clock Bayesian analyses (Table S2.3, Morphological OTU). Not all have been sequenced for mitochondrial genome, so 16S and COI (Fernholm et al., 2013) were used for those without full mitochondrial sequences. Following the morphological and molecular consensus (Gill et al., 2003; Renaud et al., 2009; Renaud, 2011; Potter et al., 2015), geotriids (*Geotria* + *Mordacia*) were constrained to form a clade, and the divergence from the rest of living lamprey lineages was set before the complete separation of Gondowana from Laurasia as they are endemic to Southern Hemisphere (Tables S2.4, S2.5). The 35 fossil taxa transferred from the morphological dataset were given tip ages (the earliest occurrences within a clade for composite taxa as available at the Paleobiology

Database), using a median of the tightest dating or correlations available for the geological horizon.

Monophyletic constraints were used in tree priors to provide topological framework. Tree priors forced the tree to conform to a strict consensus of the maximum parsimony analysis (Fig. S2.5). This left some taxa in polytomy (*Haikouella*, *Haikouichthys*, *Metaspriggina*, *Myllokunmingia*; *Achanarella*, *Ciderius*, *Cornovichthys*, *Pipiscius*; Eptatretidae) to form a fully resolved clade in the resulting MCC tree, but there is no character support for these nodes in the molecular-only clock analysis.

The sequences were aligned through multiple runs. The mitochondrial genomes were linearized using Cyclic DNA Sequence Aligner (Fernandes et al., 2009) at a highly conserved site away from 16S and COI, and then aligned with each other using KAlign (Lassmann and Sonnhammer, 2005) and Clustal Omega (Sievers et al., 2011). The accuracy was checked by whether alignment at the cut sites (beginnings and ends of linearized sequences) is recapitulated or not. The 16S and COI sequences were aligned independently first, and then incorporated with the mitochondrial genome with KAlign and Clustal Omega. The accuracy of alignment was checked by whether or not 16S and COI blocks remain intact, and whether or not 16S and COI sequences of *Eptatretus burgeri* align perfectly with the corresponding loci in the mitochondrial genome of the same taxon.

A BEAST analysis was run for 50 million generations. The dataset poses a number of computational challenges. The phylogenetic and chronological coverage is broad, but sampling is sparse. The morphological dataset is heavily weighted by characters that differentiate cyclostomes and jawless stem cyclostomes, but limited in characters that have variable states within individual lineages. Few fossil taxa are sampled from late Palaeozoic, Mesozoic, and Cenozoic times. Proportions for missing data are high: the majority (48 taxa) do not have molecular sequences; 13 of them only have tip age; five of the 11 modern cyclostome taxa only have sequence information for 16S and/or COI genes; and the majority of the living taxa with mitochondrial genome does not have morphological data. The dataset has numerous monophyly and node-age constraints. Therefore, the analysis was highly sensitive to priors, and it was difficult to predict values of priors that do not violate initialization attempts. To accommodate this, priors were set on the basis of reasonable predictions initially (e.g., a prior for origin set around molecular clock estimates of the deuterostome node) and then relaxed sequentially and

closer toward default settings of BEAUti (Bouckaert et al., 2014). Because of the low success rate for initialization attempts, the analysis was allowed to complete 50 million generations without modifying priors, once initialization was successful. The first analysis was run on the molecular data only, and the second analysis was run under total evidence (molecular + morphological).

2.8.3. Results of Phylogenetic Analyses

2.8.3a Maximum parsimony analyses

In the analysis of 52 core taxa (retained + new in Table S2.2), heuristic search found 4,869 parsimonious trees (tree length = 371; consistency index = 0.520; retention index = 0.789; rescaled consistency index = 0.411; homoplasy index = 0.488) (Fig. S2.5). The strict consensus tree resolves *Tethymyxine* as nested within the crown-group Myxinoidea, sister to the species of *Rubicundus*. Cyclostomes (myxinoids + petromyzontiforms) were recovered as a clade. Within cyclostomes, euconodonts were nested outside the crown, which was split between myxinoids and petoromyzontiforms. The relationships among myxinoids closely follow those from the previous Bayesian analysis of living myxinoids using COI gene (Fernholm et al., 2013): (***a***) *Rubicundus* was nested outside other living myxinoids; (***b***) *Neomyxine* and *Myxine* formed a clade; and (***c***) *Paramyxine* was nested among *Eptatretus*. *Myxinikela* (Bardack, 1991) was resolved as a stem myxinoid, whereas *Gilpichthys* and *Myxineidus* — two forms previously posited as potential stem hagfish — were placed among stem petromyzontiforms. In that latter clade, the Northern and Southern Hemispheric clades were recovered in accord with both morphological and molecular inferences (Hubbs and Potter, 1971; Gill et al., 2003; Renaud et al., 2009; Renaud, 2011; Potter et al., 2015). The chronologically oldest stem petromyzontiform *Priscomyzon* was closer to the crown than the Carboniferous *Hardiestilla* and *Mayomyzon*. *Mesomyzon* did not fall into Northern or Southern Hemispheric clades. In this consensus, the total group of cyclostomes is united by five unambiguous character changes (55.1 and 58.0: branchial openings closely packed and their number four or five; 86.1: dorsal midline fin initiating above or anterior to anal position; 93.2: no distinct lobe in caudal fin; 152.1: longitudinally aligned, transversely biting apparatus), and the crown group (myxinoids + petromyzontiforms) by two unambiguous character changes (142.1: keratinous feeding structure; 163.1: postotic myomeres assuming periotic position) (Table S2.6: Cyclostomi, total group).

Cephalochordates and *Pikaia* were nested outside the Olfactores (tunciates + vertebrates). The controversial Cambrian forms were recovered in a polytomy among stem vertebrates (polytomy resolved in other taxonomic combinations [*Haikouella* [[*Haikouichthys* + *Myllokunmingia*] *Metaspriggina* + crown vertebrates]]: Fig. S2.6a, c, d). Crown vertebrates consist of cyclostomes and gnathostomes (both monophyletic) in a polytomy with several Palaeozoic forms of uncertain affinity: *Achanarella*, *Ciderius*, *Cornovichthys*, and *Pipiscius*. In the gnathostome clade, anaspids formed a grade, with the 'naked' taxa nested outside the armoured taxa. The rest of the consensus tree closely follows topologies previously recovered (Donoghue et al., 2000; Gess et al., 2006; Sansom et al., 2010b; Turner et al., 2010; Conway Morris and Caron, 2014; Gabbott et al., 2016; Keating and Donoghue, 2016; McCoy et al., 2016).

Monophyletic cyclostomes were consistently supported in many of taxonomic combinations explored (Table S2.7). When the cyclostome node collapsed into a polytomy at the node of crown vertebrates, other stem gnathostome nodes lost resolution as well. The topology was stable overall across different taxonomic combinations (Tables S2.7, S2.8). A deletion of a taxon or substitution by composite taxa did not improve resolution generally — this rather collapsed some nodes. These trends suggest that the depths of taxon and character sampling were appropriate for the dataset. In all taxonomic combinations explored, anaspids were within five additional steps away from forming a clade of stem petromyzontiforms or being nested outside crown vertebrates (cyclostomes + gnathostomes). These relationships were most parsimonious in some combinations (Tables S2.7, S2.8; Fig. S2.6a, c, d). Because of this instability, Bremer and bootstrap support values were low along the stems that potentially attract anaspids (Fig. S2.5), despite large numbers of character changes supporting individual nodes (Table S2.6).

These results do not necessarily indicate that anaspids nest with cyclostomes or stem vertebrates. Rather, they illustrate instability at the nodes of the total group of gnathostomes. Anaspids nested within cyclostomes became most parsimonious when: (***a***) excluding a 'naked' anaspid (*Euphanerops* or *Jamoytius*), highly incomplete, putative 'naked' anaspids (*Achanarella*, *Ciderius*, and *Cornovichthys*), or a highly incomplete putative cyclostome (*Gilpichthys* or *Pipiscius*); or (***b***) when including *Tullimonstrum* (Table S2.7). This is counterintuitive because 'naked' anaspids have been best compared with lampreys (Janvier, 1996a; Newman and Trewin, 2001; Newman, 2002; Janvier et al., 2004, 2006; Janvier and Arsenault, 2007; van der Brugghen, 2010; Sansom et al., 2010b). In this dataset, these 'naked' anaspids were important in pulling

anaspids to the gnathostome stem. Amongst seven unambiguous character changes supporting the node of the total group Gnathostomata (Table S2.6: Gnathostomata, total group), only a single character state does not occur in cyclostomes (91.1: paired preanal skin fold).

Cyclostome monophyly has never been supported parsimoniously by morphological data before this analysis. This topological change is attributed to enhancement of contingency coding and maximum inclusion of putative fossil cyclostomes (both detailed in **2.8.4 Character and Taxon Sampling**). The topology corroborated phylogenetic inferences based on molecular data and provides topological resolution for some controversial fossil taxa. Unexpectedly, unambiguous character changes at the total and crown nodes of Cyclostomi did not include many structures considered synapomorphic to cyclostomes such as lingual apparatus and velum (Yalden, 1985; Kuratani et al., 2016) unless optimized under ACCTRAN (Table S2.6: Cyclostomi). These structures have relatively low preservation potentials in fossils (Sansom et al., 2010a, 2011, 2013a), and the characters are uninformative to parsimony as they cannot be compared outside cyclostomes (discussed in **2.8.4 Character and Taxon Sampling**). The contingency coding ruled most characters related to biomineralization inapplicable among crown cyclostomes, and redefined characters previously considered simply absent in hagfish. Thus it prevented myxinoids from slipping stemward, and the presence of several characters with relatively high consistency index (e.g., 163.1: anterior shift of postotic myomeres; CI=1.00) united them with petromyzontiforms.

Simultaneously, this topological change revealed instability of the total group node of gnathostomes as only a few soft-tissue character states are required to shift anaspids outside gnathostomes, and as optimized gnathostome synapomorphies have relatively low consistency indices. The stem cyclostome status of euconodonts is consistent with some of the recent analyses (Sansom et al., 2010b; Keating and Donoghue, 2016). With this position, mineralized skeletons may have evolved twice independently (Table S2.6: Cyclostomi, total group [characters 107, 109, 131]; Gnathostomata, total group [character 95]) or have been lost multiple times in the early phase of vertebrate evolution.

2.8.3b Bayesian inferences, non-clock

MCMC search of the morphological dataset including 52 core taxa (retained + new; Table S2.2) by MrBayes 3.2.5 found marginal majority support (51%) for the cyclostome crown group (Fig.

S2.7). As in the maximum parsimony analyses, *Tethymyxine* and *Rubicundus* were nested outside the rest of crown myxinoids, where *Tethymyxine* is sister to *Rubicundus* spp. All internal nodes of crown myxinoids had high statistical support. *Myxinikela* sat in the stem of myxinoids, whereas euconodonts had marginal majority support (51%) as a stem myxinoid lineage. Alternative positions for euconodonts were outside crown vertebrates or in a polytomy at the crown cyclostome node, as revealed by different taxonomic combinations (Tables S2.9, S2.10; Fig. S2.8b, f). The crown node of petromyzontiforms collapsed in a polytomy with *Myxineidus*, *Priscomyzon*, and *Mesomyzon* under majority rule. The crown node of cyclostomes also collapsed in a polytomy with the Carboniferous forms *Gilpichthys*, *Mayomyzon*, and *Hardistiella*.

Cyclostomes collapsed in a polytomy at the crown node of vertebrates under several taxonomic combinations (Table S2.9; Fig. S2.8a). Still, the crown vertebrate node had high support values consistently across different taxonomic combinations (Fig. S2.8). This does not necessarily mean the clade of cyclostomes had low support. As in the maximum parsimony analysis, this is likely attributed to instability in the stem of gnathostomes and conflicting signal from *Pipiscius*. A deletion of *Pipiscius* caused anaspids and their putative relatives to shift to the stem of cyclostomes (Tables S2.9, S2.10; Fig. S2.8b-f). Some combinations resolved even arandaspids, astraspids, and heterostracans as stem cyclostomes, leaving thelodonts in a polytomy at the crown node of vertebrates (Fig. S2.8d) — in a manner reminiscent of the vertebrate classification schemes before the advent of cladistics (Cope, 1889; Kiaer, 1924; Stensiö, 1964, 1968; Moy-Thomas and Miles, 1971). Some of these nodes had relatively high support values (Fig. S2.8c, d).

There is reasonable ground to reject stem cyclostome status for these “ostracoderm” lineages that are considered generally as stem gnathostomes. Likewise, it would be premature to conclude that mineralized skeletons were lost within cyclostomes as implied by these topologies. The dataset was optimized for parsimony analysis through enhanced contingency coding. It does not sample deeply for autapomorphies or variations within these lineages — especially for composite taxa (rationales for using a common dataset is provided in **2.8.4**). Nevertheless, both the parsimony principle and Bayesian inferences highlight instability in the stem of gnathostomes. This problem has been perhaps overlooked in the literature. The intense focus of cladistics in early vertebrate phylogeny has been on the cyclostome node and the origins of the jaw and other crown-group traits higher up in the gnathostome stem. Now with the recovery of

cyclostomes as a clade, it exposed the problem implied by different phylogenetic hypotheses of 'ostracoderms' since the times of Cope, Kiaer, and Stensiö (Cope, 1889; Kiaer, 1924; Stensiö, 1964, 1968; Moy-Thomas and Miles, 1971). Although the cyclostome node has been considered the problem in recent decades, the total-group node of gnathostomes may be the source of this instability.

Outside the crown node of vertebrates, relationships were relatively stable across different taxonomic combinations. In most, majority support placed *Haikouella*, *Metaspriggina*, and *Haikouichthys*/*Myllokunmingia* in crown-ward order. Pituriaspids, galeaspids/osteostracans, antiarchs, and arthrodires were recovered consistently as stem gnathostomes in that crown-ward order, although an exclusion of *Pipiscius* resulted in pituriaspids closer to crown gnathostomes than galeaspids and osteostracans (Fig. S2.8f).

2.8.3c Bayesian inferences, clock model

Divergence estimates by the molecular clock analysis using Fossilized Birth Death model (Table S2.11; Fig. S2.9) largely conformed to the estimates from previous molecular clock analyses (Wray et al., 1996; Ayala et al., 1998; Blair and Hedges, 2005a, 2005b; Hedges et al., 2006; Kuraku and Kuratani, 2006; Gaidos et al., 2007; Peterson et al., 2008; Erwin et al., 2011; Battistuzzi et al., 2015) at the crown nodes of deuterostomes, chordates, and vertebrates. The 95% highest posterior density (=HPD) intervals extended most nodes deep into Proterozoic times, but the frequency distributions were typically skewed toward younger ages (U* in Table S2.11 indicates particularly pronounced skewing). The skewed peaks may be considered more reasonable and more compatible with fossil record. This skewing is expected given that the stem of gnathostomes lacks molecular information. By mean values, divergence estimates were 983 MYA for deuterostomes; 764 MYA for chordates; 724 MYA for olfactores; 675 MYA for total vertebrates; and 606 MYA for crown vertebrates (Table S2.11). These estimates are well beyond Ediacaran times (with an exception of crown vertebrates) and may be overestimated, but preservation potentials are low for the soft-bodied taxa predicted for this stem. Although these estimates may be improved in the future, it is beyond the scope of this analysis to constrain divergence estimates peripheral to cyclostome evolution.

The divergence of crown cyclostomes was estimated between 544-417 MYA (Cambrian-earliest Devonian) with a mean of 491 MYA. These estimates largely agree with the previous

estimate (480-430 MYA) (Kuraku and Kuratani, 2006). The total node of cyclostomes (with euconodonts) was estimated close to the earliest occurrence of conodonts (mean=541 MYA), which is reasonable given high preservation potentials of the mineralized conodont elements. Crown myxinoids were estimated to have diverged in Mesozoic times between 254 to 95 MYA (mean 165 MYA), close to but deeper than the previous estimate (90-40 MYA) (Kuraku and Kuratani, 2006). The living lineages of hagfishes likely diverged from each other from late Mesozoic to early Cenozoic times (Fig. S2.9). The crown node of petromyzontiforms was estimated in early Mesozoic prior to the complete separation of Gondowana (210-163 MYA; mean=177 MYA). This is substantially younger than 280-220 MYA estimated previously (Kuraku and Kuratani, 2006) — probably because this dataset did not sample nuclear genes so it did not account for high GC content in the lamprey genome (Smith et al., 2013). Some fossil-calibrated internal nodes of cyclostomes had skewed frequency distributions of divergence estimates with mean close to the upper end of the node height estimates (U* in Table S2.11; nodes with little branch height in Fig. S2.9). These nodes were calibrated by *Myxinikela*, *Tethymyxine*, *Hardistiella*, or *Priscomyzon*. Given low preservation potentials of these soft-bodied forms, the real node ages are proably earlier than estimated by frequency distributions.

Based on mean values, the nodes of stem gnathostome lineages were predicted mostly in Cambrian and Ordovician times, whereas the estimated divergence times for crown gnathostome lineages were in Silurian times. These node ages are compatible with the vertebrate interpretation of the Late Cambrian-Early Ordovician *Anatolepis* (Smith et al., 1996; Young et al., 1996) and the Early Ordovician *Pircanchaspis* (Erdtmann et al., 2000), although their phylogenetic positions remain uncertain. The 95% HPD intervals extended deeply into Cambrian and Precambrian times. Given high preservation potential of mineralized skeletons, these nodes are not likely much deeper than the means predicted here. However, the Cambrian and Early Ordovician divergence estimates are not unreasonable for crown gnathostome nodes. The earlier dates would be compatible with the global occurrences of chondrichthyan-like scales from Ordovician horizons (Sansom et al., 1996; Young, 2009; Sansom et al., 2012; Andreev et al., 2015, 2016).

Divergence estimates under total evidence (Table S2.12; Fig. S2.10) were much deeper and wider than in the molecular-only clock analysis, consistent with other studies contrasting molecular versus total evidence/morphology in the Fossilized Birth Death model (Pyron, 2011;

Ronquist et al., 2012; Heath et al., 2014; Matzke and Wright, 2016; Puttick et al., 2016; Zhang et al., 2016). In the present analysis, the 95% HPD intervals and means for the nodes along the deuterostome-crown gnathostome stem extended unrealistically deep into Proterozoic times. These intervals are greater than the entire Phanerozoic Eon. The internal cyclostome nodes had similarly deep and wide 95% HPD intervals. These estimates are unrealistic in large part — lineages with mineralized skeletons should not remain undiscovered well beyond (by an order of magnitude in some cases) the extent of their known fossil record. Interestingly, the frequency distributions were strongly bimodal for most non-cyclostome nodes, and the upper portions of the 95% HPD intervals overlapped with the lower portions of those from the molecular-only clock analysis. These exceedingly deep estimates presumably resulted from uneven sampling of both characters and taxa in the morphological dataset. Unfortunately, the dataset was highly sensitive to priors so it is difficult to constrain the analysis from estimating node ages too deep chronologically. As a comparative reference, the divergence estimates for crown cyclostome lineages under total evidence were slightly older than under the molecular-only clock analysis in late Palaeozoic to early Mesozoic times by mean values.

2.8.3d Analysis of characters for crown cyclostomes

The parsimony and Bayesian analyses suggest *Tethymyxine* is a crown myxinoid, sister to *Rubicundus*. Under maximum parsimony, three unambiguous changes unite these genera at a node: tapering nasohypophyseal profile (21.1); nasohypophyseal barbels originating posterior to aperture (23.1); and branchial openings spaced accordingly with branchial pouches (55.1) (Table S2.6: *Tethymyxine* + *Rubicundus*; columns T and R). Character 55 cannot be scored for *Tethymyxine*, whereas characters 21 and 23 allow multiple interpretations. The nasohypophyseal morphology is difficult to assess in a compressed fossil. Possibly, the nasal cartilages could have dislocated and extended past the barbels. Assuming such taphonomic artifacts, unknown ("?") would be an alternative scoring for *Tethymyxine* in characters 21-23. After running a maximum parsimony analysis of the same dataset under this alternative coding, the *Tethymyxine* + *Rubicundus* node became fully resolved within crown myxinoids, with *R. lopheliae* nested outside the clade *Tethymyxine* + *R. eos*. The latter clade is supported by a single character (169.1: slime glands >100): the number of slime glands varies within *Rubicundus* (X in Table S2.6:

Tethymyxine+*Rubicundus*). Thus, this secondary analysis resulted in the same topology presented in Fig. S2.5b.

It still remains possible that the barbels were misidentified. Anatomically, the connection with the anterior tentacular cartilage (Fig. S2.1) makes a compelling case that the identified barbels are real. Postulating that the barbels were entirely misidentified nevertheless, characters 21-23, 159 (barbels supported by cartilage), 160 (forked subnasal cartilage, supporting the lower nasohypophsyeal barbels) were modified to unknown in *Tethymyxine*. Under maximum parsimony, this secondary analysis of the modified dataset still resulted in strict consensus identifical to the topology in Fig. S2.5b. Therefore, the position of *Tethymyxine* sister to or nested among *Rubicundus* was supported regardless of interpretations of the nasohypophyseal morphology in BHI 6445.

Among other soft tissues preserved in BHI 6445, the tooth plates and slime glands are diagnostic to myxinoids (Table S2.6). These structures were identified on the basis of their positions, morphology, and geochemical evidence (Figs. S2.2-S2.4). Accepting their identities, the number of slime glands (character 169) may be subject to interpretation. Changing the score of this character in *Tethymyxine* to unknown (while keeping characters 21-23, 159, 160 as unknown) collapsed the *Tethymyxine* + *Rubicundus* clade to the crown myxinoid node (tree not shown). Adding on to these modifications to explore alternative character coding further, a rejection of geochemical signals for keratin in the identified structures would lead to two more changes in the character scores of *Tethymyxine*: character 143 (keratinous tooth paltes) and 151 (lingual apparatus). Coding these characters as unknown in *Tethymyxine* did not impact the topology. Tethymyxine was still resolved at the crown myxinoid node. Therefore, character support is robust for the crown myxinoid status of *Tethymyxine*.

Character changes supporting the crown cyclostome node are either (***a***) umambiguous for the characters that can be scored in euconodonts (characters 142 and 163) or (***b***) optimized under DELTRAN for characters that are largely unknown in fossils (Table S2.6: Cyclostomi, crown group). Myomeres (163.1) and keratinous feeding structures (142.1) are resistant to decay relative to other soft tissues (Sansom et al., 2011, 2013a) so they have reasonable chance of being scored for fossils from localities where these tissues are known to be preserved. Other characters that may be preserved in fossils include the presence of multidenticulate/cuspid elements housed within oral cavity (141.1) and lingual apparatus (151.1), and the absence of arcualia around the

notochord (149.0). Together with character changes associated with the total-group node (Table S2.6), no particular character partitions appear to predominate in supporting the clade of cyclostomes.

2.8.3e Analysis of characters for conodonts

Intriguingly, the position of euconodonts in the stem of cyclostomes implies some combination of homoplasies in the evolution of mineralization. Given this topology, mineralized skeletons (95.1) evolved twice independently in cyclostomes and gnathostomes, or evolved once in the crown vertebrate node and became lost in the crown cyclostomes. But the characters regarding mineralized skeletons (96-100, 103-135) cannot be optimized for the crown vertebrate and total cyclostome nodes in a strict consensus of the most parsimonious trees (Fig. S2.5, Table S2.6; column C). The crown vertebrate node under strict consensus is a polytomy of the taxa without mineralization (Fig. S2.5). The characters regarding mineralized skeletons (96-100, 103-135) were scored as inapplicable in taxa lacking mineralized skeletons. The minerazed tissues present in conodonts may be optimized to the total cyclostome node under ACCTRAN (denoted with asterisk [*] in Table S2.6) and to the euconodont branch under DELTRAN. These are artifacts of inapplicable coding in crown cyclostomes. Scoring the characters (96-100, 103-135) as absence of mineralized tissues in crown cyclostomes, the mineralized skeletons (95.1) were gained once and lost in cyclostomes under ACCTRAN, and gained twice independently under DELTRAN (data not shown).

Several characters scored for conodonts may be interpreted differently (detailed discussion in **2.8.5 List of Characters**). These include putative extraocular muscles (28:?), branchial apparatus (45:-), number of branchial pouches (56:?), multidenticulate plates housed within buccal cavity (141:-), anterior element of keratinous tooth plates (143:-), lingual apparatus (151:?), and anterior extreme of myomeres (163:0). I coded these characters for conodonts conservatively because they are based on soft tissues, and because interpretations are rather polarized. For character 28, the tissue in question may be extraocular muscles (Gabbott et al., 1995) or mucocartilage-like structures (**2.8.5 List of Characters**). I accept the putative branchial pouches in *Clydagnathus* (Briggs et al., 1983; Donoghue et al., 2000). However, the number may be greater than the preserved five (character 56) and appropriate landmark structures are either absent or not preserved in the specimen (character 45). Characters regarding the feeding

apparatus (characters 141, 143, and 151) were coded as inapplicable, because I consider the evidence linking conodonts to living cyclostomes to be thin. Conodont apparati were compared to hagfish tooth plates based on detection of amelogenin in the latter (Krejsa et al., 1990). No morphological evidence was presented, and a histological comparison reveals no similarity between the two structures (Aldridge and Donoghue, 1998). Conodont feeding mechanics has been compared to the lingual apparatus of living cyclostomes (Sweet, 1988; Goudemand et al., 2011). In the absence of evidence for skeletal and muscular components of the lingual apparatus, however, this comparison could be interepreted as an implicit resurrection of a comparison between conodont elements and hagfish keratinous teeth.

Following interpretations of the preserved structures that were questioned originally in this analysis, changing these character scores (28:1, 45:0, 56:0, 141:1, 151:1) still resolved euconodonts as a stem cyclostome lineage in strict consensus of the most parsimonious trees, with the crown petromyzontiform nodes collapsed into a polytomy with *Priscomyzon* and *Myxineidus* (tree not shown).

Although euconodonts were coded conservatively overall, some characters were interpreted provisionally in this lineage. These include postoptic ectomesenchyme (66:0), preanal skin fold being absent (90:0), and keratinous feeding structures being absent (142:0). Changing these character scores to unknown ("?"), strict consensus of the most parsimonious trees recovered euconodonts in a polytomy at the crown cyclostome node with *Gilpichthys* and *Myxinikela* (tree not shown). I accept the paired, pigmented, anterior structures in euconodonts as eyes (Donoghue et al., 2000), and excluded the counterargument (Turner et al., 2010). Changing character scores related to eyes (characters 26-33) to unknown resulted in only 32 most parsimonious trees. Strict consensus (tree not shown) still yielded euconodonts as a sole stem cyclostome lineage, *Pipiscius* at the total gnathostome node, *Achanarella* and *Ciderius* nested within a clade of anaspids, and Cornovichthys as a stem gnathostome. Therefore, any particular assessment of individual character scores does not seem to impact the topology of euconodonts greatly.

2.8.3f Analysis of characters for enigmatic early vertebrates

Pipiscius is another taxon that I coded conservatively. Although consistently reconstructed as a lamprey-like animal (Bardack and Richardson, 1977; Janvier, 1996, 2008, 2015), an alternative

view compared the taxon with *Xidazoon*, a Cambrian vetulicolian (Shu et al., 1999). A survey of the list of synapomorphies (Table S2.6, column P) reveals that (***a***) *Pipiscisus* is coded as unknown or inapplicable for many characters diagnostic to cyclostomes; and (***b***) the character scores do not agree with the states shared in cyclostomes. The character scores presented here reflect a skeptical view of some traits in *Pipiscius* that have been interpreted as lamprey-like, including a perioral ring of cusps and a lingual apparatus. The cusps are not organized as in lampreys (discussed in character 144; **2.8.5 List of Characters**) and their orientations would not allow a pulley-like eversion of oral feeding structures as in the lingual apparatus of modern cyclostomes (discussed in character 151; **2.8.5 List of Characters**). The following characters merit reevaluation: neural crest (1:?), neurogenic placodes (2:?), pigmented eye (26:0), multicuspid plate within oral cavity (141:0), keratinous perioral/buccal plates (142:?), radially organized circumoral plates (144:?), lingual apparatus (151:0), longitudinally aligned, transverse-biting apparatus (152:0), and annular cartilage (157:0). Although the pigmented eyes are preserved in the majority of vertebrate fossils from the Francis Creek Shale, pigmentation cannot be confirmed in the only specimen of *Pipiscius* preserved with an eye (FMNH PF 8346), which is a small depression dorsal to the oral funnel. Still, the pigmentation may simply not have been preserved. Neural crest and neurogenic placodes were scored as unknown to accommodate the possibility that *Pipiscius* slips to the vertebrate/chordate stem (Shu et al., 1999). However, the otic capsule is identified and coded for *Pipiscius*, and this structure is derived from a placode and contributed to by neural crest in crown vertebrates (Hall, 2009). Modifying these character codings accordingly (1:1, 2:1, 26:?) resolved the polytomy at the crown vertebrate node under strict consensus of 32 most parsimonious trees — exactly the same topology as the alternative coding of euconodonts in which the eye characters (#26-33) were scored as unknown for that taxon.

Proceeding to the rest of the characters, further revision for *Pipiscius* (141:?, 142:1, 144:?, 151:?, 152:?, 157:?) resulted in 472,224 most parsimonious trees. Strict consensus of these trees largely follows the topology of the main analysis (Fig. S2.5), but internal nodes within the Petromyzontiformes were collapsed into a polytomy with an exception of *Gilpichthys*, which was nested just outside the polytomy. *Pipiscius* became nested in a polytomy at the crown petromyzontfiform node. Modeling *Pipiscius* after a living lamprey, the character scores were further modified (141:?, 142:1, 144:1, 151:?, 152:?, 157:1). This set of character scores placed

Pipiscius among stem petromyzontiforms, between *Priscomyzon* and the polytomy of *Hardistiella* and *Mayomyzon* in Fig. S2.5. These secondary analyses predict that further evidence for the conservatively coded characters would resolve *Pipiscius* as a stem petromyzontiform.

The petromyzonform position of *Gilpichthys* (Fig. S2.5) is also intriguing, as this taxon has always been compared to hagfish (Bardack and Richardson, 1977; Janvier, 1996, 2008). However, the myxinoid affinity is based on the lack of lamprey-like characters and not on the presence of characters diagnostic to myxinoids (Table S2.6, column G). The parallel anterior structures were interpreted as keratinous tooth plates (152:1), but this occurs among petromyzontiforms. In addition, *Gilpichthys* has a small proportion of characters (34.2%) scored originally by me (Suppl. 2.1). Therefore, the position is more sensistive to the inclusion/exclusion of the characters coded for *Gilpichthys* than to interpretations of the characters preserved. Two composite characters regarding overall body proportions (82:1, 83:0) were excluded from the secondary analysis. Once again, this analysis resulted in 32 most parsimonious trees, strict consensus of which is identical in topology to the secondary analyses of euconodonts and *Pipiscius*.

Similar arguments can be made about *Achanarella*, *Ciderius*, and *Cornovichthys*. These taxa contain missing or inapplicable entries for 66-83% of characters. I provide justification for individual character scoring in **2.8.5 List of Characters**. As for the first three (Table S2.6; columns A, D, V), character states are similar to stem gnathostome *Euphanerops* and *Jamoytius* (columns J and U) for unambiguous and optimized synapomorphies at the major nodes. Thus, their positions in the polytomy at the crown vertebrate node (Fig. S2.5) are likely due to missing character information rather than to conflicting signals.

Putative Cambrian stem vertebrates (*Haikouella*, *Haikouichthys*, *Metaspriggina*, *Myllokunmingia*) share several important characters with crown vertebrates, including the well-developed sensory capsules, overall head configurations, and pharyngeal and axial skeletons (Table S2.6; Vertebrata, total group; columns E, I, L, S). They consistently lack most other diagnostic character states at the internal nodes within the crown group of vertebrates, or are not preserved with them (Table S2.6). One exception is *Haikouella* (Table S2.6, column E), which was coded as lacking neural crest-derived skeleton (1:0) and endoskeletal fin supports (83:0). *Haikouichthys* and *Metaspriggina* have skeletal bars in the pharynx, but were not coded for neural crest-derived skeletons (1:?) in the absence of other correlates of neural crest (e.g., 3:1,

distinct prechordal head) and with the mesodermally derived pharyngeal cartilages in cephalochordates (Jandzik et al., 2015). The pharyngeal region of *Myllokunmingia* is not preserved well enough to assess this character. *Haikouella* — coeval with *Haikouichthys* and known from numerous well-preserved specimens (Mallatt and Chen, 2003) — still has no evidence for these elements, or any other skeletal elements known to be derived from neural crest in modern vertebrates. The character 'fin supports' was coded following the same logic. Changing these character scores in *Haikouella* to unknown (1:?, 83:?) resulted in an identical topology of strict consensus tree with Fig. S2.5.

2.8.3g Tullimonstrum *and* Palaeospondylus

Both *Tullimonstrum* and *Palaeospondylus* were treated as appendices to the phylogenetic analysis because little consensus exists on their phylogenetic positions and because proposed positions range across or even outside vertebrates (Chapter 1; Miyashita et al., in press; Joss and Johanson, 2007; Hirasawa et al., 2016; McCoy et al., 2016; Sallan et al., 2017). In the parsimony analyses, *Tullimonstrum* was resolved in a polytomy either at the crown node of cyclostomes or with putative stem vertebrates from Cambrian times (Fig. S2.6a, b). Bayesian inferences support the latter position (Fig. S2.8a). These positions are compatible with the coding scheme B and E in the reanalysis of the taxon by Sallan and colleagues (2017), respectively. However, the trees do not necessarily support the vertebrate status of *Tullimonstrum* as the dataset did not sample the protostome alternatives such as molluscs and arthropods. These trees merely suggest that *Tullimonstrum* may not fall into the lamprey stem under the current interpretation of characters, if the taxon is assumed as a chordate/vertebrate. As for *Palaeospondylus*, it formed a clade with *Euphanerops* in both maximum parsimony and Bayesian analyses (Figs. S2.6b, S2.7a) under both cyclostome and gnathostome coding schemes (discussed in **2.8.4 Character and Taxon Sampling**). These two taxa are unique in the dataset for sharing both 101.1 (hypertrophied chondrocytes) and 102.1 (mature chondrocytes remaining in pair) (Johanson et al., 2010), whereas many of the myxinoid traits posited for *Palaeospondylus* (Hirasawa et al., 2016) cannot be coded (discussed in **2.8.2 Methods** in general; **2.8.5 List of Characters** for individual characters). However, *Euphanerops* and *Palaeopondylus* are disparate from each other except for the combination of two characters (101.1, 102.1). So these trees alone do not support or reject

any of the multiple hypotheses proposed for the affinity of *Palaeospondylus*. In the very least, the quantitative analyses failed to corroborate the myxinoid hypothesis.

2.8.3h Concluding statements for secondary analyses

Based on a number of primary and secondary analyses (sections: **2.8.3a** – **2.8.3g**), the topology presented in Fig. S2.5 is robust to different taxon and character sampling methods. Stable nodes include the total/crown cyclostomes, total/crown myxinoids, and total/crown petromyzontiforms. Euconodonts represent a stem cyclostome lineage. *Tethymyxine* is a crown myxinoid. *Myxinikela* is a stem myxinoid, whereas *Gilpichthys* and *Myxineidu*s — often assigned to the same stem (Bardack and Richardson, 1977; Janvier, 1996, 2008; Poplin et al., 2001) — fell into the stem of petromyzontiforms. Putative Cambrian vertebrates are stem vertebrates.

On the other hand, some taxa remained unstable. *Pipiscius* may represent a stem petromyzontiform. *Achanarella*, *Ciderius*, and *Cornovichthys* are reminiscent of euphaneropids, but this assignment requires more character information. At the moment, these enigmatic taxa are in the polytomy at the crown vertebrate node. Anaspids were surprisingly unstable. They may form a stem assemblage near the gnathostome base, but both parsimony and Bayesian analyses recover support for anaspids as stem petromyzontiforms. These instabilities reflect insufficient character information to constrain the crown vertebrate node.

The fossil taxa tended to be coded conservatively in this analysis. However, modifications to individual character scores did not impact the overall topology significantly. A review of justifications for the chosen character scores indicates that no one measure fits all when multiple conflicting interpretations exist for the characters. Sometimes one interpretation was favored, whereas other times the character coding was compromised into equivocal state as unknown or inapplicable. One taxon may be coded using different standards of evidence from one character to another, and standards of evidence may differ from a taxon to another in the same character. These decisions were made on case-by-case basis, and are discussed in individual character descriptions (**2.8.5 List of Characters**).

2.8.4 Character and Taxon Sampling

2.8.4a Sampling strategies, overview

The character list and data matrix used for this study were mainly derived from previous analyses (Løvtrup, 1977; Janvier, 1981a, 1984, 1996b; Maisey, 1986, 1988; Gagnier, 1993a; Donoghue et al., 2000; Gess et al., 2006; Khonsari et al., 2009; Heimberg et al., 2010; Sansom et al., 2010b; Turner et al., 2010; Conway Morris and Caron, 2014; Gabbott et al., 2016; Keating and Donoghue, 2016; McCoy et al., 2016). Since Løvtrup (1977), morphological data have consistently supported cyclostome paraphyly as the most parsimonious hypothesis. This topology was reinforced by those that followed Løvtrup (1977) with fossil record and cladistic methodology (Janvier, 1981a, 1984; Maisey, 1986; Forey and Janvier, 1993; Gagnier, 1993a). Although hagfish-lamprey comparison of selected characters questioned paraphyly (Yalden, 1985; Ota et al., 2007; Oisi et al., 2013a; Kuratani et al., 2016), these comparative analyses often lacked proper outgroup comparison. Several analyses experimented with different taxon- and character-sampling schemes and topological constraint to compare cyclostome monophyly versus paraphyly (Donoghue et al., 2000; Gess et al., 2006; Gabbott et al., 2016). Monophyly still persisted as the most parsimonious hypothesis. Thus, cyclostomes have never been recovered as a clade using an inclusive cladistic dataset of morphological characters to date (see Chapter 1 for detailed review of historical context).

Recent iterations of analyses represent a series of revisions to the dataset compiled by Janvier (1996b) and reevaluated by Donoghue (2000). The most recent revisions (Conway Morris and Caron, 2014; Gabbott et al., 2016; Keating and Donoghue, 2016; McCoy et al., 2016) overlapped each other significantly in sampling but made conflicting interpretations of morphology, included slightly different suites of characters, and employed various strategies for coding the taxa. A primary purpose of these analyses is to resolve the phylogenetic position of *Tethymyxine*. Secondarily, those of putative stem cyclostomes and stem vertebrates may be affected by addition of new characters and taxa or re-interpretation of the existing characters. Resolved topologies of these problematic taxa should allow setting *Tethymyxine* in context. With these intentions, I constructed the dataset to (***a***) synthesize datasets from the recent analyses (Conway Morris and Caron, 2014; Gabbott et al., 2016; Keating and Donoghue, 2016; McCoy et al., 2016) in character and taxon sampling and (***b***) increase character and taxon sampling as necessary.

For characters, the suite from Conway Morris and Caron (2014) is used as a backbone, as this is the most recent extensive revision of Donoghue et al.'s (2000) dataset. The dataset by Conway Morris and Caron (2014) (=CMC) received sequential revisions by McCoy et al. (2016) (=MSL) and Gabbott et al. (2016) (=GDS). Both expanded the taxonomic scope. Gabbott et al. (2016) eliminated some characters and re-coded many others. Meanwhile, Keating and Donoghue (2016) (=KD) presented another parallel revision to incorporate additional histological information. All characters included in the CMC, MSL, GDS, and/or KD datasets were considered. As a general rule, coding in this dataset reflects the latest scoring so that the GDS and KD coding supersedes the MSL or CMC wherever they disagree. I supplemented this initial dataset with (***a***) characters from other past analyses (Khonsari et al., 2009; Heimberg et al., 2010; Turner et al., 2010) and (***b***) wholly new characters. Each character in the list is denoted by the latest authority.

I edited the compiled character list extensively to: (1) revise character definitions; (2) revise character coding; and (3) eliminate parsimony-uninformative characters such that at least two states provide grouping information within a character. Each of these decisions is accounted for in **2.8.4c Character Sampling** and in the notes added to each modified character description (**2.8.5**: these characters are indicated as **definition modified** or **coding modified**). Most revisions to character definitions and coding were made to reorganize hierarchically related character states through non-additive binary coding and contingency coding (Brazeau, 2011). The CMC dataset (Conway Morris and Caron, 2014) and its subsequent revisions (Gabbott et al., 2016; Keating and Donoghue, 2016; McCoy et al., 2016) already consist mostly of binary characters and contain contingency coding for 6-9% of all scores. The GDS dataset extended this approach by identifying additional characters that are hierarchical (e.g., arrangement of branchial openings [character 55] contingent on absence of single confluent branchial opening [character 53]) (Gabbott et al., 2016). However, it remains unclear how much of the contingency coding is carried over from the previous CMC and MSL datasets because the GDS matrix does not distinguish inapplicable scores due to contingency coding (-) from missing entries due to lack of information (?).

Following these previous efforts, I enhanced the coding strategies (1-3) further (Figs. S2.11-S2.13). An enforcement of the non-additive binary and contingency coding strategies is necessary as phenotype-based cladistic analysis of cyclostomes and gnathostomes has been

criticized for favouring absence of derived states over loss or degeneracy of characters (Janvier, 1996a, 2007, 2008; Kuratani and Ota, 2008; Near, 2009; Heimberg et al., 2010; Janvier, 2010; Shimeld and Donoghue, 2012; Kuratani et al., 2016). Indeed, a phenotype-based analysis tends to recover hagfish nested outside the lamprey+gnathostome clade (Løvtrup, 1977; Janvier, 1981a, 1996b, 2007; Hardisty, 1982; Forey, 1984; Maisey, 1986; Gagnier, 1993a; Donoghue et al., 2000; Gess et al., 2006; Khonsari et al., 2009; Sansom et al., 2010b; Turner et al., 2010) — a topology predicted for an artifact due to secondary conditions (loss or degeneracy) parsimoniously interpreted as primitive (absence) (Jenner, 2004a; Near, 2009). Nevertheless, the difference between cyclostome monophyly versus paraphyly is subtle in levels of statistical support (Near, 2009; Heimberg et al., 2010). A treatment of miRNAs as discrete characters (presence/absence) favours cyclostome monophyly over paraphyly (Heimberg et al., 2010). In comparison to phenotypic data, molecular datasets have almost always supported monophyly of cyclostomes (Stock and Whitt, 1992; Mallatt and Sullivan, 1998; Kuraku et al., 1999; Delarbre et al., 2000, 2002; Furlong and Holland, 2002; Winchell et al., 2002; Takezaki et al., 2003; Kuraku and Kuratani, 2006; Mallatt and Winchell, 2007; Near, 2009). Cyclostome monophyly is a topology predicted for long branch attraction, so this is an expected result of a molecular-based analysis (Near, 2009). Although the consistency of molecular inferences is not to be confused with additive reinforcement of the topology (Near, 2009), cyclostome monophyly has gained wide acceptance to the extent that recent phenotype-based analyses use monophyletic cyclostomes as a topological constraint (Donoghue et al., 2000; Sansom et al., 2010b; Conway Morris and Caron, 2014; Gabbott et al., 2016; Keating and Donoghue, 2016). Such a constraint imposes serious theoretical implications to interpreting the resulting trees. For these reasons, cyclostome paraphyly has not been ruled out entirely (Miyashita and Coates, 2016).

I followed the GDS analysis in using maximum parsimony as a primary method of phylogenetic reconstruction and using Bayesian analysis as secondary. Parsimony has predictable outcomes for optimization of non-binary additive and contingency coding strategies (Brazeau, 2011). On the other hand, these coding methods may affect Bayesian inferences computationally, but precise impacts are unknown. Although parsimony-uninformative characters are known to contribute to Bayesian inferences, such characters were still eliminated from the dataset to simplify the analytical pipeline, because: (***a***) non-additive and contingency coding strategies would require re-coding the existing characters that are contingent upon or related to the

uninformative characters added back in; and (***b***) it is beyond the scope of the present study to sample unique character states exhaustively among these deep chordate lineages, at which point the character sets will no longer be reciprocal between parsimony and Bayesian analyses. Therefore, I optimized the dataset for a maximum parsimony analysis first to generate the shortest primary phylogenetic hypothesis, and then subjected the same dataset to a Bayesian analysis to test for congruence and robustness of phylogenetic inferences supported by parsimony.

The resulting dataset contains 60 taxa and 171 characters (Tables S2.2, S2.13; Figs. S2.11, S2.12; **2.8.5 List of Characters**). Among 171 characters, 54 represent new additions (not present in the CMC, MSL, GDS, and KD datasets (Conway Morris and Caron, 2014; Gabbott et al., 2016; Keating and Donoghue, 2016; McCoy et al., 2016); 57 have modified definitions and coding from the latest datasets (Gabbott et al., 2016; Keating and Donoghue, 2016); and 38 have same definition but modified coding (Table S2.13). When coding for presence/absence of non-mineralized structures, I considered the non-random decay patterns in living analogues (Sansom et al., 2010a, 2011, 2013a; Sansom and Wills, 2013) and locality-specific trends in taphonomic bias (Gess et al., 2006; Sansom et al., 2010b; Gabbott et al., 2016; Sallan et al., 2017) to avoid stemward slippage of soft-bodied taxa (Sansom 2015; Sansom et al. 2010b; Sansom and Wills 2013), conforming the analytical strategy in the recent analyses.

Abbreviations for previous datasets: CMC, Conway Morris and Caron (2014); **GCR**, Gess et al. (2006); **GDS**, Gabbott et al. (2016); **HSM**, Heimberg et al. (2010); **KLV**, Khonsari et al. (2009); **KD**, Keating and Donoghue (2016); **MH**, Mallatt and Holland (2013); **MSL**, McCoy et al. (2016).

2.8.4b Taxonomic sampling

Among 60 taxa sampled for this dataset (Table S2.2), myxinoids and petromyzontiforms from the previous datasets were split into multiple living genera and species; jawed gnathostomes into four representative lineages; and anaspids and thelodonts into several ingroup genera. Several other new additions are taxa of uncertain affinity. The original composite taxonomic units (myxinoids, petromyzontiforms, gnathostomes, anaspids, thelodonts) were retained in the dataset so that different taxonomic combinations can be explored. The coding for these composite taxa was

modified accordingly through the rest of the dataset. *Palaeospondylus* is represented in two different coding versions of the matrix.

Palaeospondylus and *Tullimonstrum* were only included in secondary analyses. They were posited as a stem myxinoid (Hirasawa et al., 2016) and a stem vertebrate (Clements et al., 2016) or even stem petromyzontiform (McCoy et al., 2016), respectively. As for *Tullimonstrum*, a reanalysis questioned its membership as a petromyzontiform and the coding responsible for the placement (Sallan et al., 2017). No cladistic dataset available can test the full range of possible affinities for *Tullimonstrum*. So the taxon is included, but the coding was modified on the character-by-character basis by comparing the contrasting interpretations (McCoy et al., 2016; Sallan et al., 2017). The resulting coding for *Tullimonstrum* is similar to codings B and E in Sallan et al. (2017) (specific notes for some challenging character codings are listed in **2.8.5 List of Characters**).

Palaeospondylus is another problematic taxon — posited as a stem myxinoid, stem petromyzontiform, jawless stem gnathostome, placoderm, chondrichthyan, teleost, or dipnoan/amphibian larva — but no hypothesis has been tested in a rigorous cladistic analysis (Thomson, 1992; Joss and Johanson, 2007; Johanson et al., 2010, 2012; Hirasawa et al., 2016). A recent reconstruction of *Palaeospondylus* as a stem myxinoid (Hirasawa et al., 2016) is certainly provocative but contains some internal inconsistencies (Chapter 1). The comparison is tenuous for some of the characters, such as: (***a***) the purported nasal capsule basket fused to the main palatal element; (***b***) the purported velar cartilages as mineralized, displaced elements; (***c***) the purported lingual apparatus being a bilaterally paired structure; and (***d***) otic capsule, which has three semicircular canals like jawed gnathostomes (Chapter 1; Johanson et al., 2017)). Like many other problematic taxa, even the coarsest classification is difficult because *Palaeospondylus* does not exhibit multiple characters that clearly falsify alternatives. As such, I used two coding schemes. (A) The cyclostome model was coded on the assumption that *Palaeospondylus* was a cyclostome (but not necessarily a myxinoid). (B) The gnathostome was coded on the assumption that it was a gnathostome (but not necessarily jawless or jawed, nor specifically as placoderm, chondrichthyan, actinopterygian, or dipnoan).

Haikouella is the best preserved of yunnanozoans and has been interpreted varyingly. Although nearly all preserved structures of *Haikouella* generate conflicting interpretations, some anatomical characters have some degree of consensus among multiple reconstructions. These

include the oral and branchial structures, pharynx, gut, and dorsal segments. The nerve cord and dorsal and ventral blood vessels also seem to be preserved in multiple specimens in two different species (Holland and Chen, 2001; Mallatt and Chen, 2003; Shu et al., 2003a). The notochord remains contentious (Chen et al., 1995, 1999; Holland and Chen, 2001; Mallatt and Chen, 2003), and this structure does not seem to be preserved in the specimens of *H. jianshanensis* (Shu et al., 2003a). Multiple specimens of *H. lanceolatum* indicate the presence of an axial structure with a sheath at the mid-height of the trunk (Chen et al., 1999; Holland and Chen, 2001; Mallatt and Chen, 2003). On the one hand, a notochordal identity is plausible for this axial sheathed structure in *Haikouella* if similarly poorly preserved axial structures in *Cathaymyrus* are considered notochordal. On the other hand, the committal to chordate affinity by a notochord presents a risk of imposing a circular reasoning when no other definitive chordate or vertebrate synapomorphies can be discerned. Thus, the presence of a notochord in yunnanozoans is uncertain in this analysis. At the very least, it is difficult to identify irregular imprints as cranial nerves, sensory capsules, brain regions, specific arteries and veins, muscles, or arcualia as have been suggested (Chen et al., 1995, 1999; Holland and Chen, 2001; Mallatt and Chen, 2003). It was scored as either missing or inapplicable for these characters.

2.8.4c Character sampling

Non-additive binary and contingency coding strategies could buffer against secondary loss and degeneration of characters that are considered to bias a phenotype-based parsimony analysis (Shaffer et al., 1991; Jenner, 2004b; Brazeau, 2011). In principle, the characters were formulated as non-additive binary (for presence/absence) first, and specific conditions are described in separate characters with inapplicable status assigned to any that coded for absence in the foregoing character. All multistate characters were treated as unordered. For example, hemichordates (outgroup) were assigned the inapplicable status (-) as a result of contingency coding for 39.7% of the characters in the CMC dataset, 38.5% in the MSL dataset, and 81.9% in this dataset. This is not only due to the exclusion of previous characters. Many of the vertebrate characters simply do not apply to hemichordates, and those characters were re-coded.

For example, pretrematic branch in branchial nerve (CMC character 8) may be coded as absent (0) (the CMC dataset) or inapplicable (-). Given the dependence on neural crest for the organization of branchiomeric nerves in vertebrates (Lumsden et al., 1991; Hall, 2009; Trainor,

2013), branchiomeric nerves can be compared only among those that have neural crest. In the case of this particular character, assigning inapplicable status to all non-vertebrate taxa made the character constant (all the other taxa were coded with presence [1]). Therefore, I excluded the character from the analysis. Not all such characters were excluded, however. Many modifications to character definitions were designed to make them parsimony-informative under my coding strategies. New characters were sampled primarily to help sort out living hagfish and lamprey lineages and secondarily to help resolve cyclostomes near the node of the crown-group Vertebrata.

As a result, the proportion of inapplicable character values increased from previous analyses overall, per taxon (Fig S2.12a) and per character (Fig. S2.13a). The relative increase in inapplicable values occurred across both taxonomic (Fig. S2.12a, b) and character (Fig. S2.13d, g, k, n) categories, except for characters of the circulatory system. The increase is massive in non-vertebrate outgroups among taxonomic categories (Fig. S2.12b) (largely due to the high proportion of characters describing vertebrate-specific morphologies) and in skeletal and miscellaneous categories of characters (due to [***a***] the contingency coding of characters related to mineralized skeletons and [***b***] the inclusion of hagfish- and lamprey-specific characters, respectively). However, the proportion of missing values remained similar overall across different analyses (Fig. S2.2.11b). The patterns are consistent across both taxonomic (Fig. S2.2.12c, d) and character (Fig. S2.2.13e, h, l, o) categories. Proportion of missing values increased slightly in jawed vertebrates because of inclusion of placoderms, and decreased for non-vertebrate outgroups because some missing values were re-coded as inapplicable (Fig. S2.12d). It also decreased for cyclostomes, likely due to inclusion of living taxa that have fewer missing values. The magnitude of missing values is similar between the analyses for taxa with uncertain affinity, but inclusion of highly incomplete taxa in the present analysis shifted the distribution to a greater mean (Fig. S2.12c, d).

As inapplicable and missing values did not compensate for each other, the sum of inapplicable and missing values is greater in this dataset than in previous ones, both per taxon and per character (Figs. S2.12e, f, S2.13f, i, j, m, p). Among taxonomic categories, non-vertebrate outgroups and taxa with uncertain affinity had the least coded information for two different reasons: invertebrates were inapplicable to many characters, whereas taxa with

uncertain affinity tended to be poorly preserved. Despite all such differences, information content of characters was similar between the present and past datasets (Fig. S2.12g, h).

2.8.4d Excluded characters

Characters were excluded on the following basis: (***a***) definition is unclear; (***b***) character is parsimony-uninformative, or does not contribute to resolving hagfishes or lampreys (if each was treated as a natural clade) in a parsimony analysis; and (***c***) characters duplicate the same phenotypic variations. Characters in category (***b***) may have been typically coded in previous analyses as primitive (0) for chordates and hagfish, and derived (1) for lampreys and gnathostomes. Instead, many of these characters were coded for contingency as inapplicable (-) for chordates, 0 for hagfish, and 1 for lampreys and gnathostomes. In the latter coding scheme, the character does not contribute to resolving cyclostomes parsimoniously as a clade or a grade.

CMC (Conway Morris and Caron 2014) #5 (adenohypophysis, simple versus complex): definitions are unclear. This character is parsimony-uninformative unless coded for invertebrate chordates, which lack the system at an anatomical levels.

CMC #6 (optic tectum, absent or present): the character is parsimony-uninformative. Vertebrate outgroups have neither camera eyes nor morphologically unequivocal brain compartmentalization. Therefore, the outgroups were coded as inapplicable, whereas all living vertebrate taxa were scored as present.

CMC #20 (semicircular canals, absent or present): cannot be coded for the outgroups that lack an otic capsule (=parsimony-uninformative).

CMC #33 (endodermal branchial lamellae, absent or present): parsimony-uninformative when coding for hagfish is revised from absent to present.

CMC #34 (branchial lamellae with filaments, absent or present): parsimony-uninformative when the taxa lacking branchial lamellae are coded as inapplicable for this character.

CMC #36 (oral hood, absent or present): this character is redundant with the oral funnel/disc after re-coding. Cephalochordates do not have an oral hood readily comparable to lampreys. The prominent hood-like snout in lampreys arises from the posthypophyseal process anterior to the nasohypophyseal canal. The developmental attribute of this morphology is described in another character (#66, this analysis).

CMC #63 (midline retractor muscle and paired protoractor muscles, absent or present): the definition does not provide accurate description of the morphology. This character applies to both hagfish and lampreys (although the former was originally coded as absent), but in both lineages there are multiple retractors (Yalden, 1985; Miyashita, 2012). The character is inapplicable to those without a cyclostome-like lingual apparatus because the 'protractors' and 'retractors' cannot be compared with any other oropharyngeal structures outside cyclostomes. Once they are coded as such, the character is invariable.

CMC #66 (chondroitin 6-sulphate, absent or present): parsimony-uninformative when re-coded.

CMC #68 (neurocranium entirely closed dorsally, absent or present): parsimony-uninformative when re-coded. In the extant gnathostomes, the neurocranium is closed by: (***a***) dermal skull roof (cranial vault; derived from neural crest and mesoderm in various combinations) and/or (***b***) extension of chondral elements (occipitals). These two states cannot be confused.

CMC #85 (scales/denticles/teeth composed of odontodes, absent or present): this character is constant after re-coding. Odontodes assume mineralized dermal skeleton, dentine, and pulp cavity, but these attributes are already described in the existing characters. Therefore, the taxa lacking dentine or mineralized dermal skeleton altogether cannot be scored for this character and are inapplicable. All known taxa with mineralized dermal skeleton and dentine has odontodes by definition (coded as present). So no taxon can be coded as absent. In this analysis, character #115 describes monodontodes versus polyodontodes as contingent on the presence of dentine (and therefore of odontodes).

CMC #96 (hyperosmoregulation, absent or present): the character is insufficiently defined. With respect to ambient salinity that differs among taxa (e.g., freshwater lampreys versus marine hagfish), the character may be modified to contrast osmoregulator against osmoconformer, those with kidneys against those without, or those with particular ion channels against those without. However, it is difficult to formulate specific characters on different modes of osmosis because comparative studies emphasized the lack of physiological traits in hagfish that are otherwise shared across gnathostomes (Løvtrup, 1977). Hagfish may be truly primitive in physiology or secondarily specialized, but this cannot be meaningfully assessed in a cladistic

context without sufficient character-by-character comparison with anadromous lampreys and invertebrate chordates.

CMC #99 (larval phase, absent or present): the character is vaguely defined. Hemichordates have a larval phase, whereas the presence of larvae cannot be assessed reliably for stem chondrichthyans, stem osteichthyans, and stem gnathostomes. Importantly, however, it is questionable that the larval phases present in multiple lineages can be compared to each other. Different modes of feeding, locomotion, and patterning suggest that the larval forms evolved independently in each lineage. The character be reinterpreted in the vein of the physiological pathways capacitating metamorphosis (such as function of the thyroid hormone derivative, triiodothyroacetic acid; (Paris et al., 2008)), but the comparative analysis has not included some important living lineages (e.g., hagfish) so that the distribution of character states is parsimony-uninformative.

CMC #103 (neuromasts in sensory lines, absent or present): parsimony-uninformative after re-coding. Neuromasts have not been identified in the lateral lines of hagfish (Braun and Northcutt, 1997), but they cannot be ruled out because development of the lateral line suggests presence of the neuromast primordium in this taxon (Wicht and Northcutt, 1995). The lateral line is reduced in hagfish — so the absence of neuromast in the lateral line of adult hagfish should not be confused with the absence of neuromasts in invertebrate outgroups. Coding hagfish as unknown ("?") renders this character uninformative. The character is excluded provisionally.

CMC #104 (relative position of atrium and ventricle of heart, well separated or close to each other): this character is invariable. The atrium and ventricle are closely associated to each other in all known taxa with a chambered heart (on which this character is contingent).

CMC #113 (mandibular branchial bar, absent or present): invariable character. There is no compelling evidence for the presence of gills in the mandibular arch in any known vertebrate, extinct or extant (Miyashita, 2016). In *Metaspriggina*, the most anterior pair of the branhial skeleton is interpreted as the mandibular arch (Conway Morris and Caron, 2014). However, no anatomical correlates (trigeminal nerve, upper lip cartilages) exist to corroborate this identification, unless one assumes *a priori* that the ancestral mandibular arch derived a branchial skeleton or that the most anterior pharyngeal skeleton represents a mandibular arch — thereby creating a circular argument (Miyashita, 2016). Nor does any evidence rule out alternative interpretations (e.g., mandibular cartilages not preserved, and the putative mandibular branchial

bar were derived from the hyoid arch). Regardless of positional identity, no definitive branchial fillaments can be confirmed on this most anterior pair (T.M., personal observation). Even if the identification of a mandibular branchial bar in *Metaspriggina* is accepted, the character is still parsimony-uninformative because no other taxa can be scored as present.

CMC #114 (first pharyngeal bar [mandibular], undifferentiated or differentiated): the character is insufficiently defined. It contains two internal inconsistencies. First, the most anterior pharyngeal skeleton preserved does not necessarily represent a mandibular arch derivative. The most anterior pharyngeal bar in cephalochordates cannot be treated as a mandibular arch derivative based on its polarity alone. Second, the mandibular arch derivatives are differentiated from the rest of the pharyngeal skeleton in all known vertebrates, extinct or extant (Miyashita, 2012). But the degrees of differential morphology vary among taxa and cannot be confused with one another.

CMC #115 (eyes, absent/unpaired/ocelli or paired): redundant with CMC #12. The states are poorly defined. It is not clear whether eyes are intended to be an integrated photoreceptive organ with a lens, more narrowly with optic nerve, or broadly so as to include structures like ciliary eyes. There is no justification for grouping ocelli and paired eyes under the same character state..

CMC #116 (notochord, absent or present): parsimony-uninformative. *Haikouella* has yet to provide unambiguous evidence for the presence of a notochord except for a thin sheath (Shu et al., 2003a), despite extensive preservation of muscular and other soft tissues (Chen et al., 1999; Mallatt and Chen, 2003; Mallatt and Holland, 2013). The state for this taxon is unknown. The putative notochord in *Tullimosntrum* has been reinterpreted as a digestive tract (Sallan et al., 2017), an assessment consistent with preservation bias of the Mazon Creek fauna. *Tullimonstrum* is coded as unknown for this character, as a notochord is hardly preserved in coeval vertebrates. With only hemichordates scored for the absence of notochord in this dataset, this character would not have parsed putative chordates inside or outside chordates parsimoniously, regardless of how a notochord is inferred for these taxa.

GDS #109 (inflected myomeres in post-larval stage, absent or present): parsimony-uninformative after re-coding. Myomeres assume segmented organization and/or an axial rod (notochord). The character is thus inapplicable to hemichordates (and arguably to tunicates, as well) because neither the notochord nor axial musculature is retained post-metamorphosis.

2.8.4e Exceptions

The characters encoding presence/absence of placode-derived structures (adenohypophysis, nasal capsules, eyes, otic capsules, lateral line) in vertebrates cannot be decoupled from the presence of ectodermal placodes. Assigning the inapplicable status to taxa lacking neurogenic ectodermal placodes (hemichordates and cephalochordates) forces all such characters to become parsimony-uninformative. Nevertheless, these characters are coded as absent for both outgroups and retained in the present dataset. This is because: (***a***) functional or anatomical homologues of these sensory/secretory structures have been proposed in vertebrate outgroups independent of the presence/absence of placodes (Gans, 1993; Boorman and Shimeld, 2002a, 2002b; Ruppert, 2005; Wicht and Lacalli, 2005; Patthey et al., 2014); (***b***) the emergence of neurogenic ectodermal placodes is not necessarily coupled to the evolution of one particular sensory capsule (e.g., tunicates have placodes but none of vertebrate-like sensory capsules; Manni et al., 2005; Mazet et al., 2005; Schlosser et al., 2014; Abitua et al., 2015), so these characters vary independently from one another; and (***c***) some putative stem vertebrates may be argued to possess or lack one or more of these sensory capsules that are decay resistant in the living analogues (Sansom et al., 2010a, 2011, 2013a).

As discussed in the rationale for deleted characters, those that can be coded only for several extant taxa tend to be parsimony-uninformative. If multiple ingroup taxa score for different states, however, these characters may resolve some ingroup relationship. One such exception is the presence of internal taste buds (#43, this analysis) — oropharyngeal chemoreceptive structures innervated by gustatory nerves (facial, glossopharyngeal, and vagus nerves) (Northcutt, 2004; Kirino et al., 2013). Coding for presence/absence of the internal taste buds (HSM #27), hagfish, invertebrate chordates, and hemichordates would be scored as absent (Heimberg et al., 2010). However, these taxa are not equivalent in the state of absence. Hagfish have a unique chemosensory structure called Schreiner organ, which resembles internal taste buds. The organ is innervated by the trigeminal nerve and not contingent on the purinergic signaling (Braun, 1998; Kirino et al., 2013). So this character may be modified to accommodate two states (internal taste buds; Schreiner organs). As Schreiner organs are identified in two hagfish species (*Eptatretus stoutii* and *Myxine glutinosa*) (Braun, 1998), the character state may be useful as a myxinoid synapomorphy even if it does not contribute to the resolution of cyclostome mono-/paraphyly.

2.8.5 List of Characters

See **Abbreviations for previous datasets** above for the identitites of datasets abbreviated here.

2.8.5a Brain, sensory and nervous system

1. Skeletal derivatives of neural crest: 0, absent; 1, present (CMC #1: **definition modified).**

   The original definition has been modified from the presence of neural crest to that of the *derivatives* of neural crest. Robust embryological evidence indicates that neural crest gives rise to the splanchocranium, a large part of the dermatocranium, and a premandibular region of the chondrocranium (Couly et al., 1993; Hall, 2009). Teeth and scales appear to derive from neural crest ectomesenchyme (Smith and Hall, 1990; Sire et al., 2009), although experimental evidence from zebrafish suggests a mesodermal origin for their scales (Lee et al., 2013a, 2013b). The pharyngeal skeletal elements observed in myllokunmingiids (*Haikouichthys*, *Myllokunmingia*, and *Metaspriggina*) coded as unknown ('?') because pharyngeal cartilages occur as a mesodermal derivative in cephalochordates (Jandzik et al., 2015). Tunicates were originally coded as having neural crest (Conway Morris and Caron, 2014), but they lack such typical neural crest derivatives (Green et al., 2015). Although evidence points to the presence of neural crest-like cell lineages in tunicates (Abitua et al., 2012; Stolfi et al., 2015), the multi-potent differentiation of neural crest including skeletal derivatives is still unique to vertebrates.

2. Ectodermal placodes: 0, absent; 1, present (**new character**).

   The presence of neurogenic ectodermal placodes in tunicates (Manni et al., 2005; Mazet et al., 2005; Kourakis et al., 2010; Patthey et al., 2014; Schlosser et al., 2014; Abitua et al., 2015) suggests that the sensory fates of these ectodermal thickenings constitute a synapomorphy of olfactores (and the constituent cell types and gene expressions may have their evolutionary origins deeper still). For fossil taxa and those for which embryos are not known, the presence of sensory capsules was used as an indicator. The state for *Tullimonstrum* is unknown ("?") because it shows no unambiguous correlates of placodes. The camera-like eyes do not require a lens placode (as they occur in molluscs) (Clements et al., 2016) and it has been difficult to repeat the original observation of nasohypophyseal structures in this animal (McCoy et al., 2016; Sallan et al., 2017).

3. Distinct prechordal head: 0, absent or weakly developed; 1, prominent (**new character**).

One important prediction of the New Head Hypothesis is that the evolution of neural crest gave rise to the prechordal cranium (Gans and Northcutt, 1983; Northcutt and Gans, 1983; Gans, 1993). Indeed, all living vertebrates exhibit a prominent prechordal cranium to house the nasal and adenohypophyseal organs and encapsulate the forebrain. On the other hand, *Haikouichthys* and *Metaspriggina* have a notochord extending well frontally, and the nasal capsules are tucked between the eyes, whereas the mouth sits at a more posterior level (Conway Morris and Caron, 2014). The character cannot be scored in hemichordates (no notochord) or tunicates (no distinct cephalization). *Euphanerops* is superficially similar to the condition in *Metaspriggina*, but the presence of midline cartilages anterior to the notochord indicates a prechordal cranium (Janvier and Arsenault, 2007). Arandaspids have the eyes exposed at the anterior end, with the nasohypophyseal canals tucked between them (Gagnier, 1993b). However, it is more plausible to interpret the position in light of heterostracan anatomy, where the optic tectum extends anteriorly. Heterostracans tend to have the eyes exposed in anterior positions, but internal casts indicate that they had a prominent prechordal cranium (Halstead, 1973; Janvier, 1974197, 1993, 1996a).

4. Tripartite vesicles at anterior end of neural tube (prosencephalon, mesencephalon, rhombencephalon): 0, absent; 1, present (**new character**).

   Hemichordates are coded as inapplicable because they lack a fully closed, axially elongate neural tube.

5. Morphologically distinct cerebellum with corpus cerebelli: 0, absent; 1, present (CMC #7, KLV #71: **definition modified**).

   Gene expression patterns indicate cyclostomes do have the rhombic lip and medial ganglionic eminence (Sugahara et al., 2016). Previously, a cerebellar primordium has been considered present in lampreys but absent in hagfish (Nieuwenhuys et al., 1998), but new evidence (Sugahara et al., 2016) reveals that (***a***) brain development in hagfish parallels that of gnathostomes in gene expression patterns more closely than that of lampreys; and (***b***) cyclostomes do exihibit similar brain regionalization patterns at the level of gene expression. Cyclostomes still lack a clearly demarcated cerebellum with corpus cerebelli, so the original definition was modified in accordance with Khonsari et al.'s (2009) analysis. Non-vertebrates lack a tripartite brain (#4, this analysis). They are

coded as inapplicable (-) for this character.

6. Profundal nerve ganglion: 0, separate from trigeminal ganglion; 1, fused with trigeminal ganglion (HSM #46; **character addition**).

   In the galeaspid *Shuyu*, the roots for V1+0 and V2+3 are well separated (Gai et al., 2011) so the ganglia were likely independent as well. In osteostracans, these nerves share a narrow root under the myodome of the orbital cavity (Janvier, 1981b, 1985a) so the ganglia were likely fused. One conspicuous example is seen in *Belonaspis* (MNHN SVD 1005). It is difficult to assess this character in arthrodires, but the size and shape of the trigeminal canal are comparable to those in chondrichthyans (Young, 1980; Goujet, 1984; Brazeau and Friedman, 2014; Dupret et al., 2014, 2017), and they are tentatively coded as separated. This character is contingent on having a vertebrate brain and cranial nerves (#4, this analysis).

7. Tripartite division of facial nerve into pharyngeal, 'pretrematic', and 'postrematic' branches: 0, absent; 1, present (CMC #8, KLV #50: **definition modified**).

   The original definition in the CMC dataset concerned the presence of pretrematic branch in branchial nerves, where jawless vertebrates were coded as lacking the branch. Cyclostomes clearly have pretrematic branch in the glossopharyngeal and vagus nerves (Kuratani et al., 1997). The facial nerve, however, lacks the bipartite organization of pre- and post-trematic branches being separated by the hyomandibular pouch (Lindström, 1949; Khonsari et al., 2009). What appears to correspond to a pretrematic branch is a split of the postrematic branch. The lack of the pretrematic branch in the facial nerve is also consistent with the lack of pseudobranch (gill-like folded epithelium in hyomandibular position) in cyclostomes, suggesting that the structure represents a derived state acquired in the stem of gnathostomes (Miyashita, 2016).

8. Spinal cord in cross section: 0, round; 1, flattened (CMC #9: **definition modified**).

   Shape description was modified for clarity.

9. Ventral and dorsal roots of spinal nerve: 0, separated; 1, united (CMC #10: **definition modified**).

   See the next character for a rationale of modification.

10. Ventral and dorsal roots of spinal nerve originates: 0, intersegmentally; 1, intrasegmentally (**new character**).

This character supplements character #9 (ventral and dorsal roots united). Indeed, hagfish and gnathostomes are similar to each other for having the dorsal and ventral roots united (they are separate in lampreys). However, both roots originate at the intra-segmental level (medial to myomeres) in lampreys and gnathostomes, whereas the origin is at the inter-segmental level (medial to myosepta) in hagfish (Goodrich, 1930). To capture the full range of this variation, this addition to CMC #10 is required.

11. Mauthner fibres at rhombomere 4: 0, absent; 1, present (CMC #11: **definition modified**).

    The Mauthner fibres are identified primarily by their position at rhombomere 4. Therefore, the character is inapplicable (-) for outgroups without a tripartite brain (#4, this analysis).

12. Pineal organ (extra-ocular photoreceptor region expressing pineal opsins): 0, absent; 1, present (CMC #3).
13. Pineal opening: 0, covered; 1, uncovered (CMC #100; **coding modified**).

    The character is inapplicable to taxa lacking a pineal organ (#12, this analysis) and/or a skull (#3, this analysis).

14. Adenohypophysis: 0, absent; 1, present (CMC #4).
15. Olfactory peduncles: 0, absent; 1, present (CMC #2).

    Any taxon that scores for 0 in character #4 (tripartite vesicles at anterior end of neural tube, absent) is coded as inapplicable (-).

16. Encapsulated olfactory epithelium with external opening: 0, absent; 1, present (CMC #13: **definition modified**).

    Haikouichthys and *Metaspriggina* were coded as having olfactory capsules, following the original descriptions (Shu et al., 2003b; Conway Morris and Caron, 2014).

17. Position of nasohypophyseal/nasal opening: 0, terminal; 1, dorsal (CMC #16: **coding modified**).

    This character describes the extent of posthypophyseal/internasohypophyseal skeleton in the snout (Kuratani et al., 2001; Shigetani et al., 2002; Kuratani, 2012; Oisi et al., 2013b) — or, as superficially interpreted, the distance between the mouth and the nostril. If the pertinent structures in *Haikouichthys* (Shu et al., 2003b) and *Metaspriggina* (Conway Morris and Caron, 2014) are correlates of the nasohypophyseal system, the openings would have been terminal, not dorsal. Similarly, if the identification of the olfactory organ

in *Tullimosntrum* is correct, the coding for this taxon is dorsal. This character is inapplicable to those without adenohypophysis or olfactory capsules (#14 and 16, this analysis)

18. Nasohypophyseal canal: 0, blind; 1, opening into pharynx (CMC #14: **definition modified**).
Palaeospondylus is coded as having a blind nasohypophyseal canal, both under the cyclostome and gnathostome models. The cyclostome model posits a basket of longitudinal bars at the anterior end of the skull as the olfactory capsule (Hirasawa et al., 2016). If true, the olfactory cavity would be closed posteriorly by contact between this element and the neurocranium, or else the nasohypophyseal canal would have to extend below the commissure — unlike any known cyclostomes. Thus, the canal of *Palaeospondylus* was coded as blind, consistent with a cyclostome interpretation. On the other hand, galeaspids are coded as unknown ("?") for this character. The existing reconstruction of their internal anatomy (Gai et al., 2011) does not indicate whether or not the nasal cavity was open to the oropharyngeal cavity. The hypophyseal canal opened into the oral cavity, but that system is separate from the nasal passage in this lineage (Gai et al., 2011), like in crown-group gnathostomes. The character is contingent on the presence of the nasohypophyseal/nasal cavity (#14 and #16, this analysis).
19. Nasohypophyseal opening: 0, single; 1, paired (CMC #15, 101: **definition modified**).
This character likely correlates with the organization of nasal (olfactory) capsules (#20, this analysis). On the basis of paired capsules with a single aperture in stem gnathostomes and possibly in myllokunmingiids, the primitive state (single) does not assume a particular state in character #20. However, there is no example of paired apertures with a single capsule, suggesting that the derived state (paired) in this character is contingent on the derived state of character #20. One way to treat this likely contingency is to code only those with the derived state of character #20. However, multiple stem gnathostomes (anaspids, arandaspids, thelodonts, *Jamoytius*, *Athenaegis*, etc.) are not preserved with imprints of the capsules and therefore can only be scored for the organization of the aperture. Some of them are also highly incomplete with a limited number of characters scored. To compare them with the maximum range of OTUs, this character is coded without contingency on character #20.
20. Nasal (olfactory) capsule: 0, unpaired; 1, paired (CMC #17: **definition modified**).

Organization of the olfactory capsules can vary independent of the number of the nasohypophyseal opening. The olfactory tracts have paired organization in all known vertebrates, but the olfactory organ may be single or paired (Khonsari et al., 2009). Sometimes the olfactory tracts clearly split from one another as in heterostracans and crown gnathostomes.

21. Nasohypophyseal canal: 0, maintains width and height anteriorly; 1, tapers anteriorly (**new character**).

    This character only applies to myxinoids (or putative myxinoids). Among living hagfish, *Rubicundus* spp. have a tapering snout with tubular extension and with barbels originating posterior to the aperture (Fernholm, 1991; Fernholm and Quattrini, 2008; Kuo et al., 2010; Fernholm et al., 2013).

22. External opening of nasohypophyseal canal: 0, terminal aperture; 1, tubular extension (**new character**).

    This character only applies to myxinoids.

23. Nasohypophyseal barbels extend from: 0, rim of nasohypophyseal aperture; 1, posteriorly to nasohypophyseal aperture (**new character**).

    This character only applies to myxinoids.

24. Nasohypophyseal papillae, ventral element: 0, absent; 1, present (**new character**).

    This character only applies to myxinoids. The characters regarding the nasohypophyseal papillae originate from a comparative analysis by Mok (2001).

25. Nasohypophyseal papillae, dorsal element(s): 0, midline; 1, paired (**new character**).

    This character only applies to myxinoids.

26. Eyes with pigmented retinal epithelium: 0, absent; 1, present (CMC #12: **definition modified**; HSM #19).

    Pigmented retinal epithelium is characteristic of vertebrate eyes (Lamb et al., 2007; Clements et al., 2016).

27. Eyes: 0, exposed; 1, covered by dermis; 2, covered by trunk muscles (**new character**).

    This character is compound, as the state 2 assumes coverage by the dermis as well. However, the character is included in the current form as the state 2 only applies to a nested ingroup within the crown group Myxinoidea, which is the only group of taxa with covered eyes in this dataset. The character is contingent on character #26 (presence of

eye).

28. Extrinsic eye musculature: 0, absent; 1, present (CMC #18: **coding modified**).

The character is contingent on the presence of eyes (#26, this analysis). Euconodonts are typically coded as having extraocular muscles on the basis of the fibrous soft tissues preserved in the Carboniferous euconodont *Promissum* (Gabbott et al., 1995). This observation constitutes one of the prominent inferences for the vertebrate/gnathostome affinity of conodonts, but also has attracted controversy (Turner et al., 2010). Certainly, the extraocular muscles are a collection of individual bundles of muscles, whereas the supposed structure in *Promissum* shows no such organization. Two lines of evidence consistent with the original interpretation are the position close to the posited eye and the fibrous texture unlike typical cartilages (Gabbott et al., 1995).

One possible, alternative interpretation is that the 'extraocular muscles' of *Promissum* represent a patch of mucocartilage-like supporting tissue (Wright and Youson, 1982, 1983; Armstrong et al., 1987; Robson et al., 1997; Martin et al., 2009). Both interpretations are compatible with the currently available evidence, and neither can be readily ruled out. Provisionally, euconodonts were scored as unknown ('?') for this character.

29. Muscles innervated by oculomotor nerve: 0, three; 1, four (**new character**; Young, 2008).

The following characters describe three major character transitions in the extraocular muscles before the chondrichthyan-osteichthyan divergence. The oculomotor nerve innervates three muscles in lampreys (dorsal ramus: superior rectus; ventral ramus: anterior oblique, internal rectus) and four in gnathostomes (dorsal ramus: superior rectus; ventral ramus: inferior oblique, inferior rectus; internal rectus [dorsal ramus in chondrichthyans; ventral ramus in osteichthyans]) (Young, 2008). Osteostracans were coded as unknown ('?') for this character, because only two muscle attachments exist for the muscles of the oculomotor nerve and because neither provides direct evidence for multiple elements attached as in other vertebrate lineages (Janvier, 1975). This character explicitly refers only to the numbers of elements so as not to assume any one of multiple possible schemes of homology among these muscles *a priori*. A reference to number of elements (and not to interpretations of homology for the individual components) allows placoderms to be scored for this character.

Depending on the identification schemes, additional characters may be formulated to resolve ingroup relationships among gnathostomes, but this is beyond the schope of this analysis. In a brief summary, correspondence with the counterparts in crown gnathostomes is unclear for the four muscles innervated by the oculomotor nerve in placoderms. The anterior oblique (corresponding to inferior oblique in crown gnathostomes) is undisputed. The rectus inserting dorsally appears to correspond superior rectus topographically and probably received innervation from the dorsal ramus, but has been identified as internal rectus on the basis of its insertion dorsally to the anterior oblique (Young, 2008). Problematically, identification of this muscle as internal rectus assumes either: (***a***) the superior rectus was lost and one additional muscle added in placoderms; or (***b***) the superior rectus independently evolved in lampreys and gnathostomes. Transposition of the extraocular muscles is necessary no matter which assignment is followed — the internal rectus passes below the anterior oblique in lampreys, whereas it typically inserts dorsal to the inferior oblique in crown gnathostomes. Therefore, it appears most parsimonious to recognize the four muscles in placoderms as homologous to those of crown gnathostomes (anterior oblique [inferior oblique], internal rectus, inferior rectus, and superior rectus; the last probably being the only muscle innervated by the dorsal ramus). This character is contingent on the presence of extraocular muscles (#28, this analysis).

30. Oblique muscle innervated by trochlear nerve: 0, posterior; 1, superior (**new character**; Young, 2008).

    This shift of the oblique muscle correlates with the shift of another oblique muscle from anterior to inferior. This character is contingent on the presence of extraocular muscles (#28, this analysis).

31. Rectus muscles innervated by abducens nerve: 0, two; 1, one (**new character**; Young, 2008).

    Lampreys have an external and posterior rectus — only the external rectus persists in crown gnathostomes (retractor bulbi are tetrapod-specific condition). On the basis of the insertion scars, placoderms likely had two muscles innervated by the abducens nerve, although the homology of the second muscle to the posterior rectus remains unresolved (Young, 2008). In osteostracans, a single myodome sits in the corresponding position, and it remains unclear whether one or two muscles attached here despite reconstructions

typically depict two (Janvier, 1975). It is scored as unknown ('?') in the present analysis. This character is contingent on the presence of extraocular muscles (#28, this analysis).

32. Eyes: 0, laterally placed (interorbital distance equal to width of head at that position); 1, close together near midline (interorbital distance substantially less than width of head at that position); 2, on prominent eyestalk (**new character**).

    This character is contingent on the presence of eyes (#26, this analysis).

33. Cartilaginous otic capsules: 0, absent; 1, present (GDS #111; **definition modified**).

    The original definition (otic capsules, absent or present) is modified to predict distribution of the character in the stem branches with respect to general decay sequences. The otic capsules are among the most resistant skeletal structures to decay (Sansom et al., 2010a, 2011, 2013a; Sansom and Wills, 2013). Therefore, the absence of the structure may be inferred in specimens preserved with an extensive set of soft tissues that would have otherwise decayed well before the otic capsules, from the localities where cartilages and other soft tissues are readily preserved. These conditions rule out the Lesmahagow and Achanarras forms (*Achanarella*, *Ciderius*, *Cornovichthys*, *Jamoytius*) and the Miguasha forms (*Euphanerops*: most cartilages preserved in this taxon are calcified; Janvier and Arsenault, 2002, 2007) from consideration — unless the structure is clearly present in fossils (e.g., *Lasanius*: MNHN specimens under study; Miyashita in prep.; van der Brugghen, 2010). These leave several taxa from the Mazon Creek fauna (*Tullimonstrum*) and from the Chengjiang and Burgess/Marble Canyon fauna (*Haikouella*, *Haikouichthys*, *Metaspriggina*, *Myllokunmingia*, *Pikaia*) (Chen et al., 1999; Shu et al., 1999b, 2003b; Mallatt and Chen, 2003; Conway Morris and Caron, 2012, 2014). Among them, the identification of an otic capsule in *Haikouichthys* (Shu et al., 1999b) is accepted, whereas the corresponding region is not well represented in *Myllokunmingia*. For all others, the capsule is coded as absent. This does not rule out the presence of otic placodes or capsules in those taxa (*Haikouella*, *Pikaia*, and *Metaspriggina*), but if present, they are unlikely to have been extensively chondrified.

34. Vertical semicircular canals forming loops that are separate from roof of utriculus: 0, absent; 1, present (CMC #21; **coding modified**).

    All characters concerning the inner ear anatomy are inapplicable to taxa that lack an otic capsule (#33, this analysis).

35. Anterior and posterior semicircular canals: 0, share a canal toward utriculus after meeting in a confluence; 1, meet each other to form a single loop (**new character**).

    Although the single semicircular canal in hagfish is often described as a 'horizontal' canal, a series of stem gnathostome lineages (heterostracans, galeaspids, and osteostracans) clearly indicates that the horizontal canal is unique to jawed gnathostomes. So the anterior and posterior canals have broader distributions, and the condition in lampreys is compatible with that assignment. Given that hagfish have the two cristae in positions corresponding to the anterior and posterior canals in lampreys (Jørgensen et al., 1998), the 'horizontal' canal of hagfish is the fusion of the anterior and posterior canals partway in their loops. Its state is best interpreted as the loss of the confluent part of the anterior and posterior loops. This character is contingent on the presence of an otic capsule (#33, this analysis).

36. Horizontal semicircular canal: 0, absent; 1, present (**new character**).

    The character is contingent of character #33.

37. Statoliths composed of calcium phosphate: 0, absent; 1, present (HSM #38).

    Calcium phosphatic condensation in the otic capsule of *Hardiestilla* (Janvier and Lund, 1983) is accepted as a statolith.

38. Endolymphatic duct: 0, is blind; 1, opens externally (CMC #22; **definition modified**).

    The original definition (presence/absence of open endolymphatic duct) confounds the presence/absence of endolymphatic duct with its states (externally open/closed). In that original definition, presence/absence cannot be assessed for outgroups that lack an otic capsule altogether, and the character would have been parsimony-uninformative. The character definition was thus modified. The character is contingent on character #33.

39. Electroreceptive cells: 0, absent; 1, present (CMC #23).

40. Sensory lines: 0, absent; 1, present (CMC #24).

41. Sensory-lines: 0, on head only; 1, on head plus body (CMC #25).

    The character is contingent on the presence of sensory lines (#40, this analysis).

42. Sensory-line: 0, enclosed in grooves; 1, enclosed in canals (CMC #26).

    The character is contingent on the presence of sensory lines (#40, this analysis).

43. Internal taste buds, or functionally equivalent end chemosensory organs innervated by cranial nerves in head: 0, absent; 1, present; 2, lacking internal taste buds but function replaced by

Schreiner organs (HSM #27; **definition modified**).

The absence of internal taste buds in hagfish should not be confused with that in non-vertebrate chordates and hemichordates, as the function is replaced by the unique epidermal structure Schreiner organs (innervated by the non-gustatory trigeminal nerve; not requiring purinergic signaling) (Braun, 1998; Kirino et al., 2013). This is a specialization specific to hagfish and reported in multiple extant species. The implication is that internal taste buds and Schreiner organs are mutually exclusive, so these are treated as separate states in a single character.

2.8.5b Mouth and branchial system

44. Preoptic head length: 0, shorter than branchial length; 1, approximately equal to branchial length; 2, longer than branchial length (**new character**).

    This character potentially correlates with the presence/absence of the prechordal cranium and the posthypophsyeal/internasohypophyseal distance (#3 and #17, this analysis). However, states vary for this character primarily among those with a distinct prechordal cranium, and independently from the distance between the nostril and mouth. This character is inapplicable outside vertebrates as the preoptic head cannot be recognized in these forms.

45. Branchial apparatus: 0, retains arrangement of pharyngula such that first branchial opening assumes infra- to postotic position; 1, displaced anteriorly; 2, displaced posteriorly (CMC #19: **definition modified**).

    The original definition in the CMC dataset concerned position of otic capsule with respect to branchial apparatus, but the relationship is reversed. This character now describes a position of the pharyngeal arch derivatives with respect to the nervous system, where the otic capsule and roots of all cranial nerves retain their relative positions to each other. The otic capsule is intended as a landmark — so this character may be assessed by using the overall configuration of structures spatially correlated with the otic capsule (with respect to the eye, the most anterior myomeres, the notochord, and others) when the otic capsule is not preserved. This strategy is sensible only for those that are unambiguously preserved with these alternative landmark structures (e.g., Euphanerops; Janvier and Arsenault, 2006). Therefore, this character is inapplicable to taxa in which (***a***) it is uncertain whether

the otic capsule was absent or not preserved; and (***b***) other landmark structures are not comparable or not preserved (e.g., euconodonts and *Haikouella*). For *Myxineidus*, serial swellings are interpreted as an outline of the branchial region (Poplin et al., 2001). This interpretation is tentatively accepted in this analysis.

46. Branchial apparatus, displaced anteriorly such that: 0, first branchial opening assume preotic position; 1, multiple branchial arches occupy preotic position (**new character**).

    This character applies only to those taxa that score for anteriorly displaced branchial apparatus in the previous character (state 1 of character #45).

47. Branchial apparatus, displaced posteriorly such that prebranchial length is: 0, less than a quarter; 1, approximately quarter; 1, greater than a third of body length (**new character**).

    This character applies only to those taxa that score for posteriorly displaced branchial apparatus in the previous character (state 2 of character #45).

48. Pharyngeal skeleton: 0, delineates pharyngeal slits with ciliary band; 1, supports well-developed branchial lamellae (CMC #34; **definition modified**).

    In hagfish, the skeleton of the branchial region consists of the extrabranchial cartilages around the excurrent ducts of the branchial pouches. This morphology is interpreted as derived ("1") for this character.

49. Main skeletal support for branchial apparatus with respect to lamellae: 0, lateral; 1, medial (CMC #112; **definition modified**).

    The original definition (branchial bars, external or internal) was modified to allow identification of states with respect to anatomical correlates. This character is inapplicable for those taxa lacking branchial lamellae (character #48, this analysis), and for *Haikouella* and *Pikaia* in which the branchial structures appear to have been exposed externally (Conway Morris and Caron, 2012).

50. Pharyngeal skeleton: 0, skeletal arches fused with each other; 1, arches isolated (CMC #111; **definition modified**).

    The original character distinguished between 'continuous' and 'basket-like' states, but these states are indistinguishable from one another. The taxa lacking a pharyngeal skeleton are coded as inapplicable.

51. Hyomandibular pouch: 0, blind; 1, externally open (spiracle) (HSM #24; **definition modified**).

Although the adorbital opening has been interpreted as spiracular in amphiaspidiform heterostracans and pituriaspids (Halstead, 1971; Young, 1991; Miyashita, 2016), this character is conservatively coded as unknown in both taxa. Beyond its position beside the orbit and otic capsule, little evidence exists for the hyomandibular identity of this opening. An alternative interpretation for this opening is a nasohypophyseal aperture (Janvier, 1974). The amphiaspidiform condition is likely an independent derivation within heterostracans (Janvier, 1996a; Miyashita, 2016) because this clade is nested within the Heterostraci (Novitskaya, 1971, 2008; Lundgren and Blom, 2013; Randle and Sansom, 2016, 2017), and because the general condition among heterostracans is blind (0) for this character. Modifying the scores for heterostracans (0/1) and pituriaspids (1) did not affect the topology presented in Fig. S2.5.

52. Respiratory current exits through: 0, atrial space; 1, excurrent duct (=branchial pouch); 2, parabranchial cavity (CMC #27: **definition modified**).

The original character definition in the CMC dataset requires some clarification because a 'pouch-shaped gill' is a composite of two different morphological variations — whether the skeletal support is lateral or medial, and whether the excurrent passes through a duct or a cavity. A new state (atrial space) was added to contrast vertebrates and non-vertebrate chordates. *Haikouichthys* and *Metaspriggina* exhibit a mix of features consistent with any of the possible states. In *Metaspriggina*, the branchial lamellae clearly sit lateral with respect to the skeletal arches. Normally, this should preclude pouch-like anatomy in this region, but no other correlate has been identified to conform to parabranchial cavities or an atrial space. Whether or not the skeletal elements are comparable to the vertebrate branchial skeleton may also be questioned. These taxa are coded as unknown ("?") for this character. Hemichordates are coded for the primitive state ("0"). In this lineage, the external pharyngeal slits do not open directly into the pharyngeal cavity. Instead, internal pores open to the cavity partitioned by ciliated primordial and tongue bars and outlet through the external slits (Jefferies, 1987). Although the pores and the mesodermal bars have no exact anatomical counterparts outside this lineage, the hemichordate condition seems to parallel the atrial space in chordates better functionally and developmentally (e.g., mesodermal components lie between the external and internal outlets) than other states of this character.

53. Single confluent branchial opening: 0, absent; 1, present (CMC #28).

    This character is inapplicable to those with parabranchial cavities (#52).

54. Branchial excurrent duct: 0, opens roughly at position of branchial pouch; 1, extends posteriorly (**new character**).

    This character is inapplicable for those that lack branchial pouches (#52, this analysis) and for those with a single confluent branchial opening (#53). The branchial and pharyngeal pouches are not to be confused for this and other branchial characters. The branchial pouch (#52) refers to a respiratory structure, whereas the pharyngeal pouches are embryonic anlagen (Miyashita, 2016). This character seemingly overlaps with the one regarding posterior displacement of branchial apparatus (#45, 47). However, the orientation of the duct varies independently of relative position of branchial apparatus. In some taxa (such as *Athenaegis*) coding is based on the assumption that the duct must have extended posteriorly under dermal plates to have an outlet.

55. Branchial openings: 0, spaced accordingly with dimensions of branchial cavities; 1, packed closely together; 2, organized into multiple parallel rows (**new character**).

    This character was evaluated with respect to dimensions of branchial pouches to ensure some independence from the previous character (#54, this analysis). For example, osteostracans have excurrent ducts extending posteriorly, but the space between the ducts remains roughly consistent with dimensions of the pouches. This is not the case in some taxa of hagfish, which score for both excurrent ducts extending posteriorly and their openings closely packed together (Kuo et al., 2003). Multiple rows of external branchial openings occur in species of "*Paramyxine*" that are now considered as an ingroup nested within *Eptatretus* (Kuo et al., 2003; Fernholm et al., 2013).

56. Number of arches (or pouches) in branchial apparatus: 0, unconstrained to five; 1, held constant at five (CMC #29: **definition modified**).

    The arches and pouches of this definition refer to branchial arches and pouches (branchial bars and gills), respectively, and are not to be confused with pharyngeal arches and pouches (anlagen). The original character (branchial pouches/slits greater than 10 or less than 10) is clarified and split into two individual characters to reflect multiple levels of variation. Among crown gnathostomes, the number of pharyngeal arches almost never exceeds six (except for a few chondrichthyans), with five of them supporting branchial

lamellae. The number is typically greater and varies widely among jawless vertebrates (Janvier, 2004). *Myllokunmingia*, *Pipiscius*, and euconodonts are coded as unknown. These taxa have five serial impressions that appear to be related to gills. In *Myllokunmingia*, this number is at odds with the preservation of the most anterior branchial pouch (Shu et al., 1999b) but given the rest of the body the number is either four or five. Five pouch impressions are confirmed for *Pipiscius* on the observation of the specimen FMNH PF8346 (FMNH = Field Museum of Natural History), but it is unclear whether the number is fixed at five in the same way as in crown gnathostomes or is coincidental. The suspected gill impressions in the euconodont *Clydagnathus windsorensis* (Briggs et al., 1983; Donoghue et al., 2000) are elusive, but their tentative identification and comparison to the branchial pouches of *Mayomyzon* (Aldridge et al., 1993; Aldridge and Donoghue, 1998) is accepted. These three taxa are treated as unknown for this character and coded for the following character describing variations in the number of branchial pouches.

57. Number of arches (or pouches) in branchial apparatus (unconstrained to five), maximum number: 0, greater than five and fewer than 20; 1, greater than 20 (CMC #29: **definition modified**).

    This character is contingent on the previous one (#56) and therefore inapplicable for those constrained to five arches supporting branchial lamellae. Among jawless vertebrates, the number of branchial pouches varies within and between lineages. In hagfish, the number is anywhere between four to fourteen (Fernholm, 1998). The range is similar among birkeniids (Blom et al., 2001). The range is greater among galeaspids from five to 45 plus (Janvier, 2004). It is difficult to count the number of arches precisely in *Euphanerops*, but the number is at least 30 (Janvier and Arsenault, 2007). Galeaspids and *Euphanerops* are unique among vertebrates in having substantially more than twenty branchial arches. So this number is used arbitrarily to distinguish the capacity to develop an exceptionally large number of branchial arches, and composite taxa were coded for the largest number that occurs within that lineage.

58. Number of arches (or pouches) in branchial apparatus (unconstrained to five): 0, four or five; 1, six or seven; 2, eight to ten; 3, greater than ten (**new character**).

    The previous two characters (#56, 57) described whether or not the number of branchial

arches (pouches) is constrained at five and whether or not the number of the arches can exceed the count normally observed in the development of living vertebrates, respectively. These characters do not describe most variations in the number of branchial arches among jawless vertebrate lineages in which the number is not constant or tightly controlled (Janvier, 2004). Among these lineages, five and ten each breaks the distribution into discrete ranges. Few (some hagfish species) have only four branchial pouches, whereas several have five (Fernholm, 1998). Several lineages have more than ten branchial openings, including arandaspids, some anaspids (*Jamoytius* and *Pharyngolepis*), and probably *Cornovichthys* and *Achanarella* (Newman and Trewin, 2001; Newman, 2002; Janvier, 2004). Living lampreys all have seven (Renaud, 2011), whereas hagfish fall anywhere in this range from four to fourteen although most have six to eight (Fernholm, 1998). A reexamination of the holotype of *Priscomyzon* (AM 5750) revealed at least eight and as many as nine branchial arches. The count in *Hardistiella* is based on Lund and Janvier (1986). The character is inapplicable to taxa that score for either a constant number (five) (#56, this analysis) or an exceedingly large number (>20) of branchial pouches/arches (#57).

59. Branchial series extends: 0, substantially less than half the body length; 1, semiequal to or greater than half the body length (**new character**).

    This character correlates with the number of branchial arches (#56-58, this analysis) in that none of those constrained to five branchial arches score for the derived state. However, the character distinguishes a component of the variation independent from just meristics. The taxa coded for the derived state of this character (*Achanarella*, *Euphanerops*, and heterostracomorphs) vary in the number of branchial arches, whereas some forms with a large number of branchial arches are coded for the primitive state (e.g., anaspids, myxinoids, and osteostracans).

60. Lateral branchial openings: 0, at similar horizontal level; 1, in a posteroventrally inclined row (CMC #30; **definition modified**).

    The character is inapplicable for those with a highly depressiform profile (#82, this analysis) or those with parabranchial cavities (#52, this analysis).

61. Opercular flaps associated with branchial openings: 0, absent; 1, present (CMC #32).

    Coding has been revised according to Gabbott et al. (2016).

62. Branchial epithelium: 0, internal; 1, external (**new character**).

    The suggestion of externally exposed branchial structures in *Haikouella* and *Pikaia* (Conway Morris and Caron, 2012) is provisionally accepted.

63. External branchial openings, demarcated by: 0, single element entirely; 1, single element dorsally; 2, multiple plates; 3, a framework of multiple spines; 4, micromeres; 5, naked (mineralized exoskeleton locally absent around the openings) (**new character**).

    This character is contingent on the presence of mineralized integumentary skeleton (#113, this analysis). Even though inapplicable status ("-") is assigned accordingly, these character states necessarily correlate with micro-/macromeric integumentary skeletons. Nevertheless, the character is included because some variations do exist within and among lineages (e.g., anaspids). It is defined as an unordered and compound multistate character because each state is discrete from one another and because no two states can be reasonably grouped in exclusion of others. For example, birkeniids exhibit both states 0 and 3 (Blom et al., 2001). The order of character states does not reflect any discernible trend or logic of progression.

64. Position of mouth: 0, terminal; 1, subterminal (CMC #35; **definition modified**).

    Mouth orientation is correlated partly with overall body profile (#82, this analysis), but position of mouth with respect to other cranial landmarks (e.g., nasohypophyseal canal) can vary independently of the overall body profile.

65. Epidermal oral cirri: 0, absent; 1, present (**new character**).

66. Postoptically derived ectomsenchyme anterior to mandibular arch gives rise to palatal structures that: 0, meet at midline under nasal/nasohypophyseal organs; 1, meet at dorsal midline anterior to nasohypophyseal organs and form a prominent oral roof (**new character**).

    In vertebrates, three streams of neural crest cells populate the premandibular and mandibular regions (Kuratani et al., 2001, 2016; Kuratani, 2012; Oisi et al., 2013b; Miyashita, 2016). Among them, the postoptic stream gives rise to a posthypophyseal process (upper lip) in cyclostomes (Kuratani et al., 2001; Oisi et al., 2013b), whereas it forms the trabecular cartilage anterior to the adenohypophysis in crown gnathostomes (Shigetani et al., 2002; Kuratani, 2012; Kuratani et al., 2013). Although these structures differ in topology between cyclostomes and crown gnathostomes (due to a tripartite organization of the nasohypophyseal placode in the latter), the postoptic streams still meet

at the midline and extend anteriorly. The structures arising in the postoptically derived ectomesenchyme may form the palate between the nasohypophyseal canal and the oral cavity (hagfish) or shift the palate to the dorsal side into an oral hood (lampreys) (Oisi et al., 2013b). The character definition is formulated to describe these two phenotypes while reflecting topological differences in the structures derived from the postoptic ectomesenchyme. Invertebrate outgroups have neither neural crest ectomesenchyme nor explicit homologues of the structures used to identify the region (e.g., nasohypophyseal system, trigeminal nerve, mandibular arch, forebrain). Therefore, the character is inapplicable. Similarly, a specific character state cannot be assigned to *Pipiscius* and *Tullimonstrum* ("?") because neither preserves landmarks and correlates to identify the area occupied by the postoptic ectomesenchyme. *Pipiscius* has an oral funnel similar to that of a lamprey (Bardack and Richardson, 1977; Shu et al., 1999a), but no clear statement can be made about whether it was derived from the postoptic ectomesenchyme. For the same reason, *Tullimonstrum* cannot be scored for this character. The identity of putative tectal cartilages in this animal has been since questioned (Sallan et al., 2017), and no unambiguous nasohypophyseal opening has been identified (McCoy et al., 2016).

However, *Haikoichthys* and *Metaspriggina* may be scored provisionally for the character on the basis of the position of the nasal capsules, eyes, and mouth (Shu et al., 2003b; Conway Morris and Caron, 2014). Coding these taxa for this character potentially conflicts with the assessment for the characters about neural crest (#1) and prechordal cranium (#3). Both *Haikouichthys* and *Metaspriggina* were coded as unknown for having skeletal derivatives of neural crest (#1: ?) and lacking a prechordal cranium (#3: 0). By coding for the primitive state of this character, it implies either: (***a***) *Haikouichthys* and *Metaspriggina* potentially had neural crest ectomesenchyme migrating to occupy similar positions as in cyclostomes (#66: 0), but it did not differentiate into a prominent prechordal cranium (#3: 0) and might not even have acquired skeletal differentiation (#1: ?); or (***b***) both taxa did not have neural crest, but the cephalic ectoderm was patterned similarly (Shigetani et al., 2002; Kuratani et al., 2013), such that the corresponding regions may be identified. These implications are considered reasonable for this analysis.

67. Velum: 0, absent; 1, present (CMC #37; **coding modified**).

There is no velum in cephalochordates. All non-vertebrate taxa are coded as inapplicable

because a velum assumes the presence of a mandibular arch. Contrary to McCoy et al.'s assessment, hagfish do possess a velum. The functional necessity of having a valve/pump at the mandibular arch, coupled with some osteological correlates (Janvier, 1981b, 1985b; Miyashita, 2016), led to provisional coding of galeaspids and osteostracans as having a velum or velum-like structure. This assessment is consistent with Gabbott et al.'s (2016) analysis.

68. Velar cartilages: 0, at hyomandibular position; 1, extend posteriorly (**new character**).

    This character is contingent on the presence of a velum (#67).

69. Velar cartilages, functions at terminal ontogenetic stages: 0, pump and valve; 1, valve (**new character**).

    The character may partly correlate with position of velar cartilages (#68), but these characters are controlled independently to some extent, as the velum functions as both a pump and a valve in the larval stages of lampreys.

70. Velar wings: 0, absent; 1, present (**new character**).

    This character only applies to petromyzontiforms. The coding follows Gill et al. (2003) and Renaud et al. (2009).

71. Velar tentacles, papillae or tubercles: 0, absent; 1, present (**new character**).

    This character only applies to petromyzontiforms. The coding follows Gill et al. (2003) and Renaud et al. (2009).

2.8.5c Circulatory system

72. Multi-chamber heart: 0, absent; 1, present (CMC #38; **coding modified**).

    It is unknown ("?") whether the heart has multiple chambers in *Haikouichthys*, *Metaspriggina*, and *Myllokunmingia*.

73. Closed pericardium: 0, absent; 1, present (CMC #39).

74. Circulatory system: 0, open; 1, closed (CMC #40; **definition modified**).

    The original character in the CMC dataset was defined and scored as if the circulatory system was open in vertebrates. The circulatory system of hagfish is considered closed, and the extensive subcutaneous sinus is interpreted as a specialization (Davison, 2015) — perhaps associated with the cutaneous exchange and transport of various substances (Glover et al., 2011). This specialization is related to the fact that hagfish are

osmoconformers, but it is difficult to determine which character preceded (or capacitated) the other.

75. Massive subcutaneous sinus: 0, absent; 1, present (CMC #95; **definition modified**).

    The original character (high blood pressure, absent or present) was vaguely defined. In that form, the character is redundant with the closed/open circulatory system (#74) and with the absence/presence of a multichambered heart (#72). The character was modified to refer to the specialized subcutaneous blood sinus present in hagfish. As the sinus extends the entire body length (collected both from the head and tail), the presence of this sinus can be ruled out for stem gnathostomes with a dermal head skeleton with internal impressions.

76. Paired dorsal aortae: 0, absent; 1, present (CMC #41).

77. Lateral head vein: 0, drains into anterior cardinal vein or its derivative; 1, continues into (or functions as anterior extension of) anterior cardinal vein or its derivative (CMC #42; **definition modified**).

    The original character (large lateral head vein, absent or present) is vague in definition. Lampreys have (***a***) a vein collecting from the anterior and middle cerebral regions and (***b***) a vein collecting from the velar sinus, and both drain into the anterior cardinal vein (Cori, 1906). Hagfish have a cardinal heart (=velar sinus) collecting broadly from the head and draining into anterior cardinal vein (Cole, 1926). Osteostracans have a lateral head vein and an enormous marginal vein that corresponds in position to the anterior cardinal vein in other vertebrates (Janvier, 1981b, 1985a; Janvier et al., 1991). This makes galeaspids unique among jawless vertebrates for having an enormous lateral head vein collecting from the cerebral veins and continues into the anterior cardinal vein (Gai et al., 2011).

78. Lymphocytes: 0, absent; 1, present (CMC #43).

79. Lymphocytes antigen receptors: 0, VLR; 1, T and B (CMC #105; **coding modified**).

    The character is inapplicable to those that lack lymphocytes (#78, this analysis).

80. Subaponeurotic vascular plexus: 0, absent; 1, present (CMC #44; **coding modified**).

    The character is inapplicable to non-vertebrate outgroups.

2.8.5d Fins and fin-folds

81. Body forms, relative length: 0, less than five times the next largest dimension (height or

width); 1, greater than five but less than ten times; 2, greater than ten times (**new character**).

To be conservative with effects of taphonomy and decay, maximum dimension is interpreted at the plane of preservation (so it is more likely to underestimate relative length than to overestimate). Admittedly, body profile is a poorly defined composite character but also constitutes one of few biologically informative composite traits that can be observed in poorly preserved early vertebrates.

82. Body forms, width against height: 0, compressed or subcircular so that branchial openings are lateral; 1, depressed so that branchial openings are ventral (CMC #31; **definition modified**).

The original character (openings lateral or ventral) describes body proportions rather than branchial morphology.

83. Endoskeletal fin supports: 0, absent; 1, present (CMC #48; **definition modified**).

The original character (fin ray support, absent or present) is modified to distinguish endoskeletal and exoskeletal (dermal) components of the fin skeleton from one another. In the original dataset, fin rays (exoskeleton) and radials (endoskeleton) appear to have been confused. Contrary to the original coding, endoskeletal fin radials are present in hagfish ("1") (Ayers and Jackson, 1901; Cole, 1905; Janvier, 1981a). *Haikouella* is coded as absent ("0"). The exoskeletal component of the fin skeleton (rays) is described in a separate character (#116, this analysis).

84. Distinct dorsal fin: 0, absent; 1, present (CMC #45; **coding modified**).

Contrary to the assessment by McCoy et al. (2016), hagfish do not have a separate dorsal fin. Coding strategies by Gabbott et al. (2016) are followed for other taxa, except for the absence of separate dorsal fin in *Haikouella* and *Metaspriggina* ("0" in this analysis). As for *Metaspriggina*, the body outline is generally well preserved in the Burgess fauna. It is possible that this animal had a soft fin fold, but it is unlikely that *Metaspriggina* had a prominent dorsal fin as an individual unit.

85. Dorsal fins: 1, continuous or adjacent to one another; 1, set apart from each other widely (**new character**).

This character is intended to discriminate ingroup relationships of living lampreys; therefore, it is inapplicable outside the crown clade.

86. Fin(s) along dorsal midline originates: 0, above branchial series or anterior to mid-trunk; 1, above anus/anal fin or anterior; 2, posteriorly to anus/anal fin (CMC #46; **definition**

modified).

The original character (dorsal fin originates above or posterior to branchial series) is contingent on the presence of distinct dorsal fin (#84, this analysis). In the new definition, the character describes functional property (fins along the dorsal midline) rather than specialization (whether dorsal fin should be interpreted as part of fin fold or a distinct unit, and whether taxa with a midline fin extending to the dorsal side should be coded or excluded). To reflect this change, a new landmark (anus/anal fin) is added to accommodate the range of variation. For cephalochordates, *Haikouella*, *Metaspriggina*, and *Pikaia*, the fin fold is distinguished by a deflection in the outline. The fin arguably extends further anteriorly in these taxa, but it is little more than a dorsal midline ridge. By this criterion, all of them except cephalochordates are coded as unknown ("?") or inapplicable ("-"). In McCoy et al.'s (2016) analysis, *Astraspis* and galeaspids were originally coded for the derived state ("1") presumably on the assumption that the fin — if present — would have originated well posterior to the level of the branchial series, but fin morphology is poorly understood for these taxa. Therefore, the coding is unknown ("?") for the present analysis.

87. Separate anal fin, or a distinct median ventral fin in postanal tail: 0, absent; 1, present (CMC #47; **coding modified**).

In comparison to *Euphanerops* (Stensiö, 1939; Janvier et al., 2006; Janvier and Arsenault, 2007; Sansom et al., 2013b), *Achanarella* is coded for the presence of an anal fin because of the pronounced epidermal ridge anterior to the caudal fin (Newman, 2002). As for osteostracans, it is debatable whether the ventral lobe of the terminal fin represents a modified anal fin or constitutes a part of the caudal fin. This is reminiscent of the abnormal anal fin reported for a female of *Petromyzon marinus* (Vladykov, 1973). In this analysis, they are coded conservatively as absence of the anal fin.

88. Paired skin folds (epidermal ridges) at suprapharyngeal position: 0, absent; 1, present (**new character**).

This character discriminates thelodonts (Märss et al., 2007; Wilson et al., 2007) and is inapplicable to those with macromeric dermal plates forming a head shield (#133, this analysis). However, the margin of the shield in osteostracans and galeaspids may be argued as an epidermal ridge, and the position of the marginal vein (=anterior cardinal

vein) in osteostracans indicates that the margin forms in the suprapharyngeal position corresponding to the paired flaps of thelodonts. Incidentally, this domain corresponds to the circumpharyngeal crest (Kuratani, 2008), or the suprapharyngeal head-trunk boundary. In this analysis, these taxa are coded following this assessment.

89. Constricted pectoral fins with endoskeletal elements: 0, absent; 1, present (CMC #50; **coding modified**).

    McCoy et al. (2016) coded pectoral fins as present ("1") in hagfish but the correct state is absent ("0"). Among jawless vertebrates, only osteostracans provide direct evidence of endoskeletal support for the pectoral fins (Johanson, 2002; Janvier et al., 2004), but this condition is likely shared with pituriaspids (Young, 1991; Janvier, 1996a; Wilson et al., 2007).

90. Conspicuous preanal skin fold (epidermal ridge): 0, absent; 1, present (CMC #54; **definition modified**).

    Myllokunmigia is coded as present ("1") based on observations of specimens. *Tullimonstrum* is coded as unknown ("?") as the presence of skin fold is questioned (Sallan et al. 2017). To accommodate taxa with pelvic fins or with paired folds along ventral midline, the original definition (preanal median fold, absent or present) is modified. In *Cornovichthys*, the branchial series appears to extend close to the ventral fin, and the gut trace extending posteriorly above it (Newman and Trewin, 2001). The ventral fin is therefore considered preanal.

91. Preanal skin fold (epidermal ridge): 0, midline; 1, paired (CMC #49, 106; **definition modified**).

    The definition now includes pelvic fins as paired preanal epidermal ridges. The taxa without preanal skin fold (#90, this analysis) are coded as inapplicable.

92. Preanal skin fold (epidermal ridge): 0, longitudinal; 1, discrete pelvic fins (CMC #51; **definition modified**).

    As for pectoral fins, hagfish were miscoded as present in MSL dataset; this is corrected. The taxa without a preanal skin fold (#90, this analysis) are coded inapplicable. *Cornovichthys* is unique in having a single discrete preanal fin (Newman and Trewin, 2001).

93. Tail shape: 0, no distinct lobes developed; 1, ventral lobe much larger than dorsal; 2, dorsal

lobe much larger than ventral; 3, dorsal and ventral lobes almost equally developed (CMC #52; **coding modified**).

The following changes were made to the MSL dataset based on personal observations of specimens: Euconodonta, *Haikouella*, hagfish, lampreys, *Tullimonstrum* ("0"); euphaneropids and thelodonts ("1"); arandaspids ("2").

94. Chordal disposition relative to tail development: 0, isochordal; 1, hypochordal; 2, hyperchordal (CMC #53; **coding modified**)

Based on personal observation of specimens, *Achanarella* and *Cornovichthys* are coded for the hypochordal state ("1"). Character state is unknown for *Tullimonstrum* ("?").

2.8.5e Skeletal characters

95. Skeletal elements consisting of calcium phosphate: 0, absent; 1, present (CMC #55; **definition modified**).

The original definition (the endogenous ability to synthesize creatine phosphatase) (Donoghue et al., 2000) cannot be assessed adequately in living outgroups because of structural variations and diversity of creatine kinases and because of the lack of exhaustive comparison. Indeed, phosphocreatine and creatine kinase are abundant within and outside vertebrates. The modified definition distinguishes the presence/absence of mineralized skeleton consisting of calcium phosphates (which requires endogenous creatine phosphatase) (Suzuki et al., 2004; DeLigio and Ellington, 2006; Bertin et al., 2007; Ellington and Suzuki, 2007). Mineralized ossicles in hemichordates are aragonitic (Cameron and Bishop, 2012) — therefore this taxon is coded as absent. Lampreys are originally coded for the presence of this character, presumably on the basis of otolith or otolith-like structures in the crown and stem lampreys (Janvier and Lund, 1983; Avallone et al., 2007). However, crystallization of statoliths cannot be treated equally as mineralization of skeletal matrix (Avallone et al., 2007), and the experimental calcification of lamprey cartilages (Langille and Hall, 1993) occurred strictly *in vitro* under high calcium concentrations. Therefore, cyclostomes are coded for the absence of this character in the present analysis (the presence of calcium phosphatic statoliths is treated in a separate character: #37, this analysis).

The Ca signal detected in the trunk structures of *Jamoytius* (Sansom et al., 2010b)

is accepted as evidence for a mineralized skeleton, so this taxon is scored for the subsequent characters regarding mineralized skeletons unless stated otherwise. On the other hand, *Achanarella* and *Ciderius* are coded conservatively for the absence of mineralized skeletons ("0"). These taxa show no evidence of macroscopic mineralized skeletons, but have been closely compared with *Euphanerops* and *Jamoytius* and are substantially smaller in size than both. They have not been tested for the presence of mineralized elements as identified in *Jamoytius*. The structures in *Jamoytius* may also represent a size-related feature. So the alternative coding (not employed in the present analysis) is to score this character as unknown ("?") and to score the absence of skeletal tissues that are certainly missing (e.g., hypermineralized tissues such as dentine and enameloid).

96. Bone: 0, absent; 1, present (**new character**).

This character is contingent on the presence of calcification/ossification in endo- and/or exoskeleton (#95, this analysis). *Palaeospondylus* is coded conservatively as absent ("0"). The skeleton of *Palaeospondylus* does not consist of bone, but is histologically best compared to endochondral ossification in osteichthyans, implying an ontogenetically immature state (Johanson et al., 2010). So an alternative coding (not used herein) is to score unknown ("?"). Chondrichthyans are coded the presence on the basis of acanthodians (Valiukevičius, 1995; Burrow and Valiukevičius, 2005; Sire et al., 2009), even though bone is absent in the crown group (Gillis and Donoghue, 2007).

97. Cellular bone: 0, absent; 1, present (CMC #79; **coding modified**).

The character is contingent on the presence of bone (#96, this analysis). Two alternative coding strategies exist for this and the following character: (***a***) formulate one character distinguishing acellular against cellular bone or (***b***) formulate one character each for the presence/absence of acellular and cellular bone. The alternative (***a***) may be preferable in principle to not weight either of the characters; however, in many taxa acellular and cellular bones coexist (Witten et al., 2010; Hall, 2015), and both acellular and cellular bones distribute widely among stem chondrichthyans (acanthodians) and osteichthyans (Donoghue and Sansom, 2002; Sire and Huysseune, 2003; Donoghue et al., 2006; Sire et al., 2009). So these two tissue types should be treated separately as in the alternative (***b***). To make the character for acellular bone more specific, and to distinguish types of

plywood-like bone in osteichthyans, the following character for the presence/absence of acellular bone is edited to refer specifically to lamellar acellular bone seen in fossil jawless vertebrates.

98. Lamellar acellular bone (isopedine): 0, absent; 1, present (CMC #78; **definition modified**).
This character is contingent on the presence of bone (#96). The taxa lacking them are coded as inapplicable ("-").

99. Perichondral bone: 0, absent; 1, present (CMC #74; **coding modified**).
This character is contingent on the presence of cartilage and mineralized skeleton (#95, this analysis), so it is inapplicable to the taxa that lack one or both.

100. Calcified cartilage: 0, absent; 1, present (CMC #75; **coding modified**).
As in the previous character, it is contingent on the presence of cartilage and mineralized skeleton (#95).

101. Cellular cartilages with large mature chondrocytes (30-50 μm in diameter): 0, absent; 1, present (CMC #76; **definition modified**).
This character is contingent on the presence of cellular cartilages, so it is inapplicable to taxa lacking them (hemichordates and tunicates). Lacunae occupied by chondrocytes are unusually large in lampreys, *Euphanerops*, and *Palaeospondylus* (>30 μm) (Wright and Youson, 1983; Wright et al., 1988; Robson et al., 1997; Janvier and Arsenault, 2002, 2007; Johanson et al., 2010). However, hypertrophied chondrocytes in the growth plates and articular cartilages in living gnathostomes can also reach or even exceed this size (Hall, 2015). The assessment of the enlarged chondrocytes as specific to those three taxa (Johanson et al., 2010) may be influenced by the fact that chondrocyte sizes are not typically reported or systematically surveyed in extant vertebrates. The currently available data still suggest that they exhibit unusual sizes of mature chondrocytes, with the exclusion of hypertrophic chondrocytes that are either transient or specific to the growing tissues (so the character definition should not refer to hypertrophy). The original definition ("huge clumped" chondrocytes, absent or present) was modified accordingly. That original character was split into two because the nested organization of chondrocytes ("clumped") varies independently.

102. Mature chondrocytes: 0, become separated and generally even spaced by extracellular matrix; 1, remain nested in a pair (CMC #76; **definition modified**).

This character is contingent on the presence of cellular cartilages, so it is inapplicable to taxa lacking cartilages (hemichordates and tunicates). Lampreys and *Euphanerops* are unusual in having chondrocytes nested in a pair within the cartilaginous matrix (Janvier and Arsenault, 2002, 2007; Johanson et al., 2010). Although such pairing organization broadly occurs in growing cartilages within and outside vertebrates (Miyashita, 2012; Hall, 2015; Jandzik et al., 2015), retention of such organization in fully mature chondrocytes sets lampreys and *Euphanerops* apart from others. The original definition combined this feature with large sizes of the chondrocytes (see previous character), but this condition varies independently. The character was therefore split into two, and the present character is now defined on the basis of the mature status of chondrocytes.

103. Dentine: 0, absent; 1, present (CMC #80; **coding modified**).

This character is contingent on the presence of mineralized skeleton (#95, this analysis). The identification of dentine in anaspids (Keating and Donoghue, 2016) is accepted preliminarily in this analysis, although some inferences used by Keating and Donoghue (2016) are insufficiently justified. For example, they refer to Smith and Hall (1990) to state: "[cartilage] never occurs in dermal skeleton." However, cartilages form a component of dermal skeleton, exoskeleton, or intramembranously ossified bones, whichever is intended by the authors (e.g., articular cartilages on dermal or intramembranously formed elements; secondary cartilages; adventitious cartilages; callus cartilages; orbitosphenoids in amphisbaenians) (Hall, 2015). Nor can dermal bone be readily ruled out solely on the basis of histological distinctions from the underlying layer, partly because the criteria to differentiate histological features are not clear (among the cited examples, galeaspids and placoderms show some degrees of differentiation; Zhu and Janvier, 1998; Wang et al., 2005; Downs and Donoghue, 2009; Rücklin et al., 2012; Giles et al., 2013), and partly because little evidence justifies the assumption that two different types of dermal bone should not coexist in the same element. The association of enamel/oid and dentine would be a valid argument if the thin superficial layer is not an artifact of scanning but represents a true enamel/oid layer (Gillis and Donoghue, 2007). Furthermore, it is odd that tubules are lacking in the proposed dentine in birkeniids. Accepting their observations preliminarily, however, dentine is coded as present in birkeniids. *Lasanius* is coded as unknown for the lack of information.

104. Spherical/globular dentine: 0, absent; 1, present (**new character**).

This character is contigent on the presence of dentine (#103). Spherical/globular dentine occurs in anaspids and conodonts among jawless vertebrates (Sansom et al., 1994; Donoghue et al., 2000; Murdock et al., 2013; Keating and Donoghue, 2016). Spherical mineralization similar to that in anaspids also occurs in galeaspids (Zhu and Janvier, 1998; Wang et al., 2005), but there is no further support that this tissue represents true dentine. The condition in arandaspids (Sansom et al., 2005) is interpreted as tubular. As in the characters describing different types of bones, two alternatives exist for this and the following character: (***a***) formulate one character distinguishing tubular versus spherical dentines or (***b***) formulate one character each for the presence/absence of tubular and spherical dentines. The alternative (***a***) does not weight either of the characters; however, the two types coexist in conodonts and some crown gnathostomes. So these two tissue types should be treated separately as in alternative (***b***).

105. Tubular dentine: 0, absent; 1, present (CMC #80; modified by KD #84).

The original definition is modified to refer specifically to tubular dentine. Taxa lacking dentine are coded as inapplicable.

106. Tubular dentine, odontobalsts tend to: 0, retreat into pulp cavity; 1, remain in dentinous matrix (CMC #81; **definition modified**).

Given the diversity of dentinous tissues among early vertebrates, the original definition (mesodentine or orthodentine) is modified into three independent characters (#106-108, this analysis) that describe histological differences in multiple types of dentine at the level of odontoblasts. All of these three characters are contingent on the presence of tubular dentine (#105, this analysis; inapplicable to the globular/spherical dentine in anaspids). The present character distinguishes mesodentine and semidentine from other types of dentine. Different types of dentine may coexist in the same animal or within a lineage. Thus, they are coded on the basis of typical histological characteristics identified in that taxonomic unit. The character is contingent on the presence of dentine (#103, this analysis).

Conodonts are coded as having a dentine type somewhat comparable to mesodentine (Sansom et al., 1994; Donoghue, 1998; Donoghue et al., 2000). *Astraspis* is considered having the grade of meta- to orthodentine (Sire et al., 2009) (coded as 0),

although this assessment is at odds with interpretations of the canals invading from the pulp cavity (Ørvig, 1989; Sansom et al., 1997). Thelodonts exhibit a diversity of dentine histology (Janvier, 1996a; Märss et al., 2007; Sire et al., 2009). In general, however, the canaliculi show polarized but irregular branching and spacing as in *Turinia* in the grade of meta- to orthodentine. *Loganellia* is coded as having the grade of mesodentine.

107. Tubular dentine, interconnections of tubules/canaliculi for odontoblasts tend to be: 0, polarized; 1, non-polarized (CMC #81; **definition modified**).

108. Tubular dentine, interconnections of canaliculi and spacing between odontoblasts tend to be: 0, regular; 1, irregular (CMC #81; **definition modified**).

109. Enamel/oid: 0, absent; 1, present (CMC #82; **definition modified**).

As in other characters coding for skeletal tissues, the original character is split into two so that one only refers to the presence/absence and the other describes monotypic versus bitypic. The presence of enameloid is accepted preliminarily in anaspids (Keating and Donoghue, 2016) and heterostracans (Keating et al., 2015). Osteostracans are coded as present, as thyestidians unambiguously developed enameloid (Qu et al., 2015a). Although thyestidians form a nested ingroup within osteostracans (Sansom, 2008, 2009), it is more plausible to consider that the potential to secrete enamel/oid is conserved within osteostracans than to assume that enamel evolved secondarily. In a similar vein, euconodonts evolved enameloid independently from the rest of vertebrates (Murdock et al., 2013) but this lineage is coded as present.

Although enamel as a tissue likely evolved convergently, it also remains unclear how many times enamel, enameloid, and enamel-like tissues evolved within vertebrates. As this analysis does not heavily sample taxa at lower taxonomic levels, this character should be coded as the potential to secrete enamel or enamel-like tissues rather than the distribution of the tissue within each lineage. Alternatively, the character may be defined more finely to differentiate the known types of enamel and enamel-like tissues, but this is beyond the scope of this analysis as these characters will be parsimony-uninformative in the taxon sampling of this dataset. The present character is contingent on the presence of dentine (odontodes) (#103, this analysis). This contingency is not reciprocal (the character for dentine is not contingent on the presence of enamel/oid), however, as naked dentines occur in osteostracans and various crown gnathostomes (Janvier, 1996a; Sire et al., 2009;

Qu et al., 2015b).

110. Enamel/oid: 0, monotypic; 1, bitypic (CMC #82; **definition modified**).

The character is contingent on the presence of enamel/oid (#109, this analysis).

111. Calcification/ossification occurs in endoskeleton: 0, absent; 1, present (**new character**).

Given variations and overlaps in cell lineages and modes of mineralization to give rise to hard skeletal elements (Smith and Hall, 1990; Hall and Miyake, 2000; Sire and Huysseune, 2003; Witten and Huysseune, 2009; Lee et al., 2013a; Mongera and Nüsslein-Volhard, 2013; Hall, 2015), it is difficult to formulate a character to distinguish skeletal elements by either of the criteria and score fossil OTUs on the basis of information from living models. However, endo- and exo-skeleton can be clearly distinguished on the basis of anatomy alone, with predicted functional implications. Contingent on the presence of mineralized skeletons (#95).

112. Calcification/ossification occurs in exoskeleton: 0, absent; 1, present (CMC #76; **definition modified**).

Mineralization may occur in one or both of endo- and exo-skeletons, and the states may vary independently between internally and externally. This character is contingent on the presence of mineralized skeletons (#95, this analysis).

113. Mineralized integumentary skeleton (scales and plates): 0, absent in trunk; 1, present in trunk (CMC #72; **definition modified**).

This character is contingent on the presence of mineralized exoskeleton (#112, this analysis), so taxa without it are coded inapplicable. See character #116 (this analysis) for coding of fin exoskeleton. The original definition (dermal skeleton in trunk) was modified because some taxa have mineralized dermal skeletons within appendages but not on surface of the trunk (e.g., *Euphanerops*), whereas the combination is the reverse in others (e.g., osteostracans). Hemichordates are coded as absent — although they have aragonitic ossicles (Cameron and Bishop, 2012), the ossicles are neither integumentary nor calcified/ossified. So these variations appear to be independently controlled. Conodonts and *Palaeospondylus* are scored as absent for this character rather than designated inapplicable. This is because of the presence of the mineralized feeding apparatus. The apparatuses are topographically internal structures, but are generally considered dermal elements.

114. Mineralized integumentary skeleton in trunk, surface coverage: 0, extensive; 1, limited (with evidence for variation and potentials for reduction) (**new character**).

The character is contingent on the previous character (#113, this analysis) and is intended to discriminate the condition in taxa such as *Lasanius* and placoderms, which only have partial coverage of the trunk with mineralized scales/plates.

115. Odontodes: 0, monodontodes; 1, polyodontodes (CMC #108; **coding modified**).

In addition to contingency on the presence of odontodes (nested in the presence of dentine [#103], which is further nested in the presence of mineralized dermal skeletons [#95]), this character correlates with the sizes of dermal elements (e.g., #133, this analysis) because macromeric plates assume polyodontodes. Despite that overlap, both characters should be included in the analysis. That latter character (#133) has a broader range of application because the integumentary skeleton in some lineages (such as anaspids) does not contain typical odontodes with a pulp cavity. These taxa are designated as inapplicable for this character (#115), and coded for micro-/macromery (#133, this analysis). In a reverse case, euconodonts may be coded for this character (#115) while coded inapplicable for the other (#133). Tissues that compose the conodont 'teeth' (e.g., crown tissue, spheritic mineralization) appear to have evolved in stepwise fashion within the lineage (Murdock et al., 2013). Perhaps for this reason, they were coded inapplicable for this character by Gabbott et al. (2016). Nevertheless, the presence of these mineralized tissues and the pulp cavity qualify these elements morphologically as odontodes. Euconodonts are inapplicable for characters describing micro-/macromery (e.g., #133, this analysis) because they lack mineralized integumentary skeleton. All taxa that lack dentine (#103, this analysis) were scored as inapplicable.

116. Exoskeletal fin support: 0, absent; 1, present (**new character**).

The character is contingent on the presence of mineralized skeletons (#95, # 112, this analysis), so the inapplicable status has been assigned to those lacking them. Distal components of mineralized appendage skeletons appear to be independently controlled from the trunk dermal skeletons, and these are treated in the following characters separately. *Euphanerops* and *Palaeospondylus* score for the presence of this character but for the absence of the previous character.

117. Exoskeletal fin support, integumentary coverage of distal portions by tessellated scales: 0,

absent; 1, present (**new character**).

This character is contingent on the presence of fin exoskeleton (#116, this analysis). Chondrichthyans are coded on the basis of the morphology observed in acanthodians. The placoid scales covering the fins of extant chondrichthyans cannot be readily compared to the tessellate surface coverage in stem gnathostomes.

118. Exoskeletal fin support, organized into distinct rays distal to radials: 0, absent; 1, present (**new character**).

This character is contingent on having skeletal supports in the distal portions of the fins (#116, this analysis) and refers to the presence of lepidotrichia.

119. Exoskeleton, organization of superficial layer: 0, spherical; 1, tubular; 2, lamellar (CMC #83; KD #78; **definition modified**).

The character is contingent on the presence of mineralized exoskeleton (#95, #112, this analysis). All taxa lacking a mineralized exoskeleton are coded as inapplicable. The original character (three-layerd exoskeleton consisting of a basal lamella, middle spongy layer, and a superficial layer, absent or present) is split into three by Keating and Donoghue (2016), each describing the presence/absence of superficial, middle, and basal layers. The latter scheme better accommodates known variations in organization of the vertebrate exoskeleton. For this particular character in the present analysis (organization of superficial layer), the definition is modified from Keating and Donoghue (2016) to refer to specific conditions rather than to presence/absence. This is because: (***a***) all known exoskeletons have a superficial layer (thereby making the character constant); and (***b***) modes of mineralization differ among lineages in a parsimony-informative manner (e.g., anaspids and galeaspids share spherical mineralization in this layer; Wang et al., 2005; Keating and Donoghue, 2016).

Anaspids, thelodonts, and chondrichthyans lack the middle cancellar layer, but the latter two differ from anaspids in having the base as attachment and having a non-growing crown (Janvier, 1996a; Blom et al., 2001; Märss et al., 2007; Sire et al., 2009). These two variants should not be confused in a single state of the absence of the three-layerd exoskeleton. The calcium signature in the dermis of *Jamoytius* (Sansom et al., 2010b) is tentatively interpreted as a degenerate form of a typical anaspid condition of having a single tissue type forming a basal lamella and a superficial layer, but the specific

morphology has not been described. This taxon is therefore coded as inapplicable. Galeaspids are also interpreted as having a basal lamella and a superficial layer (variably invaded by sensory canals), regarding calcified cartilages as secondary endoskeletal lining (Zhu and Janvier, 1998; Wang et al., 2005). The tubercles in this lineage consist of spherical mineralization that superficially resembles spherical dentine of anaspids.

This character partly correlates with dentine characters (#104, #108, this analysis) but it has non-overlapping distributions. This character only codes for the integumentary skeleton so that teeth and other exoskeletal elements are excluded. Furthermore, the superficial layer does not always consist of dentine. For example, galeaspids are not coded as having spherical dentine (#104, this analysis), but the similarity with anaspids is accepted for this character as having a superficial layer of spherical mineralization (Zhu and Janvier, 1998; Wang et al., 2005). The coding for placoderms is based on a survey of previous works (Ørvig, 1980; Downs and Donoghue, 2009; Sire et al., 2009; Rücklin et al., 2012; Giles et al., 2013).

120. Exoskeleton, vascular/cancellar layer of osteons: 0, absent; 1, present (CMC #83; modified by KD #79).

This character is contingent on the presence of mineralized exoskeletons (#112, this analysis). *Jamoytius* conclusively lacks this layer (Sansom et al., 2010b), regardless of whether or not this animal had a mineralized exoskeleton. Similarly, pituriaspids probably lack this layer as well. Although the histology has not been described for this lineage, their endoskeletal shields are ornamented with minute tubercles without any indication of a thick canncellar middle layer (Young, 1991).

121. Exoskeleton, basal tissue: 0, basal lamella; 1, basal attachment (CMC #83; KD #80; **definition modified**).

This character is contingent on the presence of mineralized exoskeletons (#112, this analysis). As in the superficial layer, the original definition by Keating and Donoghue (2016) creates an invariable character (all mineralized exoskeletons have basal tissue). The modified version discriminates basal lamella (most) against basal attachment (thelodonts, stem chondrichthyans). The basal attachment consists of acellular bone with abundant Sharpey's fibres.

122. Cancellar layer in exoskeleton, with honeycomb-shaped cavities: 0, absent; 1,

present (CMC #84; **coding modified**).

This character only applies to those that score for having a middle cancellar layer.

123. Scale shape: 0, diamond-shaped; 1, rod-shaped (CMC #86; **coding modified**).

This character is contingent on the presence of a mineralized integumentary skeleton (#112, this analysis).

124. Oak-leaf-shaped tubercles: 0, absent; 1, present (CMC #87; **coding modified**).

This character is contingent on the presence of a mineralized integumentary skeleton (#112, this analysis).

125. Triradiate postbranchial spines: 0, absent; 1, present (KD #116).

This character is contingent on the presence of a mineralized integumentary skeleton in the trunk (#113, this analysis).

126. Median dorsal ridge scales: 0, absent; 1, present (KD #117).

This character is contingent on the presence of a mineralized integumentary skeleton in the trunk (#113, this analysis).

127. Median dorsal ridge scales: 0, simple; 1, hooked (KD #118).

This character is contingent on the presence of median dorsal ridge scales (#126, this analysis).

128. Vascular canal systems in integumentary skeleton: 0, absent; 1, present (KD #119).

This character is contingent on the presence of a mineralized integumentary skeleton in the trunk (#113, this analysis).

129. Scales: 0, without visceral ribs; 1, with visceral ribs (KD #120).

This character is contingent on the presence of a mineralized integumentary skeleton in the trunk (#113, this analysis).

130. Oral plates; 0, absent; 1, present (CMC #88; **coding modified**).

This character is contingent on the presence of a mineralized integumentary skeleton (#112, this analysis).

131. Odontodes: 0, restricted to exoskeleton; 1, extend into in oral cavity; 2, into pharynx (CMC #89; **definition modified**).

This character is contingent on the presence of odontodes (or dentine: #103, this analysis). The original definition (denticles in pharynx, absent or present) is modified to accommodate the topological distributions of dermal denticles in various vertebrate

lineages. The condition in euconodonts was evaluated on the basis of P elements (Purnell and von Bitter, 1992) and general histological information (Donoghue, 1998; Murdock et al., 2013).

132. Dermal head covering in adult state: 0, absent; 1, present (CMC #90; **coding modified**).

This character is contingent on the presence of a mineralized skeleton.

133. Dermal head covering in adult state: 0, micromeric; 1, large (macromeric) dermal plates or shield (CMC #109; **coding modified**).

The inapplicable status is assigned to all taxa lacking an integumentary skeleton in the head (#132, this analysis). Micromeric and macromeric elements coexist in the dermal head covering of birkeniids, but the former category dominates in surface area. They are coded as micromeric ("0") for this character, but are also subject to the characters about specific conditions of macromeric dermal skull elements (#134, 135, this analysis).

134. Dermal head covering, macromeric: 0, large unpaired plates covering dorsal and ventral sides; 1, covered by tesserae; 2, multiple plates (CMC #91; **definition modified**).

The original definition (large unpaired plates, absent or present) is modified to accommodate variations in the integumentary skeletons of the heads. The exact state in pituriaspids is unknown ("?"). Pituriaspids have a massive continuous endoskeletal shield, but the external morphology is poorly understood (Young, 1991). It perhaps resembled the condition in osteostracans, although there is no evidence of tessarae. Although the head integumentary skeleton of birkeniids mostly consists of micromeric scales, macromeric plates form the roof (coding for "2"). This character only applies to those that scored for having macromeric dermal head covering, with an exception of birkeniids.

135. Dermal head covering, macromeric/shield: 0, head and anterior trunk continuous; 1, head and anterior trunk decoupled (**new character**).

This character is contingent on the presence of a macromeric dermal head covering (#133, this analysis).

136. Endoskeletal contribution to dermal head covering: 0, absent; 1, present (CMC #92; **definition modified**).

This character refers to calcified or ossified endoskeletal cartilages lining the dermal elements (entirely or partially), which occur in galeaspids, osteostracans, and most jawed gnathostomes. Antiarchs have some endoskeletal components to the mainly dermal

skeleton at the exo-endoskeletal interface in the jaws, pectoral joints, and rhinocapsular element (Young, 1984; Johanson, 2002), although in general the dermal plates consist of exoskeletal components (Downs and Donoghue, 2009). The character coding does not discriminate macromery versus micromery, but is contingent on having a mineralized dermal skull and endoskeleton (#111, 133, this analysis). Thelodonts are coded as inapplicable, as no bones or calcified cartilages are known from these taxa.

137. Mineralized exoskeletal circumocular elements: 0, absent; 1, present (**new character**).

This character is intended to supplement morphological information from the exoskeletal circumocular skeleton to the following two characters about the endoskeletal circumocular elements. In addition to sclerotic ossicles, dermal/exoskeletal elements delineate the orbit in many vertebrate lineages. Chondrichthyans are coded on the basis of acanthodians for this character. Contingent on the presence of mineralized exoskeleton in the head (#133, this analysis).

138. Mineralized endoskeletal circumocular elements (sclerotic elements): 0, absent; 1, present (CMC #93; **definition modified**).

The original character (sclerotic ossicles, absent or present) is modified to accommodate different types of endoskeletal circumocular skeleton. The new definition includes sclerotic elements in arandaspids (Gagnier, 1993a) and optic pedicles in crown gnathostomes (Coates and Sequeira, 1998; Basden et al., 2000; Zhu et al., 2001; Young, 2008; Brazeau and Friedman, 2014; Coates et al., 2017). As the character is contingent on the presence of mineralized endoskeleton (#111, this analysis), the inapplicable status has been assigned accordingly.

139. Sclerotic endoskeleton: 0, isolated circumocular elements; 1, eye capsule or stalk (CMC #94; **definition modified**).

The original definition (eye capsule, absent or present) is modified to assign isolated sclera to a primitive status and make the character contingent on the presence of mineralized endoskeletal circumocular elements.

140. Fusion of visceral (pharyngeal) skeletal arches to neurocranium: 0, absent; 1, present (CMC #56; **coding modified**).

Visceral arches are broadly interpreted in this character as skeletal elements supporting the spaces between pharyngeal slits. In hagfish, the cartilages arising in the pharyngeal

arches consist of the facial cartilages (at the level of mandibular arch), visceral plate (at the level of hyoid arch), and the pharyngeal basket lateral to the velum (Miyashita, 2012; Oisi et al., 2013a; Kuratani et al., 2016). They are all fused to the parachordally derived cartilage near the otic capsule and in the vinicity of the trigeminal and facial nerve roots. *Haikouichthys* and *Metaspriggina* are coded on the basis of free pharyngeal skeletal elements (Shu et al., 2003b; Conway Morris and Caron, 2014). *Myxinikela* has the cartilaginous elements in the branchial region, which is connected to the neurocranial region by what appears to be collagenous structures (Bardack, 1991, 1998). In hemichordates and tunicates this character is inapplicable.

141. Multidenticulate/multicuspid plates housed within buccal cavity (non-odontodes): 0, absent; 1, present (CMC #58; **definition modified**).

The original definition of 'circumoral teeth' does not distinguish variants properly. For example, lampreys have multicuspid piston tooth plates within the buccal cavity and radial circumoral teeth in the oral funnel, whereas hagfish have two pairs of multicuspid tooth plates. Both were coded originally for the presence of circumoral teeth, but these variations should not be confused. Therefore, the criterion is whether the structures are housed within the buccal cavity or exposed periorally. Absence in jawless stem gnathostomes was evaluated on the basis of whether or not the perioral morphology would allow such structures. This character excludes odontodes (lip scales, gnathostomes teeth, and various perioral or oral micromeric and macromeric elements) because they are clearly not comparable to the tooth-like structures in cyclostomes (Aldridge and Donoghue, 1998; Rücklin et al., 2011; Donoghue and Rücklin, 2016) and because odontode conditions are already described by other characters (#115, 131, this analysis). The taxa meeting these latter criteria (such as conodonts and jawed gnathostomes) are coded as inapplicable.

142. Perioral/buccal feeding structure consisting of keratin: 0, absent; 1, present (CMC #57; **definition modified**).

Invertebrate outgroups are coded as inapplicable for this character. *Gilpichthys*, *Pipiscius*, and *Tullimonstrum* are coded conservatively as unknown, although geochemical comparison (McCoy et al., 2016) suggests the proposed feeding apparatus in these taxa had a similar composition. The comparison did not have a reference tissue that is clearly

keratin from the same locality.

143. Keratinous tooth plate, anterior element, number of fused cusps: 0, two; 1, three (**new character**).

This character only applies to potential myxinoids. Euconodonts are inapplicable.

144. Radially organized circumoral denticulate/cusped plates: 0, absent; 1, present (CMC #59; **definition modified**).

This character describes externally exposed, radially organized circumoral teeth. This character cannot be scored for taxa with oral plates or jaws. *Pipiscius* is coded as unknown for this character. Although the circumoral ring of cusps in this taxon superficially resembles the circumoral teeth of lampreys, it is organized in annular fashion (not radial) and embedded deeply within the oral hood as an externally open funnel. Each cusped plate is elongate and its basal tissue was probably unlike those of lampreys and hagfishes — which are organized as a cone and a cap (Marinelli and Strenger, 1954, 1956; Dawson, 1963; Krejsa et al., 1990; Miyashita, 2012).

145. Circumoral keratinous teeth, number of tooth rows in lateral field: 0, three; 1, four; 2, five or greater (**new character**).

This character applies to lampreys only. For the terminology of the circumoral filed, see Hubbs and Potter (Hubbs and Potter, 1971).

146. Cartilaginous trematic rings: 0, absent; 1, present (CMC #60; **coding modified**).

The extrabranchial cartilages in hagfish are considered provisionally as comparable to trematic rings in lampreys (Miyashita, 2012).

147. Axial skeletal condensations derived from sclerotomes: 0, absent; 1, present (CMC #61; **definition modified**).

The original character (arcualia, absent or present) does not capture the diversity of sclerotome-derived axial skeletons in vertebrates because the distribution of arcualia can be variably interpreted. Neural arches, centra, and haemal arches are the midline elements of the axial skeleton, and the centra consist of basidorsal, basiventral, interdorsal, and interventral ossification centers (Goodrich, 1930). These elements are distributed taxonomically as mosaics — lampreys have neural arches, whereas hagfish have the elements that can be interpreted as a haemal arch-like structure anatomically (Miyashita and Coates, 2016), or as vestigial vertebrae (Ota et al., 2011). *Euphanerops* appears to

have all elements as calcified cartilages (Janvier and Arsenault, 2006). Therefore, this character is more broadly defined and followed by three characters that describe contingent conditions of the axial skeletons. These subsequent characters are inapplicable to those in which the axial skeleton is absent. The 'arcualia' of *Tullimonstrum* (McCoy et al., 2016) have been since disputed (Sallan et al., 2017) so this taxon is coded as unknown ("?"). The state for this character is also unknown for *Gilpichthys*, *Metaspriggina*, and *Myllokunmingia* despite the original coding as present ("1") by McCoy et al. (2016). Heterostracans are coded on the basis of impressions of several internal casts (Janvier and Blieck, 1979). Linear rounded structures in the axial lines of *Jamoytius* (Sansom et al., 2010b) are interesting, but there is no clear evidence to indicate they are elements of the axial skeleton. There is no evidence of the axial skeleton ("?") in galeaspids.

148. Sclerotome-derived skeletons around dorsal nerve cord (=neural arches): 0, absent; 1, present (**new character**).

149. Sclerotome-derived skeletons around notochord (=centra): 0, absent; 1, present (**new character**).

150. Sclerotome-derived skeletons around dorsal aorta (=haemal arches): 0, absent; 1, present (CMC #107; **definition modified**).

In the dataset by McCoy et al. (2016), hagfish are given the state ("2") that is not explained in the character description.

151. Lingual and dental apparatus forming a pulley-like system of cartilages and protractor-retractor complex derived from mandibular arch: 0, absent; 1, present (CMC #62; **definition modified**).

The original character (piston cartilage and apical plate, absent or present) only applies to lampreys. It was therefore redefined to include the lingual and dental apparatus of hagfish. The character is inapplicable to those taxa in which no clear homologue of mandibular arch can be identified. *Pipiscius* is coded as absent, as its funnel-like arrangement of the circumoral teeth precludes a structure resembling the cyclostome lingual apparatus. Euconodonts have been suggested to have a cyclostome-like lingual apparatus (Goudemand et al., 2011), and this is functionally consistent. However, there is no anatomical evidence to indicate such a structure in a conodont. They are coded conservatively as unknown ("?"). For correlates of this morphology, see the next

character.

152. Longitudinally aligned tooth rows providing transverse bite: 0, absent; 1, present (CMC #64; **reverted to original definition** GCR #64; **coding modified**).

The coding as present in *Mayomyzon* is based on FMNH FR5687. *Myxineidus* is coded as present for this character given recent evidence (Germain et al., 2014). This character partly correlates with multidenticulate/multicuspid plates in the buccal cavity, their tissue compositions, and the associated longitudinal motions (#141, #142, #151, this analysis). However, this character concerns arrangement of the feeding apparatus, regardless of differences in and uncertainties about the other foregoing characters. The distinction of this character is important because not all such tooth-like structures are capable of a transverse bite (e.g., perioral tooth plates in living lampreys). This charater (as retained from previous analyses) also allows broader comparison. Conodonts were coded conservatively in characters #141, #142, and #151, even though they could have been coded after a cyclostome-like pattern (Goudemand et al., 2011). This character describes one aspect of the feeding apparatus in which conodonts may be compared with cyclostomes. The character is incompatible with the presence of the jaw or oral plates (#130, 153, this analysis), so it is inapplicable to any taxa having one of the two structures.

153. Jaws (dorsoventral bite): 0, absent; 1, present (CMC #65; **coding modified**).

This character is incompatible with the previous one because the transversely and vertically biting jaws cannot coexist. Therefore, those taxa scored as present for the transverse biting apparatus are scored as inapplicable for this character.

154. Parachordal cartilages: 0, absent; 1, present (**new character**).

This character describes the presence of skeletogenic paraxial mesoderm in the head. Putative cranial cartilage identified in *Metaspriggina* (Conway Morris and Caron, 2014) sits in the position of a notochord sheath (Miyashita, 2012). This is provisionally interpreted as a parachordal cartilage.

155. Braincase with lateral walls: 0, absent; 1, present (CMC #67).

The character is contingent on the presence of a tripartite brain and parachordal cartilages (#4, 154, this analysis)

156. Occiput enclosing vagus and glossopharyngeal nerves: 0, absent; 1, present (CMC #69;

coding modified).

Invertebrate outgroups are inapplicable for this character because they have no precise counterparts to cranial nerves.

157. Annular cartilage: 0, absent; 1, present (CMC #70; **coding modified**).

The structure is incompatible with the jaw (annular and jaw cartilages cannot coexist in the same animal) so jawed gnathostomes are scored as inapplicable ("-"). There is no evidence for an annular cartilage in *Pipiscius*. Although cartilages are typically represented poorly in the Mazon Creek localities (Sallan et al., 2017), the annular cartilage is fairly decay-resistant (Sansom et al., 2013a). Nothing in the circumoral ring of *Pipiscius* indicates a supporting cartilage. Even if there was one, the cartilage would not resemble the annular cartilage of a lamprey as the ring departs markedly from the morphology of the circumoral keratinous teeth in lampreys (Renaud et al., 2009). The presence of this character in *Lasanius* is on the basis of MNHN specimens under study.

158. Large oral disc: 0, absent; 1, present (CMC #71; **coding modified**).

Myxineidus is coded for the presence ("1") (Germain et al., 2014), whereas *Achanarella*, *Ciderius*, *Cornovichthys*, and *Haikouella* for the absence ("0").

159. Barbels supported by cartilages: 0, absent; 1, present (CMC #72; **definition modified**).

The character definition has been modified to allow assessment based on the outline. The cartilages supporting the barbels in living hagfish are susceptible to decay (Sansom et al., 2013a). The barbels in *Myxinikela* have been interpreted differently because the outline is not exactly well delineated in the holotype (FMNH PR15373) (Bardack, 1991, 1998, Janvier, 2008, 2015; Janvier and Sansom, 2016). The second specimen (FMNH PR8472) is currently studied, and it appears to have nasohypophyseal barbels.

160. Forked subnasal cartilage: 0, absent; 1, present (GDS #112; **coding modified**).

This character is only applicable to those in which the posthypophyseal processes meet at the midline. The presence/absence of subnasal cartilage is treated conservatively as a separate character from the presence/absence of tectal cartilages. It could be argued that the posthypophyseal processes forming a prominent oral roof in lampreys precludes rod-like cartilages supporting sensory structures in principle, and the processes forming the floor of the nasohypophyseal canal in hagfish also precludes tectal cartilages. However, this reasoning is based solely on the two living forms of cyclostomes and is therefore

circular.

161. Tectal cartilages: 0, absent; 1, present (MSL #117; **coding modified**).

This character is contingent on the presence of a posthypophyseal process meeting at the midline (cyclostome upper lip) (#66, this analysis).

2.8.5f Miscellaneous characters

162. Male gametes shed directly through the coelom: 0, absent; 1, present (CMC #97; **coding modified**).

Hagfish are coded as present for this character.

163. Postotic myomeres migrate anteriorly to the position of eye: 0, absent; 1, present absent (CMC #98; **coding modified**).

Forward migration of the anterior myomeres occurs in hagfish. The character assumes the absence of myomeres in the head and is therefore inapplicable to invertebrate chordates that lack one or more of the key attributes to assess character states. Instead, taxa with clear cephalization may be coded with the preservation of myomeric structures — these include *Metaspriggina* and conodonts. The position and orientation of spinal nerves in galeaspids and osteostracans indicate that the myomeres did not have anterior migration in a fashion similar to cyclostomes.

164. Inflected myomeres: 0, Z-shaped; 1, W-shaped (GDS #110).

The taxa lacking myomeres or having simple myomeres are designated as inapplicable. *Haikouella*, *Haikouichthys*, *Metaspriginna*, *Myllokunmingia*, and *Tullimonstrum* are coded as Z-shaped myomeres ("0"). The myomeres in *Haikouella* (Chen et al., 1999; Mallatt and Chen, 2003) show a gentle inflection also present in many specimens of *Haikouichthys* and *Metaspriggina*. The 'myomeres' in *Metapspriggina* are interpreted as unusually thick myosepta, but this does not affect identification of the state. The putative myomeric structures of *Tullimonstrum* seem to represent myosepta as well (Sallan et al., 2017), and they only show minor inflection, if at all, despite the complex shape reconstructed by McCoy et al. (2016). W-sheped myomeres are observed in some specimens of *Gilpichthys* and *Pipiscius* that are currently under study (e.g., FMNH PF8475, PF8346). This character is parsimony-informative only with both *Haikouella* and *Tullimonstrum* included.

165. Myomeric segments: 0, closely packed (typically greater than 50); 1, widely spaced (substantially fewer than 50) (**new character**).

166. Digestive tract: 0, follows pharynx; 1, passes (or loops) over branchial apparatus (**new character**).

In adult stages of lampreys, the digestive tract separates from the branchial passage and passes over the branchial region. Such separation or loop of the digestive tract dorsal to a branchial apparatus occurs in osteostracans (Janvier, 1981b, 1985a). Two conflicting interpretations have been proposed for the digestive tract of *Euphanerops*, but each reconstruction suggests either passing or looping of the tract over the branchial apparatus (Janvier and Arsenault, 2007). In furcacaudiforms, the gut trace (interpreted as stomach) extends onto the dorsal side of the branchial openings, again suggesting either passing or looping of the digestive tract over the branchial apparatus (Wilson and Caldwell, 1993, 1998). This feature is ambiguously represented in *Turinia* (coded as unknown) (Donoghue and Smith, 2001).

167. Anus, with respect to distribution of mesoderm: 0, terminal or subterminal; 1, non-terminal (**new character**).

Terminal or subterminal anus occurs in *Pikaia* (Conway Morris and Caron, 2012), *Haikouella* (Chen et al., 1995, 1999; Mallatt and Chen, 2003), and likely *Tullimonstrum* (McCoy et al., 2016; Sallan et al., 2017). The digestive tract in *Tullimonstrum* does not appear to terminate anterior to the fin flap. The tract appears to have an opening at a subterminal position in the flap, marked by a white patch (characteristic of the digestive tract in an anterior portion of the animal).

168. Globular slime glands: 0, absent; 1, present (**new character**).

Slime glands are susceptible to decay relative to other soft tissue structures (Sansom et al., 2011, 2013a), but *Tethymyxine* shows that the mechanically strong, tightly coiled, high-performance fibres of slime (α-keratin and mucin) (Ferry, 1941; Koch et al., 1991; Fudge et al., 2003, 2005, 2010; Fudge and Gosline, 2004; Winegard et al., 2014) are resistant to decay relative to other proteins. Given the high keratin composition, this character can be coded for the taxa from the localities that readily preserve keratin — structurally or chemically (Saitta et al., 2017).

169. Number of slime glands: 0, approximately 100 or fewer; 1, substantially greater than 100

(**new character**).

The character is contingent on the presence of slime glands. The number of slime glands has served as an important taxonomic character. Although there is no clear phylogenetic trend, a clear break in distribution exists around the count of 90-110 (Fernholm, 1998).

170. Slime pores: 0, overlap region of external branchial openings; 1, do not overlap region of external branchial openings (**new character**).

The character is contingent on the presence of slime glands.

171. Gular pouch in adult male: 0, absent; 1, present (**new character**).

This character is applicable only to lampreys.

2.8.6 Data Matrices

Supplementary files are available at a Dataverse depository (doi:10.7939/DVN/JGSPJN) (PDF version) or on a disc attached to the back of this thesis (print version).

Suppl. 2.1: Data matrix of morphological characters for maximum parsimony and non-clock Bayesian analyses in Nexus format.

Suppl. 2.2: Data matrix of mitogenomic sequences for Bayesian clock model analyses in Xml format.

Suppl. 2.3: Total evidence data matrix (genomics + morphology) for Bayesian clock models in Xml format.

SUPPLEMENTARY FIGURES

Fig. S2.1. The cranial anatomy of *Tethymyxine tapirostrum* (BHI 6445) in photograph (**a**) and interpretive drawing (**b**), compared to an interpretive drawing of the chondrocranium of the living hagfish *Eptatretus stoutii* (**c**) (modified from Miyashita, 2012). The lingual cartilages and nasohypophyseal barbels are distinguished as orange-coloured structures underneath dark-colored paint. They are delineated on the basis of the surface profile and geochemical signals for various elements (Figs. S2.3, S2.4). Grey areas indicate organic preservation of tissues. Stipples indicate structural preservation of soft tissues (based on surface topography).

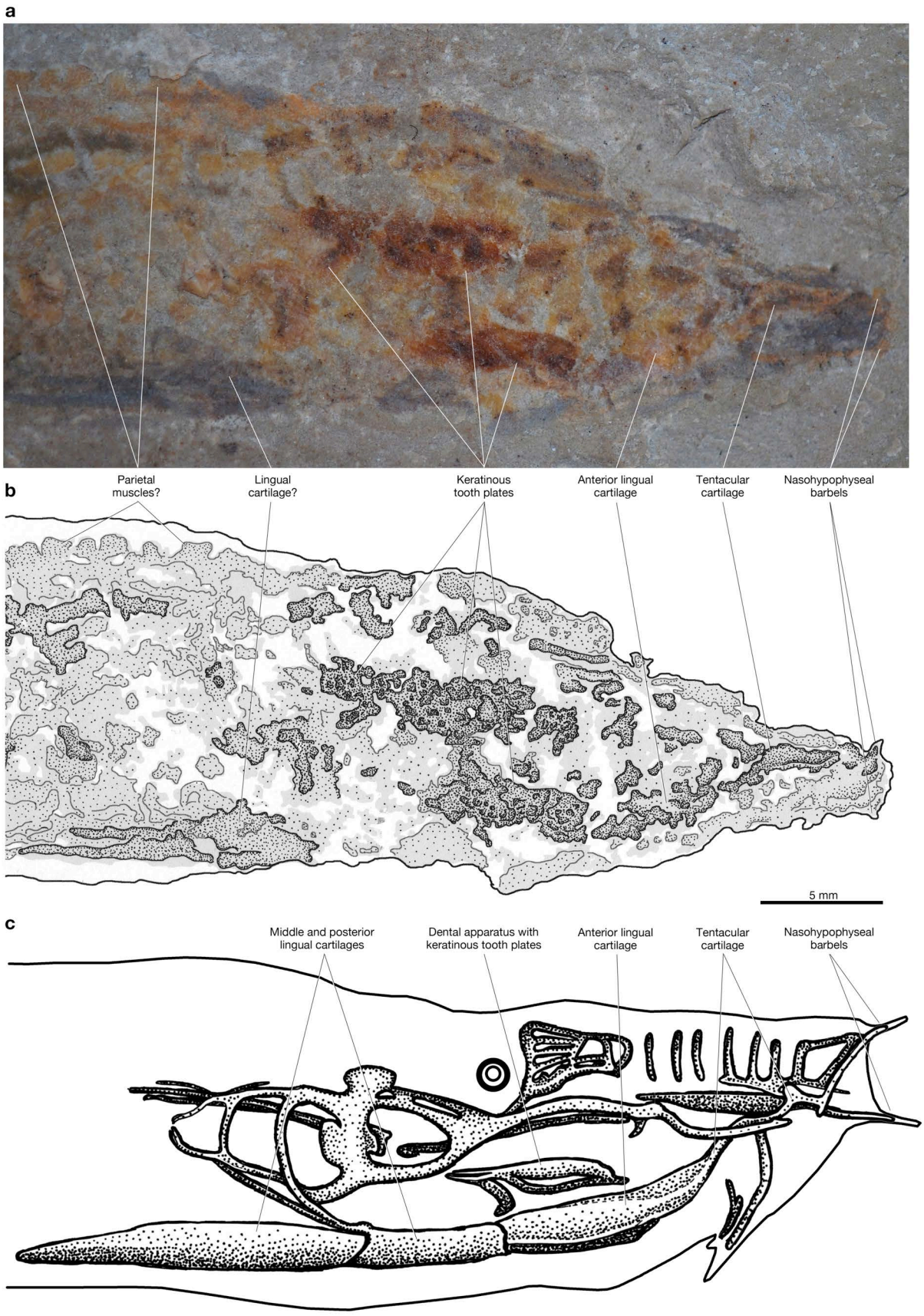
a
b
Parietal muscles?
Lingual cartilage?
Keratinous tooth plates
Anterior lingual cartilage
Tentacular cartilage
Nasohypophyseal barbels
5 mm
c
Middle and posterior lingual cartilages
Dental apparatus with keratinous tooth plates
Anterior lingual cartilage
Tentacular cartilage
Nasohypophyseal barbels

Fig. S2.2. The trunk anatomy of *Tethymyxine tapirostrum* (BHI 6445). An interpretive drawing (**a**) to indicate regions captured in individual photographic panels (**b-j**): overall visceral anatomy (**b**), anterior series of slime glands (**c**), anterior (**d**) and posterior (**e**) regions of the branchial series, posterior end of the pericardial region (**f**), liver and heart (**g**), intestine (**h**), and slime glands in the mid-trunk (**i**) and close to tail (**j**). **Abbreviations: h?**, possible heart; **int**, intestine; **lg**, left branchial pouch; **lva**, liver, anterior lobe; **lvp**, liver, posterior lobe; **rg**, right branchial pouch.

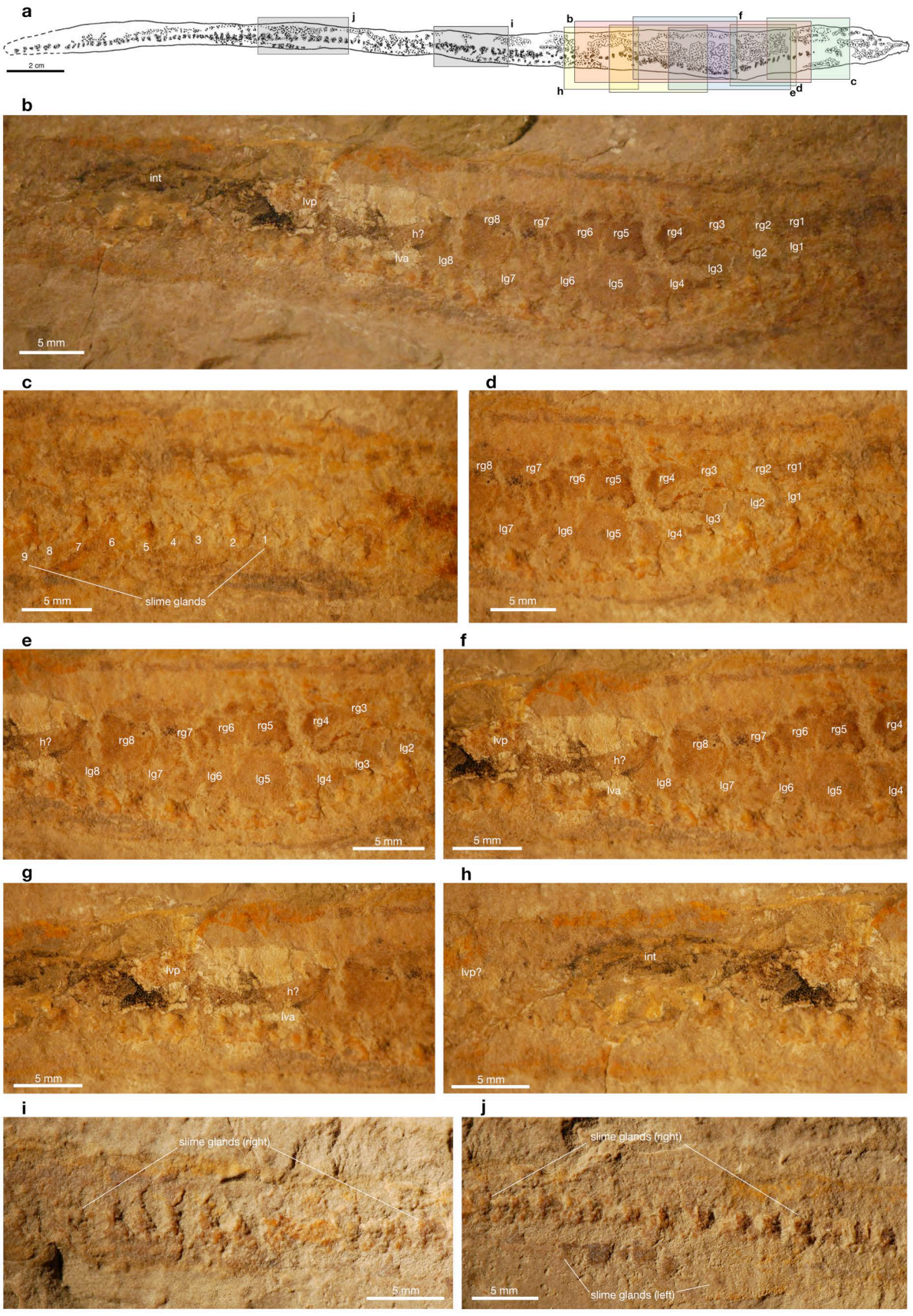
a
2 cm
j
i
b
f
h
e
d
c
b
int
lvp
h?
lva
lg8
rg8
rg7
rg6
rg5
rg4
rg3
rg2
rg1
lg2
lg1
lg3
lg7
lg6
lg5
lg4
5 mm
c
9
8
7
6
5
4
3
2
1
5 mm
slime glands
d
rg8
rg7
rg6
rg5
rg4
rg3
rg2
rg1
lg2
lg1
lg3
lg7
lg6
lg5
lg4
5 mm
e
h?
rg8
rg7
rg6
rg5
rg4
rg3
lg2
lg3
lg8
lg7
lg6
lg5
lg4
5 mm
f
lvp
h?
lva
rg8
rg7
rg6
rg5
rg4
lg8
lg7
lg6
lg5
lg4
5 mm
g
lvp
h?
lva
5 mm
h
lvp?
int
5 mm
i
slime glands (right)
5 mm
j
slime glands (right)
5 mm
slime glands (left)

Fig. S2.3. The chemical compositions of *Tethymyxine tapirostrum* (BHI 6445) in right lateral view revealed by Synchrotron Rapid-Scanning X-Ray Fluorescence (SRS-XRF). Distributions of selected elements were reconstructed through HZ mapping using a 99.9% threshold.

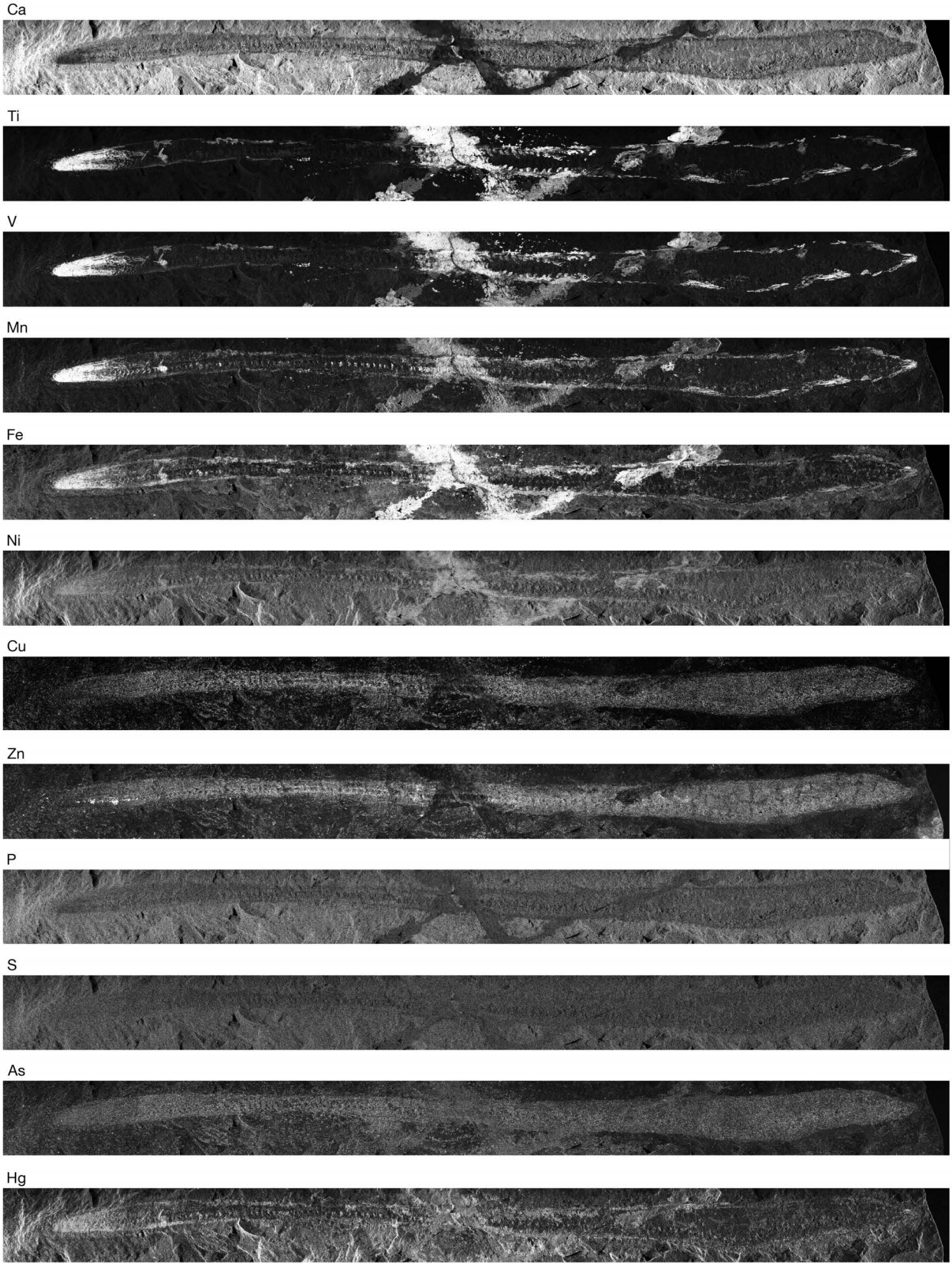
Ca
Ti
V
Mn
Fe
Ni
Cu
Zn
P
S
As
Hg

Fig. S2.4. Analyses of the output from SRS-XRF. The spatial distributions of trace elements highlight the slime glands and notochord of BHI 6445 in multiple channels: (**a**) false-color composite of Ca (blue), Zn (red), and Mn (green); (**b**) P; (**c**) S; (**d**) Fe; (**e**) Cu. Inset boxes show a part of the right series of slime glands. Red arrows indicate slime glands, whereas yellow arrows point to the notochord. Spectroscopy can be used to distinguish preserved tissues from the inorganically bound curatorial artifacts and the matrix. (**f**) K-edge XANES analyses of BHI6445 compared to the sedimentary matrix using sulfur (S).

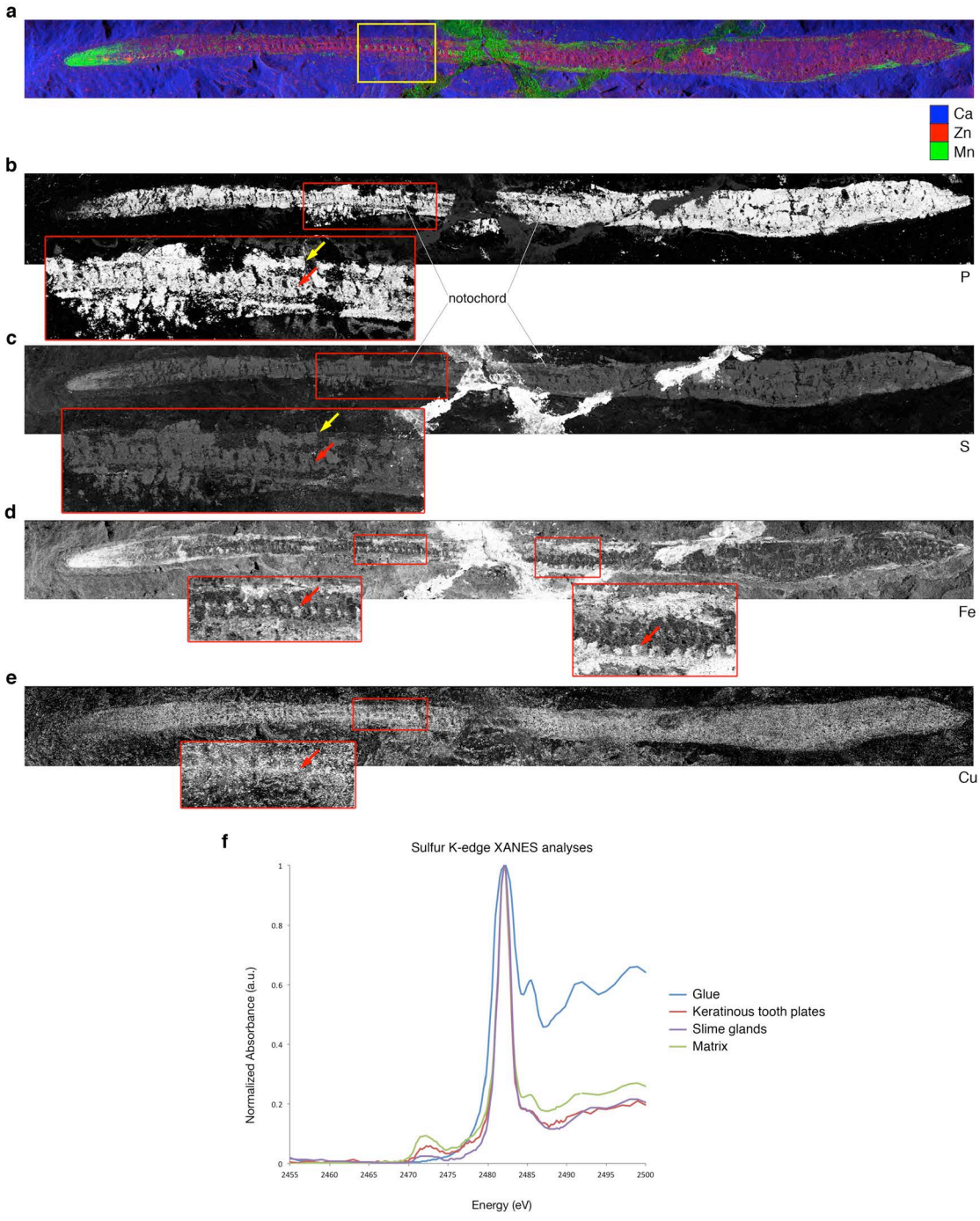
a
Ca
Zn
Mn
b
P
notochord
c
S
d
Fe
e
Cu
f
Sulfur K-edge XANES analyses
Normalized Absorbance (a.u.)
Energy (eV)
Glue
Keratinous tooth plates
Slime glands
Matrix

Fig. S2.5. Cyclostome monophyly under parsimony. Strict consensus of maximum parsimony analysis of 52 core taxa (**a**) with additional topology supported by majority rule of the bootstrap analysis (**b**). Numerical values at each node represent Bremer support (decay index) above and bootstrap values below. See Table S2.5 for the list of synapomorphies based on this strict consensus tree.

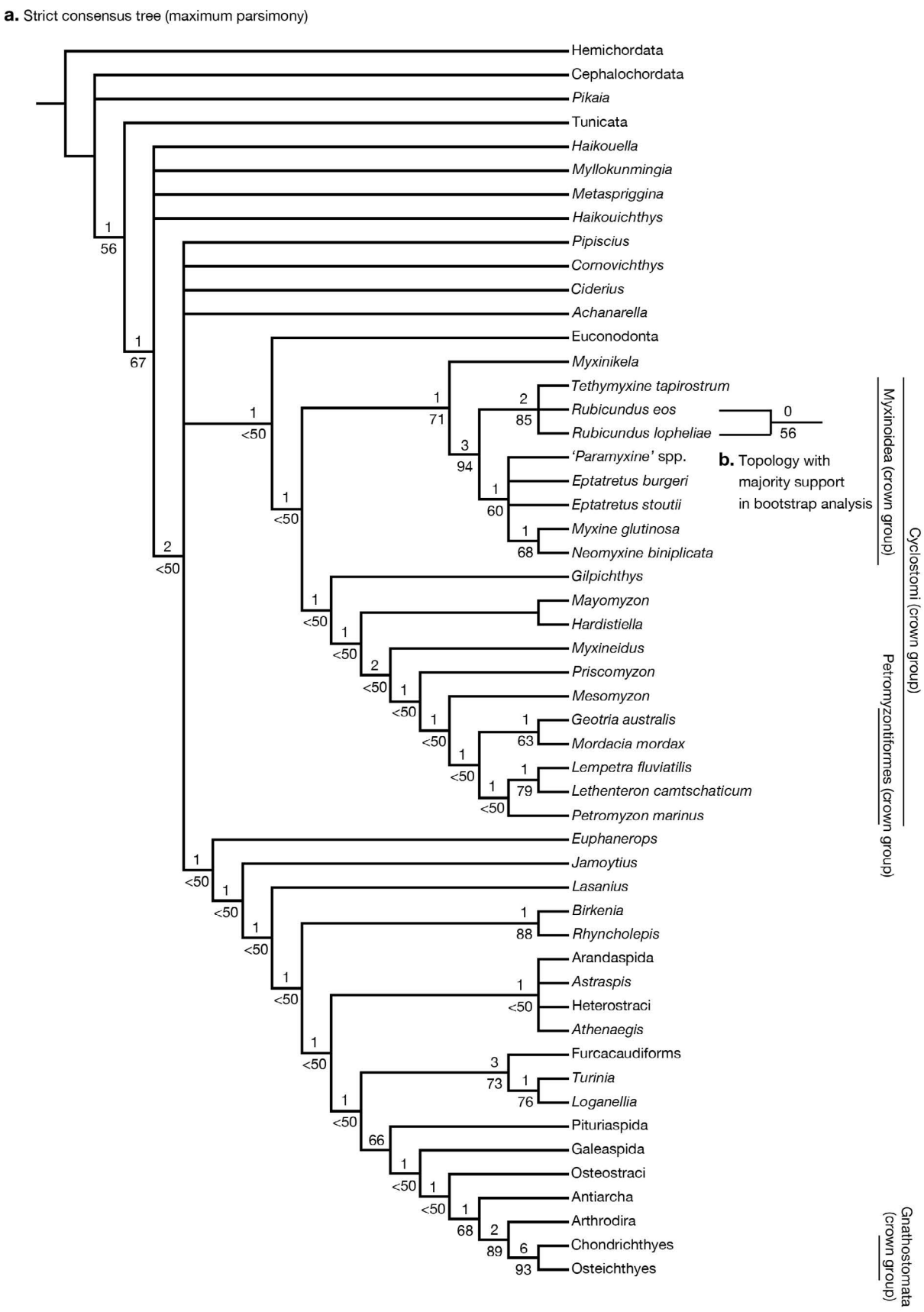
a. Strict consensus tree (maximum parsimony)
Hemichordata
Cephalochordata
Pikaia
Tunicata
Haikouella
Myllokunmingia
Metaspriggina
Haikouichthys
Pipiscius
Cornovichthys
Ciderius
Achanarella
Euconodonta
Myxinikela
Tethymyxine tapirostrum
Rubicundus eos
Rubicundus lopheliae
'Paramyxine' spp.
Eptatretus burgeri
Eptatretus stoutii
Myxine glutinosa
Neomyxine biniplicata
Gilpichthys
Mayomyzon
Hardistiella
Myxineidus
Priscomyzon
Mesomyzon
Geotria australis
Mordacia mordax
Lempetra fluviatilis
Lethenteron camtschaticum
Petromyzon marinus
Euphanerops
Jamoytius
Lasanius
Birkenia
Rhyncholepis
Arandaspida
Astraspis
Heterostraci
Athenaegis
Furcacaudiforms
Turinia
Loganellia
Pituriaspida
Galeaspida
Osteostraci
Antiarcha
Arthrodira
Chondrichthyes
Osteichthyes
b. Topology with majority support in bootstrap analysis
Myxinoidea (crown group)
Petromyzontiformes (crown group)
Cyclostomi (crown group)
Gnathostomata (crown group)

Fig. S2.6. Cyclostome monophyly is supported across different taxonomic combinations but basal gnathostome nodes are unstable. Strict consensus trees of maximum parsimony analysis under selected taxonomic combinations (full summary in Tables S2.7, S2.8): the core 52 taxa with addition of *Tullimonstrum* (**a**) and addition of *Palaeospondylus* (cyclostome coding) and *Tullimonstrum* (**b**); the original dataset with deletion of the 'naked' anaspid *Jamoytius* (**c**) and deletion of putative 'naked' anaspids (*Achanarella*, *Ciderius*, *Cornovichthys*). Anaspids are resolved as cyclostomes in **a**, **c**, **d**.

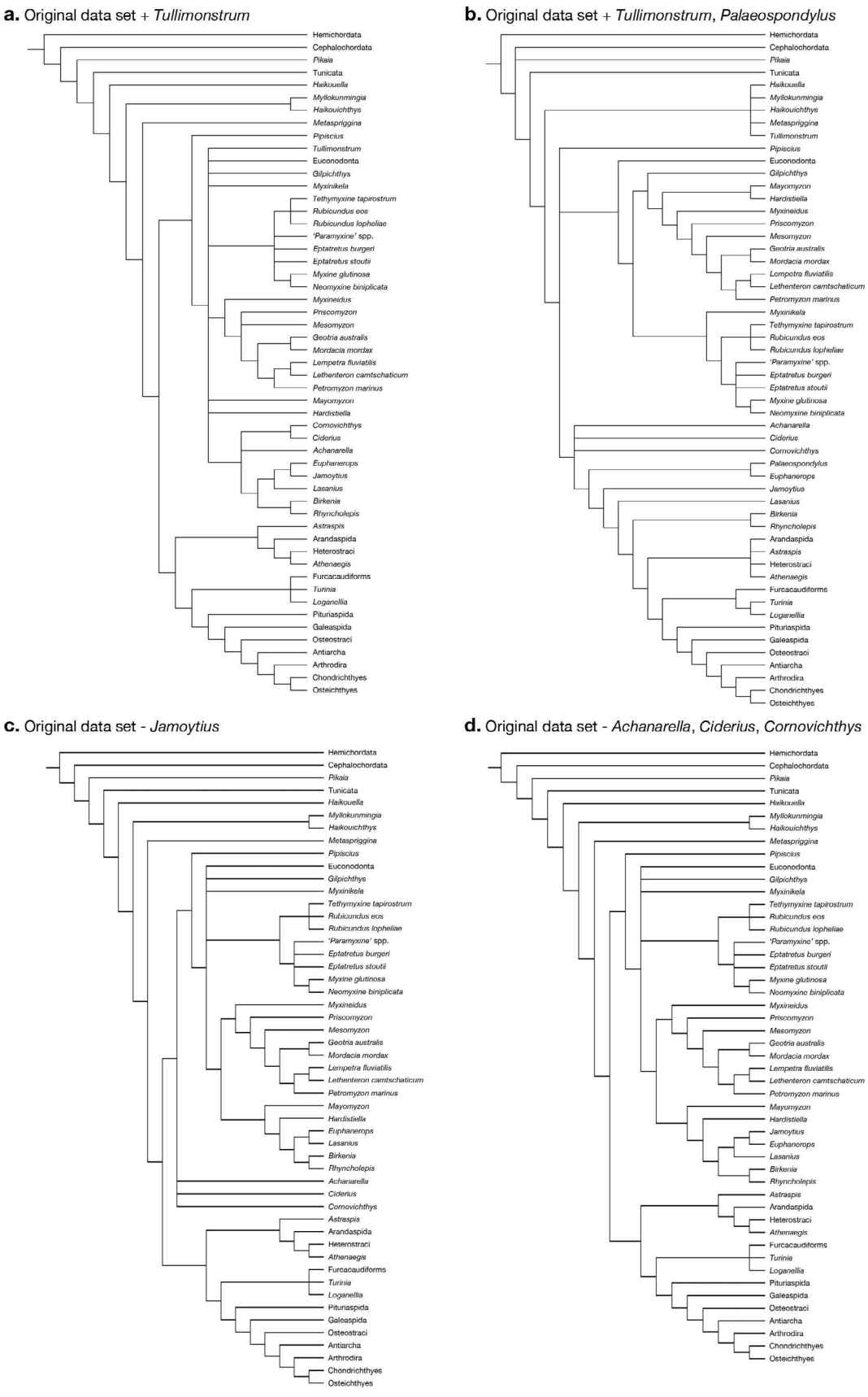
a. Original data set + Tullimonstrum
Hemichordata
Cephalochordata
Pikaia
Tunicata
Haikouella
Myllokunmingia
Haikouichthys
Metaspriggina
Pipiscius
Tullimonstrum
Euconodonta
Gilpichthys
Myxinikela
Tethymyxine tapirostrum
Rubicundus eos
Rubicundus lopheliae
'Paramyxine' spp.
Eptatretus burgeri
Eptatretus stoutii
Myxine glutinosa
Neomyxine biniplicata
Myxineidus
Priscomyzon
Mesomyzon
Geotria australis
Mordacia mordax
Lempetra fluviatilis
Lethenteron camtschaticum
Petromyzon marinus
Mayomyzon
Hardistiella
Cornovichthys
Ciderius
Achanarella
Euphanerops
Jamoytius
Lasanius
Birkenia
Rhyncholepis
Astraspis
Arandaspida
Heterostraci
Athenaegis
Furcacaudiforms
Turinia
Loganellia
Pituriaspida
Galeaspida
Osteostraci
Antiarcha
Arthrodira
Chondrichthyes
Osteichthyes
b. Original data set + Tullimonstrum, Palaeospondylus
Hemichordata
Cephalochordata
Pikaia
Tunicata
Haikouella
Myllokunmingia
Haikouichthys
Metaspriggina
Tullimonstrum
Pipiscius
Euconodonta
Gilpichthys
Mayomyzon
Hardistiella
Myxineidus
Priscomyzon
Mesomyzon
Geotria australis
Mordacia mordax
Lampetra fluviatilis
Lethenteron camtschaticum
Petromyzon marinus
Myxinikela
Tethymyxine tapirostrum
Rubicundus eos
Rubicundus lopheliae
'Paramyxine' spp.
Eptatretus burgeri
Eptatretus stoutii
Myxine glutinosa
Neomyxine biniplicata
Achanarella
Ciderius
Cornovichthys
Palaeospondylus
Euphanerops
Jamoytius
Lasanius
Birkenia
Rhyncholepis
Arandaspida
Astraspis
Heterostraci
Athenaegis
Furcacaudiforms
Turinia
Loganellia
Pituriaspida
Galeaspida
Osteostraci
Antiarcha
Arthrodira
Chondrichthyes
Osteichthyes
c. Original data set - Jamoytius
Hemichordata
Cephalochordata
Pikaia
Tunicata
Haikouella
Myllokunmingia
Haikouichthys
Metaspriggina
Pipiscius
Euconodonta
Gilpichthys
Myxinikela
Tethymyxine tapirostrum
Rubicundus eos
Rubicundus lopheliae
'Paramyxine' spp.
Eptatretus burgeri
Eptatretus stoutii
Myxine glutinosa
Neomyxine biniplicata
Myxineidus
Priscomyzon
Mesomyzon
Geotria australis
Mordacia mordax
Lempetra fluviatilis
Lethenteron camtschaticum
Petromyzon marinus
Mayomyzon
Hardistiella
Euphanerops
Lasanius
Birkenia
Rhyncholepis
Achanarella
Ciderius
Cornovichthys
Astraspis
Arandaspida
Heterostraci
Athenaegis
Furcacaudiforms
Turinia
Loganellia
Pituriaspida
Galeaspida
Osteostraci
Antiarcha
Arthrodira
Chondrichthyes
Osteichthyes
d. Original data set - Achanarella, Ciderius, Cornovichthys
Hemichordata
Cephalochordata
Pikaia
Tunicata
Haikouella
Myllokunmingia
Haikouichthys
Metaspriggina
Pipiscius
Euconodonta
Gilpichthys
Myxinikela
Tethymyxine tapirostrum
Rubicundus eos
Rubicundus lopheliae
'Paramyxine' spp.
Eptatretus burgeri
Eptatretus stoutii
Myxine glutinosa
Neomyxine biniplicata
Myxineidus
Priscomyzon
Mesomyzon
Geotria australis
Mordacia mordax
Lempetra fluviatilis
Lethenteron camtschaticum
Petromyzon marinus
Mayomyzon
Hardistiella
Jamoytius
Euphanerops
Lasanius
Birkenia
Rhyncholepis
Astraspis
Arandaspida
Heterostraci
Athenaegis
Furcacaudiforms
Turinia
Loganellia
Pituriaspida
Galeaspida
Osteostraci
Antiarcha
Arthrodira
Chondrichthyes
Osteichthyes

Fig. S2.7. Cyclostome monophyly is supported by Bayesian inferences where lineages generally considered stem gnathostomes collapse into the crown node of vertebrates. Bayesian majority-rule consensus tree of the core 52 taxa. 7502 trees were sampled overall. Numerical values indicate clade-credibility values (frequencies among sampled, supported trees).

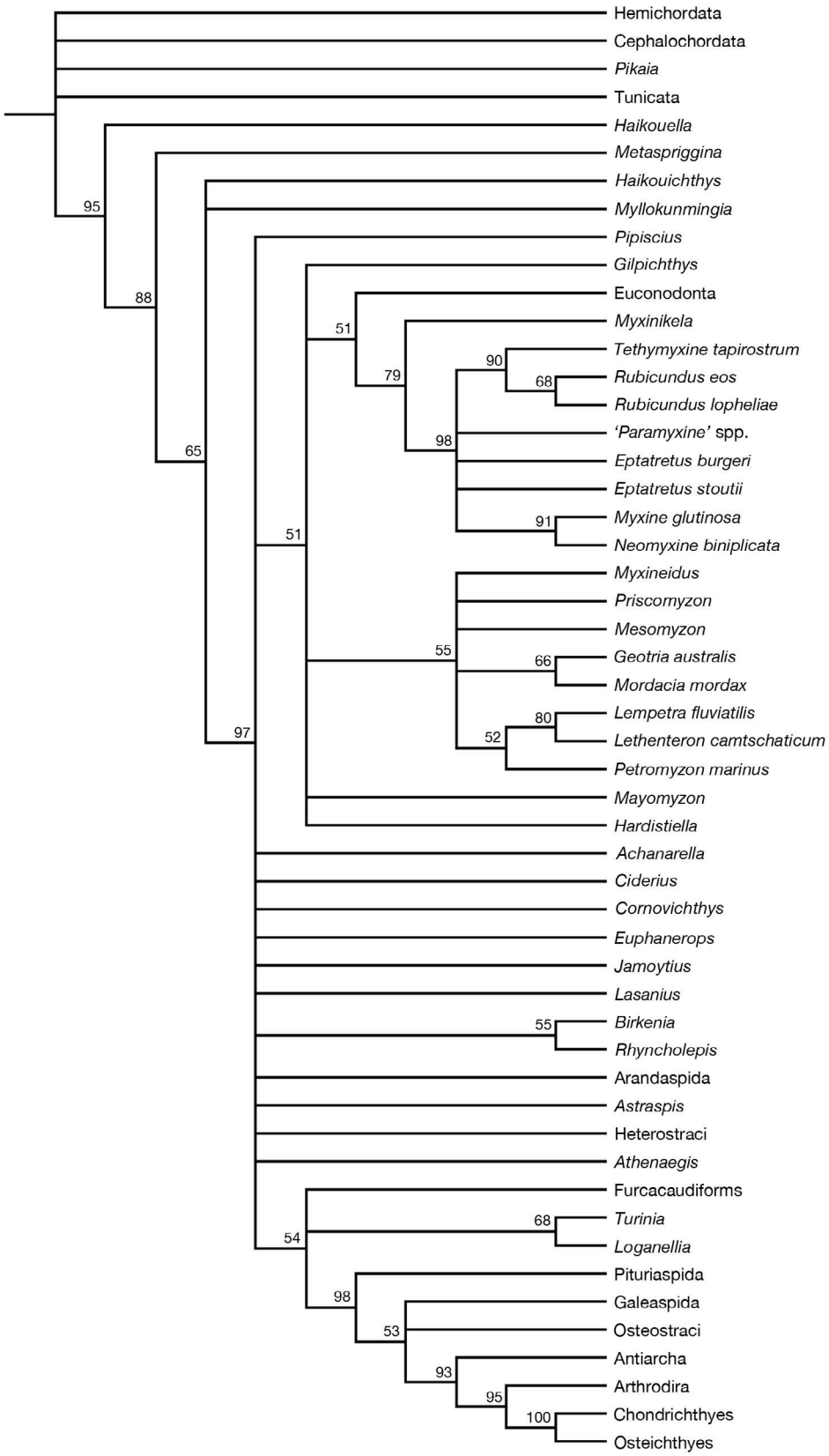
Hemichordata
Cephalochordata
Pikaia
Tunicata
Haikouella
Metaspriggina
Haikouichthys
Myllokunmingia
Pipiscius
Gilpichthys
Euconodonta
Myxinikela
Tethymyxine tapirostrum
Rubicundus eos
Rubicundus lopheliae
'Paramyxine' spp.
Eptatretus burgeri
Eptatretus stoutii
Myxine glutinosa
Neomyxine biniplicata
Myxineidus
Priscomyzon
Mesomyzon
Geotria australis
Mordacia mordax
Lempetra fluviatilis
Lethenteron camtschaticum
Petromyzon marinus
Mayomyzon
Hardistiella
Achanarella
Ciderius
Cornovichthys
Euphanerops
Jamoytius
Lasanius
Birkenia
Rhyncholepis
Arandaspida
Astraspis
Heterostraci
Athenaegis
Furcacaudiforms
Turinia
Loganellia
Pituriaspida
Galeaspida
Osteostraci
Antiarcha
Arthrodira
Chondrichthyes
Osteichthyes
95
88
65
97
51
51
79
90
68
98
91
55
66
80
52
54
68
98
53
93
95
100

Fig. S2.8. Multiple taxonomic combinations under Bayesian inferences reveal instability of the node of the total group Gnathostomata. Bayesian majority-rule consensus trees under selected taxonomic combinations (full summary in Tables S2.9, S2.10): the core 52 taxa with addition of *Palaeospondylus* (cyclostome coding) and *Tullimonstrum* (**a**); the original dataset with deletion of highly incomplete, 'naked' taxa (*Achanarella*, *Ciderius*, *Cornovichthys*, *Gilpichthys*, *Myxineidus*, and *Pipiscius*) (**b**) and with deletion of highly unstable taxa that tend to collapse multiple nodes (**c**: euconodonts, *Gilpichthys*, *Pipiscius*; **d**: *Cornovichthys*, euconodonts, *Pipiscius*; **e**: *Cornovichthys*, *Gilpichthys*, *Pipiscius*; **f**: *Pipiscius*). Cyclostomes form a clade with anaspids in the stem in **b**-**f**, whereas arandaspids, astraspids, and heterostracans become resolved as stem cyclostomes when euconodonts and *Pipiscius* are excluded (**c**, **d**). Numerical values indicate clade-credibility values.


a. Main + Tullimonstrum, Palaeospondylus (cyclostome)
Hemichordata
Cephalochordata
Pikaia
Tunicata
Haikouella
Tullimonstrum
Metaspriggina
Haikouichthys
Myllokunmingia
Pipiscius
Gilpichthys
Euconodonta
Myxinikela
Tethymyxine tapirostrum
Rubicundus eos
Rubicundus lopheliae
'Paramyxine' spp.
Eptatretus burgeri
Eptatretus stoutii
Myxine glutinosa
Neomyxine biniplicata
Myxineidus
Priscomyzon
Mesomyzon
Geotria australis
Mordacia mordax
Lempetra fluviatilis
Lethenteron camtschaticum
Petromyzon marinus
Mayomyzon
Hardistiella
Achanarella
Ciderius
Cornovichthys
Palaeospondylus
Euphanerops
Jamoytius
Lasanius
Birkenia
Rhyncholepis
Arandaspida
Astraspis
Heterostraci
Athenaegis
Furcacaudiformes
Turinia
Loganellia
Pituriaspida
Galeaspida
Osteostraci
Antiarcha
Arthrodira
Chondrichthyes
Osteichthyes
b. Main - Achanarella, Ciderius, Cornovichthys, Gilpichthys, Myxineidus, Pipiscius
c. Main - Euconodonta, Gilpichthys, Pipiscius
d. Main - Cornovichthys, Euconodonta, Pipiscius
e. Main - Cornovichthys, Gilpichthys, Pipiscius
f. Main - Pipiscius

Fig. S2.9. Time-scaled maximum clade-credibility tree from the clock-based Bayesian analysis (molecular clock) predicts the crown nodes of myxinoids and petromyzontiforms lie in early Mesozoic times. The bar at a node indicates 95% HPD interval for node age. The nodes are set at mean of the frequency distribution for node-age estimates. Summary of the node ages in Table S2.11.

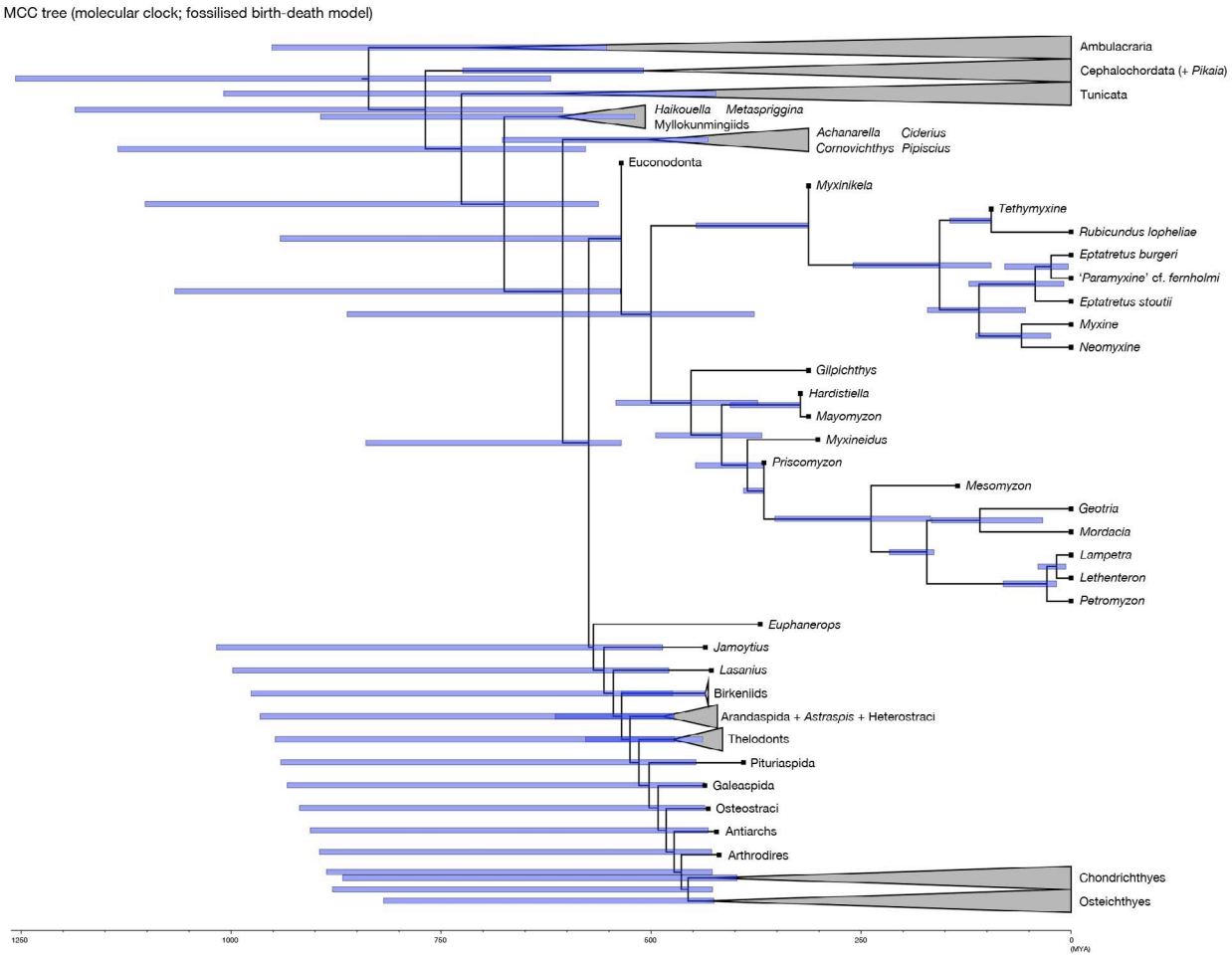
MCC tree (molecular clock; fossilised birth-death model)
Ambulacraria
Cephalochordata (+ Pikaia)
Tunicata
Haikouella Metaspriggina
Myllokunmingiids
Achanarella Ciderius
Cornovichthys Pipiscius
Euconodonta
Myxinikela
Tethymyxine
Rubicundus lopheliae
Eptatretus burgeri
'Paramyxine' cf. fernholmi
Eptatretus stoutii
Myxine
Neomyxine
Gilpichthys
Hardistiella
Mayomyzon
Myxineidus
Priscomyzon
Mesomyzon
Geotria
Mordacia
Lampetra
Lethenteron
Petromyzon
Euphanerops
Jamoytius
Lasanius
Birkenlids
Arandaspida + Astraspis + Heterostraci
Thelodonts
Pituriaspida
Galeaspida
Osteostraci
Antiarchs
Arthrodires
Chondrichthyes
Osteichthyes
1250
1000
750
500
250
0
(MYA)

Fig. S2.10. Time-scaled maximum clade-credibility tree from the clock-based Bayesian analysis (total evidence) predicts much earlier (and implausible) divergence times than the molecular clock. The bar at a node indicates 95% HPD interval for node age. The nodes are set at the mean of the frequency distribution for node-age estimates. Node ages are summarized in Table S2.12.

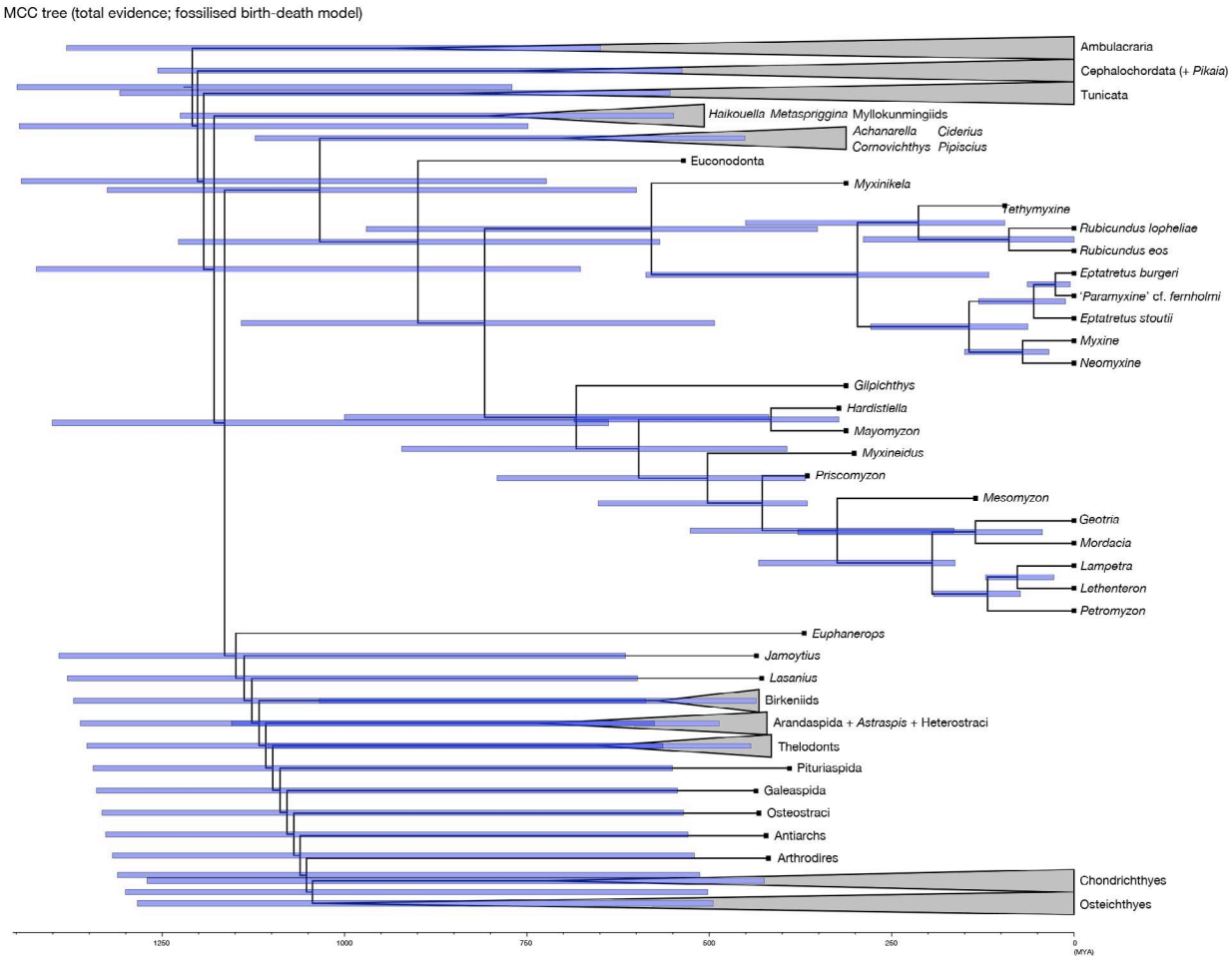
MCC tree (total evidence; fossilised birth-death model)
Ambulacraria
Cephalochordata (+ Pikaia)
Tunicata
Haikouella Metaspriggina Myllokunmingiids
Achanarella Ciderius
Cornovichthys Pipiscius
Euconodonta
Myxinikela
†Tethymyxine
Rubicundus lopheliae
Rubicundus eos
Eptatretus burgeri
'Paramyxine' cf. fernholmi
Eptatretus stoutii
Myxine
Neomyxine
Gilpichthys
Hardistiella
Mayomyzon
Myxineidus
Priscomyzon
Mesomyzon
Geotria
Mordacia
Lampetra
Lethenteron
Petromyzon
Euphanerops
Jamoytius
Lasanius
Birkeniids
Arandaspida + Astraspis + Heterostraci
Thelodonts
Pituriaspida
Galeaspida
Osteostraci
Antiarchs
Arthrodires
Chondrichthyes
Osteichthyes
1250
1000
750
500
250
0
(MYA)

Fig. S2.11. Comparison of the recent cladistic datasets (CMC, MSL, GDS, and KD; Table S2.13) for early vertebrate phylogeny. This analysis contains a greater proportion of inapplicable character values (**a**), reflecting the contingency coding strategy. Comparatively, this dataset does not differ markedly from other recent analyses in the proportions of missing character values or characters with unique values in taxa (**b**-**d**). Whiskers on box plots indicate minimum and maximum values, box ends represent 25 and 75 percentiles, and transverse lines indicate means. The GDS dataset does not distinguish inapplicable scores ('-') and missing entries ('?'); so it was thus not included in comparisons of inapplicable and missing character values (**a** and **b**). Percentiles were computed by interpolation.

A. Proportion of inapplicable values in taxon

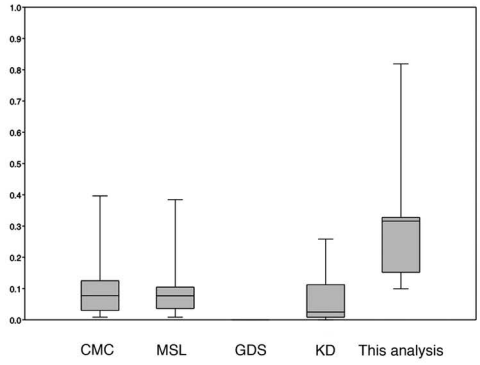

B. Proportion of missing values in taxon

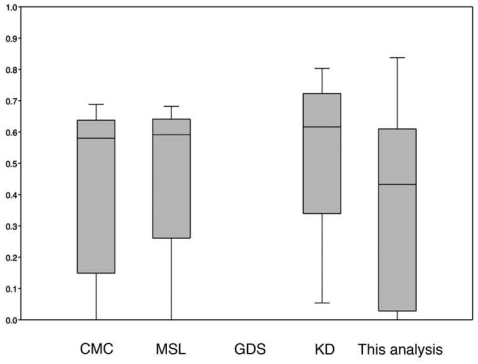

C. Proportion of inapplicable and missing values in taxon

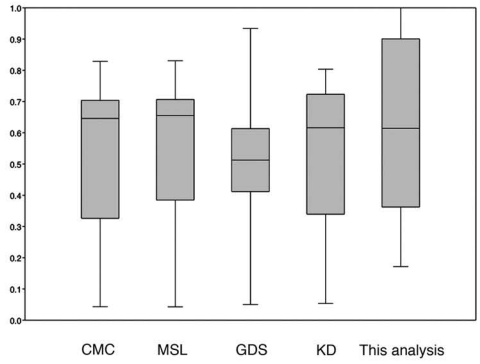

D. Proportion of characters with unique values in taxon

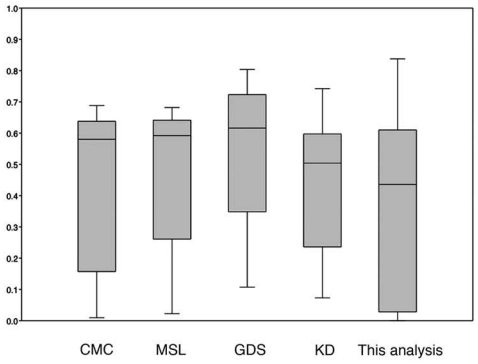

Fig. S2.12. Comparison of the recent cladistic datasets for early vertebrate phylogeny by major taxonomic categories. Increase in the proportion of inapplicable character values in this dataset is even across taxonomic categories except for non-vertebrate outgroups (hemichordates, cephalochordates, tunicates, and *Pikaia*) (**b**). Minor differences from the previous datasets in proportions of missing or unique character values are attributed to increased sampling in each of the taxonomic categories. For example, jawed vertebrates had higher proportions of inapplicable, missing, and unique character values (**b**, **d**, **f**, **h**) because of the split of the OUT "Gnathostomes" into antiarchs, arthrodires, chondrichthyans, and osteichthyans. The CMC, MSL, GDS, and KD datasets (**Table S2.13**) are more similar to each other than each is to the dataset presented here. These datasets were combined on the left column, whereas the right column represents dataset from this study. The GDS dataset was not included in calculations of inapplicable and missing values separately (as it does not distinguish the two in coding) but was considered for the sum of inapplicable and missing values. Whiskers on box plots indicate minimum and maximum values, box ends represent 25 and 75 percentiles, and transverse lines indicate means.

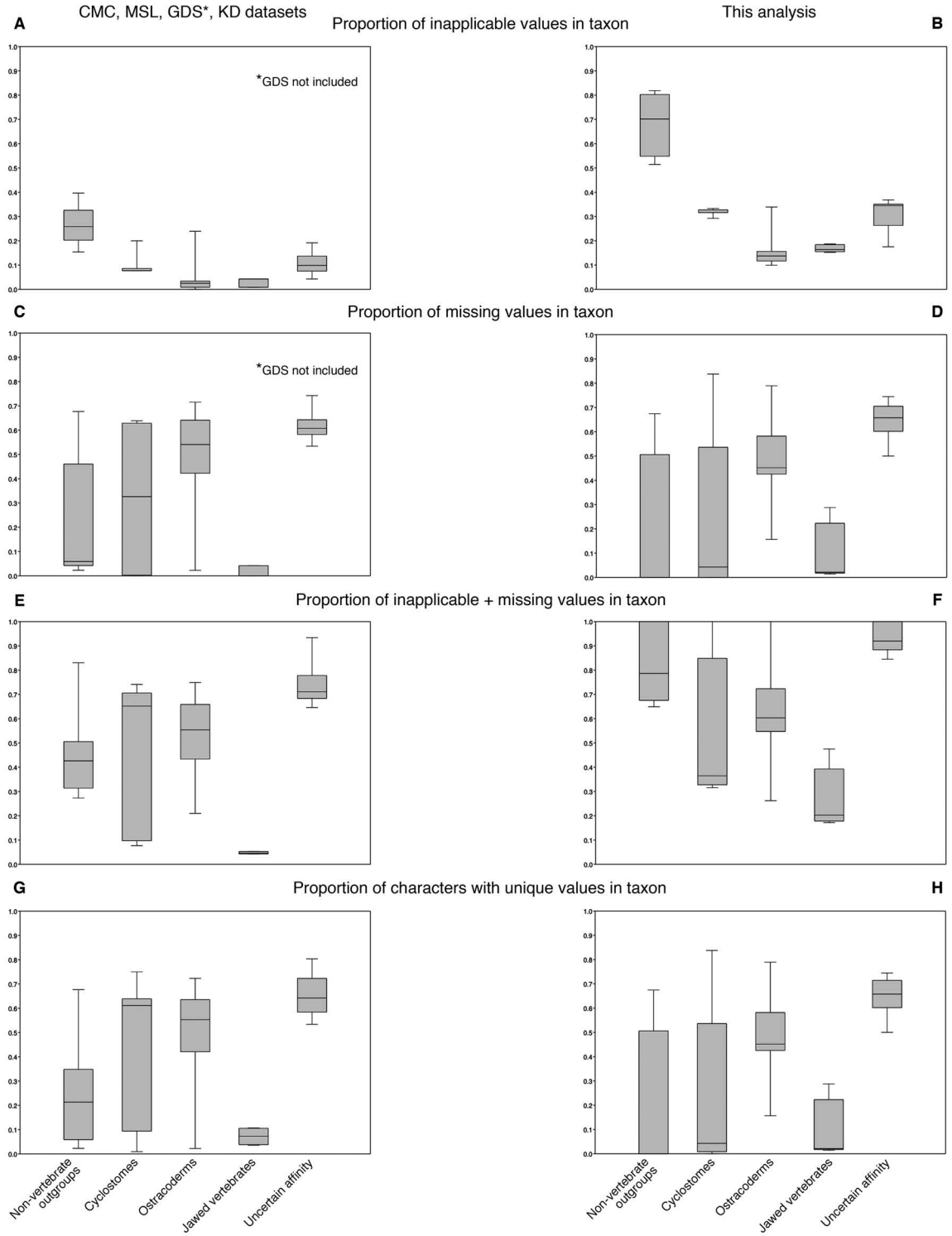
A
CMC, MSL, GDS*, KD datasets
Proportion of inapplicable values in taxon
This analysis
B
*GDS not included
C
Proportion of missing values in taxon
D
*GDS not included
E
Proportion of inapplicable + missing values in taxon
F
G
Proportion of characters with unique values in taxon
H
Non-vertebrate outgroups
Cyclostomes
Ostracoderms
Jawed vertebrates
Uncertain affinity

Fig. S2.13. Comparison of the recent cladistic datasets (CMC, MSL, GDS, and KD; Table S2.13) for early vertebrate phylogeny by major character categories. Unlike taxonomic categories, increase in proportion of inapplicable character values in this dataset is not evenly distributed across different categories of characters. From left to right, the columns represent proportions of inapplicable, missing, and inapplicable + missing values in character, respectively. Labels on the X-axis apply across the second (CMC) to sixth rows (this analysis). Character categories refer to the conventions used in character descriptions in all the compared datasets. Whiskers on box plots indicate minimum and maximum values, box ends represent 25 and 75 percentiles, and transverse lines indicate means. The GDS dataset does not distinguish inapplicable scores ('-') and missing entries ('?'); so it was thus not included in comparisons of inapplicable and missing character values (**a**, **b**, and fourth row).

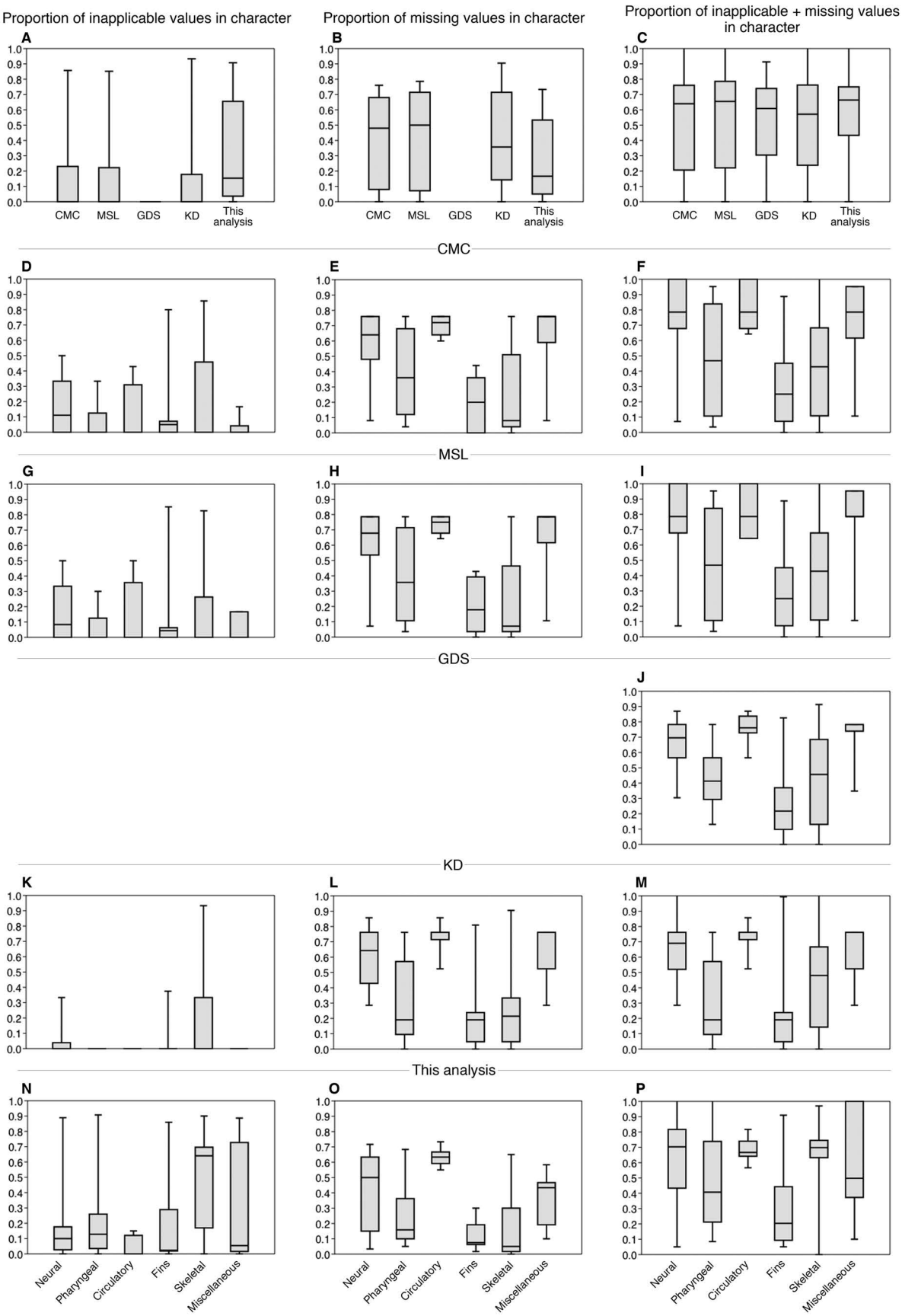
Proportion of inapplicable values in character
Proportion of missing values in character
Proportion of inapplicable + missing values in character
A
B
C
CMC
MSL
GDS
KD
This analysis
CMC
D
E
F
MSL
G
H
I
GDS
J
KD
K
L
M
This analysis
N
O
P
Neural
Pharyngeal
Circulatory
Fins
Skeletal
Miscellaneous

SUPPLEMENTARY TABLES

Table S2.1. Quantification of trace elements in the holotype of *Tethymyxine tapirostrum* gen. et sp. nov (BHI 6445) compared to the surrounding matrix and glue using synchrotron analysis. Durango (fluroapatite) was used for calibration. Concentrations are in ppm or weight percent (%). Conservative 2σ error for all quantification is ~10% of the absolute value.

Element	Fluroapatite (Durango)	Glue	Matrix	Keratinous tooth plates	Slime glands	Caudal fin
			Low *Z*			
Si	1990 ppm	2110 ppm	7.2 %	1.3 %	3.0 %	2.4 %
P	18.2 %	820 ppm	-	15.8 %	16 %	16.5 %
S	490 ppm	3.6 %	5710 ppm	2 %	2 %	2.3 %
Cl	7210 ppm	230 ppm	620 ppm	3310 ppm	2990 ppm	1520 ppm
			High *Z*			
Ca	38.1 %	-	40.1 %	16.1 %	26.5%	19.8 %
Ti	-	-	1260 ppm	1.2 %	2220 ppm	4.2 %
Mn	-	-	20 ppm	1440 ppm	420 ppm	1280 ppm
Fe	310 ppm	-	3490 ppm	7980 ppm	5650 ppm	1.7 %
Cu	-	-	100 ppm	80 ppm	300 ppm	300 ppm
Zn	-	-	90 ppm	140 ppm	170 ppm	120 ppm
As	700 ppm	-	10 ppm	20 ppm	40 ppm	40 ppm
Ba	-	-	-	3.2 %	3250 ppm	2.9 %

Table S2.2. Operational taxonomic units included in this dataset for parsimony and Bayesian analyses. Cat. = taxonomic categories (used in Fig. S2.2): C = cyclostomes; G = gnathostomes; I = non-vertebrate outgroups; O = ostracoderms; U = uncertain affinity. Status indicates whether the taxa were included in the most recent analysis (GSD) (= Retained), in one of the recent analyses (= Restored), or in none (= New). "Reserved" indicates taxa included to test different combinations and depths of taxon sampling. Percentage values are provided for inapplicable (Inappl.) and missing values for each taxon. Sources used to code the taxa include: S = first-hand observation of specimens; L = information derived from the literature or second-hand data (including photographs provided by colleagues); C = digital data derived from CT scan and other radiation or histological methods; U = information derived from unpublished specimens. *Additional taxon included only in a subset of analyses; **Composite taxa to replace terminal taxa in a subset of analyses.

Taxonomic unit	Cat.	Status	Inappl.	Missing	Sources			
					S	L	C	U
Hemichordata	I	Retained	81.9%	0.0%		X		
Cephalochordata	I	Retained	64.9%	0.0%		X		
Tunicata	I	Retained	75.4%	0.0%		X		
Pikaia	I	Restored	51.5%	67.5%	X	X		
Haikouella	U	New	36.8%	60.2%		X		
Myllokunmingia	U	Restored	33.9%	72.6%		X		
Metaspriggina	U	Restored	35.7%	52.7%	X	X		
Haikouichthys	U	Retained	34.5%	50.0%		X		
*Tullimonstrum**	U	Reserved	34.5%	70.5%		X		
Pipiscius	U	Restored	34.5%	67.9%	X	X		
Gilpichthys	U	Restored	35.1%	65.8%	X	X		X
Euconodonta	U	Retained	26.3%	63.5%	X	X		
Myxinikela	U	Retained	31.0%	61.0%	X	X		X
Myxinoidea**	C	Reserved	31.6%	1.7%	X	X	X	X
Tethymyxine	C	New	29.2%	56.2%	X		X	
Eptatretus "*Paramyxine*" spp.	C	New	31.6%	0.0%		X		

Taxonomic unit	Cat.	Status	Inappl.	Missing	Sources			
					S	L	C	U
Eptatretus burgeri	C	New	31.6%	0.9%	X	X		
Eptatretus stoutii	C	New	31.6%	0.0%	X	X	X	X
Myxine spp.	C	New	33.3%	0.0%	X	X		
Rubicundus eos	C	New	31.6%	6.8%		X		
Rubicundus lopheliae	C	New	31.6%	5.1%		X	X	X
Neomyxine biniplicata	C	New	32.7%	6.1%		X		
Priscomyzon	C	Retained	31.0%	61.0%	X	X		X
Mayomyzon	C	Retained	31.6%	54.7%	X	X		X
Hardistiella	C	New	30.4%	70.6%	X	X		
Myxineidus	U	New	31.6%	83.8%	X	X		
Mesomyzon	C	Retained	32.7%	50.4%		X		
Petromyzontida**	C	Reserved	32.7%	2.6%	X	X		X
Geotria australis	C	New	32.7%	3.5%		X		
Mordacia spp.	C	New	32.7%	6.1%		X		
Lampetra fluviatilis	C	New	32.7%	0.0%	X	X		
Lethenteron camtschaticum	C	New	32.7%	0.0%	X	X		
Petromyzon marinus	C	New	32.7%	0.0%	X	X		X
Jamoytius	O	Retained	13.5%	60.1%	X	X		
Euphanerops	O	Retained	27.5%	41.1%	X	X		X
Achanarella	O	Retained	33.9%	66.4%	X	X		
Ciderius	O	New	33.9%	68.1%		X		
Cornovichthys	O	Retained	32.7%	66.1%	X	X		
Anaspida**	O	Reserved	11.7%	42.4%	X	X		X
Lasanius	O	Restored	15.2%	52.4%	X	X		X
Birkenia	O	Restored	11.7%	43.0%	X	X		
Rhyncholepis	O	Restored	11.7%	43.0%	X	X		
Arandaspida	O	Retained	11.7%	43.0%	X	X		
Astraspis	O	Retained	11.7%	51.0%	X	X		
Heterostraci	O	Retained	11.7%	31.8%	X	X		X
Athenaegis	O	New	9.9%	48.7%	X	X		
Thelodonti**	O	Reserved	15.2%	43.4%	X	X		X

Taxonomic unit	Cat.	Status	Inappl.	Missing	Sources			
					S	L	C	U
Furcacaudiforms	O	New	14.0%	49.7%	X	X		X
Turinia	O	Retained	15.2%	44.1%	X	X		
Loganellia	O	Retained	15.2%	46.2%	X	X		
Galeaspida	O	Retained	15.8%	35.4%	X	X		
Pituriaspida	O	New	11.1%	78.9%	X	X		
Osteostraci	O	Retained	10.5%	15.7%	X	X	X	X
Gnathostomata (crown)**	G	Reserved	15.8%	1.4%	X	X		
Chondrichthyes	G	New	18.1%	2.1%	X	X		X
Osteichthyes	G	New	16.4%	2.1%	X	X		X
Antiarchs	G	New	18.7%	28.8%	X	X		X
Arthrodires	G	New	15.2%	15.9%	X	X		X
Palaeospondylus – C*	U	Reserved	17.5%	70.2%	X	X		X
Palaeospondylus – G*	U	Reserved	17.5%	74.5%	X	X		X

Table S2.3. Operational taxonomic units for the clock-based Bayesian analyses. Tip age is millions of years. Abbreviations of sequences (Seq.) are: MtG, mitochondrial genome; 16S, 16S rDNA; COI, Cytochrome Oxidase I.

Taxonomic unit	Tip age	Seq.	Morphological OTU	GenBank accession #	Notes
Neogymnocrinus richerii	0.000	MtG	-	NC_007689	
Strongylocentrotus purparatus	0.000	MtG	-	X12631	
Rhabdopleura compacta	0.000	MtG	-	FN908482	
Balanoglossus carnosus	0.000	MtG	Hemichordata	AF051097	Enteropneust node constrained prior to 306.9 MYA
Saccoglossus kowalevskii	0.000	MtG	Hemichordata	AY336131	
Asymmetron lucayanum	0.000	MtG	Cephalochordata	AP009354	Cephalochordate node (crown) constrained around 120 MYA
Branchiosotma floridae	0.000	MtG	Cephalochordata	AB478593	
Ciona intestinalis	0.000	MtG	Tunicata	AJ517314	
Doliolum nationalis	0.000	MtG	Tunicata	AB176541	
Hydrolagus lemures	0.000	MtG	-	HM147139.1	Holochephalan node constrained prior to 183 MYA
Callorhinchus milii	0.000	MtG	-	HM147137	
Scyliorhinus canicula	0.000	MtG	-	Y16067	Elasmobranch crown node constrained around 306 MYA
Leucoraja erinacea	0.000	MtG	-	JQ034406	
Polypterus endlicher	0.000	MtG	-	HM143931.1	
Polyodon spathula	0.000	MtG	-	AY510086.1	Actinopterian crown node around 354.6 MYA; holostean node around 268.6 MYA; neopterygian node around 327.8 MYA; chondrostean node around 132.5 MYA; clupeocephalan node around 245.4 MYA
Acienser transmontnus	0.000	MtG	-	AB042837	
Amia calva	0.000	MtG	-	AB042952	
Lepisosteus platyrhinchus	0.000	MtG	-	NC_029715.1	
Takifugu rubripes	0.000	MtG	-	AP006045	
Danio rerio	0.000	MtG	-	AC024175	
Latimeria chalumnae	0.000	MtG	-	U82228	
Lepidosiren paradoxa	0.000	MtG	-	AF302934	
Xenopus laevis	0.000	MtG	-	NC_001573.1	
Anolis carolinensis	0.000	MtG	-	EU747728	
Gallus gallus	0.000	MtG	-	AP003319	
Ornithorhynchus anatinus	0.000	MtG	-	X83427	
Monodelphis domestica	0.000	MtG	-	NC_006299.1	
Mus musculus	0.000	MtG	-	AP013031	Euarchontoglire node constrained around 88.8 MYA
Homo sapiens	0.000	MtG	-	GU170815	
Pikaia	509.000	-	*Pikaia*	-	

Taxonomic unit	Tip age	Seq.	Morphological OTU	GenBank accession #	Notes
Haikouella	518.000	-	*Haikouella*	-	
Myllokunmingia	518.000	-	*Myllokunmingia*	-	
Metaspriggina	507.000	-	*Metaspriggina*	-	
Haikouichthys	518.000	-	*Haikouichthys*	-	
Pipiscius	312.500	-	*Pipiscius*	-	
Gilpichthys	312.500	-	*Gilpichthys*	-	
Euconodonta	535.500	-	Euconodonta	-	
Myxinikela	312.500	-	*Myxinikela*	-	
Tethymyxine	95.000	-	*Tethymyxine*	-	
Paramyxine cf. *fernholmi*	0.000	16S + COI	*Paramyxine*' spp	JX442463; KC807333	16S and COI used to test for accuracy of alignment
Eptatretus burgeri	0.000	16S + COI; MtG	*Eptatretus burgeri*	JX442457; KC807320; AJ278504	
Eptatretus stoutii	0.000	16S + COI	*Eptatretus stoutii*	EU099456; FJ164599	
Myxine glutinosa	0.000	MtG	*Myxine glutinosa*	AJ404477	
Rubicundus lopheliae	0.000	16S + COI	*Rubicundus lopheliae*	JX442464; KC807325	
Neomyxine biniplicata	0.000	16S + COI	*Neomyxine biniplicata*	JX442447; KC807347	
Priscomyzon	365.600	-	*Priscomyzon*	-	
Mayomyzon	312.500	-	*Mayomyzon*	-	
Hardistiella	322.250	-	*Hardistiella*	-	
Myxineidus	301.450	-	*Myxineidus*	-	
Mesomyzon	135.000	-	*Mesomyzon*	-	
Geotria australis	0.000	MtG	*Geotria australis*	NC_029404	Split of Northern and Southern Hemispheric clades constrained prior to 163 MYA
Mordacia mordax	0.000	COI	*Mordacia* spp.	JN027257	
Lampetra fluviatilis	0.000	MtG	*Lampetra fluviatilis*	Y18683	
Lethenteron camtschaticum	0.000	MtG	*Lethenteron camtschaticum*	KF701113	
Petromyzon marinus	0.000	MtG	*Petromyzon marinus*	U11880	
Jamoytius	435.400	-	*Jamoytius*	-	
Euphanerops	370.000	-	*Euphanerops*	-	
Achanarella	385.000	-	*Achanarella*	-	
Ciderius	432.000	-	*Ciderius*	-	
Cornovichthys	385.000	-	*Cornovichthys*	-	
Lasanius	428.200	-	*Lasanius*	-	
Birkenia	435.400	-	*Birkenia*	-	
Rhyncholepis	431.950	-	*Rhyncholepis*	-	
Arandaspida	472.300	-	Arandaspida	-	
Astraspis	455.200	-	*Astraspis*	-	
Heterostraci	421.100	-	Heterostraci	-	

Taxonomic unit	Tip age	Seq.	Morphological OTU	GenBank accession #	Notes
Athenaegis	438.400	-	*Athenaegis*	-	
Furcacaudiforms	438.400	-	Furcacaudiforms	-	
Turinia	415.000	-	*Turinia*	-	
Loganellia	438.400	-	*Loganellia*	-	
Galeaspida	436.000	-	Galeaspida	-	
Pituriaspida	390.000	-	Pituriaspida	-	
Osteostraci	432.000	-	Osteostraci	-	
Antiarchs	422.100	-	Antiarchs	-	
Arthrodires	419.000	-	Arthrodires	-	
Graptolites	513.200	-	-	-	Hard minimum for pterobranchs (stem), hemichordates
Crinoid	482.000	-	-	-	Hard minimum for crinoids (stem), echinoderms
Ischnacanthiformes	424.300	-	Chondrichthyes	-	Hard minimum for chondrichthyans (total), gnathostomes (crown)
Ctenacanthiformes	397.600	-	-	-	Hard minimum for chondrichthyans (crown), elasmobranchs (total)
Andreolepis	425.200	-	Osteichthyes	-	Hard minimum for osteichthyans
Howqualepis	385.000	-	-	-	Hard minimum for actinopteryans (stem), actinopterygians
Guiyu	425.200	-	-	-	Hard minimum for sarcopterygians
Youngolepis	413.000	-	-	-	Hard minimum for dipnoans (stem), rhipidistians
Balanerpeton	331.200	-	-	-	Hard minimum for tetrapods
Protorosaurus	257.000	-	-	-	Hard minimum for archosauromorphs (stem), diapsids
Paleothyris	310.700	-	-	-	Hard minimum for reptiles (stem), amniotes
Juramaia	160.400	-	-	-	Hard minimum for eutherians (stem), therians
Haramiyavia	204.900	-	-	-	Hard minimum for mammals; potentially mammal outgroup

Table S2.4. A summary of priors used for the clock-based Bayesian analyses (with molecular data). To prevent initial search from collapsing, years are in tens of millions of years (1.0 = 10,000,000 years). *Initial values*: origin = 70.0; diversification rate = 1.0; turnover = 0.5; sampling proportion = 0.5; rho = 1.0.

	Model	Lower	Upper	Offset	
Diversification rate	Uniform	0.0	∞	0.0	
Turnover	Uniform	0.0	1.0	0.0	
Origin	Uniform	0.0	∞	0.0	
Sampling proportion	Uniform	0.0	1.0	0.0	
Turnover	Uniform	0.0	1.0	0.0	
ucldMean	Uniform	0.0	∞	0.0	
	Model	Mean		Offset	
Gamma shape	Exponential	1.0		0.0	
	Model	Mean	Sigma	Offset	
Kappa	Log normal	1.0	1.25	0.0	
	Model	Alpha	Beta	Offset	Mode
ucldSD	Gamma	0.5396	0.3819	0.0	ShapeScale
Node constraints	Model	Mean	Sigma	Offset	
Actinopteri (crown)	Normal	35.46	3.0	-3.0	
Chondrostei	Normal	13.25	0.65	0.5	
Clupeocephala	Normal	24.54	1.45	0.0	
Elasmobranchii (crown)	Normal	30.6	3.42	1.4	
Euarchontoglires	Normal	8.88	0.745	-0.1	
Holostei	Normal	26.86	1.5	1.0	
Neopterygii	Normal	32.78	1.6	0.0	
Petromyzontida	Log normal	0.2	1.25	16.3	
Node constraints	Model	Minimum	Maximum	Sampling gap (as minimum)	
Enteropneusta	Fossil calibration	30.69	31.14	1.0	
Holocephali	Fossil calibration	18.3	18.96	0.2	

Table S2.5. A summary of priors used for the clock-based Bayesian analyses (total evidence). To prevent the initial search from collapsing, years are in tens of millions of years (1.0 = 10,000,000 years). *Initial values*: origin = 89.6; diversification rate = 0.05; turnover = 0.5; sampling proportion = 0.01; removal probability = 0.0; rho = 5.685×10^{-4}

	Model	Lower	Upper	Offset
Diversification rate	Uniform	0.0	1.0	0.0
Turnover	Uniform	0.0	1.0	0.0

	Model	Mean	Offset
Gamma shape	Exponential	1.0	0.0
Sampling proportion	Exponential	0.001	0.0
ucldMean (molecular)	Exponential	10.0	0.0
ucldMean (morphology)	Exponential	10.0	0.0

	Model	Mean	Sigma	Offset
Kappa	Log normal	1.0	1.25	0.0
Origin	Normal	89.6	4.8	3.0

	Model	Alpha	Beta	Offset	Mode
ucldSD (molecular)	Gamma	0.5396	0.3819	0.0	ShapeScale
ucldSD (morphology)	Gamma	0.5396	0.3819	0.0	ShapeScale

Node constraints	Model	Mean	Sigma	Offset
Actinopteri (crown)	Normal	35.46	3.0	-3.0
Chondrostei	Normal	13.25	0.65	0.5
Clupeocephala	Normal	24.54	1.45	0.0
Elasmobranchii (crown)	Normal	30.6	3.42	1.4
Euarchontoglires	Normal	8.88	0.745	-0.1
Holostei	Normal	26.86	1.5	1.0
Neopterygii	Normal	32.78	1.6	0.0
Petromyzontida	Log normal	0.2	1.25	16.3

Node constraints	Model	Minimum	Maximum	Sampling gap (as minimum)
Enteropneusta	Fossil calibration	30.69	31.14	1.0
Holocephali	Fossil calibration	18.3	18.96	0.2

Table S2.6. List of synapomorphies for major nodes in a strict consensus of the most parsimonious trees generated in a maximum parsimony analysis (Fig. S2.4a) with character states for selected taxa (headed by capital letters). Due to contingency coding, the use of inapplicable state ("-") can cause ACCTRAN to ignore some character changes associated with a contingent character change closer to terminal branches. **These changes are denoted by asterisk (*)**. *These character changes are reversed toward terminal branches but ACCTRAN is blind to the changes because they are contingent on a character of higher order (e.g., mineralized skeleton is absent in crown-group cyclostomes; as attributes of mineralized skeletons are coded as inapplicable in this lineage, these individual loss events are not accounted for under ACCTRAN optimization). o=optimization of character changes, #=character number in this dataset, Trans.=transformation of character states. ***Abbreviations:*** A=ACCTRAN (accelerated character transformation, reversals preferred); D=DELTRAN (delayed character transformation; convergence preferred); O=optimization of character changes; Trans.=transformation of character states; U=unambiguous; X=polymorphism (0+1). ***Taxon abbreviations:*** (in the order of appearance) T=*Tethymyxine*; R=*Rubicundus* (*R. eos* + *R. lopheliae*); M=*Myxinikela*; G=*Gilpichthys*; P=*Pipiscius*; C=Euconodonta; E=*Haikouella*; I=*Haikoucithys*; Y=*Myllokunmingia*; S=*Metaspriggina*; J=*Jamoytius*; H=*Euphanerops*; A=*Achanarella*; D=*Ciderius*; V=*Cornovichthys*.

O	#	Trans.			Synapomorphy	*T*	*R*	*M*	*G*	*P*	C	*E*	*I*	*L*	*S*	*J*	*U*	*A*	*D*	*V*
Vertebrata, total group																				
U	16	0	=>	1	Olfactory capsule, present	1	1	1	?	?	?	?	1	?	1	1	1	1	1	?
U	26	0	=>	1	Eyes, with pigmented retinal epithelium	?	1	1	1	0	1	1	1	?	1	1	1	1	1	1
U	48	0	=>	1	Pharyngeal skeleton, supporting well-developed branchial lamellae	?	1	?	?	?	?	1	1	1	1	?	1	?	?	?
U	52	0	=>	1	Branchial pouches, present	1	1	1	1	1	?	?	?	1	?	1	1	?	1	1
U	147	0	=>	1	Sclerotome-derived axial skeletal condensations, present	?	1	?	?	?	?	?	1	?	?	?	1	?	?	?
A	4	0	=>	1	Tripartite brain, present	?	1	?	?	?	?	?	?	?	?	?	?	?	?	?
A	14	0	=>	1	Adenohypophysis, present	?	1	?	?	?	?	?	?	?	?	?	?	?	?	?
A	20	0	=>	1	Olfactory organ, paired	?	0	0	?	?	?	?	1	?	1	?	?	0	0	?
A	39	0	=>	1	Electroreceptive cells, present	?	0	?	?	?	?	?	?	?	?	?	?	?	?	?
A	40	0	=>	1	Sensory lines, present	?	1	?	?	?	?	?	?	?	?	?	?	?	?	?
A	43	0	=>	1	Internal taste buds, present	?	?	?	?	?	?	?	?	?	?	?	?	?	?	?
A	72	0	=>	1	Multi-chambered heart, present	?	1	?	?	?	?	?	?	?	?	?	?	?	?	?
A	74	0	=>	1	Circulatory system, closed	?	1	?	?	?	?	?	?	?	?	?	?	?	?	?
A	78	0	=>	1	Lymphocytes, present	?	?	?	?	?	?	?	?	?	?	?	?	?	?	?
A	83	0	=>	1	Endoskeletal fin supports, present	?	1	?	?	1	1	0	1	?	?	?	1	1	1	1
A	86	2	=>	0	Fin fold along dorsal midline, originating above branchial series	1	1	1	?	2	1	?	0	0	?	?	2	2	?	2
A	94	0	=>	1	Notochord in tail, hypochordal	?	1	?	1	?	1	?	?	?	?	?	1	1	?	1
Vertebrata, crown group																				
U	1	0	=>	1	Skeletal derivatives of neural crest, present	1	1	1	?	?	?	0	?	?	?	1	1	1	1	?
U	3	0	=>	1	Distinct prechordal head, present	1	1	1	1	?	0	?	0	?	0	1	1	1	1	1
U	17	0	=>	1	Nasohypophyseal opening, dorsal	0	0	0	?	?	?	?	0	?	0	1	1	1	1	?
U	33	0	=>	1	Cartilaginous otic capsule, present	?	1	1	1	1	?	0	1	?	0	?	?	?	?	1
U	49	1	=>	0	Pharyngeal skeleton, lateral to branchial lamellae	?	0	0	?	?	?	-	1	?	1	0	0	0	0	0
U	58	1	=>	3	Number of branchial arches (pouches), greater than ten	2	0	0	1	0	0	1	1	0	1	3	-	3	3	3
U	60	0	=>	1	Branchial openings, in a posteroventrally inclined row	?	0	?	0	1	?	0	?	?	?	?	1	?	?	1
U	90	1	=>	0	Preanal skin fold (epidermal ridge), absent	1	1	0	0	0	0	1	1	1	0	1	1	0	0	1

O	#	Trans.			Synapomorphy	*T*	*R*	*M*	*G*	*P*	C	*E*	*I*	*L*	*S*	*J*	*U*	*A*	*D*	*V*
U	93	0	=>	1	Tail, ventral lobe larger than dorsal	0	0	0	0	?	0	0	0	0	0	?	1	1	?	1
U	140	0	=>	1	Visceral skeletal arches, fused to neurocranium	1	1	1	?	?	?	?	0	?	0	?	?	?	?	?
U	154	0	=>	1	Parachordal cartilages, present	1	1	1	?	?	?	0	0	?	1	?	1	?	?	?
U	164	0	=>	1	Inflected myomeres, W-shaped	?	1	1	1	1	1	0	0	0	0	1	1	?	1	?
A	20	1	=>	0	Olfactory organ, unpaired	?	0	0	?	?	?	?	1	?	1	?	?	0	0	?
A	50	1	=>	0	Pharyngeal skeleton, arches fused to each other	?	0	0	?	?	?	?	1	?	1	0	0	0	0	0
A	81	0	=>	1	Body length, greater than five times the next largest dimension	2	2	1	1	1	2	0	1	0	0	1	1	1	1	1
A	86	0	=>	2	Dorsal midline fin, initiating posterior to anal position	1	1	1	?	2	1	?	0	0	?	?	2	2	?	2
A	155	0	=>	1	Braincase with lateral walls, present	?	0	0	?	?	?	-	-	?	0	?	1	?	?	?
D	4	0	=>	1	Tripartite brain, present	?	1	?	?	?	?	?	?	?	?	?	?	?	?	?
D	14	0	=>	1	Adenohypophysis, present	?	1	?	?	?	?	?	?	?	?	?	?	?	?	?
D	40	0	=>	1	Sensory lines, present	?	1	?	?	?	?	?	?	?	?	?	?	?	?	?
D	43	0	=>	1	Internal taste buds, present	?	?	?	?	?	?	?	?	?	?	?	?	?	?	?
D	72	0	=>	1	Multi-chambered heart, present	?	1	?	?	?	?	?	?	?	?	?	?	?	?	?
D	74	0	=>	1	Circulatory system, closed	?	1	?	?	?	?	?	?	?	?	?	?	?	?	?
D	78	0	=>	1	Lymphocytes, present	?	?	?	?	?	?	?	?	?	?	?	?	?	?	?
D	83	0	=>	1	Endoskeletal fin supports, present	?	1	?	?	1	1	0	1	?	?	?	1	1	1	1
D	94	0	=>	1	Notochord in tail, hypochordal	?	1	?	1	?	1	?	?	?	?	?	1	1	?	1
Cyclotomi, total group																				
U	55	0	=>	1	Branchial openings, closely packed	?	0	?	1	1	1	0	0	0	0	0	0	?	?	0
U	58	3	=>	0	Number of branchial pouches, four or five	2	0	0	1	0	0	1	1	0	1	3	-	3	3	3
U	86	2	=>	1	Dorsal midline fin, initiating above or anterior to anal position	1	1	1	?	2	1	?	0	0	?	?	2	2	?	2
U	93	1	=>	0	Caudal fin, no distinct lobes	0	0	0	0	?	0	0	0	0	0	?	1	1	?	1
U	152	0	=>	1	Longitudinally aligned tooth rows with transverse bite	1	1	?	1	0	1	0	0	?	0	?	?	?	?	?
A	5	0	=>	1	Profundal ganglion, fused with trigeminal ganglion	?	?	?	?	?	?	?	?	?	?	?	?	?	?	?
A	8	0	=>	1	Spinal cord, flattened in cross section	?	1	?	?	?	?	?	?	?	?	?	?	?	?	?
A	37	0	=>	1	Statolith, composed of calcium phosphate	?	?	?	?	?	?	?	?	?	?	?	?	?	?	?
A	60	1	=>	0	Branchial openings at similar horizontal level	?	0	?	0	1	?	0	?	?	?	?	1	?	?	1
A	107	0	=>	1	*Tubular dentine, non-polar interconnections of tubules/canaliculi	-	-	-	-	-	1	-	-	-	-	?	-	-	-	-

O	#	Trans.			Synapomorphy	*T*	*R*	*M*	*G*	*P*	C	*E*	*I*	*L*	*S*	*J*	*U*	*A*	*D*	*V*
A	109	0	=>	1	*Enamel/oid, bitypic	-	-	-	-	-	1	-	-	-	-	0	-	-	-	-
A	131	0	=>	2	*Odontodes in pharynx	-	-	-	-	-	2	-	-	-	-	-	-	-	-	-
A	141	0	=>	1	Multidenticulate/cuspid plates housed within buccal cavity, present	1	1	?	1	0	-	0	0	?	0	?	?	?	?	?
A	146	0	=>	1	Cartilaginous trematic rings, present	?	1	?	?	?	?	?	?	?	?	?	?	?	?	?
A	149	1	=>	0	Sclerotme-derived skeletons around notochord, absent	?	0	?	?	?	?	?	1	?	?	?	1	?	?	?
A	151	0	=>	1	Lingual apparatus, present	1	1	?	?	0	?	?	?	?	?	?	?	?	?	?
Cyclostomi, crown group																				
U	142	0	=>	1	Perioral/buccal feeding structure, keratinous	1	1	?	?	?	0	0	0	?	0	0	0	?	?	?
U	163	0	=>	1	Postotic myomeres, migrating anteriorly to position of eyes	?	1	?	?	?	0	?	?	?	0	?	?	?	?	?
D	5	0	=>	1	Profundal ganglion, fused with trigeminal ganglion	?	?	?	?	?	?	?	?	?	?	?	?	?	?	?
D	8	0	=>	1	Spinal cord, flattened in cross section	?	1	?	?	?	?	?	?	?	?	?	?	?	?	?
D	37	0	=>	1	Statolith, composed of calcium phosphate	?	?	?	?	?	?	?	?	?	?	?	?	?	?	?
D	141	0	=>	1	Multidenticulate/cuspid plates housed within buccal cavity, present	1	1	?	1	0	-	0	0	?	0	?	?	?	?	?
D	146	0	=>	1	Cartilaginous trematic rings, present	?	1	?	?	?	?	?	?	?	?	?	?	?	?	?
D	149	1	=>	0	Sclerotme-derived skeletons around notochord, absent	?	0	?	?	?	?	?	1	?	?	?	1	?	?	?
D	151	0	=>	1	Lingual apparatus, present	1	1	?	?	0	?	?	?	?	?	?	?	?	?	?
D	162	0	=>	1	Male gametes, shed directly through coelom	?	1	?	?	?	?	?	?	?	?	?	?	?	?	?
Myxinoidea, total group																				
U	17	1	=>	0	Nasohypophyseal opening, terminal	0	0	0	?	?	?	?	0	?	0	1	1	1	1	?
U	32	0	=>	1	Eyes, close together near dorsal midline	?	1	1	0	0	0	0	0	?	0	0	?	0	0	?
U	45	0	=>	2	Branchial apparatus, posteriorly shifted	2	2	2	0	1	-	-	0	0	0	1	1	0	0	0
U	159	0	=>	1	Nasohypophyseal barbells	1	1	1	0	0	?	0	0	?	0	0	0	0	0	0
A	10	1	=>	0	Ventral and dorsal roots of spinal nerve, intersegmental	?	0	?	?	?	?	?	?	?	?	?	?	?	?	?
A	11	1	=>	0	Mauthner fibres at rhombomere 4, absent	?	0	?	?	?	?	?	?	?	?	?	?	?	?	?
A	12	1	=>	0	Pineal organ, absent	?	0	?	?	?	?	?	?	?	?	?	?	?	?	?
A	18	0	=>	1	Nasohypophyseal canal, opening into pharynx	1	1	?	?	?	?	?	0	?	0	?	0	?	?	?
A	28	1	=>	0	Extrinsic eye musculature, absent	?	0	?	?	?	?	?	?	?	?	?	?	?	?	?
A	35	0	=>	1	Ant. + post. semicircular canals, loss of the confluent half loop	?	1	?	?	?	?	?	?	?	?	?	?	?	?	?

O	#	Trans.			Synapomorphy	*T*	*R*	*M*	*G*	*P*	C	*E*	*I*	*L*	*S*	*J*	*U*	*A*	*D*	*V*
A	39	1	=>	0	Electroreceptive cells, absent	?	0	?	?	?	?	?	?	?	?	?	?	?	?	?
A	41	1	=>	0	Sensory lines, on head only	?	0	?	?	?	?	?	?	?	?	?	?	?	?	?
A	43	1	=>	2	Function of internal taste buds, replaced by Schreiner's organ	?	?	?	?	?	?	?	?	?	?	?	?	?	?	?
A	68	0	=>	1	Velar cartilages, extending beyond hyomandibular position	1	1	?	?	?	?	?	?	?	?	?	?	?	?	?
A	73	1	=>	0	Pericardium, not closed	?	0	?	?	?	?	?	?	?	?	?	?	?	?	?
A	75	0	=>	1	Massive subcutaneous sinus, present	?	1	?	?	?	?	?	?	?	?	?	?	?	?	?
A	76	0	=>	1	Paired dorsal aortae, present	?	1	?	?	?	?	?	?	?	?	?	?	?	?	?
A	148	1	=>	0	Sclerotome-derived skeletons around dorsal nerve cord, absent	?	0	?	?	?	?	?	?	?	?	?	1	?	?	?
A	155	1	=>	0	Braincase with lateral walls, absent	?	0	0	?	?	?	-	-	?	0	?	1	?	?	?
A	160	0	=>	1	Forked subnasal cartilage, present	1	1	?	?	?	?	?	?	?	?	?	0	?	?	?
A	161	1	=>	0	Tectal cartilages, absent	0	0	?	?	?	?	?	?	?	?	?	1	?	?	?
Myxinoidea, crown group																				
U	27	0	=>	1	Eyes, covered by dermis	?	1	0	0	0	0	0	0	?	0	0	0	0	0	0
U	81	1	=>	2	Body length, greater than ten times the next largest dimension	2	2	1	1	1	2	0	1	0	0	1	1	1	1	1
U	90	0	=>	1	Preanal skin fold (epidermal ridge), present	1	1	0	0	0	0	1	1	1	0	1	1	0	0	1
U	168	0	=>	1	Globular slime glands, present	1	1	0	0	0	?	0	0	0	0	?	0	?	?	?
A	47	0	=>	1	Prebranchial length a quarter body length	1	1	0	-	-	-	-	-	-	-	-	-	-	-	-
D	9	0	=>	1	Ventral and dorsal roots of spinal nerve, separate	?	1	?	?	?	?	?	?	?	?	?	?	?	?	?
D	11	1	=>	0	Mauthner fibres at rhombomere 4, absent	?	0	?	?	?	?	?	?	?	?	?	?	?	?	?
D	12	1	=>	0	Pineal organ, absent	?	0	?	?	?	?	?	?	?	?	?	?	?	?	?
D	18	0	=>	1	Nasohypophyseal canal, opening into pharynx	1	1	?	?	?	?	?	0	?	0	?	0	?	?	?
D	28	1	=>	0	Extrinsic eye musculature, absent	?	0	?	?	?	?	?	?	?	?	?	?	?	?	?
D	35	0	=>	1	Ant. + post. semicircular canals, loss of the confluent half loop	?	1	?	?	?	?	?	?	?	?	?	?	?	?	?
D	41	1	=>	0	Sensory lines, on head only	?	0	?	?	?	?	?	?	?	?	?	?	?	?	?
D	60	1	=>	0	Lateral branchial openings, at similar horizontal levels	1	1	?	?	?	?	?	?	?	?	?	?	?	?	?
D	68	0	=>	1	Velar cartilages, extending beyond hyomandibular position	?	0	?	?	?	?	?	?	?	?	?	?	?	?	?
D	73	1	=>	0	Pericardium, not closed	?	1	?	?	?	?	?	?	?	?	?	?	?	?	?
D	75	0	=>	1	Massive subcutaneous sinus, present	?	1	?	?	?	?	?	?	?	?	?	?	?	?	?
D	76	0	=>	1	Paired dorsal aortae, present	?	0	?	?	?	?	?	?	?	?	?	1	?	?	?

O	#	Trans.			Synapomorphy	*T*	*R*	*M*	*G*	*P*	C	*E*	*I*	*L*	*S*	*J*	*U*	*A*	*D*	*V*
D	148	1	=>	0	Sclerotome-derived skeletons around nerve cord, absent	?	0	?	?	?	?	?	?	?	?	?	1	?	?	?
D	160	0	=>	1	Forked subnasal cartilage, present	1	1	?	?	?	?	?	?	?	?	?	0	?	?	?
D	161	1	=>	0	Tectal cartilages, absent	0	0	?	?	?	?	?	?	?	?	?	1	?	?	?
					Tethymyxine + *Rubicundus*															
U	21	0	=>	1	Nasohypophyseal canal, tapering anteriorly	1	1	0	-	-	-	-	-	-	-	-	-	-	-	-
U	23	0	=>	1	Nasohypophyseal barbells, extending from behind aperture	1	1	0	-	-	-	-	-	-	-	-	-	-	-	-
U	55	1	=>	0	Branchial openings, spaced accordingly with branchial pouches	?	0	?	1	1	1	0	0	0	0	0	0	?	?	0
A	22	0	=>	1	Nasohypophyseal aperture, tubular extension	0	1	0	-	-	-	-	-	-	-	-	-	-	-	-
A	24	0	=>	1	Nasohypophyseal papillae, ventral element present	?	1	?	-	-	-	-	-	-	-	-	-	-	-	-
A	169	0	=>	1	Number of slime glands, substantially greater than 100	1	X	-	-	-	?	-	-	-	-	?	-	?	?	?
D	47	0	=>	1	Prebranchial length a quarter body length	1	1	0	-	-	-	-	-	-	-	-	-	-	-	-
					Petromyzontiformes, total group															
U	44	0	=>	2	Preoptic head length, longer than branchial series	0	0	1	2	2	0	-	0	0	0	0	0	0	0	0
U	58	0	=>	1	Number of branchial pouches, six or seven	2	0	0	1	0	0	1	1	0	1	3	-	3	3	3
U	64	1	=>	0	Position of mouth, terminal	1	1	?	0	0	?	1	1	?	1	1	1	?	?	?
A	9	1	=>	0	Ventral and dorsal roots of spinal nerve, united	?	1	?	?	?	?	?	?	?	?	?	?	?	?	?
A	69	0	=>	1	Velar cartilages, ontogenetically terminal function as valve	?	?	?	?	?	?	?	?	?	?	?	?	?	?	?
A	101	0	=>	1	Cellular cartilages with hypertrophied chondrocytes, present	?	?	?	?	?	?	?	?	?	?	?	1	?	?	?
A	102	0	=>	1	Mature chondrocytes, nested in pair	?	?	?	?	?	?	?	?	?	?	?	1	?	?	?
A	150	1	=>	0	Sclerotome-derived skeletons around dorsal aorta, absent	?	1	?	?	?	?	?	?	?	?	?	1	?	?	?
A	166	0	=>	1	Digestive tract, passing over branchial apparatus	0	0	?	?	0	?	0	?	0	0	?	1	?	?	?
					Petromyzontiformes, crown group															
U	44	1	=>	0	Preoptic head length, shorter than branchial series	0	0	1	2	2	0	-	0	0	0	0	0	0	0	0
D	10	0	=>	1	Ventral and dorsal roots of spinal nerve, intrasegmental	?	0	?	?	?	?	?	?	?	?	?	?	?	?	?
D	69	0	=>	1	Velar cartilages, ontogenetically terminal function as valve	?	?	?	?	?	?	?	?	?	?	?	?	?	?	?
D	150	1	=>	0	Sclerotome-derived skeletons around dorsal aorta, absent	?	1	?	?	?	?	?	?	?	?	?	1	?	?	?
D	155	0	=>	1	Braincase, with lateral wall	?	0	0	?	?	?	-	-	?	0	?	1	?	?	?

O	#	Trans.			Synapomorphy	*T*	*R*	*M*	*G*	*P*	C	*E*	*I*	*L*	*S*	*J*	*U*	*A*	*D*	*V*
D	166	0	=>	1	Digestive tract, passing over branchial apparatus	0	0	?	?	0	?	0	?	0	0	?	1	?	?	?
Gnathostomata, total group																				
U	45	0	=>	1	Branchial apparatus, anteriorly shifted with respect to otic capsule	2	2	2	0	1	-	-	0	0	0	1	1	0	0	0
U	87	0	=>	1	Distinct anal fin, present	0	0	0	0	0	0	0	0	0	?	?	1	1	?	0
U	90	0	=>	1	Preanal skin fold (epidermal ridge), present	1	1	0	0	0	0	1	1	1	0	1	1	0	0	1
U	91	0	=>	1	Preanal skin fold (epidermal ridge), paired	0	0	-	-	-	-	0	0	0	-	1	1	-	-	0
U	95	0	=>	1	Calcium phosphatic (mineralized) skeleton, present	0	0	0	0	0	1	0	0	0	0	1	1	0	0	0
U	157	0	=>	1	Annular cartilage, present	0	0	0	0	0	0	?	?	?	?	1	1	?	?	?
U	166	0	=>	1	Digestive tract, passing over branchial apparatus	0	0	?	?	0	?	0	?	0	0	?	1	?	?	?
A	6	0	=>	1	Morphologically distinct cerebellum with corpus cerebelli, present	?	0	?	?	?	?	?	?	?	?	?	?	?	?	?
A	7	0	=>	1	Facial nerve, pharyngeal, pre-, and post-trematic branches	?	0	?	?	?	?	?	?	?	?	?	?	?	?	?
A	15	0	=>	1	Olfactory peduncles, present	?	0	?	?	?	?	?	0	?	0	?	?	?	?	?
A	29	0	=>	1	Muscles innervated by oculomotor nerve, four	?	-	?	?	?	?	?	?	?	?	?	?	?	?	?
A	34	0	=>	1	Vertical (ant. + post.) semicircular canals forming loops, present	?	0	?	?	?	?	-	?	?	-	?	?	?	?	?
A	77	0	=>	1	Lateral head vein, continuous with anterior cardinal vein	?	0	?	?	?	?	?	?	?	?	?	?	?	?	?
A	79	0	=>	1	Lymphocytes antigen receptors, T and B	?	0	?	?	?	?	?	?	?	?	?	?	?	?	?
A	80	0	=>	1	Subaponeurotic vascular plexus, present	?	0	?	?	?	?	?	?	?	?	?	?	?	?	?
A	156	0	=>	1	Occiput enclosing vagus and glossopharyngeal nerves, present	?	0	0	?	?	?	0	0	?	0	?	?	?	?	?
A	162	1	=>	0	Male gametes, not shed directly through coelom	?	1	?	?	?	?	?	?	?	?	?	?	?	?	?
D	155	0	=>	1	Brain case with lateral walls, present	?	0	0	?	?	?	-	-	?	0	?	1	?	?	?

Table S2.7. Summary of different taxonomic combinations for maximum parsimony analysis for selected clades showing similarities and differences using different color codes. **Topological codes:** Mo=monophyly; Pa=paraphyly; Po=polyphyly. **Taxonomic codes:** An=anaspid; CCh=crown chordate; CCy=crown cyclostome; CMy=crowm myxinoid; CPt=crown petromyzontiform; CVr=crown vertebrate; Nrt=northern hemispheric lineages; SCh=stem chordate; SCy=stem cyclostome; SGn=stem gnathostome; SMy=stem myxinoid; SPt=stem petromyzontiform; Srt=southern hemispheric lineages; SVr=stem vertebrate. **Colour codes:** grey=identical to the main analysis; black=improved resolution from polytomy; green=different topology; brown=collapsed in polytomy; yellow=anaspids resolved as cyclostomes; red=anaspids resolved outside cyclostomes and gnathostomes; blue=topology for added taxon *post hoc*. Asterisk (*) indicates internal nodes were fully resolved. When using composite taxa, the following operational taxonomic units replaced all ingroup terminal taxa: anaspids (*Birkenia*, *Euphanerops*, *Jamoytius*, *Rhyncholepis*), gnathostomes (chondrichthyans, osteichthyans), myxinoids (all living hagfish), petromyzontids (all living lampreys), thelodonts (furcacaudiforms, *Loganelia*, *Turinia*).

	Main Analysis (all core axa)	+ *Tullimonstrum*	+ *Palaeospondylus* (cyclostome)	+ *Palaeospondylus* (gnathostome)	+ *Tullimonstrum*, *Palaeospondylus* (cyclostome)	- *Achanarella*
Cyclostomes	Mo	Mo	Mo	Mo	Mo	Mo
Tethymyxine + *Rubicundus*	Mo	Mo	Mo	Mo	Mo	Mo
Crown petromyzontiids	Nrt + Sut	Nrt + Sut	Nrt + Sut	Nrt + Sut	Nrt + Sut	Nrt + Sut
Anaspida	SGn - Pa	SPt - Mo*	SGn - Pa	SGn - Pa	SGn - Pa	SGn - Pa
Heterostracomorpha	SGn - Mo	SGn - Mo	SGn - Mo	SGn - Mo	SGn - Mo	SGn - Mo
Thelodontii	SGn - Mo*	SGn - Mo	SGn - Mo*	SGn - Mo*	SGn - Mo*	SGn - Mo*
Placodermi	SGn - Pa	SGn - Pa	SGn - Pa	SGn - Pa	SGn - Pa	SGn - Pa
Crown gnathostomes	Mo	Mo	Mo	Mo	Mo	Mo
Olfactores	Mo	Mo	Mo	Mo	Mo	Mo

	- *Ciderius*	- *Cornovichthys*	- *Achanarella*, *Ciderius*, *Cornovichthys*	- *Jamoytius*	- *Euphanerops*	- *Euphanerops*, *Jamoytius*
Cyclostomes	Mo	CVr - Po	Mo	Mo	Mo	Mo
Tethymyxine + *Rubicundus*	Mo	Mo	Mo	Mo	Mo	Mo
Crown petromyzontiids	Nrt + Sut	Nrt + Sut	Nrt + Sut	Nrt + Sut	Nrt + Sut	Nrt + Sut
Anaspida	SGn - Pa	CVr - Po	SPt - Mo*	SPt - Mo*	SGn - Mo*	CVr - Po
Heterostracomorpha	SGn - Mo	SGn - Mo	SGn - Mo*	SGn - Mo*	SGn - Mo*	CVr - Mo*
Thelodontii	SGn - Mo*	SGn - Mo	SGn - Mo	SGn - Mo*	SGn - Mo*	SGn - Mo*
Placodermi	SGn - Pa	SGn - Pa	SGn - Pa	SGn - Pa	SGn - Pa	SGn - Pa
Crown gnathostomes	Mo	Mo	Mo	Mo	Mo	Mo
Olfactores	Mo	Mo	Mo	Mo	Mo	Mo

	- *Achanarella*, *Ciderius*, *Cornovichthys*, *Euphanerops*, *Jamoytius*	- *Haikouella*	- *Haikouella*, *Haikouichthys*, *Metaspriggina*, *Myllokunmingia*	- *Pipiscius*	- *Gilpichthys*	- Euconodonta
Cyclostomes	CVr - Po	Mo	Mo	CVr - Pa	Mo	CVr - Po
Tethymyxine + *Rubicundus*	Mo	Mo	Mo	Mo	Mo	Mo
Crown petromyzontiids	Nrt + Sut	Nrt + Sut	Nrt + Sut	Nrt + Sut	Nrt + Sut	Nrt + Sut
Anaspida	CVr - Po	SGn - Pa	SGn - Pa	SPt - Po	SPt - Po	CVr - Po
Heterostracomorpha	CVr - Po	SGn - Mo	SGn - Mo	SGn - Mo*	SGn - Mo*	CVr - Po
Thelodontii	SGn - Mo	SGn - Mo*	SGn - Mo*	SGn - Mo*	SGn - Mo*	SGn - Mo
Placodermi	SGn - Pa	SGn - Pa	SGn - Pa	SGn - Pa	SGn - Pa	SGn - Pa
Crown gnathostomes	Mo	Mo	Mo	Mo	Mo	Mo
Olfactores	Mo	Mo	Mo	Mo	Mo	Mo

	- *Myxineidus*	Replaced by composite taxa	Replaced by composite taxa - *Achanarella*, *Ciderius*, *Cornovichthys*	Replaced by composite taxa - Euconodonta, *Gilpichthys*, *Pipiscius*	Replaced by composite taxa - *Achanarella*, *Ciderius*, *Cornovichthys*, Euconodonta, *Gilpichthys*, *Pipiscius*
Cyclostomes	Mo	CVr - Po	CVr - Po	CVr - Po	CVr - Po
Tethymyxine + *Rubicundus*	Mo	-	-	-	-
Crown petromyzontiids	Nrt + Sut	-	-	-	-
Anaspida	SGn - Pa	CVr - Po	CVr - Po	CPt - Po	SGn - Pa
Heterostracomorpha	SGn - Mo	SGn - Mo*	SGn - Mo*	SGn - Mo*	SGn - Mo*
Thelodontii	SGn - Mo*	SGn - Mo	SGn - Mo	SGn - Mo	SGn - Mo
Placodermi	SGn - Pa	-	-	-	-
Crown gnathostomes	Mo	-	-	-	-
Olfactores	Mo	Mo	Mo	Mo	Mo

Table S2.8. Summary of different taxonomic combinations for maximum parsimony analysis for problematic stem taxa. Colour, taxonomic, and topological codes follow Table S2.7.

	Main Analysis (all core axa)	+ *Tullimonstrum*	+ *Palaeospondylus* (cyclostome)	+ *Palaeospondylus* (gnathostome)	+ *Tullimonstrum*, *Palaeospondylus* (cyclostome)	- *Achanarella*
Pikaia	CCh - Po	SCh - Mo	CCh - Po	CCh - Po	CCh - Po	CCh - Po
Tullimonstrum	-	CCy - Po	-	-	SVr - Mo	-
Palaeospondylus	-	-	SGn - Mo	SGn - Mo	SGn - Mo	-
Haikouella	SVr - Po	SVr - Mo	SVr - Po	SVr - Po	SVr - Mo*	SVr - Po
Haikouichthys	SVr - Po	SVr - Mo	SVr - Po	SVr - Po	SVr - Mo*	SVr - Po
Myllokunmingia	SVr - Po	SVr - Mo	SVr - Po	SVr - Po	SVr - Mo*	SVr - Po
Metaspriggina	SVr - Po	SVr - Mo	SVr - Po	SVr - Po	SVr - Mo*	SVr - Po
Pipiscius	CVr - Po	-	CVr - Po	CVr - Po	CVr - Po	CVr - Po
Gilpichthys	SPt - Mo	CCy - Po	SPt - Mo	SPt - Mo	SPt - Mo	SPt - Mo
Myxineidus	SPt - Mo	SPt - Mo	SPt - Mo	SPt - Mo	SPt - Mo	SPt - Mo
Myxinikela	SMy - Mo	CCy - Po	SMy - Mo	SMy - Mo	SMy - Mo	SMy - Mo
Priscomyzon	SPt - Mo	SPt - Po	SPt - Mo	SPt - Mo	SPt - Mo	SPt - Mo
Hardiestilla	SPt - Mo	CCy - Po	SPt - Mo	SPt - Mo	SPt - Mo	SPt - Mo
Mayomyzon	SPt - Mo	CCy - Po	SPt - Mo	SPt - Mo	SPt - Mo	SPt - Mo
Mesomyzon	SPt - Mo	SPt - Po	SPt - Mo	SPt - Mo	SPt - Mo	SPt - Mo
Euconodonta	SCy - Mo	CCy - Po	SCy - Mo	SCy - Mo	SCy - Mo	SCy - Mo
Achanarella	CVr - Po	An - Po	CVr - Po	SGn - Po	SGn - Po	-
Ciderius	CVr - Po	An - Po	CVr - Po	SGn - Po	SGn - Po	CVr - Po
Cornovichthys	CVr - Po	An - Po	CVr - Po	SGn - Po	SGn - Po	SGn - Mo
Euphanerops	SGn - Mo	An - Mo	SGn - Mo	SGn - Mo	SGn - Mo	SGn - Mo
Jamoytius	SGn - Mo	An - Mo	SGn - Mo	SGn - Mo	SGn - Mo	SGn - Mo
Birkeniids	SGn - Mo	An - Mo	SGn - Mo	SGn - Mo	SGn - Mo	SGn - Mo
Pturiaspida	SGn - Mo	SGn - Mo	SGn - Mo	SGn - Po	SGn - Po	SGn - Mo
Galeaspida	SGn - Mo	SGn - Mo	SGn - Mo	SGn - Po	SGn - Po	SGn - Mo
Osteostraci	SGn - Mo	SGn - Mo	SGn - Mo	SGn - Po	SGn - Po	SGn - Mo

	- *Ciderius*	- *Cornovichthys*	- *Achanarella*, *Ciderius*, *Cornovichthys*	- *Jamoytius*	- *Euphanerops*	- *Euphanerops*, *Jamoytius*
Pikaia	CCh - Po	CCh - Po	CCh - Po	CCh - Po	CCh - Po	CCh - Po
Tullimonstrum	-	-	-	-	-	-
Palaeospondylus	-	-	-	-	-	-
Haikouella	SVr - Po	SVr - Po	SVr - Mo	SVr - Mo	SVr - Mo*	SVr - Mo*
Haikouichthys	SVr - Po	SVr - Po	SVr - Mo	SVr - Mo	SVr - Mo*	SVr - Mo*
Myllokunmingia	SVr - Po	SVr - Po	SVr - Mo	SVr - Mo	SVr - Mo*	SVr - Mo*
Metaspriggina	SVr - Po	SVr - Po	SVr - Mo	SVr - Mo	SVr - Mo*	SVr - Mo*
Pipiscius	CVr - Po	CVr - Po	SCy - Mo	SCy - Mo	SGn - Mo	CVr - Po
Gilpichthys	SPt - Mo	CVr - Po	CCy - Po	CCy - Po	SPt - Mo	SPt - Mo
Myxineidus	SPt - Mo	SPt - Mo	SPt - Mo	SPt - Mo	SPt - Mo	SPt - Mo
Myxinikela	SMy - Mo	CVr - Po	CCy - Po	CCy - Po	CCy - Po	SMy - Mo
Priscomyzon	SPt - Mo	SPt - Po	SPt - Mo	SPt - Mo	SPt - Mo	SPt - Mo
Hardiestilla	SPt - Mo	CVr - Po	An - Mo	An - Mo	SPt - Mo	SPt - Mo
Mayomyzon	SPt - Mo	CVr - Po	An - Mo	An - Mo	SPt - Mo	SPt - Mo
Mesomyzon	SPt - Mo	SPt - Po	SPt - Mo	SPt - Mo	SPt - Mo	SPt - Mo
Euconodonta	SCy - Mo	CVr - Po	CCy - Po	CCy - Po	SCy - Mo	SCy - Mo
Achanarella	SGn - Po	CVr - Po	-	SCy - Po	An - Mo	CVr - Po
Ciderius	-	CVr - Po	-	SCy - Po	An - Mo	CVr - Po
Cornovichthys	SGn - Po	-	-	SCy - Po	An - Mo	CVr - Po
Euphanerops	SGn - Mo	CVr - Po	An - Mo	An - Mo	-	-
Jamoytius	SGn - Mo	CVr - Po	An - Mo	-	An - Mo	-
Birkeniids	SGn - Mo	CVr - Po	An - Mo	An - Mo	An - Mo	CVr - Po
Pturiaspida	SGn - Mo	SGn - Mo	SGn - Mo	SGn - Mo	SGn - Mo	SGn - Mo
Galeaspida	SGn - Mo	SGn - Mo	SGn - Mo	SGn - Mo	SGn - Mo	SGn - Mo
Osteostraci	SGn - Mo	SGn - Mo	SGn - Mo	SGn - Mo	SGn - Mo	SGn - Mo

	- *Achanarella*, *Ciderius*, *Cornovichthys*, *Euphanerops*, *Jamoytius*	- *Haikouella*	- *Haikouella*, *Haikouichthys*, *Metaspriggina*, *Myllokunmingia*	- *Pipiscius*	- *Gilpichthys*	- Euconodonta
Pikaia	CCh - Po	CCh - Po	CCh - Po	CCh - Po	CCh - Po	CCh - Po
Tullimonstrum	-	-	-	-	-	-
Palaeospondylus	-	-	-	-	-	-
Haikouella	SVr - Po	-	-	SVr - Mo*	SVr - Mo	SVr - Po
Haikouichthys	SVr - Po	SVr - Mo	-	SVr - Mo*	SVr - Mo	SVr - Po
Myllokunmingia	SVr - Po	SVr - Mo	-	SVr - Mo*	SVr - Mo	SVr - Po
Metaspriggina	SVr - Po	SVr - Mo	-	SVr - Mo*	SVr - Mo	SVr - Po
Pipiscius	CVr - Po	CVr - Po	CVr - Po	-	SCy - Mo	CVr - Po
Gilpichthys	CVr - Po	SPt - Mo	SPt - Mo	SMy - Mo	-	CVr - Po
Myxineidus	SPt - Mo	SPt - Mo	SPt - Mo	SPt - Po	SPt - Po	SPt -Mo
Myxinikela	CVr - Po	SMy - Mo	SMy - Mo	SMy - Po	SMy - Mo	SMy - Mo
Priscomyzon	SPt - Mo	SPt - Mo	SPt - Mo	SPt - Po	SPt - Mo	SPt - Po
Hardiestilla	SPt - Mo	SPt - Mo	SPt - Mo	SPt - Po	SPt - Po	CVr - Po
Mayomyzon	SPt - Mo	SPt - Mo	SPt - Mo	SPt - Po	SPt - Po	CVr - Po
Mesomyzon	SPt - Mo	SPt - Mo	SPt - Mo	SPt - Mo	SPt - Mo	SPt - Po
Euconodonta	CVr - Po	SCy - Mo	CVr - Po	SMy - Po	SCy - Mo	-
Achanarella	-	CVr - Po	SGn - Po	An - Po	An - Po	CVr - Po
Ciderius	-	CVr - Po	SGn - Po	An - Po	An - Po	CVr - Po
Cornovichthys	-	CVr - Po	SGn - Po	An - Po	An - Po	CVr - Po
Euphanerops	-	SGn - Mo	SGn - Mo	An - Mo	An - Mo	CVr - Po
Jamoytius	-	SGn - Mo	SGn - Mo	An - Mo	An - Mo	CVr - Po
Birkeniids	CVr - Po	SGn - Mo	SGn - Mo	An - Mo	An - Mo	CVr - Po
Pturiaspida	SGn - Mo	SGn - Mo	SGn - Mo	SGn - Mo	SGn - Mo	SGn - Mo
Galeaspida	SGn - Mo	SGn - Mo	SGn - Mo	SGn - Mo	SGn - Mo	SGn - Mo
Osteostraci	SGn - Mo	SGn - Mo	SGn - Mo	SGn - Mo	SGn - Mo	SGn - Mo

	- *Myxineidus*	Replaced by composite taxa	Replaced by composite taxa - *Achanarella*, *Ciderius*, *Cornovichthys*	Replaced by composite taxa - Euconodonta, *Gilpichthys*, *Pipiscius*	Replaced by composite taxa - *Achanarella*, *Ciderius*, *Cornovichthys*, Euconodonta, *Gilpichthys*, *Pipiscius*
Pikaia	CCh - Po	CCh - Po	SCh - Mo	SCh - Mo	SCh - Mo
Tullimonstrum	-	-	-	-	-
Palaeospondylus	-	-	-	-	-
Haikouella	SVr - Po	SVr - Po	SVr - Po	SVr - Mo	SVr - Mo
Haikouichthys	SVr - Po	SVr - Po	SVr - Po	SVr - Mo	SVr - Mo
Myllokunmingia	SVr - Po	SVr - Po	SVr - Po	SVr - Mo	SVr - Mo
Metaspriggina	SVr - Po	SVr - Po	SVr - Po	SVr - Mo	SVr - Mo
Pipiscius	CVr - Po	CVr - Po	CVr - Po	-	-
Gilpichthys	SPt - Mo	CVr - Po	CVr - Po	-	-
Myxineidus	SPt - Mo	SPt - Po	SPt - Po	CPt - Po	CPt - Po
Myxinikela	SMy - Mo	SMy - Mo	SMy - Mo	SMy - Mo	SMy - Mo
Priscomyzon	SPt - Mo	SPt - Po	SPt - Po	CPt - Po	CPt - Po
Hardiestilla	SPt - Po	CVr - Po	CVr - Po	CPt - Po	CPt - Po
Mayomyzon	SPt - Po	CVr - Po	CVr - Po	CPt - Po	CPt - Po
Mesomyzon	SPt - Mo	SPt - Po	SPt - Po	CPt - Po	CPt - Po
Euconodonta	SCy - Mo	CVr - Po	CVr - Po	-	-
Achanarella	CVr - Po	CVr - Po	-	An - Po	-
Ciderius	CVr - Po	CVr - Po	-	An - Po	-
Cornovichthys	CVr - Po	CVr - Po	-	An - Po	-
Euphanerops	SGn - Mo	CVr - Po	CVr - Po	An - Po	SGn - Mo
Jamoytius	SGn - Mo	CVr - Po	CVr - Po	An - Po	SGn - Mo
Birkeniids	SGn - Mo	-	-	-	-
Pturiaspida	SGn - Mo	SGn - Mo*	SGn - Mo*	SGn - Mo*	SGn - Mo*
Galeaspida	SGn - Mo	SGn - Mo*	SGn - Mo*	SGn - Mo*	SGn - Mo*
Osteostraci	SGn - Mo	SGn - Mo*	SGn - Mo*	SGn - Mo*	SGn - Mo*

Table S2.9. Summary of different taxonomic combinations for Bayesian analysis for selected clades. Colour, taxonomic, and topological codes follow Table S2.7.

	Main Analysis (all core axa)	+ *Tullimonstrum*, *Palaeospondylus* (cyclostome)	- *Achanarella*, *Ciderius*, *Cornovichthys*	- *Achanarella*, *Ciderius*, *Cornovichthys*, *Myxineidus*	- *Achanarella*, *Ciderius*, *Cornovichthys*, *Myxineidus*, *Hardistiella*	- *Achanarella*, *Ciderius*, *Cornovichthys*, *Myxineidus*, *Hardistiella*, *Gilpichthys*
Cyclostomes	Mo	CVr - Po	CVr - Po	CVr - Po	CVr - Po	CVr - Po
Tethymyxine + *Rubicundus*	Mo	Mo	Mo	Mo	Mo	Mo
Crown petromyzontiids	Po	Po	Po	Po	Po	Po
Anaspida	CVr - Po	CVr - Po	CVr - Po	CVr - Po	CVr - Po	CVr - Po
Heterostracomorpha	CVr - Po	CVr - Po	CVr - Po	CVr - Po	CVr - Po	CVr - Po
Thelodontii	SGn - Po	SGn - Po	SGn - Po	CVr - Po	SGn - Po	SGn - Po
Placodermi	SGn - Pa	SGn - Pa	SGn - Pa	SGn - Pa	SGn - Pa	SGn - Pa
Crown gnathostomes	Mo	Mo	Mo	Mo	Mo	Mo
Olfactores	CCh - Po	CCh - Po	CCh - Po	CCh - Po	CCh - Po	CCh - Po

	- *Achanarella*, *Ciderius*, *Cornovichthys*, *Myxineidus*, *Hardistiella*, *Gilpichthys*, *Pipiscius*, Euconodonta, *Lasanius*	- *Achanarella*, *Ciderius*, *Cornovichthys*, *Myxineidus*, *Gilpichthys*, *Pipiscius*, Euconodonta, *Lasanius*	- *Achanarella*, *Ciderius*, *Cornovichthys*, *Myxineidus*, *Gilpichthys*, *Pipiscius*, *Lasanius*	- *Achanarella*, *Ciderius*, *Cornovichthys*, *Myxineidus*, *Gilpichthys*, *Lasanius*	- *Achanarella*, *Ciderius*, *Cornovichthys*, *Myxineidus*, *Gilpichthys*, *Pipiscius*	- *Achanarella*, *Ciderius*, *Cornovichthys*, *Myxineidus*, *Pipiscius*
Cyclostomes	Mo	Mo	Mo	CVr - Po	Mo	CVr - Po
Tethymyxine + *Rubicundus*	Mo	Mo	Mo	Mo	Mo	Mo
Crown petromyzontiids	Po	Po	Po	Po	Po	Po
Anaspida	SCy - Pa	SCy - Pa	CVr - Po	CVr - Po	SCy - Pa	CVr - Po
Heterostracomorpha	SCy - Pa	SCy - Pa	CVr - Po	CVr - Po	CVr - Po	CVr - Po
Thelodontii	CVr - Po	CVr - Po	CVr - Po	CVr - Po	CVr - Po	CVr - Po
Placodermi	SGn - Pa	SGn - Pa	SGn - Pa	SGn - Pa	SGn - Pa	SGn - Pa
Crown gnathostomes	Mo	Mo	Mo	Mo	Mo	Mo
Olfactores	CCh - Po	CCh - Po	CCh - Po	CCh - Po	CCh - Po	CCh - Po

	- *Ciderius*, *Cornovichthys*, *Myxineidus*, *Pipiscius*	- *Ciderius*, *Myxineidus*, *Pipiscius*	- *Cornovichthys*, *Myxineidus*, *Pipiscius*	- *Cornovichthys*, *Pipiscius*	- Euconodonta, *Gilpichthys*, *Pipiscius*	- *Cornovichthys*, Euconodonta, *Pipiscius*
Cyclostomes	Mo	CVr - Po	Mo	Mo	Mo	Mo
Tethymyxine + *Rubicundus*	Mo	Mo	Mo	Mo	Mo	Mo
Crown petromyzontiids	Po	Po	Po	Po	Po	Po
Anaspida	SCy - Pa	CVr - Po	SCy - Pa	SCy - Pa	SCy - Pa	SCy - Pa
Heterostracomorpha	CVr - Po	CVr - Po	CVr - Po	CVr - Po	SCy - Pa	SCy - Pa
Thelodontii	CVr - Po	CVr - Po	CVr - Po	CVr - Po	CVr - Po	CVr - Po
Placodermi	SGn - Pa	SGn - Pa	SGn - Pa	SGn - Pa	SGn - Pa	SGn - Pa
Crown gnathostomes	Mo	Mo	Mo	Mo	Mo	Mo
Olfactores	CCh - Po	CCh - Po	CCh - Po	CCh - Po	CCh - Po	CCh - Po

	- *Cornovichthys*, *Gilpichthys*, *Pipiscius*	- *Pipiscius*	- *Cornovichthys*
Cyclostomes	Mo	Mo	CVr - Po
Tethymyxine + *Rubicundus*	Mo	Mo	Mo
Crown petromyzontiids	Po	Po	Po
Anaspida	SCy - Pa	SCy - Pa	CVr - Po
Heterostracomorpha	CVr - Po	CVr - Po	CVr - Po
Thelodontii	CVr - Po	SGn - Po	SGn - Po
Placodermi	SGn - Pa	SGn - Pa	SGn - Pa
Crown gnathostomes	Mo	Mo	Mo
Olfactores	CCh - Po	CCh - Po	CCh - Po

Table S2.10. Summary of different taxonomic combinations for Bayesian analysis for problematic stem taxa. Colour, taxonomic, and topological codes follow Table S2.7.

	Main Analysis (all core axa)	+ *Tullimonstrum*, *Palaeospondylus* (cyclostome)	- *Achanarella*, *Ciderius*, *Cornovichthys*	- *Achanarella*, *Ciderius*, *Cornovichthys*, *Myxineidus*	- *Achanarella*, *Ciderius*, *Cornovichthys*, *Myxineidus*, *Hardistiella*	- *Achanarella*, *Ciderius*, *Cornovichthys*, *Myxineidus*, *Hardistiella*, *Gilpichthys*
Pikaia	CCh - Po	CCh - Po	CCh - Po	CCh - Po	CCh - Po	CCh - Po
Tullimonstrum	-	SVr - Mo	-	-	-	-
Palaeospondylus	-	CVr - Mo	-	-	-	-
Haikouella	SVr - Mo	SVr - Mo	SVr - Mo	SVr - Mo	SVr - Mo	SVr - Mo
Haikouichthys	SVr - Po	SVr - Po	SVr - Po	SVr - Po	SVr - Po	SVr - Po
Myllokunmingia	SVr - Po	SVr - Po	SVr - Po	SVr - Po	SVr - Po	SVr - Po
Metaspriggina	SVr - Mo	SVr - Mo	SVr - Mo	SVr - Mo	SVr - Mo	SVr - Mo
Pipiscius	CVr - Po	CVr - Po	CVr - Po	CVr - Po	CVr - Po	CVr - Po
Gilpichthys	SCy - Po	CVr - Po	CVr - Po	CVr - Po	CVr - Po	-
Myxineidus	CPt - Po	CVr - Po	CVr - Po	-	-	-
Myxinikela	SMy - Mo	SMy - Mo	SMy - Mo	SMy - Mo	SMy - Mo	SMy - Mo
Priscomyzon	CPt - Po	CPt - Po	CPt - Po	CPt - Po	SPt - Mo	SPt - Mo
Hardiestilla	SCy - Po	CVr - Po	CVr - Po	CVr - Po	-	-
Mayomyzon	SCy - Po	CVr - Po	CVr - Po	CVr - Po	CVr - Po	CVr - Po
Mesomyzon	CPt - Po	CPt - Po	CPt - Po	CPt - Po	CPt - Po	CPt - Po
Euconodonta	SMy - Mo	CVr - Po	CVr - Po	CVr - Po	CVr - Po	CVr - Po
Achanarella	CVr - Po	CVr - Po	-	-	-	-
Ciderius	CVr - Po	CVr - Po	-	-	-	-
Cornovichthys	CVr - Po	CVr - Po	-	-	-	-
Euphanerops	CVr - Po	CVr - Mo	CVr - Mo	CVr - Mo	CVr - Mo	CVr - Mo
Jamoytius	CVr - Po	CVr - Po	CVr - Mo	CVr - Mo	CVr - Mo	CVr - Mo
Lasanius	CVr - Po	CVr - Po	CVr - Po	CVr - Po	CVr - Po	CVr - Po
Birkeniids	CVr - Po	CVr - Po	CVr - Po	CVr - Po	CVr - Po	CVr - Po
Pturiaspida	SGn - Mo	SGn - Mo	SGn - Mo	SGn - Mo	SGn - Mo	SGn - Mo
Galeaspida	SGn - Po	SGn - Po	SGn - Po	SGn - Po	SGn - Po	SGn - Po
Osteostraci	SGn - Po	SGn - Po	SGn - Po	SGn - Po	SGn - Po	SGn - Po

	- *Achanarella*, *Ciderius*, *Cornovichthys*, *Myxineidus*, *Hardistiella*, *Gilpichthys*, *Pipiscius*, Euconodonta, *Lasanius*	- *Achanarella*, *Ciderius*, *Cornovichthys*, *Myxineidus*, *Gilpichthys*, *Pipiscius*, Euconodonta, *Lasanius*	- *Achanarella*, *Ciderius*, *Cornovichthys*, *Myxineidus*, *Gilpichthys*, *Pipiscius*, *Lasanius*	- *Achanarella*, *Ciderius*, *Cornovichthys*, *Myxineidus*, *Gilpichthys*, *Lasanius*	- *Achanarella*, *Ciderius*, *Cornovichthys*, *Myxineidus*, *Gilpichthys*, *Pipiscius*	- *Achanarella*, *Ciderius*, *Cornovichthys*, *Myxineidus*, *Pipiscius*
Pikaia	CCh - Po	CCh - Po	CCh - Po	CCh - Po	CCh - Po	CCh - Po
Tullimonstrum	-	-	-	-	-	-
Palaeospondylus	-	-	-	-	-	-
Haikouella	SVr - Mo	SVr - Mo	SVr - Mo	SVr - Mo	SVr - Mo	SVr - Mo
Haikouichthys	SVr - Po	SVr - Po	SVr - Po	SVr - Po	SVr - Po	SVr - Po
Myllokunmingia	SVr - Po	SVr - Po	SVr - Po	SVr - Po	SVr - Po	SVr - Po
Metaspriggina	SVr - Mo	SVr - Mo	SVr - Mo	SVr - Mo	SVr - Mo	SVr - Mo
Pipiscius	-	-	-	CVr - Po	-	CVr - Po
Gilpichthys	-	-	-	-	-	SMy - Mo
Myxineidus	-	-	-	-	-	-
Myxinikela	SMy - Mo	SMy - Mo	SMy - Mo	SMy - Mo	SMy - Mo	SMy - Mo
Priscomyzon	CPt - Po	CPt - Po	CPt - Po	CPt - Po	CPt - Po	CPt - Po
Hardiestilla	-	CCy - Po	CCy - Po	CVr - Po	CCy - Po	CVr - Po
Mayomyzon	CCy - Po	CCy - Po	CCy - Po	CVr - Po	CCy - Po	CVr - Po
Mesomyzon	CPt - Po	CPt - Po	CPt - Po	CPt - Po	CPt - Po	CPt - Po
Euconodonta	-	-	SVr - Mo	CVr - Po	SVr - Mo	CVr - Po
Achanarella	-	-	-	-	-	-
Ciderius	-	-	-	-	-	-
Cornovichthys	-	-	-	-	-	-
Euphanerops	SCy - Mo	SCy - Mo	CVr - Po	CVr - Po	SCy - Mo	CVr - Mo
Jamoytius	SCy - Mo	SCy - Mo	CVr -Po	CVr - Po	SCy - Mo	CVr - Mo
Lasanius	-	-	-	-	SCy - Mo	CVr - Po
Birkeniids	SCy - Mo	SCy - Mo	CVr -Po	CVr - Po	SCy - Po	CVr - Po
Pturiaspida	SGn - Mo	SGn - Mo	SGn - Mo	SGn - Mo	SGn - Mo	SGn - Mo
Galeaspida	SGn - Po	SGn - Po	SGn - Po	SGn - Po	SGn - Po	SGn - Po
Osteostraci	SGn - Po	SGn - Po	SGn - Po	SGn - Po	SGn - Po	SGn - Po

	- *Ciderius*, *Cornovichthys*, *Myxineidus*, *Pipiscius*	- *Ciderius*, *Myxineidus*, *Pipiscius*	- *Cornovichthys*, *Myxineidus*, *Pipiscius*	- *Cornovichthys*, *Pipiscius*	- Euconodonta, *Gilpichthys*, *Pipiscius*	- *Cornovichthys*, Euconodonta, *Pipiscius*
Pikaia	CCh - Po	CCh - Po	CCh - Po	CCh - Po	CCh - Po	CCh - Po
Tullimonstrum	-	-	-	-	-	-
Palaeospondylus	-	-	-	-	-	-
Haikouella	SVr - Mo	SVr - Mo	SVr - Mo	SVr - Mo	SVr - Mo	SVr - Mo
Haikouichthys	SVr - Po	SVr - Po	SVr - Po	SVr - Po	SVr - Po	SVr - Po
Myllokunmingia	SVr - Po	SVr - Po	SVr - Po	SVr - Po	SVr - Po	SVr - Po
Metaspriggina	SVr - Mo	SVr - Mo	SVr - Mo	SVr - Mo	SVr - Mo	SVr - Mo
Pipiscius	-	CVr - Po	-	-	-	-
Gilpichthys	SMy - Po	-	SMy - Mo	CCy - Po	SMy - Mo	-
Myxineidus	-	-	-	CPt - Po	CCy - Po	CPt - Po
Myxinikela	SMy - Mo	SMy - Mo	SMy - Mo	SMy - Mo	SMy - Mo	SMy - Mo
Priscomyzon	CPt - Po	CPt - Po	CPt - Po	CPt - Po	CCy - Po	CPt - Po
Hardiestilla	CCy - Po	CVr - Po	CCy - Po	CCy - Po	CCy - Po	CCy - Po
Mayomyzon	CCy - Po	CVr - Po	CCy - Po	CCy - Po	CCy - Po	CCy - Po
Mesomyzon	CPt - Po	CPt - Po	CPt - Po	CPt - Po	CPt - Po	CPt - Po
Euconodonta	SMy - Po	CVr - Po	SMy - Mo	CCy - Po	-	-
Achanarella	SCy - Po	-	SCy - Mo	SCy - Mo	SCy - Po	SCy - Mo
Ciderius	-	-	SCy - Mo	SCy - Mo	SCy - Po	SCy - Mo
Cornovichthys	-	CVr - Po	-	-	SCy - Po	-
Euphanerops	SCy - Po	CVr - Po	SCy - Po	SCy - Po	SCy - Po	SCy - Po
Jamoytius	SCy - Po	CVr - Po	SCy - Mo	SCy - Po	SCy - Po	SCy - Po
Lasanius	SCy - Po	CVr - Po	SCy - Mo	SCy - Po	SCy - Mo	SCy - Mo
Birkeniids	SCy - Mo	CVr - Po	SCy - Mo	SCy - Po	SCy - Mo	SCy - Mo
Pturiaspida	SGn - Mo	SGn - Po	SGn - Mo	SGn - Mo	SGn - Mo	SGn - Mo
Galeaspida	SGn - Po	SGn - Po	SGn - Po	SGn - Po	SGn - Po	SGn - Po
Osteostraci	SGn - Po	SGn - Po	SGn - Po	SGn - Po	SGn - Po	SGn - Po

	- *Cornovichthys*, *Gilpichthys*, *Pipiscius*	- *Pipiscius*	- *Cornovichthys*
Pikaia	CCh - Po	CCh - Po	CCh - Po
Tullimonstrum	-	-	-
Palaeospondylus	-	-	-
Haikouella	SVr - Mo	SVr - Mo	SVr - Mo
Haikouichthys	SVr - Po	SVr - Po	SVr - Po
Myllokunmingia	SVr - Po	SVr - Po	SVr - Po
Metaspriggina	SVr - Mo	SVr - Mo	SVr - Mo
Pipiscius	-	-	CVr - Po
Gilpichthys	-	CCy - Po	CVr - Po
Myxineidus	CCy - Po	CPt - Po	CPt - Po
Myxinikela	SMy - Mo	SMy - Mo	SMy - Mo
Priscomyzon	CCy - Po	CPt - Po	CPt - Po
Hardiestilla	CCy - Po	CCy - Po	CVr - Po
Mayomyzon	CCy - Po	CCy - Po	CVr - Po
Mesomyzon	CPt - Po	CPt - Po	CPt - Po
Euconodonta	SVr - Mo	CCy - Po	CVr - Po
Achanarella	SCy - Po	SCy - Po	CVr - Mo
Ciderius	SCy - Po	SCy - Po	CVr - Mo
Cornovichthys	-	SCy - Po	-
Euphanerops	SCy - Po	SCy - Po	CVr - Po
Jamoytius	SCy - Po	SCy - Po	CVr - Po
Lasanius	SCy - Mo	SCy - Po	CVr - Po
Birkeniids	SCy - Mo	SCy - Po	CVr - Po
Pturiaspida	SGn - Mo	SGn - Mo	SGn - Mo
Galeaspida	SGn - Po	SGn - Po	SGn - Po
Osteostraci	SGn - Po	SGn - Po	SGn - Po

Table S2.11. Estimates of the age (millions of years ago) of the Most Recent Common Ancestor (MRCA) from a BEAST analysis using fossilized birth death model and molecular data. Mode refers to unimodal (U) or bimodal (B) frequency distribution. Asterisk (*)= distribution highly skewed toward upper height. Asterisks (**)= isolated peak frequency at upper height. SE= standard error. SD= standard deviation.

Node	Lower Age of MRCA	Upper Age of MRCA	Mean Age of MRCA	SE	SD	Variance	Median	Mode
Deuterostomia	1339.090	694.602	983.123	14.527	177.732	3158.875	950.815	U
Chordata (crown)	919.030	647.575	764.362	10.120	72.016	518.634	758.122	U
Olfactores (crown)	860.511	610.919	724.438	9.655	66.318	439.811	716.286	U
Vertebrata (total)	792.969	575.857	675.278	6.917	58.396	341.013	667.022	U
Vertebrata (crown)	685.392	540.993	606.917	4.175	41.207	169.804	599.133	U
Euconodonts + crown cyclostomes	573.947	535.500	540.967	0.753	14.520	21.083	535.500	U*
Cyclostomi (crown)	543.676	416.768	491.845	3.295	34.515	119.129	497.067	U
Myxinoidea (total)	444.529	312.500	337.999	2.031	44.761	200.351	312.500	U*
Myxinoidea (crown)	254.216	95.137	164.514	7.352	43.922	192.911	156.015	U
Tethymyxine + *Rubicundus*	143.540	95.000	101.618	0.762	19.358	37.472	95.000	U*
Eptatretus + *Myxine*	176.016	54.237	114.386	7.486	37.017	137.029	111.874	U
Myxine + *Neomyxine*	117.218	24.293	66.630	7.974	32.279	104.191	59.288	U
Petromyzontiformes (total)	519.312	384.998	451.076	2.232	36.237	131.310	449.326	U
Mayomyzon + crown petromyzontiforms	478.548	368.709	418.602	1.514	30.889	95.413	413.780	U
Myxineidus + crown petromyzontiforms	436.897	365.602	390.742	0.849	22.467	50.477	384.366	U*

Node	Lower Age of MRCA	Upper Age of MRCA	Mean Age of MRCA	SE	SD	Variance	Median	Mode
Priscomyzon + crown petromyzontif.	386.826	365.600	368.405	0.244	9.795	9.594	365.600	U*
Mesomyzon + crown petromyzontiforms	351.229	168.258	247.534	1.955	54.620	298.333	237.406	U
Petromyzontiformes (crown)	209.707	163.122	176.726	1.594	15.523	24.096	171.564	U
Geotria + *Mordacia*	166.820	33.675	106.469	9.748	42.073	177.014	114.060	B
Lampetra + *Petromyzon*	81.046	16.661	36.005	5.693	19.732	38.937	28.130	U*
Lampetra + *Lethenteron*	40.166	6.313	19.438	2.590	9.335	8.714	17.273	U*
Euphanerops + crown gnathostomes	630.763	516.704	568.529	3.582	29.789	88.737	564.785	U
Jamoytius + crown gnathostomes	615.478	503.129	555.559	3.493	28.962	83.879	552.104	U
Lasainus + crown gnathostomes	605.569	493.002	544.368	3.489	28.524	81.362	541.082	U
Birkeniids + crown gnathostomes	590.988	482.302	534.200	3.440	27.628	76.333	531.329	U
Heterostraci + crown gnathostomes	575.127	473.202	524.343	3.366	26.751	71.563	521.593	U
Arandaspida + *Astrapis* + Heterostr.	490.703	472.300	491.214	1.696	22.854	52.231	482.755	U*
Thelodonts + crown gnathostomes	523.160	438.403	475.252	1.572	25.835	66.744	471.299	U
Pituriaspida + crown gnathostomes	556.259	447.142	501.110	4.030	27.224	74.113	498.763	U
Galeaspida + crown gnathostomes	537.309	436.000	490.078	4.490	27.216	74.072	488.262	U**

Node	Lower Age of MRCA	Upper Age of MRCA	Mean Age of MRCA	SE	SD	Variance	Median	Mode
Osteostraci + crown gnathostomes	525.919	432.000	480.726	4.386	25.718	66.142	478.417	U**
Antiarchs + crown gnathostomes	515.689	429.326	472.238	4.169	23.920	57.214	469.311	U**
Arthrodires + crown gnathostomes	505.276	428.381	464.280	3.952	21.876	47.854	460.702	U
Gnathostomata (crown)	496.520	427.323	457.044	3.795	19.826	39.307	453.178	U
Chondrichthyes (crown)	471.209	397.603	425.689	3.655	21.131	44.653	421.693	U
Osteichthyes (total)	473.307	425.201	439.025	2.491	15.272	23.323	433.262	U*
Actinopterygii (crown)	425.132	385.276	407.216	1.077	12.910	16.668	406.804	U
Sarcopterygii (total)	461.358	425.200	430.982	2.246	12.515	15.663	425.200	U*

Table S2.12. Estimates of the age (millions of years ago) of the Most Recent Common Ancestor (MRCA) from a BEAST analysis using fossilized birth death model and molecular and morphological data. Mode refers to unimodal (U) or bimodal (B) frequency distribution. Asterisk (*)= distribution highly skewed toward upper height. Asterisks (**)= isolated peak frequency at upper height. SE= standard error. SD= standard deviation.

Node	Lower Age of MRCA	Upper Age of MRCA	Mean Age of MRCA	SE	SD	Variance	Median	Mode
Deuterostomia	1416.631	857.565	1136.237	49.451	173.074	2995.449	1186.759	B
Chordata (crown)	1413.576	739.301	1089.432	61.286	212.923	4533.613	1170.218	B
Olfactores (crown)	1412.178	712.818	1072.282	64.389	223.072	4976.100	1162.057	B
Vertebrata (total)	1395.365	668.713	1047.183	68.758	237.682	5649.255	1146.953	B
Vertebrata (crown)	1378.996	632.631	1023.442	72.186	248.921	6196.183	1132.510	B
Euconodonts + crown cyclostomes	1187.368	567.736	856.687	51.462	198.399	3936.206	846.595	B
Cyclostomi (crown)	1085.396	489.688	776.798	48.302	182.882	3344.597	767.596	B
Myxinoidea (total)	957.162	351.748	606.022	48.810	191.640	3672.593	557.128	B
Myxinoidea (crown)	598.589	116.797	316.509	22.687	137.026	1877.613	293.947	U
Tethymyxine + *Rubicundus*	454.475	95.000	233.448	15.298	112.182	1258.472	208.657	U
Eptatretus + *Myxine*	280.963	63.419	158.019	15.253	62.905	395.703	147.663	U
Myxine + *Neomyxine*	151.844	34.516	83.190	8.885	34.525	119.197	74.766	U
Petromyzontiformes (total)	981.242	417.392	681.308	38.464	164.932	2720.246	656.893	U
Mayomyzon + crown petromyzontiforms	890.131	386.917	600.670	30.636	146.196	2137.315	575.792	U

Node	Lower Age of MRCA	Upper Age of MRCA	Mean Age of MRCA	SE	SD	Variance	Median	Mode
Myxineidus + crown petromyzontiforms	769.725	368.583	520.012	21.766	120.546	1453.123	485.499	U
Priscomyzon + crown petromyzontif.	610.730	365.600	446.810	12.954	81.950	671.582	417.970	U*
Mesomyzon + crown petromyzontiforms	505.802	168.994	318.926	16.560	96.274	926.861	310.159	U
Petromyzontiformes (crown)	394.385	163.070	218.451	18.501	70.500	497.021	188.508	U*
Geotria + *Mordacia*	215.511	43.119	130.343	12.883	57.501	330.638	129.438	U
Lampetra + *Petromyzon*	194.559	80.102	127.802	9.184	32.593	106.231	117.597	U
Lampetra + *Lethenteron*	120.971	35.981	76.556	6.562	24.124	58.198	80.690	B
Euphanerops + crown gnathostomes	1368.571	605.035	1005.244	74.759	257.525	6631.925	1121.108	B
Jamoytius + crown gnathostomes	1365.659	595.862	993.863	75.433	259.816	6750.453	1109.441	B
Lasainus + crown gnathostomes	1355.736	581.422	983.286	75.902	261.374	6831.641	1099.924	B
Birkeniids + crown gnathostomes	1349.311	572.413	973.507	76.217	262.394	6885.048	1089.906	B
Heterostraci + crown gnathostomes	1341.618	561.141	963.778	76.602	263.653	6951.293	1079.758	B
Arandaspida + *Astrapis* + Heterostr.	1135.126	487.854	757.032	42.973	199.129	3965.248	710.931	U
Thelodonts + crown gnathostomes	1333.819	550.149	954.183	76.986	264.920	7018.236	1070.884	B

Node	Lower Age of MRCA	Upper Age of MRCA	Mean Age of MRCA	SE	SD	Variance	Median	Mode
Pituriaspida + crown gnathostomes	1329.897	541.908	944.642	77.292	265.965	7073.744	1062.179	B
Galeaspida + crown gnathostomes	1318.188	529.187	935.190	77.516	266.671	7111.316	1053.254	B
Osteostraci + crown gnathostomes	1309.757	519.909	926.376	77.600	266.982	7127.918	1044.449	B
Antiarchs + crown gnathostomes	1306.080	517.052	918.194	77.591	266.924	7124.851	1037.045	B
Arthrodires + crown gnathostomes	1299.009	511.328	910.141	77.619	266.934	7125.384	1028.367	B
Gnathostomata (crown)	1292.871	505.058	902.362	77.594	266.767	7116.463	1021.437	B
Chondrichthyes (crown)	1233.395	398.151	671.126	74.366	259.202	6718.544	587.366	B
Osteichthyes (total)	1266.016	492.771	887.988	76.727	263.858	6962.082	1010.626	B
Actinopterygii (crown)	1176.259	402.274	761.255	74.913	264.130	6976.464	774.459	B
Sarcopterygii (total)	1214.762	477.674	862.547	74.654	256.697	6589.330	986.542	B

Table S2.13. Summary of characters used in the morphological phylogenetic analyses and their source. Numbers refer to those in the dataset used for new analyses (**2.8.5 List of Characters**). The sources represent the most recent revision. CMC= Conway Morris and Caron (2014); GDS= Gabbott et al. (2016); HSM=Heimberg et al. (2010); KD= Keating and Donoghue (2016); MSL= McCoy et al. (2016).

New characters	Modified character definitions (+ coding), original sources	Modified character coding, original sources	Excluded characters, original sources
This analysis: 2-4, 10, 21-27, 29-32, 35, 36, 44, 46, 47, 54, 55, 58, 59, 62, 63, 65, 66, 68-71, 81, 85, 88, 96, 104, 111, 114, 116-118, 135, 137, 143, 145, 148, 149, 154, 165-171 HSM: 38, 46	CMC: 1, 7, 8-15, 17, 19, 22, 27, 29, 30-32, 34, 35, 40, 42, 46, 48, 49, 51, 54, 55, 58, 59, 61, 62, 72, 76, 78, 81-83, 91-95, 106, 107, 111, 112 GDS: 111 HSM: 24, 27	CMC: 16, 18, 21, 28, 37, 38, 44, 45, 47, 50, 52, 53, 56, 57, 60, 64, 65, 69-71, 74, 75, 79, 80, 84, 86-90, 97, 98, 100, 105, 108, 109 MSL: 117 GDS: 112	Unclear or insufficient definition CMC: 5, 63, 96, 99, 114 Uninformative/constant after re-coding CMC: 6, 33, 34, 66, 68, 85, 103, 104, 113, 116 GDS: 109 Redundant CMC: 36, 115

Chapter 3

A Growth Series of a Devonian Stem Lamprey and Implications for the Origin of the Filter-feeding Larvae in Vertebrate Evolution

> "But is that all you recall from your life as a lamprey—swaying to and fro at the bottom of a river?"
>
> "A former life can't be called up just like that," she said. "If you're lucky, you get a flash of what it was like. It's like catching a glimpse through a tiny hole in a wall."
>
> — *Scheherazade*, Haruki Murakami

3.1 INTRODUCTION

The ontogeny of lampreys holds a special place in the historical development of ideas about the early evolution of vertebrates. Ammocoete larvae of living lampreys have influenced scenarios about vertebrate origins since the emergence of this evolutionary problem (Haeckel, 1876; Dohrn, 1885; Gaskell, 1908; Goodrich, 1930; de Beer, 1937; Gregory, 1946; Romer and Parsons, 1977; Gee, 1996). Early comparative approaches emphasized their overall resemblance with cephalochordates to postulate an ammocoete-like vertebrate ancestor, which is frequently depicted as a sand-burrowing filter feeder with a notochord (Gaskell, 1908; Goodrich, 1930; de Beer, 1937) (or to propagate the idea that cephalochordates are 'degenerate' vertebrates; Haeckel, 1876). More recent hypotheses inferred similar ancestors on the basis of the filter-feeding habits and seemingly arrested development of adult-specific traits in ammocoetes (Gregory, 1946; Romer and Parsons, 1977; Gans, 1993; Gee, 1996; Mallatt, 1996; Jandzik et al., 2015). Implicitly or explicitly, these ammocoete-like ancestors invoke a recapitulatory scenario: ammocoetes retain primitive conditions, whereas the predatory adults represent an ontogenetically and evolutionarily derived state.

Several lines of inference challenge this view. First, gene expression patterns revealed phenotypic similarities between hagfish and lampreys at embryonic stages (Oisi et al., 2013; Sugahara et al., 2016). Second, given the morphological similarities between the two lineages at the adult stage (Kuratani et al., 2016), the direct-developing hagfish would require the loss of ammocoete-like larval stage in that lineage. Third, putative Cambrian stem vertebrates

(*Metaspriggina*, myllokunmingiids, and yunnanozoans) do not strongly corroborate an ammocoete-like morphology. For example, they lack a prominent oral hood and fused branchial basket, despite bearing general chordate/vertebrate characteristics (e.g., branchial pouches, notochord, W-shaped myomeres) that are also expressed in ammocoetes (Shu et al., 2003; Janvier, 2007; Conway Morris and Caron, 2014). Finally, the implied retention of the ancestor as a larva constitutes a classic example of Haeckelian recapitulation, which exposed early versions of this hypothesis to the same criticism as the Biogenic Law (Garstang, 1928; Gould, 1977; Gee, 1996).

None of these inferences rules out the ammocoete-first model. However, one prediction of the 'ammocoete-first' hypothesis remains to be tested fully: Did stem members of the vertebrate lineage pass through an ammocoete phase during ontogeny? Ammocoetes have been described for *Mesomyzon mengae* from the Early Cretaceous of China (Chang et al., 2014), but this taxon is nested immediately outside the crown node of petromyzontiforms (Chapter 2). A long stem extending to pre-Devonian times is occupied by several stem taxa that should better inform plesiomorphic states of the clade (Bardack and Zangerl, 1968, 1971; Bardack and Richardson, 1977; Janvier and Lund, 1983; Lund and Janvier, 1986; Gess et al., 2006; Germain et al., 2014; Janvier and Sansom, 2016).

In this chapter, I describe a newly reconstructed growth series of *Priscomyzon riniensis*, a stem lamprey from the Upper Devonian (Frasnian) Witpoort Formation of South Africa (Gess et al., 2006). The series of specimens is used to test whether *Priscomyzon* passed through an ammocoete-like phase during ontogeny. In addition to the holotype representing the adult stage, six individuals of the same taxon but of smaller body sizes were discovered from the same horizon. All the immature specimens lack ammocoete-like traits, and instead exhibit morphological features consistent with the predatory adult phase of a crown-group lamprey.

3.2 MATERIALS AND METHODS, SUMMARY

All specimens of *Priscomyzon* were collected from a single mudstone layer at Waterloo Farm in the Witpoort Formation of the Cape Supergroup, South Africa and catalogued at the Albany Museum, Rhodes University (Grahamstown, South Africa). Observations were made under a binocular microscope with low light angles. The illustrations were prepared by comparing images

taken at different light angles. The fragility of the specimens precluded any potentially corrosive methods such as alcohol immersion or ammonium chloride coating. The mudstone underwent partial metamorphosis, and the tissue remnants were completely replaced and recrystallized. Therefore, geochemical analysis using radiation or spectrometric techniques was ruled out as well.

To reinforce the inference that the immature specimens may be attributed to each coeval stem lamprey taxon (*Priscomyzon*, *Hardistiella*, and *Mayomyzon*), I used maximum parsimony analysis by adding the specimens to the recent dataset of early vertebrate phylogeny (Chapter 2). To assess morphological similarities and dissimilarities with other cyclostomes, gnathostomes, and invertebrate outgroups, I described morphological disparity within the same dataset (Chapter 2) using metric and non-metric multidimensional scaling methods. For full details on analytical methods, see **3.6 Supplementary Information**.

3.3 DESCRIPTIONS

The holotype of *Priscomyzon* (AM 5750; Figs. 3.1, S3.1, S3.2) represents the most mature specimen of the growth series. Comparable to the adult stage of modern lampreys, AM 5750 has prominent eyes, a well-developed oral disc with the annular cartilage and a ring of 14 keratinous teeth, and nine branchial arches forming a cartilaginous basket. The eyes are distinguished from other preserved organs by high densities of recrystallized tissues, which are paired and overlap the branchial basket (Fig. 3.1a). The structures were originally interpreted as otic capsules based on presumed differences in preservation potential (Gess et al., 2006). However, the anatomical positions, textures, and size relative to head, are more compatible with eyes than with otic capsules when compared with living lampreys at the adult phase. These traits remain consistent across multiple specimens (Fig. 3.2). The identification is supported by experimental taphonomy of modern lampreys, as the retina has higher preservation potentials relative to otic capsules (Sansom et al., 2010a, 2011, 2013a). The otic capsules are the patches of lower densities visible around the posterior margins of the eyes, which appear to overlap the capsules dorsally (Fig. 3.1). The otic capsules are connected with the branchial basket as in modern adult lampreys. The circumoral teeth are inferred to be keratinous as seen in modern lampreys. Similar structures may have existed in other stem lampreys, including *Hardistiella*, *Mayomyzon*, and *Mesomyzon*.

Unfortunately, specimens of these taxa are preserved in a laterally compressed manner, so the structures in *Priscomyzon* cannot be compared using these stem taxa. Among the nine branchial arches, the first branchial arch extends anterior to the eye in a manner reminiscent of osteostracans (Janvier, 1996). Although the original description (Gess et al., 2006) identified eight arches and seven branchial pouches, observations under polarized light revealed a distinct arch between the originally identified first and second arches ("2" in Fig. 2.1b). The lateral outline on the left side corroborates the total count of eight branchial pouches and nine arches through the number of swellings. The midline structure potentially represents a lingual apparatus, which is accompanied by styliform cartilages. Consistent with the original identification as a potential heart (Gess et al., 2006), the 8-shaped structure posterior to the transverse connection of the branchial basket assumes the pericardial position. The head occupies greater than a third of the total body length (42 mm).

From the smallest specimen (AM 5820) to the holotype, a number of morphological traits are present across different body sizes. All seven specimens have prominent eyes and small otic capsules behind them (Figs. 3.1, 3.2; Table 3.1). The nine branchial arches form a basket in post-metamorphosis (AM 5819) and metamorphosing (AM 5815) specimens (Fig. 3.2a, b, e, f). Although the number of arches cannot be determined, the branchial cartilages are preserved in all other larvae and form a posteriorly closed basket at least in one of the larval specimens (AM 5814) (Figs. 3.2i, j, S7). The perioral ring of keratinous teeth is present in the smallest specimen (AM 5820; Fig. 3.2k, l) and the post-metamorphosis juvenile (AM 5819; Fig. 3.2a, b). The tectal cartilages (unique to the adult phase of crown-group lampreys) are preserved in all immature specimens except AM 5816 (Table 3.1). In the holotype, the tectal cartilages and other dorsal elements of the upper lip are obscured by ventral structures. All seven specimens are dorsoventrally compressed (Figs. 3.1, 3.2). The plane of the split between part and counterpart cut across similar levels among the specimens in which dorsal structures like eyes and tectal cartilages are exposed better than ventral structures. The holotype represents an exception for having the ventral structures (like the annular cartilage) that obscure the dorsal elements. The angle of compression seems to have been oblique in AM 5819, which caused left-right misalignment of the skeletal elements (Fig. 3.1a, b). Assuming a dorsal view, the head of AM 5817 was twisted to expose the right over the left side (Fig. 3.2g, h), and the trunk in AM 5820 was rotated to show its left lateral side (Fig. 3.2k, i). Given that *Priscomyzon* (AM 5750) is the

only known jawless vertebrate from the extensively sampled Witpoort Formation (Gess et al., 2006), and given that the seven specimens show a continuum of size and morphological traits (Table 3.1), these specimens likely represent a growth series of a single taxon.

The larvae (AM 5814, 5817, 5820) range in total body lengths from one third (AM 5820: 15 mm) to greater than a half (AM 5817: 22+ mm) the length of the holotype. The smallest AM 5820 has an anteroposteriorly elliptical oral disc with the annular cartilage and keratinous teeth, a proboscis-like, elongate snout supported by anterior and posterior tectal cartilages, and remnants of branchial cartilages (Figs. 3.2k, l, S8). More than half of its length (57%) consists of the head due to large prebranchial structures relative to trunk dimensions. Unlike all other specimens of *Priscomyzon*, the body outline of AM 5820 expands in width immediately posterior to the branchial region to include an area of lower densities of preserved tissues across the bands of recrystallized organic materials (these bands appear as a result of partial metamorphosis of the mudstone at the holotype locality; Gess et al., 2006). The trunk (delineated as the area of higher tissue densities) follows the head and tapers posteriorly. The low-density region extends the entire length of the trunk. On the basis of the morphological profile, it is interpreted tentatively as a yolk sac. Modern lampreys retain yolk after hatching and as burrowing pro-larvae at which stage the body length is approximately two thirds (7.5-10 mm) of AM 5820 (Piavis, 1971). Modern hagfish hatchlings also carry a conspicuous yolk sac, and they are substantially larger than AM 5820 at a body length of approximately 30 mm (Miyashita and Coates, 2016). The oral region is not preserved in two other pre-metamorphosis larvae (AM 5814, 5817), but both specimens have tectal cartilages (Figs. 3.2g-j, S3.6, S3.7; Table 3.1). The trunk is narrow in width and elongate in the small specimens (AM 5814, 5820) but appears wider with respect to body length in larger specimens.

The onset of metamorphosis is recognized by (***a***) the snout reduced in length and becoming funnel-like, and (***b***) anterior shift of the branchial arches (Table 3.1; AM 5815, 5816). The metamorphosing larvae (transformers; AM 5815, 5816; Figs. 3.2c-f, S3.4, S3.5) are not substantially larger than the largest larval specimens. Although neither metamorphosing specimen is preserved along its entire body length, AM 5815 is similar to the larva AM 5817 in branchial length (AM 5815: 3.67 mm; AM 5817: 4.22 mm) and post-branchial trunk width (AM 5815: 4.30 mm; AM 5817: 3.63 mm) (Fig. S3.1). AM 5816 is also similar to AM 5817 in post-branchial trunk width (4.27 mm). Comparison of width measurements warrants a caveat,

however. All specimens of *Prisocmyzon* show general dorsoventral compression, but AM 5817 has a minor post-mortem twist between the head and trunk, which could affect width measurement. In this stage, the first branchial arch sits posterior to the position of eyes (Table 3.1). The nine branchial arches form a basket that is closed posteriorly. The snout is constricted and elongate. This condition is intermediate between the non-constricted, elongate proboscis in pre-metamorphosis (AM 5820) and the constricted, short snout supporting a sucker-like oral disc in post-metamorphosis (AM 5750, 5819). Paired trabecular cartilages support the elongate snout anterior to the eyes (also preserved in the larvae AM 5817 and 5820). Also reflecting the elongate snout, the posterior tectal cartilage sits well anterior to the eyes.

Metamorphosis is considered complete with the prominent oral disc, medial shift of the eyes, and branchial arches extending anterior to the eyes (Table 3.1; AM 5819, 5750). The post-metamorphosis juvenile (AM 5819) has a head length approximately two thirds that of the holotype (AM 5819: 11.42 mm; AM 5750: 16.98 mm) (Figs. 3.2a, b, S3.3). The maximum width across the branchial region (as measured parallel to the left and right eyes) shows that AM 5819 is approximately 1.5 times larger than the metamorphosing AM 5815 in this metric trait (AM 5815: 5.68 mm; AM 5819: 8.26 mm; AM 5750: 11.34 mm). One factor confounds precise comparison of the measurements: the direction of dorsoventral compression was oblique for AM 5819 (Fig. 3.1a, b). Furthermore, the head of AM 5819 is proportionally wider with respect to length than in the holotype (AM 5750). So exact size differences are difficult to assess. This is also the case when the branchial lengths (otic capsule to pericardium) are considered (AM 5815: 3.67 mm; AM 5819: 5.06 mm; AM 5750: 6.48 mm). In AM 5819, the oral disc is well developed into a large, funnel-like structure. The plane of break for AM 5819 is more dorsal than for the holotype so the keratinous teeth, except for the two positioned anteriorly, are mostly obscured by the overlying annular cartilage. The anterior and posterior tectal cartilages support the constricted, short snout. The eyes sit in intermediate position between the larvae (close to the lateral edge) and the holotype (closer to the midline). The nine branchial arches extend radially to form a cartilaginous basket. The first branchial arch extends anterolaterally below the eye, again intermediate in position between AM 5815 and the holotype. The structure preserved between the eyes represents the nasohypophyseal canal. If this identification is correct, its posterior position is likely a taphonomic artifact.

3.4 DISCUSSION

3.4.1 Ontogenetic Comparison

Strikingly, the growth series of *Priscomyzon* lacks morphological correlates of filter feeding present in extant ammocoete larvae, and instead reveals a number of features that characterize the predatory adult phase of extant lampreys. These traits include prominent eyes (ammocoete condition: primordial eyespots covered by dermis), oral disc with annular cartilage and keratinous teeth (horseshoe-shaped oral hood with cirri), tectal cartilages (absent), proximity of otic capsules to eyes (separated), anteroposteriorly short and pericardially closed branchial basket (anteroposteriorly elongate and parallel), and trabecular cartilages fusing to each other anteriorly (parallel and separate). Despite the early presence of these otherwise adult-specific traits (Table 3.1), the overall growth series parallels that of extant lampreys well. Body sizes are similar among the specimens across metamorphosis (AM 5815-5819) as in modern lampreys (Renaud, 2011). Proportional features resembling the adult phase of modern lampreys (an oral disc, constricted snout, laterally expanded branchial region) only appear post-metamorphosis.

Priscomyzon likely did not have an ammocoete-like stage before reaching the size represented by AM 5820. This is because of: (***a***) the structure identified putatively as a yolk sac in AM 5820; (***b***) the transient characters present in neither ammocoetes nor adults of extant lampreys (e.g., proboscis, radially arranged branchial arches) (Table 3.1); and (***c***) small sizes of the youngest larvae. It is unlikely that ammocoete-like traits were lost due to taphonomic bias. In living lampreys, the ammocoete-specific traits such as oral hood, endostyle, and velum are more resistant to decay than the branchial cartilages (Sansom et al., 2010b, 2011, 2013a), which are preserved in the larval specimens of *Priscomyzon*.

An analysis of morphological disparity corroborates these assessments. Ammocoetes and the immature specimens of *Priscomyzon* were each closer to adult petromyzontiforms than to one another (Figs. 3.4b, S3.12, S3.13). These inferences do not definitively rule out the presence of ammocoetes in *Priscomyzon* at a size smaller than AM 5820. Neither does the mode of preservation allow testing the ‘yolk sac’ in that specimen through radiation or spectrometric methods (**3.2 Materials and Methods, Summary**). However, if the ammocoete-like phase did exist — and if the putative yolk sac in AM 5820 is ignored — *Priscomyzon* would have to develop ammocoete traits initially, only to undergo first metamorphosis into a form represented

by AM 5820 (body length <15 mm) with an oral disc, keratinous teeth, prominent eyes, and tectal cartilages. This unlikely scenario would also assume that the immature stages described in this growth series were either lost in the crown lamprey lineage or independently derived in *Priscomyzon*. Living lampreys persist in the filter-feeding ammocoete phase for two to seven years and reach sizes of adults or greater prior to metamorphosis (Renaud, 2011). Therefore, multiple lines of inferences favor the inferred lack of an ammocoete-like phase in the ontogeny of *Priscomyzon* over a yet-to-be-discovered early phase of a minute ammocoete.

The growth series of *Priscomyzon* raises a question: whether the absence of the ammocoete-like filter-feeding stage was a general or specialized condition in the lamprey stem. With the single exception of the Cretaceous stem lamprey *Mesomyzon* (Chang et al., 2014), no ammocoete-like fossil is known from Paleozoic strata. Instead, the smallest specimens of two other Paleozoic stem lampreys resemble the larvae and juveniles of *Priscomyzon*. A comparison with the larger conspecifics identifies features consistent with the growth series of *Priscomyzon*. FMNH PF 8167 represents the smallest described specimen of the Carboniferous stem lamprey *Mayomyzon* (Bardack and Zangerl, 1971). At approximately one third of the body length (38%) of the largest specimens of *Mayomyzon*, FMNH PF 8167 has prominent eyes, an elongate snout with tectal cartilages, and anteriorly fused trabecular cartilages as in the larval *Priscomyzon* (Figs. 3.3a, b, S3.10; Table 3.1). Originally described as a larva (Lund and Janvier, 1986), CM 46123 is approximately two thirds the body length (66%) of the largest specimen of another Carboniferous stem lamprey *Hardistiella* (Figs. 3.3c, d, S3.9). CM 46123 also has prominent eyes and tectal cartilages, and the branchial region is anteroposteriorly short (almost equaling the prebranchial head length) as in larval *Priscomyzon* (Table 3.1).

In absolute sizes, FMNH PF 8167 (body length = 27.9+ mm; branchial length = 3.2 mm) is comparable overall to the small metamorphosing larva of *Priscomyzon* (AM 5815). CM 46123 (body length = 43+ mm; branchial length = 4.8 mm) is similar in body length to the mature specimen of *Priscomyzon* (AM 5750). Although little is known about size ranges of Paleozoic stem lampreys, the specimens morphologically comparable to modern adult lampreys are generally small (body lengths between 30 and 70 mm; greater than 80 mm in *Myxineidus*) (Janvier and Sansom, 2016). In living lampreys, metamorphosing larvae and sexually ripe adults both undergo reduction in body length. The larvae are larger prior to metamorphosis than during and immediately after metamorphosis, and this reduction is sometimes down to 80% of the size at

pre-metamorphosis (Damas, 1935; Youson and Potter, 1979; Youson, 1980; Renaud, 2011). So the size distributions within these species of Paleozoic stem lampreys appear consistent with metamorphosis of living lampreys, but size comparison alone may not allow correct assessment of their ontogenetic stages. At any rate, the smallest specimens of *Hardistiella* and *Mayomyzon* each have a combination of morphological traits consistent with the immature ontogenetic stages of *Priscomyzon* (Table 3.1).

As these three Paleozoic stem lampreys form a grade with respect to the crown group (Chapter 2; Gess et al., 2006; Gabbott et al., 2016; McCoy et al., 2016), the ontogenetic sequence of *Priscomyzon* may be interpreted as reflecting the primitive state of the lamprey lineage. Otherwise the loss of ammocoetes would have had to occur independently in each of the Paleozoic stem lamprey branches — and again in hagfish and gnathostomes for the ammocoete-like phase to be the last common ancestor of living vertebrates. It is possible that these three taxa form a clade united by the loss of an ammocoete phase. But this alternative interpretation has no support from phylogenetic inferences (discussed in **3.6 Supplementary Information**). Thus, the ontogenetic series of *Priscomyzon* contradicts the prediction of the 'ammocoete first' hypothesis. Instead, it is consistent with an alternative hypothesis (Hardisty, 1979, 1982) that ammocoetes of living lampreys represent a secondary innovation inserted in the life history (Fig. 3.4a). Given that the Paleozoic stem lampreys all occur in marine settings and the Mesozoic and crown-group lampreys in freshwater (with some anadromous species; Renaud, 2011), the acquisition of a filter-feeding ammocoete phase may have coincided with the marine-to-freshwater transition before the crown node.

3.4.2 Implications for Early Vertebrate Evolution

The ontogeny of *Priscomyzon* questions the utility of ammocoetes as a surrogate for the hypothetical last common ancestor of all living vertebrates. In light of the larvae and juveniles of stem lampreys presented here, the extant ammocoete traits typically regarded as primordial or primitive may be considered as secondary or reversed (Tables 3.2, 3.3). These traits include an endostyle (mucous-producing anlage of thyroid) and mucocartilage (a fibrous, mesenchymal skeletal tissue unique to ammocoetes; Hardisty, 1981). A secondary insertion of the filter-feeding larval phase explains some curious features of ammocoetes, including: (***a***) the mucocartilage becomes reduced during metamorphosis without differentiating into cellular cartilages (de Beer,

1937; Johnels, 1948); (***b***) many musculoskeletal elements of lampreys readily compared with those of hagfish and gnathostomes only form post-metamorphosis (e.g., lingual apparatus, lateral wall of braincase, neural arches) (Kuratani et al., 2016; Miyashita, 2016); and (***c***) gene expression profiles during brain regionalization are divergent in lampreys (e.g., *Nkx2.1*-positive medial ganglionic eminence of subpallium and *Pax6*-positive rhombic lip) (Sugahara et al., 2016), despite broad conservation in other vertebrates. These traits have been used to infer heterochronic shift in the evolution of lampreys (e.g., Hardisty, 1982). Assuming that the growth series of *Priscomyzon* represents a general stem condition, ammocoetes might have evolved via: (***a***) post-displacement of traits characterizing the adult phase of modern lampreys (e.g., eyes, keratinous teeth, chondrocranium, and thryroid); and (***b***) replacement of traits characterizing the larval phase of stem lampreys (e.g., proboscis) with ammocoete-specific traits (e.g., oral hood, mucocartilage, and endostyle). This scenario is internally consistent, but non-falsifiable with current evidence.

An independent origin of ammocoetes also suggests that ammocoete-cephalochordate similarities represent convergence due to filter feeding habit, rather than retention of stem chordate/vertebrate traits (Hardisty, 1979, 1982). The results of morphological disparity analyses are consistent with this, as ammocoetes were distant from invertebrate outgroups and more closely associated with adult lampreys (Figs. 3.4b, S3.12, S3.13-S3.15; detailed methods and results discussed in **3.6 Supplementary Information**). Following this line of reasoning, cyclostomes may be characterized as a clade of predators (hagfish and lampreys), whereas stem gnathostomes appear generally to be deposit feeders (Gregory, 1931; Denison, 1961; Mallatt, 1984a; Gilmore, 1992; Forey, 1995; Janvier, 1996; Janvier and Arsenault, 2007). Deposit feeding is more parsimonious as the mode of feeding at the crown vertebrate node, given the *Euphanerops*-like morphology in *Metaspriggina* (Conway Morris and Caron, 2014)..

3.5 CONCLUSION

In this chapter, I described a growth series of the stem lamprey *Priscomyzon riniensis* and tested the ammocoete-first model of vertebrate evolution. None of the seven individuals of *Priscomyzon* — ranging from a yolk-carrying larva to an adult — has any correlates of the ammocoete phase. Instead, the larvae of *Priscomyzon* have prominent eyes, an oral disc with keratinous teeth, a proboscis-like elongate snout, and an anteroposteriorly short and pericardially closed branchial

basket. In living lampreys, these characters develop only in the predatory adult phase. Similar morphological characters are also present in the smallest specimens of two other Palaeozoic stem lampreys, *Hardistiella* and *Mayomyzon*. In morphological disparity analyses, these Paleozoic larval forms and ammocoetes did not overlap in morphospace. Furthermore, ammocoetes and invertebrate outgroups (including cephalochordates) were clearly distinguished from one another. Evidence I presented in this chapter contradicts a crucial prediction of the long-held 'ammocoete-first' model that the filter-feeding larval phase was conserved along the lamprey stem.

FIGURES

Fig. 3.1. The re-interpreted anatomy of the Late Devonian stem lamprey *Priscomyzon riniensis* at the mature ontogenetic stage closely follows that of a modern lamprey at the same stage. Photograph (**a**) and interpretive drawing (**b**) of main slab of the holotype (AM 5750) from the Witpoort Formation (Upper Devonian) of South Africa. Arabic numerals indicate branchial arches, and Roman numerals indicate keratinous teeth. **Abbreviations: ac**, annular cartilage; **bb**, branchial basket; **bra**, branchial arch; **df**, dorsal fin; **dt**, digestive tract; **e**, eye; **h/eb**, hypotrematic/epitrematic bar; **hyb**, hypobranchial bar; **kt**, keratinous teeth; **la**, lingual apparatus; **nc**, notochord; **nh**, nasohypophyseal structure; **oc**, otic capsule; **od**, oral disc; **ol**, outer lip; **os**, oral structure; **pc**, pericardiac structure; **prb**, proboscis; **sc**, styliform cartilage; **tb**, transverse bridge of branchial basket; **tc**, tectal cartilage; **tca**, anterior tectal cartilage; **tcp**, posterior tectal cartilage; **tr**, trabecular cartilage; **ys**, yolk sac.

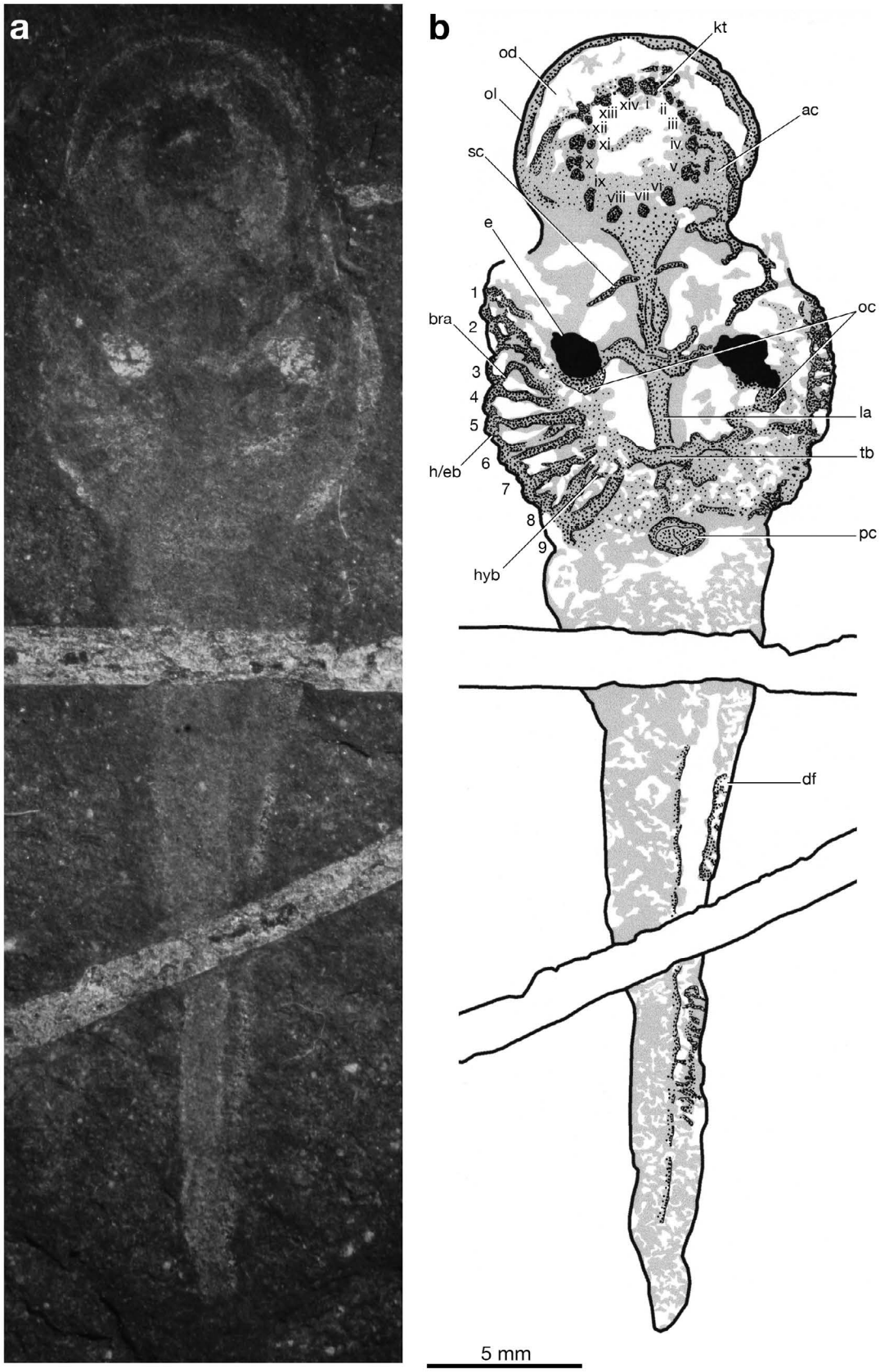
a
b
kt
od
ol
xiii
xiv
i
ii
xii
iii
xi
iv
ac
sc
x
v
ix
viii
vii
vi
e
1
oc
bra
2
3
4
la
5
tb
h/eb
6
7
8
pc
9
hyb
df
5 mm

Fig. 3.2. Immature specimens of *Priscomyzon* from the type locality comprise a growth series but present no evidence for an ammocoete-like filter-feeding phase. Photograph (**a**) and interpretive drawing (**b**) of a post-metamorphosis juvenile (AM 5819); photograph (**c**) and interpretive drawing (**d**) of the larger metamorphosing larva (AM 5816); photograph (**e**) and interpretive drawing (**f**) of the smaller metamorphosing larva (AM 5815); photograph (**g**) and interpretive drawing (**h**) of the largest pre-metamorphosis larva (AM 5817); photograph (**i**) and interpretive drawing (**j**) of the pre-metamorphosis larva (AM 5814); photograph (**k**) and interpretive drawing (**l**) of the smallest pre-metamorphosis larva (AM 5820). See Fig. 3.1 for abbreviations. Scale bars 2 mm for all panels.

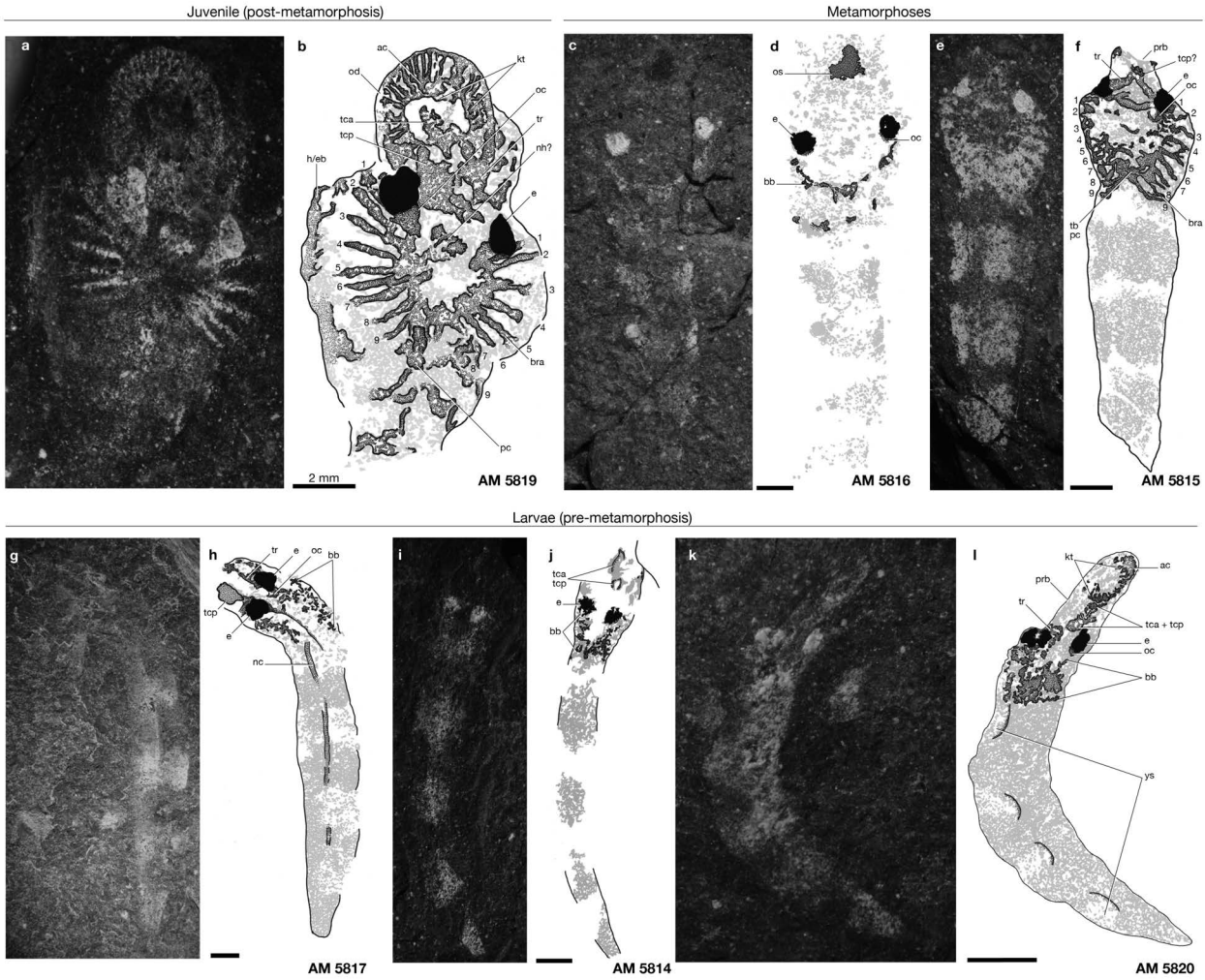
Juvenile (post-metamorphosis)
Metamorphoses
Larvae (pre-metamorphosis)
a
b
c
d
e
f
g
h
i
j
k
l
ac
od
kt
oc
tca
tcp
tr
nh?
h/eb
e
bb
os
prb
tcp?
tb
pc
bra
nc
tca + tcp
ys
2 mm
AM 5819
AM 5816
AM 5815
AM 5817
AM 5814
AM 5820

Fig. 3.3. Immature specimens of other Paleozoic stem lampreys (*Hardistiella* and *Mayomyzon*) are more similar to those of *Priscomyzon* than to ammocoete larvae of the extant lampreys. Photograph (**a**) and interpretive drawing (**b**) of the smallest specimen of *Mayomyzon* (FMNH PF 8167); photograph (**c**) and interpretive drawing (**d**) of the smallest specimen of *Hardistiella* (CM 46123); and a sketch (**e**) of the ammocoete larva (Tahara's stage 30) of *Petromyzon marinus*, modified from Tahara (1988). See Fig. 3.1 for abbreviations.

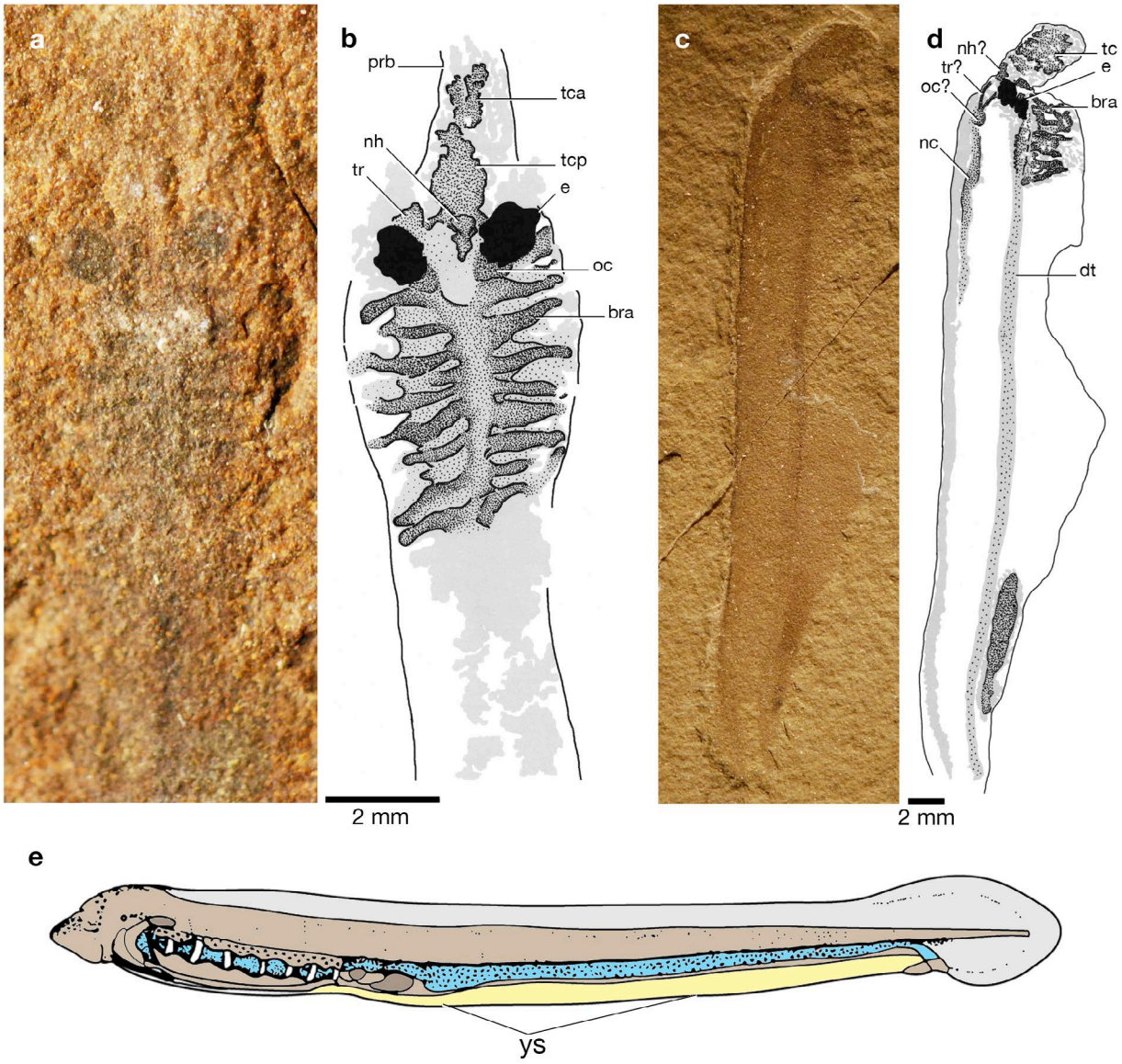
a
b
prb
tca
nh
tcp
tr
e
oc
bra
2 mm
c
d
nh?
tc
tr?
e
oc?
bra
nc
dt
2 mm
e
ys

Fig. 3.4. The lack of evidence for ammocoete-like larvae in the Paleozoic stem lampreys suggests a secondary origin of ammocoetes closer to the crown node. Phylogenetic distribution of larval forms in lampreys (**a**) suggests that the growth series of *Priscomyzon* represents a shared primitive state in lampreys. The immature specimens of the Paleozoic stem lampreys and ammocoetes of modern lampreys do not overlap each other in morphospace (first and second coordinate axes from a non-metric multidimensional scaling analysis; see **3.6.1** for methods) (**b**). In tree (**a**), nodes are indicated by dots, and terminal taxa by boxes. Nodes and terminal taxa are colour-coded for character state: red = non-ammocoete larva; blue = ammocoete larva; black = unknown. Node conditions are estimated on the basis of maximum parsimony. Tree adopted from Chapter 2.

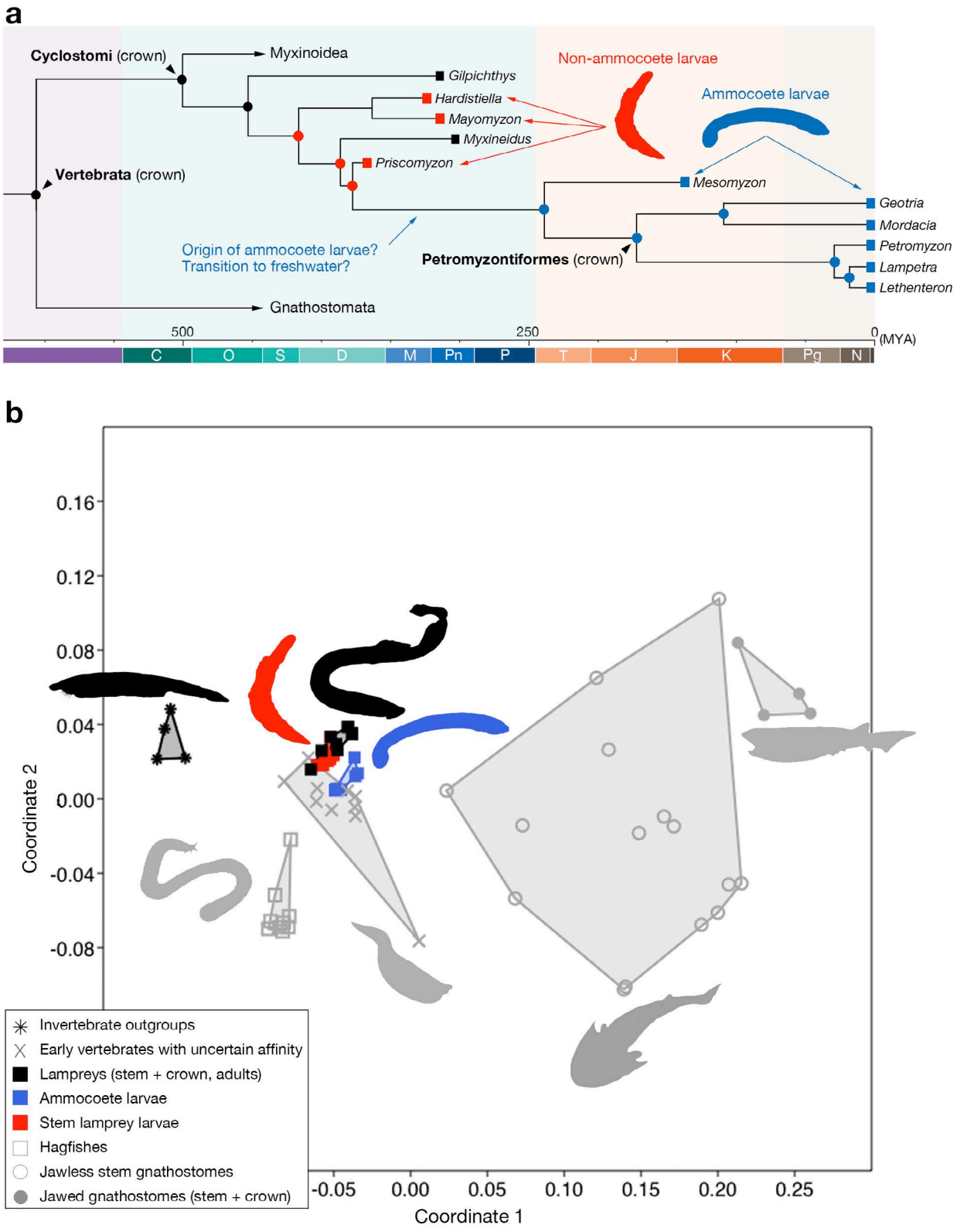
a
Cyclostomi (crown)
Myxinoidea
Gilpichthys
Hardistiella
Mayomyzon
Myxineidus
Priscomyzon
Vertebrata (crown)
Gnathostomata
Origin of ammocoete larvae?
Transition to freshwater?
Petromyzontiformes (crown)
Non-ammocoete larvae
Ammocoete larvae
Mesomyzon
Geotria
Mordacia
Petromyzon
Lampetra
Lethenteron
500
250
0
(MYA)
C
O
S
D
M
Pn
P
T
J
K
Pg
N
b
0.16
0.12
0.08
0.04
0.00
-0.04
-0.08
Coordinate 2
-0.05
0.00
0.05
0.10
0.15
0.20
0.25
Coordinate 1
Invertebrate outgroups
Early vertebrates with uncertain affinity
Lampreys (stem + crown, adults)
Ammocoete larvae
Stem lamprey larvae
Hagfishes
Jawless stem gnathostomes
Jawed gnathostomes (stem + crown)

TABLES

Table 3.1. A summary of ontogenetically variable traits in *Priscomyzon riniensis* and comparison to other Paleozoic stem lampreys (*Hardistiella* [*Hard.*] and *Mayomyzon* [*May.*]) and living lampreys (*Petromyzon marinus*; ammocoete [Amm.] and adult). The growth series of *Priscomyzon* has three categories of the seven specimens (pre-metamorphosis, metamorphosis, and post-metamorphosis), but the categories are not discrete from each other. The specimens of different categories may have overlaps of traits. **Code for traits:** - = initial state; / = intermediate state; + = terminal state; ? = unknown; * = transiently expressed.See text for institutional abbreviations.

	Priscomyzon							*May.*	*Hard.*	*Petromyzon*	
	Pre-metamorphosis			Metamorphosis		Juvenile/adult		Larva	Larva?		
	AM 5820	AM 5814	AM 5817	AM 5815	AM 5816	AM 5819	AM 5750	FMNH PF 8167	CM 46123	Amm.	Adult
Abdominal swelling (yolk sac?) (+), absent (-)	+	-	-	-	-	-	-	-	-	+*	-
Eyes, prominent (+) or primordial (/)	+	+	+	+	+	+	+	+	+	/	+
Eye and otic capsule, set apart (/) or close (+)	+	?	+	+	+	+	+	+	+	/	+
Eyes, laterally (-) or medially (+) positioned	-	-	-	-	-	+	+	-	+	-	-
Oral disc (+) or hood (/)	+	?	?	+	?	+	+	?	+	/	+
Circumoral keratinous teeth (+), absent (-)	+	?	?	+	?	+	+	?	?	-	+
Annular cartilage (+), absent (-)	+	?	?	+	?	?	+	?	?	-	+
Snout, funnel-like (+), elongate (/), or proboscis (-)	-	-	/	/	/	+	+	-	/	+	+
Tectal cartilages (+), absent (-)	+	+	+	+	+	+	?	+	+	-	+
Trabecular cartilages, fusing anteriorly (+), parallel (-)	+	?	?	+	?	+	?	+	+	-	+
Branchial basket, closed posteriorly (+) or open (-)	?	+	?	+	+	+	+	+	?	-	+
Branchial basket, short, wide (+) or long, parallel (-)	+	+	+	+	+	+	+	-	+	-	+
Branchial arch I, orientation: anterior (+), anterolateral (/) or lateral (-)	-	-	-	/	/	/	+	/	/	-	-
Head, short (-) or long (+): length relative to trunk	+	-	-	-	-	?	-	-	-	-	-

Table 3.2. Fit of evidence for the 'ammocoete-first' (H_1) versus the 'ammocoete-second' (H_2) hypotheses in the morphological similarities proposed between ammocoete larvae and cephalochordates. Proposed similarities are dissected further to delineate differences between the two lineages (A: ammocoetes; C: cephalochordates). Interpretations of the traits differ depending on whether ammocoetes represent a symplesiomorphic state ('ammocoete-first') or an autapomorphic state ('ammocoete-second') within lampreys. **Bold** typeface indicates more parsimonious interpretation, given cyclostome monophyly (Chapter 2). Similarities and observed differences were sampled from the literature (in addition to those cited in main text: Damas, 1944; Johnels, 1948; Newth, 1956; Mallatt, 1979, 1981, 1985; Jefferies, 1987; Langille and Hall, 1988; Holland et al., 1993, 1997, 2015; Lacalli et al., 1994; Holland and Garcia-Fernàndez, 1996; Harrison and Ruppert, 1997; Kuratani et al., 1997, 1999, 2001, 2004; Holland and Holland, 1998; Wada et al., 1998; Horigome et al., 1999; Boorman and Shimeld, 2002; Mallatt and Chen, 2003; McCauley and Bronner-Fraser, 2003; Lacalli, 2005; Ruppert, 2005; Wicht and Lacalli, 2005; Janvier, 2007; Janvier and Arsenault, 2007; Paris et al., 2008; Putnam et al., 2008; Miyashita, 2012, 2016; Shimeld and Donoghue, 2012; Holland, 2016; Satoh, 2016.

Potential similarities	Observed differences (C: cephalochordates; A: ammocoetes)	Interpretations	
		H_1: conserved plesiomorphy	H_2: convergent apomorphy
Indirect development	C: ontogenetically terminal state A: ontogenetically intermediate state	Recapitulation (adult phase: terminal addition); loss of ammocoetes in myxinoids and gnathostomes	**Insertion of ammocoete phase (adult phase: postdisplacement)**
Oral hood	C: mesodermal derivative A: neural crest derivative	Change in cell lineage and differentiation potentials; loss in myxinoids and gnathostomes	**Compatible with independent origins**
Oral cirri	C: perioral epidermal structure supported by cartilage A: extended sensory oral epithelium, lacking cartilaginous support	Change of topographic and functional relationships; loss in myxinoids and gnathostomes	**Compatible with independent origins**
Primordial eyespots	C: photoreceptive organ A: arrested eye development	Recapitulation; stage truncated in myxinoids and gnathostomes	**Eye development delayed to adult phase**
Branchial basket	C: asymmetric development; primary and secondary arches; mesodermally derived cartilages; all pharyngeal diverticula open externally; branchial pouches absent; atrium present A: symmetric development; primary arches only; neural crest-derived cartilages; first pharyngeal diverticulum closed; branchial pouches present; atrium absent	Either the cephalochordate or ammocoete (vertebrate) pattern represents plesiomorphic state from which the other pattern was derived. Overall similarities in the appearance of the baskets reflect evolutionary conservation.	Both cephalochordate and ammocoete (vertebrate) patterns represent independently derived apomorphic states. Overall similarities are superficial; oropharyngeal development highly modified in deuterostome evolution.

Potential similarities	Observed differences (C: cephalochordates; A: ammocoetes)	Interpretations	
		H_1: conserved plesiomorphy	H_2: convergent apomorphy
Velum	C: epithelial fold lined with cilia at buccal-branchial boundary A: musculoskeletal pump in outpocket of mandibular arch	Transitional series from one state to another; A-P identity of 'arches' conserved	Pharyngeal pumps independently evolved; no exact homology of 'arches'
Endostyle	C: ontogenetically terminal state A: ontogenetically transient state	Thyroid development recapitulates character polarity; stage truncated in myxinoids and gnathostomes	**Thyroid primordium co-opted for mucous production; development arrested**
Pterygial/hypobranchial muscles	C: obtulators; asymmetric arrangement; no segments; no circumpharyngeal migration of myoblasts A: constrictors; symmetric arrangement; segmentation; circumpharyngeal migration of myoblasts	Either the cephalochordate or ammocoete (vertebrate) pattern represents plesiomorphic state from which the other pattern was derived. Somitic muscle in hypobranchial space represents symplesiomorphy	Both cephalochordate and ammocoete (vertebrate) patterns represent independently derived apomorphic states.
Notochord	General chordate trait		
Filter-feeding habits	C: ciliary pumping A: velum and muscular constriction of branchial basket	Symplesiomorphy in lampreys; independent loss in myxinoids and gnathostomes	Autapomorphy in lampreys

Table 3.3. Fit of evidence for the 'ammocoete-first' (H_1) versus the 'ammocoete-second' (H_2) hypotheses to some representative traits in which the two different interpretations of ammocoete larvae predict opposite character polarities. Interpretations of the traits differ depending on whether ammocoetes represent a symplesiomorphic state ('ammocoete-first') or an autapomorphic state ('ammocoete-second') within lampreys. **Bold** typeface indicates more parsimonious interpretation, given cyclostome monophyly (Chapter 2).

Phenomena	Interpretations	
	H_1: conserved plesiomorphy	H_2: convergent apomorphy
Absence of ammocoete-like traits in larvae and juveniles of stem lampreys (this Chapter)	Independent losses of ammocoete phase in myxinoids, gnathostomes, and stem lampreys	**Ammocoete phase inserted in life history (replacing predatory larval stage) near the crown lamprey node**
Chondrocranial homology with other vertebrates only at adult stage (Kuratani et al. 2016)	Recapitulation; ammocoete-like chondrocranium truncated in myxinoids and gnathostomes	**Postdisplacement of chondrocranial development due to insertion of filter-feeding phase**
Tissues unique to ammocoetes, including mucocartilage (Hardisty and Potter, 1981)	Recapitulation; mucocartilage lost in myxinoids and gnathostomes	**Autapomorphic state in lampreys due to delayed development**
Unique gene expression patterns in ammocoetes; e.g., no rhombic lip expression of *Pax6* (Sugahara et al. 2016; Chapter 1)	Autapomorphic state in lampreys	Autapomorphic state in lampreys, potentially due to delayed development
Similar craniofacial patterning at embryonic stages with myxinoids (Oisi et al. 2013a)	Synapomorphic/symplesiomorphic state for cyclostomes; interrupted in myxinoids by loss of ammocoete phase	Synapomorphic/symplesiomorphic state for cyclostomes; interrupted in lampreys by insertion of ammocoete phase

3.6 SUPPLEMENTARY INFORMATION

3.6.1 Analytical Methods and Results

3.6.1a Parsimony analyses: Methods

To supplement the taxonomic identification and anatomical interpretations of the larvae and juveniles of *Priscomyzon* and other stem lampreys, I modified a matrix from Chapter 2 to perform a series of maximum parsimony analyses in PAUP* ver. 4.0a152 (Swofford, 2017). The data matrix (available from **3.6.3 Data matrices**) included all the taxa used in the previous analysis (Chapter 2) except *Palaeospondylus* and *Tullimonstrum* (Table S3.1). I added to this dataset: (***a***) specimens identified as immature individuals of *Priscomyzon*, *Hardistiella*, and *Mayomyzon*; (***b***) ammocoetes (Tahara's stage 30; (Tahara, 1988), late ammocoetes, and metamorphosing juvenile of the extant lamprey *Petromyzon marinus* (Johnels, 1948; Piavis, 1971; Youson, 1980); and (***c***) the specimens of *Mesomyzon* identified as ammocoetes and metamorphosing larvae (Chang et al., 2014) (Table S3.1). The character list from Chapter 2 was appended with three characters that describe the morphological traits of ammocoetes (characters 172-174: **3.6.2 List of characters**). All the characters were scored for these immature specimens, assuming no information from the adult stage. In principle, I consulted descriptions of the decay series of morphological characters in modern ammocoetes and adult lampreys (Sansom et al., 2010b, 2013a; Sansom and Wills, 2013; Sansom, 2015) to avoid miscoding absence of a structure prone to rapid decay post-mortem:

1) Absence of a structure can be coded only if the specimen preserves tissues that decay significantly earlier than the structure of interest (Sansom et al., 2010b, 2013a; Sansom and Wills, 2013; Sansom, 2015). For example, the absence of an oral disc (character 158:0) cannot be coded unless the specimen is preserved with structures that were lost nearly 100 days before the oral disc in the experimental taphonomy of modern adult lampreys, like branchial symmetry or otic capsule.

2) Locality-specific conditions are considered (Sallan et al., 2017). Example: a specimen that does not have otic capsules and other traits that have similar decay timelines (Sansom et al., 2010b, 2013a; Sansom and Wills, 2013; Sansom, 2015). The absence of otic capsules

(character 33:0) may be justified if sufficient evidence indicates that the preservation of the otic capsules is the norm for the locality.

3) Experimental taphonomy is a useful guide but needs not be followed precisely (Parry et al., 2017). A decay series may vary substantially at the levels of taxon, locality, and even individual. For example, skeletal morphology is largely unknown for the ammocoetes of *Mesomyzon* despite preservation of many traits that decay earlier than cartilages (e.g., shape of branchial pouches) (Chang et al., 2014) because muscles are so well preserved that they conceal internal structures, or because a decay series did not follow the prediction of experimental taphonomy. Once these distinct trends were identified, I avoided coding for absence even if the decay series predicts it.

In the first set of analyses, each run included ammocoetes of *Petromyzon marinus* and the suspected immature specimen of the Palaeozoic stem lampreys (*Hardistiella*, *Mayomyzon*, and *Priscomyzon*) (Fig. S3.11). The second set of analyses explored various combinations of ammocoetes and metamorphosing juveniles (*Mesomyzon* and *Petromyzon*) (Fig. S3.12). Each analysis ran under heuristic search with 1000 replications. The backbone tree was constrained to the strict consensus topology recovered in the original analysis (Chapter 2).

3.6.1b Parsimony analyses: Results

In all analyses but one with a highly incomplete specimen (AM 5816), the immature specimens were resolved within the total clade Petromyzontiformes, whereas the ammocoetes were nested outside of the crown group Cyclostomi (Fig. S3.11). AM 5815 and 5819 formed a clade with the holotype of *Priscomyzon*. Interestingly, FMNH PF 8167 (*Mayomyzon*; Fig. S3.11h) and CM 46123 (*Hardistiella*; Fig. S3.11i) fell outside the *Hardistiella*-*Mayomyzon* clade and nested close to the holotype of *Priscomyzon* (Fig. S3.11h, i) or within the cluster of the immature specimens of *Priscomyzon* (Fig. S3.11a). This is consistent with the tendency that immature specimens become resolved stem-ward from their adult counterparts on phylogenetic trees, mainly due to ontogenetically transient characters (Campione et al., 2013). These results indicate that the specimens represent petromyzontiforms, providing further support for a growth series of the respective coeval stem lamprey (AM: *Priscomyzon*; FMNH: *Mayomyzon*; CM: *Hardistiella*).

By contrast, ammocoetes tended to fall outside the crown group Cyclostomi and assumed positions close to or at the crown node of vertebrates (Fig. S3.12). They collapsed the petromyzontiform and cyclostome nodes when the metamorphosing larva was added to the analysis (Fig. S3.12d). Without the metamorphosing juvenile of a modern lamprey, both ammocoetes and early metamorphoses of *Mesomyzon* (Chang et al., 2014201) were nested outside the crown group Vertebrata, whereas the ammocoetes of *Petromyzon* formed either a polytomy at the crown node of vertebrates or an outgroup of the crown group Cyclostomi (Fig. S3.12b, c, e, f).

3.6.1c Parsimony analyses: Interpretations

The putative larvae and juveniles of the Paleozoic stem lampreys were nested close to the proposed parent taxa (Fig. S311). These results reinforce the assessment that the specimens represent immature ontogenetic stages of the coeval, mature stem lampreys, and not a lineage unrelated to petromyzontiforms.

Multiple interpretations are compatible with the placement of ammocoetes with respect to their adult counterparts and the immature specimens of the Paleozoic stem lampreys (Figs. S3.11, S3.12). Their positions close to or at the crown node of vertebrates do not contradict the ammocoete-first model in which ammocoetes are considered to represent the primitive conditions of crown-group vertebrates (Haeckel, 1876; Dohrn, 1885; Gaskell, 1908; Goodrich, 1930; de Beer, 1937; Mallatt, 1979, 1981, 1984b, 1984a, 1996, 2008). However, non-ammocoete-like larvae and juveniles in the Paleozoic stem lampreys suggest that ammocoetes were derived independently close to the crown node of petromyzontiforms. An alternative explanation is that the filter feeding ammocoete stage became inserted (or replaced the larval stage as seen in *Priscomyzon*) via reversals or developmental arrest of the lineage-specific features (e.g., the lack of extraocular muscles), and via convergence to cephalochordates for filter feeding (e.g., endostyle) (Hardisty, 1979, 1982).

Regardless of which interpretation may be correct, the positions of ammocoetes close to the crown vertebrate node (Fig. S3.12) are likely due to the lack of petromyzontiform synapomorphies rather than to the presence of traits shared with invertebrate outgroups. To corroborate this, in none of the characters do ammocoetes share a state exclusively with the non-vertebrate outgroup taxa. Purported similarities between ammocoetes and cephalochordates are

either symplesiomorphic (e.g., notochord), or superficial enough to be explained parsimoniously by convergence rather than by evolutionary conservation (Table 3.1). To distinguish these alternative interpretations quantitatively, I used an analysis of morphological disparity to test whether character scores are similar between ammocoetes and invertebrate outgroup taxa including cephalochordates.

3.6.1d Disparity analyses: Methods

To visualize occupation of morphospace among individual taxa, I used both nonmetric and metric multidimensional scaling methods for analysis of morphological disparity. The same matrix was used from the parsimony analysis in two different versions (**3.6.3 Data matrices**): one with the original coding scheme and the other with contingency coding removed. Early vertebrate phylogeny contains high proportions of character contingency (Chapter 2). The characters with contingency are generally coded as inapplicable ('-') and treated as missing data computationally. For an ordination analysis, however, the inapplicable coding violates the assumption that missing data distribute randomly in the dataset (Ciampaglio et al., 2001).

For the secondary analysis with contingency coding removed, three types of inapplicable codings exist in the original dataset. (**A**) One state of a character assumes particular state(s) of other character(s) (denoted with † in **3.6.2 List of Characters**). Example: Character 3 describes presence/absence of prechordal head. Hemichordates and tunicates both lack a prechordal head, but cannot be coded for the absence in this character. The character is only applicable to chordates with an axially elongate notochord. Hemichordates were initially coded as inapplicable because this clade lacks a notochord, and tunicates were also inapplicable because the notochord is restricted to the 'tail' (Chapter 2). Solution: For this type of inapplicable coding, these taxa were simply coded for the absence without considering contingency — in this particular case, contingency on the axially elongate notochord. (**B**) All states of a character assume particular state(s) of other character(s) (denoted with * in the list of characters). Example: Characters 41 and 42 (41: sensory lines, head only or head and trunk; 42: sensory lines, enclosed in grooves or canals) require presence of sensory lines (Character 40.1). So all invertebrate outgroups that lack sensory lines were initially coded as inapplicable (Chapter 2). Solution: For this type of contingency coding, a new state was added for the absence in each of the dependent characters — in this case, characters 41 and 42 now each have a tertiary state coding for the absence of sensory

lines. Finally, (**C**) as a special case of type B, all states of a character assume particular state(s) of other character(s), but not all of the original inapplicable coding is equivalent (denoted with ** or *** in the list of characters, depending on the number of additional states required). Example: Character 54 (excurrent branchial duct, extending laterally or posteriorly) is inapplicable to invertebrate outgroups, some myxinoids, heterostracans, and jawed gnathostomes. However, these taxa differ in the state of absence of the excurrent branchial duct (outgroups: no excurrent branchial duct; *Myxine* and heterostracans: common excurrent branchial duct; jawed gnathostomes: parabranchial cavity instead of excurrent duct). Solution: A new character state was added for each distinct state of the absence.

I applied (***a***) non-metric multidimensional scaling analysis (NMDS) with Hamming distance for categorical data (Cox and Cox, 2000) as similarity index and (***b***) principal coordinate analysis (PCoA) with Euclidean distance as similarity index. PCoA using Euclidean distance is a conventional ordination method used in morphological disparity analysis of cladistic datasets (Erwin, 2007; Gerber, 2013; Klingenberg, 2014; Hetherington et al., 2015). PCoA has an advantage in using ordinations of covariance matrix (unlike pairwise comparisons of covariance matrices as in principal component analysis [PCA]), thereby allowing several levels of integration. However, it is not well-studied empirically how discrete character data with multiple levels of correlations (= non-independence of variables) and large proportions of missing information impact this method as in PCA (Strauss et al., 2003). It is also problematic that character states are implicitly ordered when using Euclidean similarity index. I conducted sensitivity analysis using Hamming distance and Bray-Curtis as similarity indices for PCoA, and the results were nearly identical to those obtained with Euclidean distance (data not shown). Thus, I used the more conventional PCoA with Euclidean index to test for congruence with NMDS. NMDS yields multivariate morphospace through iterative runs until results converge in which character values are sampled as attributes, without (***a***) the use of eigenvalues and (***b***) the assumptions of normality and linearity in the dataset (Fasham, 1977; Beals, 1984; Mead, 1992; Huntley et al., 2006; Huntley, 2011; Hernández et al., 2013; Lloyd, 2016). In NMDS, however, it is not well-studied empirically how missing entries in cladistic datasets impact the result. NMDS does not produce exactly identical results between independent runs, either. Therefore, NMDS and PCoA were complementary. A one-way nonparametric PERMANOVA (Euclidean similarity index; permutation $N = 9999$) was used to test for significant overlap in occupation of

morphospace among different groups. For PERMANOVA, only PCos with eigenvalue > 1% were considered, which accounted for approximately 90% of total eigenvalue with or without contingency coding. All analyses were performed using PAST ver. 3.14 (Hammer et al., 2017).

3.6.1.e Disparity analyses: Results

In the NMDS analyses, invertebrate outgroups were separated from the rest of the dataset with or without treatment for character contingency (Fig. S3.13a, c). However, the invertebrate outgroups occupied substantially larger area of the morphospace when contingency coding was included as missing entries (Fig. S3.13a), compared to when contingency coding was replaced by discrete states (Fig. 3.13c). Similarly, an area occupied in morphospace was reduced for an assemblage of primitive vertebrates with uncertain affinity (including myllokunmingiids, conodonts, *Achanarella*, *Ciderius*, *Cornovichthys*, *Haikouella*, and *Metaspriggina*; Table S3.1) when contingency coding was replaced. The vertebrate groups formed a cluster when contingency was included (Fig. S3.13a), whereas myxinoids and jawless stem gnathostomes segregated from one another when contingency was removed (Fig. S3.13c). Still, the following groups remained in close proximity with or without inclusion of contingency: petromyzontiforms (adults), larvae of stem lampreys, ammocoete larvae, and an assemblage of primitive vertebrates. Shepard plots indicated higher stress for reaching consensus (stress = 0.2377; R^2 = 0.5995 [axis 1]; 0.1386 [axis 2]) when contingency coding was treated as missing data (Fig. S3.13b). Correlation was weak between obtained and target ranks over iterations of the analysis. On the other hand, stress is substantially lower and correlations stronger when contingency coding was replaced (Fig. 3.13d; stress = 0.1145; R^2 = 0.8678 [axis 1]; 0.2084 [axis 2]). A substantial difference in morphospace occupied by the invertebrate outgroups is consistent with the stress levels affected by inclusion/exclusion of contingency coding, because this is the group of taxa for which 70% of the characters were scored as inapplicable (Chapter 2). Thus, NMDS performed best and provided more robust results when character non-independence was corrected by replacing contingency coding with discrete states. It remains unclear, however, whether the improved performance was due to restored non-independent character state distributions or to reduction of missing entries.

One-way nonparametric PERMANOVA of the scores from the NMDS analysis corroborated these interpretations (Tables S3.3, S3.4). Separation of the taxonomic groups was highly significant ($P < 0.01$) in most pairwise comparisons. When contingency coding was

included as missing data, the larvae of Paleozoic stem lampreys could not be distinguished from jawless stem gnathostomes in morphospace (Table S3.3). Separation was marginally significant ($P = 0.044$) between the stem lamprey larvae and the adult petromyzontiforms. This is consistent with taxonomic assignment of the larvae to the adult-based stem taxa, and also with the assessment that morphological differences from the putative larvae to adults are significant enough to identify the transition as metamorphosis. When contingency coding was replaced by discrete states, separation was non-significant between ammocoetes and primitive vertebrates with uncertain affinity (Table S3.4). Perhaps surprisingly, significance was marginal between invertebrate outgroups and jawed gnathostomes, with or without contingency coding. The larvae of Paleozoic stem lampreys were set apart from ammocoetes and adult forms of the same lineage (Tables S3.3, S3.4). Similarly, ammocoetes were set apart significantly from adult petromyzontiforms, invertebrate outgroups, and primitive vertebrates. These results support: (***a***) presence of metamorphosis in the Paleozoic stem lampreys; (***b***) distinction of the stem lamprey larvae from ammocoetes in morphospace; and (***c***) dissimilarities in morphospace occupation between invertebrate outgroups and ammocoetes. Overall, these results contradict the prediction of the 'ammocoete first' model, and are consistent with the hypothesis that the ammocoete phase independently evolved near the crown petromyzontiform node.

In the PCoA, the stem larvae and ammocoetes were segregated from each other along most of the axes approximately 5% eigenvalue or greater, regardless of whether contingency coding was treated as missing entries (Fig. S3.14; Table S3.5) or corrected for discrete states (Fig. S3.15; Table S3.6). They were both closely associated and had partial overlaps with the adult petromyzontiforms. With respect to overall resemblances, ammocoetes and invertebrate outgroups were closer to each other only in some of the coordinates of significant loading (Figs S3.14a, d, e, S3.15c) but cephalochordates did not necessarily fall close to ammocoetes. Instead, ammocoetes overlapped early vertebrates of uncertain affinity (euconodonts, myllokunmingiids, yunnanozoans, and other enigmatic taxa) in morphospace occupation more extensively than others. The larvae and juveniles of the Paleozoic stem lampreys overlapped with jawless stem gnathostomes more extensively than others, when contingency coding was considered as missing entries (Fig. S3.14). When contingency coding was corrected for discrete character states, this association was not observed (Fig. S3.15). They instead associated more closely with the adult petromyzontiforms and early vertebrates of uncertain affinity than with stem gnathostomes. As

81.9% of contingency coding (inapplicable scores) in the dataset concentrated with skeletal characters (Chapter 2), the absence of mineralized skeletons contributed disproportionately to the result of the principal coordinate analysis with corrected discrete states for contingency coding (Fig. S3.15). The first coordinate explains nearly 40% of total eigenvalue (Table S3.6) along which those with mineralized skeletons were set apart from those without.

In one-way PERMANOVA test, pairwise comparisons (Tables S3.7, S3.8) supported significant segregation in most pairs identified in the counterpart analysis for NMDS. A distinct trend appeared, however. Separation between taxonomic groups was highly significant ($P < 0.01$) in more pairs when contingency coding was replaced by discrete states, compared to when it was included as missing data. When contingency coding was included, stem gnathostomes could not be distinguished from the group of primitive vertebrates with uncertain affinity (Tale S3.3). Separation was marginally significant ($P = 0.048$) between the larvae of Paleozoic stem lampreys and jawless stem gnathostomes. When contingency coding was replaced by discrete states, all pairwise comparisons showed significant differences between the groups. As in NMDS, invertebrate outgroups and jawed gnathostomes appeared to have the weakest degree of separation for having marginal significance. This is likely due to the low number of taxa included in each group.

These results from PCoA are compatible with those from NMDS. The analyses of morphological disparity reinforced that: (***a***) the Paleozoic stem lampreys underwent metamorphosis (little overlap in morphospace between the identified larvae and adult petromyzontiforms); but (***b***) they do not represent the ammocoete-like phase (highly significant separation between the identified larvae and ammocoetes in morphospace); and thus (***c***) ammocoetes evolved independently, and the overall resemblance (body forms, oral hood, filter-feeding habits) with cephalochordates likely represent convergence (highly significant separation between ammocoetes and invertebrate outgroups). They do not necessarily support that ammocoetes are generally symplesiomorphic, either.

As a final point of interest, NMDS and PCoA analyses responded differently to the treatment of contingency coding. NMDS analysis performed better with lower stress when the gap coding for contingency (inapplicable scores) was replaced by discrete states (Fig. S13b, d). There is no suitable measure of performance for this in PCoA. The distance among the groups appeared greater along the axes of significant eigenvalue (> 5%) when contingency coding was

replaced (Figs. S3.14, S3.15), correlated with increase in the levels of significance in pairwise comparison of PERMANOVA (Tables S3.7, S3.8). However, increased distance between the groups is expected. Replacing the inapplicable scores with discrete character states means weighting the matrix toward primitive character states characterized by absence. As replacement with discrete states increased distances in the morphospace in PCoA, the method is arguably sensitive to implicit weighting in the character matrix. If that is the case, the inclusion of contingency coding may be a preferable approach to PCoA.

3.6.2 List of Characters

Annotations of characters:

† = One state of a character assumes particular state(s) of other character(s); inapplicable coding replaced with dependent character state.

* = All states of a character assume particular state(s) of other character(s); inapplicable coding replaced with an additional character state.

** = All states of a character assumes particular state(s) of other character(s), but not all of the original inapplicable coding is equivalent; inapplicable coding replaced with two additional states.

*** = All states of a character assume particular state(s) of other character(s), but not all of the original inapplicable coding is equivalent; inapplicable coding replaced with three additional states.

See **3.6.1d Disparity analyses: methods** for the rationales of coding modification.

(a) Brain, sensory and nervous system

1. Skeletal derivatives of neural crest: 0, absent; 1, present.
2. Ectodermal placodes: 0, absent; 1, present.
3. †Distinct prechordal head: 0, absent or weakly developed; 1, prominent.
4. †Tripartite vesicles at anterior end of neural tube (prosencephalon, mesencephalon, rhombencephalon): 0, absent; 1, present.
5. *Morphologically distinct cerebellum with corpus cerebelli: 0, absent; 1, present.
6. †Profundal nerve ganglion: 0, separate from trigeminal ganglion; 1, fused with trigeminal ganglion.

7. *Tripartite division of facial nerve into pharyngeal, ‘pretrematic’, and ‘postrematic’ branches: 0, absent; 1, present.
8. *Spinal cord in cross section: 0, round; 1, flattened.
9. *Ventral and dorsal roots of spinal nerve: 0, separated; 1, united.
10. *Ventral and dorsal roots of spinal nerve originates: 0, intersegmentally; 1, intrasegmentally.
11. †Mauthner fibres at rhombomere 4: 0, absent; 1, present.
12. Pineal organ (extra-ocular photoreceptor region expressing pineal opsins): 0, absent; 1, present.
13. *Pineal opening: 0, covered; 1, uncovered.
14. Adenohypophysis: 0, absent; 1, present.
15. *Olfactory peduncles: 0, absent; 1, present.
16. Encapsulated olfactory epithelium with external opening: 0, absent; 1, present.
17. *Position of nasohypophyseal/nasal opening: 0, terminal; 1, dorsal.
18. *Nasohypophyseal canal: 0, blind; 1, opening into pharynx.
19. *Nasohypophyseal opening: 0, single; 1, paired.
20. *Nasal (olfactory) capsule: 0, unpaired; 1, paired.
21. **Nasohypophyseal canal: 0, maintains width and height anteriorly; 1, tapers anteriorly.
22. **External opening of nasohypophyseal canal: 0, terminal aperture; 1, tubular extension.
23. **Nasohypophyseal barbels extend from: 0, rim of nasohypophyseal aperture; 1, posteriorly to nasohypophyseal aperture.
24. **Nasohypophyseal papillae, ventral element: 0, absent; 1, present.
25. **Nasohypophyseal papillae, dorsal element(s): 0, midline; 1, paired.
26. Eyes with pigmented retinal epithelium: 0, absent; 1, present.
27. *Eyes: 0, exposed; 1, covered by dermis; 2, covered by trunk muscles.
28. *Extrinsic eye musculature: 0, absent; 1, present.
29. *Muscles innervated by oculomotor nerve: 0, three; 1, four.
30. *Oblique muscle innervated by trochlear nerve: 0, posterior; 1, superior.
31. *Rectus muscles innervated by abducens nerve: 0, two; 1, one.
32. *Eyes: 0, laterally placed (interorbital distance equal to width of head at that position); 1, close together near midline (interorbital distance substantially less than width of head at that position); 2, on prominent eyestalk.

33. †Cartilaginous otic capsules: 0, absent; 1, present.
34. *Vertical semicircular canals forming loops that are separate from roof of utriculus: 0, absent; 1, present.
35. *Anterior and posterior semicircular canals: 0, share a canal toward utriculus after meeting in a confluence; 1, meet each other to form a single loop.
36. *Horizontal semicircular canal: 0, absent; 1, present.
37. Statoliths composed of calcium phosphate: 0, absent; 1, present.
38. *Endolymphatic duct: 0, is blind; 1, opens externally.
39. Electroreceptive cells: 0, absent; 1, present.
40. Sensory lines: 0, absent; 1, present.
41. *Sensory-lines: 0, on head only; 1, on head plus body.
42. *Sensory-line: 0, enclosed in grooves; 1, enclosed in canals.
43. Internal taste buds, or functionally equivalent end chemosensory organs innervated by cranial nerves in head: 0, absent; 1, present; 2, lacking internal taste buds but function replaced by Schreiner organs.

(b) Mouth and branchial system

44. *Preoptic head length: 0, shorter than branchial length; 1, approximately equal to branchial length; 2, longer than branchial length.
45. †*Branchial apparatus: 0, retains arrangement of pharyngula such that first branchial opening assumes infra- to postotic position; 1, displaced anteriorly; 2, displaced posteriorly.
46. *Branchial apparatus, displaced anteriorly such that: 0, first branchial opening assume pretic position; 1, multiple branchial arches occupy preotic position.
47. *Branchial apparatus, displaced posteriorly such that prebranchial length is: 0, less than a quarter; 1, approximately quarter; 1, greater than a third of body length.
48. *Pharyngeal skeleton: 0, delineates pharyngeal slits with ciliary band; 1, supports well-developed branchial lamellae.
49. *Main skeletal support for branchial apparatus with respect to lamellae: 0, lateral; 1, medial.
50. *Pharyngeal skeleton: 0, skeletal arches fused with each other; 1, arches isolated.
51. *Hyomandibular pouch: 0, blind; 1, externally open (spiracle).
52. Respiratory current exits through: 0, atrial space; 1, excurrent duct (=branchial pouch); 2,

parabranchial cavity.

53. Single confluent branchial opening: 0, absent; 1, present 28).

    This character is inapplicable to those with parabranchial cavities (#52).

54. **Branchial excurrent duct: 0, opens roughly at position of branchial pouch; 1, extends posteriorly.

55. **Branchial openings: 0, spaced accordingly with dimensions of branchial cavities; 1, packed closely together; 2, organized into multiple parallel rows.

56. †Number of arches (or pouches) in branchial apparatus: 0, unconstrained to five; 1, held constant at five.

57. †Number of arches (or pouches) in branchial apparatus (unconstrained to five), maximum number: 0, greater than five and fewer than 20; 1, greater than 20.

58. †Number of arches (or pouches) in branchial apparatus (unconstrained to five): 0, four or five; 1, six or seven; 2, eight to ten; 3, greater than ten.

59. *Branchial series extends: 0, substantially less than half the body length; 1, semiequal to or greater than half the body length.

60. †**Lateral branchial openings: 0, at similar horizontal level; 1, in a posteroventrally inclined row.

61. Opercular flaps associated with branchial openings: 0, absent; 1, present.

62. Branchial epithelium: 0, internal; 1, external.

63. *External branchial openings, demarcated by: 0, single element entirely; 1, single element dorsally; 2, multiple plates; 3, a framework of multiple spines; 4, micromeres; 5, naked (mineralized exoskeleton locally absent around the openings).

64. †Position of mouth: 0, terminal; 1, subterminal.

65. Epidermal oral cirri: 0, absent; 1, present.

66. *Postoptically derived ectomsenchyme anterior to mandibular arch gives rise to palatal structures that: 0, meet at midline under nasal/nasohypophyseal organs; 1, meet at dorsal midline anterior to nasohypophyseal organs and form a prominent oral roof.

67. †Velum: 0, absent; 1, present.

68. *Velar cartilages: 0, at hyomandibular position; 1, extend posteriorly.

69. *Velar cartilages, functions at terminal ontogenetic stages: 0, pump and valve; 1, valve.

70. *Velar wings: 0, absent; 1, present.

71. *Velar tentacles, papillae or tubercles: 0, absent; 1, present.

(c) Circulatory system

72. Multi-chamber heart: 0, absent; 1, present.
73. †Closed pericardium: 0, absent; 1, present.
74. Circulatory system: 0, open; 1, closed.
75. Massive subcutaneous sinus: 0, absent; 1, present.
76. Paired dorsal aortae: 0, absent; 1, present.
77. *Lateral head vein: 0, drains into anterior cardinal vein or its derivative; 1, continues into (or functions as anterior extension of) anterior cardinal vein or its derivative.
78. Lymphocytes: 0, absent; 1, present.
79. *Lymphocytes antigen receptors: 0, VLR; 1, T and B.
80. †Subaponeurotic vascular plexus: 0, absent; 1, present.

(d) Fins and fin-folds

81. †Body forms, relative length: 0, less than five times the next largest dimension (height or width); 1, greater than five but less than ten times; 2, greater than ten times.
82. †Body forms, width against height: 0, compressed or subcircular so that branchial openings are lateral; 1, depressed so that branchial openings are ventral.
83. †Endoskeletal fin supports: 0, absent; 1, present.
84. †Distinct dorsal fin: 0, absent; 1, present.
85. *Dorsal fins: 1, continuous or adjacent to one another; 1, set apart from each other widely.
86. *Fin(s) along dorsal midline originates: 0, above branchial series or anterior to mid-trunk; 1, above anus/anal fin or anterior; 2, posteriorly to anus/anal fin.
87. †Separate anal fin, or a distinct median ventral fin in postanal tail: 0, absent; 1, present.
88. †Paired skin folds (epidermal ridges) at suprapharyngeal position: 0, absent; 1, present.
89. †Constricted pectoral fins with endoskeletal elements: 0, absent; 1, present.
90. Conspicuous preanal skin fold (epidermal ridge): 0, absent; 1, present.
91. *Preanal skin fold (epidermal ridge): 0, midline; 1, paired.
92. *Preanal skin fold (epidermal ridge): 0, longitudinal; 1, discrete pelvic fins.
93. †Tail shape: 0, no distinct lobes developed; 1, ventral lobe much larger than dorsal; 2, dorsal

lobe much larger than ventral; 3, dorsal and ventral lobes almost equally developed.

94. *Chordal disposition relative to tail development: 0, isochordal; 1, hypochordal; 2, hyperchordal.

(e) Skeletal

95. Skeletal elements consisting of calcium phosphate: 0, absent; 1, present.
96. †Bone: 0, absent; 1, present.
97. *Cellular bone: 0, absent; 1, present.
98. *Lamellar acellular bone (isopedine): 0, absent; 1, present.
99. *Perichondral bone: 0, absent; 1, present.
100. †Calcified cartilage: 0, absent; 1, present.
101. *Cellular cartilages with large mature chondrocytes (30-50 μm in diameter): 0, absent; 1, present.
102. *Mature chondrocytes: 0, become separated and generally even spaced by extracellular matrix; 1, remain nested in a pair.
103. †Dentine: 0, absent; 1, present.
104. *Spherical/globular dentine: 0, absent; 1, present.
105. *Tubular dentine: 0, absent; 1, present.
106. *Tubular dentine, odontobalsts tend to: 0, retreat into pulp cavity; 1, remain in dentinous matrix.
107. *Tubular dentine, interconnections of tubules/canaliculi for odontoblasts tend to be: 0, polarized; 1, non-polarized.
108. *Tubular dentine, interconnections of canaliculi and spacing between odontoblasts tend to be: 0, regular; 1, irregular.
109. †Enamel/oid: 0, absent; 1, present.
110. *Enamel/oid: 0, monotypic; 1, bitypic.
111. *Calcification/ossification occurs in endoskeleton: 0, absent; 1, present.
112. *Calcification/ossification occurs in exoskeleton: 0, absent; 1, present.
113. *Mineralized integumentary skeleton (scales and plates): 0, absent in trunk; 1, present in trunk.
114. *Mineralized integumentary skeleton in trunk, surface coverage: 0, extensive; 1, limited

(with evidence for variation and potentials for reduction).

115. *Odontodes: 0, monodontodes; 1, polyodontodes.

116. †Exoskeletal fin support: 0, absent; 1, present.

117. *Exoskeletal fin support, integumentary coverage of distal portions by tessellated scales: 0, absent; 1, present.

118. *Exoskeletal fin support, organized into distinct rays distal to radials: 0, absent; 1, present.

119. *Exoskeleton, organization of superficial layer: 0, spherical; 1, tubular; 2, lamellar.

120. *Exoskeleton, vascular/cancellar layer of osteons: 0, absent; 1, present.

121. *Exoskeleton, basal tissue: 0, basal lamella; 1, basal attachment.

122. *Cancellar layer in exoskeleton, with honeycomb-shaped cavities: 0, absent; 1, present.

123. *Scale shape: 0, diamond-shaped; 1, rod-shaped.

124. *Oak-leaf-shaped tubercles: 0, absent; 1, present.

125. *Triradiate postbranchial spines: 0, absent; 1, present.

126. *Median dorsal ridge scales: 0, absent; 1, present.

127. *Median dorsal ridge scales: 0, simple; 1, hooked.

128. *Vascular canal systems in integumentary skeleton: 0, absent; 1, present.

129. *Scales: 0, without visceral ribs; 1, with visceral ribs.

130. *Oral plates; 0, absent; 1, present.

131. *Odontodes: 0, restricted to exoskeleton; 1, extend into in oral cavity; 2, into pharynx.

132. *Dermal head covering in adult state: 0, absent; 1, present.

133. *Dermal head covering in adult state: 0, micromeric; 1, large (macromeric) dermal plates.

134. *Dermal head covering, macromeric: 0, large unpaired plates covering dorsal and ventral sides; 1, covered by tesserae; 2, multiple plates.

135. *Dermal head covering, macromeric/shield: 0, head and anterior trunk continuous; 1, head and anterior trunk decoupled.

136. †Endoskeletal contribution to dermal head covering: 0, absent; 1, present.

137. *Mineralized exoskeletal circumocular elements: 0, absent; 1, present.

138. *Mineralized endoskeletal circumocular elements (sclerotic elements): 0, absent; 1, present.

139. *Sclerotic endoskeleton: 0, isolated circumocular elements; 1, eye capsule or stalk.

140. *Fusion of visceral (pharyngeal) skeletal arches to neurocranium: 0, absent; 1, present.

141. †Multidenticulate/multicuspid plates housed within buccal cavity (non-odontodes): 0, absent; 1, present.

142. †Perioral/buccal feeding structure consisting of keratin: 0, absent; 1, present.

143. *Keratinous tooth plate, anterior element, number of fused cusps: 0, two; 1, three.

144. †Radially organized circumoral denticulate/cusped plates: 0, absent; 1, present.

145. *Circumoral keratinous teeth, number of tooth rows in lateral field: 0, three; 1, four; 2, five or greater.

146. †Cartilaginous trematic rings: 0, absent; 1, present.

147. Axial skeletal condensations derived from sclerotomes: 0, absent; 1, present.

148. *Sclerotome-derived skeletons around dorsal nerve cord (=neural arches): 0, absent; 1, present.

149. *Sclerotome-derived skeletons around notochord (=centra): 0, absent; 1, present.

150. *Sclerotome-derived skeletons around dorsal aorta (=haemal arches): 0, absent; 1, present.

151. †Lingual and dental apparatus forming a pulley-like system of cartilages and protractor-retractor complex derived from mandibular arch: 0, absent; 1, present.

152. †Longitudinally aligned tooth rows providing transverse bite: 0, absent; 1, present.

153. †Jaws (dorsoventral bite): 0, absent; 1, present.

154. †Parachordal cartilages: 0, absent; 1, present.

155. †Braincase with lateral walls: 0, absent; 1, present.

156. †Occiput enclosing vagus and glossopharyngeal nerves: 0, absent; 1, present.

157. †Annular cartilage: 0, absent; 1, present.

158. Large oral disc: 0, absent; 1, present.

159. †Barbels supported by cartilages: 0, absent; 1, present.

160. †Forked subnasal cartilage: 0, absent; 1, present.

161. †Tectal cartilages: 0, absent; 1, present.

(f) Miscellaneous

162. †Male gametes shed directly through the coelom: 0, absent; 1, present.

163. †Postotic myomeres migrate anteriorly to the position of eye: 0, absent; 1, present.
164. *Inflected myomeres: 0, Z-shaped; 1, W-shaped.
165. *Myomeric segments: 0, closely packed (typically greater than 50); 1, widely spaced (substantially fewer than 50).
166. Digestive tract: 0, follows pharynx; 1, passes (or loops) over branchial apparatus.
167. Anus, with respect to distribution of mesoderm: 0, terminal or subterminal; 1, non-terminal.
168. Globular slime glands: 0, absent; 1, present.
169. *Number of slime glands: 0, approximately 100 or fewer; 1, substantially greater than 100.
170. *Slime pores: 0, overlap region of external branchial openings; 1, do not overlap region of external branchial openings.
171. †Gular pouch in adult male: 0, absent; 1, present.

(*g*) *Additional characters for ammocoete morphology*

172. Eye, form: 0, ocelli/photoreceptors; 1, eyespot; 2, prominent ocular complex.
173. *Infrapharyngeal secretory organ: 0, endostyle; 1, thyroid.
174. Horseshoe-shaped oral hood: 0, absent; 1, present.

3.6.3 Data Matrices

Supplementary files are available at a Dataverse depository (doi:10.7939/DVN/JGSPJN) (PDF version) or on a disc attached to the back of this thesis (print version).

Suppl. 3.1: Data matrix for maximum parsimony analysis, NMDS, and PCoA. Contingency coding is included as missing entries.

Suppl. 3.2: Data matrix for NMDS and PCoA. Contingency coding is replaced by discrete states.

SUPPLEMENTARY FIGURES

Fig. S3.1. Comparison of *Priscomyzon riniensis* specimens to the same scale in the reverse ontogenetic order. Photograph (**a**) and interpretive drawing (**b**) of the adult (AM 5750); photograph (**c**) and interpretive drawing (**d**) of a post-metamorphosis juvenile (AM 5819); photograph (**e**) and interpretive drawing (**f**) of the larger metamorphosing larva (AM 5816); photograph (**g**) and interpretive drawing (**h**) of the smaller metamorphosing larva (AM 5815); photograph (**i**) and interpretive drawing (**j**) of the largest pre-metamorphosis larva (AM 5817); photograph (**k**) and interpretive drawing (**l**) of the pre-metamorphosis larva (AM 5814); photograph (**m**) and interpretive drawing (**n**) of the smallest pre-metamorphosis larva (AM 5820).

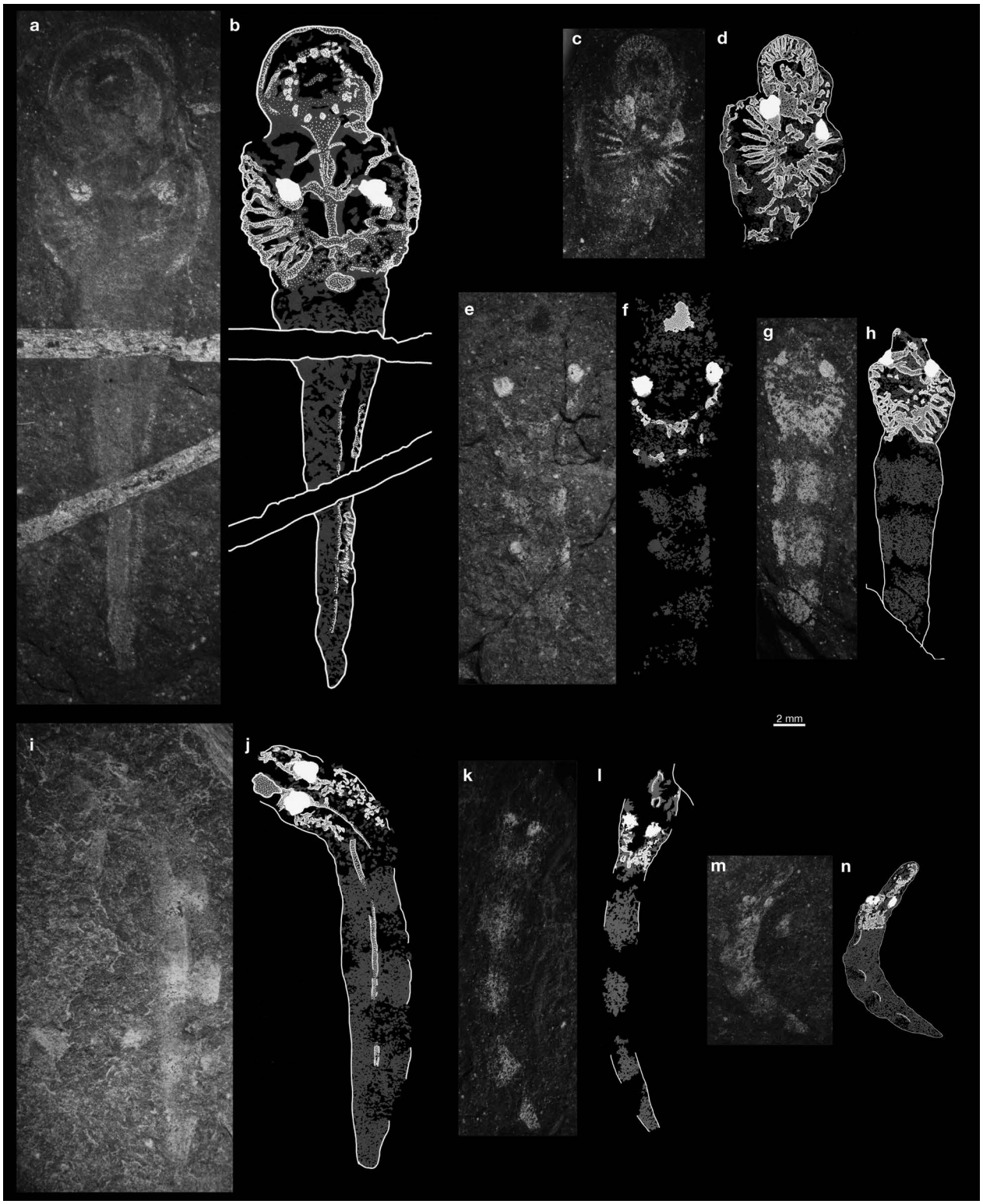
a
b
c
d
e
f
g
h
2 mm
i
j
k
l
m
n

Fig. S3.2. The holotype (AM 5750) of *Priscomyzon riniensis* representing the adult phase. Photographs (**a**, **c**) and interpretive drawings (**b**, **d**) of the slab and counter-slab, respectively. Photograph of the slab (**a**) is overlain with opaque outlines of major preserved structures (see Fig. 3.1 for an unaltered photograph). Due to the level at which the slabs were split, some of the dorsal skeletal structures in the snout (e.g., tectal cartilages) cannot be observed at the surface. **Abbreviations: ac**, annular cartilage; **bb**, branchial basket; **bra**, branchial arch; **df**, dorsal fin; **dt**, digestive tract; **e**, eye; **h/eb**, hypotrematic/epitrematic bar; **hyb**, hypobranchial bar; **kt**, keratinous teeth; **la**, lingual apparatus; **nc**, notochord; **nh**, nasohypophyseal structure; **oc**, otic capsule; **od**, oral disc; **ol**, outer lip; **os**, oral structure; **pc**, pericardiac structure; **prb**, proboscis; **sc**, styliform cartilage; **tb**, transverse bridge of branchial basket; **tc**, tectal cartilage; **tca**, anterior tectal cartilage; **tcp**, posterior tectal cartilage; **tr**, trabecular cartilage; **ys**, yolk sac.

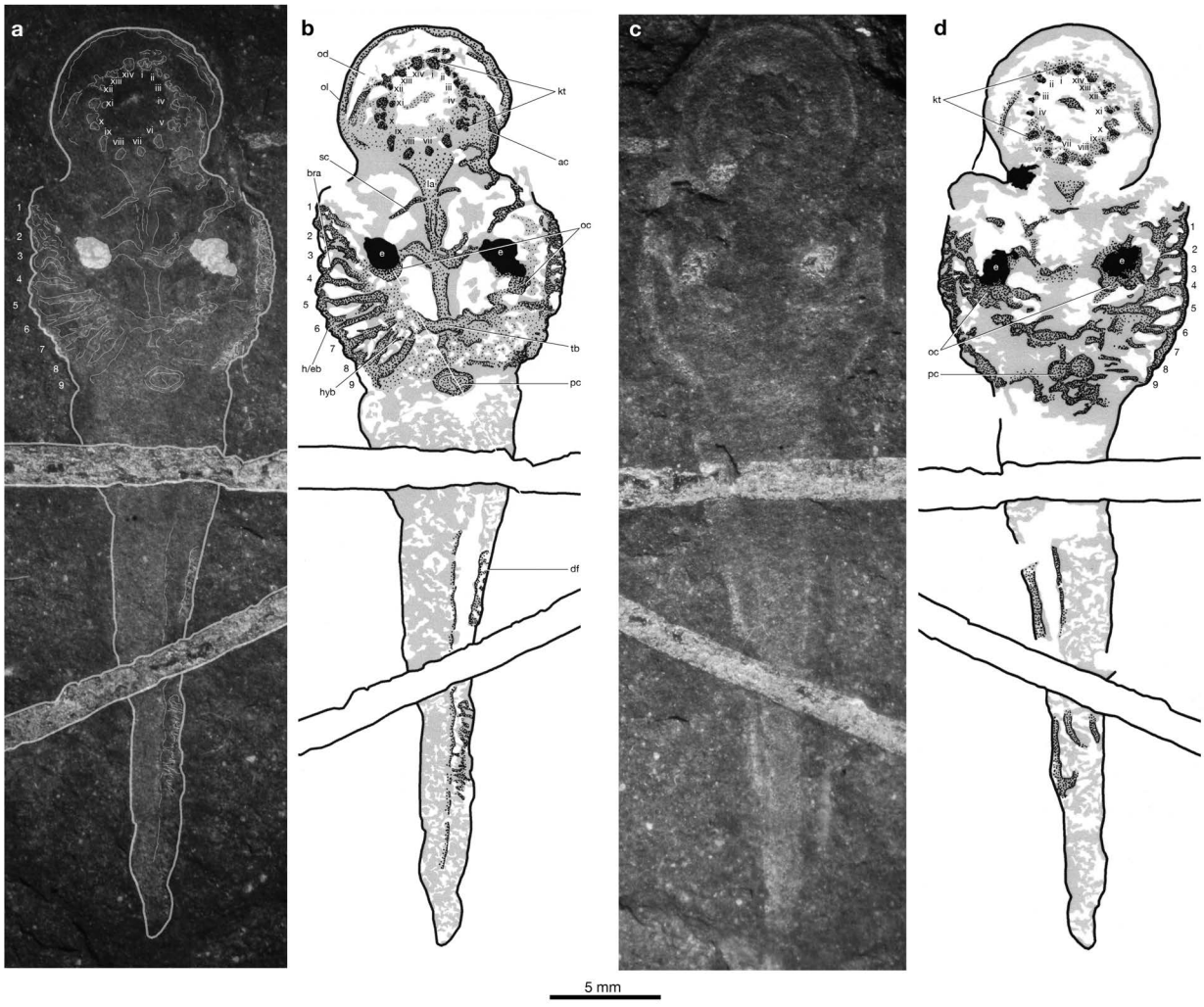
a
b
c
d
od
ol
kt
ac
sc
bra
oc
e
tb
h/eb
hyb
pc
df
5 mm

Fig. S3.3. A specimen referred to *Priscomyzon riniensis* (AM 5819) representing a post-metamorphosis juvenile. Photographs (**a**, **c**) and interpretive drawing (**b**) of the slab and counter-slab, respectively. Photograph (**a'**) is overlain by opaque outlines of major preserved tissues. Due to the level at which the slabs were split, some of the ventral skeletal structures in the snout (e.g., most of the keratinous teeth) cannot be observed at the surface. See Fig. S3.1 for anatomical abbreviations.

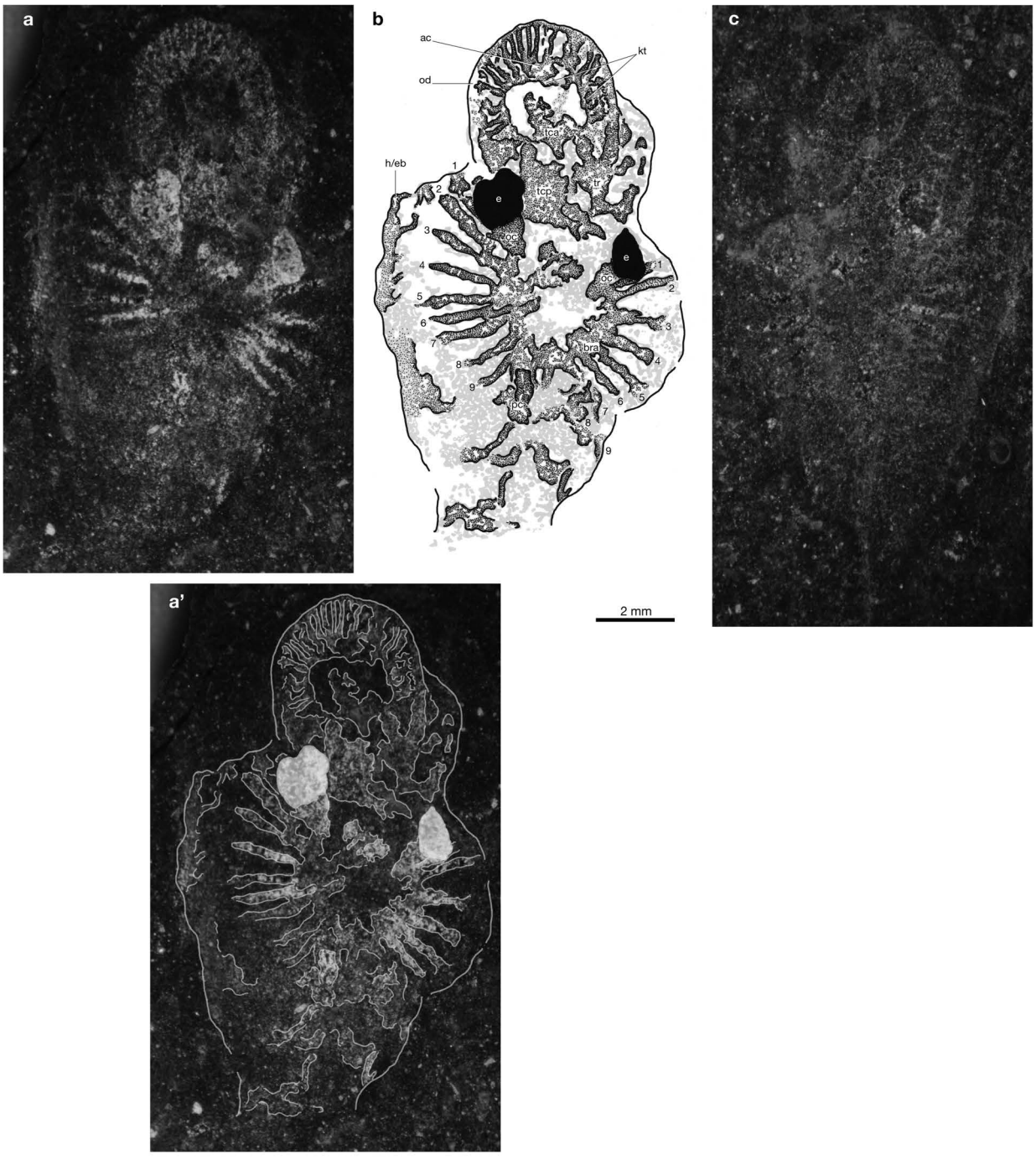
a
b
c
a'
ac
kt
od
tca
h/eb
tcp
tr
e
oc
bra
pc
2 mm

Fig. S3.4. A specimen referred to *Priscomyzon riniensis* (AM 5816) representing a metamorphosing larva. Photograph (**a**), interpretive drawing (**b**), and photograph overlain with outlines of major preserved tissues (**c**). See Fig. S3.1 for anatomical abbreviations.

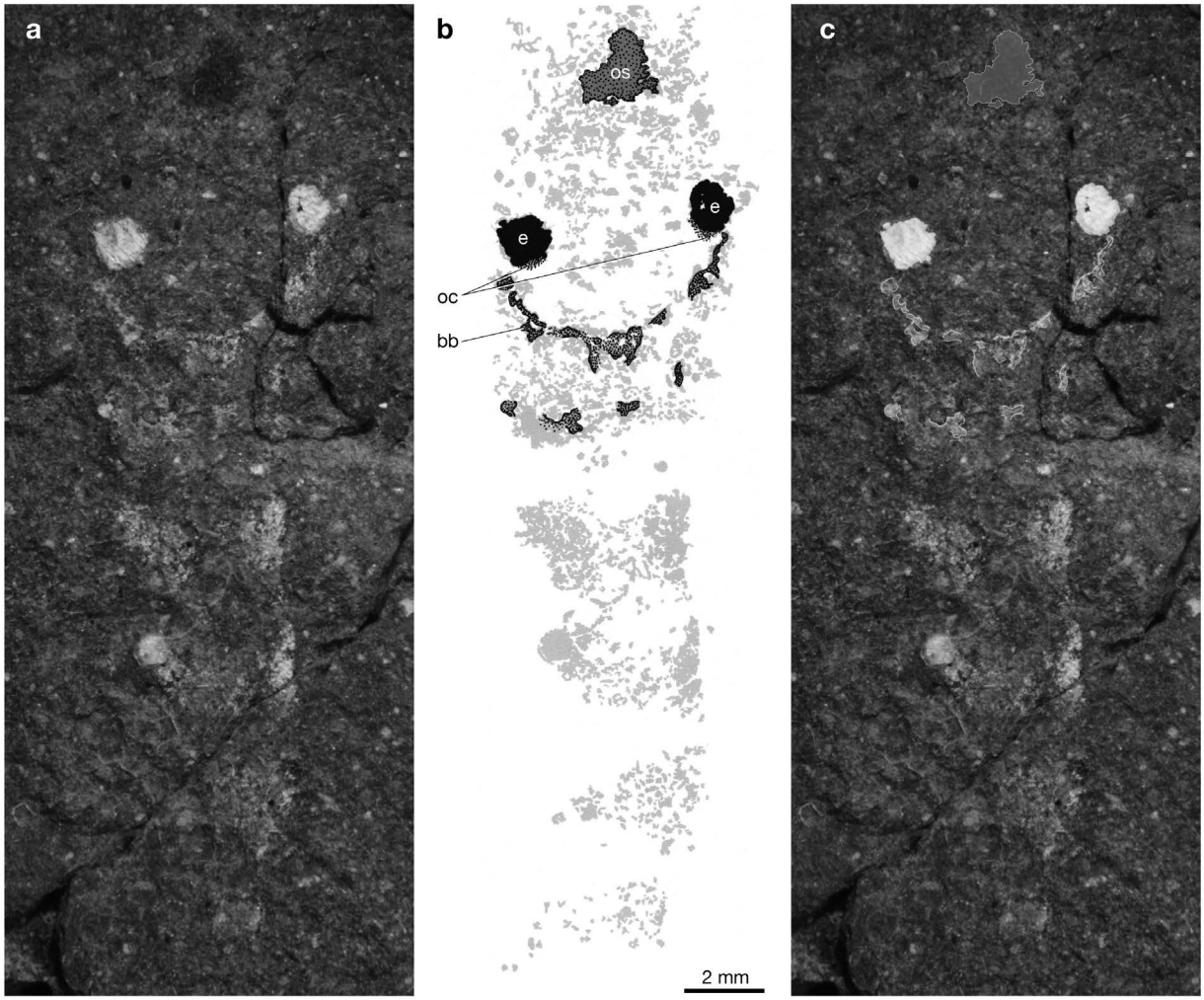
a
b
c
os
e
e
oc
bb
2 mm

Fig. S3.5. A specimen referred to *Priscomyzon riniensis* (AM 5815) representing a metamorphosing larva. Photographs (**a**), interpretive drawing (**b**), and photograph overlain with structural outlines (**c**) of the slab; photograph (**d**) of counter-slab. The snout is incomplete, and the oral region is not preserved. See Fig. S3.1 for anatomical abbreviations.

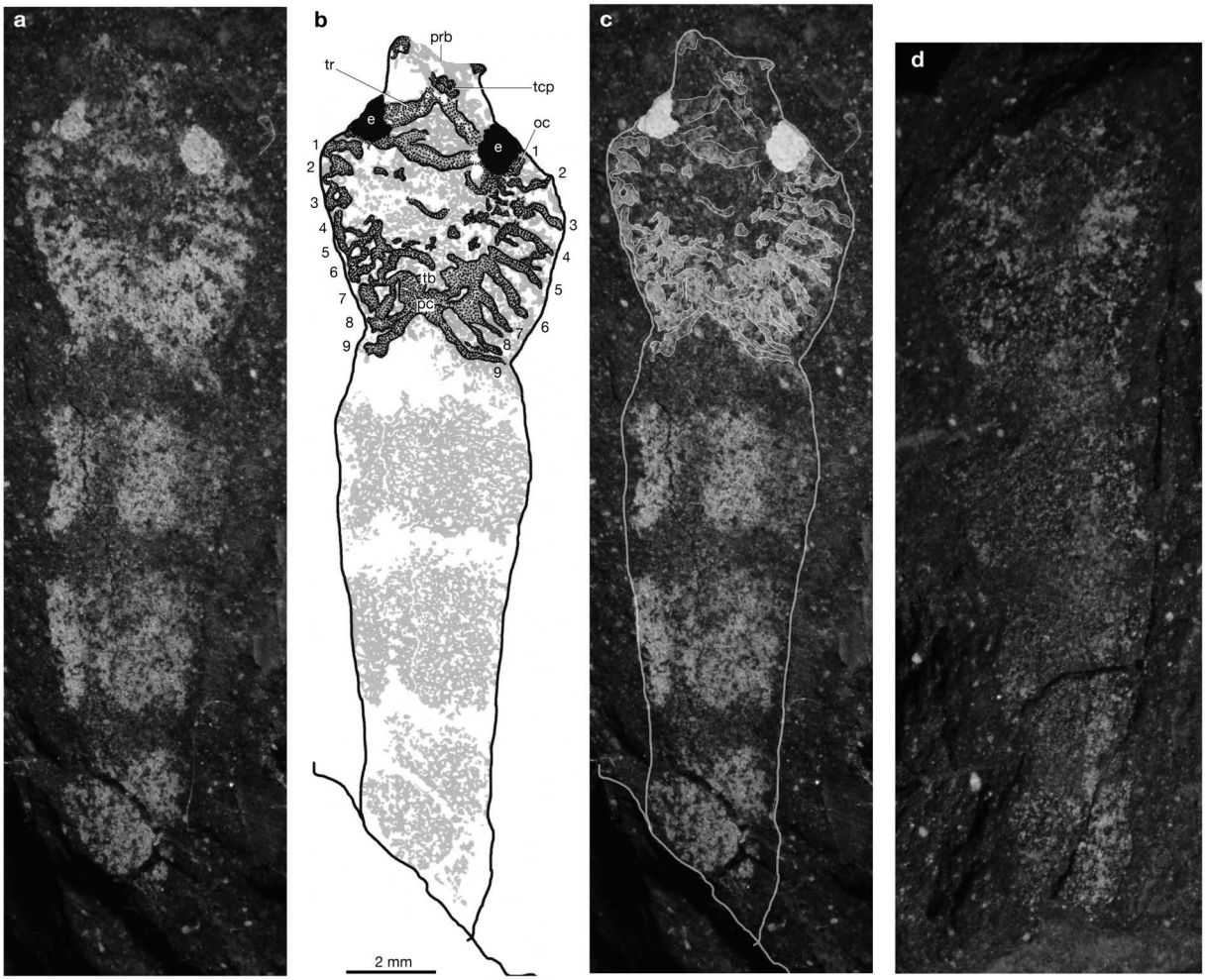
a
b
c
d
prb
tr
tcp
oc
e
e
1
2
3
4
5
6
7
8
9
tb
pc
2 mm

Fig. S3.6. A specimen referred to *Priscomyzon riniensis* (AM 5817) representing a pre-metamorphosis larva. Photograph (**a**), interpretive drawing (**b**), photograph overlain with structural outlines (**c**), and photograph of boxed area showing the head region in greater magnification (**d**). The snout is incomplete, and the oral region is not preserved. See Fig. S3.1 for anatomical abbreviations.

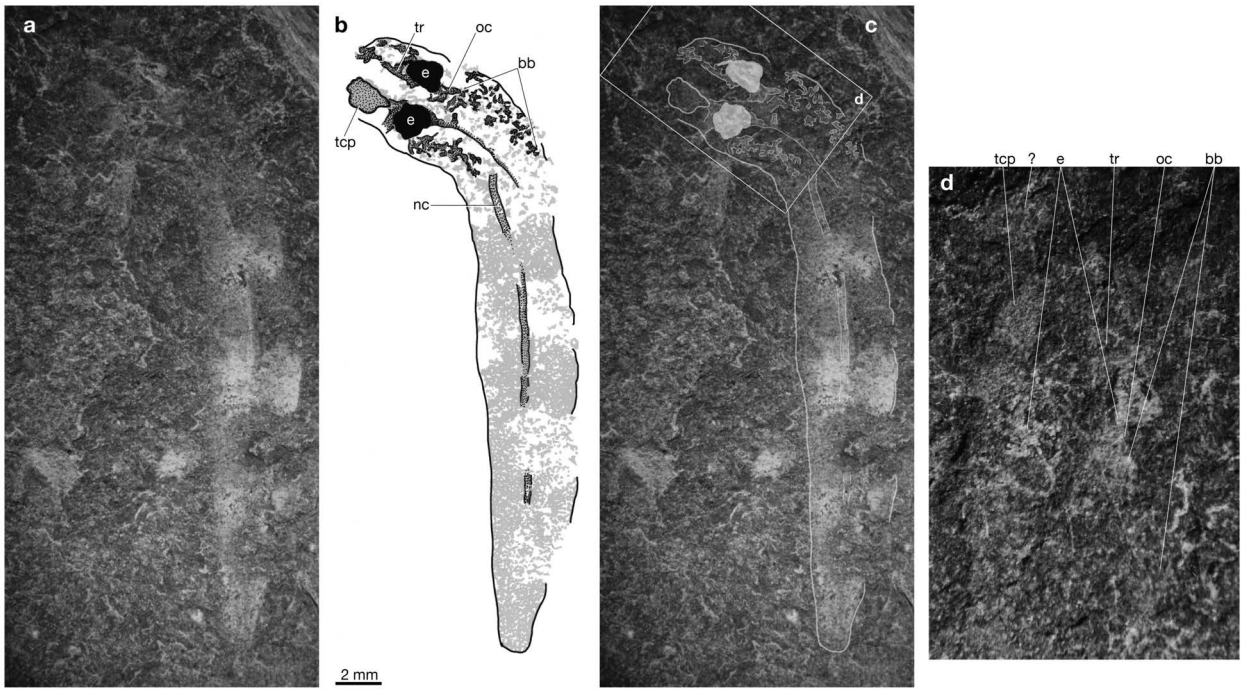
a
b
tr
oc
bb
e
e
tcp
nc
2 mm
c
d
d
tcp
?
e
tr
oc
bb

Fig. S3.7. A specimen referred to *Priscomyzon riniensis* (AM 5814) representing a pre-metamorphosis larva. Photographs (**a**, **c**) and interpretive drawings (**b**, **d**) of the slab and counter-slab, respectively. Photograph (**a**) is overlain with opaque outlines of major preserved structures. An unaltered photograph is Fig. 3.2i. See Fig. S3.1 for anatomical abbreviations.

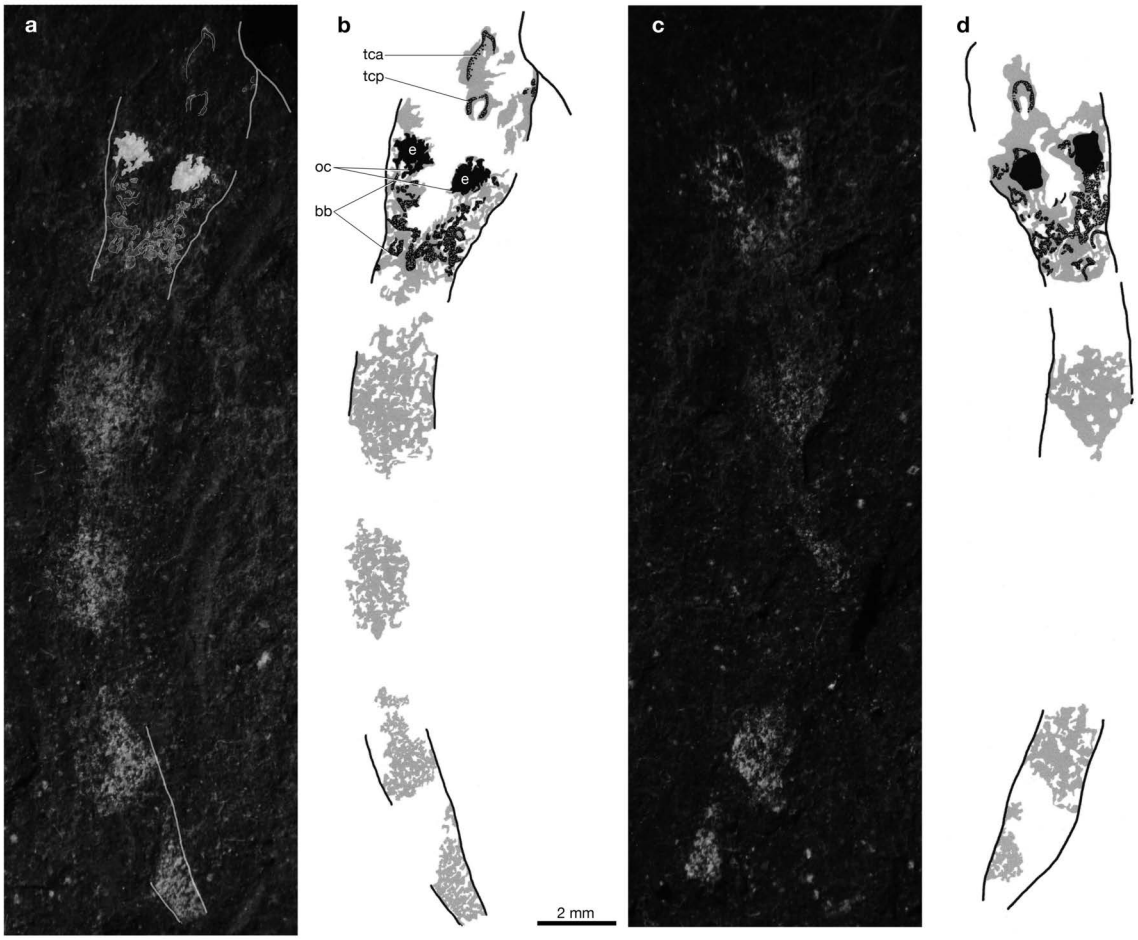
a
b
tca
tcp
oc
bb
e
e
c
d
2 mm

Fig. S3.8. A specimen referred to *Priscomyzon riniensis* (AM 5815) representing a pre-metamorphosis larva. Slab: photographs (**a**), interpretive drawing (**b**), photograph of boxed area in (**a**) showing the head region in greater magnification (**c**), photograph overlain with outlines of major preserved tissues (**d**). Counter-slab: photograph overlain with outlines of major preserve tissues (**e**), and photograph of boxed area in (**e**) showing the snout region in greater magnification (**f**). See Fig. S3.1 for anatomical abbreviations.

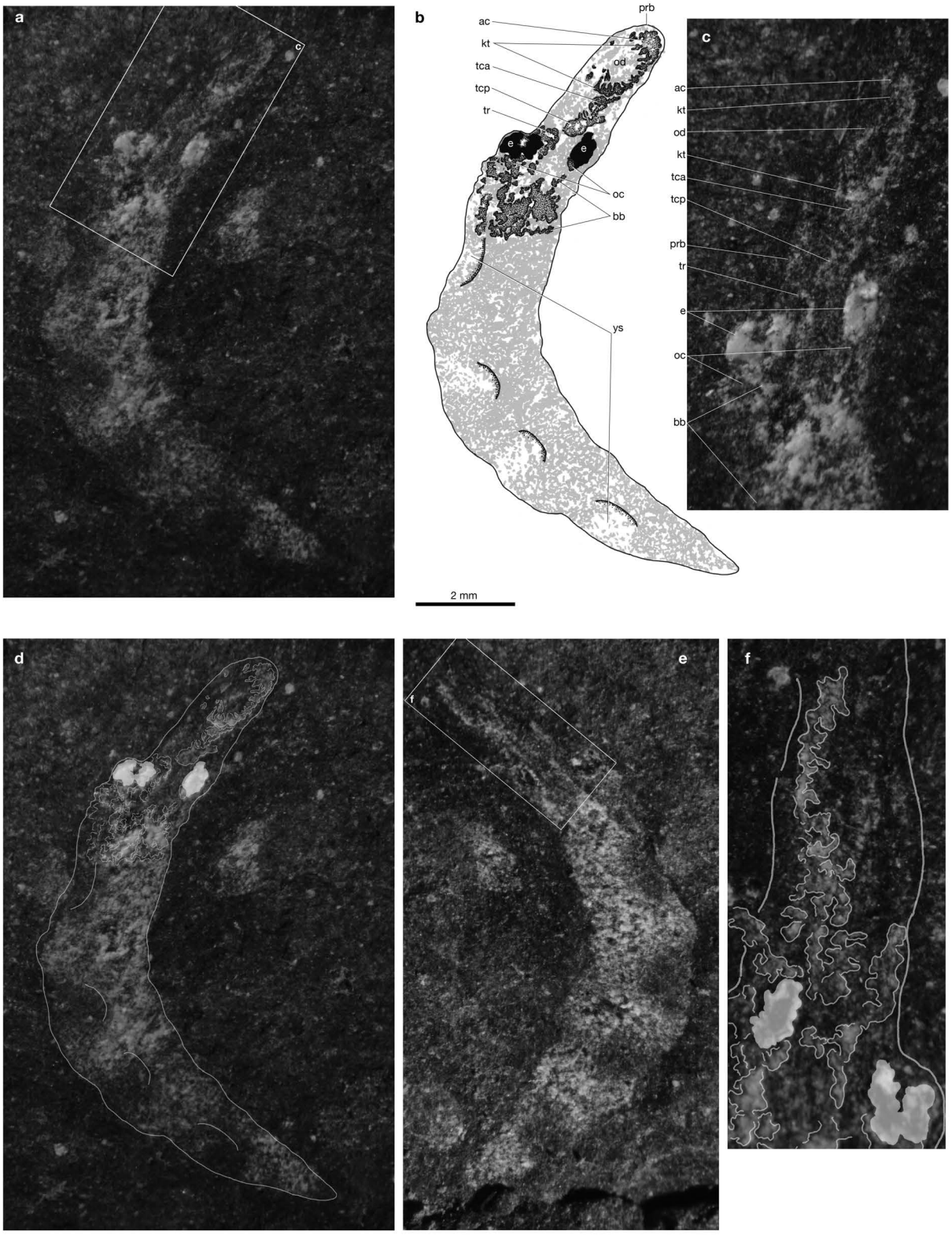
a
c
b
prb
ac
kt
od
tca
tcp
tr
e
e
oc
bb
ys
2 mm
c
ac
kt
od
kt
tca
tcp
prb
tr
e
oc
bb
d
e
f
f

Fig. S3.9. Comparison of the specimens referred to *Hardistiella montanensis*. Photograph (**a**, **c**) and interpretive drawing (**b**) of the main and counter slab of CM 46123, which represents the immature phase. Anatomical and ontogenetic interpretations are compatible with those in ref. 25. Photographs of the larger specimens UMPC (University of Montana, Paleontology Collections) 7696 (**d**) and CM 46299 (**e**), both interpreted to represent the adult phase. Panels are all to the same scale. See Fig. S3.1 for anatomical abbreviations.

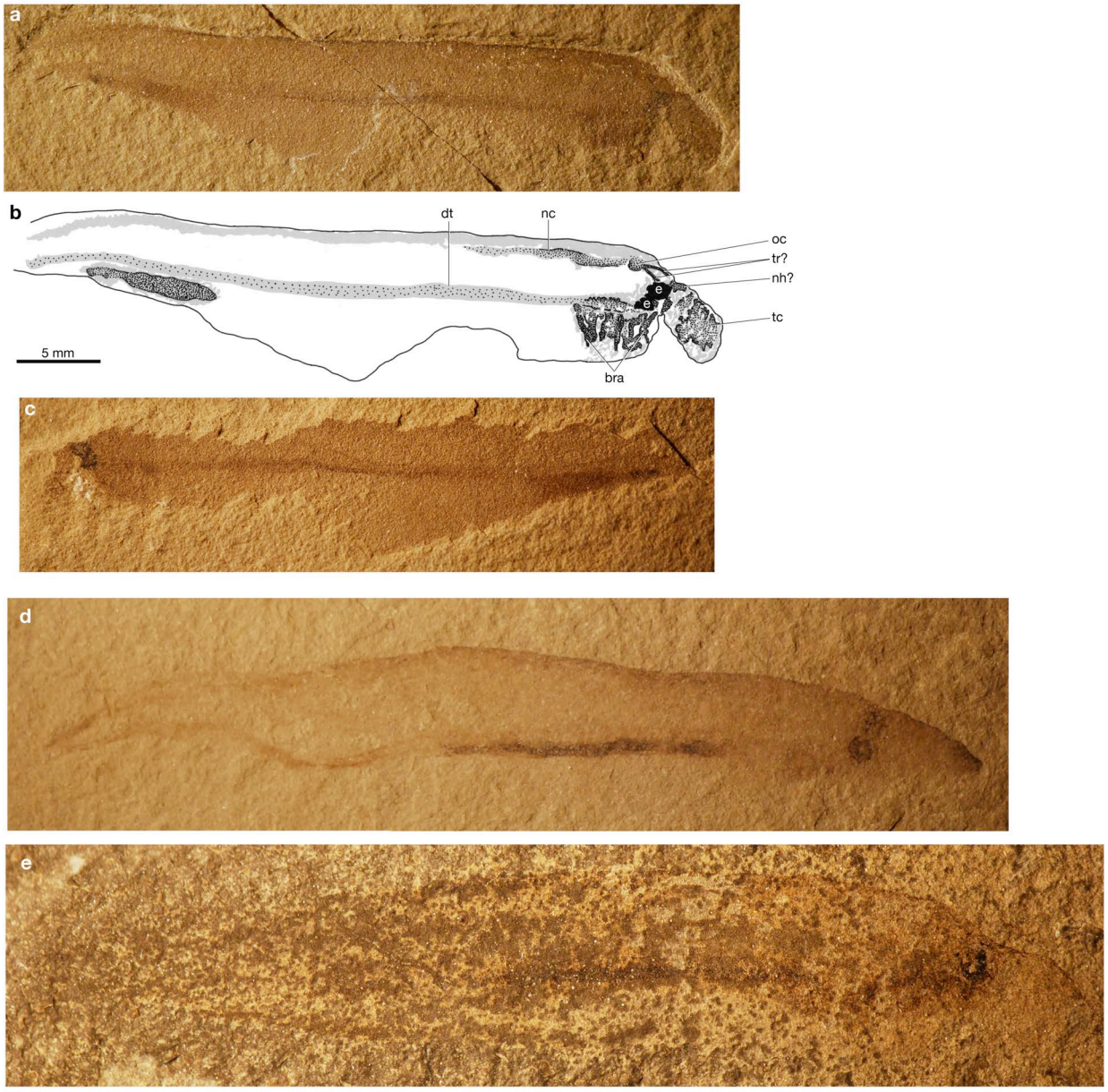
a
b
dt
nc
oc
tr?
nh?
e
e
tc
5 mm
bra
c
d
e

Fig. S3.10. Comparison of the smallest and largest specimens referred to *Mayomyzon pieckoensis*. Photograph (**a**) and interpretive drawing (**b**) of the smallest specimen FMNH PF 8167, interpreted as immature, following ref. 24. The inset shows the details of the cranial region of FMNH PF 8167 in photograph (**c**) and interpretive drawing (**d**). Photograph (**e**) of the largest specimen ROM (Royal Ontario Museum) 56787. All panels except for **c** and **d** are at the same scale. See Fig. S3.1 for anatomical abbreviations.

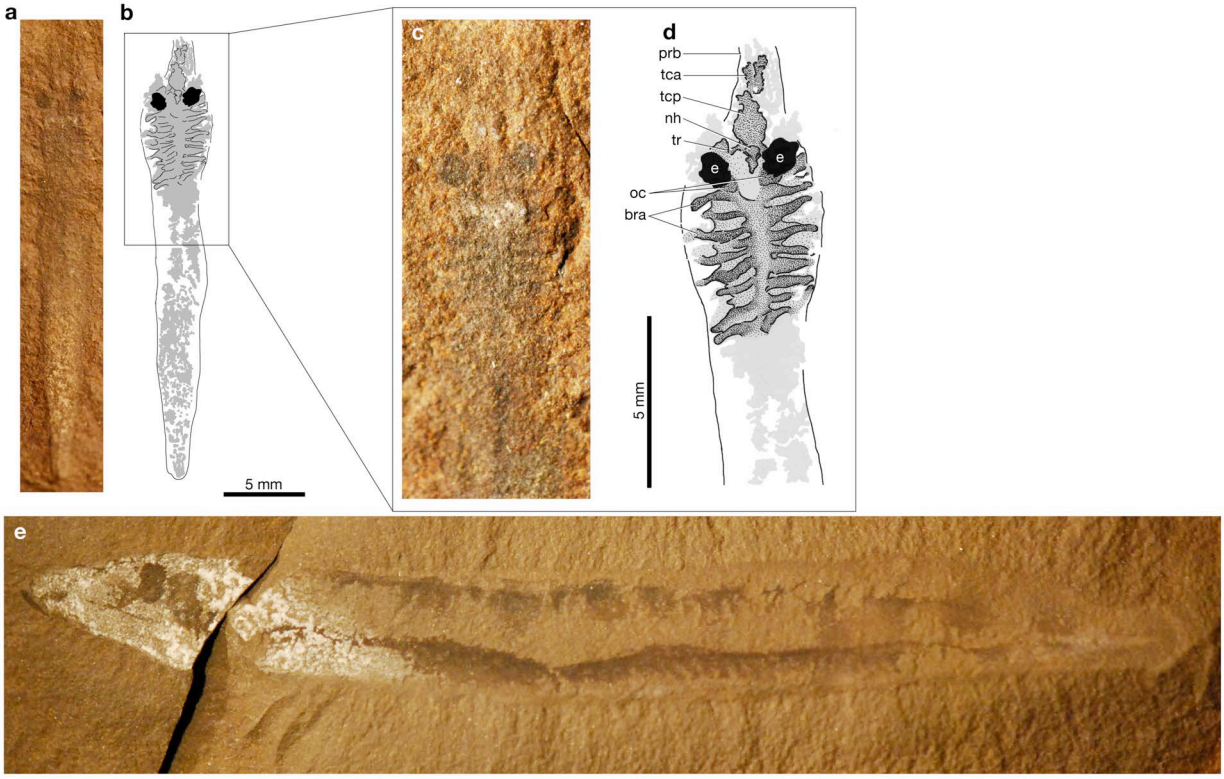
a
b
c
d
prb
tca
tcp
nh
tr
e
e
oc
bra
5 mm
5 mm
e

Fig. S3.11. Parsimony analyses were consistent with the taxonomic assignment of the specimens identified as immature individuals of coeval stem lampreys. Taxonomic combinations: (**a**) all immature specimens except AM 5816 (strict consensus: 18432 most parsimonious trees; tree length = 395); (**b**) AM 5820, *Priscomyzon riniensis* (strict consensus; 24576 most parsimonious trees; tree length = 394); (**c**) AM 5814, *Priscomyzon riniensis* (strict consensus; 18432 most parsimonious trees; tree length = 393); (**d**) AM 5817, *Priscomyzon riniensis* (strict consensus; 24573 most parsimonious trees; tree length = 393); (**e**) AM 5815, *Priscomyzon riniensis* (strict consensus; 6144 most parsimonious trees; tree length = 393); (**f**) AM 5816, *Priscomyzon riniensis* (strict consensus; 33403 most parsimonious trees; tree length = 392); (**g**) AM 5819, *Priscomyzon riniensis* (strict consensus; 6140 most parsimonious trees; tree length = 392); (**h**) FMNH PF 8167, *Mayomyzon pieckoensis* (strict consensus; 12288 most parsimonious trees; tree length = 393); (**i**) CM 46123, *Hardistiella montanensis* (strict consensus; 12288 most parsimonious trees; tree length = 393). The backbone topology was constrained using strict consensus of the most parsimonious trees resulting from the dataset of ref. 33. The trees for **b**-**e** and **g**-**i** is shown for the crown group Cyclostomi only, and the tree for **f** for the crown group Vertebrata. The topologies outside these nodes were identical.

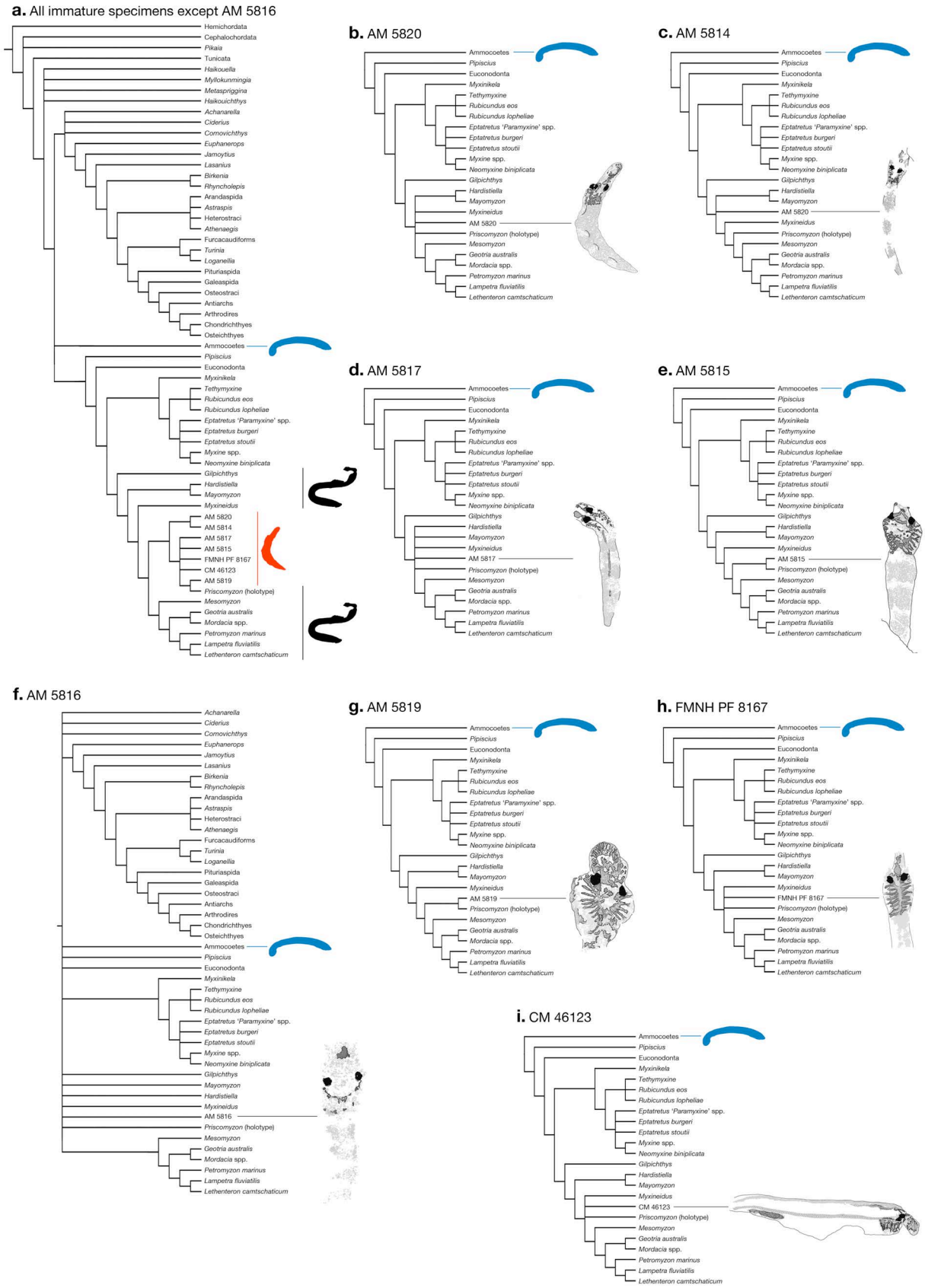
a. All immature specimens except AM 5816
b. AM 5820
c. AM 5814
d. AM 5817
e. AM 5815
f. AM 5816
g. AM 5819
h. FMNH PF 8167
i. CM 46123
Hemichordata
Cephalochordata
Pikaia
Tunicata
Haikouella
Myllokunmingia
Metaspriggina
Haikouichthys
Achanarella
Ciderius
Cornovichthys
Euphanerops
Jamoytius
Lasanius
Birkenia
Rhyncholepis
Arandaspida
Astraspis
Heterostraci
Athenaegis
Furcacaudiforms
Turinia
Loganellia
Pituriaspida
Galeaspida
Osteostraci
Antiarchs
Arthrodires
Chondrichthyes
Osteichthyes
Ammocoetes
Pipiscius
Euconodonta
Myxinikela
Tethymyxine
Rubicundus eos
Rubicundus lopheliae
Eptatretus 'Paramyxine' spp.
Eptatretus burgeri
Eptatretus stoutii
Myxine spp.
Neomyxine biniplicata
Gilpichthys
Hardistiella
Mayomyzon
Myxineidus
AM 5820
AM 5814
AM 5817
AM 5815
FMNH PF 8167
CM 46123
AM 5819
Priscomyzon (holotype)
Mesomyzon
Geotria australis
Mordacia spp.
Petromyzon marinus
Lampetra fluviatilis
Lethenteron camtschaticum
AM 5816

Fig. S3.12. Parsimony analyses of ammocoete larvae were consistent with the interpretation that none of the specimens in the growth series of a Paleozoic stem lamprey represents an ammocoete-like stage. The ammocoetes were resolved outside petromyzontiforms, unless a metamorphosing modern lamprey was included in the analysis. Taxonomic combinations: (**a**) all ammocoetes and all immature specimens of Palaeozoic stem lampreys except AM 5816 (strict consensus: 167007 most parsimonious trees; tree length = 398); (**b**) ammocoetes of *Petromyzon marinus* (Tahara's stage 30) (strict consensus: 24576 most parsimonious trees; tree length = 394); (**c**) ammocoetes (Tahara's stage 30) and late ammocoetes of *Petromyzon marinus* (strict consensus: 1920 most parsimonious trees; tree length = 398); (**d**) ammocoetes (Tahara's stage 30), late ammocoetes, and metamorphosing juveniles of *Petromyzon marinus* (strict consensus: 6816 most parsimonious trees; tree length = 402); (**e**) ammocoetes (Tahara's stage 30) and late ammocoetes of *Petromyzon marinus* and larvae of the Cretaceous stem lamprey *Mesomyzon mengae* (strict consensus: 55680 most parsimonious trees; tree length = 395); (**f**) larvae of the Cretaceous stem lamprey *Mesomyzon mengae* (strict consensus: 7872 most parsimonious trees; tree length = 385). The backbone topology was constrained using strict consensus of the most parsimonious trees resulting from the dataset presented in Chapter 2.

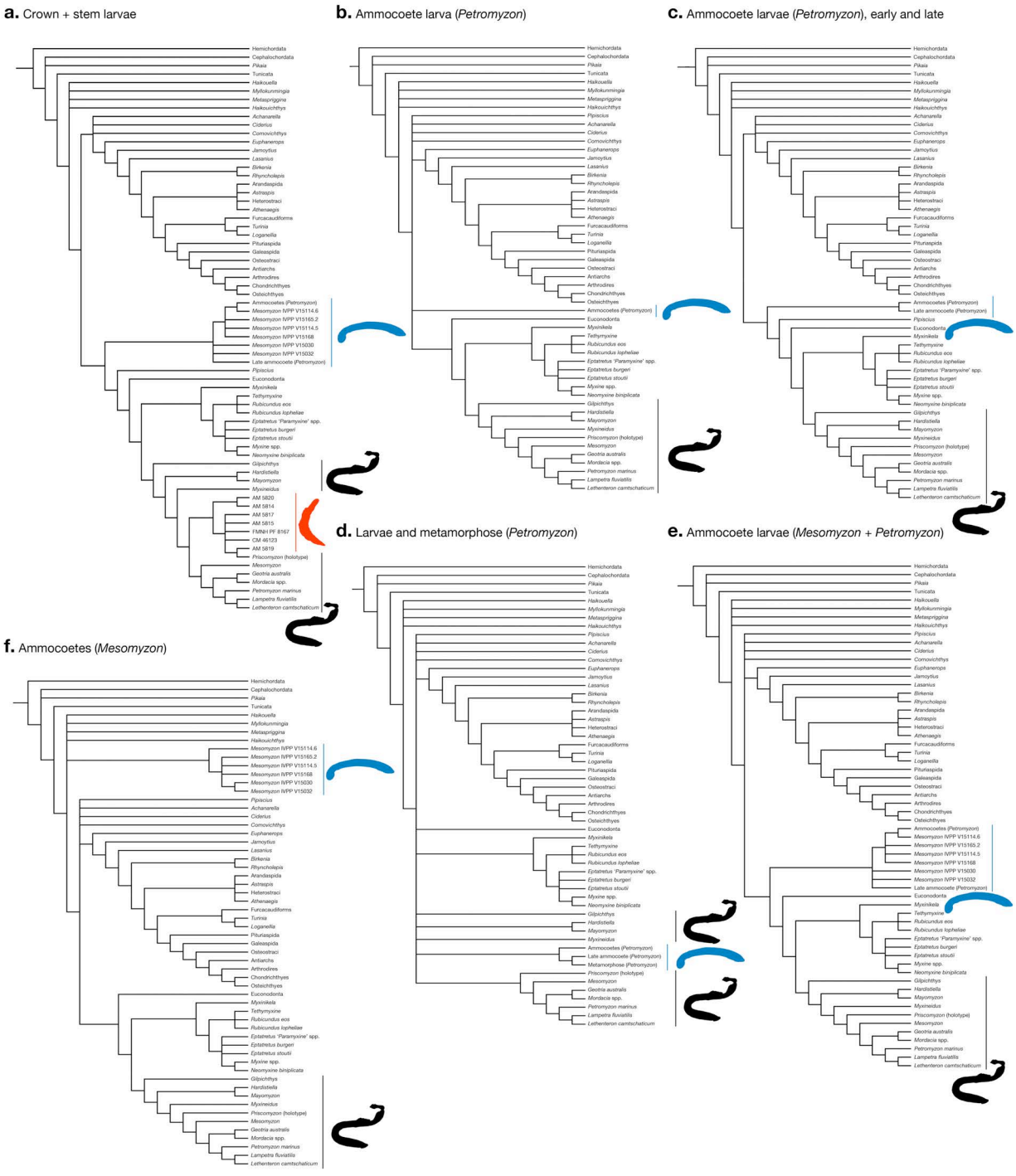
a. Crown + stem larvae
b. Ammocoete larva (Petromyzon)
c. Ammocoete larvae (Petromyzon), early and late
d. Larvae and metamorphose (Petromyzon)
e. Ammocoete larvae (Mesomyzon + Petromyzon)
f. Ammocoetes (Mesomyzon)

Fig. S3.13. Non-metric multi-dimensional scaling (NMDS) analysis of early vertebrate taxa, cyclostomes, gnathostomes, and outgroups of vertebrates. Bivariate plots of coordinates 1 and 2 (**a**, **c**) and Shepard's plots resulting from iterative runs (**b**, **d**). NMDS output of the analysis in which contingency coding was included as missing data (**a**, **b**) versus the analysis in which contingency coding was replaced by discrete states (**c**, **d**). Bivariate plots show morphospace occupied by lampreys in the adult phase, ammocoetes of modern lampreys, immature specimens of stem lampreys, and the outgroups of vertebrates with respect to other taxa in the dataset. Shepard's plots visualize a pattern of correlation between ranks obtained and ranks targeted until iterative runs of NMDS analysis converged. For PERMANOVA test scores, see Tables S3.3, S3.4.

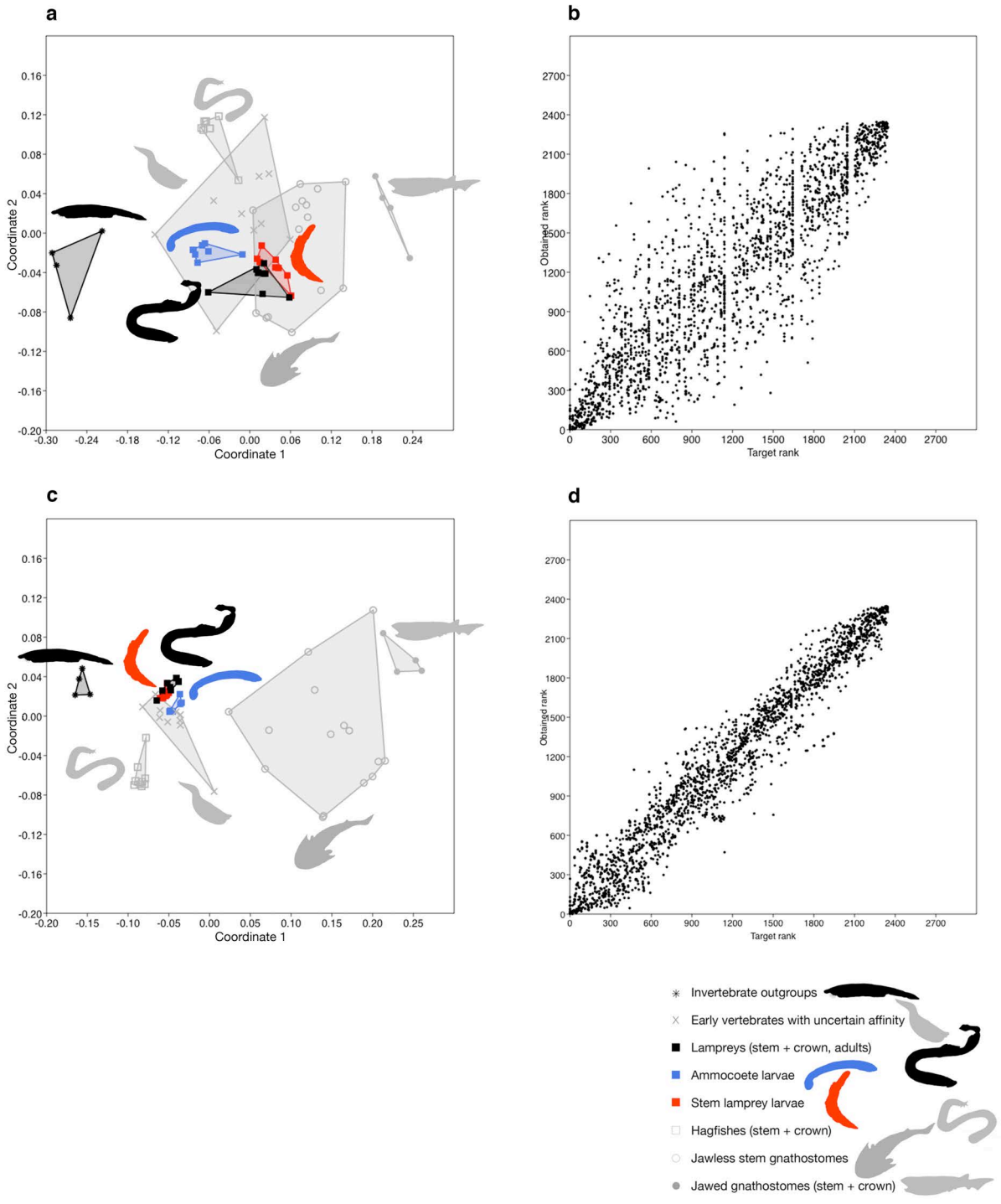
a
b
c
d
Coordinate 1
Coordinate 2
Obtained rank
Target rank
Invertebrate outgroups
Early vertebrates with uncertain affinity
Lampreys (stem + crown, adults)
Ammocoete larvae
Stem lamprey larvae
Hagfishes (stem + crown)
Jawless stem gnathostomes
Jawed gnathostomes (stem + crown)

Fig. S3.14. Principal coordinate analysis (PCoA) of early vertebrate taxa, cyclostomes, gnathostomes, and outgroups of vertebrates. Bivariate plots show morphospace occupation by lampreys in the adult phase, ammocoetes of modern lampreys, immature specimens of stem lampreys, and the outgroups of vertebrates with respect to other taxa in the dataset. (**a**) Coordinate 1 and coordinate 2; (**b**) coordinate 1 and coordinate 3; (**c**) coordinate 1 and coordinate 4; (**d**) coordinate 1 and coordinate 5; (**e**) coordinate 1 and coordinate 6. Axes with approximately or greater than 5% eigenvalue are shown. For more information on eigenvalues, see Table S3.5. For PERMANOVA test scores, see Table 3.7.

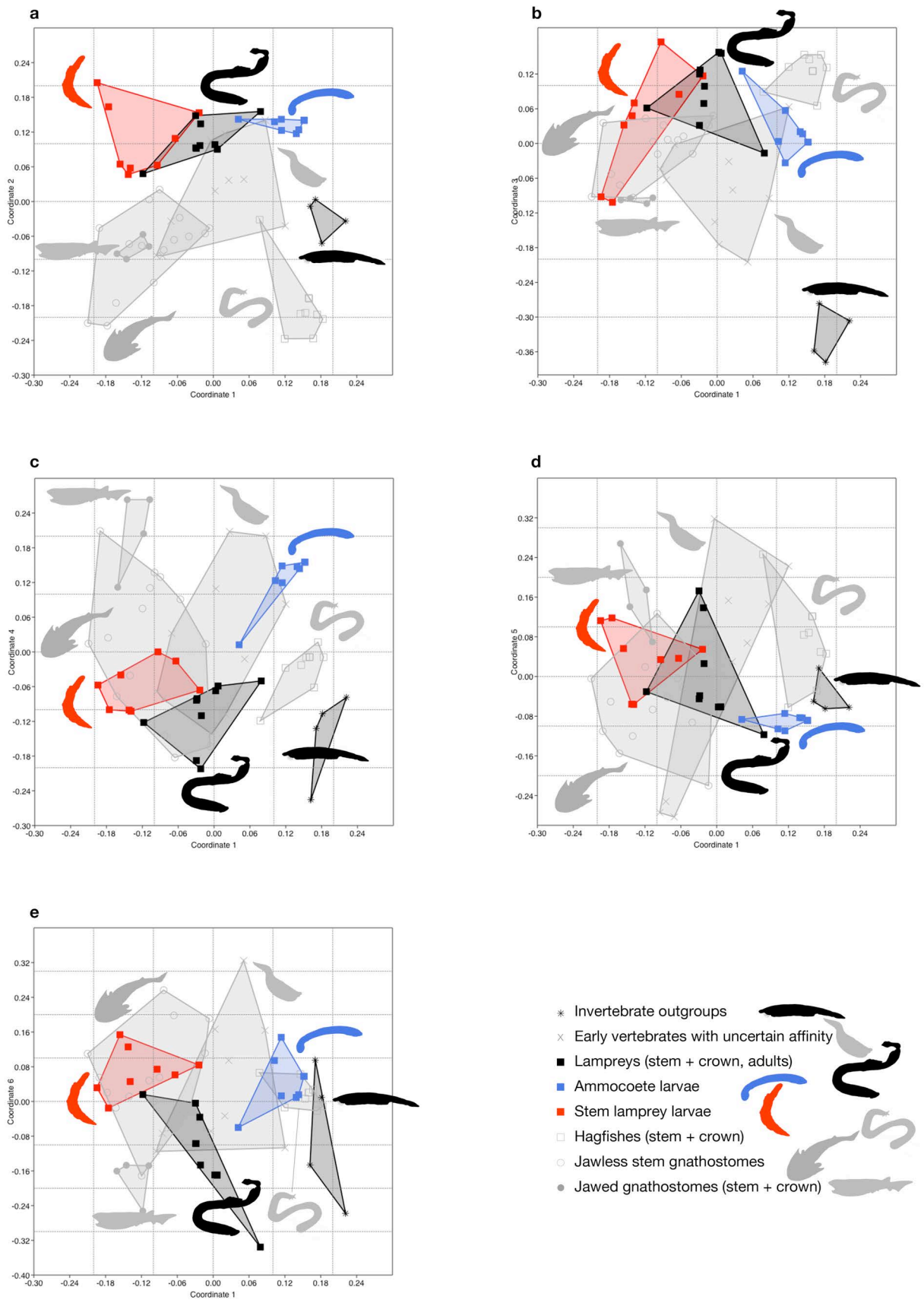
a
b
c
d
e
Coordinate 1
Coordinate 2
Coordinate 3
Coordinate 4
Coordinate 5
Coordinate 6
Invertebrate outgroups
Early vertebrates with uncertain affinity
Lampreys (stem + crown, adults)
Ammocoete larvae
Stem lamprey larvae
Hagfishes (stem + crown)
Jawless stem gnathostomes
Jawed gnathostomes (stem + crown)

Fig. S3.15. Principal coordinate analysis (PCoA) of early vertebrate taxa, cyclostomes, gnathostomes, and outgroups of vertebrates, with contingency coding accounted for. Bivariate plots show morphospace occupation by lampreys in the adult phase, ammocoetes of modern lampreys, immature specimens of stem lampreys, and the outgroups of vertebrates with respect to other taxa in the dataset. (**a**) Coordinate 1 and coordinate 2; (**b**) coordinate 1 and coordinate 3; (**c**) coordinate 1 and coordinate 4. Axes with greater than 5% eigenvalue are shown. For more information on eigenvalues, see Table S3.6. For PERMANOVA test scores, see Table 3.8.

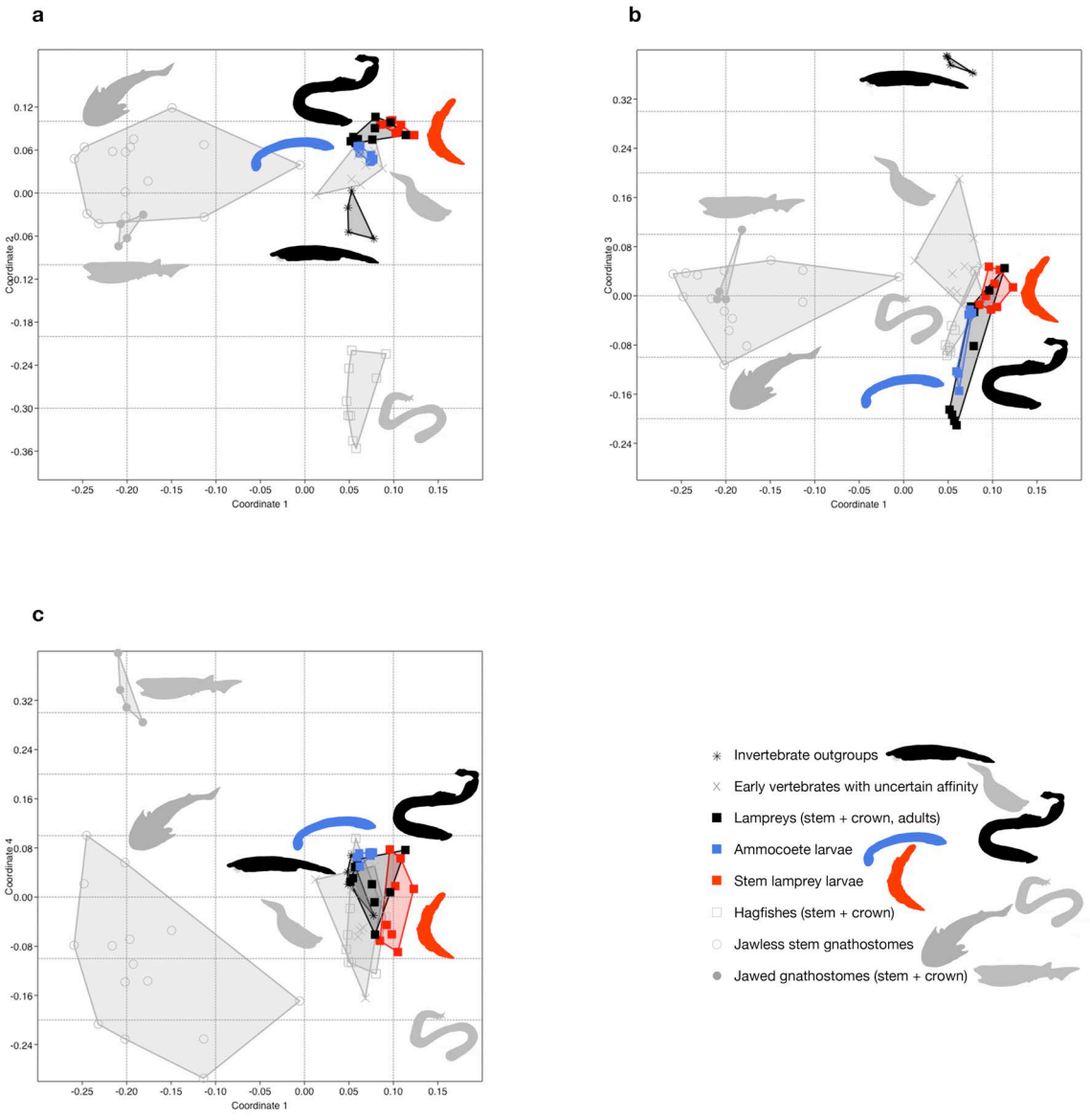
a
b
c
Coordinate 1
Coordinate 2
Coordinate 3
Coordinate 4
Invertebrate outgroups
Early vertebrates with uncertain affinity
Lampreys (stem + crown, adults)
Ammocoete larvae
Stem lamprey larvae
Hagfishes (stem + crown)
Jawless stem gnathostomes
Jawed gnathostomes (stem + crown)

SUPPLEMENTARY TABLES

Table S3.1. List of taxa used for parsimony and principal coordinate analyses.

Taxon	Group	Sources
Hemichordata	Outgroup	Specimens
Cephalochordata	Outgroup	Specimens
Tunicata	Outgroup	Specimens
Pikaia	Outgroup	Specimens
Haikouella	Uncertain affinity	Mallatt and Chen (2003)
Myllokunmingia	Uncertain affinity	Shu et al. (1996)
Metaspriggina	Uncertain affinity	Specimens
Haikouichthys	Uncertain affinity	Shu et al. (1996, 2003)
Pipiscius	Uncertain affinity	Specimens
Gilpichthys	Uncertain affinity	Specimens
Euconodonta	Uncertain affinity	Specimens
Myxinikela	Myxinoid	Specimens
Tethymyxine	Myxinoid	Specimens
Paramyxine spp.	Myxinoid	Specimens
Eptatretus burgeri	Myxinoid	Specimens
Eptatretus stoutii	Myxinoid	Specimens
Myxine spp.	Myxinoid	Specimens
Rubicundus eos	Myxinoid	Fernholm (1993)
Rubicundus lopheliae	Myxinoid	Fernholm and Quattrini (2008)
Neomyxine biniplicata	Myxinoid	Richardson and Jowett (1951)
Priscomyzon AM 5820	Stem larva - petromyzontiform	Specimens
Priscomyzon AM 5814	Stem larva - petromyzontiform	Specimens
Priscomyzon AM 5817	Stem larva - petromyzontiform	Specimens
Priscomyzon AM 5815	Stem larva - petromyzontiform	Specimens
Priscomyzon AM 5816	Stem larva - petromyzontiform	Specimens

Taxon	Group	Sources
Priscomyzon AM 5819	Stem larva - petromyzontiform	Specimens
Mayomyzon FMNH PF 8167	Stem larva - petromyzontiform	Specimens
Hardistiella CM 46123	Stem larva - petromyzontiform	Specimens
Priscomyzon - holotype	Petromyzontiform	Specimens
Mayomyzon	Petromyzontiform	Specimens
Hardistiella	Petromyzontiform	Specimens
Myxineidus	Petromyzontiform	Specimens
Mesomyzon	Petromyzontiform	Specimens
Geotria australis	Petromyzontiform	Renaud (2011)
Mordacia spp.	Petromyzontiform	Renaud (2011)
Lampetra fluviatilis	Petromyzontiform	Specimens
Lethenteron camtschaticum	Petromyzontiform	Specimens
Petromyzon marinus	Petromyzontiform	Specimens
Ammocoete *Petromyzon*	Ammocoetes	Specimens
Late ammocoete *Petromyzon*	Ammocoetes	Specimens
Metamorphose *Petromyzon*	Ammocoetes	Specimens
Mesomyzon IVPP V15114.6	Ammocoetes	Chang et al. (2015)
Mesomyzon IVPP V15165.2	Ammocoetes	Chang et al. (2015)
Mesomyzon IVPP V15114.5	Ammocoetes	Chang et al. (2015)
Mesomyzon IVPP V15168	Ammocoetes	Chang et al. (2015)
Mesomyzon IVPP V15030	Ammocoetes	Chang et al. (2015)
Mesomyzon IVPP V15032	Ammocoetes	Chang et al. (2015)
Jamoytius	Stem gnathostome	Specimens
Euphanerops	Stem gnathostome	Specimens
Achanarella	Uncertain affinity	Specimens
Ciderius	Uncertain affinity	van der Brugghen (2015)
Cornovichthys	Uncertain affinity	Specimens
Lasanius	Stem gnathostome	Specimens
Birkenia	Stem gnathostome	Specimens
Rhyncholepis	Stem gnathostome	Specimens

Taxon	Group	Sources
Arandaspida	Stem gnathostome	Specimens
Astraspis	Stem gnathostome	Specimens
Heterostraci	Stem gnathostome	Specimens
Athenaegis	Stem gnathostome	Specimens
Furcacaudiforms	Stem gnathostome	Specimens
Turinia	Stem gnathostome	Specimens
Loganellia	Stem gnathostome	Specimens
Galeaspida	Stem gnathostome	Specimens
Pituriaspida	Stem gnathostome	Specimens
Osteostraci	Stem gnathostome	Specimens
Chondrichthyes	Jawed gnathostome	Specimens
Osteichthyes	Jawed gnathostome	Specimens
Antiarchs	Jawed gnathostome	Specimens
Arthrodires	Jawed gnathostome	Specimens

Table S3.2. List of characters treated for contingency coding in the secondary analysis of morphological disparity (from **3.6.2 List of Characters**).

(a) Absence considered inapplicable (denoted †)	(b) A single state considered inapplicable (denoted *)	(c) Multiple states considered inapplicable (denoted **)
3, 4, 6, 33, 45, 56, 57, 58, 60, 64, 67, 73, 80, 81, 82, 83, 84, 87, 88, 89, 96, 100, 109, 116, 136, 141, 142, 144, 146, 151, 152, 153, 154, 155, 156, 157, 159, 160, 161, 162, 163, 171	5, 7, 8, 9, 10, 13, 15, 17, 18, 19, 20, 27, 28, 29, 30, 31, 32, 34, 35, 36, 38, 41, 42, 44, 45, 46, 47, 48, 49, 50, 51, 59, 63, 66, 68, 69, 70, 71, 77, 79, 85, 86, 91, 92, 94, 97, 98, 99, 101, 102, 104, 105, 106, 107, 108, 110, 111, 112, 113, 114, 115, 117, 118, 119, 120, 121, 122, 123, 124, 125, 126, 127, 128, 129, 130, 131, 132, 133, 134, 135, 137, 138, 139, 140, 143, 145, 148, 149, 150, 164, 165, 169, 170, 173	21, 22, 23, 24, 25, 54, 55, 60,

Table S3.3. Summary of PERMANOVA test of the scores from non-metric multidimensional scaling (NMDS) analysis in which contingency coding was included as missing data. Taxonomic codes: invertebrates = invertebrate outgroups; primitive = an assemblage of early vertebrates with uncertain affinity; stem larvae = larvae of Paleozoic stem lampreys; adult forms = adult forms of petromyzontiforms, stem and crown; stem gnath. = jawless stem gnathostomes; jawed gnath. = jawed gnathostomes. See Table S3.1 for grouping of taxa. Light grey shade indicates $0.05 > P > 0.01$; dark grey shade indicates $P < 0.01$.

PERMANOVA summary	
Permutation N:	9999
Total sum of squares:	0.9163
Within-group sum of squares:	0.1648
F:	39.73
p (same):	0.0001

Pairwise comparison (uncorrected *P*)

	Invertebrates	Primitive	Myxinoids	Stem larvae	Adult forms	Ammocoetes	Stem gnath.	Jawed gnath.
Invertebrates		0.0015	0.0020	0.0022	0.0011	0.0014	0.0004	0.0244
Primitive	0.0015		0.0002	0.0023	0.0011	0.0098	0.0004	0.0008
Myxinoids	0.0020	0.0002		0.0002	0.0002	0.0001	0.0001	0.0015
Stem larvae	0.0022	0.0023	0.0002		0.0436	0.0001	0.0903	0.0024
Adult forms	0.0011	0.0011	0.0002	0.0436		0.0001	0.0033	0.0016
Ammocoetes	0.0014	0.0098	0.0001	0.0001	0.0001		0.0001	0.0020
Stem gnath.	0.0004	0.0004	0.0001	0.0903	0.0033	0.0001		0.0003
Jawed gnath.	0.0244	0.0008	0.0015	0.0024	0.0016	0.0020	0.0003	

Table S3.4. Summary of PERMANOVA test of the scores from non-metric multidimensional scaling (NMDS) analysis in which contingency coding was replaced with discrete states. See Table S3.1 for grouping of taxa, and Table S3.4 for taxonomic codes. Light grey shade indicates 0.05 > P > 0.01; dark grey shade indicates P < 0.01.

PERMANOVA summary	
Permutation N:	9999
Total sum of squares:	0.9784
Within-group sum of squares:	0.1094
F:	69.19
p (same):	0.0001

Pairwise comparison (uncorrected *P*)

	Invertebrates	Primitive	Myxinoids	Stem larvae	Adult forms	Ammocoetes	Stem gnath.	Jawed gnath.
Invertebrates		0.0015	0.0020	0.0022	0.0011	0.0014	0.0004	0.0244
Primitive	0.0015		0.0002	0.0035	0.0002	0.0858	0.0001	0.0008
Myxinoids	0.0020	0.0002		0.0002	0.0002	0.0001	0.0001	0.0015
Stem larvae	0.0022	0.0035	0.0002		0.0195	0.0001	0.0001	0.0024
Adult forms	0.0011	0.0002	0.0002	0.0195		0.0001	0.0001	0.0016
Ammocoetes	0.0014	0.0858	0.0001	0.0001	0.0001		0.0001	0.0020
Stem gnath.	0.0004	0.0001	0.0001	0.0001	0.0001	0.0001		0.0015
Jawed gnath.	0.0244	0.0008	0.0015	0.0024	0.0016	0.0020	0.0015	

Table S3.5. Eigenvalues calculated in PCoA with no modifications for contingency coding.

Axis	Eigenvalue	%	Axis	Eigenvalue	%
1	675.06000	18.80600	36	1.54880	0.04315
2	381.38000	10.62500	37	1.09150	0.03041
3	316.26000	8.81060	38	0.61930	0.01725
4	256.36000	7.14200	39	0.36225	0.01009
5	227.37000	6.33430	40	0.00000	0.00000
6	166.72000	4.64450	41	0.00000	0.00000
7	153.15000	4.26650	42	0.00000	0.00000
8	115.71000	3.22360	43	0.00000	0.00000
9	106.63000	2.97050	44	-0.02542	-0.00071
10	92.99300	2.59070	45	-0.11066	-0.00308
11	76.04600	2.11850	46	-0.46009	-0.01282
12	73.95900	2.06040	47	-0.62381	-0.01738
13	57.81600	1.61070	48	-1.80270	-0.05022
14	48.07200	1.33920	49	-2.19270	-0.06109
15	42.49700	1.18390	50	-3.19570	-0.08903
16	32.60900	0.90845	51	-3.35760	-0.09354
17	30.67400	0.85455	52	-3.75700	-0.10467
18	25.48400	0.70995	53	-6.23270	-0.17363
19	22.94000	0.63907	54	-6.88860	-0.19191
20	21.44400	0.59741	55	-8.17660	-0.22779
21	19.63100	0.54690	56	-8.40520	-0.23416
22	17.15800	0.47801	57	-9.16430	-0.25530
23	15.67700	0.43673	58	-10.28600	-0.28656
24	12.81900	0.35713	59	-12.84000	-0.35771
25	12.39000	0.34517	60	-14.98500	-0.41746
26	9.12580	0.25423	61	-16.07400	-0.44780
27	8.45310	0.23549	62	-22.81700	-0.63566
28	6.93490	0.19320	63	-23.40800	-0.65212
29	6.41180	0.17862	64	-31.15800	-0.86801
30	5.60740	0.15621	65	-38.50100	-1.07260
31	4.69030	0.13066	66	-54.54600	-1.51960
32	4.09810	0.11417	67	-62.91700	-1.75280
33	3.64460	0.10153	68	-79.62500	-2.21830
34	3.39640	0.09462	69	-108.92000	-3.03440
35	2.23310	0.06221			

Table S3.6. Eigenvalues calculated in PCoA in which contingency coding was replaced by discrete states.

Axis	Eigenvalue	%	Axis	Eigenvalue	%
1	2242.40000	39.48800	36	2.52770	0.04451
2	774.05000	13.63100	37	1.69490	0.02985
3	477.18000	8.40310	38	1.46950	0.02588
4	307.80000	5.42040	39	1.14420	0.02015
5	191.21000	3.36720	40	0.75545	0.01330
6	181.51000	3.19630	41	0.64632	0.01138
7	136.29000	2.40000	42	0.36687	0.00646
8	128.61000	2.26490	43	0.07252	0.00128
9	108.40000	1.90900	44	0.00000	0.00000
10	97.11200	1.71010	45	0.00000	0.00000
11	90.36200	1.59130	46	0.00000	0.00000
12	81.30500	1.43180	47	0.00000	0.00000
13	60.84300	1.07140	48	-0.05529	-0.00097
14	46.13800	0.81249	49	-0.06933	-0.00122
15	44.57000	0.78487	50	-0.65298	-0.01150
16	39.68400	0.69882	51	-0.95931	-0.01689
17	32.07600	0.56486	52	-1.34940	-0.02376
18	26.59500	0.46833	53	-1.78620	-0.03146
19	24.50400	0.43151	54	-2.43770	-0.04293
20	22.15900	0.39023	55	-3.12610	-0.05505
21	19.42000	0.34199	56	-4.47060	-0.07873
22	16.86400	0.29698	57	-4.92020	-0.08664
23	15.58500	0.27445	58	-5.04350	-0.08882
24	12.03000	0.21184	59	-6.04580	-0.10647
25	11.38300	0.20046	60	-7.58910	-0.13364
26	10.73500	0.18904	61	-8.72720	-0.15369
27	9.05640	0.15948	62	-10.86800	-0.19139
28	8.95020	0.15761	63	-13.80300	-0.24307
29	8.23830	0.14508	64	-15.09200	-0.26576
30	6.45240	0.11363	65	-23.98200	-0.42233
31	5.35710	0.09434	66	-26.51400	-0.46691
32	4.24610	0.07477	67	-41.80500	-0.73617
33	3.62790	0.06389	68	-66.73600	-1.17520
34	3.38440	0.05960	69	-172.82000	-3.04340
35	2.95490	0.05204			

Table S3.7. Summary of PERMANOVA test of the scores from PCoA in which contingency coding was treated as missing entries. See Table S3.1 for grouping of taxa, and Table S3.4 for taxonomic codes. Light grey shade indicates 0.05 > P > 0.01; dark grey shade indicates P < 0.01.

PERMANOVA summary	
Permutation N:	9999
Total sum of squares:	15
Within-group sum of squares:	10.21
F:	4.084
p (same):	0.0001

Pairwise comparison (uncorrected *P*)

	Invertebrates	Primitive	Myxinoids	Stem larvae	Adult forms	Ammocoetes	Stem gnath.	Jawed gnath.
Invertebrates		0.00820	0.00200	0.00220	0.00110	0.00140	0.00040	0.02440
Primitive	0.00820		0.00010	0.01510	0.00060	0.00040	0.07690	0.00150
Myxinoids	0.00200	0.00010		0.00020	0.00020	0.00010	0.00020	0.00150
Stem larvae	0.00220	0.01510	0.00020		0.00470	0.00010	0.04800	0.00240
Adult forms	0.00110	0.00060	0.00020	0.00470		0.00010	0.00010	0.00160
Ammocoetes	0.00140	0.00040	0.00010	0.00010	0.00010		0.00010	0.00200
Stem gnath.	0.00040	0.07690	0.00020	0.04800	0.00010	0.00010		0.00050
Jawed gnath.	0.02440	0.00150	0.00150	0.00240	0.00160	0.00200	0.00050	

Table S3.8. Summary of PERMANOVA test of the scores from PCoA in which contingency coding was replaced with discrete states. See Table S3.1 for grouping of taxa, and Table S3.4 for taxonomic codes. Light grey shade indicates 0.05 > P > 0.01; dark grey shade indicates P < 0.01.

PERMANOVA summary	
Permutation N:	9999
Total sum of squares:	13
Within-group sum of squares:	7.952
F:	5.531
p (same):	0.0001

Pairwise comparison (uncorrected *P*)

	Invertebrates	Primitive	Myxinoids	Stem larvae	Adult forms	Ammocoetes	Stem gnath.	Jawed gnath.
Invertebrates		0.00150	0.00200	0.00220	0.00110	0.00140	0.00040	0.02440
Primitive	0.00150		0.00010	0.00860	0.00020	0.00020	0.00020	0.00080
Myxinoids	0.00200	0.00010		0.00020	0.00020	0.00010	0.00010	0.00150
Stem larvae	0.00220	0.00860	0.00020		0.00350	0.00010	0.00050	0.00240
Adult forms	0.00110	0.00020	0.00020	0.00350		0.00010	0.00010	0.00160
Ammocoetes	0.00140	0.00020	0.00010	0.00010	0.00010		0.00010	0.00200
Stem gnath.	0.00040	0.00020	0.00010	0.00050	0.00010	0.00010		0.00290
Jawed gnath.	0.02440	0.00080	0.00150	0.00240	0.00160	0.00200	0.00290	

Chapter 4

Testing Hypotheses about Evolutionary Origins of the Jaw Joint in Vertebrates

Nature has but little clay like that of which she moulded you.

— *To The Lighthouse*, Virginia Woolf

4.1 INTRODUCTION

4.1.1 Synovial Diarthrosis in Early Vertebrate Evolution

A hinge joint is a fundamental prerequisite for skeletal elements to yield a functional jaw (Depew and Compagnucci, 2008). In crown gnathostomes, the jaw joint is a synovial diarthrosis between the palatoquadrate and Meckel's cartilage (or their derivatives) (Fig. 4.1a-c), with the exception of mammals in which the functional jaw joint forms between two intramembranous ossifications, the temporal and mandible (the original 'jaw' joint still forms between the incus and malleus) (Hopson, 1994; Luo and Crompton, 1994; Miyashita, 2016). Although the joint must have been present in the earliest jaw skeleton, little information is available about its primitive state. The proximal ends of the palatoquadrate and Meckel's cartilage were not ossified in the antiarch *Bothriolepis* (Young, 1984) so joint morphology is unknown, whereas the palatoquadrate and Meckel's cartilage already have condyles and fossa in other placoderms with a completely ossified jaw skeleton (e.g., arthrodires and ptyctodonts) (Stensiö, 1969; Forey and Gardiner, 1986; Janvier, 1996). This phylogenetic distribution indicates the presence of synovial diarthrosis in the jaw skeleton before the crown node of gnathostomes, but it offers no information on whether or not the earliest jaw skeletons had a joint without synovium.

No synovial diarthrosis is known outside of jawed vertebrates. Cyclostomes do not have a synovial diarthrosis. As the skeleton consists of non-mineralized cartilages (Robson et al., 2000), elasticity of the cartilages and the surrounding connective tissues functions as a joint (Fig. 4.1d; Strahan, 1958; Miyashita, 2012, 2016). This is consistent with the distribution of soft cartilages in highly mobile elements such as velum (Cole, 1905; Robson et al., 2000; Miyashita, 2012). Among all jawless vertebrates extinct or extant, only osteostracans have osteological evidence for an endoskeletal joint at an interface of mineralized elements. In this lineage, a small area of unfinished bone — marked by the absence of a cortical layer — sits within the pectoral fossa to

which the main cartilaginous support of a pectoral fin is considered to have attached (Fig. 4.1e; Wängsjö, 1952; Janvier, 1981, 1985a; Johanson, 2002). It is not clear whether or not this joint represents a synovial diarthrosis, as the proximal end of the fin support is not preserved. Thus, the jaw joint probably represents one of the most ancient synovial diarthroses in vertebrates.

4.1.2 Development of Synovial Diarthrosis

Synovial diarthrosis has the following anatomical components: articular cartilages, synovial membrane, ligaments, and synovial fluid (Fig. 4.1a; Archer et al., 2003; Khan et al., 2007). Articular cartilages cap the ends of skeletal elements at the joint. The space between the articular cartilages is encapsulated by a synovial membrane and ligaments and filled with synovial fluid, the proteome of which is derived from blood plasma, synovium and articular cartilages (Bennike et al., 2014). This complex structure requires contributions from distinct cell lineages including neural crest (skeleton in splanchocranium) and mesoderm (connective tissues; skeleton in trunk and appendages and develops through cavitation (Archer et al., 2003; Khan et al., 2007).

Development of a synovial diarthrosis proceeds from establishment of an interzone to cavitation. The interzone forms either within a single condensation of chondrocytes or between two adjacent, appositionally growing condensations (Smeeton et al., 2016). The interzone chondrocytes remain in an immature state (low *Col2a1* and *Acan* expression) while the chondroprogenitors in the growth plates proliferate and mature into pre-hypertrophic state (high *Col2a1* and *Acan* expression) (Smeeton et al., 2016). During cavitation, the interzone chondrocytes differentiate into articular cartilages as they separate to the two articular surfaces, ligaments form an enthesis to encapsulate the synovium, and molecular lubricants are secreted (Figs. 4.1a, 4.2d; Pacifici et al., 2006; Decker et al., 2014). Bmp, FGF, Hedgehog, and Wnt signaling pathways are involved at various stages from interzone formation to cavitation (Figs. 4.1a, 4.2d; Guo et al., 2004; Wilson and Tucker, 2004). The role of the Bmp signaling pathway is particularly complex. A current model suggests that different fates of the chondroprogenitors are regulated by the decreasing Bmp signaling (Bmp2/4/7) and increasing Gdf (BMP ligands) toward the interzone (Smeeton et al., 2016). Cavitation requires the Hedgehog signaling (*Ihh*, *Smo*) (Koyama et al., 2008; Ray et al., 2015; Rockel et al., 2016) but the cellular mechanisms remain unclear. Filling in this cavity, synovial fluid consists of permeation through the synovial membrane and locally secreted proteins (Bennike et al., 2014). One important component of the

fluid is lubricin, and its encoding gene *Prg4* is expressed at the perichondrium of the articular cartilage and other encapsulating tissues of the joint (Fig. 4.2c, d; Askary et al., 2016).

Different transcription factors mediate formation of an interzone — a future synovial diarthrosis — in different joints. In the pharynx, these toolkit genes are Bagpipe (*Nkx3.2*, also known as *Bapx*) and Iroquois (*Irx5/7*) homologues, both homeodomain-containing, evolutionarily ancient transcription factors (Garcia-Fernàndez, 2005). In crown gnathostomes (chicks, mice, and zebrafish), *Nkx3.2* has three major expression domains: neural crest ectomesenchyme in the intermediate region of the mandibular arch (future jaw joint/middle ear) (Fig. 4.2a; Depew et al., 2002; Miller et al., 2003; Tucker et al., 2004; Wilson and Tucker, 2004); the sclerotome boundaries (future intervertebral joints) (Lettice et al., 2001; Herbrand et al., 2002); and the left or right splanchnic mesoderm (asymmetrically arranged spleen and pancreas) (Schneider et al., 1999; Murtaugh et al., 2001; Palmer, 2004). Although sclerotomal *Nkx3.2* expression is regulated by Shh signaling, mandibular expression of *Nkx3.2* is downstream of the endothelin signaling (Medeiros and Crump, 2012). Here, *Nkx3.2* is upregulated by *Edn1*/*Ednr* in the intermediate region and downregulated by ventrally expressed *Hand2* (Miller et al., 2000, 2003).

A precise function of *Nkx3.2* expression remains unclear. NKX3.2 forms a complex with HDAC1 and SMAD4, which functions as a transcriptional repressor (Kim et al., 2003; Kim and Lassar, 2003). In the middle ear joints (jaw joint in non-mammalian gnathostomes) of mice, *Nkx3.2* expression is required for the growth factor *Gdf5/6/7* and *Chd* to be expressed in the interzone at the midheight of the mandibular arch (Tucker et al., 2004). In the sclerotomes of mice, *Nkx3.2* (induced by the Hedgehog signaling) forms an autoregulatory loop with *Sox9* to inhibit chondrocyte maturation by downregulating *Runx2* (Murtaugh et al., 2001; Herbrand et al., 2002; Zeng et al., 2002; Kim and Lassar, 2003; Kim et al., 2003; Provot et al., 2006; Kerney et al., 2007; Yamashita et al., 2009; Caron et al., 2015). It has not been tested in non-tetrapod models such as zebrafish whether or not *Nkx3.2* has conserved functions and downstream pathways, and whether or not the function of *Nkx3.2* as a chondrogenesis regulator in the axial skeleton applies to the jaw joint as well. Supporting evidence from the hyoid arch of zebrafish favors broad conservation across species and body regions. Instead of *nkx3.2*, *irx5/7* performs similar functions in the hyoid joint of zebrafish by inhibiting *sox9* from activating *col2a1* expression in the interzone (Askary et al., 2015). The expression domain of *irx5/7* is regulated by the endothelin signaling and *Hand2* expression, as in the mandibular expression of *nkx3.2*

(Askary et al., 2015). As a repressor of joint formation, *Barx* is upregulated by *Hand2* in the ventral domain of the mandibular arch (Nichols et al., 2013).

These regulatory relationships are supported by a series of functional analyses. The morpholino knockdown of *nkx3.2* in zebrafish resulted in fusion of the palatoquadrate and Meckel's cartilage to eliminate the interzone, but did not affect the hyoid joints (Miller et al., 2003). Similar phenotypes were observed when the upstream endothelin signaling pathway is disrupted in knockdown or knockout experiments (Miller et al., 2000, 2007; Kimmel et al., 2003; Walker et al., 2006, 2007). Reciprocally, the *irx7* knockouts resulted in fusion of the hyomandibular, interhyal, and ceratohyal in zebrafish, but did not affect the jaw joint of the mandibular arch (Askary et al., 2015). The *barx1* knockout zebrafish developed double joints in the mandibular arch (Nichols et al., 2013), which suggests either: (***a***) *barx1* downregulates *nkx3.2* (perhaps in mutual antagonism); or (***b***) joint repression by *barx1* overrides joint promotion by *nkx3.2* — thereby allowing formation of an extra joint in the knockouts where *barx1* and *nkx3.2* expression domains would normally overlap each other.

4.1.3 Critical Questions Regarding Origins of the Jaw Joint

Thus, developmental requirements for a jaw joint are: (***a***) focal expression of *Nkx3.2* in the intermediate mandibular arch; (***b***) endothelin signaling in the intermediate region and *Hand2* expression in the ventral region to induce (***a***); and as a consequence of (***a***), (***c***) inhibition of chondrocyte maturation in the interzone (upregulation of Gdf5/6/7; downregulation of *Col2a1* and other chondrogenic genes such as *Runx2*). At what node in the vertebrate tree did these traits evolve? In lampreys dorsoventral patterning is via endothelin signaling and ventrally expressed *Hand2* (Kuraku et al., 2010; Cattell et al., 2011; Yao et al., 2011; Medeiros and Crump, 2012; Square et al., 2016), indicating that these traits are conserved from the common ancestor between cyclostomes and gnathostomes. However, interpretations of the data obtained from two different species conflict each other regarding (***a***) focal expression of *Nkx3.2*, and its regulatory relationships remain unclear in this lineage for (***b***) downstream factors and (***c***) upstream regulators. In the sea lamprey *Petromyzon marinus*, *Nkx3.2* expression appears to be lacking in the mandibular arch (Cerny et al., 2010). In the Japanese river lamprey *Lethenteron camchatsticum*, however, *Nkx3.2* is expressed in the mandibular arch at Tahara's stage 25 (Kuraku et al., 2010). To complicate matters further, two different probes were used for these *in*

situ hybridizations. This discrepancy may be attributed to taxonomic differences, experimental artifacts, or different splice forms of *Nkx3.2*, none of which can be ruled out.

The ultimate goal of this study is to test which developmental traits of the jaw joint were present in the last common ancestor between cyclostomes and gnathostomes. This chapter reports preliminary results from expression and functional analyses of the jaw joint pathway mediated by *Nkx3.2* in lampreys and zebrafish. Based on ongoing experiments, I describe expression patterns of *Nkx3.2* and its downstream targets in lampreys, compare potential *Nkx3.2* phenotypes in lampreys using partial knockouts generated by CRISPR/Cas9, and introduce a new comparative model in *nkx3.2*-knockout zebrafish.

4.2 HYPOTHESES

4.2.1 Overview

The jaw joint is considered a novel trait in jawed vertebrates (Cerny et al., 2010; Askary et al., 2016; Miyashita, 2016). The apparent absence of *Nkx3.2* expression in the mandibular arch of *Petromyzon marinus* suggested that acquisition of the mandibular expression domain represents the key innovation necessary for a jaw to evolve (Cerny et al., 2010). However, this hypothesis does not address origins of structural components of a jaw joint. The jaw joint is anatomically and developmentally a complex structure, and all components are unlikely to have evolved *de novo* by acquiring expression of a single transcription factor. Instead, evolutionary precursors should have existed in the stem of gnathostomes. Such precursors may have performed a joint-like function, may have had similar anatomy, and may have required expression of some of the jaw joint pathway genes, including *Nkx3.2* — in an unknown combination.

A co-option event to transform the evolutionary precursor into a *bona fide* jaw joint may have occurred either (***A***) at the level of tissues or (***B***) at the level of gene expressions: (***A***) co-opting a precursor tissue to the intermediate region of the mandibular arch via transposition of *Nkx3.2* expression domain; or (***B***) modifying a pre-existing structure in the mandibular arch via acquisition of *Nkx3.2* expression. In scenario (***A***), *Nkx3.2* expression should characterize the precursor tissue in outgroups of jawed vertebrates, and the tissue needs not occupy the exact anatomical position of a jaw joint. In scenario (***B***), the structure needs not express *Nkx3.2* in the outgroups, but it assumes no positional difference between a jaw joint and its evolutionary

precursor. In either scenario, the precursor tissue is predicted to perform functions similar to synovial diarthrosis. To accommodate these scenarios, three hypotheses have been proposed to identify an evolutionary precursor — or a homologue — of the jaw joint in the outgroups of jawed vertebrates (Fig. 4.3).

4.2.2 The Muscular Scaffold Hypothesis

The lingual apparatus — a pulley-like protractor-retractor complex anchored to the infrapharyngeal cartilages — is a functional analogue of the gnathostome jaw in cyclostomes (Hardisty and Rovainen, 1982; Kawasaki and Rovainen, 1988; Rovainen, 1996; Clark and Summers, 2007, 2012; Clark et al., 2010; Miyashita, 2012). The keratinous tooth plates are everted and folded back in the oral cavity by serial contraction of the protractors and retractors (Clark and Summers, 2007; Goudemand et al., 2011). During this motion, the individual muscles slide against one another, and the cartilages of the lingual apparatus are held stable by the antagonizing suspending muscles (Fig. 4.3a; Miyashita, 2012). The spatial organization of antagonizing muscles and muscle kinematics are similar to the muscular scaffold in which the jaws are embedded in polychaetes (Uyeno and Kier, 2015). Such a muscular hydrostat could function as a flexible joint not only as a hinge, but also as a repositionable pivot and a transmitter of biting forces (Uyeno and Clark, 2015). Although no evolutionary scenario was presented specifically to explain the origin of the jaw joint, the comparison raises the possibility that early jawless vertebrates relied on such muscular articulation to move a proto-jaw. Unlike the polychaete apparatuses that employ muscular hydrostats to open and close, however, the gnathostome jaw is embedded within the head. A jaw articulation as postulated by comparison with similar muscular hydrostats would require a large space for multiple antagonizing muscles relative to the head, in addition to adductor/abductor chambers. This is inconsistent with the relatively small mandibular-arch derived space covered by mineralized, dermal facial skeleton in stem gnathostomes (Miyashita, 2016).

4.2.3 The Mucocartilage Hypothesis

Mucocartilage is fibrous, mesenchymal tissue that contributes the largest component to the skulls of ammocoetes (larval lampreys) (Fig. 4.3b, c; De Beer, 1937; Johnels, 1948; Hardisty, 1981; Wright and Youson, 1982; Morrison et al., 2000; Miyashita, 2012). At this ontogenetic stage,

cellular cartilages only exist in the parachordal cartilages and branchial bars, whereas the rest of the skull is entirely composed of mucocartilage (Johnels, 1948; Langille and Hall, 1988; Wright et al., 1988). Histologically, mucocartilage appears as a mass of mesenchyme with fibrous extracellular matrix and is sometimes interpreted as undifferentiated (Wright and Youson, 1982; Armstrong et al., 1987; Martin et al., 2009; Cattell et al., 2011). Despite the assumed immature status, the mucocartilage persists throughout the larval phase (Johnels, 1948). Interpretations differ about whether the mucocartilage becomes resorbed and replaced during metamorphosis (de Beer, 1937; Johnels, 1948; Kuratani et al., 2001; Kuratani and Ota, 2008; Ohtani et al., 2008) or has the potential to differentiate into cellular cartilages (Armstrong et al., 1987). However, most mucocartilaginous components of the skull are specific to ammocoetes. As such, mucocartilage is replaced by skeletal elements made of cellular cartilage, regardless of whether or not it has the potential to differentiate. Nevertheless, properties of mucocartilage —undifferentiated appearance, high elasticity, and low matrix density — can parallel attributes of the interzone that precedes development of a synovial diarthrosis.

On that comparative basis, mucocartilage has been proposed as a potential evolutionary precursor of the synovial diarthrosis (Cattell et al., 2011; Medeiros and Crump, 2012). The expression of a *Runx2* cognate in the embryos of *Petromyzon marinus* was considered to bolster this hypothesis (Cattell et al., 2011). However, *Runx2* expression was incorrectly assumed to represent a marker of synovial diarthrosis in this comparison. Instead, it is downregulated in the interzone and upregulated in the hypertrophied chondrocytes (Später et al., 2006; Hartmann, 2009; Yamashita et al., 2009). Therefore, the Mucocartilage Hypothesis lacks support from gene regulatory and expression profiles. Anatomically, the interzone does not necessarily compare with mucocartilage because it lacks abundant fibrous extracellular matrix that the immature chondrocytes differentiate into articular cartilages, and because it is encapsulated by the collagen-rich, ligamentous connective tissues (Archer et al., 2003; Smeeton et al., 2016). Furthermore, at no ontogenetic stage of lamprey development does mucocartilage serve as a connective tissue between cartilages (Miyashita, 2012). Mucocartilage does not constitute a functional analogue of synovial diarthrosis in this regard. Finally, mucocartilage is unique to ammocoetes. Neither hagfish nor gnathostomes exhibit mucocartilage-like tissues in their skeletons (Hall, 2005, 2015). In addition, the osteological correlates of cartilages in stem gnathostomes reveal no evidence of mucocartilage-like skeletal structures (Janvier, 1993, 1996; Miyashita, 2016).

Several assumptions are required for mucocartilage to be an evolutionary precursor of a joint. These are: (***a***) ammocoetes retain primitive conditions among vertebrates; (***b***) mucocartilage was lost independently in hagfish and gnathostomes; and (***c***) mucocartilage served as connective tissues in the stem of gnathostomes rather than as supporting structures (living ammocoetes). The ontogeny of the Devonian stem lamprey *Priscomyzon riniensis* questions these assumptions (Chapter 3, this thesis) as its larval forms lack ammocoete-like traits. From that standpoint, it is more likely (and more parsimonious) to interpret the mucocartilage as developmentally transient tissues. It bridges over the secondarily inserted filter-feeding larval stage to the adult phase by deploying undifferentiated mesenchyme as supporting structures until the true chondrocranium forms during metamorphosis. To support this notion, ammocoete skeletal elements made of mucocartilage cannot be compared anatomically with the highly conserved chondrocrania of other vertebrates, whereas the adult lamprey chondrocranium (made entirely of cellular cartilages) has elements that are homologous across the rest of vertebrates (Holmgren and Stensiö, 1936; Holmgren, 1946; Johnels, 1948; Hardisty, 1982; Miyashita, 2012; Oisi et al., 2013a; Kuratani et al., 2016).

4.2.4 The Intercartilaginous Blood Sinus Hypothesis

Cyclostomes have another structure that is unique to them among vertebrates: the velar sinus (Figs. 4.1d, 4.3c). This pumping venous sinus is sometimes referred to in hagfish as a cardinal heart (Cole, 1926). A velar sinus provides a venous drainage that collects cranial circulation into the anterior cardinal vein (Cori, 1906; Hatta, 1923; Cole, 1926; Daniel, 1934; Miyashita, 2016), which persists into adulthood unlike most other vertebrates (Hyman, 1992). In hagfish, the sinus occupies the large space between the proximal end of the velar cartilage and the hyoid arch (Miyashita, 2016), and the motion of the velum pumps blood into the venous drainage (hence the cardinal ‘heart’) (Strahan, 1958). Although small relative to the hagfish counterpart, a venous sinus develops in ammocoetes between the velum and the hyoid arch to collect blood from the velum and the anterior head (Cori, 1906), and this drainage remains active in metamorphosed lampreys even as the velar-hyoid contact shifts from the dorsolateral to the ventrolateral side of the oral cavity (Marinelli and Strenger, 1954).

The velar sinus is functionally and anatomically similar to synovial diarthrosis (Miyashita, 2016). It sits between the two antagonistic cartilages and mediates their motion. The

sinus is encapsulated by ligament, and blood may be interpreted as functionally equivalent to plasma-derived synovial fluid. Both the velar and hyoid cartilages are derived from neural crest ectomesenchyme (McCauley and Bronner-Fraser, 2003, 2006; Oisi et al., 2013b), although the homology remains unclear between these cartilages in cyclostomes and the jaw cartilages in gnathostomes (Holmgren, 1946; Janvier, 1996; Kuratani and Ota, 2008; Miyashita, 2012; Oisi et al., 2013a; Kuratani et al., 2016).

To enhance this comparison, potential anatomical correlates of the velar sinus are identified in stem gnathostomes (Fig. 4.4). In several osteostracans, the endoskeletal attachment structure sits at the mandibular-hyoid interface, posterior to the prebranchial cavity and anterior to the most anterior branchial cavity (Janvier, 1981, 1985a, 1985b; Miyashita, 2016). In one specimen of the thyestiid osteostracan *Dartmuthia gemmifera* (AMNH 3871.8750), the attachment structure consists of a medial projection from the lateral margin of the cephalic shield, which is subdivided into proximal (lateral) and distal (medial) halves by a suture (Fig. 4.4a; Janvier, 1985b). The dorsal side is convex with a condyle-like ridge, implying a skeletal attachment on that side (Janvier, 1985b). The lateral margin of the shield is drained by the marginal vein, which is considered a homologue of the anterior cardinal vein (Wängsjö, 1952; Stensiö, 1958, 1964, Janvier, 1981, 1985a, 1985b). Internal casts such as MNHN SVD 1001 (*Boreaspis ceratops*) show drainage from the suspected velar attachment site into the marginal vein (Fig. 4.4b) — as expected for a cyclostome-like velar sinus (Janvier, 1985a). Among galeaspids, *Shuyu zhejiangensis* and some polybranchiaspidids have similar processes as described in osteostracans, which is consistent with velar attachment (Fig. 4.4c; Janvier, 1984; Gai et al., 2011). In polybranchiaspidids, the attachment site is associated with two to three depressions — variably interpreted as a muscular attachment site and/or a venous sinus (Janvier, 1984; Miyashita, 2016).

Osteostracans have another set of osteological correlates that bolster the comparison of an intercartilaginous blood sinus with synovial diarthrosis. In pectoral joints, the attachment site for the pectoral cartilage sits within a depression inside the pectoral fenestra, which has a distinct rim that indicates the attachment of connective tissues such as ligament (Fig. 4.1e; Janvier, 1981, 1984, 1985a). Several foramina penetrate this depression to permit passage of the brachial plexus, and brachial arteries and veins (Janvier, 1981, 1985a). Foramina for the brachial arteries are closely associated with the pectoral attachment site within the depression, implying that this site

was irrigated extensively by the subclavian artery (Janvier, 1981, 1985a). The morphology of the pectoral attachment in osteostracans was compared with that in antiarchs, where the condyles of the pectoral joint sits within a deep concavity irrigated and drained by vessels passing through the enormous axillary foramen (as large as a fifth of the area of the pectoral fenestra) (Fig. 4.1f; Janvier, 1995; Johanson, 2002).

On this anatomical basis, an intercartilaginous blood sinus such as the velar sinus may represent an evolutionary precursor to synovial diarthrosis (Miyashita, 2016). In this hypothesis, the primitive jaw joint consisted of a blood sinus encapsulated and bound by ligament between the palatoquadrate and Meckel's cartilage. This proto-joint may have been a co-opted velar sinus following loss of the velum prior to jaw origin (Miyashita, 2016), or independent from a velar sinus at the anatomical level (i.e., not draining into anterior cardinal vein) but co-opted from the velar sinus at the level of gene regulatory and expression profiles. One possible mechanism is that the velar sinus is marked by *Nkx3.2* expression primitively (Miyashita, 2016). Then *Nkx3.2* function may have changed from patterning a blood sinus between cartilages — perhaps via maintaining mural cells and through VEGF/VEGFR expression (Spice, 2015) — to patterning the interzone through regulation of *Sox9/10* and *Gdf5/6*. Alternatively, the evolutionary sequence could have been the reverse: acquisition of *Nkx3.2* expression allowed the blood sinus to be replaced with an interzone of synovial diarthrosis.

As outlined, this Blood Sinus Hypothesis is difficult to test, because it generates multiple conflicting predictions. For example, the lack of *Nkx3.2* expression in the velar sinus would falsify the change of *Nkx3.2* function from patterning a blood sinus to patterning an interzone (Miyashita, 2016), but would be consistent with replacement of a blood sinus with an interzone via acquisition of *Nkx3.2* expression. To falsify this hypothesis with confidence, *both* conditions need to be tested: (***a***) the velar sinus is not homologous with the jaw joint; and (***b***) the jaw joint pathway deploying *Nkx3.2* in gnathostomes is independent from the pathway of gene expressions for the velar sinus in cyclostomes. Otherwise, the hypothesis can be consistent with one of the predictions. Therefore, it is challenging to differentially test this hypothesis along with others dealing with the jaw joint origins. This difficulty does not reflect a deficit in the design of the hypothesis, but rather is attributed to the lack of comparative information to constrain possible states of the velar sinus in stem gnathostomes. As discussed later in this chapter, expression profiles reported in the literature conflict with each other in lampreys. Comparison with

osteological correlates of stem gnathostomes only provides indirect inferences for the presence of a velum in stem gnathostomes, and it offers little support for the presence of a velar sinus in galeaspids and osteostracans beyond depressions at the hyomandibular position in the former and drainage into the marginal vein in the latter. Given currently available information, this hypothesis cannot be tested conclusively and differentially compared to other hypotheses. Preliminary results from this chapter should help constrain the possible scenarios so that the Blood Sinus Hypothesis can be tested rigorously.

4.2.5 The Scheme of Hypothesis Testing

The scheme of hypothesis testing involves three potential precursor tissues/organs (muscular scaffold, mucocartilage, and intercartilaginous blood sinus) for a synovial diarthrosis — more specifically for the jaw joint — and two potential scenarios to transform the structure into a jaw joint: (***a***) co-option of a structure ancestrally mediated by *Nkx3.2* expression; or (***b***) co-option of *Nkx3.2* expression replacing ancestral structure. Because this scheme generates six different combinations of predictions (Table 4.1), and because these hypotheses are not fully mutually exclusive, no one hypothesis is likely to receive unambiguous support under either of the two evolutionary scenarios. Nevertheless, the three hypotheses and two evolutionary scenarios may be differentially tested in the following order.

4.2.5a Lampreys

To discriminate among the three candidate precursors first (Table 4.1), lampreys are used to describe expression profiles of *Nkx3.2* and its target genes in the jaw-joint pathway. The absence of *Nkx3.2* expression in a candidate tissue alone does not rule out that hypothesis, as the focal expression of *Nkx3.2* in the gnathostome jaw joint may be a result of co-option after the split between cyclostomes and gnathostomes. However, the absence of *Nkx3.2* and other joint marker genes (encoding growth factors, matrix proteins, lubricants) in the candidate tissue in lampreys would constitute a strong inference that contradicts the hypothesis. Next, *Nkx3.2* expression is compared with *Barx* expression in lampreys. In gnathostomes, the joint marker *Nkx3.2* and the joint repressor *Barx* have non-overlapping expression domains, the former expressed at midheight of, and the latter expressed in the ventral region of, the mandibular arch (Nichols et al., 2013). Non-overlapping expression profiles would imply that gnathostome-like regulatory

relationships exist for *Nkx3.2* and *Barx* in lampreys. Finally, *Nkx3.2* and *Barx* are knocked out in lampreys using CRISPR/Cas9. Phenotypes are analyzed using expression patterns of the suspected *Nkx3.2* target genes (homologues to components of the jaw joint pathway in gnathostomes) and morphology of the larval skeletons. This will test whether or not: (***a***) *Nkx3.2* has a patterning role in any proposed precursors to synovial diarthrosis in lampreys, just as in the jaw joint in gnathostomes; and (***b***) *Nkx3.2* had similar functions in lampreys as in the jaw-joint pathway of gnathostomes.

4.2.5b Zebrafish

To complement the information from lampreys, zebrafish are used as a gnathostome model. Comparison between wildtype and *nkx3.2* mutant zebrafish will be used to: (***a***) determine functions of *nkx3.2* in jaw joint development; (***b***) characterize expression profiles of the *nkx3.2* target genes (for comparison with lampreys); and (***c***) test regulatory relationships between *nkx3.2* and potential target genes. Furthermore, phenotypes of *nkx3.2* knockout zebrafish may parallel those of *Nkx3.2* knockout lampreys.

The role of *nkx3.2* in jaw joint development is inferred mainly on the basis of morpholino knockdowns and mutant phenotypes of other genes such as *barx1* (Miller et al., 2000, 2003; Nichols et al., 2013), but no analysis exists on knockout phenotypes of *nkx3.2* in zebrafish. *Nkx3.2* knockout phenotypes in mice include malleal/gonial fusion (Tucker et al., 2004), but the malleus and incus represent highly derived states of pharyngeal cartilages and thus are difficult to compare. Likewise, the regulatory relationships between *nkx3.2* and its predicted target genes — and functions of these target genes in jaw joint development — remain to be tested. This is possible through comparison of wildtype and *nkx3.2* mutants in zebrafish. Comparison of *nkx3.2* knockout phenotypes between lampreys and zebrafish could provide additional evidence to test the hypotheses. If both knockouts developed similar phenotypes in any of the candidate precursor tissues in lampreys and in their counterparts in zebrafish, it would suggest that evolutionarily ancient functions of *Nkx3.2* are conserved in both lineages.

4.3 METHODS, SUMMARY

To characterize gene expression profiles in the sea lamprey *Petromyzon marinus*, homologues were identified for genes that fall in the following categories: (***a***) transcription factors related to jaw joint development in gnathostomes (*Nkx3.2*, *Barx1*, *Runx2*); (***b***) transcription and growth factors that are expressed in the synovial diarthrosis and are potential target genes of *Nkx3.2* (*Trps1*, *Runx2*, *Scx*, *Irx5/7*, *Gdf6*); and (***c***) matrix protein, lubricant, and receptor genes associated with synovial diarthroses (*Col2a1*, *Prg4*, *Vegfr*).

CRISPR target sites (5'-[20N]…NGG-3') were determined for *Nkx3.2* and *BarxA* in lampreys and for *nkx3.2* in zebrafish. In lampreys, two different strategies were used. The target sites were initially identified close to the assumed 5' end of the partial coding sequences (Fig. 4.5a), but these initial designs were revised in light of updated sequence information from the Dovetail version of the *P. marinus* Genome Assembly (J. Smith and colleagues, unpublished resources) and the Trinitiy transcriptomic database (S.A. Green and colleagues, unpublished resources). The revised scheme to identify CRISPR target sites focused on homeodomains (Fig. 4.5a) and follows the accepted guideline: (***a***) 50-80% GC content; and (***b***) no off-target matches to the current genome assembly showing more than 80% similarity, or with fewer than three mismatches in the ten bases proximal to the PAM sequence (Square et al., 2015a). Similarly, mutants were chosen in zebrafish for a frame-shift deletion in a target site designed to cleave *nkx3.2* homeodomain (Fig. 4.5b). For lampreys, injected individuals cannot complete a life cycle in laboratory settings. So most, if not all, mutants are considered to be partial knockouts.

Mature males and females of *Petromyzon marinus* were obtained from Hammond Bay Biological Station and artificially spawned following published protocols (Nikitina et al., 2009). Staging of the embryos follows Tahara (1988). Embryos were fixed in MEMFA overnight at -20 ˚C and transferred into 100% EtOH for storage at -20 ˚C. Cas9 and sgRNAs were injected between 2.0 hours post fertilization (hpf) and first cleavage. Sampled embryos were photographed and processed for genotyping by extracting genomic DNA and amplifying the regions containing target sites for sequencing. Alcian blue staining of cartilages followed available protocols (Martin et al., 2009; Jandzik et al., 2014). Histological sections were made either in paraffin blocks or with a cryostat. *In situ* hybridization followed the published protocol (Nikitina et al., 2009) or the protocol developed for hemichordates by Christopher J. Lowe

(Hopkins Marine Station, Stanford University) and Stephen A. Green (California Institute of Technology) (Suppl. 4.1). Hybridization lasted from overnight to four days at 70 ˚C, with 10-50 ng/ml probe concentration. Embryos were postfixed and stored in 100% MeOH at -20 ˚C.

For zebrafish, fertilized eggs were collected from crossings of wildtype parents (AB/Wik, AB, and UA3140 ubi:switch/AB+RH). The preserved tissues, embryos, larvae, and adults were all fixed in 4% PFA, and stored in 100% EtOH or MeOH at -20 ˚C except for adults in whole mount (preserved in 70% EtOH at 4˚C). Cas9 and sgRNAs for *nkx3.2* and GFP GA5' were injected into cytoplasm between fertilization and first cleavage. The larvae were screened for reduced GFP expression with dsRed expression in the heart. Using the screened larvae as the P_0 population, *nkx3.2* mutants were identified. I selected a female with a 20 bp deletion to the homeodomain-coding region of *nkx3.2* (UA5011) (Fig. 4.5b). The UA5011 *nkx3.2* mutant was outcrossed to the *sox10*:GFP transgenic line for a F_1 population. The F_1 heterozygotes were incrossed for F_2 progenies. Phenotypes were identified using *sox10*:GFP-positive chondrocytes, alcian blue staining of cartilages, and immunostaining collagen II for confocal imaging. The homozygous UA5011 larvae were reared with a strictly small-grained diet to the adult stage.

Orthology and paralogy potentially confound identification of homologous genes. *Nkx3.2* does not appear to have a paralogue in the lamprey genome assembly. Two scaffolds exist for this gene in the genome of *Petromyzon marinus*, but they likely represent an assembly artifact (**4.8.1b *Nkx3.2***). *Barx* has at least two paralogues (*BarxA* and *BarxB*) and potentially more. I chose BarxA, which has the greater similarity to the gnathostome *Barx1* gene between the two (**4.8.1b *BarxA***). In zebrafish, there is only one annotated *nkx3.2* gene (Genbank: BC159241.1). A combination of several BLAST search did not recover any unambiguous paralogues. A phylogenetic analysis using Clustal Omega grouped coding sequences with marginal similarity (1×10^{-20} < E value < 8×10^{-32}) with other *nkx* genes from non-zebrafish vertebrates (data not shown). Therefore, *nkx3.2* is not redundant in zebrafish.

See **4.8 Supplementary Information** for full details of protocols, sequence information, and description of the ongoing experiments.

4.4 RESULTS

4.4.1 *In Situ* Hybridization: Lampreys

4.4.1a Nkx3.2

Nkx3.2 was expressed broadly in neural crest ectomesenchyme of the pharyngeal arches from Tahara's stages T26.5 to T28 (Fig. 4.6). Horizontal sections indicated that the transcripts were present in the ectomesenchyme on both lateral and medial sides of the pharyngeal arches (Fig. 4.6d). The expression domain extended anteriorly into the postoptic stream of the trigeminal ectomesenchyme (Kuratani et al., 2001; Kuratani, 2012). No conspicuous expression was detected in somites. At T30, the specific pharyngeal expression appeared to be absent, but the focal expression domain was present on the ventral side of the otic capsule (Fig. 4.6e). The probes may have been trapped broadly elsewhere, especially in the pericardial region. The otic capsule is generally prone to probe trapping (T.M., personal observation). However, *Nkx3.2* expression in the otic capsule was restricted to the lower portion of the structure. Therefore, this expression domain was not likely an artifact.

Pharyngeal ectomesenchyme expression from T26.5 to T28 appeared to correlate with the future mucocartilage (Fig. 4.6f), although the expression was no weaker in the areas that would develop cellular cartilages (branchial and hypobranchial bars). The infraotic expression in T30 corresponded in position and timing with the velar sinus, which was forming at this stage (T.M., personal observation). However, *Nkx3.2* expression did not coincide with muscular scaffolds in position and timing.

4.4.1b BarxA

BarxA was expressed in the lower lip at T26 at midheight of the mandibular arch, and was not focally restricted ventrally or dorsally (Fig. 4.7a). The transcripts appeared to be absent in later developmental stages (Fig. 4.7b, c), with extensive probe trapping in the pharyngeal pouches. However, some sub-epithelial expression may have been present at the periphery of the pouch epithelium. These expression domains did not correlate spatially with muscular scaffolds, mucocartilage, or velar sinus. Notably, however, the *BarxA* transcripts were detected where the expression of *Nkx3.2* was either absent (sub-epithelium in pharyngeal pouches) or weak (lower lip).

4.4.1c Gdf5/6/7

Gdf5/6/7 was expressed in the ectomesenchyme in the dorsal and ventral domains of the hyoid and branchial arches from T26 to T28 (Fig. 4.7d, e). In the mandibular arch, the transcripts were present in the dorsal domain but absent in the ventral domain (lower lip). In the upper lip (postoptic ectomesenchyme), *Gdf5/6/7* was expressed along the ventrolateral edge of the forebrain and in the oronasohypophyseal ectoderm anterodorsal to the mouth. An expression domain also appeared in the ventral part of the otic capsule and ectomesenchyme immediately below the capsule. As the domain did not seem to include the entire otic capsule, this signal was likely not an artifact. In T30, most of these expression domains could not be detected, but the periotic expression domain persisted (Fig. 4.7f).

Like in *Nkx3.2*, no mesodermal expression was detected for *Gdf5/6/7*. The expression domains correlated with the distribution of mucocartilage (dorsal domains of upper lip, mandibular arch, and hyoid arch; infrapharyngeal domain) and the position of the velar sinus (dorsal hyoid, infraotic domains). The mucocartilage differentiated by T30, and the velar sinus was forming at that stage. So temporal expression patterns also correlated with these structures.

4.4.1d Col2a1

Col2a1a and *Col2a1b* appeared to be expressed broadly, as expected for collagen type II (Fig. 4.8a-d). However, the true expression domains were difficult to delineate because: (***a***) extensive probe trapping likely occurred, and (***b***) *in situ* hybridization developed significant background. The riboprobes were longer than 1 kbp for both genes, and possibly had structures. This was especially the case for *Col2a1a* — the pharyngeal expression was likely an artifact due to trapping of the probe (Fig. 4.8a). The epidermis and somites were also stained strongly, but it was not clear to what extent this represented artifacts. Collagen type II is a major component of extracellular matrix in many tissues including cartilages, and its expression in these tissues is within expectations. Tentatively, however, the expression of *Col2a1a* appeared to be stronger in muscular/mesodermal tissues than in other types of tissues.

On the other hand, *Col2a1b* did not appear to suffer from pharyngeal probe trapping (Fig. 4.8b, c). The transcripts were more abundant in the ectomesenchyme in the dorsal and ventral domains of the oropharyngeal region, the periphery of trigeminal and facial ganglia, and weakly

in the somites and dermis from T26.5 to T28. Expression at T30 was weaker (Fig. 4.8d), and the transcripts seemed to be present in both the dorsal and ventral pharyngeal domains.

Taken at face value, *Col2a1a* expression was more specific to mesodermally derived tissues than *Col2a1b*, which was more strongly expressed in the ectomesenchyme. The latter was consistent with the distribution of mucocartilage and velar sinus.

4.4.1e Prg4

The perceived colour distribution for *Prg4* in the pharyngeal pouches and pericardial region likely represented probe trapping from T26.5 to T28 (Fig. 4.8e, f). At T30, however, a focal expression domain did appear at the infraotic position (Fig. 4.8g) — a future site of the velar sinus. No expression was detected in the ectomesenchyme of the pharyngeal arches and upper lip.

4.4.2 CRISPR/Cas9: Lampreys

4.4.2a Nkx3.2

Two different sets of sgRNAs were injected in various combinations (as described in Supplementary Information: **4.8.2 CRISPR/Cas9: Methods**). In 2016, three sgRNAs were injected in combinations and individually (2016_Gr1, 2016_Gr2, 2016_Gr4) but the revised gene model revealed that the target sites were (***a***) close to exon boundaries and (***b***) subject to splice variations. With a 3 kbp long intron between exons 1 and 2, it was difficult to genotype injected lampreys from the 2016 spawning season. In 2017, new target sites were identified (2017_Gr1, 2017_Hom1, 2017_Hom14). At the time of writing, data on these individuals were available up to Tahara stage T26.5, approximately two weeks prior to full differentiation of the larval skeleton (T30). Therefore, no information is available on skeletal phenotypes from the 2017 spawning season.

Alcian blue staining of specimens at T30 revealed variations in skeletal morphology, some of which may represent phenotypes due to *Nkx3.2* knockout (Fig. 4.9). Approximately 50% of CRISPR *Nkx3.2* sgRNA-injected specimens had a posteriorly hooked lateral mouth plate (red outline; Fig. 4.9c), whereas only one of ten wildtype specimens showed a similar phenotype (Table 4.2). However, the posteriorly hooked lateral mouth plate occurred in similar proportions to *Tyr* sgRNA-injected control specimens and *BarxA* sgRNA-injected specimens (Table 4.2). Therefore, this skeletal trait is likely attributed to injection phenotypes. The *Nkx3.2* sgRNA-

injected specimens also showed an elongate velar cartilage relative to wildtype (11.7%) (yellow outline; Fig. 4.9c) and dorsally shifted first branchial opening (33.3%) (orange: Fig. 4.9c; Table 4.2). These potential phenotypes appeared to be absent in wildtype, *Tyr* sgRNA-injected control, and *BarxA* sgRNA-injected specimens. However, these individuals remain to be genotyped so these potential phenotypes cannot be attributed specifically to *Nkx3.2* knockouts.

In the 2017 spawning season, different *Nkx3.2* sgRNAs were injected (Fig. 4.10). Of 21 randomly sampled at T26.5 from the first injection episode, three were indistinguishable morphologically from wildtype, and the rest had malformed heads and/or trunks. Of these abnormal specimens, 17 had malformations in the pharyngeal region (anteroposteriorly shorter pharyngeal series = 14; loss of pharyngeal arches = 3), and 18 had trunk malformations (twisted axis = 10; posteriorly truncated growth = 14). Genotypically, at least one of the three wildtype-like specimens carried a frame shift mutation (Fig. 4.10f). Among wildtypes, abnormal specimens had similar trunk malformations at frequencies between 0.5-8% per a breeding episode, depending on the healths of the parents (Fig. 4.10g). The mismatches between genotypes and phenotypes suggest: (***a***) the injected specimens represent mosaic genotypes; and (***b***) some phenotypic defects are difficult to distinguish from batch effects, which may be due to (***a***) mutations that exist in the natural populations and/or (***b***) responses to injection.

4.4.2b BarxA

Two different sets of sgRNAs were designed (described in Supplementary Information: **4.8.2 CRISPR/Cas9: Methods**). Only the set designed for the 2016 spawning season was injected (2016_Gr1, 2016_Gr2, 2016_Gr3). The availabilities of embryos during 2017 were insufficient to facilitate a CRISPR knockout experiment beyond *Nkx3.2*. The specimens injected with *BarxA* sgRNA in 2016 revealed no marked differences in skeletal morphology, except for the posteriorly hooked lateral mouth plate (Table 4.1). This skeletal trait was likely an injection phenotype.

4.4.3 CRISPR/Cas9: Zebrafish

F_2 progenies of incrossed *nkx3.2*$^{UA5011/+}$/*sox10*:GFP (Fig. 4.11) roughly followed Mendelian ratios both in genotypes (*nkx3.2*$^{+/+}$: N = 2; *nkx3.2*$^{UA5011/+}$: N = 5; *nkx3.2*$^{UA5011/UA5011}$: N = 3) and in phenotypes (normal = 34 ; abnormal = 11). RFLP analysis on subsequent progenies was consistent with these ratios, and the phenotypic screening at 4 dpf was overall accurate for

selection of homozygous mutants (85-100 % depending on breeding episodes). At 4 dpf, the chondrocytes marked by *sox10*:GFP reporter expression form a palatoquadrate and Meckel's cartilage in wildtype specimens and heterozygous mutants (Fig. 4.11c, e). The palatoquadrate and Meckel's cartilage were set apart by an approximately one-cell thick space, surrounded by collagen-rich extracellular matrix — this is the nascent jaw joint (Fig. 4.11c-e). In UA5011 homozygotes, the palatoquadrate and Meckel's cartilage were fused into a single cartilaginous structure with two anterior prongs (the palatine process of the palatoquadrate and the mandibular ramus of Meckel's cartilage) (Fig. 4.11c-e). The UA5011 homozygotes were, on average, shorter anteroposteriorly than wildtypes (Fig. 4.11a, b). Fusion of the jaw cartilages was consistent with — and qualitatively indistinguishable from — the *nkx3.2* morphants (Figs. 5d, f, h, 11e; Miller et al., 2003).

At the adult stage, the head and trunk morphology of UA 5011 homozygotes was dramatically different from that of the wildtype (Fig. 4.12). The UA5011 homozygotes (Fig. 4.12c, d) were anteroposteriorly shorter and dorsoventrally taller in overall body proportions than wildtypes (Fig. 4.12a, b). The lower jaw was depressed ventrally and fixed in position, leaving the mouth permanently open at a gape angle of 140-150°. The snout was reduced to a periocular position, with external nares positioned posteriorly on the dorsal surface between the eyes. The operculum was relatively large. It occupied 70-73% of the head height at that position and measured to 185-189% of the maximum eye diameter, compared to 57-60% and 145-148% in wildtypes, respectively. In lateral view, a small projection from the oral cavity protruded beyond the anterior margin of the lower jaw. This projection represents the anterior end of the basihyal. The element extended as anteriorly as the jaw joint in wildtypes (Schilling and Kimmel, 1997; Kimmel et al., 2001). UA5011 heterozygotes were indistinguishable morphologically from wildtypes.

4.5 DISCUSSION

4.5.1 Tests of the Hypotheses

The results presented here are insufficient to conclusively test all previous hypotheses about the origin of the jaw joint in gnathostomes (Cerny et al., 2010; Cattell et al., 2011; Uyeno and Clark, 2015; Miyashita, 2016). However, the preliminary results do provide tests of many of the

predictions arising from the hypotheses. The gene-expression data from lampreys can test whether or not they are compatible with each of the hypotheses under the first scenario: a proposed precursor tissue became co-opted to become a synovial diarthrosis at a jaw joint. However, the expression data alone cannot rule out these hypotheses under the second scenario: a proposed precursor tissue was replaced by a synovial diarthrosis through co-option of *Nkx3.2*. This is because functional analyses of *Nkx3.2* and *BarxA* using CRISPR knockout lampreys are incomplete.

Despite these caveats, the expression data of *Nkx3.2* in *Petromyzon marinus* (Fig. 4.6) is compatible with the hypothesis (Cerny et al., 2010) that the jaw joint evolved by acquisition of the focal expression domain of *Nkx3.2* at the midheight of the mandibular arch. The expression data of *Nkx3.2* in this chapter differ from those presented in Cerny et al. (2010), which showed the absence of *Nkx3.2* expression in ectomesenchyme. The difference is likely due to multiple splice variants (see **4.5.2 Discrepancies with Previously Reported Gene-Expression Profiles**). Nevertheless, *Nkx3.2* expression in the ectomesenchyme reported in this chapter is not specific or restricted to any of the proposed evolutionary precursors of the jaw joint. Therefore, these data suggest that restriction into — not *de novo* acquisition of (Cerny et al., 2010) — the focal expression domain was the likely mechanism. This is still compatible with either of the scenarios of co-option, either at the level of structures or genetic programs.

4.5.1a Expression of Nkx3.2 *in lampreys*

Ectomesenchyme expression of *Nkx3.2* in *P. marinus* (Fig. 4.6) is compatible with the predictions of the Mucocartilage and Intercartilaginous Blood Sinus hypotheses and incompatible with the Muscular Scaffold Hypothesis under the scenario of co-option at the level of structures (Table 4.1, column ***a***). The expression domains overlap with future domains of both mucocartilage and velar sinus, but are not restricted to either. *Nkx3.2* transcripts cannot be detected in any muscular tissues with the current riboprobe. *Nkx3.2* transcripts are detected in sclerotomes with the unpublished riboprobe (Cerny et al. 2010; D. Meulemans Medeiros, pers. commn., 2017; data not shown). This is likely due to multiple splice forms. Even the mesodermally expressed *Nkx3.2* transcripts are not present in any of the complex cranial muscle complexes. So, the Muscular Scaffold Hypothesis is rejected under the scenario of structural co-option.

On the other hand, if the jaw joint in crown gnathostomes represents replacement of an evolutionary precursor by acquisition (or restriction) of *Nkx3.2*, then the ectomesenchyme expression of *Nkx3.2* in lampreys does not meet the predictions of non-expression for the Mucocartilage and Intercartilaginous Blood Sinus hypotheses. However, the ectomesenchymal expression of *Nkx3.2* is not sufficiently specific to either tissues to fully reject these predictions. Ultimately, these predictions may be rejected by a functional analysis of *Nkx3.2* in lampreys.

4.5.1b Expression of potential Nkx3.2 *targets in lampreys*

Ectomesenchyme expression of *Gdf5/6/7* (Fig. 4.7d-f) is compatible with the Mucocartilage and Intercartilaginous Blood Sinus hypotheses, and incompatible with the Muscular Scaffold Hypothesis (Table 4.1). The expression domains correspond roughly with those of *Nkx3.2*. As in that gene, the expression is not specific to mucocartilage or velar sinus. Therefore, those two hypotheses cannot be distinguished from each other in the expression of *Gdf5/6/7*.

The infraotic expression of *Prg4* (Fig. 4.8e-g) is compatible with the Intercartilaginous Blood Sinus Hypothesis, and incompatible with the Mucocartilage and Muscular Scaffold hypotheses (Table 4.1). This expression is specific to the position of the velar sinus at stage T30, indicating that this structure shares expression of this proteroglycan gene with the gnathostome jaw joint (Askary et al., 2016).

The expression data for *Col2a1a* and *Col2a1b* (Fig. 4.8a-d) are not specific enough to test any of the hypotheses. These two genes should be re-characterized using new riboprobes and histological sections to provide more precise insights.

4.5.1c Expression of BarxA *in lampreys*

Expression of *BarxA* does not overlap spatially with strong expression domains of *Nkx3.2* (Fig. 4.7a). This is compatible with the scenario of co-option at the levels of structure (Table 4.1). The non-overlap implies that functions of *Nkx3.2* and *BarxA* may be antagonistic, as in crown gnathostomes where the former induces a jaw joint and the latter represses it in their respective expression domains in the mandibular arch (Miller et al., 2003; Nichols et al., 2013). To test such interactions conclusively, it will require both *Nkx3.2*- and *BarxA*-knockout lampreys in which the expression domain of the other gene is affected.

4.5.1d CRISPR knockouts in lampreys

Specimens injected with *Nkx3.2* sgRNA in the 2016 spawning season (Fig. 4.9) show potential phenotypes. Taken at face value, these candidates are compatible with the Mucocartilage and Intercartilaginous Blood Sinus hypotheses, and incompatible with the Muscular Scaffold Hypothesis, under the scenario of co-option at the level of structures (Table 4.1). Among these potential phenotypes, however, the posteriorly hooked lateral mouth plate may represent an injection-related phenotypic effect because a similar phenotype is observed in positive controls to a lesser extent (Fig. 4.9b). The elongate velar cartilages are consistent with hypertrophy of chondrocytes, whose inhibition is the likely ancestral function of *Nkx3.2*. However, the frequencies are low, and the elongation is difficult to measure quantitatively for flexibility and deep position of the velar cartilages.

The specimens injected with *Nkx3.2* sgRNA in the 2017 spawning season (Fig. 4.10) show strong evidence of mutation genotypes and of unambiguous phenotypes (defects in pharyngeal arches and axial elongation) at stage T26.5. The pharyngeal defects probably represent a failure to maintain proliferation of the neural-crest ectomesenchyme, whereas the axial defects may be related to somitogenesis and sclerotomal differentiation. Care must be taken to interpret the axial defects, however, because an axial twist — though somewhat different in form — was observed in low frequencies (0.5-8%) in wildtypes (Fig. 4.10g). Information from later developmental stages is not available yet. The specimens injected with *BarxA* sgRNAs in the 2016 spawning season did not show marked skeletal phenotypes. Gene expression data have not been generated for these potential knockouts, either. Finally, more robust controls are required to rule out injection phenotype and other artifacts as an explanation for the phenotypes observed. Therefore, the hypotheses presented here cannot be tested further using these materials.

4.5.1e Phylogenetic distributions of potential evolutionary precursors

For any of the three hypotheses to be correct, the proposed evolutionary precursors for synovial diarthrosis of the jaw joint must be present along the stem of gnathostomes. In this sense, character transitions predicted by the Mucocartilage Hypothesis are non-parsimonious because mucocartilage is a tissue unique to the ammocoete stage of lampreys. For that hypothesis to be correct, mucocartilage must have been lost at least twice independently in hagfish and crown gnathostomes. The most parsimonious scenario — also compatible with the lack of an

ammocoete-like stage or mucocartilage-like tissues in *Priscomyzon* (Chapter 3) — is that mucocartilage is a specialization that evolved within the lamprey lineage to provide skeletal support before the cartilaginous skeleton differentiates during metamorphosis. Analogous cases are known during metamorphosis in other vertebrate lineages, the most dramatic being the preoral skeletons of anuran larvae (Square et al., 2015b). Furthermore, the overall lack of differentiation from mucocartilage to cartilage across the metamorphosis of lampreys (De Beer, 1937; Johnels, 1948) suggests that they represent products of two distinct evolutionary lines of cell types. Nevertheless, the presence of mucocartilage in the stem of gnathostomes cannot be ruled out by anatomical evidence.

The Intercartilaginous Blood Sinus Hypothesis is compatible with possible correlates of a velar sinus in galeaspids and osteostracans (Fig. 4.4) and with those of a blood sinus at the pectoral joint in osteostracans and antiarchs (Fig. 4.1e, f; see **4.2 Hypotheses**). However, further work is required to determine with confidence whether or not any of these structures represents an intercartilaginous blood sinus.

Anatomical evidence is lacking to infer a muscular scaffold in the stem of gnathostomes, which may be compared to the lingual apparatus of cyclostomes and the jaws of polychaetes (Uyeno and Clark, 2015). One possible line of inference is the character polarity for primitive jaws. In primitive jawed vertebrates, the palatoquadrate did not contact the neurocranium; instead, the jaw skeleton was likely suspended in the scaffold of muscles and connective tissues (Janvier, 1996). However, this character polarity offers no clue about the specific morphology at the joint.

4.5.1f Best fit of evidence

Taken together, the preliminary results reported in this chapter are most compatible with the Intercartilaginous Blood Sinus Hypothesis (*Prg4* expression in lampreys; inferred phylogenetic distributions of velar sinus and mucocartilage; Table 4.1). Most predictions for the Muscular Scaffold Hypothesis are clearly rejected on the basis of comparative expression data. The Mucocartilage Hypothesis is difficult to evaluate. It is compatible with expression data (with the exception of *Prg4*) but supported by no anatomical evidence of mucocartilage outside the ammocoetes of living lampreys. Still, other predictions for this hypothesis have not been rejected unambiguously (Table 4.1). Therefore, the Intercartilaginous Blood Sinus Hypothesis may be

favoured tentatively by the currently available data, whereas the Mucocartilage Hypothesis has not been ruled out.

The expression data for *Nkx3.2* and *BarxA* from lampreys are more compatible with the co-option at the level of structure than at the level of genetic programs. However, this is not conclusively tested by functional evidence. Similarly, evidence from zebrafish is forthcoming. These ongoing or planned lines of research open the prospect of providing further, differential test of the hypotheses.

4.5.1g Consideration of independent evolutionary changes in lampreys

The expression data in lampreys cannot be assumed to represent a primitive state. The possibilities of independent evolution have been considered, but cannot be incorporated meaningfully in the test of hypotheses. This is the case for mucocartilage, which is thus far unique to living ammocoetes. Mucocartilage in other lineages cannot be ruled out on the basis of the lack of evidence. The velar sinus, on the other hand, exists in hagfish (Miyashita, 2016) so the structure is at least a cyclostome synapomorphy. Cyclostomes have various muscular scaffolds within which the cartilages are suspended (Miyashita, 2012; Ziermann et al., 2014). However, such an anatomy-based comparison does not apply to interpretation of gene-expression patterns. Unfortunately, comparative data are generally lacking in hagfish, and invertebrate chordate lineages (cephalochordates and tunicates) do not have relevant anatomical structures to compare with lampreys (Miyashita, 2012, 2016). Therefore, a parsimony-based test is unavailable to determine character polarity for the data from lampreys.

4.5.1h Potential alternatives

Of course, none of the hypotheses may correctly describe the evolutionary origin of the jaw joint. The evolution of synovial diarthrosis may not have required any joint-like precursor tissue as an initial stage. For example, the earliest endoskeletal joint in vertebrates may have been a zone in which immature chondroblasts/chondrocytes were maintained. It is difficult to explore all such potential alternatives and test them exhaustively. A confounding factor is that evolutionary transitions of phenotypes via a co-option event remain poorly understood. Fitted against phylogeny and fossil record, any scenarios of co-option to explain origins of novel traits appear to suggest a saltatory change, regardless of whether or not intermediate forms are required for a

functionally informed narrative of adaptation. Coupled with the fact that outgroup comparison does not necessarily provide information on ancestral states of the characters (Chapters 1-3), a hypothesis can only be rejected by testing its predictions, and cannot be singly supported for its best fit to currently available evidence.

As for the maintenance of immature chondroblasts/chondrocytes at a joint site, this recapitulation hypothesis cannot be meaningfully tested without information on the ancestral function of *Nkx3.2*. That is, whether *Nkx3.2*: (***a***) suppressed maturation of chondrocytes where skeletal tissues are patterned; or (***b***) had another function in any other pathways. Only then can it be compared with other hypotheses. Another difficulty with this recapitulation hypothesis is that information from the vertebrate fossil record is unlikely to test its predictions. For example, one prediction would be that an immediate outgroup of jawed stem gnathostomes had a single cartilaginous structure in the mandibular arch, which later split into a palatoquadrate and Meckel's cartilage in the first jawed vertebrate. No such form is known to date. Therefore, such *ad hoc* hypotheses may be compatible with currently available evidence, but are not falsifiable in principle.

4.5.2 Discrepancies with Previously Reported Gene-Expression Profiles

Expression patterns of *Nkx3.2*, *BarxA*, *Gdf5/6/7*, and *Col2a1* described in this chapter markedly differ from those reported previously in *Petromyzon marinus* and *Lethenteron camchatsticum* (Ohtani et al., 2008; Cerny et al., 2010; Kuraku et al., 2010; Cattell et al., 2011). Potential explanations are variations at taxonomic, population, or individual levels, experimental artifacts, and multiple splice forms. Among these genes, *Col2a1* expression data cannot be meaningfully compared, because the terminology for the two paralogues has not been consistent in the literature, and because expression data tend to be noisy (Fig. 4.8a-d). For *Nkx3.2*, the ectomesenchyme expression presented in this chapter contradicts the absence of ectomesenchymal expression in *Petromyzon marinus* at equivalent developmental stages (Cerny et al., 2010), but is consistent with that in *Lethenteron camchatsticum* at stage T26 (Kuraku et al., 2010). BLAST search in the Dovetail assembly of the *P. marinus* genome (see Supplementary Information: **4.8.1 Bioinformatics: Methods**) indicates that discrepancies in the reported expression domains are consistent with sequence information, where the coding sequences used in this chapter and Kuraku et al. (2010) and that used by Cerny et al. (2010) likely represent two

different splice forms close to the 3' end of Exon 1. This may also be the case for *BarxA* and *Gdf5/6/7*, although the possibility of potential paralogues has not been ruled out. In all of these genes except for *Col2a1*, expression domains are clearly delineated and reasonably specific to individual structures. The upper lip ectomesenchyme is not particularly prone to probe trapping (Stephen A. Green, pers. commn.). The otic capsules and pharyngeal epithelia are prone to probe trapping, but the infraotic expression of *Nkx3.2*, *Gdf5/6/7*, and *Prg4* appear specific enough to rule out simple trapping of riboprobes.

4.5.3 Implications of *nkx3.2* Mutant Zebrafish

The UA5011 homozygotes (*nkx3.2*$^{UA5011/UA5011}$) developed dramatic phenotypes as adults (Fig. 4.12). Intriguingly, the suite of characteristics (depressed lower lip; reduced snout; interoptic position of nasal opening; enlarged branchial region; dorsoventrally tall body profile; and potentially anteriorly extended basihyal) resemble jawless stem gnathostomes in surprising detail — particularly birkeniid anaspids (Fig. 4.12e, f; Kiaer, 1924; Janvier, 1996; Blom et al., 2001; Blom, 2008, 2012). The morphology of the basihyal in birkeniids is unknown, and the branchial series opened externally in a series of pores instead of the operculum. Nevertheless, the remaining phenotypes in the UA5011 homozygotes have their counterparts in the dermal skeleton of birkeniids. These correspondences do not necessarily mean that UA5011 homozygotes represent complete phenocopies of the stem gnathostome conditions. This is because *nkx3.2* is a highly conserved, ancient transcription factor shared between lampreys and gnathostomes. The gene likely existed in each of the jawless stem gnathostome lineages.

However, it is interesting that: (***a***) the UA5011 homozygotes provide partial phenocopies for the lack of functional *nkx3.2* expression in the mandibular arch, which may have been a stem condition for gnathostomes; (***b***) the depressed lower lip implies that *nkx3.2* has a patterning role in the jaw skeleton beyond specifying a jaw joint, potentially through functions of downstream genes; and (***c***) phenotypes affected by the loss of functional *nkx3.2* expression distribute beyond the mandibular arch (expression domain of *nkx3.2*), which hints at extensive phenotypic plasticity that likely modified the wildtype skeletal morphology. The data at hand are insufficient to address these implications.

Nonetheless, enhanced comparison and characterization of implied phenotypic plasticity may provide a living model in the UA5011 homozygotes to understand poorly understood

biological aspects of the gnathostome stem (e.g., growth and patterning of the skull and feeding and ventilation mechanics). For example, mutant craniofacial phenotypes that appear in the adult stage of UA5011 are linked to feeding and ventilation (depressed lower lip; enlarged operculum; anteriorly extended basihyal). These morphological conditions were not observed in the larval stage following *nkx3.2* expression (Fig. 4.11), and the latter two phenotypes do not occur near *nkx3.2* expression domains. Thus, these traits are likely — at least in part — to represent phenotypic plasticity. To feed without a functional jaw joint, UA5011 homozygous adults have been observed in the aquarium to: (***a***) ram-feed and (***b***) pump vigorously through the operculum (T.M., personal observation). These behaviours, coupled with muscular activities in the mandibular-hyoid domains in the absence of a joint, may have contributed to the dramatic craniofacial phenotypes. The observation that these phenotypes parallel jawless stem gnathostomes implies potentially similar feeding and ventilation mechanics in the latter.

Notably, the UA5011 homozygotes add another case study in which morphant and mutant phenotypes are compatible with one another. Numerous cases of incompatibilities have generated a considerable debate in zebrafish about the efficacies of morpholino and the mechanisms of gene regulation at different stages of transcription and translation (Bill et al., 2009; Schulte-Merker and Stainier, 2014; Kok et al., 2015; Lawson, 2016). As a frame shift deletion was introduced in the homeodomain sequence in UA5011, the prediction is that binding functions of *nkx3.2* were impaired and could not be compensated during development. These interpretations, and comparison with lampreys, will be enhanced in the ongoing and planned experiments using the UA5011 homozygotes.

4.6 FUTURE DIRECTIONS FOR ONGOING EXPERIMENTS

4.6.1 Lampreys: Gene Expression Patterns

Priorities among the planned and ongoing experiments include identification of multiple splice forms of *Nkx3.2* in lampreys, which could explain different expression patterns reported by different riboprobes (Cerny et al., 2010; this chapter; D. Meulemans Medeiros, pers. commn.). With the inputs from new genomic resources, it is now possible to redesign and optimize riboprobes for other genes of interest. These include *BarxB*, *Irx5/7*, *RunxA*, *RunxB*, *RunxC*, *Scx*,

Trps1, *Vegfr*, *Prg4*, *Col2a1a*, and *Col2a1b*. Rather than cloning directly from cDNAs, it may be more feasible to construct templates for riboprobes.

4.6.2 Lampreys: CRISPR/Cas9 Knockouts

Analyses of phenotypes and genotypes in the specimens injected with *Nkx3.2* sgRNAs in the 2017 spawning season are critical to the test of hypothesis. Phenotypes may be analyzed by *in situ* hybridization of potential *Nkx3.2* target genes such as *Gdf5/6/7* and a homologue of the gnathostome joint repressor *BarxA* (sampled at stages T26.5, T28, T30) and by alcian blue cartilage staining (T30). A recent study of cadherin expression in lampreys demonstrates that it is possible to genotype specimens used for *in situ* hybridization (York et al., 2017). Preliminary results presented in this chapter suggest that a significant proportion of *Nkx3.2* partial knockouts represent genetic mosaics. This confounding factor is difficult to rule out. Quantitative and statistical comparison of phenotypes may be crucial to delineate the effects of *Nkx3.2* knockouts.

New sgRNAs designed to knock out *BarxA* have not been injected. Once these specimens become available, in situ hybridization of *Nkx3.2* and alcian blue staining of cartilages are among the priorities for an analysis of phenotype.

4.6.3 Zebrafish: *nkx3.2* Mutants

The UA5011 homozygotes (*nkx3.2*$^{UA5011/UA5011}$) are now available for crossing. Multiple experiments are either underway or planned to: (***a***) conduct additional phenotypic analysis by μCT scanning (adults), alcian blue staining of cartilages (adults), and immunostaining of skeletal, muscular, and connective tissues (embryos, larvae); (***b***) test penetrance of the jaw joint phenotype; (***c***) describe the skeletal growth of UA5011 homozygotes using morphometrics; and (***d***) characterize feeding mechanics. The UA5011 homozygotes will be used produce a pool of 100% homozygous mutants for *in situ* hybrization of: (***a***) *nkx3.2* to test that the transcripts are absent; and (***b***) selected genes such as *gdf6a* to describe the interactions between *nkx3.2* and its suggested downstream genes. The *nkx3.2* transcripts may be best tested by qPCR among the wildtypes, the UA5011 heterozygotes, and the UA5011 homozygotes.

4.7 CONCLUSION

The gnathostome jaw joint represents one of the earliest examples of a synovial diarthrosis, but it has remained difficult to test hypotheses that explain evolutionary origins of this functional prerequisite for a biting jaw. To differentially test the three previously proposed hypotheses, comparative data on gene expression profiles were combined with functional analyses using gene knockouts in lampreys and zebrafish. The lack of muscular expression of the jaw joint-patterning *Nkx3.2* and its potential target genes in lampreys reject the Muscular Scaffold Hypotheses. On the basis of no spatial overlap between *Nkx3.2* and *BarxA* expressions in lampreys, the co-option to pattern synovial diarthrosis at the jaw joint likely occurred at the levels of structure (ancestrally linked with *Nkx3.2* and its downstream genes). Although the preliminary results are more compatible with the Intercartilaginous Blood Sinus Hypothesis over the Mucocartilage Hypothesis, these comparisons do not provide fully rigorous tests. Neither do they necessarily support the single best-fit hypothesis (Intercartilaginous Blood Sinus Hypothesis under the scenario of co-option of structure) yet.

Homozygous mutants of *nkx3.2* in zebrafish developed skeletal phenotypes reminiscent of jawless stem gnathostomes, particularly birkeniid anaspids. The similar traits include depressed lower lip, reduced snout, interoptic position of nasal opening, enlarged branchial region, dorsoventrally tall body profile, and potentially anteriorly extended basihyal. These mutants provide an interesting model to understand the evolution of craniofacial patterning in stem gnathostomes and the potentials of phenotypic plasticity that exist in the lineage of highly derived jawed vertebrates.

FIGURES

Fig. 4.1. Synovial diarthrosis in the jaw joint of crown gnathostomes and synovial joint-like structures in stem gnathostomes (adapted from Miyashita, 2016). (**a**) Schematic drawing for development of a synovial joint in gnathostomes. (**b**) Three-dimensional reconstruction of a jaw joint of the gecko *Eublepharis macularius* using X-ray microcomputed tomography (from Payne et al., 2011), showing the gross anatomy of a typical gnathostome synovial joint. (**c**) Transverse histological section of the jaw joint of a gecko (from Payne et al. 2011), showing the fine-scale anatomy of a typical gnathostome synovial joint. Hyaline cartilage caps the element as an articular cartilage. The synovial cavity is encapsulated within ligamentous tissue, and the cavity filled with synovial fluid acts as a lubricant and shock-absorbing agent. (**d**) Transverse histological section of the head of an adult hagfish (*Eptatretus stoutii*) at the level of the cardinal heart. The cardinal heart is an intercartilaginous venous sinus between the velar and facial cartilages that is functionally and anatomically similar to a synovial joint. The cardinal heart lacks myofibrils, and its wall consists of ligament. The movement of the velum aids in circulation, while blood acts as a lubricant. (**e**) Pectoral fenestra of the osteostracan *Norselaspis glacialis* in left lateral view (modified from Janvier, 1984), showing the attachment area of the pectoral fin. The pectoral fenestra is shaded green, and the external surface of the head shield light brown. The attachment of the pectoral fin is a pad of perichondrally ossified cartilage (blue) within a fossa irrigated and drained by several major vascular foramina (red). (**f**) The area of pectoral fin attachment in the antiarch *Bothriolepis mcpharsoni* in left lateral view (modified from Janvier, 1995). The pectoral articulation is *via* perichondrally ossified cartilaginous pads divided dorsoventrally by the funnel pit, which may have hosted a blood sinus irrigated and drained by the axillary foramen. Colour codes as in E.

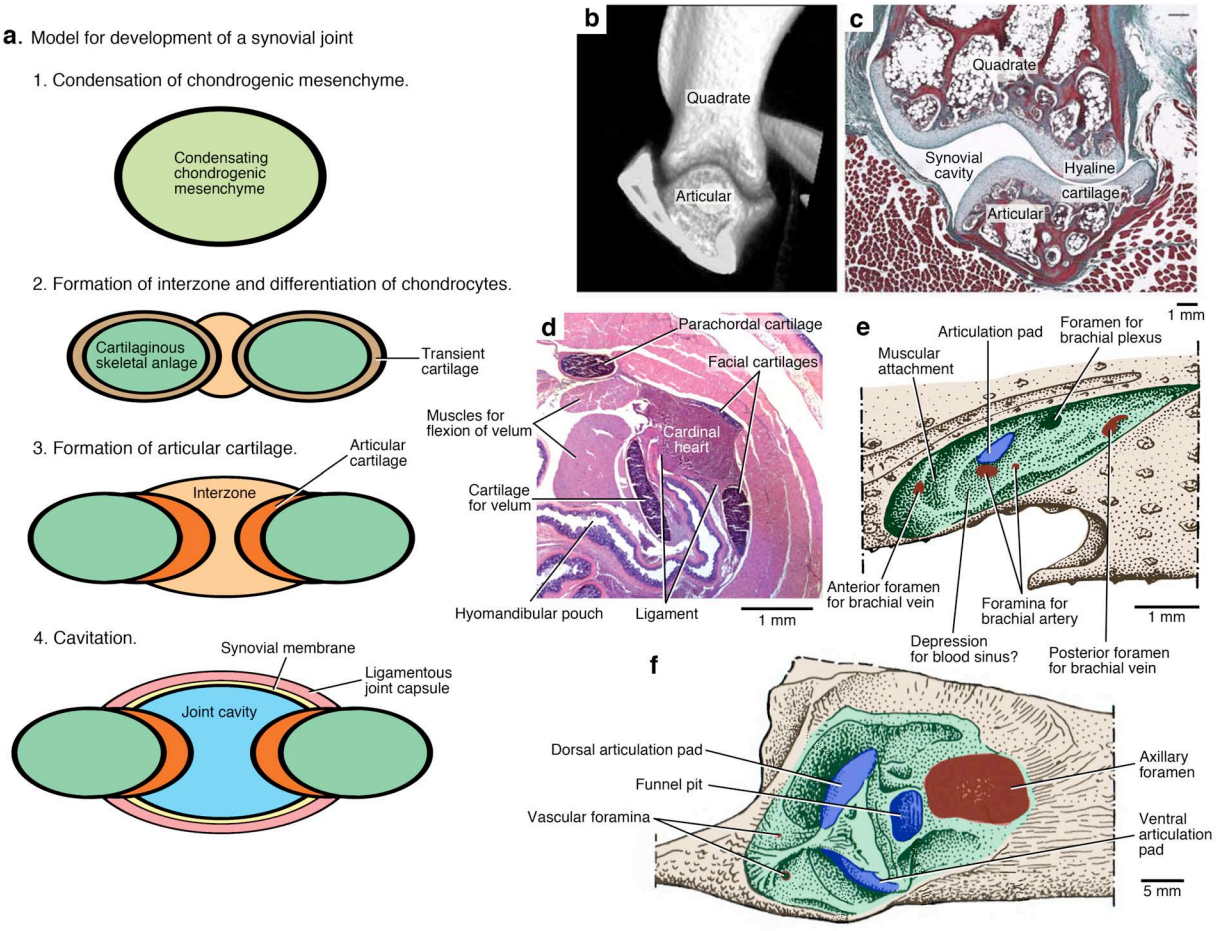
a. Model for development of a synovial joint
1. Condensation of chondrogenic mesenchyme.
Condensating chondrogenic mesenchyme
2. Formation of interzone and differentiation of chondrocytes.
Cartilaginous skeletal anlage
Transient cartilage
3. Formation of articular cartilage.
Articular cartilage
Interzone
4. Cavitation.
Synovial membrane
Ligamentous joint capsule
Joint cavity
b
Quadrate
Articular
c
Quadrate
Synovial cavity
Hyaline cartilage
Articular
d
Parachordal cartilage
Facial cartilages
Muscles for flexion of velum
Cardinal heart
Cartilage for velum
Hyomandibular pouch
Ligament
1 mm
e
Articulation pad
Foramen for brachial plexus
Muscular attachment
1 mm
Anterior foramen for brachial vein
Foramina for brachial artery
Depression for blood sinus?
Posterior foramen for brachial vein
1 mm
f
Dorsal articulation pad
Funnel pit
Vascular foramina
Axillary foramen
Ventral articulation pad
5 mm

Fig. 4.2. Function of *Nkx3.2* in the development of synovial diarthrosis. (**a**) A chondrogenic ectomesenchyme in the mandibular arch of zebrafish at 24 hpf (adopted from Nichols et al., 2013). Patterning the jaw joint, *nkx3.2* is expressed in the intermediate domain of the mandibular arch in gnathostomes, downstream of endothelin signals and *hand2*. (**b**) In the sclerotomes of mice, function of *Nkx3.2* in is down-regulation of factors promoting chondrogenesis (adopted from Hartman, 2009). (**c**) In the development of synovial diarthrosis, inhibition of chondrocyte hypertrophy by *Nkx3.2* induces formation of an interzone (adopted from Smeeton et al., 2016). (**d**) The development of a synovial joint requires formation of an interzone, followed by cavitation (adopted from Smeeton et al., 2016). Colour codes are shared between panels **c** and **d**.

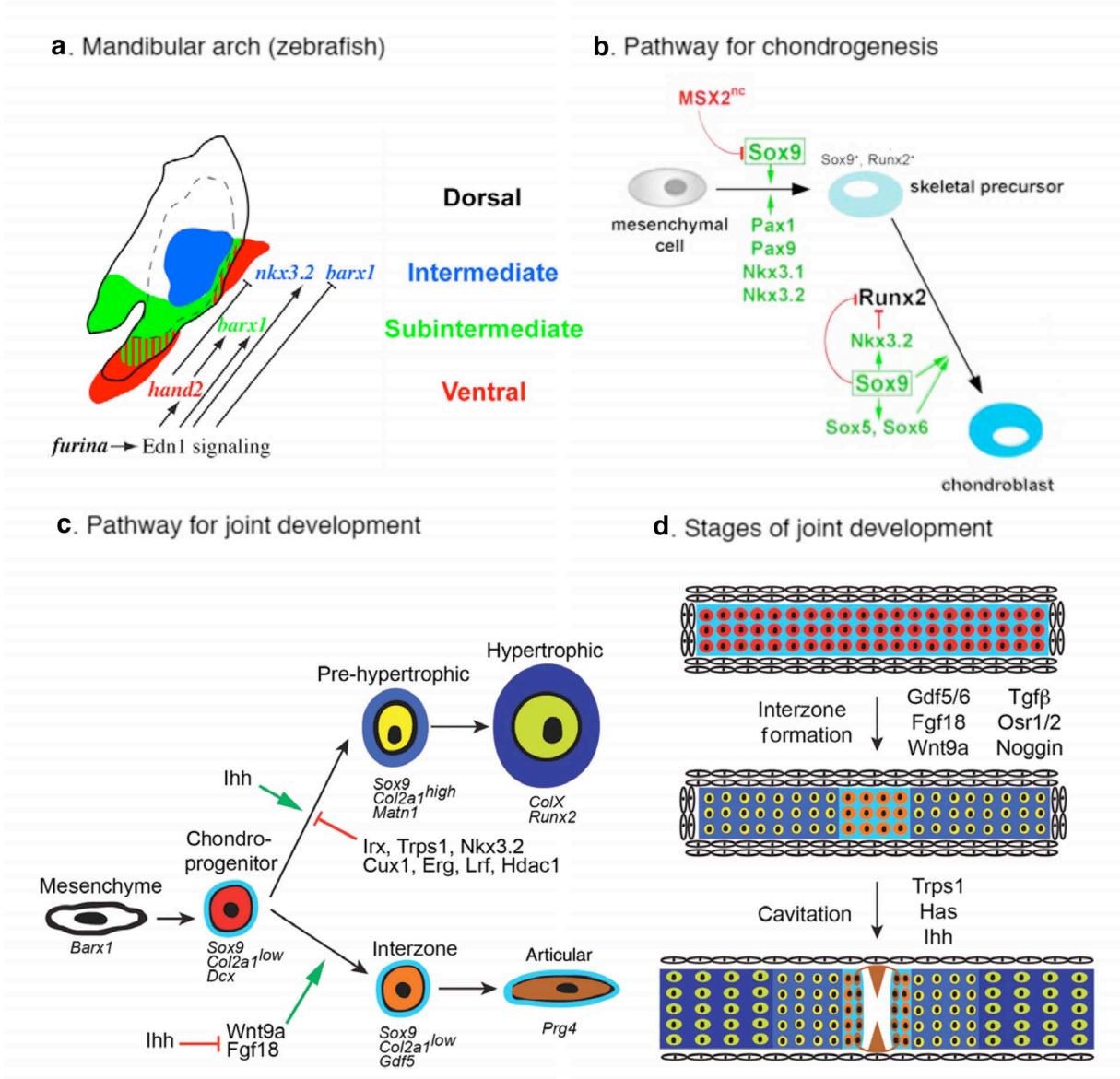
a. Mandibular arch (zebrafish)
Dorsal
Intermediate
Subintermediate
Ventral
nkx3.2
barx1
barx1
hand2
furina
Edn1 signaling
b. Pathway for chondrogenesis
MSX2nc
Sox9
Sox9+, Runx2+
skeletal precursor
mesenchymal cell
Pax1
Pax9
Nkx3.1
Nkx3.2
Runx2
Nkx3.2
Sox9
Sox5, Sox6
chondroblast
c. Pathway for joint development
Hypertrophic
Pre-hypertrophic
Sox9
Col2a1high
Matn1
ColX
Runx2
Ihh
Chondro-progenitor
Irx, Trps1, Nkx3.2
Cux1, Erg, Lrf, Hdac1
Mesenchyme
Barx1
Sox9
Col2a1low
Dcx
Interzone
Articular
Ihh
Wnt9a
Fgf18
Sox9
Col2a1low
Gdf5
Prg4
d. Stages of joint development
Interzone formation
Gdf5/6
Fgf18
Wnt9a
Tgfβ
Osr1/2
Noggin
Cavitation
Trps1
Has
Ihh

Fig. 4.3. Three hypotheses for an evolutionary precursor of synovial diarthrosis at the jaw joint. (**a**) The *Muscular Scaffold Hypothesis* predicts the earliest jaw elements to have been embedded in a muscular complex. A notable example in cyclostomes is the lingual apparatus. In this figure, muscles sharing same colour form a pair of antagonists to suspend and stabilize the lingual apparatus in the Northeastern Pacific hagfish *Eptatretus stoutii* (adopted from Miyashita, 2012). (**b**) The *Mucocartilage Hypothesis* predicts mucocartilage as an evolutionary precursor of the synovial diarthrosis. In this panel, anatomical distributions of mucocartilage are indicated by pale green (modified after Johnels, 1948 by Miyashita, 2012). (**c**) The *Intercartilaginous Blood Sinus Hypothesis* postulates that a structure like the velar sinus in cyclosotmes may have preceded the synovial diarthrosis. In this panel, a parasagittal histological section with hematoxylin and eosin staining indicates the position and morphology of the velar sinus with respect to some of the surrounding tissues such as mucocartilage.

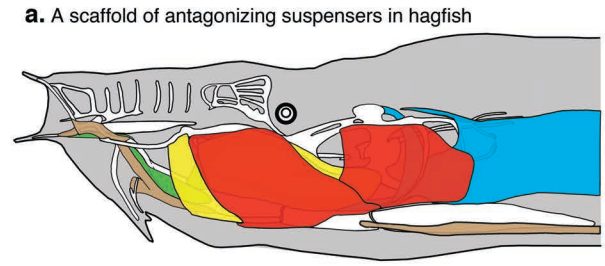
a. A scaffold of antagonizing suspensers in hagfish

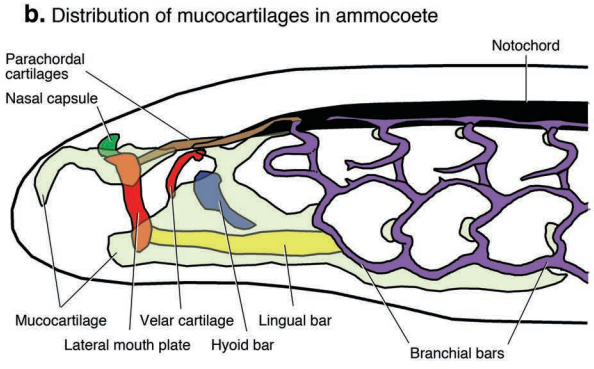
b. Distribution of mucocartilages in ammocoete
Notochord
Parachordal cartilages
Nasal capsule
Mucocartilage
Velar cartilage
Lingual bar
Lateral mouth plate
Hyoid bar
Branchial bars

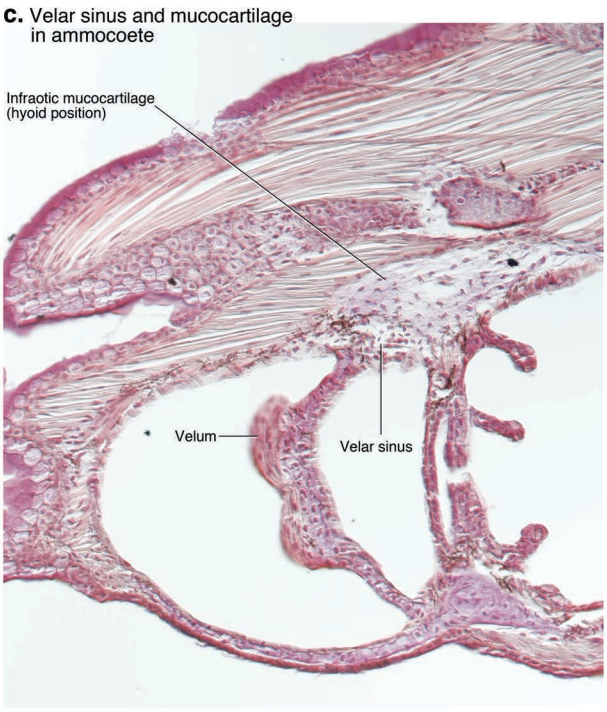
c. Velar sinus and mucocartilage in ammocoete
Infraotic mucocartilage (hyoid position)
Velum
Velar sinus

Fig. 4.4. Potential skeletal correlates of velum and velar sinus in stem gnathostomes. (**a**) Right side of the head of the osteostracan *Dartmuthia gemmifera* in ventral view [AMNH (American Museum of Natural History) Patten Collections 38.71.8750; modified from Janvier, 1985b; as reproduced by Miyashita, 2016] with sketches of sections at positions indicated by the thick lines, showing the attachment site with a suture for the velar skeleton in the hyomandibular position. (**b**) Anterior part of an internal cast of the headshield of *Boreaspis ceratops* (MNHN [Muséum national d'Histoire naturelle] SVD1001) in dorsal view, showing the marginal vein draining from the proximal end of the velar chamber. (**c**) Right half of the head shield of the galeaspid *Duyunaspis paoyangensis* in ventral view (modified from Janvier, 1984; reproduced by Miyashita, 2016), showing the attachment site for endoskeletal elements in the hyomandibular position and associated depressions that presumably represent muscular attachment and a sinus connected with the lateral head vein.

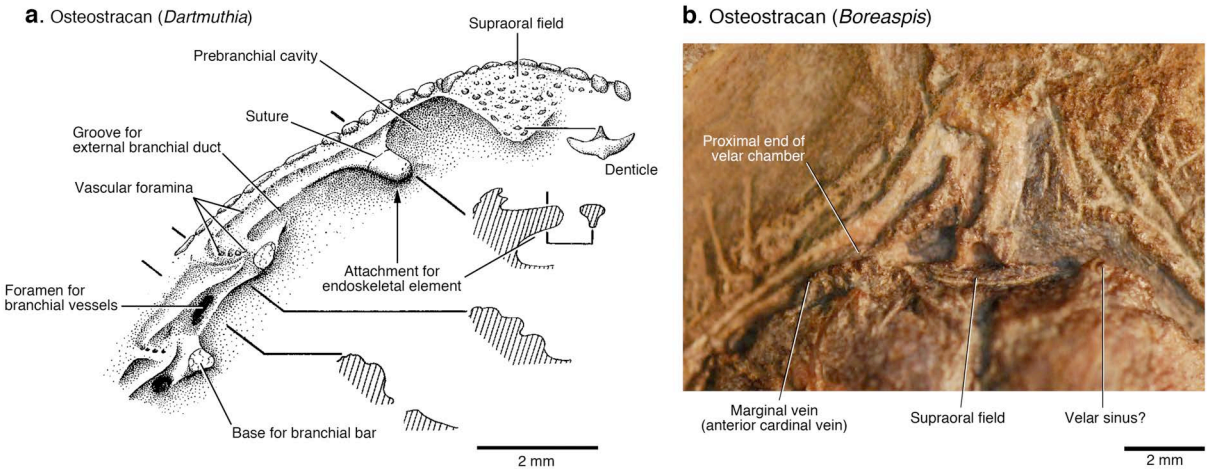
a. Osteostracan (Dartmuthia)
Supraoral field
Prebranchial cavity
Suture
Groove for external branchial duct
Denticle
Vascular foramina
Attachment for endoskeletal element
Foramen for branchial vessels
Base for branchial bar
2 mm
b. Osteostracan (Boreaspis)
Proximal end of velar chamber
Marginal vein (anterior cardinal vein)
Supraoral field
Velar sinus?
2 mm
c. Galeaspid (Duyunaspis)
Depressions (muscular attachment + venous sinus?)
Lateral head vein
Neural canal
Spinal nerves
Nasal aperture
Prebranchial cavity
Attachment for endoskeletal elements
Foramina for branchial vessels
Base for branchial bar
Branchial fossae
Interbranchial ridges
10 mm

Fig. 4.5. Schematic functional analyses of *Nkx3.2* in lampreys and zebrafish. (**a**) The model of *Nkx3.2* in *Petromyzon marinus* based on Scaffold_00015 of the Dovetail assembly (Smith et al., unpublished) showing the position of homeodomain and aligned with partial coding sequences retrieved from Genbank (blue). (**b**) The model of *nkx3.2* in *Danio rerio* (zebrafish) showing the position of homeodomain. The mutant genotype UA5011 is 20 bp deletion near the start of homeodomain (yellow bar). For **b** and **c**, triangles in magenta indicate locations of CRISPR target sequences, and black arrows show locations of primers used for genotyping. (**c**, **e**, **g**) Alcian blue staining of cartilages in non-injected, wildtype AB zebrafish at 4 dpf (**c**) *in situ*, (**e**) dissected for mandibular and hyoid arches, and (**g**) close-up of the interface between the palatoquadrate and Meckel's cartilage, showing the jaw joint. (**d**, **f**, **h**) Alcian blue staining of cartilages in *nkx3.2* morpholino-injected AB zebrafish at 4 dpf (**d**) *in situ*, (**f**) dissected for mandibular and hyoid arches, and (**h**) close-up of the interface between the palatoquadrate and Meckel's cartilage, showing fusion of the two elements. Panels **c**-**h** adopted from Miller et al. (2003). Scale bar = 50 μm.

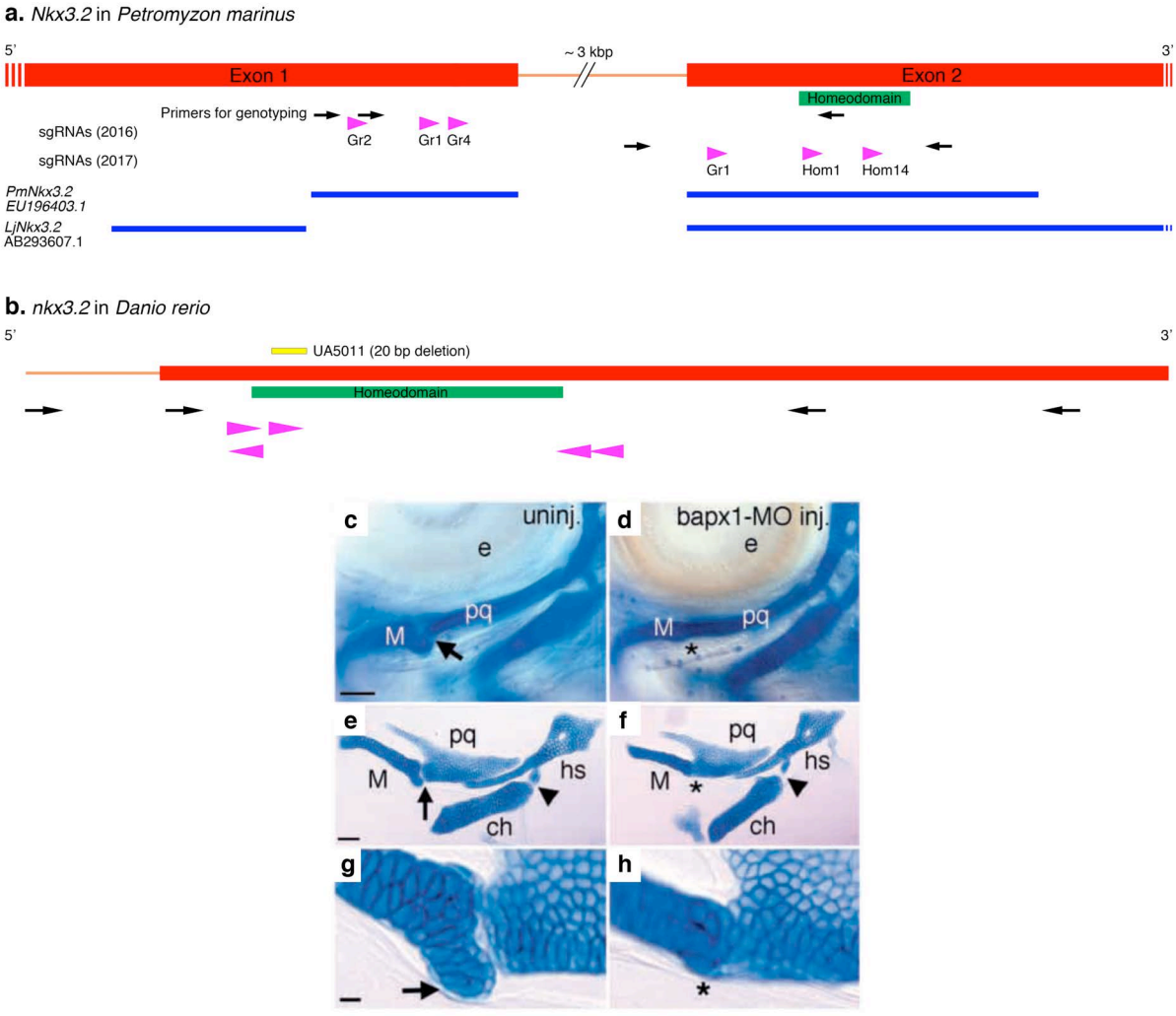
a. Nkx3.2 in Petromyzon marinus
5'
~ 3 kbp
3'
Exon 1
Exon 2
Homeodomain
Primers for genotyping
sgRNAs (2016)
sgRNAs (2017)
Gr2
Gr1 Gr4
Gr1
Hom1
Hom14
PmNkx3.2
EU196403.1
LjNkx3.2
AB293607.1
b. nkx3.2 in Danio rerio
5'
3'
UA5011 (20 bp deletion)
Homeodomain
c
uninj.
e
pq
M
d
bapx1-MO inj.
e
M
pq
*
e
pq
M
hs
ch
f
pq
M
*
hs
ch
g
h
*

Fig. 4.6. Expression patterns of *Nkx3.2* in *Petromyzon marinus*, all in left lateral view except for d. (**a**) Tahara stage T26.5; (**b**) T27; (**c**) T28; (**d**) T28 in horizontal section; (**e**) T30; (**f**) same specimen with overlay of schematized skeletal elements. Red arrows indicate areas of enhanced expression. See main text for description.

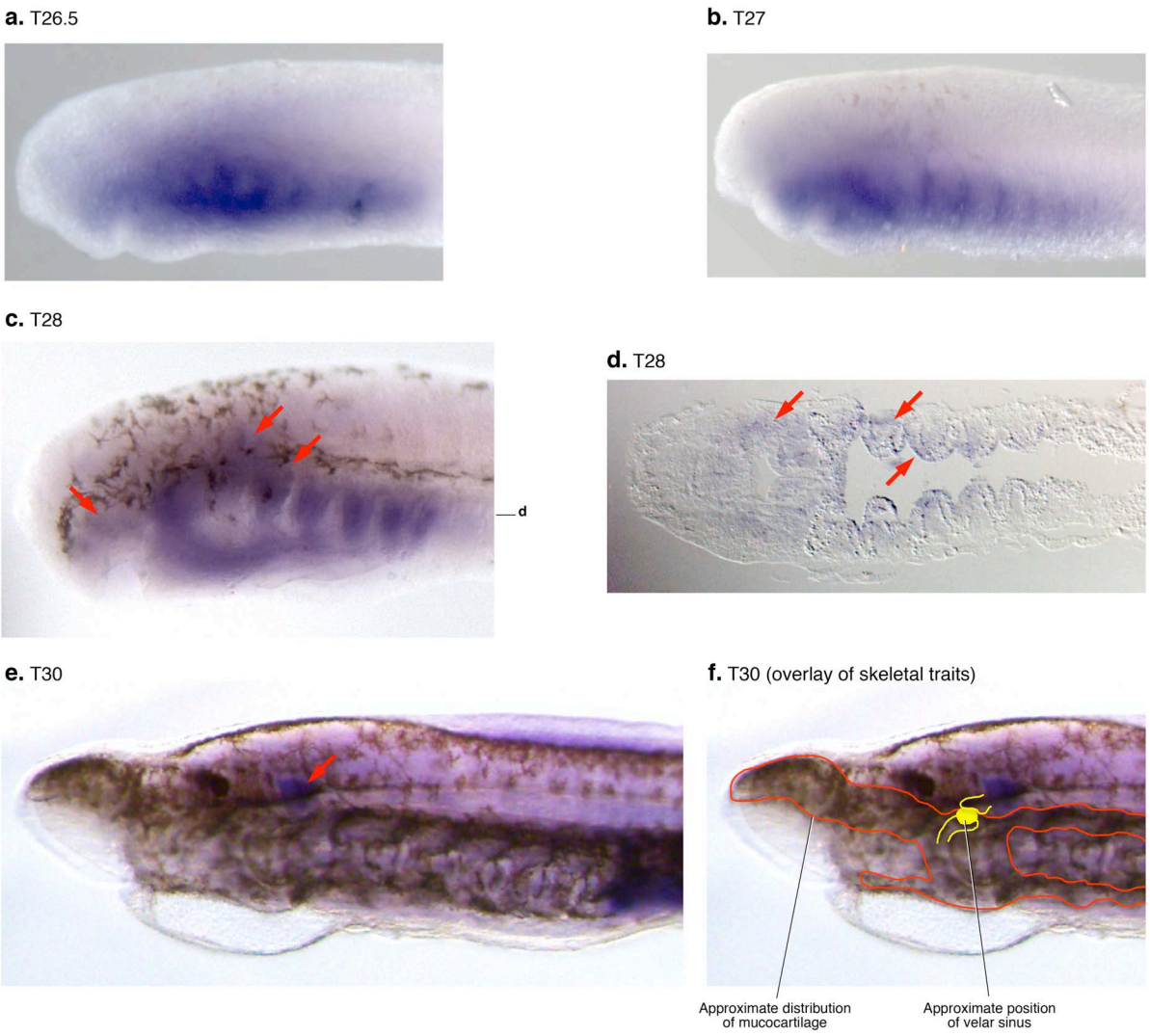
a. T26.5
b. T27
c. T28
d
d. T28
e. T30
f. T30 (overlay of skeletal traits)
Approximate distribution of mucocartilage
Approximate position of velar sinus

Fig. 4.7. Expression patterns of genes that potentially interact with *Nkx3.2* in *Petromyzon marinus*, all in left lateral view except c. (**a**-**c**) *BarxA*: (**a**) Tahara stage T26; (**b**) T29; (**c**) same specimen in ventral view. (**e**-**f**) *Gdf5/6/7*: (**d**) T27; (**e**) T28; (**f**) T30. Red arrows indicate areas of enhanced expression. See main text for description.

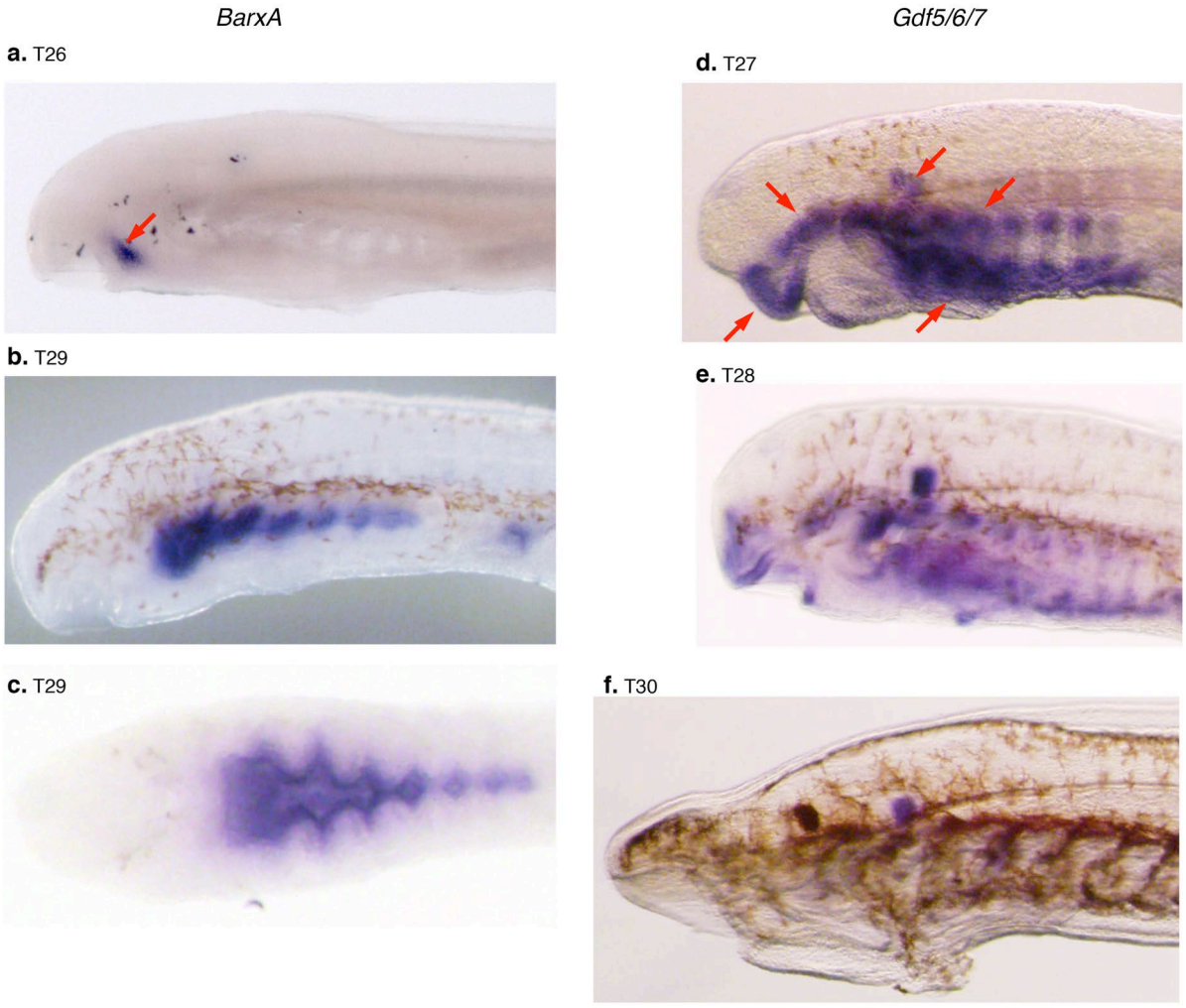
BarxA
Gdf5/6/7
a. T26
b. T29
c. T29
d. T27
e. T28
f. T30

Fig. 4.8. Expression patterns of effector genes that are potentially downstream of *Nkx3.2* in *P. marinus*, all in left lateral view. (**a**) *Col2a1a* at Tahara stage T30. (**b**-**d**) *Col2a1b*: (**b**) T26.5; (**c**) T28; (**d**) T30. (**e**-**g**) *Prg4*: (**e**) T27; (**f**) T28; (**g**) T30. Purple areas show potential probe trapping. See main text for description.

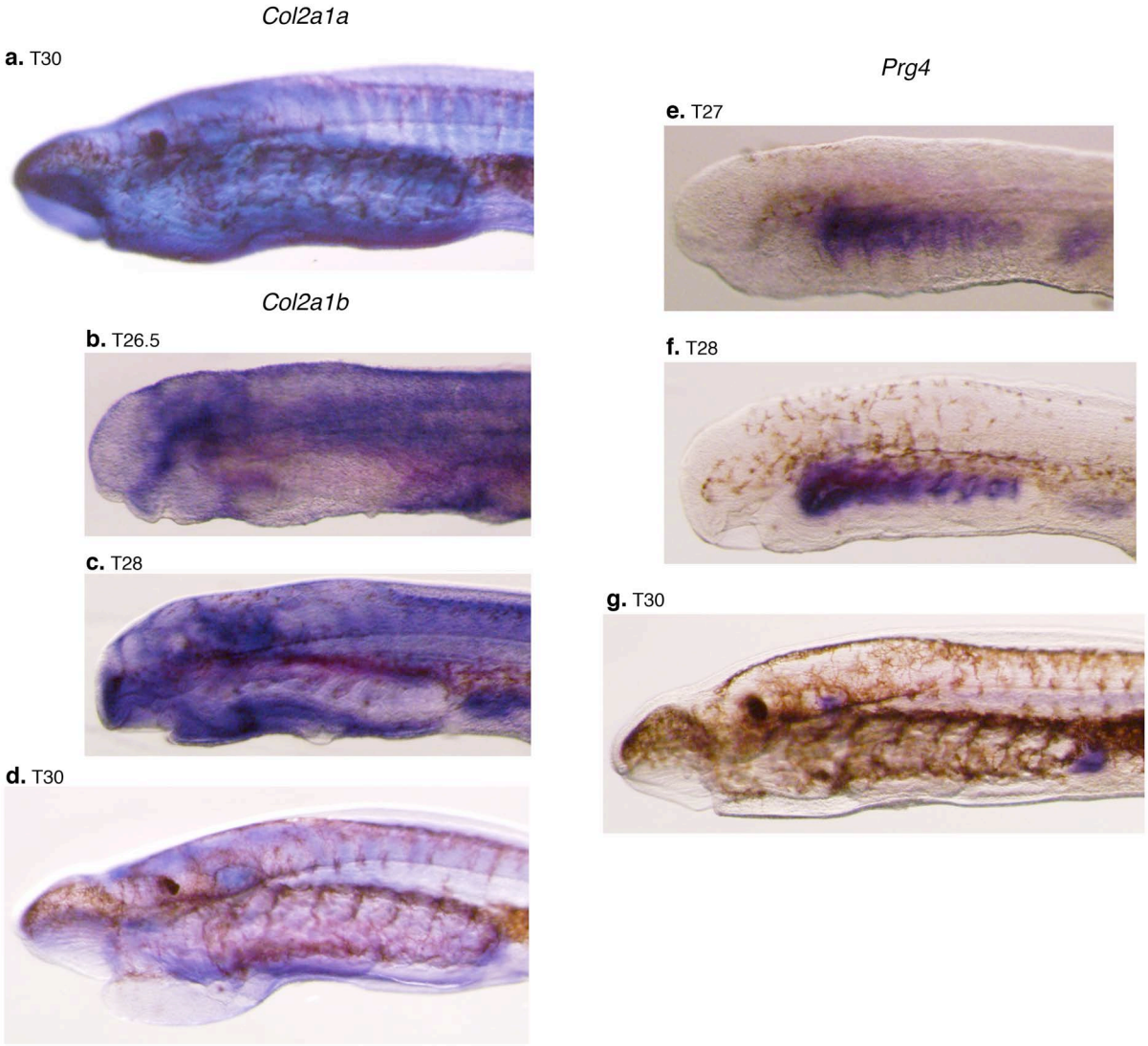
Col2a1a
a. T30
Col2a1b
b. T26.5
c. T28
d. T30
Prg4
e. T27
f. T28
g. T30

Fig. 4.9. Potential skeletal phenotypes resulting from *Nkx3.2* sgRNA injections (2016) in *Petromyzon marinus*. See Fig. 4.5a for design of the sgRNAs. (**a**-**c**) Alcian blue staining of cartilages at Tahara stage T30. (**a**) Wildtype (non-injected). (**b**) Control (injected with *Tyr* sgRNA). (**c**) Potential mutants (injected with *Nkx3.2* sgRNAs). Original specimens in left column, and same specimens in right column with schematic overlay of skeletal elements to illustrate potential morphological variations. (**d**) Distribution of chondrocytes in the same specimen as the panel a, using endogenous fluorescence of alcian blue.

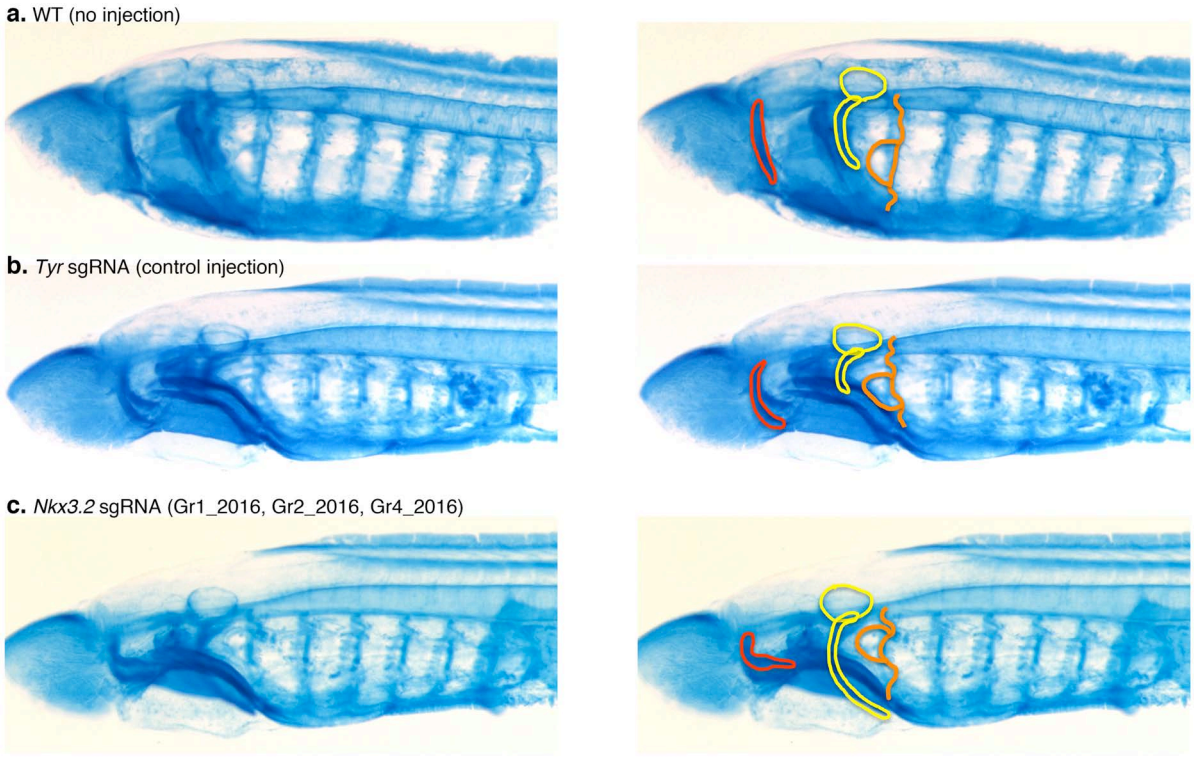
a. WT (no injection)
b. Tyr sgRNA (control injection)
c. Nkx3.2 sgRNA (Gr1_2016, Gr2_2016, Gr4_2016)

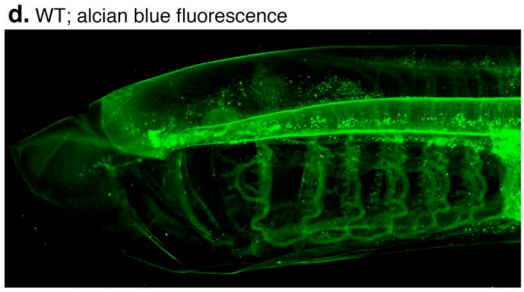
d. WT; alcian blue fluorescence

Fig. 4.10. Phenotypes and genotypes of *Petromyzon marinus* at Tahara stage T26.5, resulting from *Nkx3.2* sgRNA injections (2017). See Fig. 4.5a for design of the sgRNAs. (**a**-**g**) Photographs of individuals with representative phenotypes, with sequence information in the right column. The mutants were selected from those with frame-shift deletions. In panel a, the target sequences are indicated by bold typeface and PAM sites by red font. See text for description.

a. WT (non-injected)

```
AGTGCCCTGGCTCCTCTATTAAAGATCGTTGCCCCGGCTCCGCTGTGCGCGTCCCTGCAGAGCGACTCTGCGGCTCCATGGACGAGGACGACGACGCCGG
CCCCGCCTCCGGGGGACAGACTCAGCCCGGGCGCCGAGCCGCCGCTGGCTGAGGGAGGTGCCGTGGTGCTGGGGGGCAGCACCGGGCCCCCCGCGGAGATG
CCGCTGCTCACGCCGCAAGCGAAGCCGCGCAAGAAGCGCTCCCGCGCCGCCTTTTCGCACGCGCAGGTGTTCGAGTTGGAGCGGCGCTTCAACCAGCAGC
GCTACCTGTCGGGCCCCGAGCGGGCCGACCTGGCCGCGGCGCTCAAACTCACGGAGACCCAGGTGAAGATCTGGTTCCAGAACCGACGCTACAAGACC
```

b. *Nkx3.2* sgRNA (short pharynx)

```
AGTGCCCTGGCTCCTCTATTAAAGATCGTTGCCCCGGCTCCGCTGTGCGCGTCCCTGCAGAGCGACTCTGCGGCTCCATGGACGAGGACGACGAC-----
----------GGGGACAGACTCAGCCCGGGCGCCGAGCCGCCGCTGGCTGAGGGAGGTGCCGTGGTGCTGGGGGGCAGCACCGGGCCCCCCGCGGAGATG
CCGCTGCTCACGCCGCAAGCGAAGCCGCGCAAGAAGCGCTCCCGCGCCGCCTTTTCGCACGCGCAGGTGTTCGAGTTGGAGCGGCGCTTCAACCAGCAGC
GCTACCTGTCGGGCCCCGAGCGGGCCGACCTGGCCGCGGCGCTCAAACTCACGGAGACCCAGGTGAAGATCTGGTTCCAGAACCGACGCTACAAGACC

AGTGCCCTGGCTCCTCTATTAAAGATCGTTGCCCCGGCTCCGCTGTGCGCGTCCCTGCAGAG----------------------------------------
----------GACTCAGCCCGGGCGCCGAGCCGCCGCTGGCTGAGGGAGGTGCCGTGGTGCTGGGGGGCAGCACCGGGCCCCCCGCGGAGATG
CCGCTGCTCACGCCGCAAGCGAAGCCGCGCAAGAAGCGCTCCCGCGCCGCCTTTTCGCACGCGCAGGTGTTCGAGTTGGAGCGGCGCTTCAACCAGCAGC
GCTACCTGTCGGGCCCCGAGCGGGCCGACCTGGCCGCGGCGCTCAAACTCACGGAGACCCAGGTGAAGATCTGGTTCCAGAACCGACGCTACAAGACC
```

c. *Nkx3.2* sgRNA (short pharynx; axial defects)

```
AGTGCCCTGGCTCCTCTATTAAAGATCGTTGCCCCGGCTCCGCTGTGCGCGTCCCTGCAGAGCGACTCTGCGGCTCCATGGACGAGGACGACGACGCCGG
CCCCGCCT----------
----------AAGAAGCGCTCCCGCGCCGCCTTTTCGCACGCGCAGGTGTTCGAGTTGGAGCGGCGCTTCAACCAGCAGC
GCTACCTGTCGGGCCCCGAGCGGGCCGACCTGGCCGCGGCGCTCAAACTCACGGAGACCCAGGTGAAGATCTGGTTCCAGAACCGACGCTACAAGACC
```

d. *Nkx3.2* sgRNA (loss of PAs; axial defects)

```
AGTGCCCTGGCTCCTCTATTAAAGATCGTTGCCCCGGCTCCGCTGTGCGCGTCCCTGCAGAGCGACTCTGCGGCTCCATGGACGAGGACGACGACG----
--------CCGGGGACAGACTCAGCCCGGGCGCCGAGCCGCCGCTGGCTGAGGGAGGTGCCGTGGTGCTGGGGGGCAGCACCGGGCCCCCCGCGGAGATG
CCGCTGCTCACGCCGCAAGCGAAGCCGCGCAAGAAGCGCTCCCGCGCCGCCTTTTCGCACGCGCAGGTGTTCGAGTTGGAGCGGCGCTTCAACCAGCAGC
GCTACCTGT----------GCGGGCCGACCTGGCCGCGGCGCTCAAACTCACGGAGACCCAGGTGAAGATCTGGTTCCAGAACCGACGCTACAAGACC

AGTGCCCTGGCTCCTCTATTAAAGATCGTTGCCCCGGCTCCGCTGTGCGCGTCCCTGCAGAGCGACTCTGCGGCTCCATGGACGAGGACGACGACGCCGG
CCCCGC----------GCTGGGGGGCAGCACCGGGCCCCCCGCGGAGATG
CCGCTGCTCACGCCGCAAGCGAAGCCGCGCAAGAAGCGCTCCCGCGCCGCCTTTTCGCACGCGCAGGTGTTCGAGTTGGAGCGGCGCTTCAACCAGCAGC
GCTACCTGT----------GCGGGCCGACCTGGCCGCGGCGCTCAAACTCACGGAGACCCAGGTGAAGATCTGGTTCCAGAACCGACGCTACAAGACC
```

e. *Nkx3.2* sgRNA (loss of PAs; axial defects)

```
AGTGCCCTGGCTCCTCTATTAAAGATCGTTGCCCCGGCTCCGCTGTGCGCGTCCCTGCAGAGCGACTCTGCGGCTCCATGGACGAGGACGACGACGCCGG
CCCCGC--------------TCAGCCCGGGCGCCGAGCCGCCGCTGGCTGAGGGAGGTGCCGTGGTGCTGGGGGGCAGCACC------CCCGCGGAGATG
CCGCTGCTCACGCCGCAAGCGAAGCCGCGCAAGAAGCGCTCCCGCGCCGCCTTTTCGCACGCGCAGGTGTTCGAGTTGGAGCGGCGCTTCAACCAGCAGC
GCTACCTGTCGGGCC-----------GACCTGGCCGCGGCGCTCAAACTCACGGAGACCCAGGTGAAGATCTGGTTCCAGAACCGACGCTACAAGACC

AGTGCCCTGGCTCCTCTATTAAAGATCGTTGCCCCGGCTCCGCTGTGCGCGTCCCTGCAGAGCGACTCTGCGGCTCCATGGACGAGGACGACGACGCCGG
CCCCGCCTCCGGGGGACAGACTCAGCCCGGGCGCCGAGCCGCCGCTGGCTGAGGGAGGTGCCGTGGTGCTGGGGGGCAGCAC-------------------
----------
----------TCAAACTCACGGAGACCCAGGTGAAGATCTGGTTCCAGAACCGACGCTACAAGACC
```

f. *Nkx3.2* sgRNA (no apparent phenotype)

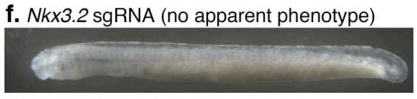

```
AGTGCCCTGGCTCCTCTATTAAAGATCGTTGCCCCGGCTCCGCTGTGCGCGTCCCTGCAGAGCGACTCTGCGGCTCCATGGACGAGGACGACGACGCCGG
CCCCGCCTCCGGGGGACAGACTCAGCCCGGGCGCCGAGCCGCCGCTGGCTGAGGGAGGTGCCGTGGTGCTGGGGGGCAGCACCGGGCCCCCCGCGGAGATG
CCGCTGCTCACGCCGCAAGCGAAGC-----------CGCTCCCGCGCCGCCTTTTCGCACGCGCAGGTGTTCGAGTTGGAGCGGCGCTTCAACCAGCAGC
GCTACCTGTCGGGCCCCGAGCGGGCCGACCTGGCCGCGGCGCTCAAACTCACGGAGACCCAGGTGAAGATCTGGTTCCAGAACCGACGCTACAAGACC
```

g. WT (non-injected; batch effect)

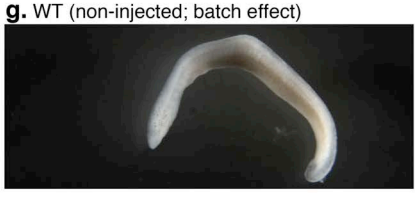

```
AGTGCCCTGGCTCCTCTATTAAAGATCGTTGCCCCGGCTCCGCTGTGCGCGTCCCTGCAGAGCGACTCTGCGGCTCCATGGACGAGGACGACGACGCCGG
CCCCGCCTCCGGGGGACAGACTCAGCCCGGGCGCCGAGCCGCCGCTGGCTGAGGGAGGTGCCGTGGTGCTGGGGGGCAGCACCGGGCCCCCCGCGGAGATG
CCGCTGCTCACGCCGCAAGCGAAGCCGCGCAAGAAGCGCTCCCGCGCCGCCTTTTCGCACGCGCAGGTGTTCGAGTTGGAGCGGCGCTTCAACCAGCAGC
GCTACCTGTCGGGCCCCGAGCGGGCCGACCTGGCCGCGGCGCTCAAACTCACGGAGACCCAGGTGAAGATCTGGTTCCAGAACCGACGCTACAAGACC
```

Fig. 4.11. Comparison of *nkx3.2* mutants (F_2) with wildtype in zebrafish larvae (*Danio rerio*). (**a**) AB wildtype and *nkx3.2*$^{UA5011/UA5011}$ (20 bp deletion; see Fig. 4.5b) at 4 dpf (treated with PTU; reduced pigments). (**b**) Same specimens under fluorescence, showing *sox10*:GFP expression in cartilages. (**c**) Comparison of chondrocrania among wildtype AB (*nkx3.2*$^{+/+}$), F_2 heterozygous mutant (*nkx3.2*$^{+/UA5011}$), and F_2 homozygous mutant (*nkx3.2*$^{UA5011/UA5011}$) at 4 dpf, showing *sox10*:GFP expression in cartilages. The palatoquadrate and Meckel's cartilage are fused to each other and the jaw joint is lost only in homozygous mutants. (**d**) Skeletons of mandibular arches in wildtype AB (*nkx3.2*$^{+/+}$) and F_2 homozygous mutant (*nkx3.2*$^{UA5011/UA5011}$) at 4 dpf, with *sox10*:GFP expression in chondrocytes. An interzone (a future jaw joint) is forming between the palatoquadrate and Meckel's cartilage in the wildtype, whereas this interzone is absent in the homozygous mutant. (**e**) Comparison of chondrocrania stained with alcian blue among wildtype AB (*nkx3.2*$^{+/+}$), F_2 heterozygous mutant (*nkx3.2*$^{+/UA5011}$), and F_2 homozygous mutant (*nkx3.2*$^{UA5011/UA5011}$) at 4 dpf. White arrow indicates interzone (jaw joint). Yellow asterisk indicates fusion between palatoquadrate and Meckel's cartilage.

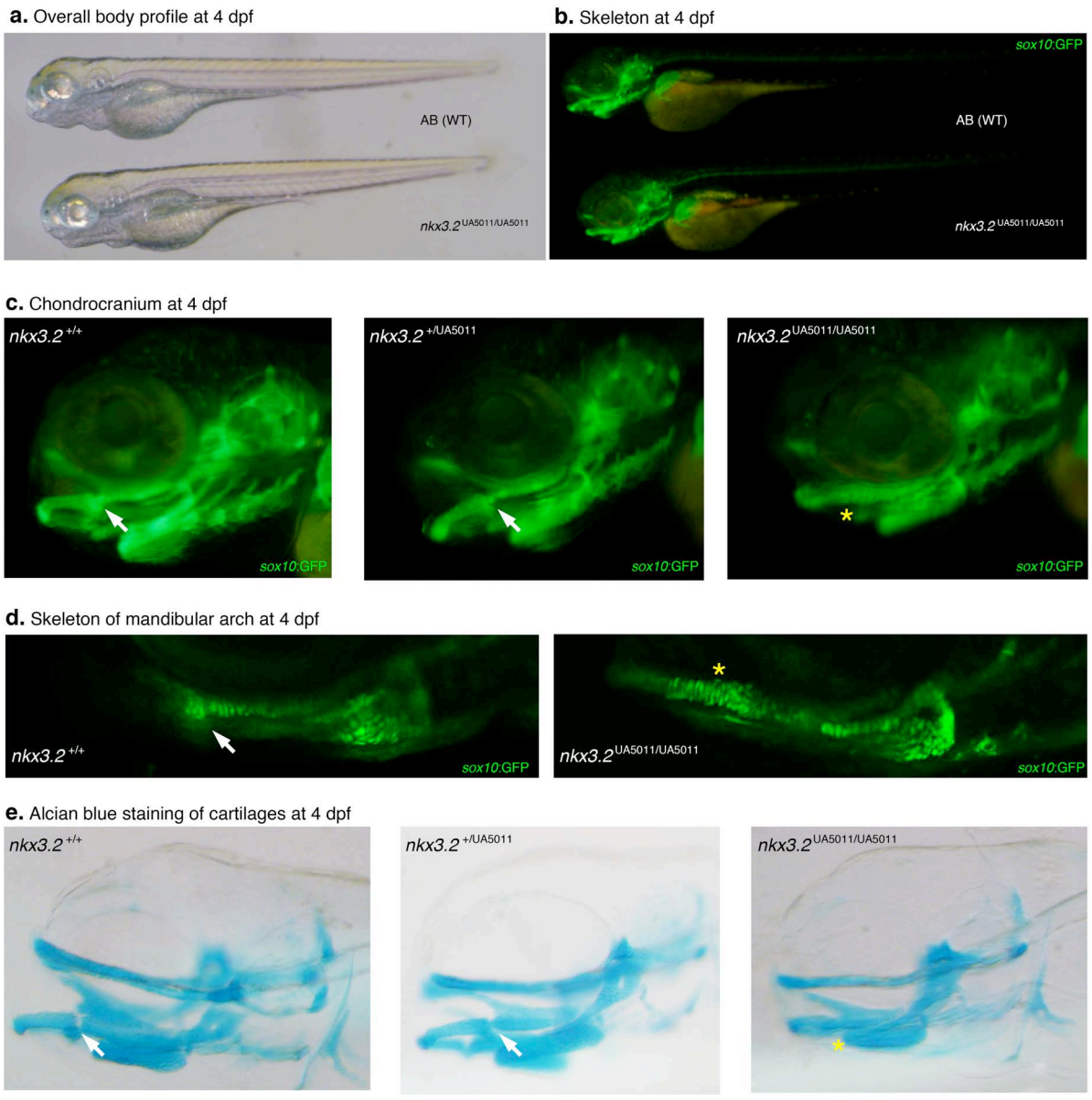
a. Overall body profile at 4 dpf
AB (WT)
nkx3.2UA5011/UA5011
b. Skeleton at 4 dpf
sox10:GFP
AB (WT)
nkx3.2UA5011/UA5011
c. Chondrocranium at 4 dpf
nkx3.2+/+
sox10:GFP
nkx3.2+/UA5011
sox10:GFP
nkx3.2UA5011/UA5011
sox10:GFP
d. Skeleton of mandibular arch at 4 dpf
nkx3.2+/+
sox10:GFP
nkx3.2UA5011/UA5011
sox10:GFP
e. Alcian blue staining of cartilages at 4 dpf
nkx3.2+/+
nkx3.2+/UA5011
nkx3.2UA5011/UA5011

Fig. 4.12. Phenotypes of wild type (WT) and *nkx3.2* mutants (F_2) in adult zebrafish (*Danio rerio*). (**a**, **c**, **e**) Head and trunk morphology; (**b**, **d**, **f**) close-up of head region of same specimen in the left column, all in left lateral view. (**a**, **b**) wildtype, AB strain, 2.5 months old. (**c**, **d**) *nkx3.2*$^{UA5011/UA5011}$, 2.5 month old. (**e**, **f**) an undescribed birkeniid anaspid (GSC [Geological Survey of Canada] 026-003) from the Cape Phillips Formation (Upper Silurian), Cornwallis Island. Red arrows indicate the height of the operculum (zebrafish) or the length of the branchial series (birkeniid). White arrows indicate depth of body.

a. WT

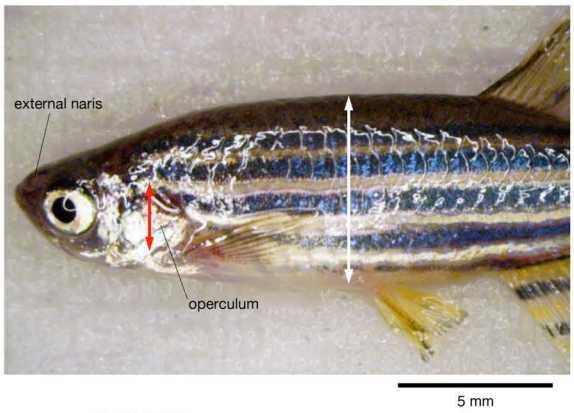

b. WT

c. *nkx3.2* UA5011/UA5011

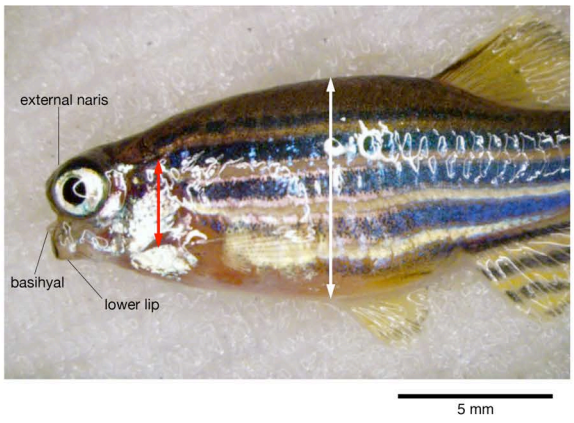

d. *nkx3.2* UA5011/UA5011

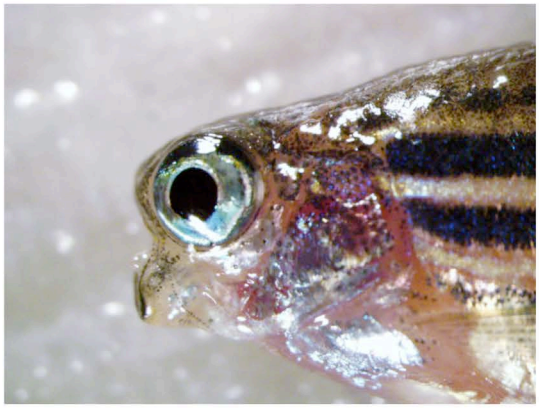

e. Birkeniida gen. et sp. nov.

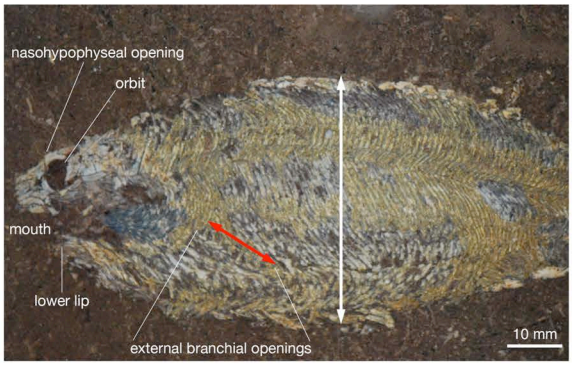

f. Birkeniida gen. et sp. nov.

TABLES

Table 4.1. Comparison of hypotheses about the evolutionary precursor of synovial diarthrosis at the jaw joint. Predictions are different under two potential evolutionary scenarios (***a***: co-option of a structure with conserved gene interactions; ***b***: co-option of genetic programs to replace a proposed precursor tissue with a jaw joint). L = lampreys; Z = zebrafish. Mucocart.- mucocartilage.

	Phenomenon to test	***a***. Structure co-opted	***b***. Program co-opted
Muscular Scaffolds	Expression: *Nkx3.2* (L)	Present in muscles	Absent in muscles
	Expression: Potential *Nkx3.2* targets (L)	Present in muscles	Present in muscles
	Expression: *BarxA* (L)	No overlap with *Nkx3.2*	—
	Nkx3.2 knockouts (L)	Muscle defects	No muscle defects
	BarxA knockouts (L)	Muscle defects	No muscle defects
	Nkx3.2 knockouts (Z)	Muscular phenotypes	No muscular phenotype
	Expression of targets in *nkx3.2* knockouts (Z)	Lamprey-like	Non-lamprey-like
	Distribution of structure in stem gnathostomes	Jawless	Jawless + jawed

	Phenomenon to test	***a***. Structure co-opted	***b***. Program co-opted
Mucocartilage	Expression: *Nkx3.2* (L)	Present in mucocart.	Absent in mucocart.
	Expression: Potential *Nkx3.2* targets (L)	Present in mucocart.	Present in mucocart.
	Expression: *BarxA* (L)	No overlap with *Nkx3.2*	—
	Nkx3.2 knockouts (L)	Mucocart. defects	No mucocart. defects
	BarxA knockouts (L)	Mucocart. defects	No mucocart. defects
	Nkx3.2 knockouts (Z)	Chondroblasts	—
	Expression of targets in *nkx3.2* knockouts (Z)	Lamprey-like	Non-lamprey-like
	Distribution of structure in stem gnathostomes	Jawless	Jawless + jawed
Intercartilaginous Blood Sinus	Expression: *Nkx3.2* (L)	Present in velar sinus	Absent in velar sinus
	Expression: Potential *Nkx3.2* targets (L)	Present in velar sinus	Present in velar sinus
	Expression: *BarxA* (L)	No overlap with *Nkx3.2*	—
	Nkx3.2 knockouts (L)	Velar defects	Velar defects
	BarxA knockouts (L)	Velar defects	Velar defects
	Nkx3.2 knockouts (Z)	Vascular/circulatory	—
	Expression of targets in *nkx3.2* knockouts (Z)	Lamprey-like	Non-lamprey-like
	Distribution of structure in stem gnathostomes	Jawless	Jawless + jawed

Table 4.2. Patterns of phenotypic variations in sgRNA-injected and non-injected *P. marinus* during 2016 spawning season. Numbers indicate individuals.

	Total *n*	Hooked lateral mouth plate	Long velar cartilage	Dorsal branchial opening
Wildtype (non-injected)	10	1	0	0
Tyr control	6	3	0	0
Nkx3.2 Gr1, Gr2, Gr4	21	10	4	10
Nkx3.2 Gr1	20	10	0	2
Nkx3.2 Gr2	19	12	3	8
Barx Gr1, Gr2, Gr3	32	14	0	0
Barx Gr1	25	0	0	0

4.8 SUPPLEMENTARY INFORMATION

4.8.1 Methods: Bioinformatics

I identified homologues for genes in the sea lamprey *Petromyzon marinus* for genes that fall under the following categories: (***a***) transcription factors related to jaw joint development in gnathostomes (*Nkx3.2*, *Barx1*, *Runx2*); (***b***) transcription and growth factors that are expressed in synovial diarthrosis and are potential target genes of *Nkx3.2* (*Trps1*, *Runx2*, *Scx*, *Irx5/7*, *Gdf6*); and (***c***) effector and receptor genes associated with synovial diarthrosis or vascular patterning (*Col2a1*, *Prg4*, *Vegfr*). Some of these genes were successfully cloned, and some others have not been cloned yet.

4.8.1a Confounding factors for lampreys

The draft genome of *Petromyzon marinus* (Smith et al., 2013) has low coverage, and many genes listed above are not included in this assembly. This is partly due to genome reorganization that occurs during ontogeny (Smith et al., 2010; Sémon et al., 2012) and partly due to multiple factors that confound cloning and scaffolding. Notably, the genome of *P. marinus* has markedly high GC contents (averaged at 61% in protein coding regions and 75% in third codon positions) and an abundance of repeats with high sequence identity (accounting 34.7% of the draft genome) (Smith et al., 2013). These features of the lamprey genome and the incompleteness of the genomic/transcriptomic resources presented formidable challenges to isolating and cloning the listed genes. Published descriptions of gene-expression profiles in lampreys do not always accompany sequence information, and it was often unavailable for various logistical reasons.

To aid in isolating and cloning the listed genes, unpublished transcriptomic datasets (prefix: Trinity) assembled at Marianne E. Bronner's laboratory (California Institute of Technology) were utilized in June 2017. In addition, access was granted to the Dovetail version of the unpublished, new assembly of *P. marinus* genome (Smith et al., unpublished) in late July 2017. These resources were not available for the earlier design of riboprobes and CRISPR sgRNAs. Currently, initial probe designs are being revised.

4.8.1b Nkx3.2

Nkx3.2 is not included in the published draft genome of *Petromyzon marinus* but has been cloned independently in two different lamprey species (*P. marinus* and *Lethenteron camchatsticum*). Two partial coding sequences are available, one each for *P. marinus* (Genbank: EU196403.1; 723 bp) and *L. camchatsticum* (GenBank: AB293607.1; 1012 bp) (Fig. 4.5a). These two partial coding sequences are contiguous over 427 bp, with 94% of that being identical. The sequence information for the description of *Nkx3.2* expression in *P. marinus* (Cerny et al., 2010) did not accompany the original publication, and was not available to the author at the time of writing this chapter. These sequences were cloned at Daniel Meulemans Medeiros's laboratory (University of Colorado, Boulder). They combine to a 1987 bp long transcript with a coding region 1356 bp long (sequence data undisclosed in this thesis; provided to the defense committee). Another transcript was identified in the Trinity transcriptomic database (TRINITY_DN315643_c5_g5_i1; 2735 bp). In the Dovetail version of the *P. marinus* genome assembly, two scaffolds contain *Nkx3.2* cognates (scaf_00015, scaf_00721) but they likely represent an assembly artifact rather than two paralogues. The coding sequences are nearly identical, but the exons were reconstructed differently. Therefore, *Nkx3.2* in *P. marinus* is considered as a single orthologous gene in this chapter.

Comparison among these independently obtained *Nkx3.2* sequences suggests different splice forms of the *Nkx3.2* transcript. Scaf_00015 of the Dovetail assembly contains two exons of *Nkx3.2* set apart by approximately 3 kbp (2894 bp) (Fig. 4.5a). The 250 bp-long 5'end sequence of the *P. marinus* EU196403.1 does not align with the *L. camchatsticum* AB293607.1. The non-overlapping sequences each align to different regions near the 3' end of Exon 1 in Scaf_00015. Detailed information to support this preliminary bioinformatic analysis will be provided upon publication of this chapter, and upon the publication of the Dovetail assembly (unpublished sequence data available to the defense committee).

In the absence of insights into splice variants, a riboprobe was initially designed using the partial coding sequence from *P. marinus* (EU196403.1). The riboprobe sequence straddles the region of splice variant between the exons, and it aligns only to exon 2 in the Trinity Nkx3.2 transcript (TRINITY_DN315643_c5_g5_i1) with its 250 bp-long 5' end not represented in the Trinity transcript. Therefore, the probe is sensitive to splice forms.

The same partial coding sequence (EU196403.1) was used initially to design CRISPR/Cas9 sgRNAs, without information from the Dovetail assembly and assuming that the sequence represents a single coding region (Fig. 4.5a). On the basis of scaf_00015, these sgRNA target sites are close to the 5' end of Exon 2. A forward primer was designed toward the 5' end of EU196403.1 for genotyping these CRISPR target sites — a region that is more than 3 kbp away from the CRISPR target sites on scaf_00015. This accounts for the difficulty of genotyping (see **4.5 Discussion**). Given new information from the Dovetail assembly (July 2017), three CRISPR target sites were re-identified (***a***) in the homeodomain-coding region and (***b***) close to the start codon of the homeodomain-containing Exon 2 (methods discussed under **4.8.2 Methods: CRISPR/Cas9**).

4.8.1c Barx

Similarly, *Barx* is not included in the draft genome of *Petromyzon marinus*. A 522 bp long partial coding sequence from *P. marinus* (Genbank: HQ248098.1) was used to design a riboprobe and identify potential CRISPR target sites. Protein translation indicates that the first 144 bp of HQ248098.1 represents 5' UTR. In the Dovetail assembly, HQ248098.1 aligns to scaf_00022, and the boundary between exons 1 and 2 is adjacent to the 3' end of the homeodomain. Three CRISPR target sites were initially identified close to the start codon of Exon 1. These sites were revised in July 2017 with the Dovetail assembly to reduce the number of potential off targets (methods discussed under **4.8.2 Methods: CRISPR/Cas9**). Due to the presence of a likely paralogue, HQ248098.1 and the Dovetail scaf_00022 are referred to as *BarxA*. This gene is also present in *Lethenteron camchatsticum* (Genbank: AB920564.1; partial coding sequence, 509 bp).

Another *Barx*-like transcript was identified in the transcriptomic dataset of *P. marinus* (TRINITY_DN257460_c0_g1_i1). This 400 bp-long partial coding sequence is referred to as *BarxB*. It aligns with scaf_00065 of the Dovetail assembly of *P. marinus* genome. No riboprobes or CRISPR sgRNAs have been created for this gene.

4.8.1d Trps1

A non-annotated transcript was identified in cDNA resources at Marianne E. Bronner's laboratory using highly conserved sequences of *Trps1* from other vertebrate taxa. This coding sequence aligns identically to scaf_00001 of the Dovetail assembly of *Petromyzon marinus*. The

sequence has repeats and high GC contents, and remains difficult to clone for the purpose of riboprobe synthesis. In addition, several transcripts highly similar to *Trps1* from other vertebrate taxa were identified in the Trinity transcriptomic database (TRINITY_DN310467_c4_g2_i1, TRINITY_DN310467_c4_g3_i1, TRINITY_DN310467_c4_g4_i2).

4.8.1e Runx2

Several cognates exist for *Runx* proteins in *Petromyzon marinus*. Three transcripts have been identified in the Trinity database (TRINITY_DN317163_c0_g1_i1, TRINITY_DN312686_c0_g1_i6, TRINITY_DN174209_c0_g1_i1), with matched scaffolds in the Dovetail assembly (scaf_00050, scaf_00058, scaf_00097) and registered partial coding sequences from *L. camchatsticum* in Genbank (AJM44878.1, AJM44879.1, AJM44886.1). Orthology for these cognates with members of the gnathostome *Runx* family remain unclear.

4.8.1f Scx

Scleraxis (*Scx*) has a patterning role in tendons and ligaments (Murchison et al., 2007; Schweitzer et al., 2010; Sugimoto et al., 2013) so its expression is predicted for a homologue of synovial diarthrosis. This gene has not been cloned. One partial coding sequence recovered from the trace archive of the *Petromyzon marinus* draft genome (GL484724; predicted as same with scaf_00045 in the Dovetail assembly) has nearly 90% congruence with *Scx* from other vertebrate taxa over a 150-200 bp long region. Further work is required to identify *Scx* homologue in *P. marinus* with confidence.

4.8.1g Irx5/7

A single homologue of *Irx5/7* has been identified (scaf_00008 in the Dovetail assembly) and several transcripts with high similarities exist in the Trinity database and the trace archive of the draft genome. The expression of *Irx5/7* appears to be restricted to joints in the hyoid arch, and its knockout phenotypes do not affect the jaw joint (Askary et al., 2015). For these reasons, the gene is of low priority and treated as of secondary interest, set aside in case expression patterns of the other genes depart markedly from predictions of the Hypotheses.

4.8.1h Gdf5/6/7

A complete transcript (Genbank: HQ248100.1) was used to clone and design a riboprobe.

4.8.1i Col2a1

Two approximately 2 kbp-long transcripts were cloned, using the full transcript from *Petromyzon marinus* (Genbank: DQ136024). They are 99% identical to each other and referred to as *Col2a1a* and *Col2a1b*, respectively. *Col2a1* expression patterns have been described previously (Zhang et al., 2006; Sauka-Spengler et al., 2007; McCauley, 2008; Ohtani et al., 2008; Cattell et al., 2011). Unfortunately, due to the lack of published information, references to the two paralogues are unclear, and the designation of two *Col2a1* paralogues may not be consistent across studies.

4.8.1j Prg4

Prg4 is expressed in the articular cartilages in synovial diarthrosis (Askary et al., 2016). A partial transcript was identified in the cDNA resources using highly conserved regions of *Prg4* in other vertebrate taxa.

4.8.1k Vegfr

Vegfr homologue has been identified and cloned by Stephen A. Green (California Institute of Technology). The data are not included in this chapter.

4.8.2 Methods: CRISPR/Cas9

CRISPR target sites (5'-[20N]…NGG-3') were initially identified close to the assumed 5' end of the partial coding sequences of *Nkx3.2* and *BarxA* in lampreys and close to the 5' and 3' ends of the *nkx3.2*-coding sequence in zebrafish, which were also highlighted with low frequencies of potential off-targets (Fig. 4.5a, b). This initial design was revised, respectively, for different reasons. In lampreys, these target sites straddle exon boundaries, and genotyping was highly challenging. The Dovetail assembly of the *P, marinus* genome returned larger numbers of potential offtargets for the initially designed sgRNA sequences. In zebrafish, the success rates were low, and a complete truncation of *nkx3.2* homeodomain was unlikely.

The revised scheme to identify CRISPR target sites focused on homeodomains (Fig. 4.5a, b), and follows the accepted guideline: (***a***) 50-80% GC content; and (***b***) no off-target matches to

the current genome assembly showing more than 80% similarity, or with fewer than three mismatches in the ten bases proximal to the PAM sequence (Square et al., 2015a). In *Nkx3.2* of lampreys, one target sequence was identified 23 bp away from the start codon of Exon 2, and two sites in the homeodomain (3 bp away from the 5' start of homeodomain; 92 bp away from the 5' start of homeodomain). In zebrafish, these resulted in five target sites flanking the homeodomain. The sgRNA design was similarly modified for *BarxA* of lampreys. Due to the low availabilities of embryos during the 2017 spawning season, however, these revised sgRNAs for *BarxA* were never injected. For sgRNA sequences, see Supplementary Information.

sgRNAs were generated following the published protocol (Gagnon et al., 2014). To synthesize sgRNAs, HiScribe™ T7 RNA Synthesis Kit (NEB: E2040) was used for lampreys and MegaScript™ SP6 Transcription Kit (Ambion: AM1330) for zebrafish. The RNAs were precipitated in ammonium acetate solution, suspended in UltraPure™ H_2O, and stored in 2-3 µl aliquots at -80 ˚C. For injection, sgRNA(s) were diluted to 400-600 ng/µl, with 1 µl mixed with 1 µl aliquot of Cas9 nuclease from *Streptococcus pyogenes* (NEB: #M0646) at 1 µg/ml. In lampreys, this solution was mixed with 1 µl of dextran aliquot (see **4.8.3 Methods: Lampreys**) and 2 µl of ddH_2O. In zebrafish, it was mixed with 3 µl of 0.2M KCl, 0.2 % phenol red, and ddH_2O. The final injection volume per embryo was approximately 5 nl, with 400-600 pg sgRNA and 1 ng Cas9 nuclease. For control, the published sgRNA designs for *Tyr* were used in lampreys, which can be detected by reduction of pigments (Square et al., 2015a). For zebrafish, GFP 5'GA was used at the stage (P_0) when ubi:switch/RH+AB was crossed, which can be phenotyped by reduction of ubiquitous GFP in the progenies with dsRed expression in heart (information available from A. Phil Oel and W. Ted Allison, the University of Alberta).

4.8.3 Methods: Lampreys

Mature males and females of the sea lamprey *Petromyzon marinus* were obtained from Hammond Bay Biological Station and artificially spawned following published protocols (Nikitina et al., 2009). Fertilized eggs were kept in Sparkletts® water overnight at 18 ˚C and transferred to 0.1x MMR (Marc's Modified Ringer's: 11.0 mM NaCl; 0.2 mM KCl; 0.1 mM $MgCl_2$; 0.2 mM Ca Cl_2; 0.2 mM $NaHCO_3$; 0.5 mM Hepes pH 7.8) at 18 ˚C. Staging of the embryos follows Tahara (1988). Embryos were fixed in MEMFA (0.1 M MOPS, pH 7.4; 2.0 mM

EGTA; 1.0 mM $MgSO_4$; 3.7% formaldehyde) overnight at -20 ˚C and transferred into 100% EtOH for storage at -20 ˚C.

Cas9 and sgRNAs were injected between 2.0 hours post fertilization (hpf) and first cleavage, with Fluorescein isothiocyanate–dextran solution (Sigma 46945) as a tracer. Embryos that were dead or without dextran fluorescence were removed at 24 and 36 hpf. As injected lamprey embryos are sensitive to vibration and rolling, viable embryos were transferred individually to 94 well plates filled with 0.1x MMR before gastrulation. Embryos were recovered from the plates into a dish of fresh 0.1x MMR around Tahara's stage (T-) 23. They continued to be incubated at 18 ˚C. Sampled embryos were photographed and processed for genotyping by extracting genomic DNA and amplifying the regions containing target sites for sequencing.

Alcian blue staining of cartilages followed available protocols (Martin et al., 2009; Jandzik et al., 2014). Histological sections were made either in paraffin blocks or with a cryostat. For paraffin sectioning, embryos were washed in grading solutions of Histosol® from 100% EtOH to Histosol® to paraffin. The sections were stained with hematoxylin and eosin. For cryosectioning, the embryos were dehydrated in 5% and 15% sucrose overnight, incubated in 7.5% gelatin, and flash-frozen in gelatin by liquid nitrogen (stored at -80 ˚C). After sectioning, the slides were washed in PBS at 37 ˚C to remove gelatin, washed in ddH_2O to remove salt, and dehydrated through EtOH series. Genomic DNA was extracted by incubating tissues in 0.05 M NaOH at 95 ˚C for 15 minutes, followed by addition of 5-10 % volume of 1.0 M Tris-HCl buffer pH 8.0.

For riboprobe synthesis, plasmids were linearized using SP6- or T7-specific restriction enzymes (NotI or Spe1; depending on directions of cloned sequences) and purified through precipitation by sodium acetate solution. Sp6- or T7- RNA polymerases (M0207, M0251, New England Biotechnology) were used to synthesize the probes, depending on the promoters and following the standard protocol. The products were precipitated in ammonium acetate solution and resuspended in UltraPure™ H_2O. *In situ* hybridization followed the published protocol partly (Nikitina et al., 2009) or the protocol developed for hemichordates by Christopher J. Lowe (Hopkins Marine Station, Stanford University) and Stephen A. Green (California Institute of Technology) mostly. To reduce probe trapping, embryos were perforated at the level of the second to fourth pharyngeal arch and incised along the ventral midline across endostyle. Embryos were rehydrated through a graded series of PBST, digested in 20 μg/ml Proteinaise K for 10

minutes, incubated in 0.25% acetic anhydride in 0.1 M triehanolamine, refixed in 5 % formaldehyde, and incubated in hybridization buffer (100 μg/ml heparin; 1x Denhardt's solution; 5x SSC; 0.1% Tween; 5 mM EDTA; 50% formamide; 1 mg/ml tRNA in DEPC H_2O). Hybridization lasted from overnight to four days at 70 ˚C, with 10-50 ng/ml probe concentration. After a series of washes through 2x and 0.2x SSC, embryos were rinsed in MABT several times, blocked in 2% blocking agent/MABT solution overnight at 4 ˚C, and incubated with antibody solution (1:1500 antibody for DIG probes) overnight at 4 ˚C. Following rinsing in MABT and AP buffer, embryos were incubated in chromogenic solution. The chromogenic reaction was halted by several MABT rinses. Embryos were postfixed through a graded series of EtOH/MABT to 100% MeOH and 1:1 37% formaldehyde:MABT overnight at room temperature and stored in 100% MeOH at -20 ˚C.

4.8.4 Methods: Zebrafish

Fertilized eggs were collected from crossings of wildtype parents (AB/Wik, AB, and UA3140 ubi:switch/AB+RH). Embryos were incubated at 28 ˚C, and treated with 0.003% PTU (1-phenyl-2-thiourea) in 10% Hank's saline starting at 24 hpf. Larvae were introduced to the nursery at 1 week to 10 dpf. Genomic DNA was extracted from clipped fins of 3-5 dpf larvae or from adults, following the same protocol as lampreys (see **4.8.3 Methods: Lampreys**). The preserved tissues, embryos, larvae, and adults were all fixed in 4% PFA, and stored in 100% EtOH or MeOH at -20 ˚C except for adults (preserved in 70% EtOH at 4˚C).

Cas9 and sgRNAs for *nkx3.2* and GFP GA5' were injected between fertilization and first cleavage to fertilized eggs collected from the crossing of UA3140 ubi:switch/AB+RH and AB. At 3 dpf, injected larvae were sorted for reduced expression of ubiquitous GFP and the presence of red fluorescent heart. These larvae provided the P_0 population. At the adult stage, sorted individuals were in-crossed, and progenies from each cross was subjected to High Resolution Melt (HRM) analysis for genotyping, using MeltDoctor™ and following the protocols attached to the reagent. The HRM analysis did not provide conclusive results to identify *nkx3.2* mutants. Sequencing of genomic DNA extracted from fin clips of the P_0 adults identified a female with a 20 bp deletion to the homeodomain-coding region of *nkx3.2* (UA5011). The deleted sequence included one XmaI (NEB: R01805) restriction site and thus allowed genotyping by RFLP analysis. The P_0 female carrying this mutation was crossed to the *sox10*:GFP transgenic line, and

progenies were sorted at 3 dpf for the presence of *sox10*:GFP expression and the absence of the two markers (ubiquitous GFP expression and red fluorescent heart), and fin-clipped to extract genomic DNA at that stage, or at the adult stage. UA5011 heterozygotes were identified by both sequencing and RFLP analysis, representing the F_1 population. The F_1 heterozygotes were incrossed for F_2 embryos, which were genotyped by RFLP analysis and phenotyped at 4 dpf by identifying *sox10*:GFP-positive chondrocytes, staining cartilages using alcian blue, and immunostaining collagen II for confocal imaging. The homozygous UA5011 larvae were reared with a strictly small-grained diet to the adult stage. The F_1 UA5011 heterozygotes were also out-crossed to *flk*:mCherry and *gata1*:dsRed transgenic lines to test for vascular/circulatory phenotypes. In addition, the *gdf6a* heterozygotes (DuVal et al., 2014) were out-crossed to the *sox10*:GFP transgenic line to test whether *gdf6a*$^{-/-}$ replicate *nkx3.2* phenotypes, given that *gdf6a* is a predicted target gene of *nkx3.2* (Miller et al., 2003).

Alcian blue staining of cartilages partly followed the protocol provided by Michael Shapiro (University of Utah). Four-dpf larvae fixed in 4% PFA were rinsed with ddH_2O and transferred to 70% EtOH. Once equilibrated, larvae were immersed in alcian blue solution (0.167 mg/ml alcian blue; 15% acetic acid; 70% EtOH), rinsed through EtOH/ddH_2O series, and washed in a saturated sodium borate solution. Specimens were immersed in trypsin solution (0.125% trypsin; 30% sodium borate) overnight, washed in 1% KOH solution, bleached in 0.15% H_2O_2 0.1% KOH, 25% glycerol solution, immersed through a 1% KOH/glycerol graded series into 100% glycerol for storage. Immunostaining followed the published protocol (DuVal et al., 2014), using collagen II antibody purchased from Developmental Studies Hybridoma Bank (II-II6B3), DAPI nuclear stain (Invitrogen: D1306), and endogenous *sox10:GFP* expression. Morpholinos were used to replicate knockdown phenotypes previously reported for *nkx3.2* (Miller et al., 2003). Morpholino injections were made between fertilization and first cleavage. The oligonucleotide purchased from Gene Tools, Inc. (5'-GCGCACAGCCATGTCGAGCAGCACT-3') follows the previously published *nkx3.2* MO1 (Miller et al., 2003). Oligonucleotides were diluted to 25 mg/ml in Milli-Q® H_2O for storage at room temperature, and diluted further in 0.2 M KCl and 0.2% phenol red. The injected volume was 5-10 nl.

4.8.5 CRISPR Target Sites

4.8.5a Lamprey: Nkx3.2 *(2016 spawning season)*

2017_Gr1	CCTCGACCAAGGATCAGTGCCCT
2017_Gr2	ACCCGTCTCTCCCTTGAGAGCAC
2017_Gr4	CCCTGACTTCTCTATCGAGGATC

4.8.5b Lamprey: Nkx3.2 *(2017 spawning season)*

2017_Hom1	CCGCGCAAGAAGCGCTCCCGCGC
2017_Hom14	CCCCGAGCGGGCCGACCTGGCCG
2017_Gr1	TGAGTCTGTCCCCGGAGGCGGGG

4.8.5c Lamprey: BarxA *(2016 spawning season)*

2016_Gr1	GCGTGACAAACAATCGGAAAAGG
2016_Gr2	GCGAGTGCGTGACAAACAATCGG
2016_Gr3	GAATTCACGTCGCGGTCGCGAGG

4.8.5d Lamprey: BarxA *(2017 spawning season)*

2017_Hom1	CCCCGTAGGATCGATCTTGCCGA
2017_Hom2	CCAGGTGAAGACTTGGTACCAGA
2017_Gr1	CCGACTCGGGCCCAGCCAACCTT

4.8.5e Zebrafish: nkx3.2

Exon1_gRNA1	GATGGCGAGACTCCTCTTTT
Exon1_gRNA2	AAGAACTACGATTCCGACTC
Exon1_gRNA3	GGATCAGCAATCCGCGGCCA
Homeo1	GGCGGCCATCTGACGTCGCT
Homeo2	GGCTGACGCCAGCAGATCGG
Homeo3	AAGCAGCGGAAGAAGCGCTC
Homeo4	GAGCGCTTCTTCCGCTGCTT
Homeo5	GGCCGCGTTCTCCCACGCGC

4.8.6 Primers For Genotyping

4.8.6a Lamprey: Nkx3.2 *(2016 spawning season)*

Fwd: CAACGAGTGTTGCTGTCTGT

Rev: ACCTGGGTCT CCGTGAGTTT

4.8.6b Lamprey: Nkx3.2 *(2017 spawning season)*

Fwd1: AGTGCCCTGGCTCCTCTATT

Fwd2: GAGAGCACTGGCTCCTCTGTA

Rev: GGTCTTGTAGCGTCGGTTCT

4.8.6c Zebrafish: nkx3.2

Fwd: GGACGAGACGGATCAGGAATC

Rev: CACTCGGCGTGTTCGGTAAA

4.8.7 Registered Coding Sequences

Supplementary sequence files are available at a Dataverse depository (doi:10.7939/DVN/JGSPJN) or on a disc attached to the back of this thesis (print version).

4.8.7a Nkx3.2

Zebrafish / *nkx3.2*/ Genbank: BC159241.1

V_4-01_zebrafish_nkx3.2_BC159241.1

Petromyzon marinus / *Nkx3.2* / Genbank: EU196403.1

V_4-02_Pmarinus_Nkx3.2_EU196403.1

Lethenteron camchatsticum / *Nkx3.2* / GenBank: AB293607.1

V_4-03_Lcamchat_Nkx3.2_AB293607.1

4.8.7b Barx

Petromyzon marinus / *BarxA* / Genbank: HQ248098.1

V_4-04_Pmarinus_BarxA_HQ248098.1

Lethenteron camchatsticum / *BarxA* / Genbank: AB920564.1

V_4-05_Lcamchat_BarxA_AB920564.1

4.8.7c Runx

Lethenteron camchatsticum / *RunxA* / GenBank: AJM44878.1

V_4-06_Lcamchat_RunxA_AJM44878.1

Lethenteron camchatsticum / *RunxB* / GenBank: AJM44879.1

V_4-07_Lcamchat_RunxB_AJM44879.1

Lethenteron camchatsticum / *RunxC* / GenBank: AJM44886.1

V_4-08_Lcamchat_RunxC_AJM44886.1

4.8.7d Scx

Petromyzon marinus / *Scx* / GL484724 (scaffold of draft genome assembly)

V_4-09_Pmarinus_Scx_GL484724

4.8.7e Gdf5/6/7

Petromyzon marinus / *Gdf5/6/7* / Genbank: HQ248100.1

V_4-10_Pmarinus_Gdf567_HQ248100.1

4.8.7f Col2a1

Petromyzon marinus / *Col2a1* / Genbank: DQ136024

V_4-11_Pmarinus_Col2a1_DQ136024

4.8.8 Transcriptomic Sequences from *Petromyzon marinus*

Supplementary sequence files are available at a Dataverse depository (doi:10.7939/DVN/JGSPJN) or on a disc attached to the back of this thesis (print version).

4.8.8a Nkx3.2

TRINITY_DN315643_c5_g5_i1

W_4-01_Pmarinus_Nkx3.2_DN315643

4.8.8b BarxB

TRINITY_DN257460_c0_g1_i1

W_4-02_Pmarinus_BarxB_DN257460

4.8.8c Trps1

trps1-201 cdna:KNOWN_BY_PROJECTION_protein_coding

W_4-03_Pmarinus_trps1-201

TRINITY_DN310467_c4_g2_i1

W_4-04_Pmarinus_Trps1_DN310467c4g2

TRINITY_DN310467_c4_g3_i1

W_4-05_Pmarinus_Trps1_DN310467c4g3

TRINITY_DN310467_c4_g4_i1

W_4-06_Pmarinus_Trps1_DN310467c4g4

4.8.8d Prg4

TRINITY_DN100665_c0_g1_i1

W_4-07_Pmarinus_Prg4_DN100665

TRINITY_DN305732_c0_g2_i1

W_4-08_Pmarinus_Prg4_DN305732c0g2

TRINITY_DN305732_c0_g1_i1

W_4-09_Pmarinus_Prg4_DN305732c0g1

4.8.8e Runx

TRINITY_DN317163_c0_g1_i1

W_4-10_Pmarinus_Runx_DN317163c0g1

TRINITY_DN312686_c0_g1_i6

W_4-11_Pmarinus_Runx_DN312686

TRINITY_DN174209_c0_g1_i1

W_4-12_Pmarinus_Runx_DN174209

TRINITY_DN317163_c0_g1_i1

W_4-13_Pmarinus_Runx_DN317163c0g1

4.8.9 Cloned Sequences and Probes for Lampreys

Supplementary sequence files are available at a Dataverse depository (doi:10.7939/DVN/JGSPJN) or on a disc attached to the back of this thesis (print version).

4.8.9a Nkx3.2

X_4-01_Pmarinus_Nkx3.2

4.8.9b BarxA

X_4-02_Pmarinus_BarxA

4.8.9c Gdf5/6/7

X_4-03_Pmarinus_Gdf567

4.8.9d Prg4

X_4-04_Pmarinus_Prg4

4.8.9e Col2a1a

X_4-05_Pmarinus_Col2a1a

4.8.9f Col2a1b

X_4-06_Pmarinus_Col2a1b

4.8.9g Irx5/7

X_4-07_Pmarinus_Irx57

4.8.10 Scaffolds of the Genome Assembly for *Petromyzon marinus*

Sequence information for scaffolds of the Dovetail Assembly of the genome of *Petromyzon marinus* (Smith et al., unpublished) is available from the author upon request. In this thesis, BLASTN outputs are provided. Supplementary files are available at a Dataverse depository (doi:10.7939/DVN/JGSPJN) or on a disc attached to the back of this thesis (print version).

4.8.10a Nkx3.2

Y_4-01_BLASTN_Dovetail_Nkx3.2

4.8.10b BarxA

Y_4-02_BLASTN_Dovetail_BarxA_HQ248098.1

Y_4-03_BLASTN_Dovetail_BarxA_AB920564.1

4.8.10c BarxB

Y_4-04_BLASTN_Dovetail_BarxB_ DN257460

4.8.10d Trps1

Y_4-05_BLASTN_Dovetail_Trps1_trps1-201

4.8.10e Runx2

Y_4-06_BLASTN_Dovetail_Runx_DN317163

Y_4-07_BLASTN_Dovetail_Runx_DN312686

Y_4-08_BLASTN_Dovetail_Runx_DN174209

Y_4-09_TBLASTN_Dovetail_Runx_AJM44878.1

Y_4-10_TBLASTN_Dovetail_Runx_AJM44879.1

Y_4-11_TBLASTN_Dovetail_Runx_AJM44886.1

4.8.10f Scx

Y_4-12_TBLASTN_Dovetail_Scx_ConservedDomain

Y_4-13_TBLASTN_Dovetail_Scx_Danio_ NP_001076538.2

4.8.10g Irx5/7

Y_4-14_BLASTN_Dovetail_Irx57_cDNA201

4.8.11 Sequences for Genotyping

Full sequence information for each genotyping experiment is available from the author upon request. Supplementary sequence files are available at a Dataverse depository (doi:10.7939/DVN/JGSPJN) or on a disc attached to the back of this thesis (print version).

4.8.11a Zebrafish / nkx3.2

Z_4-01_Zebrafish_CRISPR_nkx3.2_genotypes

4.8.11b Lamprey / Nkx3.2

Z_4-02_Pmarinus_CRISPR_nkx3.2_genotyping_August17_2017

*Zip archive of sequence files from one genotyping experiment from August 17, 2017.

4.8.12 Protocol for *In Situ* Hybridization

Supplementary file is available at a Dataverse depository (doi:10.7939/DVN/JGSPJN) (PDF version) or on a disc attached to the back of this thesis (print version).

Suppl. 4.1: Protocol for *in situ* hybridization for lampreys (developed by Stephen A. Green, California Institute of Technology).

Chapter 5
Conclusions: Early Vertebrate Supertrees as a Platform for an Extensive Character Analysis

> A complete system is made clear to us by a bit of mosaic,
> just as a whole past order of things is implied by the skeleton of an ichthyosaur.
>
> — *La Recherche de l'Absolu*, Honoré de Balzac

5.1 SUMMARY OF QUESTIONS GENERATED

Phylogeny underpins all questions in evolutionary biology. From the ancestral state of vertebrate development (Chapter 1), to interrelationships among cyclostomes (Chapter 2), to reconstruction of life history modes in early vertebrate lineages (Chapter 3), to the evolutionary origins of the jaw and jaw joint (Chapter 4 and Appendix I), phylogenetic trees provide the basis at every step of a dialectic spiral of generating, testing, and synthesizing hypotheses. However, phylogeny-based hypothesis testing is not only about questions of tree topology. It is intimately linked to evolutionary patterns of characters fitted to the best-supported trees. Cyclostome monophyly versus paraphyly has remained a central debate of early vertebrate phylogeny since the proposal of the Agnatha-Pisces dichotomy (Cope, 1889), but this Cyclostome Problem did not assume such importance just because it concerns the basic systematic scheme of vertebrates. The Problem has compelled numerous analyses[1] because it has profound implications for: (***a***) whether or not embryonic traits in hagfish and lampreys represent the primitive state of vertebrate development (Chapter 1); (***b***) how relevant cyclostomes and stem gnathostomes each are to

[1] These past analyses may be categorized into pre-cladistic classifications (Kiaer, 1924; Stensiö, 1927, 1932, 1958; Romer, 1945; Obruchev, 1964; Halstead, 1973); cladistics using selected morphological traits (Løvtrup, 1977; Janvier, 1978, 1981, 1984, 1996b; Janvier and Blieck, 1979; Hardisty, 1982; Forey, 1984; Yalden, 1985; Forey and Janvier, 1993; Gagnier, 1993b; Forey, 1995); quantitative cladistics using phenotypic datasets (Maisey, 1986, 1988; Janvier, 1996b; Donoghue et al., 2000; Donoghue and Smith, 2001; Gess et al., 2006; Khonsari et al., 2009; Sansom et al., 2010b; Turner et al., 2010; Conway Morris and Caron, 2014; Gabbott et al., 2016; Keating and Donoghue, 2016; Sallan et al., 2017); and quantitative cladistincs using molecular datasets (Stock and Whitt, 1992; Mallatt and Sullivan, 1998; Kuraku et al., 1999; Delarbre et al., 2000, 2002; Winchell et al., 2002; Takezaki et al., 2003; Blair and Hedges, 2005; Kuraku and Kuratani, 2006; Mallatt and Winchell, 2007; Yu et al., 2008; Near, 2009; Heimberg et al., 2010).

reconstructing vertebrate synapomorphies (Chapter 2); (***c***) whether a larval lamprey provides a recapitulatory model of primitive vertebrates or an inference for radical life history evolution that resulted in extensive convergence with invertebrate chordates (Chapter 3); and (***d***) to what extent cyclostomes may be considered as a surrogate for a suite of traits that existed prior to the origin of the jaw (Chapter 4 and Appendix I). The phylogeny of crown and stem gnathostomes has also generated numerous parallel questions, with placoderms, stem chondrichthyans, and stem osteichthyans swapping and collapsing different internal nodes in every new analysis[2]. Even then, differences in the proposed interrelationships would be of little interest without characters to map onto the trees. Tree topology is therefore a backdrop to develop and address questions regarding character evolution.

Despite intensive research, two interrelated problems persist: (***a***) tree topology is prone to be unstable, partly because of asymmetries in the distribution of unambiguous homologies (creating few robustly supported nodes, long branches, and numerous weakly supported internal nodes) (Janvier, 1996a, 2007, 2008; Brazeau and Friedman, 2014; Janvier, 2015; Miyashita, 2016) and partly because of non-random loss of characters (leading to loss of phylogenetic signals) (Sansom et al., 2010b, 2011, 2013a; Sansom, 2015; Sansom and Wills, 2013); and (***b***) only a small number of characters are systematically useful across early vertebrate phylogeny, because most characters vary within a subset of early vertebrate taxa or may even be inapplicable outside that subset, and because soft-tissue characters are inherently underrepresented (a case study of these confounding factors is presented in Chapter 2). To complicate the matter further, molecular inferences cannot help with this problem beyond recovering a handful of crown nodes. The crown node of vertebrates (or 'craniates') is among the deepest nodes (>550 MYA) that can be adequately addressed with morphological characters (Janvier, 2008, 2015). Thus, crown-group members of the three lineages extending close to this node — myxinoids, petromyzontiforms, and gnathostomes — each have a long stem populated by a grade of morphologically disparate forms. It is along these stems and among the stem lineages that many key traits of vertebrates such as neural crest, jaw, and paired fins evolved.

[2] Zhu et al., 2001, 2009, 2013, 2016a; Johanson, 2002; Zhu and Yu, 2002; Zhu and Ahlberg, 2004; Brazeau, 2009; Friedman and Brazeau, 2010; Davis et al., 2012; Brazeau and Friedman, 2014, 2015; Dupret et al., 2014; Pradel et al., 2014; Giles et al., 2015, 2017; Long et al., 2015; Lu et al., 2016; Qiao et al., 2016; Coates et al., 2017; King et al., 2017.

Herein, I revisit fundamental questions generated by Chapters 1-4 and other synthetic reviews of early vertebrates. Then, I outline an analytical scheme to address these questions by grouping cladistic characters into anatomical, functional, and developmental categories. The key, unanswered questions include:

- Is character evolution modular among early vertebrates, or do characters co-vary significantly between different cell lineages, body parts, tissue types, or functional contexts?
- Do rates of character evolution remain stable overall, or do asymmetric distributions* of synapomorphies reflect significantly accelerated or decelerated rates of character change? (*Disproportionately higher density of changes constrained to just a handful of nodes; e.g., crown vertebrate node versus the least inclusive node of *Euphanerops* + other gnathostomes; Chapter 2)
- What are the impacts of key novel traits (such as neural crest, jaw, and paired fins) on rates, magnitudes, and directions of state change in other characters?
- Are any categories of morphological characters more predisposed to homoplasies than others?
- Do characters co-vary more strongly among structures that express the same gene than those that do not?
- Do seemingly 'primitive' lineages (e.g., cyclostomes, chondrichthyans) have slower rates of character change overall, or do faster rates of character change result in convergence with outgroups? Are suites of characters in lineages linked to state changes in particular categories of characters?

These questions are not exhaustive, and remain largely unanswered. They have been addressed quantitatively in a small subset of taxa and characters (Sansom, 2009a; Anderson et al., 2011; Sansom et al., 2015; Larouche et al., 2017; Sansom and Wills, 2017) and discussed qualitatively to a much greater extent[3]. But no single published dataset is adequate to explore them over such

[3] Maisey, 1986; Smith and Hall, 1990; Gans, 1993; Forey, 1995; Gee, 1996; Janvier, 1996b, 2007; Chen et al., 1999; Donoghue, 2002; Donoghue and Sansom, 2002; Sire and Huysseune, 2003; Donoghue et al., 2006, 2008a; Kuratani and Ota, 2008; Hall, 2009, 2015; Sire et al., 2009; Rücklin et al., 2012; Trinajstic et al., 2013, 2014; Brazeau and Friedman, 2015; Green et al., 2015; Qu et al., 2015; Donoghue and Rücklin, 2016; Kuratani et al., 2016; Miyashita, 2016.

great breadths of morphological disparity and taxonomic diversity. Typically, datasets addressing interrelationships of jawless vertebrate lineages (cyclostomes and stem gnathostomes) sample shallowly for characters that could resolve the topology within each of major lineage[4]. On the other hand, datasets focused on relationships within individual lineages do not overlap each other in character sampling[5]. Merging these datasets collapses weakly supported nodes both within and among the major lineages (T.M., pers. obs.).

Among jawed vertebrates, most characters do not overlap with the 'jawless' grade of vertebrates. Some tree topologies have been consistent overall from one analysis to another (e.g., placoderm paraphyly, stem chondrichthyan status of acanthodians) but only weakly supported — and thus unstable — in many of them (Brazeau, 2009; Davis et al., 2012; Zhu et al., 2013, 2016a; Dupret et al., 2014; Giles et al., 2015; Long et al., 2015; Qiao et al., 2016). So placoderm monophyly is within several steps of the shortest trees, or even shorter than paraphyly in one dataset (King et al., 2017). As the character set has changed little, the analyses are likely sensitive to the unforeseen character combinations introduced by new taxa added to the dataset or by taxa with modified codings. As in jawless stem gnathostomes, increased sampling of terminal taxa nested within various placoderm or acanthodian branches will not reinforce overall topology; it will likely undermine the support that currently exists for the stems of gnathostome clades.

To circumvent the unrealistic task of generating sufficiently resolved and reasonably supported trees of early vertebrates with a single comprehensive dataset, I present in this chapter supertrees of early vertebrates as a platform for future character analyses. A supertree approach offers several advantages over a conventional phylogenetic analysis. Character and taxon sampling need not overlap extensively from one subset to another (Bininda-Emonds et al., 2002). Tree topology reflects areas of consensus and preserves tree structure supported by individual subsets of data (Bininda-Emonds, 2004a). Previously published datasets can be utilized, and they form the basis for character analyses (Bininda-Emonds, 2004b). Therefore, a supertree frees the

[4] Janvier, 1984, 1996a; Gagnier, 1993; Donoghue et al., 2000; Donoghue and Smith, 2001; Gess et al., 2006; Heimberg et al., 2010; Sansom et al., 2010b; Turner et al., 2010; Conway Morris and Caron, 2014; Gabbott et al., 2016; Keating and Donoghue, 2016; McCoy et al., 2016; Sallan et al., 2017.

[5] Janvier, 1984; Fernholm, 1998; Gill et al., 2003; Wilson and Märss, 2004, 2009; Zhu and Gai, 2007; Blom, 2008, 2012; Donoghue et al., 2008b; Sansom, 2008, 2009b; Renaud et al., 2009; Scott and Wilson, 2012, 2015; Fernholm et al., 2013; Lundgren and Blom, 2013; Mallatt and Holland, 2013; Potter et al., 2015; Randle and Sansom, 2017a, 2017b.

analysis from the challenging task of constructing a comprehensive dataset across the lineages with high morphological disparity and taxic diversity. Conversely, insights gained from character mapping on a supertree can be utilized to construct such a dataset in the future.

Conveniently, multiple areas of early vertebrate phylogeny have been converging toward an overall consensus topology. Cyclostomes are inferred to form a clade based on molecular data (Near, 2009; Heimberg et al., 2010; Janvier, 2010), and this clade was as close as two steps away from the shortest trees based on recent morphological datasets. At present, the most recent revision of the continually updated dataset supports cyclostome monophyly under both maximum parsimony and Bayesian inferences (Chapter 2). Interrelationships of stem gnathostomes supported by these datasets are consistent overall from one analysis to another. These analyses disagree about: (***a***) the placement of conodonts and other putative cyclostomes; (***b***) positions of anaspids versus heterostracomorphs (arandaspids, astraspids, and heterostracans); and (***c***) the order of galeaspids, pituriaspids, and osteostracans along the stem leading to jawed vertebrates. But these differences are considered minor (discussed in more detail in **5.2 Methods**).

The phylogeny of jawed vertebrates has been continuously refined with additions of new taxa and characters. Most of these analyses agree that: (***a***) placoderms form a stem assemblage with respect to the crown node of gnathostomes; (***b***) acanthodians represent a grade of stem chondrichthyans; and (***c***) various primitive osteichthyans fall along the stems of actinopterygians and sarcopterygians while leaving the stem of osteichthyans relatively unoccupied[6]. Minor differences in topology are mainly attributed to taxa where large proportions of characters are missing, except for the placement of *Guiyu* and its relatives (Qiao et al., 2016). Perhaps the most acute point of disagreement is the status of placoderms. At least one recent dataset found support for 'placoderms' as a clade rather than a grade (King et al., 2017), and similar trees are explored concurrently. But even in these recent analyses, *Entelognathus*, *Janusiscus*, and *Qilinyu* tend to be nested outside as successive stem taxa leading to crown gnathostomes. Therefore, placoderm interrelationships should be viewed not so much in light of the monophyly versus paraphyly dichotomy (which inevitably induces a semantic discussion of what constitutes 'placoderms') but rather as in a continuum of alternative topologies. Specific relationships of placoderm clades

[6] Zhu et al., 2001, 2009, 2013, 2016a; Johanson, 2002; Zhu and Yu, 2002; Zhu and Ahlberg, 2004; Brazeau, 2009; Friedman and Brazeau, 2010; Davis et al., 2012; Brazeau and Friedman, 2014, 2015; Dupret et al., 2014; Pradel et al., 2014; Giles et al., 2015, 2017; Long et al., 2015; Lu et al., 2016; Qiao et al., 2016; Coates et al., 2017; King et al., 2017.

differ markedly even among the analyses supporting paraphyletic placoderms (Johanson, 2002; Brazeau, 2009; Davis et al., 2012; Zhu et al., 2013, 2016a; Dupret et al., 2014; Giles et al., 2015; Long et al., 2015; Lu et al., 2016; Qiao et al., 2016). Whether they form a clade or not, 'placoderms' (as recognized morphologically) are still likely stem gnathostomes. So, the major questions remain focused on interrelationships among major placoderm lineages (acanthothoracids, antiarchs, arthrodires, brindabellaspidids, petalichthyiids, phyllolepids, pseudopetalichthyiids, ptyctodonts, rhenanids, *Stensioella*, and osteichthyan-like forms including *Entelognathus*, *Janusiscus*, and *Qilinyu*) and successive outgroups of crown gnathostomes.

The goal of the supertree analysis presented here is to establish a platform on which to address the questions about evolutionary patterns of characters in early vertebrates. It is not to present an optimized tree topology for these taxa. High degrees of resolution in tree topology were not a priority, and polytomies were tolerated within each of the major lineages insofar as character changes can be mapped reasonably among internal nodes (e.g., the polytomy of scolenaspidids, superciliaspidids, and zenaspidids). Therefore, patterns of character evolution as mapped onto the supertree should be robust to minor modifications of tree topology. This expectation will be tested using two radically different phylogenetic hypotheses of placoderms (Zhu et al., 2016a; King et al., 2017).

5.2 METHODS

5.2.1 Supertrees

Two supertrees (ST1 and ST2) were generated with nearly identical sets of source trees. The only difference in the source trees concerns the topology in stem gnathostomes: the latest version of placoderms as a stem assemblage (ST1; Zhu et al., 2016a) or a revision that supported most placoderms as a sister group to the clade of *Entelognathus* + crown gnathostomes (ST2; King et al., 2017). This was done to test the robustness of inferred character changes against markedly different topologies. I constructed two supermatrices using the matrix representation method (Bininda-Emonds et al., 2002; Bininda-Emonds, 2004b, 2004a). For example, each node in one tree was entered as a column ('character') in the supermatrix and the states for that 'character' scored as 'present' for all taxa inferred to descend from that node but 'absent' for all other taxa in the tree. This was repeated for all nodes in a tree, and repeated again for all additional source

trees. The consensus topology was obtained via a maximum parsimony analysis of the supermatrix (MRP: Matrix Representation using Parsimony; Bininda-Emonds 2004a).

Source trees were collected from the latest analyses focused on different areas of early vertebrate phylogeny. My choice of sources is justified in the following section under each taxonomic category. I did not include all previously published phylogenies as source trees because they do not represent independent analyses based on different datasets. These analyses rather represent continual updates to an original dataset, and the latest, most broadly sampled version was chosen as source. From 'placoderms' to crown gnathostomes, several source trees overlap each other extensively in taxon composition. When tree topology was markedly incongruent among source trees, conflicting character blocks were pruned from the supermatrix, leaving one source tree focused on that particular portion of the phylogeny in full matrix representation. An example of this is the acanthodian grade along the chondrichthyan stem, which was resolved differently between Lu et al. (2016) and Zhu et al. (2016a) (ST1)/King et al. (2017) (ST2), where I chose to use only the latter.

The purpose of supertree analysis is to provide a robust framework for character analysis. Thus, it does not strive to find consensus among multiple competing analyses when they focus on different portions of the tree. The osteichthyan portion of the supertree was one exception where apparent conflict was not resolved between contributing source trees *a priori*. Differences among the selected source trees were minor in this part of the tree. Outside the node of jawed gnathostomes, taxon sampling in source trees overlapped only for outgroup taxa, or for a small subset of taxa, with no marked internal incongruence. Supermatrices and character matrices were compiled in Mesquite version 3.31 (Maddison and Maddison, 2017), and the analysis was conducted in PAUP* version 4.0a157 (Swofford, 2017).

5.2.1a Stem Vertebrates, Cyclostomes, and Stem Gnathostomes

Chapter 2 presents the latest version of the dataset originally compiled by Janvier (1996a). Therefore, I included the tree and matrix from Chapter 2 as sources and excluded all previous versions of the dataset (Løvtrup, 1977; Janvier, 1981, 1996b; Gagnier, 1993; Donoghue et al., 2000; Donoghue and Smith, 2001; Gess et al., 2006; Heimberg et al., 2010; Sansom et al., 2010b; Turner et al., 2010; Conway Morris and Caron, 2014; Gabbott et al., 2016; Keating and Donoghue, 2016; McCoy et al., 2016). All characters included in one or more versions of this

dataset were vetted by subsequent authors, and reevaluated in Chapter 2. Keating and Donoghue (2016) included novel histological and scale characters, but these characters were introduced originally to resolve interrelationships of anaspids. I considered them separately in the source dataset of anaspids. The dataset presented in Chapter 2 samples broadly across jawless vertebrates. It includes the Cambrian stem vertebrates (myllokunmingiids, *Haikouella*, and *Metaspriggina*), stem and crown cyclostomes, enigmatic Silurian/Devonian forms posited as primitive vertebrates (*Achanarella*, *Ciderius*, *Cornovichthys*, *Euphanerops*, and *Jamoytius*), euconodonts, and all major stem gnathostome lineages. Tree topology was congruent overall with previous morphology-based analyses except for supporting cyclostome monophyly and for placing euconodonts as a stem cyclostome lineage. These results were interpreted and discussed in details in Chapter 2. Therefore, this source tree serves as a backbone for the jawless grade of vertebrates.

The source tree does not include three Groups: (***a***) some enigmatic early Palaeozoic vertebrates such as *Anatolepis*, *Eriptychius*, *Kodinskaspis*, *Pircanchaspis*, *Tesakoviaspis*, and an unnamed form from the Manlius Formation of New York (Janvier and Busch, 1984); (***b***) terminal taxa within arandaspids (*Andinaspis*, *Arandaspis*, *Porophoraspis*, and *Sacabambaspis*) or pituriaspids (*Neeyambaspis* and *Pituriaspis*); or (***c***) highly controversial taxa such as *Palaeospondylus* and *Tullimonstrum*. The enigmatic taxa of Group (***a***) are only known from isolated scales or from imprints so they add little character information. With the exception of *Eriptychius* (Turner et al., 2010), they have never been included in a cladistic dataset. Given that their systematic positions are uncertain, it would be reasonable to exclude these taxa from the analysis. For Group (***b***), *Arandaspis* and *Sacabambaspis* are the only arandaspids with relatively complete materials. These taxa code identically in the dataset from Chapter 2. No cladistic analysis has focused on ingroup relationships of arandaspids so this problem cannot be addressed by adding another source tree. Pituriaspids were not split into two genera on the basis of the same rationales. For Group (***c***), *Palaeospondylus* and *Tullimonstrum*, rationales for excluding them from the analysis are given in Chapter 2.

5.2.1b Conodonts

The source tree does not include terminal taxa among conodonts. Several phylogenies of conodonts could be used as source trees (Sweet, 1988; Dzik, 1991; Donoghue, 2001; Sweet and

Donoghue, 2001; Donoghue et al., 2008b; Mazza et al., 2012). However, the cladograms or trees presented in some of these analyses (Sweet, 1988; Dzik, 1991; Sweet and Donoghue, 2001) do not have accompanying cladistic data matrices, whereas the rest focus on specific portions of the conodont tree (Donoghue, 2001; Donoghue et al., 2008b; Mazza et al., 2012). The characters used in these analyses are sampled exclusively from the conodont apparatus, which is unique to this clade. This isolated character block could present logistical problems for a character analysis based on supertrees. First, the conodont-based characters cannot be classified under most anatomical and developmental categories of characters because little is known about their homology and development. Second, these characters could skew the character analysis in the conodont portion of the supertree — and consequently inferences for the entire supertree — toward oropharyngeal characters of mineralized extracellular matrix, given their role in feeding. For these reasons, euconodonts were treated as a single terminal taxon in this supertree analysis.

5.2.1c Anaspids

For anaspids, the source tree is derived from analysis 2 of Blom (2012), which represents an updated version of the analysis by Blom and Märss (2010). This dataset omits taxa based on disarticulated materials as they contribute little character information. These omitted taxa consist of those either named or reviewed by Blom et al. (2001). Several characters and taxa introduced by Keating and Donoghue (2016) to their dataset of jawless vertebrates are already present in the dataset by Blom (2012).

5.2.1d Heterostracans

For heterostracans, the source tree is derived from a strict consensus in the most recent analysis in which quantitative characters were discretized into multiple states (Randle and Sansom, 2017a). In their analyses, the strict consensus tree based on continuous characters has higher resolution than the strict consensus tree based on discretized characters, but continuous characters cannot be compared with conventional characters with discrete states in other source phylogenies on the same platform. The dataset from Randle and Sansom (2017b) has broader taxon and character sampling than the previous version published by the same authors (Randle and Sansom, 2017b). An independent analysis focused on interrelationships of cyathaspidiforms (Lundgren and Blom, 2013). The internal nodes of cyathaspidiforms are better resolved in this latter analysis, whereas

many of them are collapsed into polytomies in Randle and Sansom (2017a, b). However, the taxon and character sets overlap significantly between these analyses, and tree topology is nearly congruent (except for the placement of *Homalaspidella borealis* and the ariaspid affinity of *Listraspis*). Cyathaspidiforms collapsed into a grade with respect to pteraspidiforms in Randle and Sansom (2017a, b) whereas its clade versus grade status was not explicitly tested in Lundgren and Blom (2013). There currently is little reason to sample a source tree and a matrix from Lundgren and Blom (2013), but this may be reconsidered in the future.

One potential disadvantage of the dataset by Randle and Sansom (2017b) is that taxon sampling is not exhaustive and geographically biased. Some well-preserved North American heterostracans were not included (e.g., *Cardipeltis*, *Corvaspis*, *Homaspis*, etc.). However, a comprehensive sampling is logistically challenging for such a speciose clade with broad geographical and stratigraphic distributions, and no better alternative exists among other phylogenetic analyses.

5.2.1e Thelodonts

For thelodonts, the strict consensus from Wilson and Märss (2009) was used as a source tree. This dataset is an updated version from earlier studies (Wilson and Märss, 2004; Märss et al., 2007) and includes 14 representative taxa known from isolated scales in addition to the taxa with body fossils. The thelodont and galeaspid source datasets are distinct from the others in that a well-resolved topology was obtained despite a low character/taxon ratio (thelodonts: 52 characters for 39 taxa).

5.2.1f Galeaspids

The only cladistic dataset with a matrix for galeaspids was provided by Zhu and Gai (2007). Following reconstruction of the internal anatomy in *Shuyu* (included in the Zhu and Gai dataset under its former taxonomic name as '*Sinogaleaspis*' *zhejiangensis*), the coding for this taxon was updated, and the new streamlined galeaspid *Rhegmaspis xiphoidea* (Gai et al., 2015) was coded into the source dataset as it adds character information for the poorly understood gantarostrataspidiids. Like the thelodont source matrix, the galeaspid dataset has a well-resolved topology with low character/taxon ratio (53 characters for 39 taxa).

5.2.1g Osteostracans

For osteostracans, the dataset from Scott and Wilson (2015) is the most comprehensive and most recent. This is a revision of the dataset presented by Sansom (2008, 2009b). A 50% majority consensus tree was presented by Scott and Wilson (2015) because superciliaspidids were resolved as sister to the clade of scolenaspidids + zenaspidids. However, strict consensus collapses this node, while each of the three lineages remained intact as a clade. To account for all most parsimonious trees, strict consensus was used as the source tree. Several independent analyses have been published on osteostracan relationships (Janvier, 1984, 1985; Mark-Kurik and Janvier, 1997). These were excluded, however, because congruence is low with the trees from Sansom (2008, 2009b) and because taxonomic and character sampling is shallower than, and overlapped with, later analyses. Some well-preserved taxa have not been included in any of these datasets, such as *Janaspis* (Keating et al., 2012), and individual genera were each treated as a single OTU without being split into species. I did not code these species into the source matrix, however, because (***a***) the character scores are typically uniform among species within individual genera (Sansom, 2009b) (or among taxa classified under some of the traditionally recognized genera such as *Zenaspis*) and (***b***) revisions are still ongoing for some genera (e.g., *Yvonaspis*; Miyashita, in prep.).

5.2.1h Stem gnathostomes ('placoderms' and 'acanthodians')

I used two different source trees to test effects of placoderm monophyly versus paraphyly. Among recently published datasets, the strict consensus of the most parsimonious trees from Zhu et al. (2016) was used as a source tree for the main supertree (ST1) in which placoderms represent a stem assemblage. The analysis by Zhu et al. (2016) represents the most recent update to the dataset originally compiled by Brazeau (2009) and has the greatest taxon coverage by including *Qilinyu*. The source tree represents a gnathostome backbone for this supertree analysis, so it fixed interrelationships of major placoderm lineages and positions of acanthodian OTUs. I supplemented this backbone by adding ingroup datasets for several placoderm lineages, stem chondrichthyans, stem actinopterygians, and stem sarcopterygians.

For the alternative supertree (ST2) in which most placoderms form a clade, I used the strict consensus of the most parsimonious trees from King et al. (2017). As for the source tree from Zhu et al. (2016), I used the source for the alternative supertree from King et al. (2017) as a

gnathostome backbone, fixing interrelationships of major placoderm lineages and positions of acanthodian OTUs. In the osteichthyan portion, the source tree from King et al. (2017) places several forms on the osteichthyan stem, even though they are conventionally considered stem actinopterygians (*Dialipina*, *Ligualalepis*, *Meemania*) or stem sarcopterygians (*Achoania*, *Guiyu*, *Psarolepis*). Their positions in the osteichthyan stem were subject to Matrix Representation using Parsimony to reach a consensus with the topology of the other published source tree (Lu et al., 2016).

Both the main and alternative gnathostome backbone trees (ST1, ST2; Zhu et al., 2016a; King et al., 2017) lack several stem gnathostome taxa that may have impacted tree topology. These include the purportedly primitive placoderms like *Pseudopetalichthys*, *Stensioella*, and various acanthothoracids in addition to *Romundina*. Also missing from these source datasets are *Andreolepis* and other putative stem osteichthyans known from disarticulated materials (*Lophosteus* is omitted in King et al., 2017 so it is not included in the alternative supertree ST2). With this omission, the dental and histological characters recently reported from these taxa (Qu et al., 2015; Chen et al., 2016) cannot be mapped precisely. However, none of the previous versions of the source datasets contained these taxa either. Therefore, no attempts were made to incorporate them in either supertree.

5.2.1i Antiarchs

For the intrarelationships among antiarchs, I used the dataset from Pan et al. (2017). This dataset is an updated version from Zhu (1996), and includes all genera of antiarchs that are represented by associated materials. This dataset adds to several antiarchs included by Zhu et al. (2016) or by King et al. (2017). The internal topology is congruent with the gnathostome backbone trees (Zhu et al., 2016a; King et al., 2017).

5.2.1j Ptyctodonts

The only available cladistic dataset for ptyctodonts is that of Trinajstic and Long (2009). They presented two most parsimonious trees that differ from each other only in the positions of *Kimbryanodus* and *Materpiscis*. Therefore, I used the strict consensus of these two trees as a source. As in antiarchs, this dataset adds to a few ptyctodonts included by Zhu et al. (2016) or by King et al. (2017). The position of ptyctodonts on the gnathostome stem is fixed by either of

those backbone trees. The internal topology within ptyctodonts is fully congruent between Trinajstic and Long (2009) and the backbone analyses.

5.2.1k Arthrodires

Two sources were used for arthrodires — one focuses on the basal grade of non-brachythoracian arthrodires (or 'actinolepidoids') (Dupret et al., 2017) and the other on brachithoracians (Zhu et al., 2016b). The source dataset from Dupret et al. (2017) represents the updated version of Dupret et al. (2009), whereas the source from Zhu et al. (2016b) is the most recent and more broadly sampled version of Carr and Hlavin (2010) with modifications by Zhu and Zhu (2013). Additional updates to Carr and Hlavin (2010) and Zhu and Zhu (2013) have been published by Boyle and Ryan (2017), but these are omitted because of overall congruence in topology and nearly complete overlap in taxon and character sampling. The source trees from Dupret et al. (2017) and Zhu et al. (2016b) are congruent with each other in topology, but some minor differences exist against the gnathostome backbone trees (Zhu et al., 2016a; King et al., 2017). These differences in internal topology were resolved in favor of the sources from Dupret et al. (2017) and Zhu et al. (2016b).

5.2.1l Stem chondrichthyans

The supertree topology for stem chondrichthyans (with exclusion of 'acanthodians') follows that of Coates et al. (2017). This source does not overlap extensively with other phylogenies (Grogan et al., 2012; Lund et al., 2014) in taxonomic sampling among stem holocephalans and stem elasmobranchs. Although the topological differences are numerous, the parallel phylogenies (Grogan et al., 2012; Lund et al., 2014) are not accompanied by numerical matrices. There is no sensible way to merge these phylogenies unless the taxa sampled by Grogan et al. (2012) and Lund et al. (2014) are recoded into the matrix of Coates et al. (2017). For the purpose of this analysis, these parallel analyses were excluded, but the taxa sampled for those analyses will be considered in the future as potential supplements, if not to balance with the osteicthyan portion of the supertrees.

Acanthodians underwent major topological changes from one analysis to another (Hanke and Wilson, 2004, 2006; Brazeau, 2009; Davis et al., 2012; Zhu et al., 2013; Brazeau and Friedman, 2014; Brazeau and Winter, 2015), but recent analyses converged on their stem

chondrichthyan status (Dupret et al., 2014; Giles et al., 2015; Long et al., 2015; Lu et al., 2016; Zhu et al., 2016a; Coates et al., 2017; King et al., 2017). Topologies among terminal acanthodian taxa vary between these analyses. All acanthodians sampled by Coates et al. (2017) are included in the larger, jawed stem-gnathostome backbones (Zhu et al., 2016a; King et al., 2017), which also contain the taxa excluded by Coates et al. (2017). For this reason, I used the jawed stem-gnathostome backbone for the 'acanthodian' grade.

5.2.1m Osteichthyans

The osteichthyan portion of the dataset was based on Lu et al. (2016). This dataset overlaps extensively with the gnathostome backbone trees (Zhu et al., 2016a; King et al., 2017) both in taxa and characters. Therefore, the original sources were subjected to Matrix Representation using Parsimony to establish consensus in the osteichthyan topology of ST1 and ST2.

Ideally, the dataset from Giles et al. (2017) should have been used as the source for actinopterygians. However, supplementary information including the dataset was not available from the publisher's website as of October 2, 2017. The dataset was provided by the original author at the time of writing this chapter. The use of this dataset as a source for the supertree, however, would have added a large number of actinopterygians (n = 85), which may skew the analysis. This actinopterygian overrepresentation can be balanced by adding additional sources for chondrichthyans and sarcopterygians (Zhu et al., 2017). For the purpose of this chapter, however, the current dataset without these crown-ward source trees provides well-sampled coverage from the total node of vertebrates to the crown nodes of chondrichthyans and osteichthyans.

5.2.1n Supermatrices

Compilation and integration of these source matrices produced two supermatrices: (***a***) main supermatrix (ST1: with Zhu et al. 2016a as a gnathostome backbone) of 512 taxa and 442 node characters; and (***b***) alternative supermatrix (ST2: with King et al. 2017 as a gnathostome backbone) of 509 taxa with 452 node characters (matrices available from **5.5 Supplementary Information**). These two supermatrices were analyzed separately under maximum parsimony (Matrix Representation using Parsimony).

5.2.2 Character Analysis

A complete analysis of characters to address the listed questions (see **5.1 Summary of Questions Generated**) is beyond the scope of this chapter. So only the jawless vertebrate backbone was used for a preliminary analysis, and the matrices are presented as a platform for future analyses. I compiled and integrated all character matrices associated with the source trees. This resulted in the main character matrix of 512 taxa and 1608 characters (associated with the main supertree ST1 with placoderm paraphyly) and the alternative character matrix of 509 taxa and 1733 characters (associated with the alternative supertree ST2 with placoderm monophyly) (matrices available from **5.5 Supplementary Information**). I recoded several outgroup taxa when source matrices had: (***a***) only a single outgroup taxon or (***b***) multiple outgroup taxa that were not immediate sisters to the ingroup in the supertrees. I also recoded representative individual taxa when a suprageneric taxon in one source matrix was split into multiple ingroup taxa. The recoding of characters was based on observations and photographs of the type and referred specimens, and on the literature in the absence of personally collected data.

5.2.2a Categorical information and character attributes

To facilitate future analyses, all characters will be tagged with categorical information (Table 5.1). This information will allow character changes to be mapped onto each supertree (ST1, ST2) under distinct categories of cell lineages, body regions, tissue types, functional contexts, gene expression patterns, and character types. Among these categories, cell lineages, gene expression patterns, and functional contexts cannot be tested conclusively for fossil taxa. I will use the Extant Phylogenetic Bracket (EPB; Bryant and Russell, 1992; Witmer, 1997), which shows strength of inference, to assign individual characters to particular categories: inference level I — category assigned without extant analogue; inference level II — category assigned assuming that the condition was shared with one of the phylogenetically bracketing taxa; inference level III — category assigned assuming that the condition was shared with both of phylogenetically bracketing taxa. To illustrate this planned character tagging scheme, I use three characters selected from the ST1 and ST2 matrices. The characters were chosen from the pool of numbers generated by combining uniform numbers of some of my favorite Major League Baseball players (Example 1: Ichiro Suzuki OF #51; Example 2: Josh Donaldson IF #20, Yadier Molina C #4; Example 3: Pat Neshek P #37, Hunter Pence OF #8).

Example 1. Character 51: Hyomandibular pouch: 0, blind; 1, externally open (spiracle).

Cell lineage: Endoderm (gut endoderm)

Body regions: Head (splanchocranium [premandibular/mandibuar] [hyoid])

Tissue types: Epithelial

Functional contexts: Respiratory; tissue induction

Gene expression patterns: Signaling pathways (Wnt) (FGF) (TGFβ); transcription factors (*Hox*)

Character type: Presence/absence

EPB, level of inference: III — cell lineages, functional contexts, gene expression patterns

Comments: The hyomandibular pouch is blind in cyclostomes, whereas it gives rise to a spiracle in gnathostomes (functions in ventilation). The pouch is required to induce pharyngeal cartilages (Crump et al., 2004). So this character is tagged with "tissue induction" for the category "functional contexts".

Example 2. Character 204: Pre-oral surface (ornamented medial area on the ventral side of rostral plate): 0, absent; 1, present.

Cell lineage: Mesoderm/neural crest (dermal mesenchyme)

Body regions: Head (dermatocranial)

Tissue types: Extracellular matrix (enamel/-oid) (dentine) (bone, acellular)

Functional contexts: Feeding

Gene expression patterns: Unassigned.

Character type: Presence/absence

EPB, level of inference: II — cell lineages, functional contexts.

Comments: This is a character coded for heterostracans. "Cell lineage" is assigned based on the dermal skeleton of living gnathostomes. "Functional contexts" are predictions based on anatomical position. As no living lineages have a homologous plate, the character is not tagged for gene expression patterns.

Example 3. Character 378: Arrangement of lateral line system on body: 0, longitudinal lines; 1, short segments forming right-angled network.

Cell lineage: Ectoderm (neural crest)

Body regions: Head (dermatocranial); trunk (epidermal)

Tissue types: Nerves/sensory epithelia

Functional contexts: Sensory

Gene expression patterns: Signaling pathways (Wnt) (FGF) (TGFβ); transcription factors (*Hox*) (*Sox*)

Character type: Shape

EPB, level of inference: III — cell lineages, functional contexts; II — gene expression patterns.

Comments: This character is specific to thelodonts and other stem gnathostomes (Wilson and Märss, 2009). Although this character is recognized in the dermal skeleton, it describes the morphology of the lateral line. So only the lateral line is considered to assign character attributes. Lateral lines are known from cyclostomes (Braun and Northcutt, 1997; Gelman et al., 2007, 2009); thus, the level of inference is III for "cell lineage" and "functional contexts". "Gene expression patterns" are predicted based on zebrafish (compiled by ZFIN [The Zebrafish Information Network]).

Once labeled by attribute, characters will be grouped into separate submatrices by attributes and mapped onto the supertrees. Some characters will be left unlabeled for one or more attributes where evidence is ambiguous. In particular, functions may not be explicit, and developmental data are often ambiguous or lacking.

For the preliminary analysis, Table 5.2 provides character attributes for the data matrix associated with the jawless vertebrate backbone tree of ST1 and ST2.

5.2.2b Assigning cell lineage to characters

Each cell lineage has distinct differentiation potentials, and developmental fates are known with experimental evidence in both living cyclostomes and gnathostomes. For cyclostomes, this is reviewed in Chapter 1. For gnathostomes, numerous syntheses are available as starting

references[7]. With the exception of neural crest and other vertebrate-specific organs, the embryology of living chordates and ambulacrarians supports the view that developmental fates of each major cell lineage remain conserved overall across the phylogenetic range (Jefferies, 1987; Gilbert and Raunio, 1997; Harrison and Ruppert, 1997; Satoh, 2016). Therefore, the character attributes of cell lineages will be assigned based on the following criteria: (***a***) cell lineages are described for structures coded by the character in the bracketing crown clades (cyclostomes or gnathostomes); (***b***) experimental evidence exists for contribution of that cell lineage to that structure (including, but not limited to, fate mapping, cell labeling, cell ablation, tissue transplant, gene expression, transcriptomic, knockdown/knockout, or pharmacological experiment); and (***c***) anatomical observations and experimental evidence are consistent across the crown vertebrates (no significant exception is known).

For example, these criteria are not satisfied for one major component of the character set: dermal skeleton. Anatomical observations and experimental evidence continue to conflict over contributions and distributions of neural crest- and mesoderm-derived mesenchyme to the dermal skeleton both among — and even within — living gnathostome models. This conflict is acute in the skull roof (Chai et al., 2000; Jiang et al., 2002; Gross and Hanken, 2005, 2008a; Kague et al., 2012; Maddin et al., 2016), where multiple conflicting lineage maps have been proposed in the chick model (Lievre, 1974; Noden, 1978; Couly et al., 1992, 1993; Le Douarin et al., 1993, 2004; Kontges and Lumsden, 1996; Lee et al., 2001; Richman and Lee, 2003; Noden and Trainor, 2005; Evans and Noden, 2006). The lateral facial elements, on the other hand, appear to have consensus as neural-crest-derived. Still, unambiguous evidence is lacking in the mouse model. As a subset of this problem, different streams of neural crest cells may contribute to the same skeletal elements. *Xenopus* illustrates this point. In that taxon, the hyoid stream of crest cells migrate to the anterior end of the head to give rise to anterior facial elements such as the premaxilla, which are normally derived from the trigeminal stream (Gross and Hanken, 2005, 2008b). In this case, the skeletal elements are still composed of neural crest cells so it does not affect assigning cell lineage information to the pertinent characters. The lesson is rather that

[7] Gegenbaur, 1859; Balfour, 1880; Goodrich, 1909, 1930; Edgeworth, 1935; de Beer, 1937; Holmgren, 1942, 1942, 1946; Romanoff, 1960; Romer and Parsons, 1977; Jarvik, 1980; Le Douarin, 1982; Jefferies, 1987; Hall and Hörstadius, 1989; Smith and Hall, 1990; Hyman, 1992; Hanken and Hall, 1993; Gee, 1996; Janvier, 1996a; Gilbert and Raunio, 1997; Hall, 1998, 2009, 2015; Nieuwenhuys et al., 1998; Kuratani, 2004, 2016, 2017; Gilbert, 2013; Trainor, 2013; Gilbert and Barresi, 2016.

spatial association with a particular cell lineage may not be as tightly conserved as often expected. Now that a survey of just a handful of vertebrate model taxa reveals significant departures from the supposedly conserved patterns, exceptions may not be so exceptional. Thus, anatomically informed arguments (e.g., premaxilla sits in the area typically occupied by the trigeminal stream) should not be followed blindly.

The difficulty of extrapolating the cell lineage analyses of extant taxa is not limited to the skull. Scales and fin rays are often considered as neural crest derivatives (Smith and Hall, 1990). Lineage mapping in skate embryos appears to support this view (Gillis et al., 2017). However, lineage mapping in teleost models recently revealed that these elements are derived from mesoderm (Lee et al., 2013b, 2013a; Mongera and Nüsslein-Volhard, 2013). In the absence of experimental evidence from other gnathostome models, it remains unclear whether the mesodermal origin represents a secondarily derived trait restricted to some teleosts or an evolutionarily conserved trait. Overall, cell fates and lineages may be decoupled from each other evolutionarily, and the variations appear greater in the dermal skeletons. To accommodate these confounding factors, characters of the dermal skeletal elements will be assigned to a distinct attribute "dermal mesenchyme" for the cell lineage category, and not to either neural crest and mesoderm (Table 5.1; see examples in the previous section **3.5.1a**).

5.2.2c Assigning functional contexts and gene expression patterns to characters

Similarly, I will assign attributes under functional contexts and gene expression profiles through comparison with living taxa. For gene expression patterns, major signaling pathways and transcription factors will be selected from those described from a broad range of taxa and discussed extensively in evolutionary contexts, such as Hedgehog signaling and *Hox* (Table 5.1). Thus, this is not an exhaustive list. All of them — with the exception of *MyoD*/*Myf5*, which are specific to musculature — are expressed pleiotropically to varying extents. Therefore, comparison of characters tagged with these attributes will add another dimension to character analyses by contrasting evolutionary patterns between different genetic pathways. Gene-expression data will be mined from the literature and several model-specific databases (Geisha - A Chicken Embryo Gene Expression Database; MGI-Mouse Genome Informatics; Xenbase - the Xenopus Model Organism Database; ZFIN - The Zebrafish Information Network). Terminal genes of a pathway and tissue-specific pathways will not be included, because they would likely

duplicate attributes of tissue types and/or body regions. In the previous section, Example 3 (Character 378: Arrangement of lateral line system on body: 0, longitudinal lines; 1, short segments forming right-angled network) describes stem gnathostome-specific lateral line morphology. Of course, gene expression is unknown for the lateral lines of stem gnathostomes. However, the lateral line has been extensively studied in zebrafish with a long list of genes that have well-characterized phenotypes. Therefore, gene expression patterns will be assigned based on this information. The level of inference under EPB is II, as no expression data are available from cyclostomes.

Functional contexts will be inferred by bracketing living lineages with a structure coded by the character (Table 5.1). In the case of the lateral line character (Example 3, Character 378), the lateral line has a sensory function in both cyclostomes and gnathostomes. Bracketed by these two lineages, function of the lateral line is predicted to be sensory in thelodonts and other stem gnathostomes.

5.3 SUPERTREES

The main supertree (ST1: placoderm paraphyly) is a strict consensus of 16 trees (Figs. 5.1, 5.2). Each of the 16 most parsimonious trees has tree length = 4792, consistency index = 0.389, and retention index = 0.813 (strict consensus: tree length = 4792; consistency index = 0.389; retention index = 0.813). The alternative supertree (ST2: placoderm monophyly) is a strict consensus of 697101 trees (Figs. 5.3, 5.4). Each of those shortest trees has tree length = 4953, consistency index = 0.402, and retention index = 0.810 (strict consensus: tree length = 4949; consistency index = 0.403; retention index = 0.810). These supertrees differ from each other in several ways, including: supporting or collapsing the placoderm node, internal topologies among placoderms (acanthothoracids, antiarchs, brindabellaspidids, macropetalichthyids, and ptyctodonts), *Ramirosuarezia* being a stem or crown gnathostome lineage, *Meemania* nested outside or inside the crown osteichthyan node, and *Guiyu* and its relatives (*Achoania*, *Psarolepis*) lying within or outside of the sarcopterygian stem. Despite these topological differences, the tree statistics are nearly identical. Plotting consistency and retention indices against step numbers per character did not reveal any notable differences (data not shown). This high similarity implies that conflicting

topologies among jawed gnathostomes will likely not impact inferences about character evolution significantly.

5.4 PRELIMINARY ANALYSIS OF CHARACTERS

I present preliminary results of a character analysis in this section as a proof of concept of the approach proposed here. Although a full analysis of complete datasets is beyond the scope of this thesis, I conducted a series of pilot analyses on a portion of the datasets (Suppls. 5.3, 5-6) across the early jawless vertebrate backbone of ST1 and ST2 (Figs. 5.1-5.4). This portion of the dataset comes from Chapter 2 (**2.8.5 List of Characters**; Suppl. 2.1). ST1 and ST2 are identical to each other in this part of the supertree. To avoid the majority of internal branches becoming zero-length, I only used the taxon set included in the analysis of Chapter 2. Before the analysis, each character was given attributes (Table 5.2). This information was used to sort character information into submatrices by categories. Although numerous combinations are possible, in this particular case study I will focus on cell lineages code 1B and non-1Bs: neural-crest versus non-neural-crest characters. The matrix (Suppl. 2.1) was divided into two submatrices, neural-crest and non-neural-crest characters. Scale-related characters and other integumentary skeletal traits (2, cell lineages; Table 5.2) are excluded from this comparison, due to uncertainty about the cell lineage contribution to these elements (discussed in **5.2.2b Assigning Cell Lineage to Characters**). These characters contributed to neither submatrix.

Neural-crest and non-neural-crest characters performed similarly in the early jawless vertebrate backbone when compared by consistency and retention indices (Fig. 5.5a). This similarity is expected because of high interaction potentials of neural crest cells with tissues derived from any germ layers (Hall, 2009), and may be explained by correlated character changes between the two character sets. When mapped onto the jawless early vertebrate backbone of ST1/2, some differences became apparent. Fewer terminal branches have zero length in the non-neural-crest characters than in the neural-crest characters (Fig. 5.5b). This difference indicates that neural-crest characters had more character changes along the stems than within crowns, whereas non-neural-crest characters accumulated state changes among ingroup lineages. Qualitatively, the evolution of neural-crest characters appears to be more punctuated (some stems are substantially longer than others). The changes are more or less unimodal in the non-neural-

crest characters. These patterns may underscore the link postulated between neural-crest-derived traits and novel body plans of vertebrates (Janvier, 1996a, 2007; Kuratani and Ota, 2008; Green et al., 2015; Kuratani, 2017).

A striking difference between neural-crest and non-neural-crest characters emerged in the states/steps curves, where each novel derived state was plotted against tree steps (Fig. 5.5c; Wagner, 2000; Wagner et al., 2006). Neural crest is a vertebrate novelty (Gans and Northcutt, 1983; Hall, 2009; Green et al., 2015).Reflecting this, every character change is novel in the initial phase of its evolution. This isometric linear relationship extended well past 45 total steps, almost uninterrupted by homoplasies. Neural crest did not appear to exhaust its repertoire completely toward jawed gnathostomes, as the curve never reached a plateau. In contrast, the non-neural-crest characters were punctuated with homoplasies to a greater extent from near the base of the tree toward jawed gnathostomes. Although it did not quite bend into a plateau either, some notable flat shoulders (clustered homoplasies) occurred. The most prominent one sits approximately between 100-125 tree steps, closer to the basal part of the stem gnathostome assemblage (anaspids, heterostracomorphs, thelodonts).

Despite these straightforward interpretations, the narrative becomes complex once curves are labeled by major character transitions. For example the origin of the jaw — when mapped with other neural-crest characters — sits close to the endpoint of the states/steps curve of the neural-crest characters (jaw with arrow, Fig. 5.5c). By this point, the neural-crest characters appear to have exhausted much of their repertoire (increased frequencies of homoplasies). Only several character changes remained until all tree steps were accounted for. On the other hand, the non-neural-crest characters did not appear to exhaust novel character states before the origin of the jaw despite higher frequencies of homoplasies. The states/steps curve continues well past the origin of the jaw. This result is puzzling because jaw cartilages are derived from neural crest cells (Couly et al., 1993). Co-options and tissue interactions can explain this paradox. As predicted by the Mandibular Confinement Hypothesis (Miyashita, 2016), character changes preceding and following the origin of the jaw concern shifting spatial relationships of the progenitor populations rather than the acquisition of novel genetic pathways or cell fates of the skeletogenic neural crest. Such spatial shifts likely created novel tissue interactions (e.g., confined space for the mandibular arch; facilitated by the trabecular cartilages, hyoid arch, and hypobranchial muscles) (Miyashita, 2016). This fits the test of hypotheses for the origin of the jaw joint, because each of the

hypotheses requires a co-option event, and because the jaw joint — though forming at the ends of the neural crest-derived cartilages — can only develop with contributions of other cell lineages (e.g., mesodermal mesenchyme for the connective tissues). Therefore, the origin of the novel, neural-crest-derived skeleton (jaw) correlated with greater character changes in non-neural crest tissues.

Even though the characters may perform similarly between the neural-crest and non-neural-crest submatrices (Fig. 5.5a), patterns of character changes tangibly differ from each other. A complete dataset is required to test the preliminary interpretations presented here, to calculate rates of character evolution, to quantify correlations among characters of different categories, and to generate further insights.

5.5 SUMMARY, PROSPECTUS, AND CONCLUDING REMARKS

The two supertrees (Figs. 5.1-5.4) provide a platform for future analyses of character evolution across early vertebrate lineages. To address the questions outlined at the start of this chapter, a complete set of analyses will describe: (***a***) covariance of character states within and among different character attributes; (***b***) rates of character evolution for each category of characters; (***c***) patterns of character exhaustions; (***d***) ancestral state reconstruction; and (***e***) morphological disparity (Maddison, 2000; Wagner, 2000; Wagner et al., 2006; Hernández et al., 2013; Pennell and Harmon, 2013; Pennell et al., 2016). Despite omissions and underrepresentation of some lineages like conodonts, this chapter provides the sole comprehensive dataset to date that covers jawless and jawed vertebrate lineages extending into the early half of Paleozoic times.

The stem from which these lineages branched represents the elusive early evolutionary history of vertebrates. Comparison of living vertebrate lineages produces a long list of synapomorphies acquired prior to the crown vertebrate node and the crown gnathostome node (Janvier, 1996a, 2007; Hall, 1998; Kuratani, 2004, 2016, 2017; Brazeau and Friedman, 2014, 2015; Miyashita, 2016; King et al., 2017). Comparison of stem vertebrate lineages provides some inferences to constrain evolutionary changes in the characters, and a glimpse into morphological disparity exploited by multiple episodes of radiations off the stem (Janvier, 1996a, 2007; Donoghue et al., 2000; Miyashita, 2016). However, long branches leading to the living lineages

restrict the power of comparative approaches to constrain conditions at nodes, whereas the fossil record is too incomplete to break down those branches to resolve character changes at every segment (Janvier, 2007, 2015; Donoghue and Purnell, 2009; Sansom, 2015). To stretch the limits of comparative methods further, vertebrate anatomy is devilishly complex — it is highly modular and yet highly integrated, and outscores all other metazoan lineages in number of cell types, anatomical parts, and functional connectivity (Schlosser and Wagner, 2004; Wagner, 2007, 2014; Arendt, 2008; Hallgrímsson and Hall, 2011; Wagner and Zhang, 2011; Hallgrimsson et al., 2014; Arendt et al., 2016). Challenging as it may be, a study of early vertebrate evolution is synonymous with an endeavor to understand the evolution of vertebrate body plans (Gee, 1996; Kuratani, 2004, 2016, 2017). The endeavor has stood among the core pursuits of zoology since the infancy of the field (Hanken and Hall, 1993; Gee, 1996; Janvier, 1996a; Hall, 1998; Holland et al., 2015; Kuratani, 2016), and it will remain a great challenge far into the foreseeable future.

My contributions to the study of early vertebrate evolution used fossils and embryos reciprocally, and utilized synergies of insights from comparative anatomy and comparative development, to maximize inferences about character evolution. The chapters included in the thesis focused on cyclostomes as critical lineages that constrain primitive vertebrate conditions because (***a***) they represent the lesser understood — and the only living jawless — vertebrates compared to gnathostomes; (***b***) their interrelationships with the rest of vertebrates remain unstable and controversial; and (***c***) the fossil record is so poor that only a handful of putative stem taxa are available with little character information to constrain states at their respective crown nodes (Janvier, 2007, 2008, 2015).

In Chapter 1, I introduced the conceptual basis of this thesis by reviewing the embryonic development of living cyclostomes. My synthesis: (***a***) classified the identified developmental traits as synapomorphies for vertebrates, cyclostomes, or myxinoids/petromyzontiforms; (***b***) tested congruence of controversial fossil forms proposed recently as a stem myxinoid or petromyzontiform; and (***c***) delineated remaining areas of uncertainties, including the identity of vertebra-like elements in hagfish.

In Chapter 2, I described a new fossil myxinoid from the Cenomanian of Lebanon. The new taxon, *Tethymyxine tapirostrum*, was inferred to nest within crown myxinoids and provides a hard minimum calibration point for this clade. Through a comprehensive analysis of characters, I presented a revision to the previously published phylogenetic datasets for the relationships among

jawless vertebrate lineages. My maximum parsimony and Bayesian analyses based on the newly revised dataset supported monophyletic cyclostomes, which was consistent with molecular inferences and departed from previous morphology-based analyses that consistently supported cyclostome paraphyly. The Cyclostome Problem has its root in the classification proposed in the 19th century (Duméril, 1806) — or in the misclassification of hagfish as a non-vertebrate (Linnaeus, 1758) — and was reignited in recent times with the advent of cladistics (Løvtrup, 1977; Janvier, 2007, 2010; Near, 2009). Although a single phylogenetic analysis will certainly not close the debate, the significance of my result lies in its demonstration that morphological and molecular inferences converge on a similar topology in this textbook case where morphology- and sequence-based phylogenies usually conflict (Hillis, 1987; Patterson, 1987; Jenner, 2004a, 2004b; Wiens and Collins, 2004; Janvier, 2007; Near, 2009). This congruence provides additional confidence in the topology of stem gnathostomes obtained in the same analysis. Thus it adds to the series of recent analyses showing that a complementary relationship between morphology and molecules is important to reconstruct what would have been long ghost lineages in the absence of fossils (Wiens and Collins, 2004; Wiens et al., 2010; Dávalos et al., 2014; Heath et al., 2014; Heikkilä et al., 2014; Reeder et al., 2015; Zhang et al., 2016).

In Chapter 3, I described seven specimens of *Priscomyzon riniensis*, a stem petromyzontiform from the Late Devonian of South Africa. I interpreted these specimens to represent an ontogenetic series from pre-metamorphosis larvae to adults. However, the larvae of *Priscomyzon* do not have skeletal traits comparable to the filter-feeding larval stage (ammocoetes) in living lampreys. Instead, immature specimens of *Priscomyzon* have traits that more closely resemble the predatory adult stage seen in living lampreys, including prominent eyes, an oral sucker, keratinous teeth, and an anteroposteriorly short and pericardially closed branchial basket. This morphology lies in a continuum leading to the adult stage. This combination of traits is also consistent with the specimens of other Paleozoic stem petromyzontiforms (*Hardistiella* and *Mayomyzon*) that were also thought to be potential larvae. The lack of ammocoete-like morphology has profound implications for evolutionary scenarios about the origin of vertebrates. Ammocoetes have been considered to retain primitive conditions within vertebrates, and thus are often used as a surrogate or model for the last common ancestor of all living vertebrates (Gaskell, 1908; Garstang, 1928; Goodrich, 1930; de Beer, 1937; Romer, 1972; Romer and Parsons, 1977; Gans, 1993; Forey, 1995; Gee, 1996; Janvier, 1996a; Mallatt,

1996; Northcutt, 2005; Cattell et al., 2011; Holland et al., 2015; Jandzik et al., 2015; Kuratani, 2017). However, these immature specimens of stem petromyzontiforms contradict the prediction from this ammocoete-first model that a filter-feeding larval phase was conserved along the petromyzontiform stem. They are consistent, however, with the hypothesis that ammocoetes represent a secondary innovation within the lamprey lineage (Hardisty, 1982; Janvier, 2007). This ammocoete-second model suggests that superficial but long-recognized similarities between ammocoetes and cephalochordates are convergences. Although it cannot be ruled out that the Paleozoic stem petromyzontiforms secondarily lost an ammocoete phase, the ammocoete-second model is more parsimonious than the ammocoete-first model (Tables 3.1, 3.2).

Chapter 4 presents partial results from an ongoing project. In it, I am using lampreys and zebrafish as comparative models to test hypotheses about the evolutionary origin of the jaw joint — a prerequisite structure for a jaw to evolve. I presented comparative evidence supporting three hypotheses proposed in the literature (Cattell et al., 2011; Uyeno and Clark, 2015; Miyashita, 2016) that the jaw joint evolved from: (***a***) muscular scaffold; (***b***) mucocartilage; and (***c***) intercartilaginous blood sinus. Gene-expression profiles in lampreys reject predictions of the Muscular Scaffold Hypothesis and are compatible with both Mucocartlaige and Intercartilaginous Blood Sinus hypotheses, with perhaps the latter slightly favoured. The data also suggest that the origin of the jaw joint occurred through a co-option event at the level of structures rather than via acquisition of expression of the jaw joint marker *Nkx3.2* alone. In zebrafish, *nkx3.2*-knockout mutants developed craniofacial morphology similar to jawless stem gnathostomes like birkeniid anaspids. This ongoing project has the potential to constrain evolutionary scenarios for the jaw joint, and to reveal insights about the poorly understood mechanisms of co-option events and the role of plasticity in craniofacial morphology.

Although not included this thesis, my published synthesis on the evolutionary origin of the jaw (Miyashita, 2016) forms an integral part of this thesis project. It provided a novel conceptual framework in which problems linked to the origin of the jaw should be considered in future.. A developing vertebrate head is a whole of many serial structures: hindbrain rhombomeres, neural crest streams, head cavities, pharyngeal arches and pouches, epibranchial placodes, and others. Although the traditional view of a unified segmentation scheme no longer holds, it remained a puzzle whether these serial structures originated all at once or independently. A long-standing challenge to differentially test these alternative hypotheses is to identify more

than one evolutionary event in which significant additions or modifications occurred to the serial patterns. I provided fossil and developmental evidence for such modifications in the pharyngeal apparatus at the origin of jawed vertebrates. Comparison between cyclostomes and gnathostomes revealed that the mandibular region does not have a typical pharyngeal arch organization in cyclostomes. Mapping of musculoskeletal elements in multiple jawless stem gnathostomes revealed similar patterns to cyclostomes in general, but also suggests that diffuse boundaries around 'mandibular' elements independently evolved in the hyoid or hypobranchial positions in some lineages. A synthesis of the evidence indicates that the mandibular arch (typically labeled as PA I or BA I) acquired a pattern serial to the rest of the pharyngeal apparatus only at the origin of the jaw. This Mandibular Confinement Hypothesis leads to an emerging view that (***a***) in the last common ancestor of all living vertebrates, only hindbrain rhombomeres and pharyngeal pouches were truly segmented in the head; and (***b***) serial patterns in the head of living jawed vertebrates gradually evolved through interdependent tissue interactions facilitated by multipotency of neural crest ectomesenchyme.

Thus, this thesis contributes novel data, insights, and hypotheses to three critical nodes in the early evolution of vertebrates: crown nodes of vertebrates (Chapters 1, 3), crown nodes of cyclostomes (Chapters 1, 2), and the node of jawed vertebrates, inclusive of placoderms and crown gnathostomes and exclusive of osteostracans and galeaspids (Chapter 4; Miyashita, 2016). These contributions all bring discussion back to the questions of character evolution. Given the increasing information for topology and synapomorphies at each node, what insights can be gained from patterns of character changes? What trends and processes of character evolution explain the transitions in a set of symplesiomorphies and synapomorphies inferred from one node to another? Do character covariances, rates of state changes, and availabilities of character space reveal significant biological factors that shaped the observed great morphological variations of early vertebrates? Although this ongoing analysis was not included in this thesis, the supertrees, accompanying datasets, and preliminary analysis are presented here as a platform for future analyses.

I plan to address this final set of questions through supertree analysis so that I can complete the first round of an intellectual circuit that originally began with the comparative anatomy of myxinoids (Miyashita, 2012). The project was initiated in the hope of reconstructing the last common ancestor of all living vertebrates. As the project unfolded, however, that initial

goal has become less appealing. Because cyclostomes form a clade (Chapter 2), and because the ancestral status of the ammocoetes form is in doubt (Chapter 3), such attempts to reconstruct the common ancestor will result in either: (***a***) a list of synapomorphies and symplesiomorphies inferred for that crown node; or (***b***) a hypothetical ancestor informed by an arbitrarily chosen living model — but not both, as the two results appear to be incompatible with one another.

For comparison, the quest for the elusive Urbilateria illustrates this dilemma well. Multiple versions of the hypothetical urbilateria differ in suite of characters and in choice of 'model' taxa used to infer its character states (Knoll and Carroll, 1999; Arendt and Wittbrodt, 2001; Balavoine and Adoutte, 2003; Raible and Arendt, 2004; Arendt et al., 2008; Hejnol and Martindale, 2008; Hejnol and Lowe, 2014). However, these hypothetical ancestors have one thing in common: each hypothesis is a minimalistic assembly of arbitrarily chosen characters to achieve internal consistency. Regardless of whether it was modeled mainly after an acoelomorph, a polychaete, or a hemichordate, it does not represent just a collection of synapomorphies. This practice could create an unlikely — and misleading — scenario in which all bilaterians diverged from an ancestor that is essentially a polychaete (Arendt et al., 2008; Tomer et al., 2010; Lauri et al., 2014; Brunet et al., 2015), or all vertebrates were derived from an ancestor that is indistinguishable from a cephalochordate (Mallatt, 1996; Holland et al., 2008). By using quantitative phylogenetic inferences alone, however, a list of inferred synapomorphies and symplesiomorphies will contain internal inconsistencies, for example: Urbilateria without a central nervous system (Northcutt, 2010) but with the *Hox* code and paraxially organized, segmented muscles (Balavoine and Adoutte, 2003; Butts et al., 2008).

Indeed, the narratives for key events in metazoan evolution have historically tended to focus on terminal taxa rather than on characters, whereas inferred character states at successive nodes often fail to contribute to a coherent narrative. Patterns of character changes link these two conceptually different approaches: a set of character states observed at a branch tip versus inferred for a node. Thus, the proposed character analysis (outlined in this chapter) promises mechanistic insights into the set of shared traits inferred to have evolved at a given node. They are not simply constrained to that node by statistical inferences based on tree shape. The dynamics of character evolution may provide explanations for correlated character changes, asymmetric distributions of synapomorphies, and observed phenotypic disparity that make early vertebrates such challenging but appealing taxa to work on.

5.6 DATA MATRICES AND CHARACTERS

Supplementary files are available at a Dataverse depository (doi:10.7939/DVN/JGSPJN) (PDF version) or on a disc attached to the back of this thesis (print version).

Suppl. 5.1: A supermatrix for the main supertree (ST1), using Zhu et al. (2016a) as a backbone for gnathostomes in Nexus format.

Suppl. 5.2: A list of characters compiled from source matrices/trees for the main supertree (ST1), using Zhu et al. (2016a) as a backbone for gnathostomes.

Suppl. 5.3: A character matrix accompanying the main supertree (ST1), using Zhu et al. (2016a) as a backbone for gnathostomes, in Nexus format.

Suppl. 5.4: A supermatrix for the alternative supertree (ST2), using King et al. (2017) as a backbone for gnathostomes in Nexus format.

Suppl. 5.5: A list of characters compiled from source matrices/trees for the alternative supertree (ST2), using King et al. (2017) as a backbone for gnathostomes.

Suppl. 5.6: A character matrix accompanying the alternative supertree (ST2), using King et al. (2017) as a backbone for gnathostomes, in Nexus format.

FIGURES

Fig. 5.1. A strict consensus of 16 supertrees generated by matrix representation parsimony, using Zhu et al. (2016a) as a backbone for gnathostomes (16 most parsimonious trees: tree length = 4792, consistency index = 0.389, and retention index = 0.813). Placoderms were resolved as a grade of stem gnathostomes. Colour codes for branches are consistent throughout Figs. 5.1-5.4. In clockwise: black = invertebrate chordates; dark brown = stem vertebrates and unstable early vertebrate lineages (including conodonts); green = myxinoids; cyan = petromyzontiforms; red = anaspids; grey brown = arandaspids; grey = astraspids; light brown = heterostracans; light yellow green = thelodonts; blue = pituriaspids; light cyan = galeaspids; magenta = osteostracans; dark grey brown = primitive placoderms (acanthothoracids, brindabellaspidids, rhenanids); light purple = macropetalichthyids; orange = ptyctodonts; yellow green = antiarchs; pink = arthrodires; dark red = *Entelognathus*, *Janusciscus*, *Qilinyu*; dark green = acanthodians; olive green = *Doliodus*, *Gladbachus*, *Pucapampella*; cyan green = crown chondrichthyians; light blue = stem osteichthyeans; purple = actinopterygians; red purple = sarcopterygians.

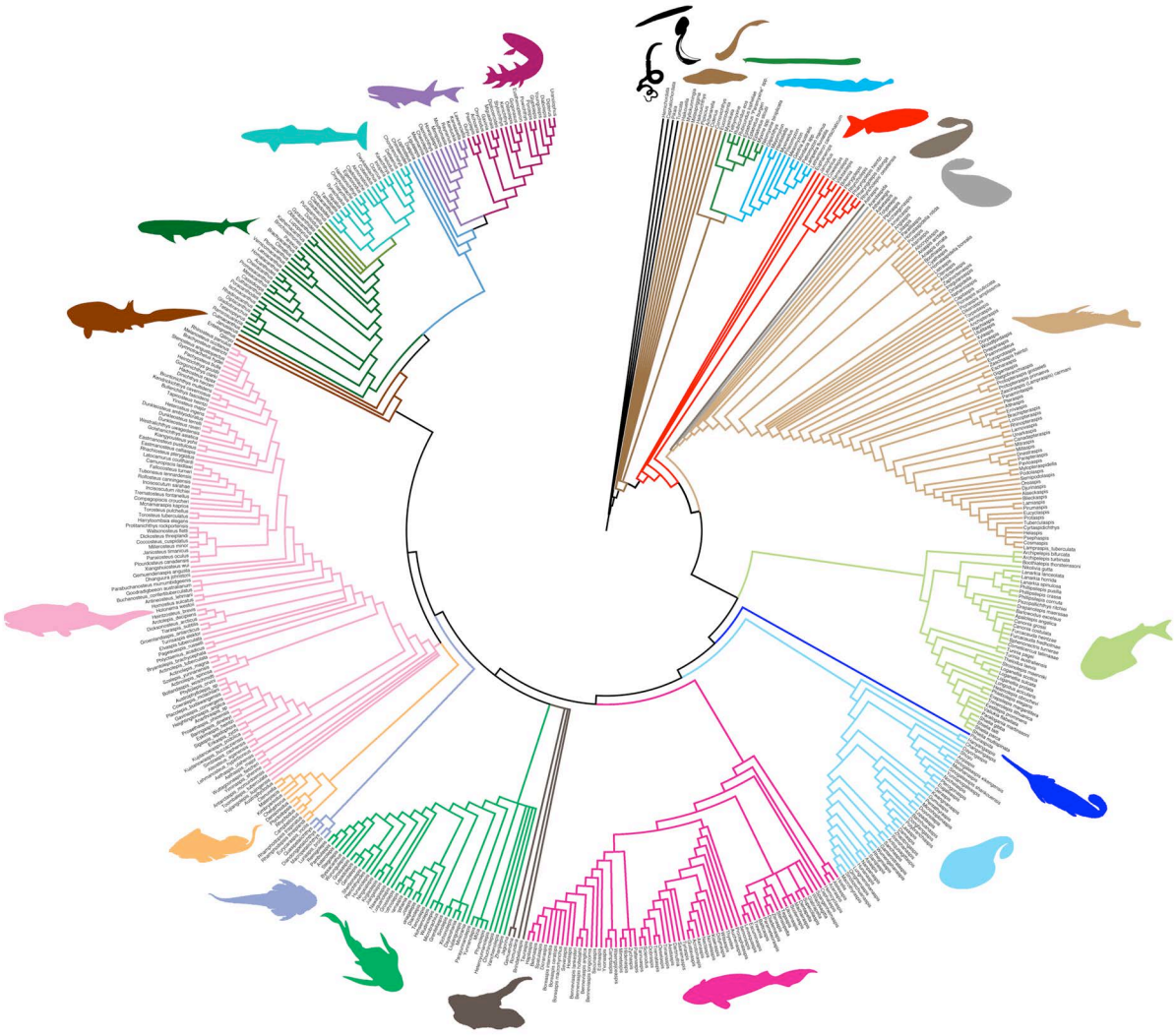

Fig. 5.2. Details of strict consensus of 16 supertrees generated by matrix representation parsimony, using Zhu et al. (2016a) as a backbone for gnathostomes (tree length = 4792, consistency index = 0.389, and retention index = 0.813). For colour codes, see Fig. 5.1.


a
b
c
Chordata (crown)
Vertebrata (total)
Vertebrata (crown)
Gnathostomata (total)
Myxinoidea (total)
Cyclostomi (crown)
Petromyzontiformes (total)
Heterostraci
Thelodonti
'Anaspida'
Galeaspida
Osteostraci
Antiarcha
Unnamed clade (jawed vertebrates)
'Placodermi'
Macropetalichthyida
Ptyctodonta
Arthrodira
Chondrichthyes (total)
Gnathostomata (crown)
Chondrichthyes (crown)
Osteichthyes (total)
Actinopterygii (total)
Osteichthyes (crown)
Sarcopterygii (total)
'Placodermi'
'Acanthodii'

Fig. 5.3. A strict consensus of 697101 supertrees generated by matrix representation parsimony, using King et al. (2017) as a backbone for gnathostomes (697101 most parsimonious trees: tree length = 4953, consistency index = 0.402, and retention index = 0.810). Most placoderms were nested within a clade. Note topological differences in positions of 'primitive' placoderms, a grade of macropetalichthyids with respect to ptyctodonts, *Ramirosuarezia* as a stem gnathostome, relationships of acanthodians, *Meemania* as a stem osteichthyan, and Guiyu and its relatives in a polytomy at the crown osteichthyan node. For colour codes, see Fig. 5.1.

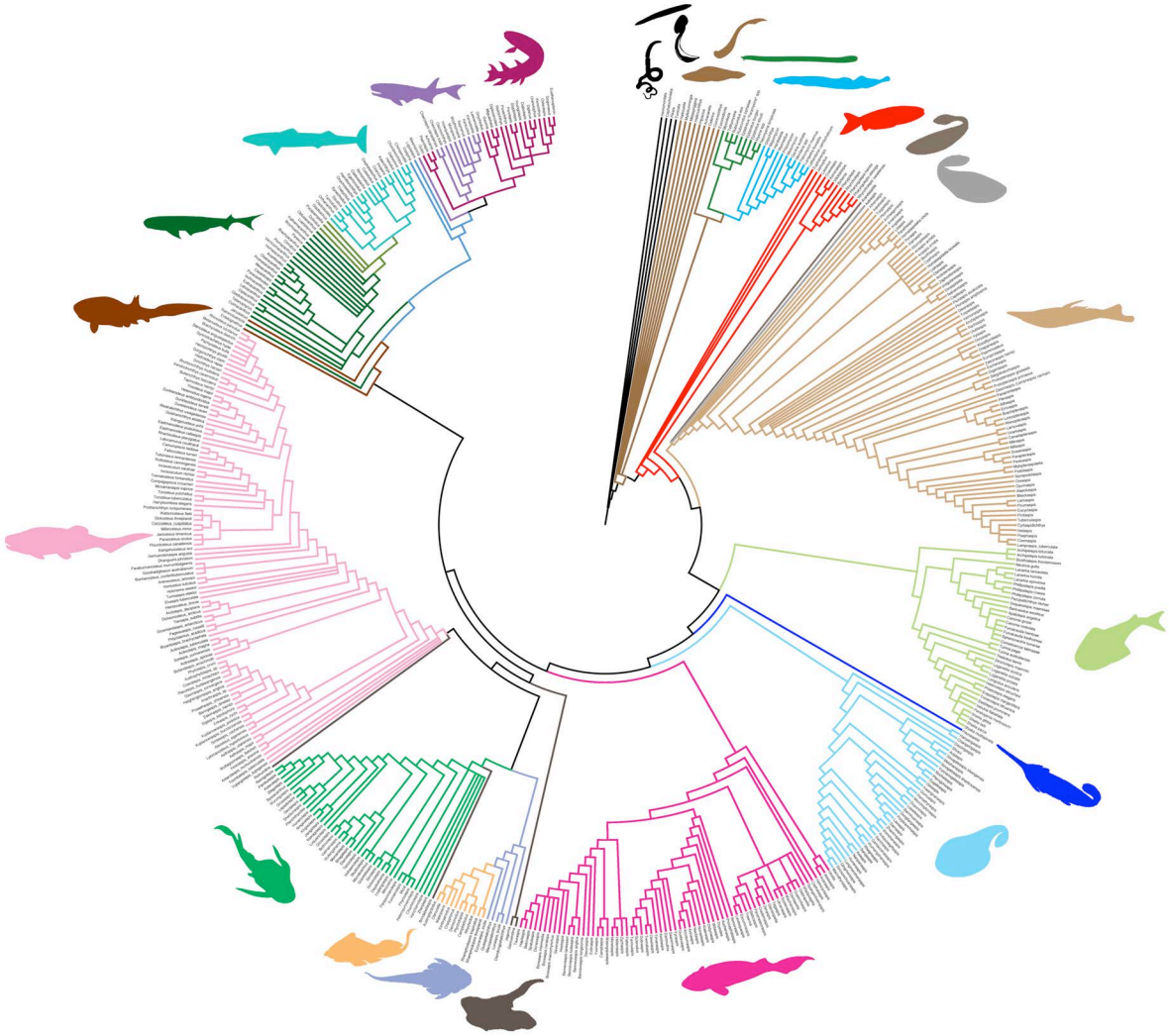

Fig. 5.4. Details of a strict consensus of 697101 supertrees generated by matrix representation parsimony, using King et al. (2017) as a backbone for gnathostomes (tree length = 4953, consistency index = 0.402, and retention index = 0.810). Most placoderms were nested within a clade. Note topological differences in positions of 'primitive' placoderms, a grade of macropetalichthyids with respect to ptyctodonts, *Ramirosuarezia* as a stem gnathostome, relationships of acanthodians, *Meemania* as a stem osteichthyan, and Guiyu and its relatives in a polytomy at the crown osteichthyan node. For colour codes, see Fig. 5.1.

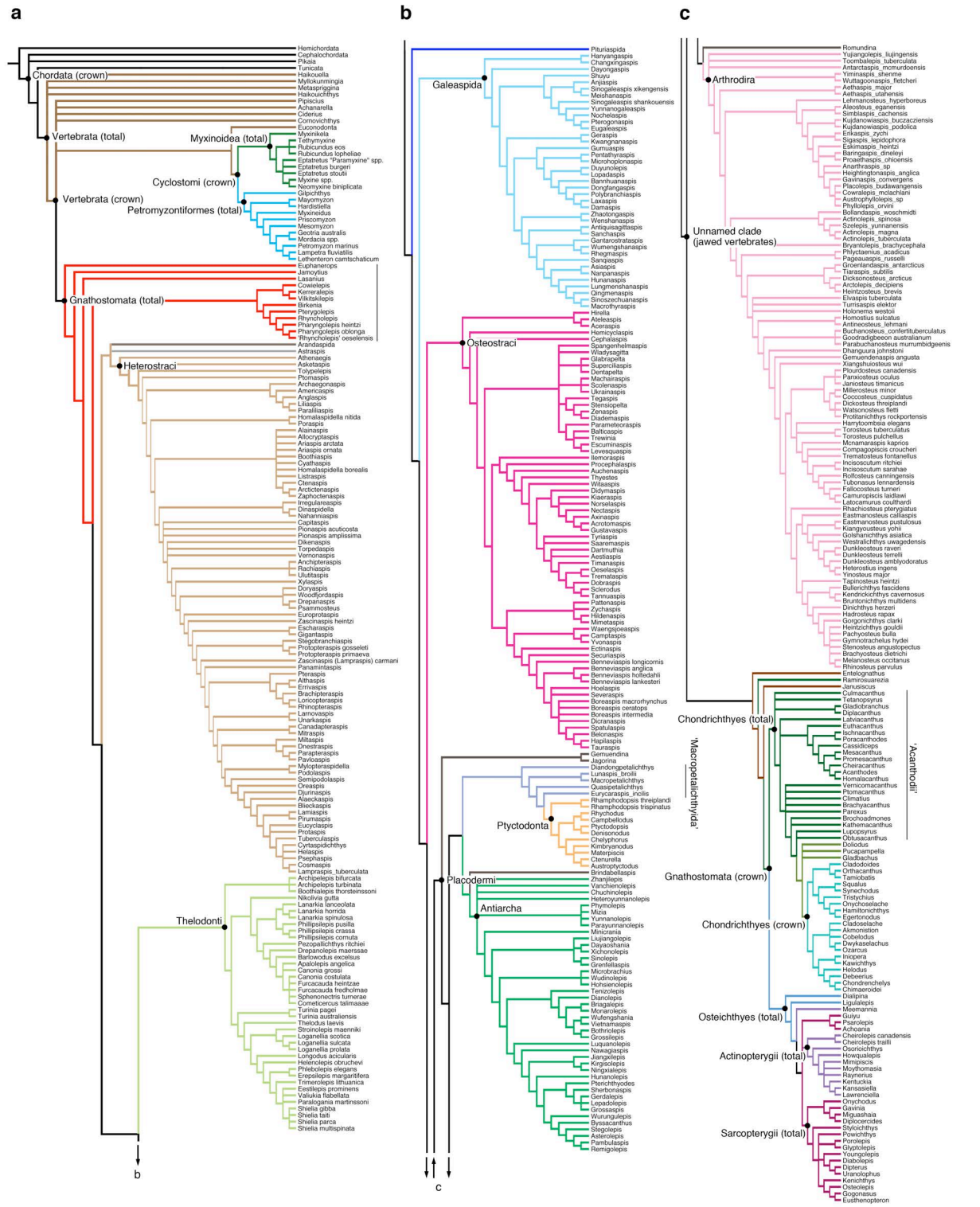
a
b
c
Chordata (crown)
Vertebrata (total)
Myxinoidea (total)
Cyclostomi (crown)
Vertebrata (crown)
Petromyzontiformes (total)
Gnathostomata (total)
Heterostraci
Thelodonti
Galeaspida
Osteostraci
Placodermi
Ptyctodonta
Antiarcha
Arthrodira
Unnamed clade
(jawed vertebrates)
Chondrichthyes (total)
'Macropetalichthyida'
'Acanthodii'
Gnathostomata (crown)
Chondrichthyes (crown)
Osteichthyes (total)
Actinopterygii (total)
Sarcopterygii (total)

Fig. 5.5. Analysis of neural-crest and non-neural-crest characters from Chapter 2 (**2.8.5 List of Characters**; Table 5.2) on the jawless vertebrate backbone of ST1 and ST2. Comparison between neural-crest and non-neural-crest characters in (**a**) consistency and retention indices; (**b**) tree shapes in which branch lengths are proportional to character changes; (**c**) states/steps curves. Whiskers on box plots indicate minimum and maximum values, box ends represent 25 and 75 percentiles, and transverse lines indicate means.

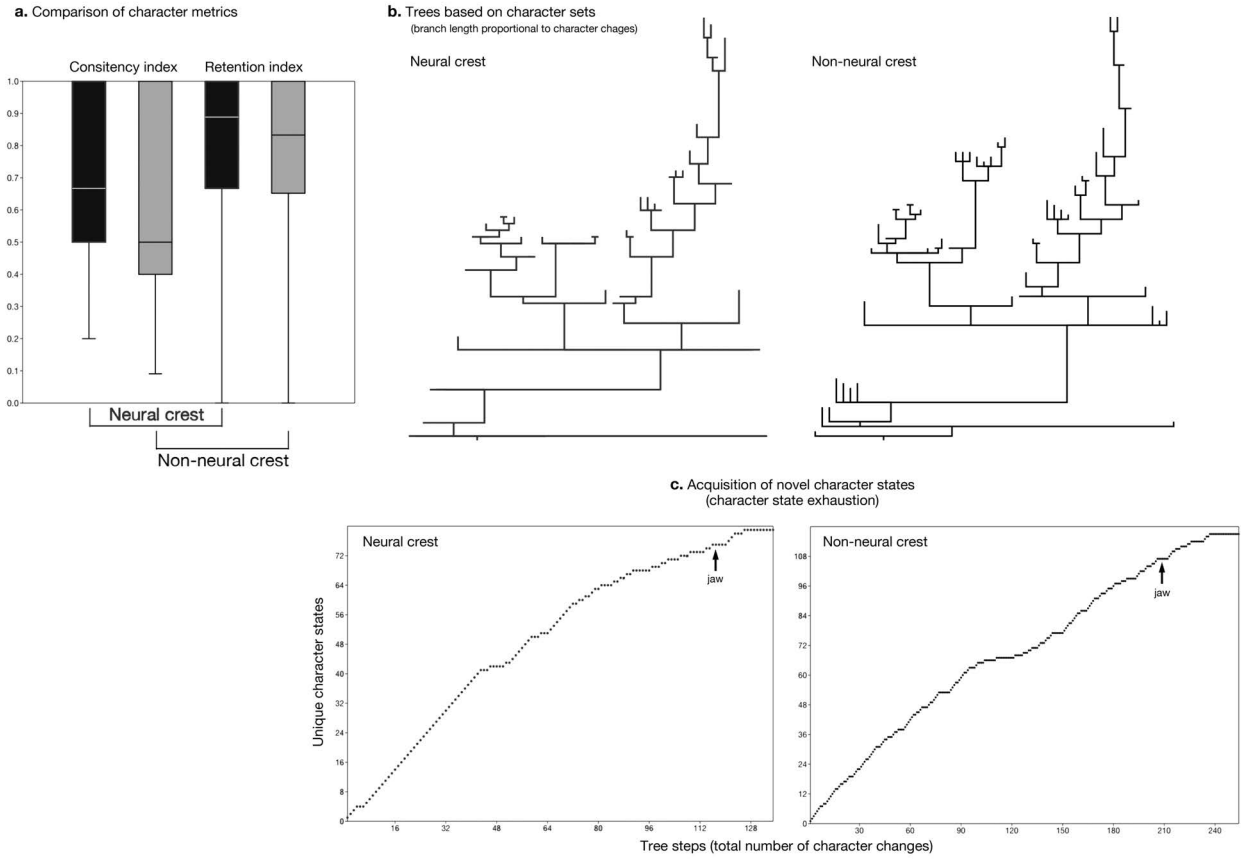
a. Comparison of character metrics
Consitency index
Retention index
Neural crest
Non-neural crest
b. Trees based on character sets
(branch length proportional to character chages)
Neural crest
Non-neural crest
c. Acquisition of novel character states
(character state exhaustion)
Neural crest
jaw
Non-neural crest
jaw
Unique character states
Tree steps (total number of character changes)

TABLE

Table 5.1. Attributes of characters for the supertree analysis of early vertebrates. Broken lines separate primary categories, whereas secondary categories are shaded alternately for clarity. Each character is tagged with one or more attributes in each of cell lineages, body regions, tissue types, functional contexts, gene expression patterns, and character types. Among these attributes, many characters are inapplicable to gene expression patterns, which are predicted by the Extant Phylogenetic Bracket procedure (Bryant and Russell, 1992; Witmer, 1997).See main text for details. Each attributed is coded for Table 5.2: primary category = Arabic numerals; secondary category = upper case letters; tertiary category = lower case letters. Example: 1A, cell lineages = neural tube; 1Cb, body regions = hyoid; 4, functional contexts = feeding.

Primary category	Secondary category	Tertiary category
Cell lineages		
Ectoderm (1)	Neural tube (A)	
	Neural crest (B)	
	Epidermal (C)	
Mesoderm/neural crest (2) (dermal mesenchyme)		
Mesoderm (3)	Axial and paraxial mesoderm (A)	
	Lateral plate mesoderm (B)	
Endoderm (4)	Gut endoderm (A)	
	Endothelium (B)	
Germ line (5)		

Primary category	Secondary category	Tertiary category
Cell lineages		
Ectoderm (1)	Neural tube (A)	
	Neural crest (B)	
	Epidermal (C)	
Mesoderm/neural crest (2) (dermal mesenchyme)		
Mesoderm (3)	Axial and paraxial mesoderm (A)	
	Lateral plate mesoderm (B)	
Endoderm (4)	Gut endoderm (A)	
	Endothelium (B)	
Germ line (5)		

Primary category	Secondary category	Tertiary category
Body regions		
Head (1)	Neurocranial (A)	
	Dermatocranial (B)	
	Splanchocranium (oropharyngeal) (C)	Pre-/mandibular (a)
		Hyoid (b)
		Branchial (c)
Trunk (2)	Epidermal (A)	
	Axial/paraxial/epidermal (B)	Postotic/suprapharyngeal (a)
		Hypobranchial (b)
		Cardium/pericardium (c)
		Trunk (d)
		Postanal (e)
	Appendages (C)	Pectoral fin (a)
		Pelvic fin (b)
		Anal fin (c)
		Dorsal fin (d)
		Caudal fin (e)
	Gut/viscera (D)	Digestive tract (a)
		Reproductive organs (b)
		Other organs (c)
Circulatory (3)		

Primary category	Secondary category	Tertiary category
Tissue types		
Epithelial (1)	Epidermal (A)	
	Endodermal (B)	
	Endothelial (C)	
Nerves/sensory epithelia (2)		
Mesenchymal (3)		
Extracellular matrix (4)	Cartilage (A)	
	Calcified cartilage (B)	
	Enamel/-oid (C)	
	Dentine (D)	
	Bone, acellular (intramembranous) (E)	
	Bone, cellular (F)	Endochondral/perichondral (a)
		Intramembranous (b)
	Keratin (G)	
Connective tissues (5)	Muscle, tendon, ligament (A)	
	Joint/diarthrosis (B)	
Glands/mucosa (6)		
Hematopoietic (7)		
Germ line (8)		

Primary category	Secondary category	Tertiary category
Functional contexts		
Neural coordination (1)		
Sensory (2)		
Locomotion (3)		
Feeding (4)		
Respiration (5)		
Digestive (6)		
Urogenital (7)		
Circulatory (8)		
Structural support (9)		
Secretory (10)		
Defense (11)		
Ornamentation (12)		
Tissue induction (13)		
Immunity (14)		

Primary category	Secondary category	Tertiary category
Gene expression patterns		
Signaling pathways	Hedgehog	
	Wnt	
	FGF	
	TGFβ (BMP and GDF)	
	Endothelin	
	Retinoic acid	
	Notch	
Transcription factors	Homeodomain	*Hox*
		Dlx
		Otx
		Sox
		Pax
		Pitx
		Nkx
	Basic helix-loop-helix	*MyoD/Myf5*

Character types
Presence/absence (1)
Position (2)
Shape (3)
Ratio/size (4)
Meristic (5)

Table 5.2. Attributes assigned to the character set from Chapter 2 (**2.8.5 List of Characters**; subset of the data matrix associated with ST1; **Suppl. 5-2**). Characters were sorted to create submatrices for analysis. Codes are explained in Table 5.1. Header: # = character number from **2.8.5 List of Characters**.

#	Cell lineages	Body regions	Tissue types	Functional contexts	Gene expression patterns	Ch.
1	1B	1, 2	4	2, 3, 4, 5, 11, 12	FGF, Wnt, TGF, Dlx, Pax, Hox	1
2	1B, 1C	1, 2	2	2	FGF, TGF, Wnt, Dlx, Pax, Ptx	1
3	1B	1A	4A	9	Hedgehog, FGF, TGF	1
4	1A	1A	2	1	Hedgehog, Wnt, FGF, TGF, Dlx, Otx,Hox	1
5	1A	1A	2	1	Hedgehog, FGF	1
6	1A, 1B	1A	2	1		1
7	1A, 1B	1A, 1Ca, 1Cb	2	1		1
8	1A	2B	2	1		3
9	1A	2B	2	1		2
10	1A	2B	2	1		2
11	1A	1A	2	1	Hox	1
12	1A	1A	2	2		1
13	1B, 3A	1A, 1B	4	2		1
14	1A, 1C	1A	2, 6	2, 10	Hedgehog, Pitx	1
15	1A	1A	2	2	FGF, Wnt, TGF	1
16	1A, 1C	1A	2	2	FGF, Wnt, TGF	1
17	1C	1B	1B	2	FGF, Wnt, TGF	2
18	1C	1B	1B	2		1
19	1B, 1C	1B	1B	2		1
20	1B, 1C	1A	2	2		1
21	1C	1B	1B	2		3
22	1C	1B	1B	2		3
23	1C	1B	1B, 4A	2		2
24	1C	1B	1B, 4A	2		1
25	1C	1B	1B, 4A	2		1
26	1A	1A	2	2		1
27	1A	1A	2	2	FGF, TGF, Wnt, Pax	1
28	3A	1A	5A	2	MyoD	1
29	3A	1A	5A	2	MyoD	5
30	3A	1A	5A	2	MyoD	2
31	3A	1A	5A	2	MyoD	5
32	1A	1A	2	2		2

#	Cell lineages	Body regions	Tissue types	Functional contexts	Gene expression patterns	Ch.
33	1C	1A	4A	2		1
34	1C	1A	2	2	FGF, Hedgehog	1
35	1C	1A	2	2	FGF, Hedgehog	1
36	1C	1A	2	2	FGF, Hedgehog	1
37	1C	1A	4B	2		1
38	1C	1A	1B	2		1
39	1B	1A, 2A	2	2	Wnt	1
40	1B, 3B	1B, 2A	2, 4	2	Wnt	1
41	1B, 3B	1B, 2A	2, 4	2	Wnt	2
42	1B, 3B	1B, 2A	2, 4	2	Wnt	3
43	1B	1C	2	2		1
44	1A, 1B, 3A	1		2, 4, 5, 9		4
45	4A	1Cc	1B	4, 5	TGF	2
46	4A	1Cc	1B	4, 5	TGF	2
47	4A	1Cc	1B	4, 5	TGF	2
48	1B	1Cc	4A, 4B, 4Fa	4, 5		1
49	1B	1Cc	4A, 4B, 4Fa	4, 5		1
50	1B	1Cc	4A, 4B, 4Fa	4, 5		1
51	4A	1Cb	1B	5	Hox, TGF, Wnt	1
52	4A	1Cc	1B	4, 5	Wnt	1
53	4A	1Cc	1B	5	Wnt	1
54	4A	1Cc	1B	5	Wnt	2
55	4A	1Cc	1B	5	Wnt	2
56	4A	1Cc	1B	4, 5	TGF	5
57	4A	1Cc	1B	4, 5	TGF	5
58	4A	1Cc	1B	4, 5	TGF	5
59	4A	1Cc	1B	4, 5	TGF	4
60	4A	1Cc	1B	4, 5	Wnt	2
61	1B	1Cc	1A, 4Fb	4, 5		1
62	4A	1Cc	1B	5		2
63	1B, 2	1Cc	4C, 4D, 4E, 4Fb	5, 9, 12		1, 5
64	4A	1Ca	1B	4, 5	Wnt	2
65	1C	1Ca	1A	2		1
66	1B, 1C	1Ca	3	13		1
67	1B, 3B, 4A	1Ca	4A, 5A, 5B	4, 5		1
68	1B	1Ca	4A	4, 5		2
69	1B	1Ca	4A	4, 5		2, 3, 4
70	1B	1Ca	4A	4, 5		1
71	4A	1Ca	1B	4, 5		1
72	3B, 4B	2Bc	1C, 5A	8	MyoD	1

#	Cell lineages	Body regions	Tissue types	Functional contexts	Gene expression patterns	Ch.
73	1B, 3B	2Bc	4A, 4Fa, 4Fb, 5A	8		1
74	4B	1, 2	1C	8		1
75	4B	1, 2	1C	8		1
76	4B	2B	1C	8		1
77	4B	1A	1C	8		1
78	3	3	7	14		1
79	3	3	7	14		1
80	4B	3	1C	8		1
81	3A	2B		3		4
82	1B, 3B	2		3		4
83	3B	2C	4A, 4B, 4Fa	3	FGF	1
84	1C, 3A	2Cd	1A, 4A, 4B, 4Fa, 5A	3	FGF	1
85	1C, 3A	2Cd	1A, 4A, 4B, 4Fa, 5A	3	FGF	1
86	1C, 3A	2Cd	1A, 4A, 4B, 4Fa, 5A	3	FGF	2
87	1C, 3A	2Cc	1A, 4A, 4B, 4Fa, 5A	3	FGF	1
88	1C, 3A	2Ca	1A, 4A, 4B, 4Fa, 5A	3	FGF	1
89	1C, 3A	2Ca	1A, 4A, 4B, 4Fa, 5A	3	FGF	1
90	1C, 3A	2Cb	1A, 4A, 4B, 4Fa, 5A	3	FGF	1
91	1C, 3A	2Cb	1A, 4A, 4B, 4Fa, 5A	3	FGF	1
92	1C, 3A	2Cb	1A, 4A, 4B, 4Fa, 5A	3	FGF	3
93	1C, 3A	2Ce	1A, 4A, 4B, 4Fa, 5A	3	FGF	3
94	3A	2Ce	5c	3		3
95	1B, 2, 3	1, 2A, 2B, 2C	4B, 4C, 4D, 4E, 4F	3, 4, 5, 9, 11, 12		1
96	1B, 2, 3	1, 2A, 2B, 2C	4E, 4F	3, 4, 5, 9, 11		1
97	1B, 2, 3	1, 2A, 2B, 2C	4F	3, 4, 5, 9, 11		1
98	1B, 2, 3	1B, 2A	4E	9, 11		1
99	1B, 2, 3	1A, 1C, 2B	4Fa	3, 4, 5, 9, 11		1
100	1B, 3	1A, 1C, 2B, 2C	4B	3, 4, 5, 9, 11		1
101	1B, 3	1A, 1C, 2B, 2C	4A, 4B	3, 4, 5, 9, 11		1
102	1B, 3	1A, 1C, 2B, 2C	4A, 4B	9		2
103	1B, 2	1B, 2A	4D	4, 9, 11, 12	Hedgehog	1
104	1B, 2	1B, 2A	4D	4, 9, 11, 12	Hedgehog	1
105	1B, 2	1B, 2A	4D	4, 9, 11, 12	Hedgehog	1
106	1B, 2	1B, 2A	4D	4, 9, 11, 12	Hedgehog	1
107	1B, 2	1B, 2A	4D	4, 9, 11, 12	Hedgehog	1

#	Cell lineages	Body regions	Tissue types	Functional contexts	Gene expression patterns	Ch.
108	1B, 2	1B, 2A	4D	4, 9, 11, 12	Hedgehog	1
109	1B, 2	1B, 2A	4C	4, 9, 11, 12	Hedgehog	1
110	1B, 2	1B, 2A	4C	4, 9, 11, 12	Hedgehog	1
111	1B, 2, 3	1A, 1C, 2B, 2C	4B, 4E, 4F	3, 4, 5, 9, 11		1
112	1B, 2, 3	1B, 2A, 2C	4B, 4E, 4Fb	3, 4, 5, 9, 11		1
113	2	1B, 2A	4C, 4D, 4E, 4Fb	9, 11, 12	Hedgehog	1
114	2	2A	4C, 4D, 4E, 4Fb	9, 11, 12	Hedgehog	1
115	1B, 2	1B, 2A	4D, 4E	4, 9, 11, 12	Hedgehog	1
116	2	2C	4C, 4D, 4E, 4Fb	3, 9, 11, 12		1
117	2	2C	4C, 4D, 4E, 4Fb	3, 9, 11, 12		1
118	2	2C	4Fb	3, 9, 11, 12		1
119	2	1B, 2A	4C, 4D, 4E, 4Fb	3, 4, 9, 11, 12		1
120	2	1B, 2A	4E, 4Fb	4, 9, 11		1
121	2	1B, 2A	4E, 4Fb	4, 9, 11		1
122	2	1B, 2A	4E, 4Fb	4, 9, 11		1
123	2	1B, 2A	4C, 4D, 4E, 4Fb	9, 11, 12		3
124	2	1B, 2A	4C, 4D, 4E, 4Fb	9, 11, 12		3
125	2	2A, 2Bb	4C, 4D, 4E, 4Fb	9, 11, 12		3
126	2	2A	4C, 4D, 4E, 4Fb	3, 9, 11, 12		1
127	2	2A	4C, 4D, 4E, 4Fb	3, 9, 11, 12		3
128	2, 4B	2B, 2A	1C, 4C, 4D, 4E, 4Fb	8, 9, 11		1
129	2	1B, 2A	2C. 2D, 2E, 2fb	3, 9, 11, 12		3
130	2	1C	4C, 4D, 4E, 4Fb	4, 5, 9		1
131	1B, 2	1B, 1C, 2A	4D	3, 4, 11, 12	Hedgehog	1
132	1B, 2, 3	1B	4C, 4D, 4E, 4Fb	9, 11, 12		1
133	1B, 2, 3	1B	4C, 4D, 4E, 4Fb	9, 11, 12		1
134	1B, 2, 3	1B	4C, 4D, 4E, 4Fb	9, 11, 12		1
135	1B, 2, 3	1B	4C, 4D, 4E, 4Fb	9, 11, 12		1
136	2	1B	4A, 4B, 4Fa	9, 11, 12		1
137	1B, 2	1B	4C, 4D, 4Fb	9, 11		1
138	1B, 2	1Ca	4A, 4B, 4Fa	2, 9, 11		1
139	1B, 2	1Ca	4A, 4B, 4Fa	2, 9, 11		1
140	1B	1C	4A, 4B, 4Fa	4, 5, 9	Dlx, Hox	1
141	1B	1Ca	4G	4		1
142	1B	1Ca	4G	4		1
143	1B	1Ca	4G	4		5
144	1B	1Ca	4G	4		1
145	1B	1Ca	4G	4		5
146	1B	1Cc	4A	5, 9		5
147	3A	2B	4A, 4B, 4E, 4Fa	3, 9	Hox	1

#	Cell lineages	Body regions	Tissue types	Functional contexts	Gene expression patterns	Ch.
148	3A	2B	4A, 4B, 4E, 4Fa	3, 9	Hox	1
149	3A	2B	4A, 4B, 4E, 4Fa	3, 9	Hox	1
150	3A	2B	4A, 4B, 4E, 4Fa	3, 9	Hox	1
151	1B, 3B	1Ca	4A, 4G, 5A	4	MyoD	1
152	1B	1Ca	4C, 4D, 4E, 4G	4		1
153	1B, 3B	1Ca	4A, 4B, 4Fa, 5A, 5B	4	Dlx	1
154	3A	1A	4A, 4B, 4Fa	1, 9		1
155	3A	1A	4A, 4B, 4Fa	1, 9		1
156	3A	1A	4A, 4B, 4Fa	1, 9		1
157	1B	1Ca	4A	4, 5, 9		1
158	1A, 1B	1Ca	1A, 4A, 5A	4		1
159	1A, 1B	1Ca	1A, 2, 4A	2		1
160	1B	1Ca	2, 4A	2, 9		1
161	1B	1Ca	4A	4, 9		1
162	4A, 5	2Db	1B, 8	7		2
163	3A	2Ba	5A	3, 9	MyoD	2
164	3A	2B	5A	3, 9	MyoD	3
165	3A	2B	5A	3, 9	MyoD	3
166	4A	2Da	1B	4, 5, 6		2
167	4A	2Da	1B	6		2
168	3B	2Dc	6	11		1
169	3B	2Dc	6	11		5
170	3B	1Cc, 2Dc	6	11		2
171	1C	1Ca	6	7		1

REFERENCES

Abitua, P. B., Gainous, T. B., Kaczmarczyk, A. N., Winchell, C. J., Hudson, C., Kamata, K., et al. (2015). The pre-vertebrate origins of neurogenic placodes. *Nature*, *524*(7566), 462–465.

Abitua, P. B., Wagner, E., Navarrete, I. A., & Levine, M. (2012). Identification of a rudimentary neural crest in a non-vertebrate chordate. *Nature*, *492*(7427), 104–107.

Ahlborn, F. (1883). Untersuchungen über das gehirn der Petromyzonten. *Zeitschrift für wissenschaftliche Zoologie*, *39*, 191–294.

Ahlborn, F. (1884). Über den ursprung und austritt der hirnnerven von *Petromyzon*. *Zeitschrift für Wissenschaftliche Zoologie*, *40*, 286–308.

Alcock, R. (1898). The peripheral distribution of the cranial nerves of ammocœtes. *Journal of Anatomy and Physiology*, *33*(Pt 1), 131.

Aldridge, R. J., Briggs, D. E. G., Clarkson, E. N. K., & Smith, M. P. (1986). The affinities of conodonts: New evidence from the Carboniferous of Edinburgh, Scotland. *Lethaia*, *19*, 1–14.

Aldridge, R. J., Briggs, D. E. G., Smith, M. P., Clarkson, E. N. K., & Clark, N. D. L. (1993). The anatomy of conodonts. *Philosophical Transactions of the Royal Society B: Biological Sciences*, *340*(1294), 405–421.

Aldridge, R. J., Purnell, M. A., Gabbott, S. E., & Theron, J. N. (1995). The apparatus architecture and function of *Promissum pulchrum* Kovacs-Endrody (Conodonta, Upper Ordovician) and the prioniodontid plan. *Philosophical Transactions of the Royal Society of London B: Biological Sciences*, *347*, 275–291.

Aldridge, R. J., & Donoghue, P. C. J. (1998). Conodonts: A sister group to hagfishes? In J. M. Jørgensen, J. P. Lonholt, R. E. Weber, & H. Malte (Eds.), *The Biology of Hagfishes* (pp. 15–31). London: Chapman.

Allen, W. F. (1916). Studies on the spinal cord and medulla of cyclostomes with special refernce to the formation and expansion of the roof plate and the flattening of the spinal cord. *The Journal of Comparative Neurology*, *26*(1), 9–77.

Anderson, P. S. L., Friedman, M., Brazeau, M. D., & Rayfield, E. J. (2011). Initial radiation of jaws demonstrated stability despite faunal and environmental change. *Nature*, *476*(7359), 206–209.

Andreev, P., Coates, M. I., Karatajūtė-Talimaa, V., Shelton, R. M., Cooper, P. R., Wang, N.-Z., & Sansom, I. J. (2016). The systematics of the Mongolepidida (Chondrichthyes) and the Ordovician origins of the clade. *PeerJ*, *4*, e1850.

Andreev, P. S., Coates, M. I., Shelton, R. M., Cooper, P. R., Smith, M. P., & Sansom, I. J. (2015). Upper Ordovician chondrichthyan-like scales from North America. *Palaeontology*, *58*(4), 691–704.

Antia, D. D. J. (1981). Faunas from the Upper Silurian (upper Ludlovian) in the Ludlow-much Wenlock district, England. *Geological Journal*, *16*(2), 137–147.

Archer, C. W., Dowthwaite, G. P., & Francis-West, P. (2003). Development of synovial joints. *Birth Defects Research Part C: Embryo Today: Reviews*, *69*(2), 144–155.

Arendt, D. (2003). Evolution of eyes and photoreceptor cell types. *International Journal of Developmental Biology*, *47*(7-8), 563–571.

Arendt, D. (2008). The evolution of cell types in animals: Emerging principles from molecular studies. *Nature Reviews Genetics*, *9*(11), 868–882.

Arendt, D., Denes, A. S., Jékely, G., & Tessmar-Raible, K. (2008). The evolution of nervous system centralization. *Philosophical Transactions of the Royal Society B: Biological Sciences*, *363*(1496), 1523–1528.

Arendt, D., Musser, J. M., Baker, C. V. H., Bergman, A., Cepko, C., Erwin, D. H., et al. (2016). The origin and evolution of cell types. *Nature Reviews Genetics*, *17*(12), 744–757.

Arendt, D., & Wittbrodt, J. (2001). Reconstructing the eyes of Urbilateria. *Philosophical Transactions of the Royal Society B: Biological Sciences*, *356*(1414), 1545–1563.

Armstrong, L. A., Wright, G. M., & Youson, J. H. (1987). Transformation of mucocartilage to a definitive cartilage during metamorphosis in the sea lamprey, *Petromyzon marinus*. *Journal of Morphology*, *194*(1), 1–21.

Ayers, H., & Worthington, J. (1908). The finer anatomy of the brain of *Bdellostoma dombeyi*. I. The acustico-lateral system. *American Journal of Anatomy*, *8*(1), 1–16.

Askary, A., Mork, L., Paul, S., He, X., Izuhara, A. K., Gopalakrishnan, S., et al. (2015). Iroquois proteins promote skeletal joint formation by maintaining chondrocytes in an immature state. *Developmental Cell*, *35*(3), 358–365.

Askary, A., Smeeton, J., Paul, S., Schindler, S., Braasch, I., Ellis, N. A., et al. (2016). Ancient origin of lubricated joints in bony vertebrates. *eLife*, *5*, e16415.

Avallone, B., Fascio, U., Balsamo, G., Bianco, P. G., Balassone, G., & Marmo, F. (2007). Morphogenesis of otoliths during larval development in brook lamprey, *Lampetra planeri. Italian Journal of Zoology*, *74*(3), 247–258.

Ayala, F. J., Rzhetsky, A., & Ayala, F. J. (1998). Origin of the metazoan phyla: Molecular clocks confirm paleontological estimates. *Proceedings of the National Academy of Sciences*, *95*(2), 606–611.

Ayers, H., & Jackson, C. M. (1901). Morphology of the Myxinoidei. I. Skeleton and musculature. *Journal of Morphology*, *17*, 185–225.

Balavoine, G., & Adoutte, A. (2003). The segmented Urbilateria: A testable scenario. *Integrative and Comparative Biology*, *43*(1), 137–147.

Balfour, F. M. (1878). The development of the elasmobranchial fishes. *Journal of Anatomy and Physiology*, *11*, 405–706.

Balfour, F. M. (1880). *A Treatise on Comparative Embryology*. London: Macmillan and Co.

Bardack, D. (1991). First fossil hagfish (Myxinoidea): A record from the Pennsylvanian of Illinois. *Science*, *254*(5032), 701–703.

Bardack, D. (1998). Relationships of living and fossil hagfishes. In J. M. Jørgensen, J. P. Lomholt, R. E. Weber, & H. Malte (Eds.), *The Biology of Hagfishes* (pp. 3–14). London: Chapman.

Bardack, D., & Richardson, E. S. (1977). New agnathous fishes from the Pennsylvanian of Illinois. *Fieldiana (Geology)*, *33*(26), 489–510.

Bardack, D., & Zangerl, R. (1968). First fossil lamprey: A record from the Pennsylvanian of Illinois. *Science*, *162*(3859), 1265–1267.

Bardack, D., & Zangerl, R. (1971). Lampreys in the fossil record. In M. W. Hardisty & I. C. Potter (Eds.), *The Biology of Lampreys. Volume 1.* (Vol. 1, pp. 1–65). New York: Academic Press.

Basden, A. M., Young, G. C., Coates, M. I., & Ritchie, A. (2000). The most primitive osteichthyan braincase? *Nature*, *403*(6766), 185–188. doi:10.1038/35003183

Battistuzzi, F. U., Billing-Ross, P., Murillo, O., Filipski, A., & Kumar, S. (2015). A protocol for diagnosing the effect of calibration priors on posterior time estimates: A case study for the Cambrian Explosion of animal phyla. *Molecular Biology and Evolution*, *32*(7), 1907–1912.

Beals, E. W. (1984). Bray-Curtis ordination: An effective strategy for analysis of multivariate ecological data. In A. MacFadyen & E. D. Ford (Eds.), *Advances in Ecological Research* (Vols. 1-Supplement C, Vol. 14, pp. 1–55). Academic Press.

Beard, J. (1888). Morphological studies. I. The parietal eye of the cyclostome rishes. *Quarterly Journal of Microscopical Science*, *s2-29*(113), 55–74.

Bennike, T., Ayturk, U., Haslauer, C. M., Froehlich, J. W., Proffen, B. L., Barnaby, O., et al. (2014). A normative study of the synovial fluid proteome from healthy porcine knee joints. *Journal of Proteome Research*, *13*(10), 4377–4387.

Bergmann, U., Manning, P. L., & Wogelius, R. A. (2012). Chemical mapping of paleontological and archeological artifacts with synchrotron X-rays. *Annual Review of Analytical Chemistry*, *5*(1), 361–389.

Bertin, M., Pomponi, S. M., Kokuhuta, C., Iwasaki, N., Suzuki, T., & Ellington, W. R. (2007). Origin of the genes for the isoforms of creatine kinase. *Gene*, *392*(1–2), 273–282.

Betancur-R, R., Broughton, R. E., Wiley, E. O., Carpenter, K., López, J. A., Li, C., et al. (2013). The tree of life and a new classification of bony fishes. *PLOS Currents Tree of Life*. doi:10.1371/currents.tol.53ba26640df0ccaee75bb165c8c26288

Bever, G. S., Gauthier, J. A., & Wagner, G. P. (2011). Finding the frame shift: digit loss, developmental variability, and the origin of the avian hand. *Evolution & Development*, *13*(3), 269–279.

Bill, B. R., Petzold, A. M., Clark, K. J., Schimmenti, L. A., & Ekker, S. C. (2009). A primer for morpholino use in zebrafish. *Zebrafish*, *6*(1), 69–77.

Bininda-Emonds, O. R. P. (2004a). The evolution of supertrees. *Trends in Ecology & Evolution*, *19*(6), 315–322.

Bininda-Emonds, O. R. P. (2004b). *Phylogenetic Supertrees: Combining information to reveal the Tree of Life*. Springer Science & Business Media.

Bininda-Emonds, O. R. P., Gittleman, J. L., & Steel, M. A. (2002). The (super)tree of life: Procedures, problems, and prospects. *Annual Review of Ecology and Systematics*, *33*(1), 265–289.

Blair, J. E., & Hedges, S. B. (2005a). Molecular phylogeny and divergence times of deuterostome animals. *Molecular Biology and Evolution*, *22*(11), 2275–2284.

Blair, J. E., & Hedges, S. B. (2005b). Molecular clocks do not support the Cambrian Explosion. *Molecular Biology and Evolution*, *22*(3), 387–390.

Blom, H. (2008). A new anaspid fish from the Middle Silurian Cowie Harbour Fish Bed of Stonehaven, Scotland. *Journal of Vertebrate Paleontology*, *28*(3), 594–600.

Blom, H. (2012). New birkeniid anaspid from the Lower Devonian of Scotland and its phylogenetic implications. *Palaeontology*, *55*(3), 641–652.

Blom, H., & Märss, T. (2010). The interrelationships and evolutionary history of anaspid fishes. In D. K. Elliott, J. G. Maisey, X. Yu, & D. Miao (Eds.), *Morphology, Phylogeny and Palaeogeography of Fossil Fishes – honoring Meemann Chang*. Munich: Verlag Dr. Fredrich Pfeil.

Blom, H., Märss, T., & Miller, C. G. (2001). Silurian and earliest Devonian birkeniid anaspids from the Northern Hemisphere. *Earth and Environmental Science Transactions of The Royal Society of Edinburgh*, *92*(3), 263–323.

Boorman, C. J., & Shimeld, S. M. (2002a). Pitx homeobox genes in *Ciona* and amphioxus show left–right asymmetry is a conserved chordate character and define the ascidian adenohypophysis. *Evolution & Development*, *4*(5), 354–365.

Boorman, C. J., & Shimeld, S. M. (2002b). The evolution of left–right asymmetry in chordates. *BioEssays*, *24*(11), 1004–1011.

Bouckaert, R., Heled, J., Kühnert, D., Vaughan, T., Wu, C.-H., Xie, D., et al. (2014). BEAST 2: A software platform for Bayesian evolutionary analysis. *PLOS Computational Biology*, *10*(4), e1003537.

Boyle, J., & Ryan, M. J. (2017). New information on *Titanichthys* (Placodermi, Arthrodira) from the Cleveland Shale (Upper Devonian) of Ohio, USA. *Journal of Paleontology*, *91*(2), 318–336.

Braun, C. B. (1998). Schreiner organs: A new craniate chemosensory modality in hagfishes. *The Journal of Comparative Neurology*, *392*(2), 135–163.

Braun, C. B., & Northcutt, R. G. (1997). The lateral line system of hagfishes (Craniata: Myxinoidea). *Acta Zoologica*, *78*(3), 247–268.

Brazeau, M. D. (2009). The braincase and jaws of a Devonian “acanthodian” and modern gnathostome origins. *Nature*, *457*(7227), 305–308.

Brazeau, M. D. (2011). Problematic character coding methods in morphology and their effects. *Biological Journal of the Linnean Society*, *104*(3), 489–498.

Brazeau, M. D., & Friedman, M. (2014). The characters of Palaeozoic jawed vertebrates. *Zoological Journal of the Linnean Society*, *170*(4), 779–821.

Brazeau, M. D., & Friedman, M. (2015). The origin and early phylogenetic history of jawed vertebrates. *Nature*, *520*(7548), 490–497.

Brazeau, M. D., & de Winter, V. (2015). The hyoid arch and braincase anatomy of *Acanthodes* support chondrichthyan affinity of 'acanthodians.' *Proceedings of the Royal Society of London. Series B: Biological Sciences*, *282*(1821), 20152210.

Briggs, D. E. G. (1992). Conodonts: A major extinct group added to the vertebrates. *Science*, *256*, 1285–1286.

Briggs, D. E. G., Clarkson, E. N. K., & Aldridge, R. J. (1983). The conodont animal. *Lethaia*, *16*(1), 1–14.

Brooks, D. R., & Wiley, E. O. (1985). Theories and methods in different approaches to phylogenetic systematics. *Cladistics*, *1*(1), 1-11.

Broughton, R. E., Betancur-R, R., Li, C., Arratia, G., & Ortí, G. (2013). Multi-locus phylogenetic analysis reveals the pattern and tempo of bony fish evolution. *PLOS Currents Tree of Life*. doi:10.1371/currents.tol.2ca8041495ffafd0c92756e75247483e

Brunet, T., Lauri, A., & Arendt, D. (2015). Did the notochord evolve from an ancient axial muscle? The axochord hypothesis. *BioEssays*, *37*(8), 836–850.

Bryant, H. N., & Russell, A. P. (1992). The role of phylogenetic analysis in the inference of unpreserved attributes of extinct taxa. *Philosophical Transactions of the Royal Society of London. Series B: Biological Sciences*, *337*(1282), 405–418.

Burrow, C. J., & Valiukevičius, J. (2005). Diversity of tissues in acanthodians with Nostolepis-type histological structure. *Acta Palaeontologica Polonica*, *50*(3), 635–649.

Butts, T., Holland, P. W. H., & Ferrier, D. E. K. (2008). The Urbilaterian Super-Hox cluster. *Trends in Genetics*, *24*(6), 259–262.

Calberla, E. (1877). Zur entwicklung des Medullarrohres und der Chorda dorsalis der Teleostier und der Petromyzonten. *Morphologisches Jahrbuch, Leipzig*, *3*, 227–270.

Cameron, C. B. (2016). Saccoglossus testa from the Mazon Creek fauna (Pennsylvanian of Illinois) and the evolution of acorn worms (Enteropneusta: Hemichordata). *Palaeontology*, *59*(3), 329–336.

Cameron, C. B., & Bishop, C. D. (2012). Biomineral ultrastructure, elemental constitution and genomic analysis of biomineralization-related proteins in hemichordates. *Proceedings of the Royal Society of London B: Biological Sciences*, *279*(1740), 3041–3048.

Campione, N. E., Brink, K. S., Freedman, E. A., McGarrity, C. T., & Evans, D. C. (2013). "*Glishades ericksoni*", an indeterminate juvenile hadrosaurid from the Two Medicine Formation of Montana: Implications for hadrosauroid diversity in the latest Cretaceous (Campanian-Maastrichtian) of western North America. *Palaeobiodiversity and Palaeoenvironments*, *93*(1), 65–75.

Carine, M. A., & Scotland, R. W. (1999). Taxic and transformational homology: different ways of seeing. *Cladistics*, *15*(2), 121–129.

Caron, M. M. J., Emans, P. J., Surtel, D. A. M., van der Kraan, P. M., van Rhijn, L. W., & Welting, T. J. M. (2015). BAPX-1/NKX-3.2 acts as a chondrocyte hypertrophy molecular switch in osteoarthritis. *Arthritis & Rheumatology*, *67*(11), 2944–2956.

Carr, R. K., & Hlavin, W. J. (2010). Two new species of *Dunkleosteus*, from the Ohio Shale Formation (USA, Famennian) and the Kettle Point Formation (Canada, Upper Devonian), and a cladistic analysis of the Eubrachythoraci (Placodermi, Arthrodira). *Zoological Journal of the Linnean Society*, *159*(1), 195–222.

Carroll, R. L. (1969). A Middle Pennsylvanian captorhinomorph, and the interrelationships of primitive reptiles. *Journal of Paleontology*, *43*(1), 151–170.

Cattell, M., Lai, S., Cerny, R., & Medeiros, D. M. (2011). A new mechanistic scenario for the origin and evolution of vertebrate cartilage. *PLoS ONE*, *6*(7), e22474.

Cerny, R., Cattell, M., Sauka-Spengler, T., Bronner-Fraser, M., Yu, F., & Medeiros, D. M. (2010). Evidence for the prepattern/cooption model of vertebrate jaw evolution. *Proceedings of the National Academy of Sciences*, *107*(40), 17262–17267.

Chai, Y., Jiang, X., Ito, Y., Bringas, P., Han, J., Rowitch, D. H., et al. (2000). Fate of the mammalian cranial neural crest during tooth and mandibular morphogenesis. *Development*, *127*(8), 1671–1679.

Chang, M. M. (1981). A new crossopterygian, *Youngolepis praecursor*, gen. et sp. nov., from lower Devonian of E. Yunnan, China. *Scientia Sinica*, *24*, 89–97.

Chang, M., Wu, F., Miao, D., & Zhang, J. (2014). Discovery of fossil lamprey larva from the Lower Cretaceous reveals its three-phased life cycle. *Proceedings of the National Academy of Sciences*, *111*(43), 15486–15490.

Chang, M., Zhang, J., & Miao, D. (2006). A lamprey from the Cretaceous Jehol biota of China. *Nature*, *441*(7096), 972–974.

Chen, D., Blom, H., Sanchez, S., Tafforeau, P., & Ahlberg, P. E. (2016). The stem osteichthyan *Andreolepis* and the origin of tooth replacement. *Nature*, *539*(7628), 237–241.

Chen, J.-Y., Dzik, J., Edgecombe, G. D., Ramsköld, L., & Zhou, G.-Q. (1995). A possible Early Cambrian chordate. *Nature*, *377*(6551), 720–722.

Chen, J.-Y., Huang, D.-Y., & Li, C.-W. (1999). An early Cambrian craniate-like chordate. *Nature*, *402*(6761), 518–522.

Chiu, K.-H., & Mok, H.-K. (2011). Study on the accumulation of heavy metals in shallow-water and deep-sea hagfishes. *Archives of Environmental Contamination and Toxicology*, *60*(4), 643–653.

Ciampaglio, C. N., Kemp, M., & McShea, D. W. (2001). Detecting changes in morphospace occupation patterns in the fossil record: Characterization and analysis of measures of disparity. *Paleobiology*, *27*(4), 695–715.

Clark, A. J., Maravilla, E. J., & Summers, A. P. (2010). A soft origin for a forceful bite: Motor patterns of the feeding musculature in Atlantic hagfish, *Myxine glutinosa*. *Zoology*, *113*(5), 259–268.

Clark, A. J., & Summers, A. P. (2007). Morphology and kinematics of feeding in hagfish: Possible functional advantages of jaws. *Journal of Experimental Biology*, *210*(22), 3897–3909.

Clark, A. J., & Summers, A. P. (2012). Ontogenetic scaling of the morphology and biomechanics of the feeding apparatus in the Pacific hagfish *Eptatretus stoutii*. *Journal of Fish Biology*, *80*(1), 86–99.

Clements, T., Dolocan, A., Martin, P., Purnell, M. A., Vinther, J., & Gabbott, S. E. (2016). The eyes of *Tullimonstrum* reveal a vertebrate affinity. *Nature*, *532*(7600), 500–503.

Coates, M. I., Gess, R. W., Finarelli, J. A., Criswell, K. E., & Tietjen, K. (2017). A symmoriiform chondrichthyan braincase and the origin of chimaeroid fishes. *Nature*, *541*(7636), 208–211.

Coates, M. I., & Sequeira, S. E. K. (1998). The braincase of a primitive shark. *Earth and Environmental Science Transactions of The Royal Society of Edinburgh*, *89*(2), 63–85.

Cohn, M. J. (2002). Lamprey Hox genes and the origin of jaws. *Nature*, *416*(6879), 386–387.

Cole, A. G., & Hall, B. K. (2004). The nature and significance of invertebrate cartilages revisited: Distribution and histology of cartilage and cartilage-like tissues within the Metazoa. *Zoology*, *107*(4), 261–273.

Cole, F. J. (1905). A monograph on the general morphology of the myxinoid fishes, based on a study of *Myxine*. Part I. The anatomy of the skeleton. *Transactions of the Royal Society of Edinburgh*, *41*, 749–791.

Cole, F. J. (1926). A monograph on the general morphology of the myxinoid fishes, based on a study of *Myxine*. Part VI. The morphology of the vascular system. *Transactions of the Royal Society of Edinburgh*, *54*, 683–757.

Conel, J. L. (1929). The development of the brain of *Bdellostoma stouti*. I. External growth changes. *The Journal of Comparative Neurology*, *47*(3), 343–403.

Conel, J. L. (1931). The development of the brain of *Bdellostoma stouti*. II. Internal growth changes. *The Journal of Comparative Neurology*, *52*(3), 365–499.

Conel, J. L. (1942). The origin of the neural crest. *The Journal of Comparative Neurology*, *76*(2), 191–215.

Conway Morris, S., & Caron, J.-B. (2012). *Pikaia gracilens* Walcott, a stem-group chordate from the Middle Cambrian of British Columbia. *Biological Reviews*, *87*(2), 480–512.

Conway Morris, S., & Caron, J.-B. (2014). A primitive fish from the Cambrian of North America. *Nature*, *512*(7515), 419–422.

Cox, T. F., & Cox, M. A. A. (2000). *Multidimensional Scaling*, *Second Edition*. CRC Press: Boca Raton. 332 pp.

Cope, E. D. (1886). An interesting connecting genus of Chordata. *The American Naturalist*, *20*(12), 1027–1031.

Cope, E. D. (1889). Synopsis of the families of Vertebrata. *The American Naturalist*, *23*(274), 849–877.

Cori, C. I. (1906). Das Blutgefäßsystem des jungen Ammocoetes. *Arbeiten aus den Zoologischen Instituten der Universität Wien*, *16*, 217–312.

Couly, G. F., Coltey, P. M., & Douarin, N. M. L. (1992). The developmental fate of the cephalic mesoderm in quail-chick chimeras. *Development*, *114*(1), 1–15.

Couly, G. F., Coltey, P. M., & Douarin, N. M. L. (1993). The triple origin of skull in higher vertebrates: A study in quail-chick chimeras. *Development*, *117*(2), 409–429.

Criswell, K. E., Coates, M. I., & Gillis, J. A. (2017a). Embryonic development of the axial column in the little skate, *Leucoraja erinacea*. *Journal of Morphology*, *278*(3), 300–320.

Criswell, K. E., Coates, M. I., & Gillis, J. A. (2017b). Embryonic origin of the gnathostome vertebral skeleton. *Proceedings of the Royal Society of London. Series B: Biological Sciences*,, *284*(1867), 20172121.

Crump, J. G., Maves, L., Lawson, N. D., Weinstein, B. M., & Kimmel, C. B. (2004). An essential role for Fgfs in endodermal pouch formation influences later craniofacial skeletal patterning. *Development*, *131*(22), 5703–5716.

Damas, H. (1935). Contribution à l'étude de la metamorphose de la tête de la lamproie. *Archives de Biologie Paris*, *46*, 171–227.

Damas, H. (1942). Le developpement de la tete de la lamproie (*Lampetra fluviatilis* L.). *Annales de la Société Royale Zoologique de Belgique*, *73*, 201–211.

Damas, H. (1944). Recherches sur le dévelopment de *Lampetra fluviatilis* L. Contribution à l'étude de la cephalogénèse des vertébrés. *Archives de Biologie Paris*, *55*, 1–289.

Damas, H. (1948). L'influence de la lumière sur la segmentation et la gastrulation chez *Lampetra fluviatilis*. *Bulletin de la Société Royale des Sciences de Liège*, *7–10*, 286–292.

Damas, H. (1951). Observations sur le développement des ganglions crâniens chez *Lampetra fluviatillis* (L.). *Archives de Biologie Paris*, *62*, 65–95.

Daniel, J. F. (1934). The circulation of blood in ammocoetes. *University of California Publications in Zoology*, *39*, 311–340.

Dávalos, L. M., Velazco, P. M., Warsi, O. M., Smits, P. D., & Simmons, N. B. (2014). Integrating incomplete fossils by isolating conflicting signal in saturated and non-independent morphological characters. *Systematic Biology*, *63*(4), 582–600.

Davis, S. P., Finarelli, J. A., & Coates, M. I. (2012). *Acanthodes* and shark-like conditions in the last common ancestor of modern gnathostomes. *Nature*, *486*(7402), 247–250.

Davison, W. (2015). The hagfish heart. In S. L. Edwards & G. G. Goss (Eds.), *Hagfish Biology* (Vols. 1-0, pp. 149–160). CRC Press.

Dawson, J. A. (1963). The oral cavity, the "jaws" and the horny teeth of *Myxine glutinosa*. In A. Brodal & R. Fänge (Eds.), *The Biology of Myxine* (pp. 231–255). Oslo: Universtetsforlaget.

De Beer, G. (1937). *The Development of the Vertebrate Skull*. Oxford: Clarendon Press.

Dean, B. (1898). On the development of the Californian hagfish, *Bdellostoma stouti*. *Quarterly Journal of Microscopical Science*, *40*, 269–279.

Dean, B. (1899). On the embryology of *Bdellostoma stouti*. A general account of myxinoid development from the egg and segmentation to hatching. In *Festschrift zum 70ten Geburstag Carl von Kupffer* (pp. 220–276). Jena: Gustav Fischer Verlag.

Decker, R. S., Koyama, E., & Pacifici, M. (2014). Genesis and morphogenesis of limb synovial joints and articular cartilage. *Matrix Biology*, *39*(Supplement C), 5–10.

Delarbre, C., Escriva, H., Gallut, C., Barriel, V., Kourilsky, P., Janvier, P., et al. (2000). The complete nucleotide sequence of the mitochondrial DNA of the agnathan *Lampetra fluviatilis*: Bearings on the phylogeny of cyclostomes. *Molecular Biology and Evolution*, *17*(4), 519–529.

Delarbre, C., Gallut, C., Barriel, V., Janvier, P., & Gachelin, G. (2002). Complete mitochondrial DNA of the hagfish, *Eptatretus burgeri*: The comparative analysis of mitochondrial DNA sequences strongly supports the cyclostome monophyly. *Molecular Phylogenetics and Evolution*, *22*(2), 184–192.

DeLigio, J. T., & Ellington, W. R. (2006). The capacity for the *de novo* biosynthesis of creatine is present in the tunicate *Ciona intestinalis* and is likely widespread in other protochordate and invertebrate groups. *Comparative Biochemistry and Physiology Part D: Genomics and Proteomics*, *1*(2), 167–178.

Denes, A. S., Jékely, G., Steinmetz, P. R., Raible, F., Snyman, H., Prud'Homme, B., Ferrier, D. E., Balavoine, G., & Arendt, D. (2007). Molecular architecture of annelid nerve cord supports common origin of nervous system centralization in Bilateria. *Cell*, *129*(2), 277–288.

Denison, R. H. (1961). Feeding mechanisms of Agnatha and early gnathostomes. *American Zoologist*, *1*(2), 177–181.

Depew, M. J., & Compagnucci, C. (2008). Tweaking the hinge and caps: Testing a model of the organization of jaws. *Journal of Experimental Zoology Part B: Molecular and Developmental Evolution*, *310B*(4), 315–335.

Doflein, F. (1898). Bericht über eine wissenschaftliche Reise nach Californien. *Sitzungsber Gesellsch Morph Physiol München*, *14*, 105–118.

Dohrn, A. (1885). Thyroidea bei *Petromyzon*, Amphioxus und den Tunicaten. *Mittheilungen aus der Zoologischen Station zu Naepel*, *6*, 49–92.

Dohrn, A. (1886). Studien zur Urgeschichte des Wirbelthierkorpers. VII. Entstehung und differenzirung des zungenbein- und Kiefer-apparates de Selachier. VIII. Die Thyroidea bei *Petromyzon*, *Amphioxus* und Tunicaten. *Mittheilungen aus der Zoologischen Station zu Naepel*, *6*, 1–92.

Donoghue, P. C. J. (1998). Growth and patterning in the conodont skeleton. *Philosophical Transactions of the Royal Society of London B: Biological Sciences*, *353*(1368), 633–666.

Donoghue, P. C. J. (2001). Conodonts meet cladistics: Recovering relationships and assessing the completeness of the conodont fossil record. *Palaeontology*, *44*(1), 65–93.

Donoghue, P. C. J. (2002). Evolution of development of the vertebrate dermal and oral skeletons: Unraveling concepts, regulatory theories, and homologies. *Paleobiology*, *28*(4), 474–507.

Donoghue, P. C. J., Forey, P. L., & Aldridge, R. J. (2000). Conodont affinity and chordate phylogeny. *Biological Reviews*, *75*(2), 191–251.

Donoghue, P. C. J., Graham, A., & Kelsh, R. N. (2008a). The origin and evolution of the neural crest. *BioEssays*, *30*(6), 530–541.

Donoghue, P. C. J., & Purnell, M. A. (2009). Distinguishing heat from light in debate over controversial fossils. *BioEssays*, *31*(2), 178–189.

Donoghue, P. C. J., Purnell, M. A., Aldridge, R. J., & Zhang, S. (2008b). The interrelationships of "complex" conodonts (Vertebrata). *Journal of Systematic Palaeontology*, *6*(2), 119–153.

Donoghue, P. C. J., & Rücklin, M. (2016). The ins and outs of the evolutionary origin of teeth. *Evolution & Development*, *18*(1), 19–30.

Donoghue, P. C. J., & Sansom, I. J. (2002). Origin and early evolution of vertebrate skeletonization. *Microscopy Research and Technique*, *59*(5), 352–372.

Donoghue, P. C. J., Sansom, I. J., & Downs, J. P. (2006). Early evolution of vertebrate skeletal tissues and cellular interactions, and the canalization of skeletal development. *Journal of Experimental Zoology Part B: Molecular and Developmental Evolution*, *306B*(3), 278–294.

Donoghue, P. C. J., & Smith, M. P. (2001). The anatomy of *Turinia pagei* (Powrie), and the phylogenetic status of the Thelodonti. *Earth and Environmental Science Transactions of The Royal Society of Edinburgh*, *92*(1), 15–37.

Dornburg, A., Townsend, J. P., Friedman, M., & Near, T. J. (2014). Phylogenetic informativeness reconciles ray-finned fish molecular divergence times. *BMC Evolutionary Biology*, *14*, 169.

Downs, J. P., & Donoghue, P. C. J. (2009). Skeletal histology of *Bothriolepis canadensis* (Placodermi, Antiarchi) and evolution of the skeleton at the origin of jawed vertebrates. *Journal of Morphology*, *270*(11), 1364–1380.

Duboule, D. (1994). Temporal colinearity and the phylotypic progression: A basis for the stability of a vertebrate Bauplan and the evolution of morphologies through heterochrony. *Development*, *1994*(Supplement), 135–142.

Dudgeon, C. L., Coulton, L., Bone, R., Ovenden, J. R., & Thomas, S. (2017). Switch from sexual to parthenogenetic reproduction in a zebra shark. *Scientific Reports*, *7*, 40537.

Duméril, A. M. C. (1806). *Zoologie Analytique, ou Mèthode Naturelle de Classi cation des Animaux*. Paris: Didot.

Dupret, V., Sanchez, S., Goujet, D., & Ahlberg, P. E. (2017). The internal cranial anatomy of *Romundina stellina* Ørvig, 1975 (Vertebrata, Placodermi, Acanthothoraci) and the origin of jawed vertebrates—Anatomical atlas of a primitive gnathostome. *PLOS ONE*, *12*(2), e0171241.

Dupret, V., Sanchez, S., Goujet, D., Tafforeau, P., & Ahlberg, P. E. (2014). A primitive placoderm sheds light on the origin of the jawed vertebrate face. *Nature*, *507*(7493), 500–503.

Dupret, V., Zhu, M., & Wang, J.-Q. (2009). The morphology of *Yujiangolepis liujingensis* (Placodermi, Arthrodira) from the Pragian of Guangxi (south China) and its phylogenetic significance. *Zoological Journal of the Linnean Society*, *157*(1), 70–82.

Dupret, V., Zhu, M., & Wang, J.-Q. (2017). Redescription of *Szelepis* Liu, 1981 (Placodermi, Arthrodira), from the Lower Devonian of China. *Journal of Vertebrate Paleontology*, *37*(2), e1312422.

DuVal, M. G., Oel, A. P., & Allison, W. T. (2014). gdf6a is required for cone photoreceptor subtype differentiation and for the actions of tbx2b in determining rod versus cone photoreceptor fate. *PLOS ONE*, *9*(3), e92991.

Dzik, J. (1991). Evolution of oral apparatuses in the conodont chordate. *Acta Palaeontologica Polonica*, *36*(3), 265–323.

Edgeworth, F. H. (1935). *The Cranial Muscles of the Vertebrates* (1st edition.). Cambridge: Cambridge University Press.

Ellington, W. R., & Suzuki, T. (2007). Early evolution of the creatine kinase gene family and the capacity for creatine biosynthesis and membrane transport. In G. S. Salomons & M. Wyss (Eds.), *Creatine and Creatine Kinase in Health and Disease* (pp. 17–26). Springer Netherlands.

Erdtmann, B.-D., Weber, B., Schultze, H.-P., & Egenhoff, S. (2000). A possible agnathan plate from the lower arenig (lower ordovician) of south Bolivia. *Journal of Vertebrate Paleontology*, *20*(2), 394–399.

Erwin, D. H. (2007). Disparity: Morphological pattern and developmental context. *Palaeontology*, *50*(1), 57–73.

Erwin, D. H., Laflamme, M., Tweedt, S. M., Sperling, E. A., Pisani, D., & Peterson, K. J. (2011). The Cambrian conundrum: Early divergence and later ecological Success in the early history of animals. *Science*, *334*(6059), 1091–1097.

Evans, D. J. R., & Noden, D. M. (2006). Spatial relations between avian craniofacial neural crest and paraxial mesoderm cells. *Developmental Dynamics*, *235*(5), 1310–1325.

Fasham, M. J. R. (1977). A comparison of nonmetric multidimensional scaling, principal components and reciprocal averaging for the ordination of simulated coenoclines, and coenoplanes. *Ecology*, *58*(3), 551–561.

Feldheim, K. A., Clews, A., Henningsen, A., Todorov, L., McDermott, C., Meyers, M., et al. (2016). Multiple births by a captive swellshark *Cephaloscyllium ventriosum* via facultative parthenogenesis. *Journal of Fish Biology*, *90*(3), 1047–1053.

Fernandes, F., Pereira, L., & Freitas, A. T. (2009). CSA: An efficient algorithm to improve circular DNA multiple alignment. *BMC Bioinformatics*, *10*, 230.

Fernholm, B. (1991). *Eptatretus eos*: A new species of hagfish (Myxinidae) from the Tasman Sea. *Japanese Journal of Ichthyology*, *38*, 115–118.

Fernholm, B. (1998). Hagfish systematics. In J. M. Jørgensen, J. P. Lomholt, R. E. Weber, & H. Malte (Eds.), *The Biology of Hagfishes* (pp. 33–44). London: Chapman.

Fernholm, B., Norén, M., Kullander, S. O., Quattrini, A. M., Zintzen, V., Roberts, C. D., et al. (2013). Hagfish phylogeny and taxonomy, with description of the new genus *Rubicundus* (Craniata, Myxinidae). *Journal of Zoological Systematics and Evolutionary Research*, *51*(4), 296–307.

Fernholm, B., & Quattrini, A. M. (2008). A new species of hagfish (Myxinidae: *Eptatretus*) associated with deep-sea coral habitat in the western North Atlantic. *Copeia*, *2008*(1), 126–132.

Ferry, J. D. (1941). A fibrous protein from the slime of the hagfish. *Journal of Biological Chemistry*, *138*(1), 263–268.

Forey, P. L. (1984). Yet more reflections on agnathan-gnathostome relationships. *Journal of Vertebrate Paleontology*, *4*(3), 330–343.

Forey, P. L. (1995). Agnathans recent and fossil, and the origin of jawed vertebrates. *Reviews in Fish Biology and Fisheries*, *5*, 267–303.

Forey, P. L., & Gardiner, B. G. (1986). Observations on *Ctenurella* (Ptyctodontida) and the classification of placoderm fishes. *Zoological Journal of the Linnean Society*, *86*(1), 43–74.

Forey, P. L., & Janvier, P. (1993). Agnathans and the origin of jawed vertebrates. *Nature*, *361*(6408), 129–134.

Forey, P. L., Yi, L., Patterson, C., & Davies, C. E. (2003). Fossil fishes from the Cenomanian (Upper Cretaceous) of Namoura, Lebanon. *Journal of Systematic Palaeontology*, *1*(4), 227–330.

Fox, W. T. (1968). Quantitative paleoecologic analysis of fossil communities in the Richmond Group. *The Journal of Geology*, *76*(6), 613–640.

Freud, S. (1877). Über den ursprung der hinteren nervenwurzeln im rückenmarke von ammocötes (*Petromyzon planeri*). *Akademie der Wissenschaften in Wien. Sitzungsberichte (Mathematisch-Naturwissenschaftliche Klasse), 3. Abteilung*, *75*, 15–27.

Freud, S. (1878). Über spinalganglien und rückenmark des *Petromyzon*. *Akademie der Wissenschaften in Wien. Sitzungsberichte (Mathematisch-Naturwissenschaftliche Klasse), 3. Abteilung*, *78*, 81–167.

Friedman, M. (2015). The early evolution of ray-finned fishes. *Palaeontology*, *58*(2), 213–228.

Friedman, M., & Brazeau, M. D. (2010). A reappraisal of the origin and basal radiation of the Osteichthyes. *Journal of Vertebrate Paleontology*, *30*(1), 36–56.

Fudge, D. S., Gardner, K. H., Forsyth, V. T., Riekel, C., & Gosline, J. M. (2003). The mechanical properties of hydrated intermediate filaments: Insights from hagfish slime threads. *Biophysical Journal*, *85*(3), 2015–2027.

Fudge, D. S., & Gosline, J. M. (2004). Molecular design of the α–keratin composite: Insights from a matrix–free model, hagfish slime threads. *Proceedings of the Royal Society of London B: Biological Sciences*, *271*(1536), 291–299.

Fudge, D. S., Hillis, S., Levy, N., & Gosline, J. M. (2010). Hagfish slime threads as a biomimetic model for high performance protein fibres. *Bioinspiration & Biomimetics*, *5*(3), 35002.

Fudge, D. S., Levy, N., Chiu, S., & Gosline, J. M. (2005). Composition, morphology and mechanics of hagfish slime. *Journal of Experimental Biology*, *208*(24), 4613–4625.

Fujimoto, S., Oisi, Y., Kuraku, S., Ota, K. G., & Kuratani, S. (2013). Non-parsimonious evolution of hagfish Dlx genes. *BMC Evolutionary Biology*, *13*(1), 15.

Furlong, R. F., & Holland, P. W. H. (2002). Bayesian phylogenetic analysis supports monophyly of Ambulacraria and of cyclostomes. *Zoological Science*, *19*(5), 593–599.

Gabbott, S. E., Aldridge, R. J., & Theron, J. N. (1995). A giant conodont with preserved muscle tissue from the Upper Ordovician of South Africa. *Nature*, *374*(6525), 800–803.

Gabbott, S. E., Donoghue, P. C. J., Sansom, R. S., Vinther, J., Dolocan, A., & Purnell, M. A. (2016). Pigmented anatomy in Carboniferous cyclostomes and the evolution of the vertebrate eye. *Proceedings of the Royal Society of London. Series B: Biological Sciences*, *283*(1836), 20161151.

Gagnier, P.-Y. (1993a). *Sacabambaspis janvieri*, Vertébré ordovicien de Bolivie. 1. Analyse morphologique. *Annales de Paléontologie (Vertébrés)*, *79*, 19–69.

Gagnier, P.-Y. (1993b). *Sacabambaspis janvieri*, Vertébré ordovicien de Bolivie. 2. Analyse phylogénétique. *Annales de Paléontologie (Vertébrés)*, *79*, 119–166.

Gagnon, J. A., Valen, E., Thyme, S. B., Huang, P., Ahkmetova, L., Pauli, A., et al. (2014). Efficient mutagenesis by Cas9 protein-mediated oligonucleotide insertion and large-scale assessment of single-guide RNAs. *PLOS ONE*, *9*(5), e98186.

Gai, Z., Donoghue, P. C. J., Zhu, M., Janvier, P., & Stampanoni, M. (2011). Fossil jawless fish from China foreshadows early jawed vertebrate anatomy. *Nature*, *476*(7360), 324–327.

Gai, Z., Zhu, M., Jia, L., & Zhao, W. (2015). A streamlined jawless fish (Galeapida) from the Lower Devonian of Yunnan, China and its taxonomic and paleoecological implications. *Vertebrata PalAsiatica*, *53*, 93–109.

Gaidos, E., Dubuc, T., Dunford, M., Mcandrew, P., Padilla-Gamiño, J., Studer, B., et al. (2007). The Precambrian emergence of animal life: a geobiological perspective. *Geobiology*, *5*(4), 351–373.

Gans, C. (1993). Evolutionary origin of the vertebrate skull. In J. Hanken & B. K. Hall (Eds.), *The Skull. Volume 2. Patterns of Structural and Systematic Diversity* (pp. 1–35). Chicago: The University of Chicago Press.

Garcia-Fernàndez, J. (2005). The genesis and evolution of homeobox gene clusters. *Nature Reviews Genetics*, *6*(12), 881–892.

Gans, C., & Northcutt, R. G. (1983). Neural crest and the origin of vertebrates: A new head. *Science*, *220*(4594), 268–273.

Garstang, W. (1928). The morphology of the Tunicata, and its bearings on the phylogeny of the Chordata. *Quarterly Journal of Microscopical Science*, *s2-72*(285), 51–187.

Gaskell, W. H. (1898). On the origin of vertebrates, deduced from the study of ammocœtes. *Journal of Anatomy and Physiology*, *33*(Pt 1), 154–188.2.

Gaskell, W. H. (1900). Origin of vertebrates, deduced from the study of ammocœtes. *Journal of Anatomy and Physiology*, *34*(Pt 4), 465–588.3.

Gaskell, W. H. (1901). On the origin of vertebrates, deduced from the study of ammocœtes. *Journal of Anatomy and Physiology*, *35*(Pt 2), 224.

Gaskell, W. H. (1902). The origin of vertebrates, deduced from the study of ammocœtes. *Journal of Anatomy and Physiology*, *36*(Pt 2), 164–208.

Gaskell, W. H. (1903). On the origin of vertebrates deduced from the study of ammocœtes. *Journal of Anatomy and Physiology*, *37*(Pt 2), 168–219.

Gaskell, W. H. (1908). *On the Origin of Vertebrates*. London and New York: Longmans, Green.

Gee, H. (1996). *Before the Backbone. Views on the origin of vertebrates* (1996 edition.). London ; New York: Springer.

Gegenbaur, C. (1859). *Grundzüge der Vergleichenden Anatomie*. Leipzig: Wilhelm Engelmann.

Geisha. http://geisha.arizona.edu/geisha/. Accessed 2 October 2017

Gelman, S., Ayali, A., Tytell, E. D., & Cohen, A. H. (2007). Larval lampreys possess a functional lateral line system. *Journal of Comparative Physiology A*, *193*(2), 271–277.

Gelman, S., Cohen, A. h., & Sanovich, E. (2009). Developmental changes in the ultrastructure of the lamprey lateral line nerve during metamorphosis. *Journal of Morphology*, *270*(7), 815–824.

Germain, D., Sanchez, S., Janvier, P., & Tafforeau, P. (2014). The presumed hagfish *Myxineidus gononorum* from the Upper Carboniferous of Montceau-les-Mines (Saône-et-Loire, France): New data obtained by means of Propagation Phase Contrast X-ray Synchrotron Microtomography. *Annales de Paléontologie*, *100*(2), 131–135.

Gerber, S. (2013). On the relationship between the macroevolutionary trajectories of morphological integration and morphological disparity. *PLOS ONE*, *8*(5), e63913.

Gess, R. W., Coates, M. I., & Rubidge, B. S. (2006). A lamprey from the Devonian period of South Africa. *Nature*, *443*(7114), 981–984.

Gilbert, S. F. (2013). *Developmental Biology, Tenth Edition* (10 edition.). Sunderland, MA, USA: Sinauer Associates, Inc.

Gilbert, S. F., & Barresi, M. J. F. (2016). *Developmental Biology* (11 edition.). Sunderland, Massachusetts: Sinauer Associates is an imprint of Oxford University Press.

Gilbert, S. F., & Raunio, A. M. (Eds.). (1997). *Embryology: Constructing the Organism* (1 edition.). Sunderland, MA: Sinauer Associates.

Giles, S., Friedman, M., & Brazeau, M. D. (2015). Osteichthyan-like cranial conditions in an Early Devonian stem gnathostome. *Nature*, *520*(7545), 82–85.

Giles, S., Rücklin, M., & Donoghue, P. C. J. (2013). Histology of "placoderm" dermal skeletons: Implications for the nature of the ancestral gnathostome. *Journal of Morphology*, *274*(6), 627–644.

Giles, S., Xu, G.-H., Near, T. J., & Friedman, M. (2017). Early members of "living fossil" lineage imply later origin of modern ray-finned fishes. *Nature*, *549*(7671), 265–268.

Gill, H. S., Renaud, C. B., Chapleau, F., Mayden, R. L., Potter, I. C., & Douglas, M. E. (2003). Phylogeny of living parasitic lampreys (Petromyzontiformes) based on morphological data. *Copeia*, *2003*(4), 687–703.

Gillis, J. A., Alsema, E. C., & Criswell, K. E. (2017). Trunk neural crest origin of dermal denticles in a cartilaginous fish. *Proceedings of the National Academy of Sciences*, *114*(50), 13200–13205.

Gillis, J. A., & Donoghue, P. C. J. (2007). The homology and phylogeny of chondrichthyan tooth enameloid. *Journal of Morphology*, *268*(1), 33–49.

Gilmore, B. (1992). Scroll coprolites from the Silurian of Ireland and the feeding of early vertebrates. *Palaeontology.*, *35*, 319–333.

Glaesner, L. (1910). Studien zur Entwicklungsgeschichte von *Petromyzon fluviatilis*. *Zoologische Jahrbücher (Anatomie)*, *24*, 139–190.

Glover, C. N., Blewett, T. A., & Wood, C. M. (2015). Novel route of toxicant exposure in an ancient extant vertebrate: Nickel uptake by hagfish skin and the modifying effects of slime. *Environmental Science & Technology*, *49*(3), 1896–1902.

Glover, C. N., Bucking, C., & Wood, C. M. (2011). Adaptations to in situ feeding: Novel nutrient acquisition pathways in an ancient vertebrate. *Proceedings of the Royal Society of London B: Biological Sciences*, *278*(1721), 3096–3101.

Goette, A. (1890). *Entwicklungsgeechichte des Flussneunauges, Petromyzon fluviatilis*. Leipzig.

Goodrich, E. S. (1901). On the excretory organs of amphioxus. *Proceedings of the Royal Society of London*, *69*, 350–351.

Goodrich, E. S. (1902). On the structure of the excretory organs of amphioxus. Part I. *Quarterly Journal of Microscopical Science*, *s2-45*(180), 493–501.

Goodrich, E. S. (1909a). On the structure of the excretory organs of amphioxus. *Quarterly Journal of Microscopical Science*, *s2-54*(214), 185–205.

Goodrich, E. S. (1909b). *Vertebrata Craniata*. London: Adam and Charles Black.

Goodrich, E. S. (1930). *Studies on the Structure and Development of Vertebrates* (Vols. 1-2). London: Dover Publishing.

Gorbman, A. (1983). Early development of the hagfish pituitary gland: Evidence for the endodermal 0rigin of the adenohypophysis. *American Zoologist*, *23*(3), 639–654.

Gorbman, A., & Tamarin, A. (1985). Early development of oral, olfactory and adenohypophyseal structures of agnathans and its evolutionary implications. In R. E. Foreman, A. Gorbman, J. M. Dodd, & R. Olsson (Eds.), *Evolutionary Biology of Primitive Fishes* (pp. 165–185). Springer US.

Goudemand, N., Orchard, M. J., Urdy, S., Bucher, H., & Tafforeau, P. (2011). Synchrotron-aided reconstruction of the conodont feeding apparatus and implications for the mouth of the first vertebrates. *Proceedings of the National Academy of Sciences*, *108*(21), 8720–8724.

Goujet, D. (1984). *Les poissons placodermes du Spitsberg. Arthrodires Dolichothoraci de la Formation de Wood Bay (Devonien Inferieur)*. Paris: Centre national de la Recherche scientifique.

Gould, S. J. (1977). *Ontogeny and Phylogeny*. Cambridge: Belknap Press. 520 pp.

Grande, L., & Rieppel, O. (1994). (Eds.) *Interpreting the Hierarchy of Nature: From Systematic Patterns to Evolutionary Process Theories*. San Diego: Academic Press. 298 pp.

Green, S. A., Simoes-Costa, M., & Bronner, M. E. (2015). Evolution of vertebrates as viewed from the crest. *Nature*, *520*(7548), 474–482.

Green, S. A., Uy, B. R., & Bronner, M. E. (2017). Ancient evolutionary origin of vertebrate enteric neurons from trunk-derived neural crest. *Nature*, *544*(7648), 88–91.

Gregory, W. K. (1931). Certain critical stages in the evolution of the vertebrate jaws. *International Journal of Orthodontia, Oral Surgery and Radiography*, *17*(12), 1138–1148.

Gregory, W. K. (1946). The roles of motile larvae and fixed adults in the origin of the vertebrates. *The Quarterly Review of Biology*, *21*(4), 348–364.

Griffith, R. W., & Thomson, K. S. (1973). *Latimeria chalumnae*: Reproduction and conservation. *Nature*, *242*(5400), 617–618.

Grogan, E. D., Lund, R., & Greenfest-Allen, E. (2012). The origin and relationships of early chondrichthyans. In J. C. Carrier, J. A. Musick, & M. R. Heithaus (Eds.), *Biology of Sharks and Their Relatives* (pp. 3–29). CRC Press.

Gross, J. B., & Hanken, J. (2005). Cranial neural crest contributes to the bony skull vault in adult Xenopus laevis: Insights from cell labeling studies. *Journal of Experimental Zoology Part B: Molecular and Developmental Evolution*, *304B*(2), 169–176.

Gross, J. B., & Hanken, J. (2008a). Review of fate-mapping studies of osteogenic cranial neural crest in vertebrates. *Developmental Biology*, *317*(2), 389–400.

Gross, J. B., & Hanken, J. (2008b). Segmentation of the vertebrate skull: neural-crest derivation of adult cartilages in the clawed frog, *Xenopus laevis*. *Integrative and Comparative Biology*, *48*(5), 681–696.

Gross, W. (1968). Fragliche Actinopterygier-Schuppen Aus Dem Silur Gotlands. *Lethaia*, *1*(2), 184–218.

Guo, X., Day, T. F., Jiang, X., Garrett-Beal, L., Topol, L., & Yang, Y. (2004). Wnt/β-catenin signaling is sufficient and necessary for synovial joint formation. *Genes & Development*, *18*(19), 2404–2417.

Haeckel, E. (1876). *The Evolution of Man: A popular exposition of the principal points of human ontogney phylogeny. 3rd edition.* (Vols. 1-2). Akron: The Werner Company.

Hall, B. K. (1994). (Ed.) *Homology: The Hierarchical Basis of Comparative Biology.* San Diego: Academic Press. 483 pp.

Hall, B. K. (2005). *Bones and Cartilage: Developmental and Evolutionary Skeletal Biology* (1 edition.). Australia; San Diego, Calif: Academic Press.

Hall, B. K. (2009). *The Neural Crest and Neural Crest Cells in Vertebrate Development and Evolution*. New York: Springer.

Hall, B. K. (2015). *Bones and Cartilage: Developmental and Evolutionary Skeletal Biology. 2nd edition.* London: Academic Press.

Hall, B. K., & Hörstadius, S. (1989). *The Neural Crest*. New York: Oxford University Press.

Hall, B. K., & Miyake, T. (2000). All for one and one for all: Condensations and the initiation of skeletal development. *BioEssays*, *22*(2), 138–147.

Hallgrímsson, B., & Hall, B. K. (2011). *Variation: A Central Concept in Biology*. Academic Press.

Hallgrimsson, B., Mio, W., Marcucio, R. S., & Spritz, R. (2014). Let's face it—Complex traits are just not that simple. *PLOS Genetics*, *10*(11), e1004724.

Halstead, L. B. (1971). The presence of a spiracle in the Heterostraci (Agnatha). *Zoological Journal of the Linnean Society*, *50*(2), 195–197.

Halstead, L. B. (1973a). The heterostracan fishes. *Biological Reviews*, *48*(3), 279–332.

Halstead, L. B. (1973b). Affinities of the Heterostraci (Agnatha). *Biological Journal of the Linnean Society*, *5*(4), 339–349.

Häming, D., Simoes-Costa, M., Uy, B., Valencia, J., Sauka-Spengler, T., & Bronner-Fraser, M. (2011). Expression of sympathetic nervous system genes in lamprey suggests their recruitment for specification of a new vertebrate feature. *PLOS ONE*, *6*(10), e26543

Hammer, Ø., Harper, D. A. T., & Ryan, P. D. (2017). *PAST. Paleontological Statistics software package for education.* Oslo. https://folk.uio.no/ohammer/past/

Hammond, K. L., Baxendale, S., McCauley, D. W., Ingham, P. W., & Whitfield, T. T. (2009). Expression of patched, prdm1 and engrailed in the lamprey somite reveals conserved responses to Hedgehog signaling. *Evolution & Development*, *11*(1), 27–40.

Hammond, K. L., & Whitfield, T. T. (2006). The developing lamprey ear closely resembles the zebrafish otic vesicle: otx1 expression can account for all major patterning differences. *Development*, *133*(7), 1347–1357.

Hanke, G. F., & Wilson, M. V. H. (2004). New teleostome fishes and acanthodian systematics. In G. Arratia, M. V. H. Wilson, & R. Cloutier (Eds.), *Recent Advances in the Origin and Early Radiation of the Vertebrates, Honoring Hans-Peter Schultze* (pp. 189–216). Munich: Verlag Dr. Friedrich Pfeil.

Hanke, G. F., & Wilson, M. V. H. (2006). Anatomy of the early Devonian acanthodian *Brochoadmones milesi* based on nearly complete body fossils, with comments on the evolution and development of paired fins. *Journal of Vertebrate Paleontology*, *26*(3), 526–537.

Hardisty, M. W. (1979). *Biology of the Cyclostomes*. Springer.

Hardisty, M. W. (1981). The skeleton. In M. W. Hardisty & I. C. Potter (Eds.), *The Biology of Lampreys* (Vol. 3, pp. 118–124).

Hardisty, M. W. (1982). Lampreys and hagfishes: Analysis of cyclostome relationships. In M. W. Hardisty & I. C. Potter (Eds.), *The Biology of Lampreys* (Vol. 4b, pp. 165–259). New York: Academic Press.

Hardisty, M. W., & Rovainen, C. M. (1982). Morphological and functional aspects of the muscular system. In M. W. Hardisty & I. C. Potter (Eds.), *The Biology of Lampreys* (Vol. 4a, pp. 137–231). New York: The Academic Press.

Harrison, F. W., & Ruppert, E. E. (Eds.). (1997). *Microscopic Anatomy of Invertebrates, Hemichordata, Chaetognatha, and the Invertebrate Chordates* (1 edition.). New York, NY: Wiley-Liss.

Hartmann, C. (2009). Transcriptional networks controlling skeletal development. *Current Opinion in Genetics & Development*, *19*(5), 437–443.

Hasse, C. (1893). Die Entwicklung der Wirbelsäule der Cyclostomen. *Zeitschrift für wissenschaftliche Zoologie*, *57*, 290–305.

Hatta, S. (1897). Contributions to the morphology of Cyclostomata. I. On the formation of the heart in *Petromyzon*. *Journal of the College of Science, Imperial University of Tokyo*, *10*, 225–237.

Hatta, S. (1900). Contributions to the morphology of Cyclostomata. II: The development of pronephros and segmental duct in *Petromyzon*. *Journal of the College of Science, Imperial University of Tokyo*, *13*, 311–425.

Hatta, S. (1907). On the gastrulation in *Petromyzon*. *Journal of the College of Science, Imperial University of Tokyo*, *21*, 1–44.

Hatta, S. (1915). The fate of the peristomal mesoderm and the tail in *Petromyzon*. *Annotationes Zoologicae Japonenses*, *9*, 49–62.

Hatta, S. (1923). Über die entwicklung des gefäßsytems des neunauges, *Lampetra mitsukurii* Hatta. *Zoologische Jahrbücher (Anatomie)*, *44*, 1–264.

Heath, T. A., Huelsenbeck, J. P., & Stadler, T. (2014). The fossilized birth–death process for coherent calibration of divergence-time estimates. *Proceedings of the National Academy of Sciences*, *111*(29), E2957–E2966.

Hedges, S. B., Battistuzzi, F. U., & Blair, J. E. (2006). Molecular timescale of evolution in the Proterozoic. In S. Xiao & A. J. Kaufman (Eds.), *Neoproterozoic Geobiology and Paleobiology* (pp. 199–229). Springer Netherlands.

Heikkilä, M., Mutanen, M., Kekkonen, M., & Kaila, L. (2014). Morphology reinforces proposed molecular phylogenetic affinities: A revised classification for Gelechioidea (Lepidoptera). *Cladistics*, *30*(6), 563–589.

Heimberg, A. M., Cowper-Sal·lari, R., Sémon, M., Donoghue, P. C. J., & Peterson, K. J. (2010). microRNAs reveal the interrelationships of hagfish, lampreys, and gnathostomes and the nature of the ancestral vertebrate. *Proceedings of the National Academy of Sciences*, *107*(45), 19379–19383.

Hejnol, A., & Lowe, C. J. (2014). Animal evolution: Stiff or squishy notochord origins? *Current Biology*, *24*(23), R1131–R1133.

Hejnol, A., & Martindale, M. Q. (2008). Acoel development supports a simple planula-like urbilaterian. *Philosophical Transactions of the Royal Society B: Biological Sciences*, *363*(1496), 1493–1501.

Herbrand, H., Pabst, O., Hill, R., & Arnold, H.-H. (2002). Transcription factors *Nkx3.1* and *Nkx3.2* (*Bapx1*) play an overlapping role in sclerotomal development of the mouse. *Mechanisms of Development*, *117*(1), 217–224.

Hernández, C. E., Rodríguez-Serrano, E., Avaria-Llautureo, J., Inostroza-Michael, O., Morales-Pallero, B., Boric-Bargetto, D., et al. (2013). Using phylogenetic information and the comparative method to evaluate hypotheses in macroecology. *Methods in Ecology and Evolution*, *4*(5), 401–415.

Hetherington, A. J., Sherratt, E., Ruta, M., Wilkinson, M., Deline, B., & Donoghue, P. C. J. (2015). Do cladistic and morphometric data capture common patterns of morphological disparity? *Palaeontology*, *58*(3), 393–399.

Higashiyama, H., Hirasawa, T., Oisi, Y., Sugahara, F., Hyodo, S., Kanai, Y., & Kuratani, S. (2016). On the vagal cardiac nerves, with special reference to the early evolution of the head–trunk interface. *Journal of Morphology*, *277*(9), 1146–1158.

Higashiyama, H., & Kuratani, S. (2014). On the maxillary nerve. *Journal of Morphology*, *275*(1), 17–38.

Hillis, D. M. (1987). Molecular versus morphological approaches to systematics. *Annual Review of Ecology and Systematics*, *18*(1), 23–42.

Hirasawa, T., Oisi, Y., & Kuratani, S. (2016). *Palaeospondylus* as a primitive hagfish. *Zoological Letters*, *2*, 20.

Holland, L. Z., & Holland, N. D. (1998). Developmental gene expression in amphioxus: New insights into the evolutionary origin of vertebrate brain regions, neural crest, and rostrocaudal segmentation. *Integrative and Comparative Biology*, *38*(4), 647–658.

Holland, L. Z., Holland, N. D., & Gilland, E. (2008). Amphioxus and the evolution of head segmentation. *Integrative and Comparative Biology*, *48*(5), 630–646.

Holland, L. Z., Kene, M., Williams, N. A., & Holland, N. D. (1997). Sequence and embryonic expression of the amphioxus engrailed gene (AmphiEn): The metameric pattern of transcription resembles that of its segment-polarity homolog in *Drosophila*. *Development*, *124*(9), 1723–1732.

Holland, N. D. (2016). Nervous systems and scenarios for the invertebrate-to-vertebrate transition. *Philosophical Transactions of the Royal Society of London. Series B*, *371*(1685), 20150047.

Holland, N. D., & Chen, J. (2001). Origin and early evolution of the vertebrates: New insights from advances in molecular biology, anatomy, and palaeontology. *BioEssays*, *23*(2), 142–151.

Holland, N. D., Holland, L. Z., & Holland, P. W. H. (2015). Scenarios for the making of vertebrates. *Nature*, *520*(7548), 450–455.

Holland, N. D., Holland, L. Z., Honma, Y., & Fujii, T. (1993). Engrailed expression during development of a lamprey, *Lampetra japonica*: A possible clue to homologies between agnathan and gnathostome muscles of the mandibular arch. *Development, Growth & Differentiation*, *35*(2), 153–160.

Holland, P. W. H., & Garcia-Fernàndez, J. (1996). Hox genes and chordate evolution. *Developmental Biology*, *173*(2), 382–395.

Holmgren, N. (1942). Studies on the Head of Fishes. *Acta Zoologica*, *23*(1–3), 129–261.

Holmgren, N. (1946). On two embryos of *Myxine glutinosa*. *Acta Zoologica*, *27*, 1–90.

Holmgren, N., & Stensiö, E. (1936). Kranium and visceralskelett der akranier, cyclostomen und fische. In L. Bolk, E. Göppert, E. Kallius, & W. Lubosch (Eds.), *Handbuch der vergleichenden Anatomie der Wirbeltiere* (Vol. Bd. 4, pp. 233–500). Berlin: Urban & Schwarzenberg.

Hopson, J. A. (1994). Synapsid evolution and the radiation of non-eutherian mammals. *Short Courses in Paleontology*, *7*, 190–219.

Horigome, N., Myojin, M., Ueki, T., Hirano, S., Aizawa, S., & Kuratani, S. (1999). Development of cephalic neural crest cells in embryos of *Lampetra japonica*, with special reference to the evolution of the jaw. *Developmental Biology*, *207*(2), 287–308.

Hubbs, C. L., & Potter, I. C. (1971). Distribution, phylogeny and taxonomy. In M. W. Hardisty & I. C. Potter (Eds.), *The Biology of Lampreys. Volume 1*. pp. 1–65. New York: Academic Press

Hückel, U. (1970). Die Fischschiefer von Haqel und Hjoula in der Oberkreide des Libanon. *Neues Jahrbuch für Geologie und Paläontologie, Abhandlungen*, *135*(2), 113–149.

Huelsenbeck, J., Ronquist, F., & Teslenko, M. (2015). *MrBayes: Bayesian Inference of Phylogeny*. http://mrbayes.sourceforge.net/index.php

Huntley, J. W. (2011). Exploratory multivariate techniques and their utility for understanding ancient ecosystems. In *Quantifying the Evolution of Early Life* (pp. 23–48). Springer, Dordrecht.

Huntley, J. W., Xiao, S., & Kowalewski, M. (2006). 1.3 Billion years of acritarch history: An empirical morphospace approach. *Precambrian Research*, *144*(1), 52–68.

Hurley, I. A., Mueller, R. L., Dunn, K. A., Schmidt, E. J., Friedman, M., Ho, R. K., et al. (2007). A new time-scale for ray-finned fish evolution. *Proceedings of the Royal Society of London B: Biological Sciences*, *274*(1609), 489–498.

Huxley, T. H. (1874). Preliminary note upon the brain and skull of *Amphioxus lanceolatus*. *Proceedings of the Royal Society of London*, *23*, 127–132.

Hyman, L. H. (1992). *Hyman's Comparative Vertebrate Anatomy*. (M. H. Wake, Ed.) (3rd edition.). Chicago: University of Chicago Press.

Inoue, J. G., Miya, M., Lam, K., Tay, B.-H., Danks, J. A., Bell, J., et al. (2010). Evolutionary origin and phylogeny of the modern holocephalans (Chondrichthyes: Chimaeriformes): A mitogenomic perspective. *Molecular Biology and Evolution*, *27*(11), 2576–2586.

Irie, N., & Kuratani, S. (2011). Comparative transcriptome analysis reveals vertebrate phylotypic period during organogenesis. *Nature Communications*, *2*, 248.

Irie, N., & Kuratani, S. (2014). The developmental hourglass model: A predictor of the basic body plan? *Development*, *141*(24), 4649–4655.

Jandzik, D., Garnett, A. T., Square, T. A., Cattell, M. V., Yu, J.-K., & Medeiros, D. M. (2015). Evolution of the new vertebrate head by co-option of an ancient chordate skeletal tissue. *Nature*, *518*(7540), 534–537.

Jandzik, D., Hawkins, M. B., Cattell, M. V., Cerny, R., Square, T. A., & Medeiros, D. M. (2014). Roles for FGF in lamprey pharyngeal pouch formation and skeletogenesis highlight ancestral functions in the vertebrate head. *Development*, *141*(3), 629–638.

Janečka, J. E., Miller, W., Pringle, T. H., Wiens, F., Zitzmann, A., Helgen, K. M., et al. (2007). Molecular and genomic data identify the closest living relative of primates. *Science*, *318*(5851), 792–794.

Janvier, P. (1974). The structure of the naso-hypophysial complex and the mouth in fossil and extant cyclostomes, with remarks on amphiaspiforms. *Zoologica Scripta*, *3*(4), 193–200.

Janvier, P. (1975). Les yeux des Cyclostomes fossiles et le problème de l'origine des Myxinoïdes. *Acta Zoologica*, *56*(1), 1–9. doi:10.1111/j.1463-6395.1975.tb00077.x

Janvier, P. (1978). Les nageoires paires des Ostéostracés et la position systématique des Céphalaspidomorphes. *Annales de Paléontologie*, *64*, 113–142.

Janvier, P. (1981a). The phylogeny of the Craniata, with particular reference to the significance of fossil "agnathans." *Journal of Vertebrate Paleontology*, *1*(2), 121–159.

Janvier, P. (1981b). *Norselaspis glacialis* n.g., n.sp. et les relations phylogénétiques entre les Kiaeraspidiens (Osteostraci) du Dévonien inféerieur du Spitsberg. *Palaeovertebrata*, *11*, 19–131.

Janvier, P. (1984). The relationships of the Osteostraci and Galeaspida. *Journal of Vertebrate Paleontology*, *4*, 344–358.

Janvier, P. (1985a). *Les Céphalaspides du Spitsberg. Anatomie, phylogénie et systématique des Ostéostracés siluro-dévoniens. Révision des Ostéostracés de la Formation de Wood Bay (Dévonien inférieur du Spitsberg).* Paris: Centre national de la Recherche scientifique.

Janvier, P. (1985b). Les Thyestidiens (Ostéostraci) du Silurien de Saaremaa (Estonie). Première partie: Morphologie et anatomie. *Annales de Paléontologie*, *71*, 83–147.

Janvier, P. (1993). Patterns of diversity in the skull of jawed fishes. In J. Hanken & B. K. Hall (Eds.), *The Skull. Volume II. Patterns of Structural and Systematic Diversity*. Chicago: University of Chicago Press.

Janvier, P. (1995). The brachial articulation and pectoral fin in antiarchs (Placodermi). *Bulletin du Museum national d'Histoire Naturelle 4 e serie*, *17*, 143–162.

Janvier, P. (1996a). *Early Vertebrates*. Oxford: Clarendon Press.

Janvier, P. (1996b). The dawn of vertebrates: Characters versus common ascent in the rise of current vertebrate phylogenies. *Palaeontology*, *39*, 259–287.

Janvier, P. (2004). Early specializations in the branchial apparatus of jawless vertebrates: A consideration of gill number and size. In G. Arratia, M. V. H. Wilson, & R. Cloutier (Eds.), *Recent Advances in the Origin and Early Radiation of Vertebrates* (pp. 29–52). Munich: Verlag Dr. Friedrich Pfeil.

Janvier, P. (2007). Homologies and evolutionary transitions in early vertebrate history. In J. S. Anderson & H.-D. Sues (Eds.), *Major Transitions in Vertebrate Evolution* (pp. 57–121). Bloomington: Indiana University Press.

Janvier, P. (2008). Early jawless vertebrates and cyclostome origins. *Zoological Science*, *25*(10), 1045–1056.

Janvier, P. (2010). microRNAs revive old views about jawless vertebrate divergence and evolution. *Proceedings of the National Academy of Sciences of the United States of America*, *107*(45), 19137–19138.

Janvier, P. (2015). Facts and fancies about early fossil chordates and vertebrates. *Nature*, *520*(7548), 483–489.

Janvier, P., & Arsenault, M. (2002). Palaeobiology: Calcification of early vertebrate cartilage. *Nature*, *417*(6889), 609–609.

Janvier, P., & Arsenault, M. (2007). The anatomy of *Euphanerops longaevus* Woodward, 1900, an anaspid-like jawless vertebrate from the Upper Devonian of Miguasha, Quebec, Canada. *Geodiversitas*, *29*(1), 143–216.

Janvier, P., Arsenault, M., & Desbiens, S. (2004). Calcified cartilage in the paired fins of the osteostracan *Escuminaspis laticeps* (Traquair 1880), from the Late Devonian of Miguasha (Québec, Canada), with a consideration of the early evolution of the pectoral fin endoskeleton in vertebrates. *Journal of Vertebrate Paleontology*, *24*(4), 773–779.

Janvier, P., & Blieck, A. (1979). New data on the internal anatomy of the Heterostraci (Agnatha), with general remarks on the phytogeny of the Craniota. *Zoologica Scripta*, *8*(1–4), 287–296.

Janvier, P., & Busch, R. M. (1984). *Jamoytius*-like vertebrates from the Lower Devonian Manlius Formation of New York State. *Journal of Vertebrate Paleontology*, *4*(4), 501–506.

Janvier, P., Desbiens, S., Willett, J. A., & Arsenault, M. (2006). Lamprey-like gills in a gnathostome-related Devonian jawless vertebrate. *Nature*, *440*(7088), 1183–1185.

Janvier, P., & Lund, R. (1983). *Hardistiella montanensis* n. gen. et sp. (Petromyzontida) from the Lower Carboniferous of Montana, with Remarks on the Affinities of the Lampreys. *Journal of Vertebrate Paleontology*, *2*(4), 407–413.

Janvier, P., Lund, R., & Grogan, E. D. (2004). Further consideration of the earliest known lamprey, *Hardistiella montanensis* Janvier and Lund, 1983, from the Carboniferous of Bear Gulch, Montana, U.S.A. *Journal of Vertebrate Paleontology*, *24*(3), 742–743.

Janvier, P., Percy, L. R., & Potter, I. C. (1991). The arrangement of the heart chambers and associated blood vessels in the Devonian osteostracan *Norselaspis glacialis*. A reinterpretation based on recent studies of the circulatory system in lampreys. *Journal of Zoology*, *223*(4), 567–576.

Janvier, P., & Sansom, R. S. (2016). Fossil hagfishes, fossil cyclostomes, and the lost world of "ostracoderms." In S. L. Edwards & G. G. Goss (Eds.), *Hagfish Biology* (pp. 73–93). Boca Raton: CRC Press.

Jarvik, E. (1980). *Basic Structure and Evolution of Vertebrates* (Vols. 1-2). London: Academic Press.

Jefferies, R. P. S. (1987). *The Ancestry of the Vertebrates*. Cambridge ; New York: Cambridge University Press.

Jenkins, F. A., Gatesy, S. M., Shubin, N. H., & Amaral, W. W. (1997). Haramiyids and Triassic mammalian evolution. *Nature*, *385*(6618), 715–718.

Jenner, R. A. (2004a). When molecules and morphology clash: Reconciling conflicting phylogenies of the Metazoa by considering secondary character loss. *Evolution & Development*, *6*(5), 372–378.

Jenner, R. A. (2004b). Accepting partnership by submission? Morphological phylogenetics in a molecular millennium. *Systematic Biology*, *53*(2), 333–359.

Jensen, D. D. (1960). Hoplonemertines, myxinoids, and deuterostome origins. *Nature*, *187*, 649–650.

Jensen, D. D. (1963). Hoplonemertines, myxinoids and vertebrate origins. In E. C. Dougherty (Ed.), *The Lower Metazoa: Comparative Biology and Phylogeny* (pp. 113–126). Berkeley: University of California Press.

Jiang, X., Iseki, S., Maxson, R. E., Sucov, H. M., & Morriss-Kay, G. M. (2002). Tissue origins and interactions in the mammalian skull vault. *Developmental Biology*, *241*(1), 106–116.

Johanson, Z. (2002). Vascularization of the osteostracan and antiarch (Placodermi) pectoral fin: Similarities, and implications for placoderm relationships. *Lethaia*, *35*(2), 169–186.

Johanson, Z., Kearsley, A., den Blaauwen, J., Newman, M., & Smith, M. M. (2010). No bones about it: An enigmatic Devonian fossil reveals a new skeletal framework—A potential role of loss of gene regulation. *Seminars in Cell & Developmental Biology*, *21*(4), 414–423.

Johanson, Z., Kearsley, A., den Blaauwen, J., Newman, M., & Smith, M. M. (2012). Ontogenetic development of an exceptionally preserved Devonian cartilaginous skeleton. *Journal of Experimental Zoology Part B: Molecular and Developmental Evolution*, *318B*(1), 50–58.

Johanson, Z., Smith, M., Sanchez, S., Senden, T., Trinajstic, K., & Pfaff, C. (2017). Questioning hagfish affinities of the enigmatic Devonian vertebrate *Palaeospondylus*. *Royal Society Open Science*, *4*(7), 170214.

Johnels, A. G. (1948). On the development and morphology of the skeleton of the head of *Petromyzon*. Acta Zoologica, *29*(1), 139–279.

Johnston, J. B. (1905). The cranial nerve components of *Petromyzon*. *Morphologisches Jahrbuch, Leipzig*, *34*, 149–203.

Jørgensen, J. M., Shichiri, M., & Geneser, F. A. (1998). Morphology of the hagfish inner ear. *Acta Zoologica*, *79*(3), 251–256.

Joss, J., & Johanson, Z. (2007). Is *Palaeospondylus gunni* a fossil larval lungfish? Insights from *Neoceratodus forsteri* development. *Journal of Experimental Zoology Part B: Molecular and Developmental Evolution*, *308B*(2), 163–171.

Julin, C. (1887). Des origines de l'aorta et des carotides chez les poissons Cyclostomes. *Anatomischer Anzeiger*, *1887*, 228–238.

Kague, E., Gallagher, M., Burke, S., Parsons, M., Franz-Odendaal, T., & Fisher, S. (2012). Skeletogenic fate of zebrafish cranial and trunk neural crest. *PLOS ONE*, *7*(11), e47394.

Kano, S., Xiao, J.-H., Osório, J., Ekker, M., Hadzhiev, Y., Müller, F., et al. (2010). Two lamprey Hedgehog genes share non-coding regulatory sequences and expression patterns with gnathostome Hedgehogs. *PLOS ONE*, *5*(10), e13332.

Kawasaki, R., & Rovainen, C. M. (1988). Feeding behavior by parasitic phase lampreys, *Ichthyomyzon unicuspis*. *Brain, Behavior and Evolution*, *32*(6), 317–329.

Keating, J. N., & Donoghue, P. C. J. (2016). Histology and affinity of anaspids, and the early evolution of the vertebrate dermal skeleton. *Proceedings of the Royal Society of London B: Biological Sciences*, *283*(1826), 20152917.

Keating, J. N., Marquart, C. L., & Donoghue, P. C. J. (2015). Histology of the heterostracan dermal skeleton: Insight into the origin of the vertebrate mineralised skeleton. *Journal of Morphology*, *276*(6), 657–680.

Keating, J. N., Sansom, R. S., & Purnell, M. A. (2012). A new osteostracan fauna from the Devonian of the Welsh Borderlands and observations on the taxonomy and growth of Osteostraci. *Journal of Vertebrate Paleontology*, *32*(5), 1002–1017.

Keibel, F. (1906). *Die Entwickelung der äusseren Körperform der Wirbeltierembryonen, insbesondere der menschlichen Embryonen aus den ersten 2 Monaten*. Jena: Gustav Fischer.

Keibel, F. (1928). Beiträge zur anatomie, zur entwicklungsgeschichte und zur stammesgeschichte der sehorgane der Cyklostomen. *Zeitschrift fur mikroskopisch-anatomische Forschung*, *12*, 391–456.

Keiser, W. (1914). Untersuchungen über die erste anlage des herzens, der beiden längsgefäßstämme und des blutes bei embryonen von *Petromyzon planeri*. *Vierteljahrsschrift der Naturforschenden Gesellschaft in Zürich*, *58*, 269–275.

Kennedy, J. F. (1986). *Carbohydrate Chemistry: Macrmolecules* (Vol. 15). London: Royal Society of Chemistry.

Kerney, R., Gross, J. B., & Hanken, J. (2007). Runx2 is essential for larval hyobranchial cartilage formation in *Xenopus laevis*. *Developmental Dynamics*, *236*(6), 1650–1662.

Khan, I. M., Redman, S. N., Williams, R., Dowthwaite, G. P., Oldfield, S. F., & Archer, C. W. (2007). The development of synovial joints. In B.-C. T. in D. Biology (Ed.), (Vol. 79, pp. 1–36). Academic Press.

Khonsari, R. H., Li, B., Vernier, P., Northcutt, R. G., & Janvier, P. (2009). Agnathan brain anatomy and craniate phylogeny. *Acta Zoologica*, *90*, 52–68.

Kiaer, J. (1924). The Downtonian fauna of Norway. I. Anaspida with a geological introduction. *Videnskapsselskapets Skrifter, I. Matematisk-naturvidenskapslige Klasse*, *6*, 1–139.

Kieckebusch, H.-H. (1928). Bau und entwicklung der schildrüse bei neunaugenlarven (*Lampetra fluviatilis* L. und *Lampetra planeri* Bl.). *Zeitschrift für Morphologie und Ökologie der Tiere*, *11*, 247–360.

Kim, D.-W., Kempf, H., Chen, R. E., & Lassar, A. B. (2003). Characterization of *Nkx3.2* DNA binding specificity and its requirement for somitic chondrogenesis. *Journal of Biological Chemistry*, *278*(30), 27532–27539.

Kim, D.-W., & Lassar, A. B. (2003). Smad-dependent recruitment of a histone deacetylase/sin3A complex modulates the Bone Morphogenetic Protein-dependent transcriptional repressor activity of *Nkx3.2*. *Molecular and Cellular Biology*, *23*(23), 8704–8717.

Kimmel, C. B., T. Miller, C., & J. Keynes, R. (2001). Neural crest patterning and the evolution of the jaw. *Journal of Anatomy*, *199*(1&2), 105–119.

Kimmel, C. B., Miller, C. T., & Moens, C. B. (2001). Specification and morphogenesis of the zebrafish larval head skeleton. *Developmental Biology*, *233*(2), 239–257.

Kimmel, C. B., Ullmann, B., Walker, M., Miller, C. T., & Crump, J. G. (2003). Endothelin 1-mediated regulation of pharyngeal bone development in zebrafish. *Development*, *130*(7), 1339–1351.

King, B., Qiao, T., Lee, M. S. Y., Zhu, M., & Long, J. A. (2017). Bayesian morphological clock methods resurrect placoderm monophyly and reveal rapid early evolution in jawed vertebrates. *Systematic Biology*, *66*(4), 499–516.

Kirino, M., Parnes, J., Hansen, A., Kiyohara, S., & Finger, T. E. (2013). Evolutionary origins of taste buds: Phylogenetic analysis of purinergic neurotransmission in epithelial chemosensors. *Open Biology*, *3*(3), 130015.

Klingenberg, C. P. (2014). Studying morphological integration and modularity at multiple levels: Concepts and analysis. *Philosophical Transactions of the Royal Society of London. Series B*, *369*(1649), 20130249.

Knoll, A. H., & Carroll, S. B. (1999). Early animal evolution: Emerging views from comparative biology and geology. *Science*, *284*(5423), 2129–2137.

Koch, E. A., Spitzer, R. H., & Pithawalla, R. B. (1991). Structural forms and possible roles of aligned cytoskeletal biopolymers in hagfish (slime eel) mucus. *Journal of Structural Biology*, *106*(3), 205–210.

Kohrs, D. G. (2013). *Hopkins Seaside Laboratory of Natural History*. Pacific Grove: Hopkins Marine Station. http://seaside.stanford.edu/

Kok, F. O., Shin, M., Ni, C.-W., Gupta, A., Grosse, A. S., van Impel, A., et al. (2015). Reverse genetic screening reveals poor correlation between morpholino-induced and mutant phenotypes in zebrafish. *Developmental Cell*, *32*(1), 97–108.

Kokubo, N., Matsuura, M., Onimaru, K., Tiecke, E., Kuraku, S., Kuratani, S., & Tanaka, M. (2010). Mechanisms of heart development in the Japanese lamprey, *Lethenteron japonicum*. *Evolution & Development*, *12*(1), 34–44.

Koltzoff, N. K. (1901). Entwicklungsgeschichte des Kopfes von *Petromyzon planeri*. *Bulletin de la Société das naturalists, Moscow*, *15*, 259–589.

Kontges, G., & Lumsden, A. (1996). Rhombencephalic neural crest segmentation is preserved throughout craniofacial ontogeny. *Development*, *122*(10), 3229–3242.

Kourakis, M. J., Newman-Smith, E., & Smith, W. C. (2010). Key steps in the morphogenesis of a cranial placode in an invertebrate chordate, the tunicate *Ciona savignyi*. *Developmental Biology*, *340*(1), 134–144.

Koyama, E., Shibukawa, Y., Nagayama, M., Sugito, H., Young, B., Yuasa, T., et al. (2008). A distinct cohort of progenitor cells participates in synovial joint and articular cartilage formation during mouse limb skeletogenesis. *Developmental Biology*, *316*(1), 62–73.

Kowalevsky, A. (1866a). Entwickelungsgeschichte der einfachen Ascidien. *Mémoires de l'Académie des sciences de St Pétersbourg*, *7(10)*(15), 1–19.

Kowalevsky, A. (1866b). Entwickelungsgeschichte des *Amphioxus lanceolatus*. *Mémoires de l'Académie des sciences de St Pétersbourg*, *7(11)*(4), 1–17.

Krejsa, R. J., Bringas, P., & Slavkin, H. C. (1990). A neontological interpretation of conodont elements based on agnathan cyclostome tooth structire function, and development. *Lethaia*, *23*(4), 359–378.

Kuo, C.-H., Huang, S., & Lee, S.-C. (2003). Phylogeny of hagfish based on the mitochondrial 16S rRNA gene. *Molecular Phylogenetics and Evolution*, *28*(3), 448–457.

Kuo, C.-H., Lee, S. C., & Mok, H.-K. (2010). A new species of hagfish *Eptatretus rubicundus* (Myxinidae: Myxiniformes) from Taiwan, with reference to its phylogenetic position based on its mitochondrial DNA sequence. *Zoological Studies*, *49*(6), 855–864.

Kuraku, S., Hoshiyama, D., Katoh, K., Suga, H., & Miyata, T. (1999). Monophyly of lampreys and hagfishes supported by nuclear DNA–coded genes. *Journal of Molecular Evolution*, *49*(6), 729–735.

Kuraku, S., & Kuratani, S. (2006). Time scale for cyclostome evolution inferred with a phylogenetic diagnosis of hagfish and lamprey cDNA sequences. *Zoological Science*, *23*(12), 1053–1064.

Kuraku, S., Takio, Y., Sugahara, F., Takechi, M., & Kuratani, S. (2010). Evolution of oropharyngeal patterning mechanisms involving Dlx and endothelins in vertebrates. *Developmental Biology*, *341*(1), 315–323.

Kuratani, S. (2004). *Evolutionary Morphology - Bauplan and Embryonic Development of Vertebrates*. Tokyo: University of Tokyo Press.

Kuratani, S. (2008). Evolutionary developmental studies of cyclostomes and the origin of the vertebrate neck. *Development, Growth & Differentiation*, *50*, S189–S194.

Kuratani, S. (2012). Evolution of the vertebrate jaw from developmental perspectives. *Evolution & Development*, *14*(1), 76–92.

Kuratani, S. (2016). *The Illusions of Segmentation. A history of scientific ideas about the origins of animal body plans*. Tokyo: Kohsaku-sha.

Kuratani, S. (2017). *Evolutionary Morphology - Bauplan and Embryonic Development of Vertebrates. 2nd edition.* Tokyo: University of Tokyo Press.

Kuratani, S., Adachi, N., Wada, N., Oisi, Y., & Sugahara, F. (2013). Developmental and evolutionary significance of the mandibular arch and prechordal/premandibular cranium

in vertebrates: Revising the heterotopy scenario of gnathostome jaw evolution. *Journal of Anatomy*, *222*(1), 41–55.

Kuratani, S., Horigome, N., & Hirano, S. (1999). Developmental morphology of the head mesoderm and reevaluation of segmental theories of the vertebrate head: Evidence from embryos of an agnathan vertebrate, *Lampetra japonica*. *Developmental Biology*, *210*(2), 381–400.

Kuratani, S., Murakami, Y., Nobusada, Y., Kusakabe, R., & Hirano, S. (2004). Developmental fate of the mandibular mesoderm in the lamprey, *Lethenteron japonicum*: Comparative morphology and development of the gnathostome jaw with special reference to the nature of the trabecula cranii. *Journal of Experimental Zoology Part B: Molecular and Developmental Evolution*, *302B*(5), 458–468.

Kuratani, S., Nobusada, Y., Horigome, N., & Shigetani, Y. (2001). Embryology of the lamprey and evolution of the vertebrate jaw: Insights from molecular and developmental perspectives. *Philosophical Transactions of the Royal Society of London. Series B*, *356*(1414), 1615–1632.

Kuratani, S., Oisi, Y., & Ota, K. G. (2016). Evolution of the vertebrate cranium: Viewed from hagfish developmental studies. *Zoological Science*, *33*(3), 229–238.

Kuratani, S., & Ota, K. G. (2008). Primitive versus derived traits in the developmental program of the vertebrate head: Views from cyclostome developmental studies. *Journal of Experimental Zoology Part B: Molecular and Developmental Evolution*, *310B*(4), 294–314.

Kuratani, S., Ueki, T., Aizawa, S., & Hirano, S. (1997). Peripheral development of cranial nerves in a cyclostome, *Lampetra japonica*: Morphological distribution of nerve branches and the vertebrate body plan. *The Journal of Comparative Neurology*, *384*(4), 483–500.

Kusakabe, R., Kuraku, S., & Kuratani, S. (2011). Expression and interaction of muscle-related genes in the lamprey imply the evolutionary scenario for vertebrate skeletal muscle, in association with the acquisition of the neck and fins. *Developmental Biology*, *350*(1), 217–227.

Kusakabe, R., & Kuratani, S. (2005). Evolution and developmental patterning of the vertebrate skeletal muscles: Perspectives from the lamprey. *Developmental Dynamics*, *234*(4), 824–834.

Kusakabe, R., & Kuratani, S. (2007). Evolutionary perspectives from development of mesodermal components in the lamprey. *Developmental Dynamics*, *236*(9), 2410–2420.

Kusakabe, R., Takechi, M., Tochinai, S., & Kuratani, S. (2004). Lamprey contractile protein genes mark different populations of skeletal muscles during development. *Journal of Experimental Zoology Part B: Molecular and Developmental Evolution*, *302B*(2), 121–133.

Kusakabe, R., Tochinai, S., & Kuratani, S. (2003). Expression of foreign genes in lamprey embryos: An approach to study evolutionary changes in gene regulation. *Journal of Experimental Zoology Part B: Molecular and Developmental Evolution*, *296B*(1), 87–97.

Lacalli, T. C. (2005). Protochordate body plan and the evolutionary role of larvae: Old controversies resolved? *Canadian Journal of Zoology*, *83*(1), 216–224.

Lacalli, T. C., Holland, N. D., & West, J. E. (1994). Landmarks in the anterior central nervous system of amphioxus larvae. *Philosophical Transactions of the Royal Society of London. Series B*, *344*(1308), 165–185.

Lakiza, O., Miller, S., Bunce, A., Lee, E. M.-J., & McCauley, D. W. (2011). SoxE gene duplication and development of the lamprey branchial skeleton: Insights into development and evolution of the neural crest. *Developmental Biology*, *359*(1), 149–161.

Lamb, T. D., Collin, S. P., & Pugh, E. N. (2007). Evolution of the vertebrate eye: Opsins, photoreceptors, retina and eye cup. *Nature Reviews Neuroscience*, *8*(12), 960–976.

Langille, R. M., & Hall, B. K. (1988). Role of the neural crest in development of the trabeculae and branchial arches in embryonic sea lamprey, *Petromyzon marinus* (L). *Development*, *102*(2), 301–310.

Langille, R. M., & Hall, B. K. (1993). Calcification of cartilage from the lamprey *Petromyzon marinus* (L.) in vitro. *Acta Zoologica*, *74*(1), 31–41.

Lankester, E. R. (1875). On some new points in the structure of amphioxus, and their bearing on the morphology of Vertebrata. *Quarterly Journal of Microscopical Science*, *15*, 257–267.

Larouche, O., Zelditch, M. L., & Cloutier, R. (2017). Fin modules: An evolutionary perspective on appendage disparity in basal vertebrates. *BMC Biology*, *15*, 32.

Lassmann, T., & Sonnhammer, E. L. (2005). Kalign – an accurate and fast multiple sequence alignment algorithm. *BMC Bioinformatics*, *6*, 298.

Lauri, A., Brunet, T., Handberg-Thorsager, M., Fischer, A. H. L., Simakov, O., Steinmetz, P. R. H., et al. (2014). Development of the annelid axochord: Insights into notochord evolution. *Science*, *345*(6202), 1365–1368.

Lawson, N. D. (2016). Reverse genetics in zebrafish: Mutants, morphants, and moving forward. *Trends in Cell Biology*, *26*(2), 77–79.

Le Douarin, N. M. (1982). *The Neural Crest*. Cambridge Cambridgeshire ; New York: Cambridge University Press.

Le Douarin, N. M., Creuzet, S., Couly, G., & Dupin, E. (2004). Neural crest cell plasticity and its limits. *Development*, *131*(19), 4637–4650.

Le Douarin, N. M., Ziller, C., & Couly, G. F. (1993). Patterning of neural crest derivatives in the avian embryo: *In vivo* and *in vitro* studies. *Developmental Biology*, *159*(1), 24–49.

Le Lievre, C. (1974). Rôle des cellules mésectodermiques issues des crêtes neurales céphaliques dans la formation des arcs branchiaux et du squelette viscéral. *Development*, *31*(2), 453–477.

Leach, W. J. (1944). The archetypal position of amphioxus and ammocoetes and the role of endocrines in chordate evolution. *The American Naturalist*, *78*(777), 341–357.

Lee, E. M., Yuan, T., Ballim, R. D., Nguyen, K., Kelsh, R. N., Medeiros, D. M., & McCauley, D. W. (2016). Functional constraints on SoxE proteins in neural crest development: The

importance of differential expression for evolution of protein activity. *Developmental Biology*, *418*(1), 166–178.

Lee, R. T. H., Knapik, E. W., Thiery, J. P., & Carney, T. J. (2013a). An exclusively mesodermal origin of fin mesenchyme demonstrates that zebrafish trunk neural crest does not generate ectomesenchyme. *Development*, *140*(14), 2923–2932.

Lee, R. T. H., Thiery, J. P., & Carney, T. J. (2013b). Dermal fin rays and scales derive from mesoderm, not neural crest. *Current Biology*, *23*(9), R336–R337.

Lee, S.-H., Bédard, O., Buchtová, M., Fu, K., & Richman, J. M. (2004). A new origin for the maxillary jaw. *Developmental Biology*, *276*(1), 207–224.

Lee, S.-H., Fu, K. K., Hui, J. N., & Richman, J. M. (2001). Noggin and retinoic acid transform the identity of avian facial prominences. *Nature*, *414*(6866), 909–912.

Lettice, L., Hecksher-Sørensen, J., & Hill, R. (2001). The role of Bapx1 (Nkx3.2) in the development and evolution of the axial skeleton. *Journal of Anatomy*, *199*(1–2), 181–187.

Licht, M., Schmuecker, K., Huelsken, T., Hanel, R., Bartsch, P., & Paeckert, M. (2012). Contribution to the molecular phylogenetic analysis of extant holocephalan fishes (Holocephali, Chimaeriformes). *Organisms Diversity & Evolution*, *12*(4), 421–432.

Lindström, T. (1949). On the cranial nerves of the cyclostomes with special reference to n. trigeminus. *Acta Zoologica*, *30*, 315–458.

Linnaeus, C. (1758). *Systema Naturae per Regna Tria Naturae. Regnum Animale.* Stockholm: Laurentii Salvii.

Lloyd, G. T. (2016). Estimating morphological diversity and tempo with discrete character-taxon matrices: Implementation, challenges, progress, and future directions. *Biological Journal of the Linnean Society*, *118*(1), 131–151.

Long, J. A. (1988). New palaeoniscoid fishes from the Late Devonian - Early Carboniferous of Victoria, Australia. *Memoirs of the Association of Australasian Palaeontologists*, *7*(7), 1–64.

Long, J. A., Mark-Kurik, E., Johanson, Z., Lee, M. S. Y., Young, G. C., Min, Z., et al. (2015). Copulation in antiarch placoderms and the origin of gnathostome internal fertilization. *Nature*, *517*(7533), 196–199.

Løvtrup, S. (1977). *The Phylogeny of the Vertebrata.* New York: Wiley.

Lu, J., Giles, S., Friedman, M., den Blaauwen, J. L., & Zhu, M. (2016). The oldest actinopterygian highlights the cryptic early history of the hyperdiverse ray-finned fishes. *Current Biology*, *26*(12), 1602–1608.

Lumsden, A., Sprawson, N., & Graham, A. (1991). Segmental origin and migration of neural crest cells in the hindbrain region of the chick embryo. *Development*, *113*(4), 1281–1291.

Lund, R., Grogan, E. D., & Fath, M. (2014). On the relationships of the Petalodontiformes (Chondrichthyes). *Paleontological Journal*, *48*(9), 1015–1029.

Lund, R., & Janvier, P. (1986). A second lamprey from the Lower Carboniferous (Namurian) of Bear Gulch, Montana (U.S.A.). *Geobios*, *19*(5), 647–652.

Lundgren, M., & Blom, H. (2013). Phylogenetic relationships of the cyathaspidids (Heterostraci). *GFF*, *135*(1), 74–84.

Lüning, S., Kolonic, S., Belhadj, E. M., Belhadj, Z., Cota, L., Barić, G., & Wagner, T. (2004). Integrated depositional model for the Cenomanian–Turonian organic-rich strata in North Africa. *Earth-Science Reviews*, *64*(1), 51–117.

Luo, Z., & Crompton, A. W. (1994). Transformation of the quadrate (incus) through the transition from non-mammalian cynodonts to mammals. *Journal of Vertebrate Paleontology*, *14*(3), 341–374.

Luo, Z.-X., Gatesy, S. M., Jenkins, F. A., Amaral, W. W., & Shubin, N. H. (2015). Mandibular and dental characteristics of Late Triassic mammaliaform *Haramiyavia* and their ramifications for basal mammal evolution. *Proceedings of the National Academy of Sciences*, *112*(51), E7101–E7109.

Luo, Z.-X., Yuan, C.-X., Meng, Q.-J., & Ji, Q. (2011). A Jurassic eutherian mammal and divergence of marsupials and placentals. *Nature*, *476*(7361), 442–445.

Maddin, H. C., Piekarski, N., Sefton, E. M., & Hanken, J. (2016). Homology of the cranial vault in birds: New insights based on embryonic fate-mapping and character analysis. *Royal Society Open Science*, *3*(8), 160356.

Maddison, W. P. (2000). Testing character correlation using pairwise comparisons on a phylogeny. *Journal of Theoretical Biology*, *202*(3), 195–204.

Maddison, W. P., & Maddison, D. R. (2017). *Mesquite: A modular system for evolutionary analysis*. https://mesquiteproject.wikispaces.com/home

Maisey, J. G. (1986). Heads and tails: A chordate phylogeny. *Cladistics*, *2*(4), 201–256.

Maisey, J. G. (1988). Phylogeny of early vertebrate skeletal induction and ossification patterns. In M. K. Hecht, B. Wallace, & G. T. Prance (Eds.), *Evolutionary Biology* (pp. 1–36). Springer US.

Maletz, J. (Ed.). (2017). *Graptolite Paleobiology*. John Wiley & Sons.

Mallatt, J. (1979). Surface morphology and functions of pharyngeal structures in the larval lamprey Petromyzon marinus. *Journal of Morphology*, *162*(2), 249–273.

Mallatt, J. (1981). The suspension feeding mechanism of the larval lamprey *Petromyzon marinus*. *Journal of Zoology*, *194*(1), 103–142.

Mallatt, J. (1982). Pumping rates and particle retention efficiencies of the larval lamprey, an unusual suspension feeder. *The Biological Bulletin*, *163*(1), 197–210.

Mallatt, J. (1984a). Early evolution: Pharyngeal structure and the origin of gnathostomes. *Journal of Zoology*, *204*(2), 169–183.

Mallatt, J. (1984b). Feeding ecology of the earliest vertebrates. *Zoological Journal of the Linnean Society*, *82*(3), 261–272.

Mallatt, J. (1985). Reconstructing the life cycle and the feeding of ancestral vertebrates. In R. E. Foreman, A. Gorbman, J. M. Dodd, & R. Olsson (Eds.), *Evolutionary Biology of Primitive Fishes* (pp. 59–68). Springer US.

Mallatt, J. (1996). Ventilation and the origin of jawed vertebrates: A new mouth. *Zoological Journal of the Linnean Society*, *117*(4), 329–404.

Mallatt, J. (2008). The origin of the vertebrate jaw: Neoclassical ideas versus newer, development-based ideas. *Zoological Science*, *25*(10), 990–998.

Mallatt, J., & Chen, J. (2003). Fossil sister group of craniates: Predicted and found. *Journal of Morphology*, *258*(1), 1–31.

Mallatt, J., & Holland, N. (2013). *Pikaia gracilens* Walcott: Stem chordate, or already specialized in the Cambrian? *Journal of Experimental Zoology Part B: Molecular and Developmental Evolution*, *320*(4), 247–271.

Mallatt, J., & Sullivan, J. (1998). 28S and 18S rDNA sequences support the monophyly of lampreys and hagfishes. *Molecular Biology and Evolution*, *15*(12), 1706–1718.

Mallatt, J., & Winchell, C. J. (2007). Ribosomal RNA genes and deuterostome phylogeny revisited: More cyclostomes, elasmobranchs, reptiles, and a brittle star. *Molecular Phylogenetics and Evolution*, *43*(3), 1005–1022.

Manni, L., Agnoletto, A., Zaniolo, G., & Burighel, P. (2005). Stomodeal and neurohypophysial placodes in *Ciona Intestinalis*: Insights into the origin of the pituitary gland. *Journal of Experimental Zoology Part B: Molecular and Developmental Evolution*, *304B*(4), 324–339.

Mark-Kurik, E., & Janvier, P. (1997). A new trematapidid (Vertebrata, Osteostraci, Thyestiida) from the Devonian of northern Urals, with remarks on tannuaspids. *Neues Jahrbuch für Geologie und Paläontologie Abhandlungen*, *206*, 405–421.

Marinelli, W., & Strenger, A. (1954). *Vergleichende Anatomie und Morphologie der Wirbeltiere. I Lieferung*. Petromyzon marinus *(L).* Vienna: Franz Deuticke Wien.

Marinelli, W., & Strenger, A. (1956). *Vergleichende Anatomie und Morphologie der Wirbeltiere. II Lieferung*. Myxine glutinosa *(L).* Vienna: Franz Deuticke Wien.

Märss, T., Turner, S., & Karatajūtė-Talimaa, V. (2007). *Handbook of Paleoichthyology / "Agnatha" II. Thelodonti.* (Vol. 1B). München: Verlag Dr. Friedrich Pfeil.

Martin, W. M., Bumm, L. A., & McCauley, D. W. (2009). Development of the viscerocranial skeleton during embryogenesis of the sea lamprey, *Petromyzon marinus*. *Developmental Dynamics*, *238*(12), 3126–3138.

Martini, F. H. (1998). The ecology of hagfishes. In J. M. Jørgensen, J. P. Lomholt, R. E. Weber, & H. Malte (Eds.), *The Biology of Hagfishes* (pp. 57–77). London: Chapman.

Martini, F. H., & Beulig, A. (2013). Morphometics and gonadal eevelopment of the hagfish *Eptatretus cirrhatus* in New Zealand. *PLOS ONE*, *8*(11), e78740.

Martini, F., Heiser, J. B., & Lesser, M. P. (1997). A population profile for Atlantic hagfish, *Myxine glutinosa* (L.), in the Gulf of Maine. Part I: morphometrics and reproductive state. *Fisheries Bulletin*, *95*, 311–320.

Matsuura, M., Nishihara, H., Onimaru, K., Kokubo, N., Kuraku, S., Kusakabe, R., et al. (2008). Identification of four Engrailed genes in the Japanese lamprey, *Lethenteron japonicum*. *Developmental Dynamics*, *237*(6), 1581–1589.

Matzke, N. J., & Wright, A. (2016). Inferring node dates from tip dates in fossil Canidae: The importance of tree priors. *Biology Letters*, *12*(8), 20160328.

Mazet, F., Hutt, J. A., Milloz, J., Millard, J., Graham, A., & Shimeld, S. M. (2005). Molecular evidence from *Ciona intestinalis* for the evolutionary origin of vertebrate sensory placodes. *Developmental Biology*, *282*(2), 494–508.

Mazza, M., Cau, A., & Rigo, M. (2012). Application of numerical cladistic analyses to the Carnian–Norian conodonts: a new approach for phylogenetic interpretations. *Journal of Systematic Palaeontology*, *10*(3), 401–422.

McBurney, K. M., Keeley, F. W., Kibenge, F. S. B., & Wright, G. M. (1996). Spatial and temporal distribution of lamprin mRNA during chondrogenesis of trabecular cartilage in the sea lamprey. *Anatomy and Embryology*, *193*(5), 419–426.

McBurney, K. M., & Wright, G. M. (1996). Chondrogenesis of a non-collagen-based cartilage in the sea lamprey, *Petromyzon marinus*. *Canadian Journal of Zoology*, *74*(12), 2118–2130.

McCauley, D. W. (2008). SoxE, type II collagen, and evolution of the chondrogenic neural crest. *Zoological Science*, *25*(10), 982–989.

McCauley, D. W., & Bronner-Fraser, M. (2002). Conservation of Pax gene expression in ectodermal placodes of the lamprey. *Gene*, *287*(1–2), 129–139.

McCauley, D. W., & Bronner-Fraser, M. (2003). Neural crest contributions to the lamprey head. *Development*, *130*(11), 2317–2327.

McCauley, D. W., & Bronner-Fraser, M. (2006). Importance of SoxE in neural crest development and the evolution of the pharynx. *Nature*, *441*(7094), 750–752.

McCoy, V. E., Saupe, E. E., Lamsdell, J. C., Tarhan, L. G., McMahon, S., Lidgard, S., et al. (2016). The "Tully monster" is a vertebrate. *Nature*, *532*(7600), 496–499.

Mead, A. (1992). Review of the development of multidimensional scaling methods. *Journal of the Royal Statistical Society. Series D (The Statistician)*, *41*(1), 27–39.

Medeiros, D. M., & Crump, J. G. (2012). New perspectives on pharyngeal dorsoventral patterning in development and evolution of the vertebrate jaw. *Developmental Biology*, *371*(2), 121–135.

Melo, J. H. G. de. (1988). The Malvinokaffric Realm in the Devonian of Brazil. In *Devonian of the World: Proceedings of the 2nd International Symposium on the Devonian System* (pp. 669–703).

Meulemans, D., & Bronner-Fraser, M. (2002). Amphioxus and lamprey AP-2 genes: Implications for neural crest evolution and migration patterns. *Development*, *129*(21), 4953–4962.

Meulemans, D., McCauley, D., & Bronner-Fraser, M. (2003). Id expression in amphioxus and lamprey highlights the role of gene cooption during neural crest evolution. *Developmental Biology*, *264*(2), 430–442.

MGI-Mouse Genome Informatics-The international database resource for the laboratory mouse. (n.d.). http://www.informatics.jax.org/. Accessed 2 October 2017

Miller, C. T., Schilling, T. F., Lee, K., Parker, J., & Kimmel, C. B. (2000). sucker encodes a zebrafish Endothelin-1 required for ventral pharyngeal arch. *Development*, *127*(17), 3815–3828.

Miller, C. T., Swartz, M. E., Khuu, P. A., Walker, M. B., Eberhart, J. K., & Kimmel, C. B. (2007). mef2ca is required in cranial neural crest to effect Endothelin1 signaling in zebrafish. *Developmental Biology*, *308*(1), 144–157.

Miller, C. T., Yelon, D., Stainier, D. Y. R., & Kimmel, C. B. (2003). Two endothelin 1 effectors, hand2 and bapx1, pattern ventral pharyngeal cartilage and the jaw joint. *Development*, *130*(7), 1353–1365.

Milner, A. R., & Sequeira, S. E. K. (1993). The temnospondyl amphibians from the Viséan of East Kirkton, West Lothian, Scotland. *Earth and Environmental Science Transactions of The Royal Society of Edinburgh*, *84*(3–4), 331–361.

Miyashita, T. (2012). *Comparative Analysis of the Anatomy of the Myxinoidea and the Ancestry of Early Vertebrate Lineages* (Unpublished M.Sc. thesis). University of Alberta, Edmonton.

Miyashita, T. (2016). Fishing for jaws in early vertebrate evolution: A novel hypothesis of mandibular confinement. *Biological Reviews*, *91*(3), 611–657.

Miyashita, T., & Coates, M. I. (2016). The embryology of hagfishes and the evolution and development of vertebrates. In S. L. Edwards & G. G. Goss (Eds.), *Hagfish Biology* (pp. 95–127). Boca Raton: CRC Press.

Miyashita, T., Green, S. A., & Bronner, M. E. (in press). Comparative development of cyclostomes. In Z. Johanson, M. Richter, & C. J. Underwood (Eds.), *Evolution and Development of Fishes*. Cambridge: University of Cambridge Press.

Modrell, M. S., Hockman, D., Uy, B., Buckley, D., Sauka-Spengler, T., Bronner, M. E., & Baker, C. V. H. (2014). A fate-map for cranial sensory ganglia in the sea lamprey. *Developmental Biology*, *385*(2), 405–416.

Mok, H.-K. (2001). Nasal-sinus papillae of hagfishes and their taxonomic implications. *Zoological Studies*, *40*, 355–364.

Mongera, A., & Nüsslein-Volhard, C. (2013). Scales of fish arise from mesoderm. *Current Biology*, *23*(9), R338–R339.

Moore, J. W., & Mallatt, J. M. (1980). Feeding of larval lamprey. *Canadian Journal of Fisheries and Aquatic Sciences*, *37*(11), 1658–1664.

Morrison, S. L., Campbell, C. K., & Wright, G. M. (2000). Chondrogenesis of the branchial skeleton in embryonic sea lamprey, *Petromyzon marinus*. *The Anatomical Record*, *260*(3), 252–267.

Moy-Thomas, J. A., & Miles, R. S. (1971). *Palaeozoic Fishes* (2nd edition.). London: Chapman.

Müller, A. (1856). Über die Entwicklung der Neunaugen. *Archiv für Anatomie, Physiologie und Wissenschaftliche Medicin*.

Murakami, Y., Ogasawara, M., Satoh, N., Sugahara, F., Myojin, M., Hirano, S., & Kuratani, S. (2002). Compartments in the lamprey embryonic brain as revealed by regulatory gene

expression and the distribution of reticulospinal neurons. *Brain Research Bulletin*, *57*(3–4), 271–275.

Murakami, Y., Ogasawara, M., Sugahara, F., Hirano, S., Satoh, N., & Kuratani, S. (2001). Identification and expression of the lamprey Pax6 gene: Evolutionary origin of the segmented brain of vertebrates. *Development*, *128*(18), 3521–3531.

Murakami, Y., Pasqualetti, M., Takio, Y., Hirano, S., Rijli, F. M., & Kuratani, S. (2004). Segmental development of reticulospinal and branchiomotor neurons in lamprey: Insights into the evolution of the vertebrate hindbrain. *Development*, *131*(5), 983–995.

Murakami, Y., Uchida, K., Rijli, F. M., & Kuratani, S. (2005). Evolution of the brain developmental plan: Insights from agnathans. *Developmental Biology*, *280*(2), 249–259.

Murchison, N. D., Price, B. A., Conner, D. A., Keene, D. R., Olson, E. N., Tabin, C. J., & Schweitzer, R. (2007). Regulation of tendon differentiation by scleraxis distinguishes force-transmitting tendons from muscle-anchoring tendons. *Development*, *134*(14), 2697–2708.

Murdock, D. J. E., Dong, X.-P., Repetski, J. E., Marone, F., Stampanoni, M., & Donoghue, P. C. J. (2013). The origin of conodonts and of vertebrate mineralized skeletons. *Nature*, *502*(7472), 546–549.

Murtaugh, L. C., Zeng, L., Chyung, J. H., & Lassar, A. B. (2001). The chick transcriptional repressor *Nkx3.2* acts downstream of *Shh* to promote BMP-dependent axial chondrogenesis. *Developmental Cell*, *1*(3), 411–422.

Myojin, M., Ueki, T., Sugahara, F., Murakami, Y., Shigetani, Y., Aizawa, S., et al. (2001). Isolation of Dlx and Emx gene cognates in an agnathan species, *Lampetra japonica*, and their expression patterns during embryonic and larval development: Conserved and diversified regulatory patterns of homeobox genes in vertebrate head evolution. *Journal of Experimental Zoology*, *291*(1), 68–84.

Near, T. J. (2009). Conflict and resolution between phylogenies inferred from molecular and phenotypic data sets for hagfish, lampreys, and gnathostomes. *Journal of Experimental Zoology Part B: Molecular and Developmental Evolution*, *312B*(7), 749–761.

Near, T. J., Dornburg, A., Tokita, M., Suzuki, D., Brandley, M. C., & Friedman, M. (2014). Boom and bust: Ancient and recent diversification in bichirs (Polypteridae: Actinopterygii), a relictual lineage of ray-finned fishes. *Evolution*, *68*(4), 1014–1026.

Near, T. J., Eytan, R. I., Dornburg, A., Kuhn, K. L., Moore, J. A., Davis, M. P., et al. (2012). Resolution of ray-finned fish phylogeny and timing of diversification. *Proceedings of the National Academy of Sciences*, *109*(34), 13698–13703.

Neidert, A. H., Virupannavar, V., Hooker, G. W., & Langeland, J. A. (2001). Lamprey Dlx genes and early vertebrate evolution. *Proceedings of the National Academy of Sciences*, *98*(4), 1665–1670.

Nelson, J. S., Grande, T. C., & Wilson, M. V. H. (2016). *Fishes of the World. 5th edition.* New York: Wiley.

Nestler, K. (1890). Anatomie und Entwicklungsgeschichte von *Petromyzon planeri*. *Archiv für Naturgeschichte*, *56*, 81–112.

Neumayr, L. (1938). Die entwicklung des kopskelettes von *Bdellostoma* St. L. *Archivio Italiano di Anatomica e di Embriologia*, *40*(suppl.), 1–222.

Newman, M. J. (2002). A new naked jawless vertebrate from the Middle Devonian of Scotland. *Palaeontology*, *45*(5), 933–941.

Newman, M. J., & Trewin, N. H. (2001). A new jawless vertebrate from the Middle Devonian of Scotland. *Palaeontology*, *44*(1), 43–51.

Newth, D. R. (1950). Fate of the neural crest in lampreys. *Nature*, *165*(4190), 284–284.

Newth, D. R. (1951). Experiments on the neural crest of the lamprey embryo. *Journal of Experimental Biology*, *28*(3), 247–260.

Newth, D. R. (1956). On the neural crest of the lamprey embryo. *Development*, *4*(4), 358–375.

Nichols, J. T., Pan, L., Moens, C. B., & Kimmel, C. B. (2013). barx1 represses joints and promotes cartilage in the craniofacial skeleton. *Development*, *140*(13), 2765–2775.

Nieuwenhuys, R., Ten Donkelaar, H. J., & Nicholson, C. (1998). *The Central Nervous System of Vertebrates* (Vols. 1-3). Berlin: Springer.

Nikitina, N., Bronner-Fraser, M., & Sauka-Spengler, T. (2009). The sea lamprey *Petromyzon marinus*: A model for evolutionary and developmental biology. *Cold Spring Harbor Protocols*, *2009*(1), pdb.emo113.

Noden, D. M. (1978). The control of avian cephalic neural crest cytodifferentiation: I. Skeletal and connective tissues. *Developmental Biology*, *67*(2), 296–312.

Noden, D. M., & Trainor, P. A. (2005). Relations and interactions between cranial mesoderm and neural crest populations. *Journal of Anatomy*, *207*(5), 575–601.

Norell, M. A., & Novacek, M. J. (1992). Congruence between superpositional and phylogenetic patterns: Comparing cladistic patterns with fossil records. *Cladistics*, *8*(4), 319–337.

Northcutt, R. G. (2004). Taste buds: Development and evolution. *Brain, Behavior and Evolution*, *64*(3), 198–206.

Northcutt, R. (2005). The New Head Hypothesis revisited. *Journal of Experimental Zoology Part B: Molecular and Developmental Evolution*, *304B*(4), 274–297.

Northcutt, R. G. (2010). Cladistic analysis reveals brainless Urbilateria. *Brain, Behavior and Evolution*, *76*(1), 1–2.

Northcutt, R. G., & Gans, C. (1983). The genesis of neural crest and epidermal placodes: A reinterpretation of vertebrate origins. *The Quarterly Review of Biology*, *58*(1), 1–28.

Novitskaya, L. (1971). *Les Amphiaspides (Heterostraci) de Dévonien de la Sibérie.* Cahiers de Paléontologie. 127 pp.

Novitskaya, L. (2008). Evolution of taxonomic diversity in amphiaspids (Agnatha, Heterostraci: Amphiaspidiformes) and the causes of extinction in ecologically favorable conditions. *Paleontological Journal*, *42*(2), 181-191.

Nuel, P. (1881). Quelques phases du développement du *Petromyzon planeri*. *Archives de Biologie*, *2*, 403–454.

Obruchev, D. V. (1964). *Agnathans and Fishes.* Moscow: Nauka.

Ogasawara, M., Shigetani, Y., Hirano, S., Satoh, N., & Kuratani, S. (2000). Pax1/Pax9-related genes in an agnathan vertebrate, *Lampetra japonica*: Expression pattern of LjPax9 implies sequential evolutionary events toward the gnathostome body plan. *Developmental Biology*, *223*(2), 399–410.

Ogasawara, M., Shigetani, Y., Suzuki, S., Kuratani, S., & Satoh, N. (2001). Expression of Thyroid transcription factor-1 (TTF-1) gene in the ventral forebrain and endostyle of the agnathan vertebrate, *Lampetra japonica*. *genesis*, *30*(2), 51–58.

Ohtani, K., Yao, T., Kobayashi, M., Kusakabe, R., Kuratani, S., & Wada, H. (2008). Expression of Sox and fibrillar collagen genes in lamprey larval chondrogenesis with implications for the evolution of vertebrate cartilage. *Journal of Experimental Zoology Part B: Molecular and Developmental Evolution*, *310B*(7), 596–607.

Oisi, Y., Fujimoto, S., Ota, K. G., & Kuratani, S. (2015). On the peculiar morphology and development of the hypoglossal, glossopharyngeal and vagus nerves and hypobranchial muscles in the hagfish. *Zoological Letters*, *1*(1), 6.

Oisi, Y., Ota, K. G., Fujimoto, S., & Kuratani, S. (2013a). Development of the chondrocranium in hagfishes, with special reference to the early evolution of vertebrates. *Zoological Science*, *30*(11), 944–961.

Oisi, Y., Ota, K. G., Kuraku, S., Fujimoto, S., & Kuratani, S. (2013b). Craniofacial development of hagfishes and the evolution of vertebrates. *Nature*, *493*(7431), 175–180.

Okkelberg, P. (1921). The early history of the germ cells in the brook lamprey, *Entosphenus wilderi* (Gage), up to and including the period of sex differentiation. *Journal of Morphology*, *35*(1), 1–151.

Onimaru, K., Shoguchi, E., Kuratani, S., & Tanaka, M. (2011). Development and evolution of the lateral plate mesoderm: Comparative analysis of amphioxus and lamprey with implications for the acquisition of paired fins. *Developmental Biology*, *359*(1), 124–136.

Ørvig, T. (1980). Histologic studies of ostracoderms, placoderms and fossil elasmobranchs. *Zoologica Scripta*, *9*(1–4), 219–239.

Ørvig, T. (1989). Histologic studies of ostracoderms, placoderms and fossil elasmobranchs. 6. Hard tissues of Ordovician vertebrates. *Zoologica Scripta*, *18*(3), 427–446.

Ota, K. G., Fujimoto, S., Oisi, Y., & Kuratani, S. (2011). Identification of vertebra-like elements and their possible differentiation from sclerotomes in the hagfish. *Nature Communications*, *2*, 373. doi:10.1038/ncomms1355

Ota, K. G., Fujimoto, S., Oisi, Y., & Kuratani, S. (2013). Late development of hagfish vertebral elements. *Journal of Experimental Zoology Part B: Molecular and Developmental Evolution*, *320*(3), 129–139.

Ota, K. G., Kuraku, S., & Kuratani, S. (2007). Hagfish embryology with reference to the evolution of the neural crest. *Nature*, *446*(7136), 672–675.

Ota, K. G., & Kuratani, S. (2006). The history of scientific endeavors towards understanding hagfish embryology. *Zoological Science*, *23*(5), 403–418.

Ota, K. G., & Kuratani, S. (2007). Cyclostome embryology and early evolutionary history of vertebrates. *Integrative and Comparative Biology*, *47*(3), 329–337.

Ota, K. G., & Kuratani, S. (2008). Developmental biology of hagfishes, with a report on newly obtained embryos of the Japanese inshore hagfish, *Eptatretus burgeri*. *Zoological Science*, *25*(10), 999–1011.

Ota, K. G., & Kuratani, S. (2010). Expression pattern of two collagen type 2 α1 genes in the Japanese inshore hagfish (*Eptatretus burgeri*) with special reference to the evolution of cartilaginous tissue. *Journal of Experimental Zoology Part B: Molecular and Developmental Evolution*, *314B*(2), 157–165.

Owen, R. (1848). *On the Archetype and Homologies of the Vertebrate Skeleton*. London: Red Lion Court. 203pp.

Owsjannikow, P. (1893). On the embryology of the river-lamprey. *Annals And Magazine of Natural History*, *11*, 30–43.

Pacifici, M., Koyama, E., Shibukawa, Y., Wu, C., Tamamura, Y., Enomoto-Iwamoto, M., & Iwamoto, M. (2006). Cellular and molecular mechanisms of synovial joint and articular cartilage formation. *Annals of the New York Academy of Sciences*, *1068*(1), 74–86.

The Paleobiology Database. https://paleobiodb.org/#/. Accessed 15 June 2017

Palmer, A. R. (2004). Symmetry breaking and the evolution of development. *Science*, *306*(5697), 828–833.

Pan, Z., Zhu, M., Zhu, Y., & Jia, L. (2017). A new antiarch placoderm from the Emsian (Early Devonian) of Wuding, Yunnan, China. *Alcheringa: An Australasian Journal of Palaeontology*, 1–12 (Advance online publication).

Pani, A. M., Mullarkey, E. E., Aronowicz, J., Assimacopoulos, S., Grove, E. A., & Lowe, C. J. (2012). Ancient deuterostome origins of vertebrate brain signalling centres. *Nature*, *483*(7389), 289–294.

Paris, M., Escriva, H., Schubert, M., Brunet, F., Brtko, J., Ciesielski, F., et al. (2008). Amphioxus postembryonic development reveals the homology of chordate metamorphosis. *Current Biology*, *18*(11), 825–830.

Parker, H. J., Bronner, M. E., & Krumlauf, R. (2014). A Hox regulatory network of hindbrain segmentation is conserved to the base of vertebrates. *Nature*, *514*(7523), 490–493.

Parker, H. J., Bronner, M. E., & Krumlauf, R. (2016). The vertebrate Hox gene regulatory network for hindbrain segmentation: Evolution and diversification. *BioEssays*, *38*(6), 526–538.

Parker, H. J., & Krumlauf, R. (2017). Segmental arithmetic: Summing up the Hox gene regulatory network for hindbrain development in chordates. *Wiley Interdisciplinary Reviews: Developmental Biology*, advance online publication. doi:10.1002/wdev.286

Parker, H. J., Piccinelli, P., Sauka-Spengler, T., Bronner, M., & Elgar, G. (2011). Ancient Pbx-Hox signatures define hundreds of vertebrate developmental enhancers. *BMC Genomics*, *12*, 637.

Parker, H. J., Sauka-Spengler, T., Bronner, M., & Elgar, G. (2014). A reporter assay in lamprey embryos reveals both functional conservation and elaboration of vertebrate enhancers. *PLoS ONE*, *9*(1), e85492.

Parry, L. A., Smithwick, F., Nordén, K. K., Saitta, E. T., Lozano-Fernandez, J., Tanner, A. R., et al. (2018). Soft-bodied fossils are not simply rotten carcasses – Toward a holistic understanding of exceptional fossil preservation. *BioEssays*, *40*(1), 1700176.

Patten, W. (1890). On the origin of vertebrates from arachnids. *Quarterly Journal of Microscopical Science*, *2–31*(123), 317–378.

Patten, W. M. (1912). *The Evolution of the Vertebrates and Their Kin*. Philadelphia: The Blakiston Co.

Patterson, C. (1982). Morphological characters and homology. In K. A. Joysey & A. E. Friday (Eds.), *Problems of Phylogenetic Reconstruction* (pp. 21–74). San Diego: Academic Press.

Patterson, C. (1987). *Molecules and Morphology in Evolution: Conflict or Compromise?* Cambridge University Press.

Patthey, C., Schlosser, G., & Shimeld, S. M. (2014). The evolutionary history of vertebrate cranial placodes – I: Cell type evolution. *Developmental Biology*, *389*, 82–97.

Patzner, R. A. (1998). Gonads and reproduction in hagfishes. In J. M. Jørgensen, J. P. Lomholt, R. E. Weber, & H. Malte (Eds.), *The Biology of Hagfishes* (pp. 378–395). London: Chapman.

Payne S. L., Holliday, C. M., & Vickaryous, M. K. (2011). An osteological and histological investigation of cranial joints in geckos. *The Anatomical Record* **294**, 399-405.

Pennell, M. W., FitzJohn, R. G., & Cornwell, W. K. (2016). A simple approach for maximizing the overlap of phylogenetic and comparative data. *Methods in Ecology and Evolution*, *7*(6), 751–758.

Pennell, M. W., & Harmon, L. J. (2013). An integrative view of phylogenetic comparative methods: Connections to population genetics, community ecology, and paleobiology. *Annals of the New York Academy of Sciences*, *1289*(1), 90–105.

Peterson, K. J., Cotton, J. A., Gehling, J. G., & Pisani, D. (2008). The Ediacaran emergence of bilaterians: Congruence between the genetic and the geological fossil records. *Philosophical Transactions of the Royal Society B: Biological Sciences*, *363*(1496), 1435–1443.

Piavis, G. W. (1961). Embryological stages in the sea lamprey and effects of temperature on development. *Fishery Bulletin of the U.S. Fish and Wildlife Service*, *61*(182), 111–143.

Piavis, G. W. (1971). Embryology. In M. W. Hardisty & I. C. Potter (Eds.), *The Biology of Lampreys. Volume 1.* (Vol. 1, pp. 361–400). New York: Academic Press.

de Pinna, M. C. (1991). Concepts and tests of homology in the cladistic paradigm. *Cladistics*, *7*(4), 367–394.

Poplin, C., Sotty, D., & Janvier, P. (2001). Un Myxinoïde (Craniata, Hyperotreti) dans le Konservat-Lagerstätte Carbonifère supérieur de Montceau-les-Mines (Allier, France).

Comptes Rendus de l'Académie des Sciences - Series IIA - Earth and Planetary Science, *332*(5), 345–350.

Potter, I. C., Gill, H. S., Renaud, C. B., & Haoucher, D. (2015). The taxonomy, phylogeny, and distribution of lampreys. In M. F. Docker (Ed.), *Lampreys: Biology, Conservation and Control* (pp. 35–73). Springer Netherlands.

Pradel, A., Maisey, J. G., Tafforeau, P., Mapes, R. H., & Mallatt, J. (2014). A Palaeozoic shark with osteichthyan-like branchial arches. *Nature*, *509*(7502), 608–611.

Price, G. (1896a). Zur Ontogenie eines Myxinoiden (*Bdellostoma stouti* Lockington). *Sitzungsberichte der Mathematisch—Physikalischen Classe der KB Akademie der Wissenschaften zu München*, *36*, 167–174.

Price, G. (1896b). Some points in the development of a myxinoid (*Bdellostoma stouti* Lockington). *Anatomischer Anzeiger*, *12*, 81–86.

Price, G. (1896c). Development of the excretory organs of a myxinoid, *Bdellostoma stoutii* Lockington. *Zoologische Jahrbücher (Anatomie)*, *10*, 205–226.

Price, G. (1904). A further study of the development of the excretory organs in *Bdellostoma stouti*. *American Journal of Anatomy*, *4*, 117–138.

Provot, S., Kempf, H., Murtaugh, L. C., Chung, U., Kim, D.-W., Chyung, J., et al. (2006). *Nkx3.2*/*Bapx1* acts as a negative regulator of chondrocyte maturation. *Development*, *133*(4), 651–662.

Purnell, M. A. (1994). Skeletal ontogeny and feeding mechanisms in conodonts. *Lethaia*, *27*, 129–138.

Purnell, M. A. (1995). Microwear on conodont elements and macrophagy in the first vertebrates. *Nature*, *374*, 798–800.

Purnell, M. A., & Donoghue, P. C. J. (1997). Architecture and functional morphology of the skeletal apparatus of ozarkodinid conodonts. *Philosophical Transactions of the Royal Society of London B: Biological Sciences*, *352*(1361), 1545–1564.

Purnell, M. A., & von Bitter, P. H. (1992). Blade-shaped conodont elements functioned as cutting teeth. *Nature*, *359*(6396), 629–631.

Putnam, N. H., Butts, T., Ferrier, D. E. K., Furlong, R. F., Hellsten, U., Kawashima, T., et al. (2008). The amphioxus genome and the evolution of the chordate karyotype. *Nature*, *453*(7198), 1064–1071.

Puttick, M. N., Thomas, G. H., & Benton, M. J. (2016). Dating Placentalia: Morphological clocks fail to close the molecular fossil gap. *Evolution*, *70*(4), 873–886.

Pyron, R. A. (2011). Divergence time estimation using fossils as terminal taxa and the origins of Lissamphibia. *Systematic Biology*, *60*(4), 466–481.

Qiao, T., King, B., Long, J. A., Ahlberg, P. E., & Zhu, M. (2016). Early gnathostome phylogeny revisited: Multiple method consensus. *PLOS ONE*, *11*(9), e0163157.

Qu, Q., Blom, H., Sanchez, S., & Ahlberg, P. (2015). Three-dimensional virtual histology of Silurian osteostracan scales revealed by synchrotron radiation microtomography. *Journal of Morphology*, *276*(8), 873–888.

Qu, Q., Haitina, T., Zhu, M., & Ahlberg, P. E. (2015). New genomic and fossil data illuminate the origin of enamel. *Nature*, *526*(7571), 108–111.

Raff, R. A. (1996). *The Shape of Life: Genes, Development, and the Evolution of Animal Form*. Chicago: University of Chicago Press. 544 pp.

Raible, F., & Arendt, D. (2004). Metazoan evolution: Some animals are more equal than others. *Current Biology*, *14*(3), R106–R108.

Randle, E., & Sansom, R. S. (2017a). Exploring phylogenetic relationships of Pteraspidiformes heterostracans (stem-gnathostomes) using continuous and discrete characters. *Journal of Systematic Palaeontology*, *15*(7), 583–599.

Randle, E., & Sansom, R. S. (2017b). Phylogenetic relationships of the "higher heterostracans" (Heterostraci: Pteraspidiformes and Cyathaspididae), extinct jawless vertebrates. *Zoological Journal of the Linnean Society*. doi:10.1093/zoolinnean/zlx025

Ray, A., Singh, P. N. P., Sohaskey, M. L., Harland, R. M., & Bandyopadhyay, A. (2015). Precise spatial restriction of BMP signaling is essential for articular cartilage differentiation. *Development*, *142*(6), 1169–1179.

Reeder, T. W., Townsend, T. M., Mulcahy, D. G., Noonan, B. P., Jr, P. L. W., Jr, J. W. S., & Wiens, J. J. (2015). Integrated analyses resolve conflicts over squamate reptile phylogeny and reveal unexpected placements for fossil taxa. *PLOS ONE*, *10*(3), e0118199.

Renaud, C. B. (2011). *Lampreys of the World. An annotated and illustrated catalogue of lamprey species known to date.* Rome: Food and Agriculture Organization of the United Nations.

Renaud, C. B., Gill, H. S., & Potter, I. C. (2009). Relationships between the diets and characteristics of the dentition, buccal glands and velar tentacles of the adults of the parasitic species of lamprey. *Journal of Zoology*, *278*(3), 231–242.

Renz, A. J., Meyer, A., & Kuraku, S. (2013). Revealing less derived nature of cartilaginous fish genomes with their evolutionary time scale inferred with nuclear genes. *PLOS ONE*, *8*(6), e66400.

Richardson, M. K., Admiraal, J., & Wright, G. M. (2010). Developmental anatomy of lampreys. *Biological Reviews*, *85*(1), 1–33.

Richardson, M. K., & Wright, G. M. (2003). Developmental transformations in a normal series of embryos of the sea lamprey *Petromyzon marinus* (linnaeus). *Journal of Morphology*, *257*(3), 348–363.

Richman, J. M., & Lee, S.-H. (2003). About face: Signals and genes controlling jaw patterning and identity in vertebrates. *BioEssays*, *25*(6), 554–568.

Riedl, R. (1978). *The Order in Living Organisms: Systems Analysis of Evolution*. London: John Wiley & Sons. 313 pp.

Robson, P., Wright, G. M., & Keeley, F. W. (2000). Distinct non-collagen based cartilages comprising the endoskeleton of the Atlantic hagfish, *Myxine glutinosa*. *Anatomy and Embryology*, *202*(4), 281–290.

Robson, P., Wright, G. M., Sitarz, E., Maiti, A., Rawat, M., Youson, J. H., & Keeley, F. W. (1993). Characterization of lamprin, an unusual matrix protein from lamprey cartilage.

Implications for evolution, structure, and assembly of elastin and other fibrillar proteins. *Journal of Biological Chemistry*, *268*(2), 1440–1447.

Robson, P., Wright, G. M., Youson, J. H., & Keeley, F. W. (1997). A family of non–collagen-based cartilages in the skeleton of the sea lamprey, *Petromyzon marinus*. *Comparative Biochemistry and Physiology Part B: Biochemistry and Molecular Biology*, *118*(1), 71–78.

Rockel, J. S., Yu, C., Whetstone, H., Craft, A. M., Reilly, K., Ma, H., et al. (2016). Hedgehog inhibits β-catenin activity in synovial joint development and osteoarthritis. *The Journal of Clinical Investigation*, *126*(5), 1649–1663.

Romanoff, A. (1960). *The Avian Embryo: Structural and Functional Development* (First Edition edition.). The Macmillan Co.

Romer, A. S. (1945). *Vertebrate Paleontology. 2nd edition.* Chicago: University of Chicago Press.

Romer, A. S. (1972). The vertebrate as a dual animal: Somatic and visceral. *Evolutionary Biology*, *6*, 121–156.

Romer, A. S., & Parsons, T. S. (1977). *The Vertebrate Body. 5th edition.* Philadelphia: Saunders.

Ronquist, F., Klopfstein, S., Vilhelmsen, L., Schulmeister, S., Murray, D. L., & Rasnitsyn, A. P. (2012). A total-evidence approach to dating with fossils, applied to the early radiation of the Hymenoptera. *Systematic Biology*, *61*(6), 973–999.

Rovainen, C. M. (1996). Feeding and breathing in lampreys. *Brain, Behavior and Evolution*, *48*(5), 297–305.

Rücklin, M., Donoghue, P. C. J., Johanson, Z., Trinajstic, K., Marone, F., & Stampanoni, M. (2012). Development of teeth and jaws in the earliest jawed vertebrates. *Nature*, *491*(7426), 748–751.

Rücklin, M., Giles, S., Janvier, P., & Donoghue, P. C. J. (2011). Teeth before jaws? Comparative analysis of the structure and development of the external and internal scales in the extinct jawless vertebrate Loganellia scotica. *Evolution & Development*, *13*(6), 523–532.

Ruppert, E. E. (2005). Key characters uniting hemichordates and chordates: Homologies or homoplasies? *Canadian Journal of Zoology*, *83*, 8–23.

Saitta, E. T., Rogers, C., Brooker, R. A., Abbott, G. D., Kumar, S., O'Reilly, S. S., et al. (2017). Low fossilization potential of keratin protein revealed by experimental taphonomy. *Palaeontology*, *60*(4), 547–556.

Sallan, L., Giles, S., Sansom, R. S., Clarke, J. T., Johanson, Z., Sansom, I. J., & Janvier, P. (2017). The "Tully Monster" is not a vertebrate: Characters, convergence and taphonomy in Palaeozoic problematic animals. *Palaeontology*, *60*(2), 149–157.

Sansom, I. J., Davies, N. S., Coates, M. I., Nicoll, R. S., & Ritchie, A. (2012). Chondrichthyan-like scales from the Middle Ordovician of Australia. *Palaeontology*, *55*(2), 243–247.

Sansom, I. J., Donoghue, P. C. J., & Albanesi, G. (2005). Histology and affinity of the earliest armoured vertebrate. *Biology Letters*, *1*(4), 446–449.

Sansom, I. J., Smith, M. M., & Smith, M. P. (1996). Scales of thelodont and shark-like fishes from the Ordovician of Colorado. *Nature*, *379*(6566), 628–630.

Sansom, I. J., Smith, M. P., & Smith, M. M. (1994). Dentine in conodonts. *Nature*, *368*(6472), 591–591.

Sansom, I. J., Smith, M. P., Smith, M. M., & Turner, P. (1997). *Astraspis*: The anatomy and histology of an Ordovician fish. *Palaeontology*, *40*(3), 625–643.

Sansom, R. S. (2008). The origin and early evolution of the Osteostraci (Vertebrata): A phylogeny for the Thyestiida. *Journal of Systematic Palaeontology*, *6*(3), 317–332.

Sansom, R. S. (2009a). Endemicity and palaeobiogeography of the Osteostraci and Galeaspida: A test of scenarios of gnathostome evolution. *Palaeontology*, *52*(6), 1257–1273.

Sansom, R. S. (2009b). Phylogeny, classification and character polarity of the Osteostraci (Vertebrata). *Journal of Systematic Palaeontology*, *7*(1), 95–115.

Sansom, R. S. (2015). Bias and sensitivity in the placement of fossil taxa resulting from interpretations of missing data. *Systematic Biology*, *64*(2), 256–266.

Sansom, R. S., Freedman, K., Gabbott, S. E., Aldridge, R. J., & Purnell, M. A. (2010b). Taphonomy and affinity of an enigmatic Silurian vertebrate, *Jamoytius kerwoodi* White. *Palaeontology*, *53*(6), 1393–1409.

Sansom, R. S., Gabbott, S. E., & Purnell, M. A. (2010a). Non-random decay of chordate characters causes bias in fossil interpretation. *Nature*, *463*(7282), 797–800.

Sansom, R. S., Gabbott, S. E., & Purnell, M. A. (2011). Decay of vertebrate characters in hagfish and lamprey (Cyclostomata) and the implications for the vertebrate fossil record. *Proceedings of the Royal Society of London B: Biological Sciences*, *278*(1709), 1150–1157.

Sansom, R. S., Gabbott, S. E., & Purnell, M. A. (2013a). Atlas of vertebrate decay: A visual and taphonomic guide to fossil interpretation. *Palaeontology*, *56*(3), 457–474.

Sansom, R. S., Gabbott, S. E., & Purnell, M. A. (2013b). Unusual anal fin in a Devonian jawless vertebrate reveals complex origins of paired appendages. *Biology Letters*, *9*(3), 20130002.

Sansom, R. S., & Wills, M. A. (2013). Fossilization causes organisms to appear erroneously primitive by distorting evolutionary trees. *Scientific Reports*, *3*.

Sansom, R. S., & Wills, M. A. (2017). Differences between hard and soft phylogenetic data. *Proceedings of the Royal Society of London. Series B: Biological Sciences*, *284*(1869), 20172150.

Santini, F., Harmon, L. J., Carnevale, G., & Alfaro, M. E. (2009). Did genome duplication drive the origin of teleosts? A comparative study of diversification in ray-finned fishes. *BMC Evolutionary Biology*, *9*, 194.

Satoh, N. (2016). *Chordate Origins and Evolution* (1st ed.). San Diego: Academic Press.

Sauka-Spengler, T., Le Mentec, C., Lepage, M., & Mazan, S. (2002). Embryonic expression of Tbx1, a DiGeorge syndrome candidate gene, in the lamprey *Lampetra fluviatilis*. *Gene Expression Patterns*, *2*(1–2), 99–103.

Sauka-Spengler, T., Meulemans, D., Jones, M., & Bronner-Fraser, M. (2007). Ancient evolutionary origin of the neural crest gene regulatory network. *Developmental Cell*, *13*(3), 405–420.

Schaffer, J. (1896). Über das knorpelige Skelett van *Ammocoetes branchialis* nebst Bemerkungen über das knorpelgewebe im Allgemeinen. *Zeitschrift für wissenschaftliche Zoologie*, *61*, 606–659.

Schalk, A. (1913). Die entwicklung des cranial-und visceralskeletts von *Petromyzon fluviatilis*. *Archiv für mikroskopische Anatomie*, *83*(1), A43–A67.

Schilling, T. F., & Kimmel, C. B. (1997). Musculoskeletal patterning in the pharyngeal segments of the zebrafish embryo. *Development*, *124*(15), 2945–2960.

Schlichting, C. D., & Pigliucci, M. (1998). *Phenotypic Evolution: A Reaction Norm Perspective*. Sunderland: Sinauer Associates. 387 pp.

Schlosser, G., Patthey, C., & Shimeld, S. M. (2014). The evolutionary history of vertebrate cranial placodes II. Evolution of ectodermal patterning. *Developmental Biology*, *389*(1), 98–119.

Schlosser, G., & Wagner, G. P. (2004). *Modularity in Development and Evolution*. University of Chicago Press.

Schneider, A., Mijalski, T., Schlange, T., Dai, W., Overbeek, P., Arnold, H.-H., & Brand, T. (1999). The homeobox gene NKX3.2 is a target of left–right signalling and is expressed on opposite sides in chick and mouse embryos. *Current Biology*, *9*(16), 911-S1.

Schulte-Merker, S., & Stainier, D. Y. R. (2014). Out with the old, in with the new: Reassessing morpholino knockdowns in light of genome editing technology. *Development*, *141*(16), 3103–3104.

Schultze, M. S. (1856). *Die Entwickelungs-Geschichte von* Petromyzon planeri. Haarlem: Loosjes.

Schweitzer, R., Zelzer, E., & Volk, T. (2010). Connecting muscles to tendons: Tendons and musculoskeletal development in flies and vertebrates. *Development*, *137*(17), 2807–2817.

Scott, B. R., & Wilson, M. V. H. (2012). A new species of *Waengsjoeaspis* (Cephalaspidomorpha, Osteostraci) from the Early Devonian of Northwestern Canada, with a redescription of *W. nahanniensis* and implications for growth, variation, morphology, and phylogeny. *Journal of Vertebrate Paleontology*, *32*(6), 1235–1253.

Scott, B. R., & Wilson, M. V. H. (2015). The Superciliaspididae, a new family of Early Devonian Osteostraci (jawless vertebrates) from northern Canada, with two new genera and three new species. *Journal of Systematic Palaeontology*, *13*(3), 167–187.

Scott, W. B. (1880). Vorläufige mittheilung über die entwickelungsgeschichte der Petromyzonten. *Zoologischer Anzeiger*, *1880*(64), 443–449.

Scott, W. B. (1881). Preliminary account of the development of the lampreys. *Quarterly Journal of Microscopical Science*, *s2-21*(81), 146–153.

Scott, W. B. (1882). Beiträge zur entwicklungsgeschichte der Petromyzonten. *Morphologisches Jahrbuch, Leipzig*, *7*, 101–172.

Scott, W. B. (1883). On the development of the pituitary body in *Petromyzon*, and the significance of that organ in other types. *Science*, *2*(28), 184–186.

Scott, W. B. (1887). Notes on the development of *Petromyzon*. *Journal of Morphology*, *1*(2), 253–310.

Sémon, M., Schubert, M., & Laudet, V. (2012). Programmed genome rearrangements: In lampreys, all cells are not equal. *Current Biology*, *22*(16), R641–R643.

Servais, T., Owen, A. W., Harper, D. A. T., Kröger, B., & Munnecke, A. (2010). The Great Ordovician Biodiversification Event (GOBE): The palaeoecological dimension. *Palaeogeography, Palaeoclimatology, Palaeoecology*, *294*(3), 99–119.

Sewertzoff, A. N. (1899). Studien zur entwicklungsgeschichte der wirbeltierkopfes. I. Die metamerie des kopfes des elektrischen Rochen. *Bulletin de la Société Impériale des naturalistes de Moscou*, *1899*, 197–263.

Sewertzoff, A. N. (1913). Das visceralskelet der Cyclostomen. *Anatomischer Anzeiger*, *82*, 280–283.

Sewertzoff, A. N. (1916). Études sur l'évolution des vertébrés inférieurs. I. Morphologie du squelette et de la musculature de le tête des Cyclostomes. *Archives of Russian Anatomy, Histology, and Embryology*, *1*, 1–104.

Sewertzoff, A. N. (1927). Études sur l'évolution des vertébrés inférieurs: Structure primitive de l'appareil viscéral des Elasmobranches. *Pubblcazioni Stazione Zoologica di Napoli*, *8*, 475–554.

Sewertzoff, A. N. (1931). *Morphologische Gesetzmässigkeiten der Evolution*. Jena: Gustav Fischer.

Shaffer, H. B., Clark, J. M., & Kraus, F. (1991). When molecules and morphology clash: A phylogenetic analysis of the North American ambystomatid salamanders (Caudata: Ambystomatidae). *Systematic Biology*, *40*(3), 284–303.

Shigetani, Y., Sugahara, F., Kawakami, Y., Murakami, Y., Hirano, S., & Kuratani, S. (2002). Heterotopic shift of epithelial-mesenchymal interactions in vertebrate jaw evolution. *Science*, *296*(5571), 1316–1319.

Shimeld, S. M., & Donoghue, P. C. J. (2012). Evolutionary crossroads in developmental biology: Cyclostomes (lamprey and hagfish). *Development*, *139*(12), 2091–2099.

Shipley, A. E. (1885). On the formation of the mesoblast, and the persistence of the blastopore in the lamprey. *Proceedings of the Royal Society of London*, *39*, 244–248.

Shipley, A. E. (1887). On some points in the development of *Petromyzon fluviatilis*. *Quarterly Journal of Microscopical Science*, *s2-27*(107), 325–377.

Shu, D., Zhang, X., & Chen, L. (1996). Reinterpretation of *Yunnanozoon* as the earliest known hemichordate. *Nature*, *380*(6573), 428–430.

Shu, D., Morris, S. C., Zhang, X.-L., Chen, L., Li, Y., & Han, J. (1999a). A pipiscid-like fossil from the Lower Cambrian of south China. *Nature*, *400*(6746), 746–749.

Shu, D., Morris, S. C., Zhang, Z. F., Liu, J. N., Han, J., Chen, L., et al. (2003). A new species of Yunnanozoan with implications for deuterostome evolution. *Science*, *299*(5611), 1380–1384.

Shu, D.-G., Luo, H.-L., Conway Morris, S., Zhang, X.-L., Hu, S.-X., Chen, L., et al. (1999b). Lower Cambrian vertebrates from south China. *Nature*, *402*(6757), 42–46.

Shu, D.-G., Morris, S. C., Han, J., Zhang, Z.-F., Yasui, K., Janvier, P., et al. (2003). Head and backbone of the Early Cambrian vertebrate *Haikouichthys*. *Nature*, *421*(6922), 526–529.

Shubin, N., Tabin, C., & Carroll, S. (1997). Fossils, genes and the evolution of animal limbs. *Nature*, *388*(6643), 639-648.

Shubin, N., Tabin, C., & Carroll, S. (2009). Deep homology and the origins of evolutionary novelty. *Nature*, *457*(7231), 818–823.

Sievers, F., Wilm, A., Dineen, D., Gibson, T. J., Karplus, K., Li, W., et al. (2011). Fast, scalable generation of high-quality protein multiple sequence alignments using Clustal Omega. *Molecular Systems Biology*, *7*(1), 539.

Sire, J.-Y., Donoghue, P. C. J., & Vickaryous, M. K. (2009). Origin and evolution of the integumentary skeleton in non-tetrapod vertebrates. *Journal of Anatomy*, *214*(4), 409–440.

Sire, J.-Y., & Huysseune, A. (2003). Formation of dermal skeletal and dental tissues in fish: A comparative and evolutionary approach. *Biological Reviews*, *78*(2), 219–249.

Smeeton, J., Askary, A., & Gage Crump, J. (2016). Building and maintaining joints by exquisite local control of cell fate. *Wiley Interdisciplinary Reviews: Developmental Biology*, *6*(1), e245.

Smith, A. J., Howell, J. H., & Piavis, G. W. (1968). Comparative embryology of five species of lampreys of the Upper Great Lakes. *Copeia*, *1968*(3), 461–469.

Smith, C. L., Rand, C. S., Schaeffer, B., & Atz, J. W. (1975). *Latimeria*, the living coelacanth, Is ovoviviparous. *Science*, *190*, 1105–1106.

Smith, J. J., Kuraku, S., Holt, C., Sauka-Spengler, T., Jiang, N., Campbell, M. S., et al. (2013). Sequencing of the sea lamprey (*Petromyzon marinus*) genome provides insights into vertebrate evolution. *Nature Genetics*, *45*(4), 415–421.

Smith, J. J., Saha, N. R., & Amemiya, C. T. (2010). Genome biology of the cyclostomes and insights into the evolutionary biology of vertebrate genomes. *Integrative and Comparative Biology*, *50*(1), 130–137.

Smith, M. M., & Hall, B. K. (1990). Development and evolutionary origins of vertebrate skeletogenic and odontogenic tissues. *Biological Reviews*, *65*(3), 277–373.

Smith, M. P., Sansom, I. J., & Repetski, J. E. (1996). Histology of the first fish. *Nature*, *380*(6576), 702–704.

Song, J., & Boord, R. L. (1993). Motor components of the trigeminal nerve and organization of the mandibular arch muscles in vertebrates. *Acta Anatomica*, *148*(2-3), 139-149.

Später, D., Hill, T. P., O'Sullivan, R. J., Gruber, M., Conner, D. A., & Hartmann, C. (2006). Wnt9a signaling is required for joint integrity and regulation of Ihh during chondrogenesis. *Development*, *133*(15), 3039–3049.

Spice, P. J. (2015). *Nkx3.2 regulates zebrafish vascular stabilization through recruitment of mural cells* (Unpublished M.Sc. thesis). University of Calgary, Calgary.

Square, T., Jandzik, D., Cattell, M., Coe, A., Doherty, J., & Medeiros, D. M. (2015a). A gene expression map of the larval *Xenopus laevis* head reveals developmental changes underlying the evolution of new skeletal elements. *Developmental Biology*, *397*(2), 293–304.

Square, T., Jandzik, D., Cattell, M., Hansen, A., & Medeiros, D. M. (2016a). Embryonic expression of endothelins and their receptors in lamprey and frog reveals stem vertebrate origins of complex Endothelin signaling. *Scientific Reports*, *6*, 34282.

Square, T., Jandzik, D., Romášek, M., Cerny, R., & Medeiros, D. M. (2017). The origin and diversification of the developmental mechanisms that pattern the vertebrate head skeleton. *Developmental Biology*, *427*(2), 219–229.

Square, T., Romášek, M., Jandzik, D., Cattell, M. V., Klymkowsky, M., & Medeiros, D. M. (2015b). CRISPR/Cas9-mediated mutagenesis in the sea lamprey *Petromyzon marinus*: A powerful tool for understanding ancestral gene functions in vertebrates. *Development*, *142*(23), 4180–4187.

Stensiö, E. A. (1927). The Devonian and Downtonian vertebrates of Spitsbergen. Part I. Family Cephalaspidae. *Skrifter om Svalbard og Nordishavet*, *12*, 1–391.

Stensiö, E. A. (1932). *The Cephalaspids of Great Britain*. London: Trustees of the British Museum.

Stensiö, E. A. (1939). A new anaspid from the Upper Devonian of Scaumenac Bay in Canada with remakrs on the other anaspids. *Kungliga Svenska Ventenskapsakademiens Handlingar*, *18*, 1–25.

Stensiö, E. A. (1958). Les Cyclostomes fossiles ou Ostracodermes. In P. P. Grassé (Ed.), *Traité de Zoologie* (Vol. 13, pp. 173–425). Paris: Masson et Cie.

Stensiö, E. A. (1964). Les Cyclostomes fossiles ou Ostracodermes. In J. Piveteau (Ed.), *Traité de Paléontologie* (Vol. 4, pp. 96–383). Paris: Masson et Cie.

Stensiö, E. A. (1968). The cyclostomes with special reference to the diphyletic origin of the Petromyzontida and the Myxinoidea. In T. Ørvig (Ed.), *Current Problems in Lower Vertebrate Phylogeny* (pp. 13–71). Stockholm: Almqvist and Wiksell.

Stensiö, E. A. (1969). Elasmobranchiomorphi Placodermata Arthrodires. In J. Piveteau (Ed.), *Traité de Paléontologie* (Vols. 1-2, Vol. 4, pp. 71–692). Paris: Masson et Cie.

Stock, D. W., & Whitt, G. S. (1992). Evidence from 18S ribosomal RNA sequences that lampreys and hagfishes form a natural group. *Science*, *257*(5071), 787–789.

Stockard, C. R. (1906a). The development of the thyroid gland in *Bdellostoma stoutii*. *Anatomischer Anzeiger*, *29*, 91–99.

Stockard, C. R. (1906b). The development of the mouth and gills in *Bdellostoma stouti*. *American Journal of Anatomy*, *5*(4), 481–517.

Stolfi, A., Ryan, K., Meinertzhagen, I. A., & Christiaen, L. (2015). Migratory neuronal progenitors arise from the neural plate borders in tunicates. *Nature*, *527*(7578), 371–374.

Strahan, R. (1958). The velum and the respiratory current of *Myxine*. *Acta Zoologica*, *39*(2–3), 227–240.

Strauss, R. E., Atanassov, M. N., & De Oliveira, J. A. (2003). Evaluation of the principal-component and expectation-maximization methods for estimating missing data in morphometric studies. *Journal of Vertebrate Paleontology*, *23*(2), 284–296.

Sugahara, F., Aota, S., Kuraku, S., Murakami, Y., Takio-Ogawa, Y., Hirano, S., & Kuratani, S. (2011). Involvement of Hedgehog and FGF signalling in the lamprey telencephalon: Evolution of regionalization and dorsoventral patterning of the vertebrate forebrain. *Development*, *138*(6), 1217–1226.

Sugahara, F., Pascual-Anaya, J., Oisi, Y., Kuraku, S., Aota, S., Adachi, N., et al. (2016). Evidence from cyclostomes for complex regionalization of the ancestral vertebrate brain. *Nature*, *531*(7592), 97–100.

Sugimoto, Y., Takimoto, A., Akiyama, H., Kist, R., Scherer, G., Nakamura, T., et al. (2013). Scx+/Sox9+ progenitors contribute to the establishment of the junction between cartilage and tendon/ligament. *Development*, *140*(11), 2280–2288.

Suzuki, D. G., Fukumoto, Y., Yoshimura, M., Yamazaki, Y., Kosaka, J., Kuratani, S., & Wada, H. (2016). Comparative morphology and development of extra-ocular muscles in the lamprey and gnathostomes reveal the ancestral state and developmental patterns of the vertebrate head. *Zoological Letters*, *2*, 10.

Suzuki, T., Mizuta, C., Uda, K., Ishida, K., Mizuta, K., Sona, S., et al. (2004). Evolution and divergence of the genes for cytoplasmic, mitochondrial, and flagellar creatine kinases. *Journal of Molecular Evolution*, *59*(2), 218–226.

Sweet, W. C. (1988). *The Conodonta. Morphology, taxonomy, paleoecology, and evolutionary history of a long-extinct animal phylum*. Oxford: Clarendon Press. 212 pp.

Sweet, W. C., & Donoghue, P. C. J. (2001). Conodonts: Past, present, future. *Journal of Paleontology*, *75*(6), 1174–1184.

Swofford, D. L. (2017). *PAUP**. Sinauer Associates.

Szarski, H. (1949). The concept of homology in the light of the comparative anatomy of vertebrates. *The Quarterly Review of Biology*, *24*(2), 124–131.

Tahara, Y. (1988). Normal stages of development in the lamprey, *Lampetra reissneri* (Dybowski). *Zoological Science*, *5*, 109–118.

Takechi, M., Adachi, N., Hirai, T., Kuratani, S., & Kuraku, S. (2013). The Dlx genes as clues to vertebrate genomics and craniofacial evolution. *Seminars in Cell & Developmental Biology*, *24*(2), 110–118.

Takechi, M., Takeuchi, M., Ota, K. G., Nishimura, O., Mochii, M., Itomi, K., et al. (2011). Overview of the transcriptome profiles identified in hagfish, shark, and bichir: Current

issues arising from some nonmodel vertebrate taxa. *Journal of Experimental Zoology Part B: Molecular and Developmental Evolution*, *316B*(7), 526–546.

Takezaki, N., Figueroa, F., Zaleska-Rutczynska, Z., & Klein, J. (2003). Molecular phylogeny of early vertebrates: Monophyly of the agnathans as revealed by sequences of 35 genes. *Molecular Biology and Evolution*, *20*(2), 287–292.

Takio, Y., Kuraku, S., Murakami, Y., Pasqualetti, M., Rijli, F. M., Narita, Y., et al. (2007). Hox gene expression patterns in *Lethenteron japonicum* embryos—Insights into the evolution of the vertebrate Hox code. *Developmental Biology*, *308*(2), 606–620.

Takio, Y., Pasqualetti, M., Kuraku, S., Hirano, S., Rijli, F. M., & Kuratani, S. (2004). Evolutionary biology: Lamprey Hox genes and the evolution of jaws. *Nature*, *429*(6989).

Tamura, K., Nomura, N., Seki, R., Yonei-Tamura, S., & Yokoyama, H. (2011). Embryological evidence identifies wing digits in birds as digits 1, 2, and 3. *Science*, *331*(6018), 753–757.

Tautz, D. (1998). Evolutionary biology: Debatable homologies. *Nature*, *395*(6697), 17-19.

Thomson, K. S. (1992). The puzzle of "*Palaeospondylus*." *American Scientist*, *80*(3), 216–219.

Tiecke, E., Matsuura, M., Kokubo, N., Kuraku, S., Kusakabe, R., Kuratani, S., & Tanaka, M. (2007). Identification and developmental expression of two Tbx1/10-related genes in the agnathan *Lethenteron japonicum*. *Development Genes and Evolution*, *217*(10), 691–697.

Tomer, R., Denes, A. S., Tessmar-Raible, K., & Arendt, D. (2010). Profiling by image registration reveals common origin of annelid mushroom bodies and vertebrate pallium. *Cell*, *142*(5), 800–809.

Tomsa, J. M., & Langeland, J. A. (1999). Otx expression during lamprey embryogenesis provides insights into the evolution of the vertebrate head and jaw. *Developmental Biology*, *207*(1), 26–37.

Trainor, P. (Ed.). (2013). *Neural Crest Cells: Evolution, Development and Disease* (1 edition.). Amsterdam: Academic Press.

Tretjakoff, D. (1909a). Das nervensystem von ammocoetes. I. Das Rückenmark. *Archiv für mikroskopische Anatomie*, *73*, 607–680.

Tretjakoff, D. (1909b). Das nervensystem von ammocoetes. II. Gehirn. *Archiv für mikroskopische Anatomie*, *74*, 636–779.

Tretjakoff, D. (1909c). Nervus mesencephalicus bei ammocoetes. *Anatomischer Anzeiger*, *34*, 151–157.

Tretjakoff, D. (1913). Die zentralen Sinnesorgane bei *Petromyzon*. *Archiv für mikroskopische Anatomie*, *83*(1), A68–A117.

Tretjakoff, D. (1926a). Das skelett und die muskulatur im kopfe des flüssneunauges. *Zeitschrift für Wissenschaftliche Zoologie*, *128*, 267–304.

Tretjakoff, D. (1926b). Die wirbelsäule des neunauges. *Anatomischer Anzeiger*, *61*, 387–396.

Tretjakoff, D. (1927). Das periphere nervensystem de flussneunauges. *Zeitschrift für Wissenschaftliche Zoologie*, *129*, 359–452.

Tretjakoff, D. (1929). Die schleimknorpeligen bestandteile in kopfskelett von ammocoetes. *Zeitschrift für Wissenschaftliche Zoologie*, *133*, 470–516.

Trinajstic, K., Boisvert, C., Long, J., Maksimenko, A., & Johanson, Z. (2014). Pelvic and reproductive structures in placoderms (stem gnathostomes). *Biological Reviews*, *90*(2), 467–501.

Trinajstic, K., & Long, J. A. (2009). A new genus and species of Ptyctodont (Placodermi) from the Late Devonian Gneudna Formation, Western Australia, and an analysis of Ptyctodont phylogeny. *Geological Magazine*, *146*(5), 743–760.

Trinajstic, K., Sanchez, S., Dupret, V., Tafforeau, P., Long, J., Young, G., et al. (2013). Fossil musculature of the most primitive jawed vertebrates. *Science*, *341*(6142), 160–164.

True, J. R., & Haag, E. S. (2001). Developmental system drift and flexibility in evolutionary trajectories. *Evolution & Development*, *3*(2), 109–119.

Tsuneki, K., Ouji, M., & Saito, H. (1983). Seasonal migration and gonadal changes in the hagfish *Eptatretus burgeri*. *Japanese Journal of Ichthyology*, *29*, 429–440.

Tucker, A. S., Watson, R. P., Lettice, L. A., Yamada, G., & Hill, R. E. (2004). Bapx1 regulates patterning in the middle ear: Altered regulatory role in the transition from the proximal jaw during vertebrate evolution. *Development*, *131*(6), 1235–1245.

Tulenko, F. J., McCauley, D. W., MacKenzie, E. L., Mazan, S., Kuratani, S., Sugahara, F., et al. (2013). Body wall development in lamprey and a new perspective on the origin of vertebrate paired fins. *Proceedings of the National Academy of Sciences*, *110*(29), 11899–11904.

Turner, S., Burrow, C. J., Schultze, H.-P., Blieck, A., Reif, W.-E., Rexroad, C. B., et al. (2010). False teeth: Conodont-vertebrate phylogenetic relationships revisited. *Geodiversitas*, *32*(4), 545–594.

Uchida, K., Murakami, Y., Kuraku, S., Hirano, S., & Kuratani, S. (2003). Development of the adenohypophysis in the lamprey: Evolution of epigenetic patterning programs in organogenesis. *Journal of Experimental Zoology Part B: Molecular and Developmental Evolution*, *300B*(1), 32–47.

Ueki, T., Kuratani, S., Hirano, S., & Aizawa, S. (1998). Otx cognates in a lamprey, *Lampetra japonica*. *Development Genes and Evolution*, *208*(4), 223–228.

Uy, B. R., Simoes-Costa, M., Koo, D. E. S., Sauka-Spengler, T., & Bronner, M. E. (2015). Evolutionarily conserved role for SoxC genes in neural crest specification and neuronal differentiation. *Developmental Biology*, *397*(2), 282–292.

Uy, B. R., Simoes-Costa, M., Sauka-Spengler, T., & Bronner, M. E. (2012). Expression of Sox family genes in early lamprey development. *The International Journal of Developmental Biology*, *56*(5), 377–383.

Uyeno, T. A., & Clark, A. J. (2015). Muscle articulations: Flexible jaw joints made of soft tissues. *Integrative and Comparative Biology*, *55*(2), 193–204.

Uyeno, T. A., & Kier, W. M. (2015). The structure and function of a muscle articulation-type jaw joint of a polychaete worm. *Journal of Morphology*, *276*(4), 403–414.

Valiukevičius, J. (1995). Acanthodian histology: Some significantaspects in taxonomical and phylogenetical research. *Geobios*, *28*, 157–159.

van der Brugghen, G. (2010). New observations on the Silurian anaspid *Lasanius problematicus* Traquair. *Fossil Quarry Articles*, *1*, 1–10.

Van Otterloo, E., Li, W., Garnett, A., Cattell, M., Medeiros, D. M., & Cornell, R. A. (2012). Novel *Tfap2*-mediated control of *soxE* expression facilitated the evolutionary emergence of the neural crest. *Development*, *139*(4), 720–730.

van Whijhe, J. W. (1882). Über die mesodermsegmente und die entwicklung der nerven des selachierkopfes. *Verhandelingen der Koninklijke Akademie van Wetenschappen*, *22*, 1–50.

Van Valen, L. M. (1982). Homology and causes. *Journal of Morphology*, *173*(3), 305–312.

Veit, O. (1939). Beiträge zur kenntnis des kopfes der wirbelthiere. *Morphologisches Jahrbuch, Leipzig*, *84*, 86–107.

Vladykov, V. D. (1973). A female sea lamprey (*Petromyzon marinus*) with a true anal fin, and the question of the presence of an anal fin in Petromyzonidae. *Canadian Journal of Zoology*, *51*(2), 221–224.

von Kupffer, C. (1890). Entwicklung von *Petromyzon planeri*. *Archiv. für. Mik. Anat.*, *35*, 469–558.

von Kupffer, C. (1899). Zur kopfentwicklung von *Bdellostoma*. *Sitzungsberichte der Geselleschaft fur Morpholigie und Physioligie*, *15*, 21–35.

von Kupffer, C. (1900). *Studien zur vergleichenden Entwicklungsgeschichte des Kopfes der Kranioten, Heft 4: Zur Kopfentwicklung von Bdellostoma*. München: Verlag von J. F. Lehmann.

von Kupffer, C. (1906). Die morphogenie des centralnervensystems. *Handbuch der vergleichenden und experimentellen Entwicklungslehre der Wirbeltiere*, *2 (Part 3)*, 1–272.

Wada, H., Saiga, H., Satoh, N., & Holland, P. W. (1998). Tripartite organization of the ancestral chordate brain and the antiquity of placodes: Insights from ascidian Pax-2/5/8, Hox and Otx genes. *Development*, *125*(6), 1113–1122.

Wagner, G. P. (1989). The biological homology concept. *Annual Review of Ecology and Systematics*, *20*(1), 51–69.

Wagner, G. P. (1994). Homology and the mechanisms of development. In B. K. Hall (Ed.), *Homology: The Hierarchical Basis of Comparative Biology* (pp. 273–299). San Diego: Academic Press.

Wagner, G. P. (2007). The developmental genetics of homology. *Nature Reviews Genetics*, *8*(6), 473–479.

Wagner, G. P. (2014). *Homology, Genes, and Evolutionary Innovation*. Princeton: Princeton University Press.

Wagner, G. P., & Zhang, J. (2011). The pleiotropic structure of the genotype–phenotype map: The evolvability of complex organisms. *Nature Reviews Genetics*, *12*(3), 204–213.

Wagner, G. P., & Gauthier, J. A. (1999). 1, 2, 3= 2, 3, 4: A solution to the problem of the homology of the digits in the avian hand. *Proceedings of the National Academy of Sciences*, *96*(9), 5111–5116.

Wagner, P. J. (2000). Exhaustion of morphologic character states among fossil taxa. *Evolution*, *54*(2), 365–386.

Wagner, P. J., Ruta, M., & Coates, M. I. (2006). Evolutionary patterns in early tetrapods. II. Differing constraints on available character space among clades. *Proceedings of the Royal Society of London B: Biological Sciences*, *273*(1598), 2113–2118.

Walker, M. B., Miller, C. T., Coffin Talbot, J., Stock, D. W., & Kimmel, C. B. (2006). Zebrafish furin mutants reveal intricacies in regulating Endothelin1 signaling in craniofacial patterning. *Developmental Biology*, *295*(1), 194–205.

Walker, M. B., Miller, C. T., Swartz, M. E., Eberhart, J. K., & Kimmel, C. B. (2007). phospholipase C, beta 3 is required for Endothelin1 regulation of pharyngeal arch patterning in zebrafish. *Developmental Biology*, *304*(1), 194–207.

Wang, N.-Z., Donoghue, P. C. J., Smith, M. M., & Sansom, I. J. (2005). Histology of the galeaspid dermoskeleton and endoskeleton, and the origin and early evolution of the vertebrate cranial endoskeleton. *Journal of Vertebrate Paleontology*, *25*(4), 745–756.

Wängsjö, G. (1952). The Downtonian and Devonian vertebrates of Spitsbergen. IX, Morphologic and systematic studies of the Spitsbergen Cephalaspids. *Norsk Polarinstitutt Skrifter*, *97*, 1–611.

Wedin, A. B. (1949). *The Anterior Mesoblast in some Lower Vertebrates. A comparative study of the ontogenetic development of the anterior mesoblast in Petromyzon, Etmopterus, Torpedo, et al.* (G. Åkerman & K. Koch, Trans.). Lund: Håkan Ohlssons Boktryckeri.

Wheeler, W. M. (1900). The development of the urogenital organs of the lamprey. *Zoologische Jahrbücher (Anatomie)*, *13*, 1–88.

Wicht, H., & Lacalli, T. C. (2005). The nervous system of amphioxus: Structure, development, and evolutionary significance. *Canadian Journal of Zoology*, *83*, 122–150.

Wicht, H., & Northcutt, R. G. (1995). Ontogeny of the head of the Pacific hagfish (*Eptatretus stouti*, Myxinoidea): Development of the lateral line system. *Philosophical Transactions of the Royal Society of London B: Biological Sciences*, *349*, 119–134.

Wiedersheim, R. (1880). Das Gehirn von *Ammocoetes* und *Petromyzon planeri*. *Morph. Studien I. Jenaische Zeitschr.*, *14*, 1–38.

Wiens, J. J., & Collins, T. (2004). The role of morphological data in phylogeny reconstruction. *Systematic Biology*, *53*(4), 653–661.

Wiens, J. J., Kuczynski, C. A., Townsend, T., Reeder, T. W., Mulcahy, D. G., & Sites, J. W. (2010). Combining phylogenomics and fossils in higher-level squamate reptile phylogeny: Molecular data change the placement of fossil taxa. *Systematic Biology*, *59*(6), 674–688.

Wiley, A. (1894). *Amphioxus and the Ancestry of the Vertebrates*. London: Macmillan and Co.

Williston, A. D. (2016). Charles Minot and the Harvard Embryological Collection: Over a century of development. *Breviora*, *547*(1), 1–13.

Willmer, E. N. (1974). Nemertines as possible ancestors of the vertebrates. *Biological Reviews*, *49*(3), 321–363.

Wills, M. A. (1998). Crustacean disparity through the Phanerozoic: Comparing morphological and stratigraphic data. *Biological Journal of the Linnean Society*, *65*(4), 455–500.

Wilson, J., & Tucker, A. S. (2004). Fgf and Bmp signals repress the expression of Bapx1 in the mandibular mesenchyme and control the position of the developing jaw joint. *Developmental Biology*, *266*(1), 138–150.

Wilson, M. V. H., & Caldwell, M. W. (1993). New Silurian and Devonian fork-tailed "thelodonts" are jawless vertebrates with stomachs and deep bodies. *Nature*, *361*(6411), 442–444.

Wilson, M. V. H., & Caldwell, M. W. (1998). The Furcacaudiformes: A new order of jawless vertebrates with thelodont scales, based on articulated Silurian and Devonian fossils from northern Canada. *Journal of Vertebrate Paleontology*, *18*(1), 10–29.

Wilson, M. V. H., Hanke, G. F., & Märss, T. (2007). Paired fins of jawless vertebrates and their homologies across the "agnathan"-gnathostome transition. In J. S. Anderson & H.-D. Sues (Eds.), *Major Transitions in Vertebrate Evolution* (pp. 122–149). Bloomington: Indiana University Press.

Wilson, M. V. H., & Märss, T. (2004). Toward a phylogeny of the thelodonts. In G. Arratia, M. V. H. Wilson, & R. Cloutier (Eds.), *Recent Advances in the Origin and Early Radiation of the Vertebrates, Honoring Hans-Peter Schultze* (pp. 95–108). Munich: Verlag Dr. Friedrich Pfeil.

Wilson, M. V. H., & Märss, T. (2009). Thelodont phyogeny revisted, with inclusion of key scale-based taxa. *Estonian Journal of Earth Sciences*, *58*(4), 297–310.

Winchell, C. J., Sullivan, J., Cameron, C. B., Swalla, B. J., & Mallatt, J. (2002). Evaluating hypotheses of deuterostome phylogeny and chordate evolution with new LSU and SSU ribosomal DNA data. *Molecular Biology and Evolution*, *19*(5), 762–776.

Winegard, T., Herr, J., Mena, C., Lee, B., Dinov, I., Bird, D., et al. (2014). Coiling and maturation of a high-performance fibre in hagfish slime gland thread cells. *Nature Communications*, *5*, 3534.

Witmer, L. M. (1997). The extant phylogenetic bracket and the importance of reconstructing soft tissues in fossils. In J. Thomason (Ed.), *Functional Morphology in Vertebrate Paleontology* (pp. 19–33). Cambridge: Cambridge University Press.

Witten, P. E., & Huysseune, A. (2009). A comparative view on mechanisms and functions of skeletal remodelling in teleost fish, with special emphasis on osteoclasts and their function. *Biological Reviews*, *84*(2), 315–346.

Witten, P. E., Huysseune, A., & Hall, B. K. (2010). A practical approach for the identification of the many cartilaginous tissues in teleost fish. *Journal of Applied Ichthyology*, *26*(2), 257–262.

Wray, G. A., Levinton, J. S., & Shapiro, L. H. (1996). Molecular evidence for deep Precambrian divergences among metazoan phyla. *Science*, *274*(5287), 568–573. doi:10.1126/science.274.5287.568

Wright, G. M. (1989). Ultrastructure of the adenohypophysis in the anadromous sea lamprey, *Petromyzon marinus*, during metamorphosis. *Journal of Morphology*, *202*(2), 205–223.

Wright, G. M., Armstrong, L. A., Jacques, A. M., & Youson, J. H. (1988). Trabecular, nasal, branchial, and pericardial cartilages in the sea lamprey, *Petromyzon marinus*: Fine structure and immunohistochemical detection of elastin. *American Journal of Anatomy*, *182*(1), 1–15.

Wright, G. M., Keeley, F. W., & Robson, P. (2001). The unusual cartilaginous tissues of jawless craniates, cephalochordates and invertebrates. *Cell and Tissue Research*, *304*(2), 165–174.

Wright, G. M., Keeley, F. W., & Youson, J. H. (1983). Lamprin: A new vertebrate protein comprising the major structural protein of adult lamprey cartilage. *Experientia*, *39*(5), 495–497.

Wright, G. M., & Youson, J. H. (1976). Transformation of the endostyle of the anadromous sea lamprey, *Petromyzon marinus* L., during metamorphosis: I. Light microscopy and autoradiography with 125I. *General and Comparative Endocrinology*, *30*(3), 243–257.

Wright, G. M., & Youson, J. H. (1980). Transformation of the endostyle of the anadromous sea lamprey, *Petromyzon marinus* L., during metamorphosis. II. Electron microscopy. *Journal of Morphology*, *166*(2), 231–257.

Wright, G. M., & Youson, J. H. (1982). Ultrastructure of mucocartilage in the larval anadromous sea lamprey, *Petromyzon marinus* L. *American Journal of Anatomy*, *165*(1), 39–51.

Wright, G. M., & Youson, J. H. (1983). Ultrastructure of cartilage from young adult sea lamprey, *Petromyzon marinus* L: A new type of vertebrate cartilage. *American Journal of Anatomy*, *167*(1), 59–70.

Xenbase Home. http://www.xenbase.org/entry/. Accessed 2 October 2017

Yalden, D. W. (1985). Feeding mechanisms as evidence for cyclostome monophyly. *Zoological Journal of the Linnean Society*, *84*(3), 291–300.

Yamashita, S., Andoh, M., Ueno-Kudoh, H., Sato, T., Miyaki, S., & Asahara, H. (2009). Sox9 directly promotes Bapx1 gene expression to repress Runx2 in chondrocytes. *Experimental Cell Research*, *315*(13), 2231–2240.

Yamazaki, Y., Fukutomi, N., Takeda, K., & Iwata, A. (2003). Embryonic development of the Pacific lamprey, *Entosphenus tridentatus*. *Zoological Science*, *20*(9), 1095–1098.

Yao, T., Ohtani, K., Kuratani, S., & Wada, H. (2011). Development of lamprey mucocartilage and its dorsal–ventral patterning by endothelin signaling, with insight into vertebrate jaw evolution. *Journal of Experimental Zoology Part B: Molecular and Developmental Evolution*, *316B*(5), 339–346.

York, J. R., Yuan, T., Zehnder, K., & McCauley, D. W. (2017). Lamprey neural crest migration is Snail-dependent and occurs without a differential shift in cadherin expression. *Developmental Biology*, *428*(1), 176–187.

Young, G. C. (1980). A new Early Devonian placoderm from New South Wales, Australia, with a discussion of placoderm phylogeny. *Palaeontographica Abteilung A*, 10–76.

Young, G. C. (1984). Reconstruction of the jaws and braincase in the Devonian placoderm fish Bothriolepis. *Palaeontology*, *27*(3), 635–661.

Young, G. C. (1991). The first armoured agnathan vertebrates from the Devonian of Australia. In M. M. Chang, Y. H. Liu, & G. R. Zhang (Eds.), *Early Vertebrates and Related Problems of Evolutionary Biology* (pp. 67–85). Beijing: Science Press.

Young, G. C. (2008). Number and arrangement of extraocular muscles in primitive gnathostomes: Evidence from extinct placoderm fishes. *Biology Letters*, *4*(1), 110–114.

Young, G. C. (2009). An Ordovician vertebrate from western New South Wales, with comments on Cambro-Ordovician vertebrate distribution patterns. *Alcheringa: An Australasian Journal of Palaeontology*, *33*(1), 79–89.

Young, G. C., Karatajute-Talimaa, V. N., & Smith, M. M. (1996). A possible Late Cambrian vertebrate from Australia. *Nature*, *383*(6603), 810–812.

Youson, J. H. (1980). Morphology and physiology of lamprey metamorphosis. *Canadian Journal of Fisheries and Aquatic Sciences*, *37*(11), 1687–1710.

Youson, J. H., & Potter, I. C. (1979). A description of the stages in the metamorphosis of the anadromous sea lamprey, *Petromyzon marinus* L. *Canadian Journal of Zoology*, *57*(9), 1808–1817.

Yu, S., Zhang, W., Li, L., Huang, H., Ma, F., & Li, Q. (2008). Phylogenetic analysis of 48 gene families revealing relationships between hagfishes, lampreys, and gnathostomata. *Journal of Genetics and Genomics*, *35*(5), 285–290.

Yue, J.-X., Yu, J.-K., Putnam, N. H., & Holland, L. Z. (2014). The Transcriptome of an amphioxus, *Asymmetron lucayanum*, from the Bahamas: A window into chordate evolution. *Genome Biology and Evolution*, *6*(10), 2681–2696.

Zeng, L., Kempf, H., Murtaugh, L. C., Sato, M. E., & Lassar, A. B. (2002). Shh establishes an *Nkx3.2*/*Sox9* autoregulatory loop that is maintained by BMP signals to induce somitic chondrogenesis. *Genes & Development*, *16*(15), 1990–2005.

ZFIN: The Zebrafish Information Network. https://zfin.org/. Accessed 2 October 2017

Zhang, C., Stadler, T., Klopfstein, S., Heath, T. A., & Ronquist, F. (2016). Total-evidence dating under the fossilized birth–death process. *Systematic Biology*, *65*(2), 228–249.

Zhang, G., Miyamoto, M. M., & Cohn, M. J. (2006). Lamprey type II collagen and Sox9 reveal an ancient origin of the vertebrate collagenous skeleton. *Proceedings of the National Academy of Sciences of the United States of America*, *103*(9), 3180–3185.

Zhu, M. (1996). The phylogeny of the Antiarcha (Placodermi, Pisces), with the description of Early Devonian antiarchs from Qujing, Yunnan, China. *Bulletin du Muséum national d'Histoire naturelle, 4e série, section C*, *18*, 233–347.

Zhu, M., & Ahlberg, P. E. (2004). The origin of the internal nostril of tetrapods. *Nature*, *432*(7013), 94–97.

Zhu, M., Ahlberg, P. E., Pan, Z., Zhu, Y., Qiao, T., Zhao, W., et al. (2016). A Silurian maxillate placoderm illuminates jaw evolution. *Science*, *354*(6310), 334–336.

Zhu, M., Ahlberg, P. E., Zhao, W.-J., & Jia, L.-T. (2017). A Devonian tetrapod-like fish reveals substantial parallelism in stem tetrapod evolution. *Nature Ecology & Evolution*, *1*(10), 1470.

Zhu, M., & Gai, Z. (2007). Phylogenetic relationships of galeaspids (Agnatha). *Frontiers of Biology in China*, *2*(2), 151–169.

Zhu, M., & Janvier, P. (1998). The histological structure of the endoskeleton in galeaspids (Galeaspida, Vertebrata). *Journal of Vertebrate Paleontology*, *18*(3), 650–654.

Zhu, M., & Yu, X. (2002). A primitive fish close to the common ancestor of tetrapods and lungfish. *Nature*, *418*(6899), 767–770.

Zhu, M., Yu, X., & Ahlberg, P. E. (2001). A primitive sarcopterygian fish with an eyestalk. *Nature*, *410*(6824), 81–84.

Zhu, M., Yu, X., Ahlberg, P. E., Choo, B., Lu, J., Qiao, T., et al. (2013). A Silurian placoderm with osteichthyan-like marginal jaw bones. *Nature*, *502*(7470), 188–193.

Zhu, M., Zhao, W., Jia, L., Lu, J., Qiao, T., & Qu, Q. (2009). The oldest articulated osteichthyan reveals mosaic gnathostome characters. *Nature*, *458*(7237), 469–474.

Zhu, Y.-A., & Zhu, M. (2013). A redescription of *Kiangyousteus yohii* (Arthrodira: Eubrachythoraci) from the Middle Devonian of China, with remarks on the systematics of the Eubrachythoraci. *Zoological Journal of the Linnean Society*, *169*(4), 798–819.

Zhu, Y.-A., Zhu, M., & Wang, J.-Q. (2016). Redescription of *Yinostius major* (Arthrodira: Heterostiidae) from the Lower Devonian of China, and the interrelationships of Brachythoraci. *Zoological Journal of the Linnean Society*, *176*(4), 806–834.

Ziermann, J. M., Miyashita, T., & Diogo, R. (2014). Cephalic muscles of Cyclostomes (hagfishes and lampreys) and Chondrichthyes (sharks, rays and holocephalans): Comparative anatomy and early evolution of the vertebrate head muscles. *Zoological Journal of the Linnean Society*, *172*(4), 771–802.